UPDATE OF THE STATE PAVEMENT MANAGEMENT SYSTEM AND IMPLEMENTATION OF THE MECHANISTIC-EMPIRICAL PAVEMENT DESIGN GUIDE

FINAL REPORT

PRINCIPAL INVESTIGATOR:
Adrian Ricardo Archilla, Ph.D.
Associate Professor

PREPARED IN COOPERATION WITH:
State of Hawaii, Department of Transportation,
Materials Testing and Research Branch and
U.S. Department of Transportation, Federal Highway Administration

Honolulu, Hawaii
March 25, 2014

Technical Report Documentation Page

1. Report No. FHWA/HI-15-53463	2. Government Accession No.	3. Recipient's Catalog No.
4. Title and Subtitle *Update of the State Pavement Management System and Implementation of the Mechanistic-Empirical Pavement Design Guide*		5. Report Date March 25, 2014 6. Performing Organization Code
7. Author(s) Adrian Ricardo Archilla, Phillip S. Ooi, and Luis G. Diaz Vasquez		8. Performing Organization Report No.
9. Performing Organization Name and Address Department of Civil & Environmental Engineering University of Hawaii at Manoa 2540 Dole Street, Holmes Hall 383 Honolulu, HI, 96825		10. Work Unit No. (TRAIS) 11. Contract or Grant No.
12. Sponsoring Agency Name and Address Hawaii Department of Transportation Highways Division 869 Punchbowl Street, Honolulu, HI, 96813		13. Type of Report and Period Covered FINAL 8/1/2005 to 8/1/2012 14. Sponsoring Agency Code

15. Supplementary Notes
Prepared in cooperation with the U.S. Department of Transportation, Federal Highway Administration

16. Abstract

The Hawaii Department of Transportation (HDOT) needs to update its pavement design procedure and pavement management system (PMS). For new pavement sections, calibration of the Mechanistic-Empirical Pavement Design Guide (MEPDG) was performed with the help of tools developed for development of Historical Pavement Structural Information (HPSI); development of axle load spectra (ALS), number of axles per vehicle, and lane distribution factors; and processing of roughness. Testing of material characteristics was performed, including dynamic modulus (|E*|) of Hot Mix Asphalt (HMA), HMA permanent deformation and fatigue cracking, resilient modulus (Mr), binder testing, permeability of permeable base material, and coefficient of thermal expansion of Portland Cement Concrete (PCC). Local models of |E*| and Mr are examined and the difficulties for selecting Mr, created by non-linearities and environmental effects, are analyzed. Simple rules are presented to select Mr input values. A procedure is presented to limit the number of simulations needed for calibration of the MEPDG for cracking and roughness. In addition, a mechanism for top-down fatigue cracking is postulated. Overall, it is shown that the MEPDG can produce reasonable results for Hawaiian conditions. For implementation, after personnel training, it is recommended to use the MEPDG for a few years in tandem with the current procedure to develop calibration data and getting experience with it. Changes to the HDOT design procedure (e.g., traffic loading) are proposed.

For the PMS, it is found that although pavement condition has been collected for years, there has been a lack of consistency in terms of the protocols used, the length and location of the pavement segments, and the calculation of the Pavement Condition Index (PCI). The capabilities of StreetSaver©, RoadSoft©, and PAVER™ were analyzed in detail. It is found that any of these programs (and others) can satisfy HDOT needs if some data issues discussed are overcome. This research advanced the most with PAVER™, for which a network of almost 2,000 pavement sections for Oahu was created and populated. Guidelines for the use of PAVER™ that complement the Users' Manual have been created as well as a program to prepare the data for import into PAVER™. Consequently, if HDOT select a low cost software for its PMS, the suggested order or preference for adoption is 1) PAVER™, 2) StreetSaver®, and 3) RoadSoft®.

Recommendations are provided for solving many PMS and MEPDG issues.

17. Key Words	18. Distribution Statement
Pavement Management, Mechanistic-Empirical Pavement Design, Resilient Modulus, Dynamic Modulus, Permanent Deformation, Fatigue	Document is available to the U.S. public through the National Technical Information Service, Springfield, VA 22161.

19. Security Classif. (of this report)	20. Security Classif. (of this page)	21. No. of Pages	22. Price
Unclassified	Unclassified	646	

Form DOT F 1700.7 (8-72) **Reproduction of completed page authorized**

ACKNOWLEDGEMENTS AND DISCLAIMER

The authors are grateful for the funding and support provided by the **Hawaii Department of Transportation** (HDOT) and the **Federal Highway Administration** (FHWA).

The authors greatly appreciate the support and patience of Casey Abe (HDOT) and Steve Ege (HDOT). Without it, some of the most useful contributions in this report could not have been accomplished. The authors are also grateful for the many contributions and interactions at different stages of the project of the following individuals at HDOT's Material Testing and Research Branch: Herbert Chu, Brandon Hee, Kwok Ming Ng, Wayne Kawahara, Joanne Nakamura, and Loy Kuo (C&CH, formerly at HDOT).

A substantial portion of this report is based on field data provided by the HDOT Planning Branch. The authors are thankful to Goro Sulijoadikusumo (HDOT) for his contributions, for giving them remote access to the Road Information System and for assisting in delivering other data not available online. The delivery of some of these latter data items by Richard Akana (HDOT) and Jennifer Arinaga (HDOT) and the troubleshooting of RIS and Photo log connection problems by Thomas Giguere (Intergraph Corporation) is greatly appreciated.

The authors are also grateful to the following individuals and organizations for providing complimentary assistance to the project in the form of materials, mix design, invitations to participate in industry meetings, advise, etc.: Richard Levins of Grace Pacific Corporation (GPC), Jeromy Castro (GPC), Rich Gribbin of Jas W. Glover Ltd., Arist de Wolf of Alakona Corporation, Kimo Scott of OK Hardware, Jon Young of the Hawaii Asphalt Pavement Industry (HAPI), Wayne Kawano of the Portland Cement Concrete Industry (PCCI) and Cyndy Aylett and James Matsusaki from the City and County of Honolulu (C&CH).

The contributions of former graduate research assistants Jayanth Kumar Rayapeddi Kumar, Angel Panizo Espuelas, Diego Munar Castaneda, Letizia de Lannoy Kobayashi, Steve Havel, Scott Kauai, and Chao Huang are acknowledged and appreciated. In some cases, part of their theses directly form part of this research report and in others, their work provided a starting

point for work presented in this report. The project also benefitted from the thesis and dissertation work of the co-PI students Michelle Sagario and Dr. Yonghui Song.

Finally, the authors would like to thank the Transportation Engineering colleagues at the UH Department of Civil and Environmental Engineering, Dr. Panos Prevedouros for helping with a traffic survey and Dr. Constantinos Papacostas for allowing the participation on a large number LTAP workshop trainings and advisory committee meetings, which in addition to the knowledge acquired on them provided a venue for interacting with many of the people in the industry.

TABLE OF CONTENTS

LIST OF TABLES

LIST OF FIGURES

CHAPTER 1. INTRODUCTION

1.1 BACKGROUND

The main goal of this project was to update the Hawaii Department of Transportation (HDOT) pavement design and pavement management practices. In particular, for pavement design, an effort towards calibration of the recently developed Guide for Mechanistic-Empirical Design of New and Rehabilitated Pavement Structures [1] for Hawaiian conditions was to be performed. The guide is also widely known as the Mechanistic-Empirical Pavement Design Guide (MEPDG), which is the term most often used in this report. The MEPDG software was released for research purposes in 2004. The first commercial version of the software was named DARWin ME, and as of 2013, it has been renamed Pavement ME Design [2].

The pavement design procedure currently used by HDOT for *flexible pavements* is based on the Gravel Equivalent (GE) concept developed by Francis Hveem for the California Department of Transportation (CALTRANS). The procedure relies on an empirical approach to pavement design. It does not have an explicit mechanism to evaluate the use of new materials, such as Stone Matrix Asphalt (SMA) mixes, Polymer Modified Asphalt (PMA) mixes, or mixes with some other type of additives. The contribution of Hot Mix Asphalt (HMA) to the pavement structure is taken into account through a "gravel factor", which does not depend on the HMA characteristics. Furthermore, the traffic loading factors (known as ESAL constants or ESALC in the HDOT procedure, as explained later in section 3.2) were based on traffic loading from the 1970's. Thus, there was a need to evaluate whether new values for these constants were warranted if the procedure continues to be used.

HDOT's personnel and consultants are very familiar with this design procedure, which for the most part produces long lived pavement structures. However, the current HDOT design procedure has no formal mechanism to calibrate it for local conditions. In contrast, a main advantage of a Mechanistic-Empirical (ME) approach is that it allows for calibration to local conditions and consideration of factors other than layer thicknesses, thus potentially allowing the study of more cost-effective designs. Of course, these procedures also demand a better

understanding of pavement design, geotechnical engineering, mix design, and traffic loading analysis. Therefore, their successful implementation requires substantially more training.

With respect to pavement management, existing data, data collection technologies, and different software for Pavement Management Systems (PMS) needed to be evaluated.

For a PMS to function and serve the agency´s objectives, it is necessary to properly address the obstacles and difficulties that could hamper its smooth operation. Multiple reasons could make implementation of a PMS difficult; among those reported in the literature are specific interests of particular stakeholders, organizational internal barriers, inappropriate funding, poor commitment from upper management, and poorly trained personnel to run the system to name a few ([3], [4], [5]). The existence and success of a PMS also relies on the information contained in a properly designed database ([4], [6]), which ideally should contain detailed information about Historical Pavement Structural Information (HPSI), traffic volumes, climatic data, number of lanes, deterioration history, etc. Appropriate integration and management of these pieces of information can provide a sound basis for determining homogeneous pavement management sections and defining families with similar deterioration patterns [7]. Although all information is desired for the correct functioning of the PMS, inventory information (HPSI), condition data, and costs are critical [5].

Pavement Management at HDOT has been performed largely by use of Excel® spreadsheets and apparently ad-hoc procedures for treatment selection and timing. As indicated in [8], the scope and complexity of managing a network of the size managed by HDOT (approximately 1,100 centerline-miles) require a more sophisticated system. However, no software will be useful without feeding it with adequate and timely data. One of the obstacles for the use of any formal procedure is the availability of data adequate for pavement management. Currently, data are available at different locations at HDOT and they are not always readily available for easy access or analysis. For example, some pavement structural information is available on as-built plans (which are accessible on-line for HDOT personnel), but often these only show the material and thickness for the latest overlay or for the layers of the last reconstruction and little, if anything is indicated about the rest of the pavement structure. Although the exact pavement structure is not often needed at the network level, still some

indication of the overall structure is useful for some analyses. The recent update to the Highway Performance Monitoring System (HPMS) requirements for pavement thicknesses appears to be an attempt to capture similar information for the nation's highways [9].

Different types of performance indicators are needed for a successful implementation of a PMS. At a minimum, some form of pavement condition indicator based on the measurement of specific pavement distresses is needed. Typically, the indicators are obtained by measuring individual distresses such as alligator cracking, longitudinal cracking, rutting, raveling, etc. for flexible pavements and faulting, cracking, spalling, etc. for rigid pavements and combining them through formal procedures into a single index. Dealing with a single index is typically easier for communicating the results to the public although individual distresses are also used for some other purposes such as the definition of treatment trigger values in some PMS. Examples of such indexes are the Pavement Condition Index (PCI) standardized in ASTM D6433 and the PASER (Pavement Surface Evaluation and Rating) system [10]. Pavement condition information is usually complemented with roughness measurements, a kind of user serviceability index, as provided by the International Roughness Index (IRI) and to a lesser degree by friction measurements for safety assessment and deflection measurements for structural evaluation. Ground Penetrating Radar has also been used for estimating as-built layer thicknesses by some agencies.

HDOT has been routinely collecting IRI information. As with any large data collection effort, one may find some localized problems with the data but for the most part IRI measurements are reliable and repeatable. Another piece of information that has been collected regularly at HDOT is pavement condition. Unfortunately, although pavement condition information has been collected for years, there has been a lack of consistency in terms of the protocols used to collect the information, the length and location of the pavement segments, and the calculation of the index. For example, for years, the pavement condition was collected on one mile segments. These segments are typically too long to be homogeneous in terms of pavement structure, number of lanes/traffic loading, subgrade conditions, etc. For this and other reasons that will be explained later in the report, the use of the historical information has been too limited to develop pavement performance curves or for calibration of the MEPDG. In terms of pavement structural information, although HDOT has a Falling Weight Deflectometer (FWD) to measure

pavement deflections, it is not used regularly for network monitoring. Nevertheless, not all highway agencies use it for this purpose. However, currently the FWD is rarely used also for structural design. If a ME design approach is adopted, it would be desirable to change this situation (actually, this is desirable whether or not a ME design approach is used.) Friction information is not currently collected at all.

There is a need for HDOT to select and start using a modern commercial PMS software, to streamline the procedures and communication protocols for collecting and storing the PMS data.

This project was intended to advance in the implementation of both the MEPDG and the PMS. Although significant work still needs to be performed to fully implement a PMS and calibrate the MEDPG, considerable progress has been made in several areas. This report documents the advances made, many of the challenges that were encountered along the way, and discusses areas that required further study.

1.2 PROJECT SCOPE

This project deals with the improvement of two very different but intrinsically related tools. The MEPDG and the PMS in general involve different activities. Nevertheless, ideally these two should interact with each other. PMS data should provide feedback for calibration of the MEPDG and the MEPDG could help in predicting pavement condition. At the outset of the project, it was recognized that much of the information available could potentially be useful for both. Therefore, a significant effort was directed towards evaluation and processing of existing information that could potentially help both activities.

Along the way, several tools were developed to process data to put it in a more usable format for the intended use. In particular, tools that were created for this purpose include a pavement inventory processing tool that allows the re-creation of the pavement structure from spreadsheets with thickness and material information that were mined by HDOT personnel; a roughness processing tool that allows the visualization of the voluminous roughness information, automatic segmentation into statistically homogeneous segments, and correction (shifting/compression/ stretching) of the roughness series to correct locational problems; a traffic loading processing tool to obtain axle load spectra and the average number of axles of different

configurations (single, tandem, tridem, and quad) from Weigh-in-Motion (WIM) data; and a tool to compute the Pavement Condition Index (PCI) outside of any specific PMS software such as MicroPAVER® (now referred to and marketed as PAVER™ by the developer) and to transform the distress information so that it can be imported into PAVER™. Some of the tools, such as the traffic loading processing tool were developed out of necessity because of issues encountered with existing software. A new piece of software for data preparation for the MEPDG is currently under development by University of Oklahoma researchers. Since the PI is helping HDOT in this pool fund study, a limited evaluation of that software capabilities has also been performed.

At the outset of the project it was recognized that the existing pavement condition information and pavement structural information was probably too limited to perform a thorough calibration of the MEPDG. Therefore, significant effort was directed to measure material properties needed as input. This also meant instrumenting a pavement laboratory at the University of Hawaii at Manoa (UHM) for which a significant portion of the effort and budget of this project was spent (complemented with funding from UHM for some equipment). In particular, testing capabilities were added for measuring dynamic modulus, permanent deformation, indirect tensile resilient modulus, and fatigue cracking of Hot Mix Asphalt (HMA), viscosity, dynamic shear modulus, creep and recovery, and aging of asphalt binders, permeability of coarse aggregate gradations (to evaluate an alternative to the existing untreated permeable base specification), resilient modulus of base and subbase materials, and coefficient of thermal expansion (CTE) of concrete specimens.

The equipment described above was used to carry out a thorough evaluation of 12.5-mm Nominal Maximum Aggregate Size (NMAS) Superpave mixes with varying air voids, asphalt contents, and binder types from which models for dynamic modulus and permanent deformation were developed. The 12.5 NMAS mixes have basically the same gradation as the State Mix Type IV, which appears to have been the most prevalent mix used throughout the State in recent years. A more limited study of fatigue cracking characteristics was also conducted for these mixes. Some limited binder testing was performed, including viscosity and dynamic shear modulus determinations as well as creep and recovery characteristics. In addition, some unbound base materials and foamed asphalt bases have been tested for resilient modulus. Finally, a study of the CTE of Portland Cement Concrete (PCC) specimens of three field mixes was also performed.

There reasons why much more effort was put into evaluating properties of HMA than of PCC are that first, flexible pavements currently represent about 80% of the HDOT network and second, that until very recently no data was available for one of the most relevant distresses for Hawaiian conditions, namely faulting. The MEPDG calibration for PCC pavements essentially requires cracking, faulting, and roughness information. Thus, without faulting information, which is probably the main reason that some PCC pavements have recently been retrofitted with dowels in Oahu, calibration of the MEPDG was not really possible. If the collection of faulting information that was started in 2010 as part of the pavement condition information survey by the planning branch is continued, then calibration of the MEPDG for PCC pavements may be possible in the future.

Based on the structural information available, new pavements or reconstructions were identified to perform a calibration effort of the MEPDG for new pavement sections. Sections have also been identified for calibration of HMA overlays of flexible pavements. Since in the design of overlays some of the same calibration parameters derived for new pavements are used, attention was first directed towards the calibration for new HMA pavements. Only a limited number of sections were found with data available for this purpose. Furthermore, after some initial unsuccessful calibration efforts, particularly of the fatigue cracking predictions, a review of the available fatigue cracking information was deemed necessary. Fortunately, remote access for the principal investigator (PI) to the HDOT Roadway Information System (RIS) and photo log was restored in 2013[1], which was useful for accessing valuable information. A review of the photo log allowed the estimation of new cracking data that was finally used for the calibration effort. On the one hand, the process was so slow that it was not possible to collect the cracking information for overlays. Because of this and the lack of reliable information about the conditions of pavements before they were overlaid, calibration of the MEPDG for rehabilitation projects has not been possible. On the other hand, performing this activity (obtaining cracking information from the photo log) was very beneficial as it allowed the observation of how fatigue cracking evolves over time for state roads, particularly those with substantial HMA thickness (10

[1] The access had been lost for technical reasons.

to 16 inches of HMA over untreated base or subbase, which were the most common in the sample.) Most of the fatigue cracking on these pavements appears as longitudinal cracks over a short time span and it rarely evolves into a typical pattern of fatigue cracking. Over a long period of time, several longitudinal cracks may appear on a wheel path which are occasionally joined by transverse cracks. Still, the pattern does not resemble the typical alligator cracking pattern associated with structural base failures. On the thinner pavements (on the order of 6 inches of HMA), the same pattern is observed initially but then it is followed by the formation of transverse cracks between both wheel paths forming a pattern that resembles that of block cracking (note that this observation is based on a very limited number of sections). The reason for the formation of the transverse cracks in this case it is not entirely clear, but it is believed that the most likely cause is asphalt aging/oxidation than thermal cracking. Although this is based on a very limited sample, many pavement sections throughout the State appear to display that type cracking. With Hawaii's relatively small temperature fluctuations, it is difficult to believe that this would be related to thermal cracking, except perhaps on very thin pavements (~ 2 to 3 inches of HMA), which provide a very small cross section to resist tensional forces caused by the friction between the base and the HMA with thermal contractions.

With the limited available information collected, a first calibration of the MEPDG was performed for new pavements. The initial calibration shows that with reasonable accurate inputs, the MEPDG can produce reasonable results for Hawaiian condition. In the process, several issues that need further study have been identified. In addition, a procedure that allows calibration of the MEPDG with a limited number of runs has been developed.

It is recognized that full implementation of the MEPDG, if HDOT decides to do so, would take several years. In the interim, it is necessary to continue using the HDOT design procedure. Thus, although the procedure is left largely unchanged, a few recommended changes are proposed. The most salient one is the use of new traffic loading factors.

The capabilities of three different PMS programs were also studied at different points in time using available data: StreetSaver©, RoadSoft©, and PAVER™. As indicated earlier, a PMS is much more than just the software. It is believed that in terms of their capabilities all three of the programs evaluated (as well as a few other that were not evaluated in detail) could be used by

HDOT. For reasons explained later in the report, the efforts with PAVER™ were most fruitful in this research project. A network of almost 2,000 pavement sections for Oahu has been created and populated with basic information within PAVER™. Sectioning was performed based on an analysis of several of the pieces of information described above. Also guidelines for the use of PAVER™ that complement the Users' Manual have been created.

Although most the effort in this project was spent on the analysis of data and software capabilities, it has been observed that HDOT faces the same type of implementation difficulties reported in the literature. Specifically, conflicting interests of particular stakeholders, lack of buy-in, staffing challenges, and the need for better communication.

1.3 REPORT ORGANIZATION

The report is organized as follows. Chapter 2 describes efforts to create an inventory of pavement structural information using mined data from as-built plans. Chapter 3 describes the analysis of the traffic loading information from the Weigh-In-Motion (WIM) stations and how the data were used to develop axle load spectra (ALS) for ME pavement design and derive of the updated ESALC used in the current HDOT flexible pavement design procedure. This chapter also presents a study of the distribution of trucks by lane at the WIM locations. Then, chapter 4 deals with the analysis of the historical pavement distress and roughness information. Distress data are essential for both the PMS and calibration of the MEPDG. Chapter 5 provides an overview of ME pavement design procedures in general and the MEPDG approach in particular. The concepts discussed in this chapter provide a context for the material presented in the two subsequent chapters. In chapter 6, the results of material characterization testing performed in this study as well as the information from previous local studies and elsewhere are analyzed. In chapter 7, an extensive description of the challenges found to calibrate the MEPDG are described along with the calibration results. In particular, a procedure to reduce the number of simulations needed during calibration for fatigue cracking is presented. Several simulations outside the MEPDG are performed to illustrate the effects of material non-linearities and temperature distribution with depths. The latter may help to explain the pervasive occurrence of longitudinal fatigue cracking observed on Hawaii roads. Chapter 8 describes in detail the three PMS pieces of

software evaluated and provides suggestions for implementation. The last chapter summarizes the findings and provides recommendations for implementation and future research.

CHAPTER 2. PAVEMENT STRUCTURE INVENTORY

2.1 INTRODUCTION

As discussed in the previous chapter, Historical Pavement Structural Information (HPSI) and pavement condition data are critical for the correct functioning of a PMS [5]. Pavement structural information is typically an important factor in sectioning the network into approximately homogeneous segments. This is an important consideration in the development of deterioration models that rely on the similarity between sections to define families of pavements with similar deterioration patterns. Obviously, pavement sections with similar pavement structures, similar traffic loading, with the same number of lanes, same highway type (e.g.: local, arterial, freeway), located in similar environments and constructed on similar subgrades are more likely to behave more similarly than pavements with differences in one or more of these features.

Reliable information on traffic, number of lanes and highway type are available in HDOT's Planning Branch databases and therefore, with proper manipulation, these are readily available for use in the PMS. Other information such subgrade soil is not yet readily available. Subgrade information could be added over time as the information is obtained from new projects. The structural information may still be useful even if HDOT decided to perform a Ground Penetrating Radar (GPR) survey and/or a Falling Weight Deflectometer (FWD) survey for the whole network. In the case of GPR, the historical structural information would help in the understanding of the layering that may have been created over time with consecutive overlay and/or mill-and-overlay activities and also provide some information of unbound layers that may not be known without coring. An FWD study at the pavement section level should be accompanied by some coring. However, for decisions at the network level, coring would be prohibitively expensive. Thus, the historical information, along with traffic loading, may shed light on places with large deflections and distress differences between sections.

At the start of this project, it was recognized that reliable pavement structural information at the network level was not readily available. Thus, after identification of this shortcoming, HDOT personnel undertook the mining of data on pavement structural information

from as-built plans. Unfortunately, for reasons beyond the control of the principal investigator, the data were stored in spreadsheets with inconsistent formatting for the different islands. More importantly, however, are the complications encountered for reconstructing the pavement history.

Although the process of reconstructing the pavement structure history is in principle simple for a given road segment, several challenges needed to be overcome to simplify the task and make it practical at the network level. To facilitate the processing of information available in HDOT´s archives, a Pavement Structure Processing Tool (PSPT) was developed. The present chapter describes the development of the Pavement Structure Processing Tool (PSPT), and describes its capabilities to generate Historical Pavement Structural Information (HPSI), along with challenges encountered and potential room for improvements in future software versions. Most of the information provided in this chapter was presented in Archilla & Diaz [11].

2.2 NATURAL SECTIONING OF A HIGHWAY OVER TIME

Highways are usually designed and constructed through projects of limited length. Usually, there are differences in the structural design from project to project or even within the length of a project due to changes in one or more factors such as changes in traffic loading (e.g., changes after an entry or exit ramp), changes in subgrade materials, changes from fill to cut sections, etc. This leads to a natural sectioning of the route.

In addition to the above, further sectioning occurs when maintenance and rehabilitation (M&R) activities are carried out on only portions of the original sections or over lengths comprising more than one section, generating many shorter sections each with unique pavement structural history. As illustrated in Figure 2-1, where three different pavement sections are converted into five new structural sections after a simple mill-and-overlay operation (represented schematically by the dash lines), situations like these are actually quite common.

In addition to changes along the alignment, changes in pavement structural history can also occur across lanes because of either lane additions or rehabilitation activities on selected lanes only.

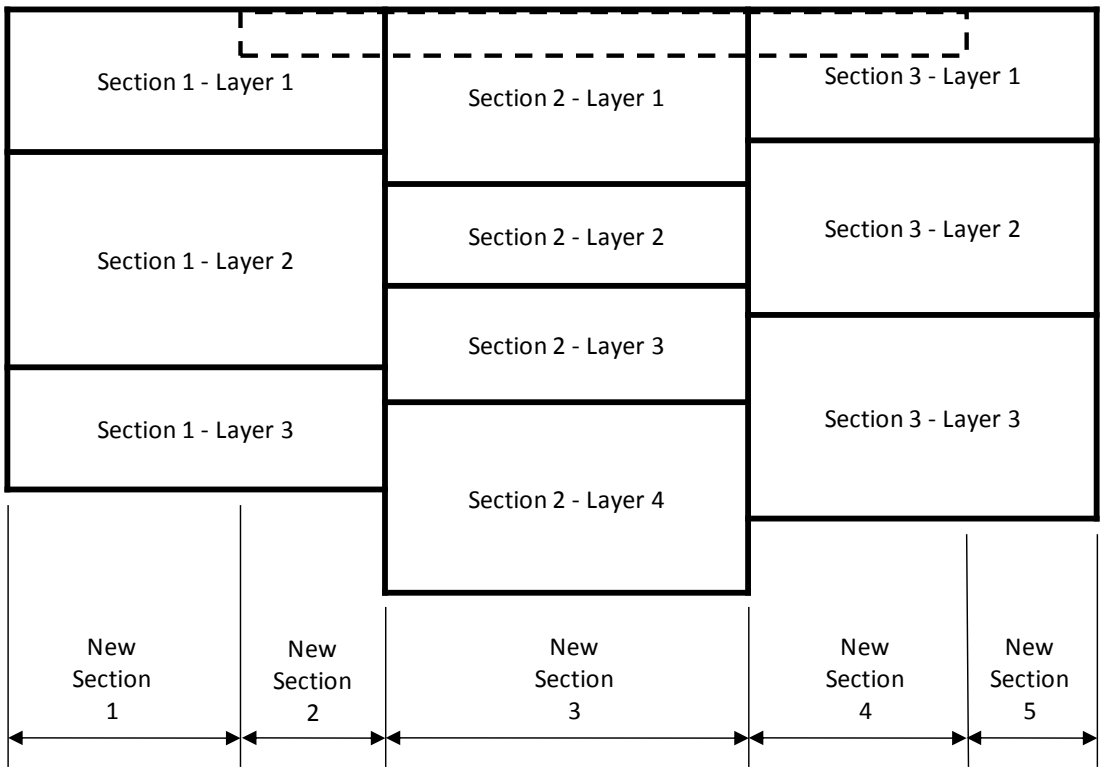

Figure 2-1. Additional sectioning resulting from M&R activity (mill-and-fill represented by the dashed lines).

2.3 BACKGROUND OF DATA MINING ACTIVITIES

Personnel from HDOT's Materials Testing and Research (MT&R) Branch mined data containing pavement structural information. The information consists mainly of material types and layer thicknesses extracted from as-built plans. Due to personnel changes over the data collection period, different technicians were involved in the task. As a consequence, the data were stored in different spreadsheets for different counties with slight differences in format among the spreadsheets.

The structure of the spreadsheets was similar for all counties. However, there were differences and other details that made their automated or semi-automated processing challenging such as:

- Information collected on a project basis. In most cases, a project contains relatively good information on layers that were added, some information on removed or milled

layers and often little or no information on existing layers; as a result, very often an engineer would need to search the pavement history to get an approximation to the existing pavement structure or obtain field cores for more detailed information.

- Minor differences in the structure of the different files (e.g., different number of columns and different layer types, differences in the convention used to designate lanes and directions affected in a given project (e.g., identifying all lanes affected by a project in a single column or on separate columns), placement of non-numeric fields with potentially useful information where only numeric information should be, and the consideration of a comments' field often carrying other useful structural information).
- No information about the location of the layers within the pavement structure. In most situations the application of common sense by an engineer can recreate the order of the layers in the field (for example bound layers are above unbound layers, materials labeled as bases should be above materials labeled as subbases, finer Hot Mix Asphalt (HMA) mixes should be above coarser mixes (if built in the same year), etc. However, forcing an engineer to perform such an analysis for each section would make the process too inefficient (or it would simply not be done.)

Appropriate labeling of the materials used within the pavement structure is useful, but identification of similar material types with different labels should be avoided. For instance, for all practical purposes, Untreated Base Course, Untreated AB (Aggregate Base), AB, and Base Course may all refer to very similar materials complying with the agency´s specifications; in this case, it would be advisable to identify all of them with a standard name. Although this appears to be a logic assumption, it is common to encounter this situation where different personnel is involved in data gathering activities.

Each spreadsheet contains four sets of columns plus a column with comments. The first set of columns contains general information for each project whereas the next three sets of columns contain the layer thicknesses for existing layers (if such information was available in the as-built plans), removed layers, and added layers, respectively. Layers names were in the first row of the original spreadsheets.

Figure 2-2 shows portions of a worksheet as mined by HDOT personnel corresponding to the Big Island illustrating the set of columns with general information and part of the set of columns with thickness information for existing layers (which are shown in the figure with a heading "Existing" in yellow). Notice that there is a column for each material encountered in any project (columns were apparently added to the existing, removed, or added categories as new materials were found in the plans). For a given project, most of the columns will be empty as clearly illustrated in Figure 2-2. Furthermore, all valid projects should have some non-empty "added layer" information but may or may not have "existing and removed layer" information.

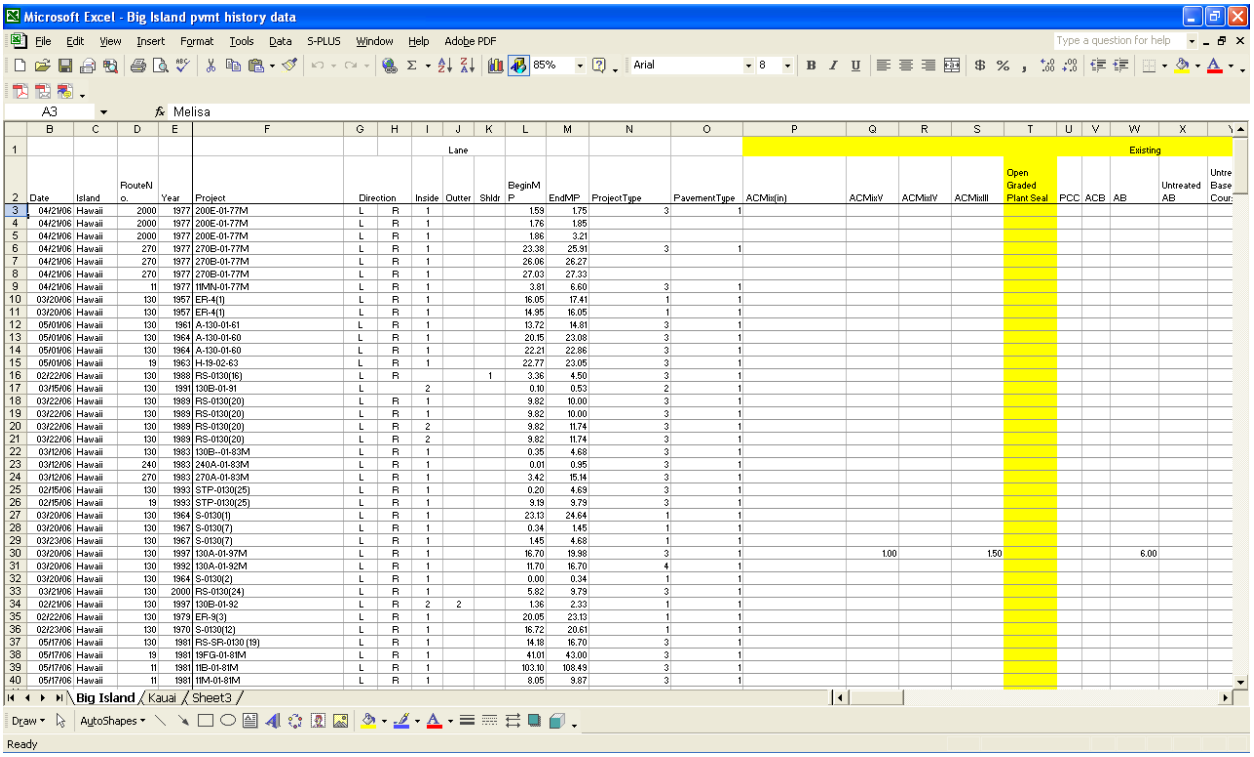

Figure 2-2. Pavement history data worksheet for the Big Island.

Figure 2-3 shows another snapshot of the same worksheet illustrating the added layer information. Clearly, the materials do not always appear in the same order for the existing, removed and added layers. In fact, one material that may appear in the "added" category may not be present in the "existing" or the "removed" categories. Furthermore, the headings are not always spelled equally. The differences are even more pronounced when one compares

worksheets for different islands. Figure 2-4 shows a snapshot of the Oahu worksheet. Contrasting Figure 2-2 with Figure 2-4, it can be observed that in Figure 2-2 there is a column for "Open Graded Plant **Seal**" whereas in Figure 2-4 there is a column for "Open Graded Plant **Mix**". Figure 2-4 shows an "ACmix unspecified" for Oahu but no such column is found in the existing category in the Big Island worksheet. These are just two examples of the differences between worksheets. There are too many others to list them here.

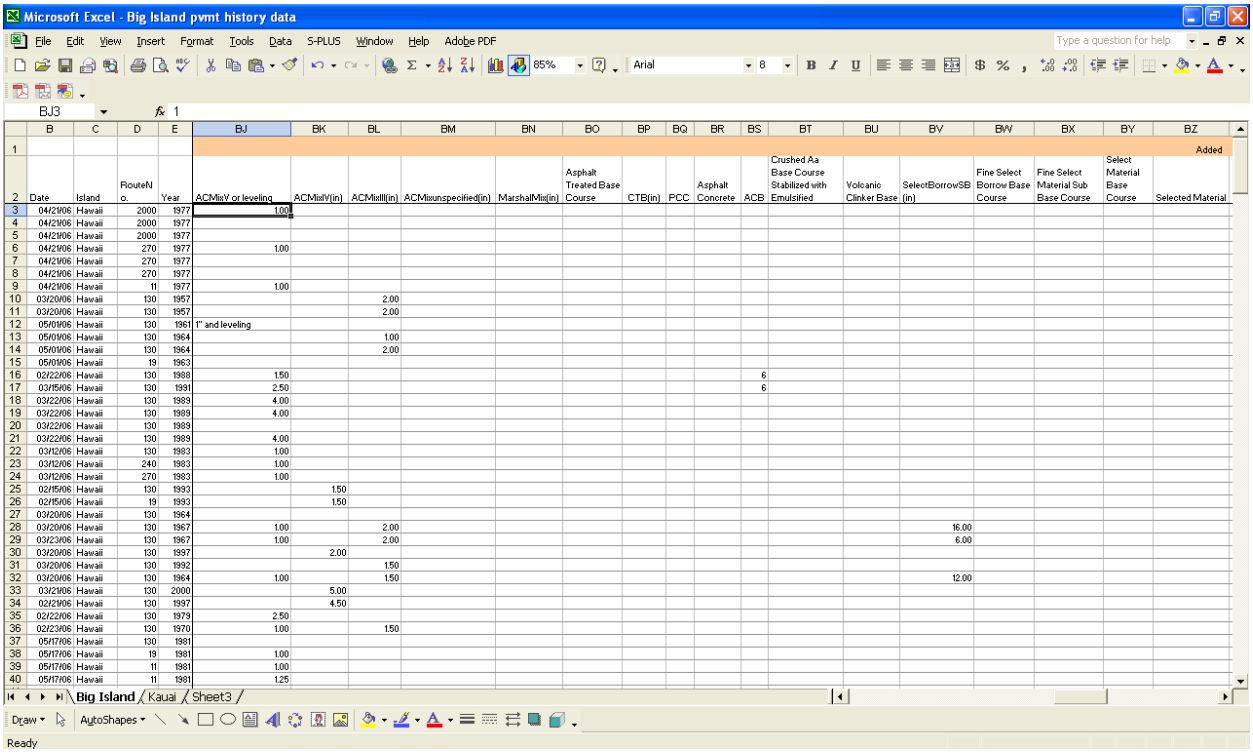

Figure 2-3. Another view of the pavement history data worksheet for the Big Island.

Since different materials (and/or description of materials) were used in the different islands, most worksheets contain a different number of columns. Obviously this makes the automated processing of the data complex. Figure 2-3 illustrates another problem found in many cases. As can be observed in row 12 under the heading "ACMix V or leveling", in many occasions the worksheet contains text (***1" or leveling*** in this example) instead of a numeric value. This again makes automated processing of the information quite challenging.

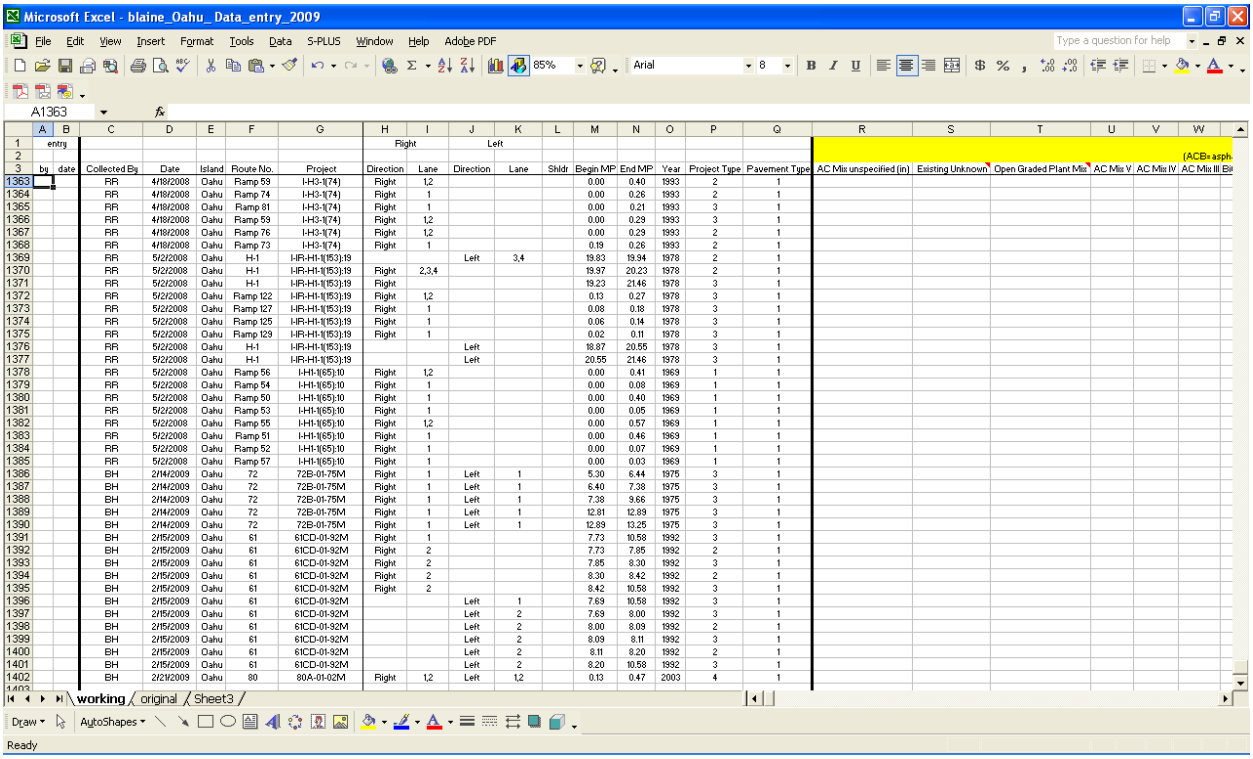

Figure 2-4. Pavement history data worksheet for the Oahu.

A more important difference between the worksheets (compare again Figure 2-2 and Figure 2-4) is that not all general information columns are the same. In order to deal with the most problematic differences, the worksheets were modified manually with the structure shown in Figure 2-5 and Figure 2-6. Obviously, a minimum number of changes were performed to the structure of the spreadsheets. In terms of columns, the main difference is the consideration of the direction and lane affected. As illustrated in Figure 2-5, now the three or four columns used in the original worksheets have been converted into 14 columns. An entry of "Right" in the column labeled "DirectionRight" (or MP+) indicates that work was done in that direction. This column is followed by six lane columns containing a non-zero number for each lane affected by the project (1 for lane 1, 2 for lane 2, etc.). The same logic was applied for the left direction. Most two-lane two-way highways would contain only a 1 under Lane1R and Lane1L if work was performed in both directions. Although additional columns were needed with this structure, it makes reading the data simpler and consistent between worksheets.

Another important modification was done to the top rows. The top-most row now contains either a zero (nothing is also acceptable in this case) or the words “Existing”, “Removed”, and “Added” for the different layer categories. The purpose of this modification is to be able to discriminate the category of the layer in the column (i.e., “Existing”, “Removed”, and “Added”) or whether the column contains other type of general information. A restriction is that the existing layers category has to be followed by the removed layers category and this in turn must be followed by the added layers category (that is, the order of the categories cannot be changed). Nevertheless, the number of material types in each category can be arbitrary, which provides significant flexibility.

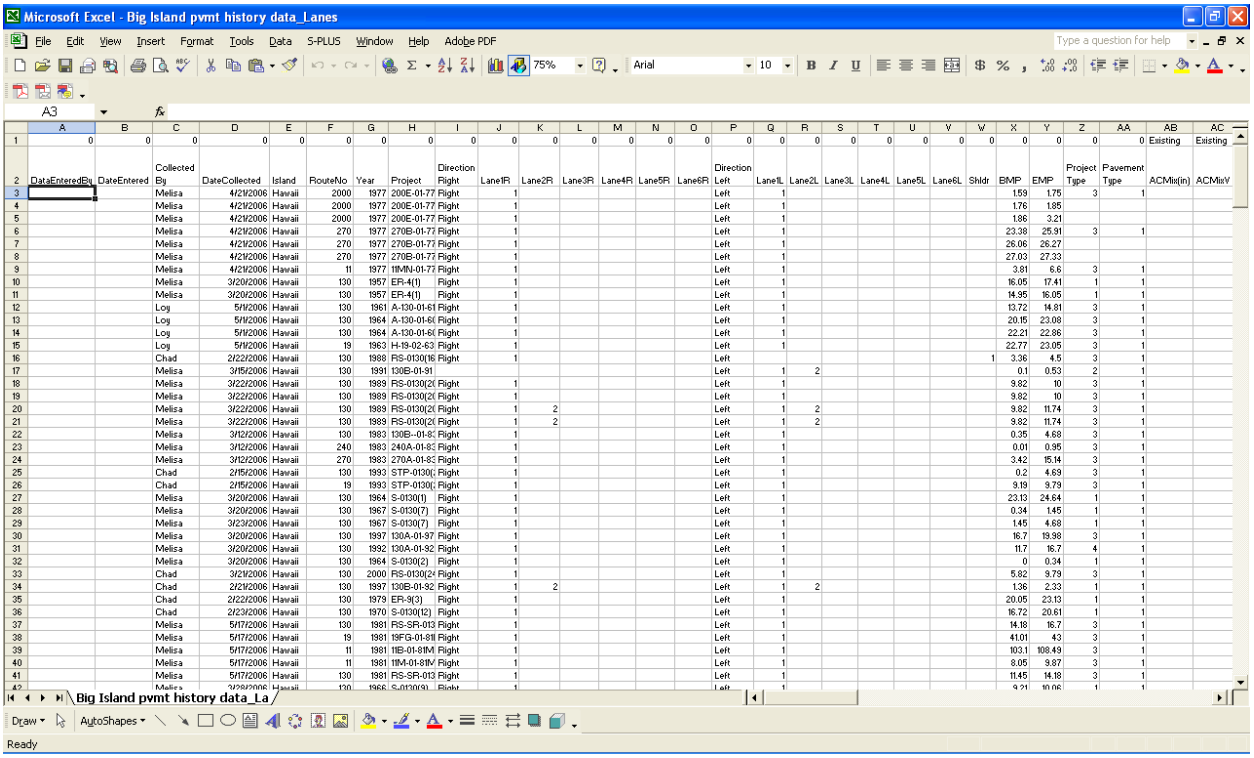

Figure 2-5. Modified worksheet for pavement history for the Big Island.

Figure 2-6 provides another view of the modified spreadsheet showing some of the existing, removed, and added layers. It also illustrates again examples of fields containing non-numeric information.

In order to read the files with the PSPT, the excel file has to be exported as a comma delimited file (CSV).

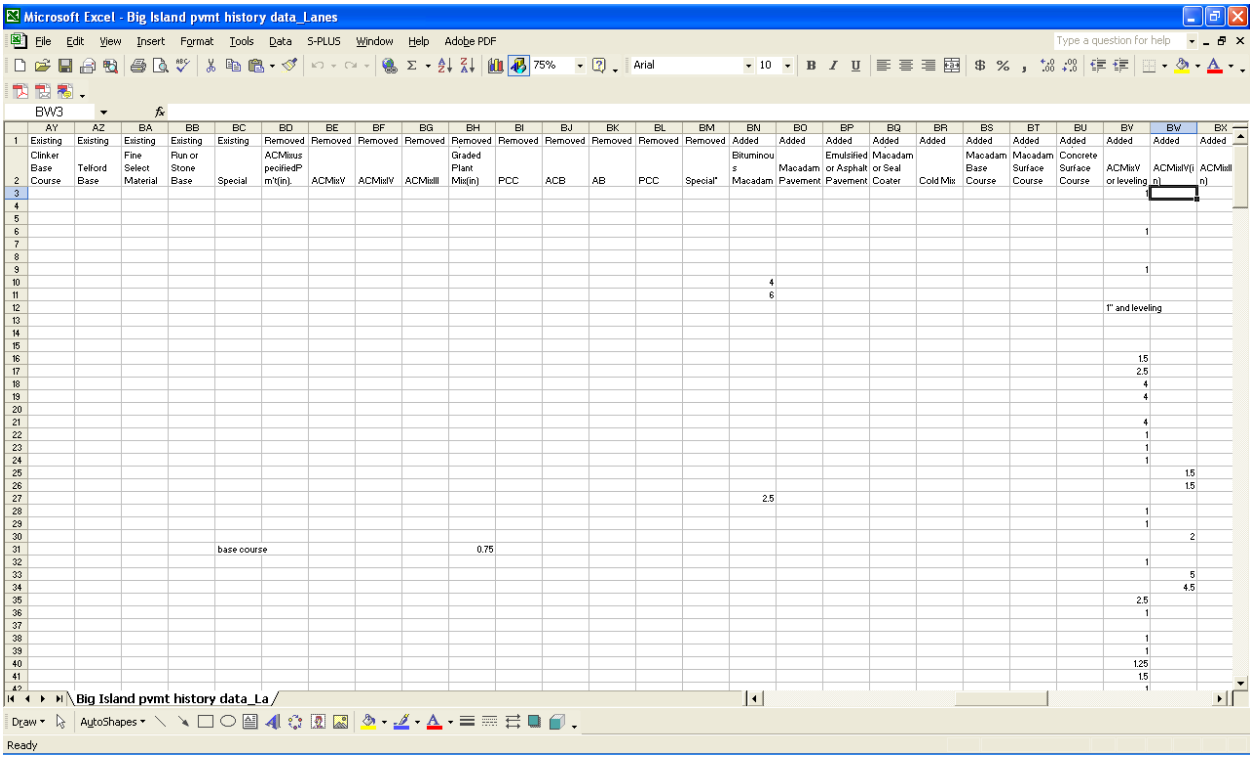

Figure 2-6. Another snapshot of the modified worksheet for pavement history for the Big Island.

It is important to note that subgrade information was not available in the recorded data; however, this information could be added to the database over time as the information is obtained from new projects or existing soil reports.

2.4 PAVEMENT STRUCTURE PROCESSING TOOL (PSPT)

As discussed earlier, there are many challenges that need to be overcome to process the mined pavement structural information automatically. This section describes some of the most important features of the Pavement Structure Processing Tool (PSPT) developed to use the mined data to generate Historical Pavement Structural Information (HPSI), thus facilitating the organization and interpretation of such information for the state´s Pavement Management System.

2.4.1 General Layout

Figure 2-7 shows a snapshot of the main program screen, which is divided in three main areas. On the left, a docking panel labeled “Inventory Section Selection” is located. This panel contains three parts, identified as “Route & Direction” (for selecting a route and direction for analysis), “Begin MP – End MP” (for selecting a mile point range for analysis from the list of available mile points for the selected route and direction), and “Structure History” (for observing and editing pavement structural history). Although only one of the parts is visible at a time, the second and third panels have been overlaid in Figure 2-7 for the reader´s clarity).

On the top center of the screen there is room for a chart that shows the pavement structural history graphically. Finally, on the top right side there is another docking panel that contains options for the chart. A docking panel is a panel that can be docked to different locations of the interface or be converted into a floating window. Although this is mostly a cosmetic interface issue, it provides tremendous flexibility for the user to adopt their preferred configuration layout.

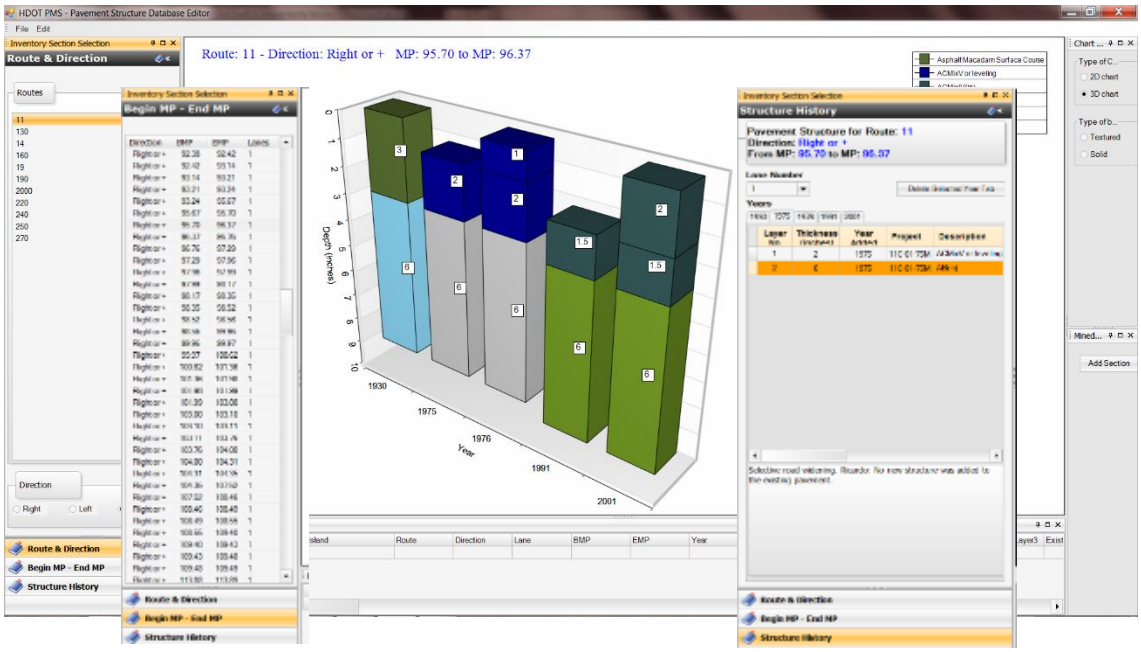

Figure 2-7. Initial screen of the pavement structure database editor.

2.4.2 Importing Data

The PSPT provides a menu option for importing the pavement structure data files. After selecting the option, the PSPT presents a standard Windows "File Open" dialog box that allows the user to select an appropriately formatted input file (generally a comma delimited file, i.e., *.csv). After a confirmation message indicating that the file has been read successfully, the list of routes will be updated with the routes imported as shown on the left panel in Figure 2-7. It must be pointed out that this step involves a lot more than just simply reading the data file. In fact, after reading the file, the information is sorted by route, then by direction within a route, then by lane and finally, the information for the lane is segmented into sections with unique pavement structural history. The segmentation for each route involves creating a list with "begin" and "end" mile points for all the M&R and reconstruction projects related to the route (including all lanes), sorting the mile points, eliminating all the duplicates, and then creating the segments.

The reconstruction of the pavement history is done on the fly when the user selects a route and, within a route, a section between two mile points. Initially, no route is selected in the list of routes. After selecting a route from the list and a direction to be analyzed from the radio buttons at the bottom of the pane (as shown in Figure 2-7), a list of subsections available for the route is created under the pane labeled "Begin MP – End MP", as indicated in the left overlay in Figure 2-7 (when the PSPT is running, activating the "Begin MP – End MP" information will hide the list of routes).

Once the user clicks on a given "subsection", the pavement structural history is created on the fly based on the input information and is immediately displayed in the chart. Figure 2-8 displays the chart together with the "Structure History" pane (described later) instead of the "Begin MP – End MP" pane (note that before selecting a subsection the chart would not be visible). The material for each layer is displayed on the chart legend (upper corner in the right); while the thicknesses are displayed in the data labels on each layer in whatever units were used in the input file (inches in the examples discussed here.) The chart also displays a title with the information for the route, direction, and begin- and end-mile points. Options for two- and three-dimensional charts are provided as well as tooltips describing the layer names (the latter feature being very useful when many layers appear on the legend).

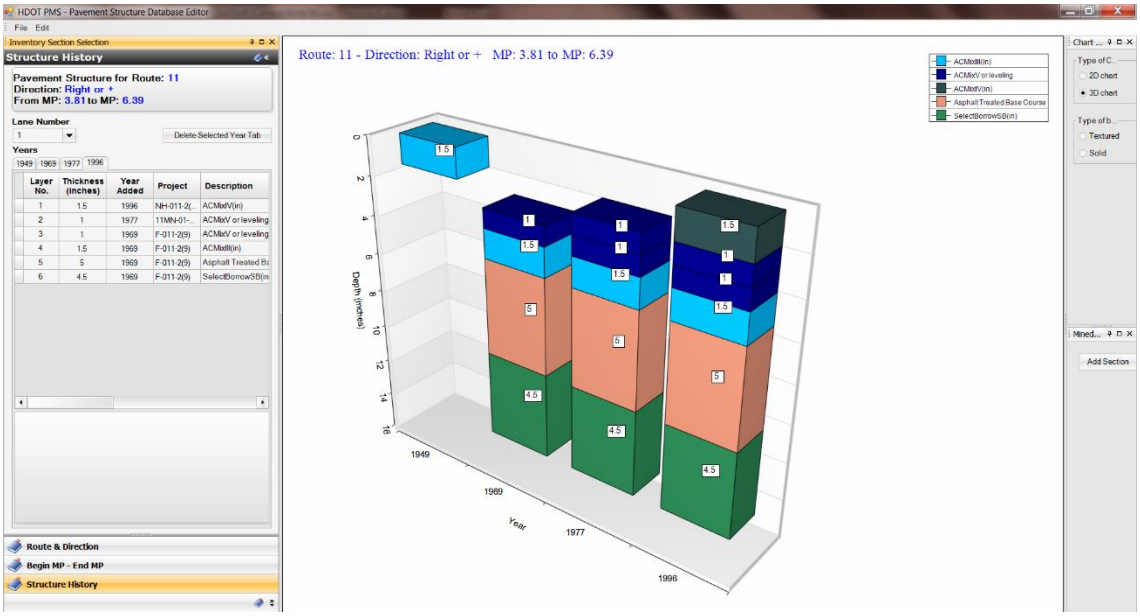

Figure 2-8. Structure history pane and pavement structural history chart.

The "Structure History" pane displays the details of the recreated pavement structure history (Figure 2-8). The subsection´s general information is presented at the top of the pane (essentially the same information presented in the chart title), followed by a set of tabs created on the fly for each year in which an M&R or reconstruction activity occurred.

Each tab contains a grid with the pavement structural information. Except for the layer number, which is automatically assigned, all other fields are editable by the user. Notice that the program produces an automated ordering of the layers based on some engineering common sense rules involving a large number of substring comparisons to produce a logical ordering. However, the ordering is produced for each year. That is, layers from different years are not interchanged since that would produce an illogical chronological ordering. For example, in Figure 2-8 the layer with Mix Type IV, which was constructed in 1996, is correctly shown above the layers with Mix Type V that were created in previous years. If these same materials had been used in the same year, the ordering would have been reversed since Mix Type V has a smaller nominal maximum aggregate size (NMAS) than Mix Type IV, and it would be logical that a mix with smaller NMAS be used as a surface course on top of a coarser asphalt mixture.

The position of the structure for each year with respect to the top of the chart also deserves explanation. In order to explain the process, the concept of a reconstruction sequence is introduced. A reconstruction sequence starts with a year corresponding to either new construction or reconstruction of a pavement section and ends in the last recorded year before another reconstruction occurs. Consider for example the case in Figure 2-8. According to the existing records, that section was first constructed in 1949 with only 1.5 in. of AC Mix III (no information for lower layers is available). Since the section was then reconstructed in 1969, the first reconstruction sequence consists only of year 1949 (that is the last year with an activity before a new reconstruction.) To date, there is no record of other reconstruction of that section; consequently the second sequence includes all recorded years since 1969, that is, 1969, 1977, and 1996. It is now relatively simple to explain the positioning of the layers in the chart. For a given reconstruction sequence, the top of the thickest pavement section is arbitrarily located at the zero depth whereas the top of the layers for the other years in the sequence are located so that the position of the layers appearing in several years are the same for all years in the sequence. Thus, in the example, the thickest pavement structure in the first sequence is the only pavement structure in that sequence, that is, the one for 1949; so its top is located at zero depth. However, the thickest structure for the second sequence occurs in 1996 and thus the top of the structure for that year is located at the zero depth. It is clearly seen in the figure how the other layers align in previous years. This allows the appreciation of the changes in grade occurring over time due to overlays. Unfortunately, there is no information in the file for determining the relative grade when reconstruction occurs, and therefore, jumps like the one shown in Figure 2-8 that are clearly related to reconstructions should not be interpreted as changes in grade (it simply shows that there is no information indicating the relative grade before and after the reconstruction). Notice that in this particular example it is possible that the 1.5 in AC Mix III layers shown for 1949 and 1969 had the same grade but there is really no way of knowing this from the information provided.

2.4.3 Editing Options

As shown before, the program is able to distinguish between reconstructions (in which case the information from previous years is not carried forward) and overlays (in which case the

information from previous years is used to recreate the pavement structure when information for existing layers is not present). However, there are occasions where the user may need to make some changes. This section describes some features that have been added for editing the pavement structure information.

Figure 2-9 shows a case in which the history recreation may be dubious. As shown in the figure, a 3-in asphalt Macadam surface course on top of a 6-in stone base course was built in 1930. Then, based on the information in the input file the pavement was rehabilitated by constructing on top of the existing structure a 6-in aggregate base (AB) and a 2-in AC Mix V. However, although possible, the raising of the grade at once by 8 inches raises doubts of whether the information in the input file is correct. Furthermore, it is unlikely that the aggregate base would have been laid out directly on top of a bound material. In addition, the similarities of the added and existing structures may also raise some concern. In fact, for this section the original information was not entirely appropriate. This project corresponds to a selective widening as shown in the comment section below the grids under the "Years" label in Figure 2-9.

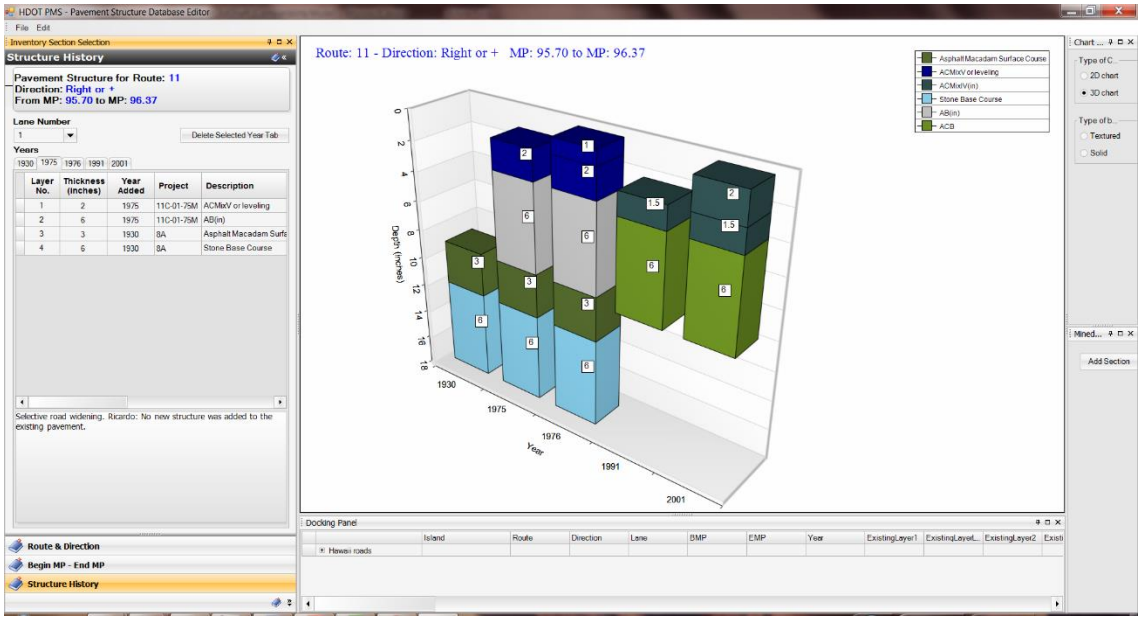

Figure 2-9. Case where history may be dubious.

In this particular example the comment also provided the information that for this project no new structure was added to the original section. However it must be pointed out that in this

particular case this part of the comment was added by the authors during a rapid check of the plans. The point is that even if this part of the comment had not been present, a simple analysis like the one presented above could prompt the user to double check the information in the as-built plans. In this case, since it is known that the structure is basically unchanged, either the new layer information or the existing layer information must be deleted and/or modified. Notice also that apparently, the whole structure was completed in two consecutive years. Several options are provided to make changes relatively simple. First note that the values in the grid can be edited by simply selecting a cell and start typing the new values (standard rules, such as pressing "F2" to start editing the information in the cell also work.)

Another option is to right click on a row that needs modification. As shown in Figure 2-10 several options are presented to the user. The selected layer can be moved up (this option will not be active if the selected layer is the top layer), moved down (not active if the selected layer is the bottom layer as shown in the figure), and deleted. In addition, another empty line can be added above or below the selected layer. Added lines should then be edited to add meaningful information.

Clearly, as illustrated in this case, the deleted layers in 1975 also need to be deleted in subsequent years. This could become tedious and repetitive for the user if the information propagates to several subsequent years. Thus, in order to avoid repetitive work the program recognizes that when the user chooses to delete or move a layer in a given year, it wants to do so in the following years as well (note that the layer information in years prior to the selected one will not be altered). Of course, in order for a layer to be deleted or moved in several years at once, it is required that all the layer information (except for the layer number) be identical in subsequent years, and the layer must be in the same place with respect to the layer used as alignment reference (only the first matching layer is used for layer alignment). It is important to note that the layer information may not match up exactly if the user has previously edited the information in one year.

Suppose that in the current example, the user decided to delete the 6-in stone base course and the 3-in asphalt Macadam surface course in 1975; these two layers would also need to be

deleted in 1976. Figure 2-10 shows the resulting structure with those two deletions in 1975 (done automatically by the program).

Since the HDOT may wish to standardize the layer descriptions (for example, eliminating the "(in)" from the descriptions or combining different names that describe similar materials), a last editing option "Select Layer Description" is provided in a pop-up menu that appears when the user clicks a row on the "Description" column. Notice that a new option for selecting a layer description is given at the bottom of the list. When clicked, a list with standardized names is displayed (lower right corner of Figure 2-10). At this point, this list contains a few names just for testing, but HDOT should develop a more comprehensive list containing most cases of interest. Selecting a layer description from the list and pressing the OK button changes the description to the selected standardized name.

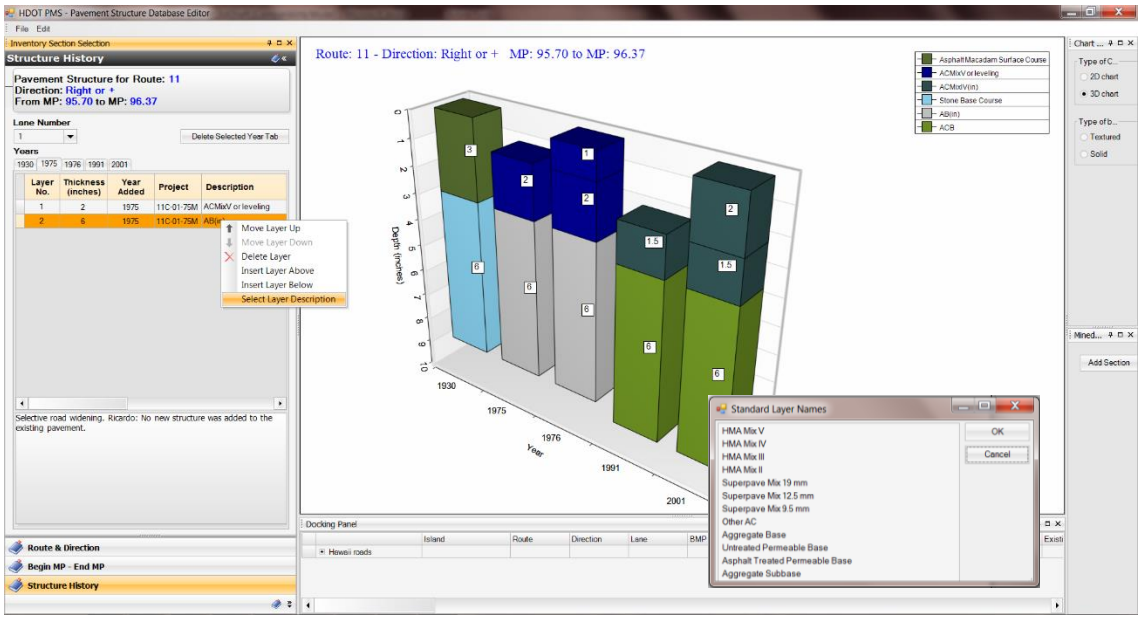

Figure 2-10. Pavement structure after deletion operation and editing options.

When the input file contains non-numeric information in places where numeric information is expected, this information is appended to the comments of the project by adding three pieces of information: the first is the layer type, which is taken from the heading of the cell where information is found; the second, labeled "Other info", is the information found on the cell

being read from the input file (particularly useful when it contains some information about likely thickness); and the third is the project number.

Whenever numeric information is provided for removed layers in the input files, this information is taken into account automatically. Figure 2-11 shows an example in which the top 2-in of the existing layers built in 1969 are milled before being overlaid in 1990 with 2.5-in of asphalt concrete base and 3.5-in of Mix Type IV.

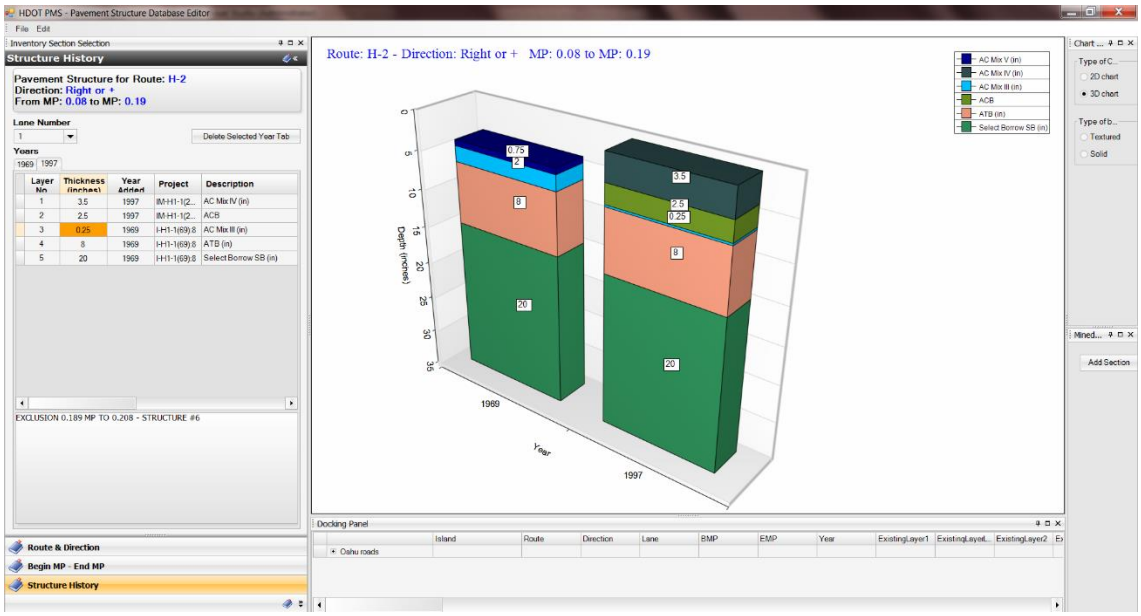

Figure 2-11. Automatic handling of partially removed layers.

2.4.4 Pavement Structure Processing Tool (PSPT) Potential Improvements

Although the current version of the PSPT is already operational and can greatly reduce time and effort in generating HPSI for the entire state´s road network, there are some areas that need to be enhanced and further developed in order to serve its purpose in a broader way. Some of the desired features include:

- Provision of the capability for saving the changes performed by the user in a permanent and carefully designed database.
- Ability to make the number of sections more easily manageable.

- Ability to identify and correct small errors in the locations of the “begin” or “end” mile points of some sections while importing data, as they lead to the creation of non-existing small sections. It would be desirable for the PSPT to be able to analyze a significant number of sections on a given route for all lanes and directions simultaneously, allowing the user to make decisions about sectioning the network based on pavement structure.
- Ability to create and export HPSI in formats that can readily be used in commercially available PMS software.
- Integration of HPSI with other geometric and traffic information.
- Development of a process to perform periodic updates of the database without unduly significant effort.

2.5 DISCUSSION AND SUMMARY

The existence and success of a PMS relies on the information contained in a properly designed database with different types of data from the road network. An important piece of information is the Historical Pavement Structural Information (HPSI). Although the process of reconstructing the pavement structural history is in principle simple for a given road segment, several challenges need to be overcome to simplify the task and make it practical at the network level.

In order to generate the HPSI from as-built plans and visual surveys already available in the Hawaii Department of Transportation, a Pavement Structure Processing Tool (PSPT) was developed. With the PSPT, a sound basis for rational sectioning of the State of Hawaii pavement network can be established, which is fundamental in the development of deterioration models that rely on the similarity between sections to define families of pavements with similar deterioration processes.

The reconstruction of the HPSI obtained with the Pavement Structure Processing Tool (PSPT) also provides a basis for the analysis of the historical distributions of times between maintenance and rehabilitation activities (M&R) and reconstructions for different types of pavements, which can be useful for monitoring actual practices within the agency, for analyzing

potential M&R policy changes and for assuming realistic scenarios during Life Cycle Cost Analyses (LCCA). HPSI could also be useful for interpretation of Ground Penetrating Radar (GPR) surveys since it could assist in the understanding of the layering that may have been created over time with consecutive overlay and/or mill-and-overlay activities, and also provide some information of unbound layers that may not be known without coring. Additionally, the PSPT could also be helpful for the agency in fulfilling the Highway Performance Monitoring System (HPMS) reporting requirements, which now include pavement structural information.

Although there is significant room for improvements in future versions of the PSPT, its current version can greatly reduce time and effort in generating HPSI for Hawaii´s road network.

CHAPTER 3. TRAFFIC LOADING ANALYSIS

3.1 INTRODUCTION

Traffic loading information is essential for any pavement design procedure; yet, it is often difficult to characterize accurately. Traffic loads, primarily those of heavy vehicles, cause stresses/strains in pavement structures whose effects accumulate over time resulting in pavement deterioration such as plastic deformation in Hot Mix Asphalt (HMA), fatigue cracking in HMA and Portland Cement Concrete (PCC), and faulting in PCC.

This chapter presents the development of some traffic inputs required by the design procedures using information from Weigh-In-Motion (WIM) and Automated Vehicle Classification (AVC) stations located across the state.

3.2 USE OF TRAFFIC LOADING DATA IN PAVEMENT DESIGN

Traffic loading data are typically available for different heavy vehicle classes. Classification of heavy vehicles is typically done following the Federal Highway Administration (FHWA) 13 vehicle classes. Figure 3-1 shows vehicle classes 4 to 13, which represent the heavy vehicles. Vehicle classes 1, 2 and 3 represent motorcycles, autos, and four tired trucks (pick-ups), respectively and their effects on pavement design are negligible.

Traffic loads and their impact on pavements are quantified primarily in terms of:

- number of axles of a given configuration,
- configuration of these axles, and
- axle load magnitudes.

Other factors that affect pavements are:

- timing of load applications (time of day and season within the year),
- vehicle/axle lateral placement (wander),
- vehicle/axle speed, and
- tire pressure.

Vehicle Class	Schema	Description
4		Buses
5		Two–axle, six–tire, single–unit trucks
6		Three–axle single–unit trucks
7		Four– or more than four–axle single–unit trucks
8	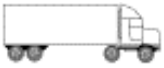	Four– or less than four–axle single trailer trucks
9	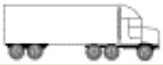	Five–axle single trailer trucks
10	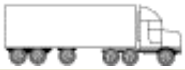	Six– or more than six–axle single trailer trucks
11		Five– or less than five–axle multi–trailer trucks
12		Six–axle multi–trailer trucks
13		Seven– or more than seven–axle multi–trailer trucks

Figure 3-1. FHWA vehicle classes 4-13.

Axle configuration is defined by the number of axles sharing the same suspension system and the number of tires in each axle. Multiple axles involve two, three, or four axles spaced 4 ft. (1.2 m) to 6.5 ft. (2.0 m) apart, and are referred to as tandem, triple, or quad respectively. The stresses and strains imposed by each axle in a multiple axle configuration overlap at certain depths and therefore must be treated differently from single axles.

One common approach to quantify traffic loading is by classifying traffic into different vehicle classes for which the average number of axles of each configuration (single, tandem, tridem, and quad) are determined and deriving the axle load spectrum or distribution for each axle configuration on each vehicle class. This is the approach used in the MEPDG and used implicitly in one way or another by all roadway pavement design procedures.

For example, in the widely used 1993 AASHTO Pavement Design Guide procedure [12] all traffic loading is reduced to an equivalent number of load repetitions of an Equivalent Single

Axle Load (ESAL) of 18,000 lb. In order to find that single number of ESALs, the number of repetitions expected over the design period of each axle configuration within a load interval of the spectrum is multiplied by a Load Equivalency Factor (LEF) appropriate for the axle configuration/load interval combination. The LEF transforms the number of applications of the axle configuration in the particular load interval into an equivalent number of repetitions of the standard single axle load that would have the same effect on the pavement structure. The total number of ESALs over the design period is then obtained by adding the contributions of each axle configuration/load interval combination for each vehicle class over the design period.

The axle load spectrum for a given axle configuration (single, tandem, tridem, or quad) of a particular vehicle class (4, 5, .., or 13) is defined by the percentage of the total axle applications of the axle configuration in the particular vehicle class that fall within the particular load interval. The definition of load intervals typically used is provided below:

- Single axles – 0 to 3 kips, 3 to 4 kips,…, 39 to 40 kips (beyond 3 kips, the intervals are of 1 kip).
- Tandem axles – 0 to 6 kips, 6 to 8 kips,…, 78 to 80 kips (beyond 6 kips, the intervals are of 2 kips).
- Tridem and quad axles – 0 to 15 kips, 15 to 18 kips,…, 99 to 102 kips (beyond 15 kips, the intervals are of 3 kips).

As can be seen, computation of ESALs requires knowledge of the axle load spectrum of each axle configuration of each vehicle class. In addition, the percentage of heavy vehicles (commonly referred to as trucks although they include buses) in the traffic stream as well as the percentage of each heavy vehicle class relative to the total of heavy vehicles are also needed. Since basic traffic information typically available includes the Annual Average Daily Traffic (AADT) or Annual Average Daily Truck Traffic (AADTT = AADT x percentage of trucks) in both directions, a directional distribution factor as well as a lane distribution factor for multilane facilities in one direction are also needed. Of course, traffic growth factors are also required to properly quantify traffic over the design life.

3.2.1 Truck Factor

Historically, dealing with traffic loading spectra (and in turn with load equivalency factors for each axle configuration/interval) was cumbersome for routine pavement design. Therefore, the calculations were typically simplified using the concept of a truck factor (TF). The TF for a given vehicle class represents the average number of ESALs applied by one passage of the vehicle class in question. To illustrate, consider a semi-trailer truck with a single steering axle of 12,000 lb. and LEF = 0.19 and two tandem axles each with 34,000 lbs. and LEF = 1.10. Thus, for this hypothetical truck, the TF is simply computed as 0.19 + 1.10 +1.10 = 2.39 ESALs. Of course, for real highway traffic, each passage of the same truck class would most likely have different loads for the single and the tandem axles. Thus, the TF is derived by using axle load distributions of the single and tandem axles on the vehicle class to compute the total number of ESALs applied by a large sample of that truck and diving it by the corresponding number of trucks in the sample. This is a calculation that is done only once in a while for a given WIM station or stations in a region. When this TF is then used in a particular project, the implicit assumption is that the axle load distributions at the design site are the same as those used to obtain the truck factor.

3.2.2 ESALC or ESAL Constants

Computation of ESALs in the HDOT design procedure relies on a factor called ESALC or ESAL Constant. The ESALC is simply the TF multiplied by 365. In other words, the value of the ESALC represents the average number of ESALS contributed by one passage of the truck in question on every day of the year. The only difference in the calculation of ESALs with the use of TF or ESALC is that for the TF the value of 365 has to be used explicitly in the calculations to convert daily loading calculations into annual calculations whereas the 365 factor is already embedded in the ESALC.

3.3 MEPDG TRAFFIC LOADING INFORMATION REQUIREMENTS

Traffic loading information is used by the MEPDG to estimate the strains induced by the different traffic loads and the frequency with which those strains are induced throughout the pavement's design life. As for other inputs in the MEPDG, traffic loading can be characterized

using a hierarchical approach that allows using better information for important projects and default values for smaller projects. This is done to facilitate the use of the MEPDG regardless of the level of detail of available traffic data. The MEPDG defines three broad levels of traffic data input (Levels 1 through 3) based on how well future truck traffic characteristics can be estimated. The three levels are defined in the MEPDG as:

- Level 1 – There is very good knowledge of past and future traffic characteristics.
- Level 2 – There is modest knowledge of past and future traffic characteristics.
- Level 3 – There is poor knowledge of past and future traffic characteristics.

For Level 1, the traffic data measured at or near a site must include *counting and classifying* the number of trucks traveling over the roadway, along with the breakdown by lane and direction, and *measuring the axle loads* for each class to determine the truck traffic for the first year after construction.

Level 2 requires the collection of enough truck *volume* information at a site to measure truck volumes accurately. This includes being able to account for any weekday/weekend volume variation, and any significant seasonal trends in truck loads (e.g., in areas affected by heavy, seasonal, agricultural hauls).

Level 3 uses a regional or statewide average load distribution (or other default distribution table).

The MEPDG requires some basic traffic (or traffic related) input data, including:

- Initial two-way Annual Average Daily Truck Traffic (AADTT).
- Number of lanes in the design direction.
- Percent of trucks in the design direction (directional distribution factor).
- Percent of trucks in the design lane (lane distribution factor).
- Operational speed.
- Vehicle class distribution and growth.

All these factors are site specific and should be estimated for each particular project. For HDOT projects, AADTT (or AADT and percentage of trucks), (heavy) vehicle class distribution,

and an overall traffic growth factor are typically furnished by the HDOT Planning Branch. Operational speed can be estimated from speed limits or reasonable estimates for roadways with recurrent congestion and/or traffic signals. For the percent of trucks in the design direction, except for special situations, the assumption of the 2002 HDOT Pavement Design Manual [13] of 50% on each direction is still reasonable.

Currently, the most problematic parameter is the percentage of trucks in the design lane. The 2002 Pavement Design Manual [13] assumes 100% for 2 lanes in one direction, 80% for 3 lanes in one direction and 75% for 4 lanes in one direction. These values appear to be very conservative. Values of percentage of trucks in the design lane based on the most recent WIM and AVC measurements are presented with the analysis of WIM data later in this chapter.

Developing an estimate of vehicle operational speed is important for flexible pavement design using the MEPDG. As discussed later in section 6.2, frequency of loading (or equivalently the duration of the stress pulse or load duration) directly influences the stiffness response of the asphalt concrete layers within the pavement structure. The magnitude and duration of the stress pulses caused by the passage of a load depend on the *vehicle speed*, type, and geometry of the pavement structure, and the location of the element under consideration. Thus, the speed of the vehicle can result in a different load frequency, resulting in different moduli values for the HMA layers.

In addition to the basic information, the MEPDG requires the following inputs:

- Traffic volume adjustment factors.
  - Monthly adjustment.
  - Vehicle class distribution.
  - Hourly truck distribution.
  - Traffic growth factors.
- Axle load distribution factors.
- General traffic inputs
  - Number axles/trucks.
  - Axle configuration.
  - Wheel base.

Obviously, to be practical, only a few of the inputs can be project specific. The following sections describe the efforts to determine the most important of these inputs for Hawaiian conditions that can be used for different roads throughout the State.

3.4 ANALYSIS OF HAWAIIAN WEIGH-IN-MOTION DATA

This section describes the analysis of data from the weigh-in-motion (WIM) stations located throughout the State. The analysis is based on millions of heavy vehicle records from 11 Weigh-In-Motion (WIM) and Automatic Vehicle Classification (AVC) stations located on the islands of Hawaii (2 stations), Maui (1 station), and Oahu (8 stations). The data used for the analysis were collected by the HDOT Planning Branch from 2006 to 2012 (though a variable number of years with valid data were available for the different stations). Figure 3-2 shows the locations of all the stations and Figure 3-3 shows the stations in Oahu only.

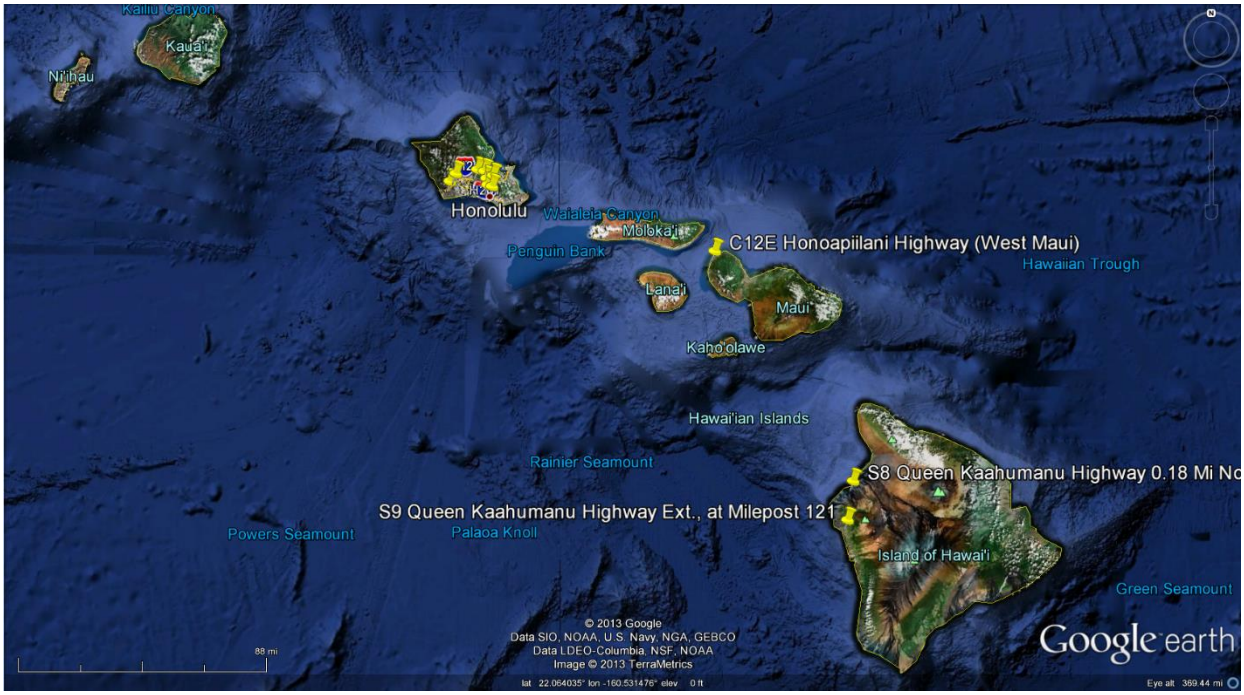

Figure 3-2. Locations of WIM stations as of 2012 in Hawaii.

Figure 3-3. Location of WIM stations as of 2012 in the island of Oahu.

The emphasis of the analysis is on those factors that are routinely required for pavement design but that are not easy to characterize for each single project. Specifically, the analysis concentrates on the factors needed for the characterization of the axle load spectra (axle load weight distributions) for the new MEPDG design procedures (which are also useful in the HDOT design procedure for new rigid pavements) and in the update of the ESAL Constants (ESALC) used in the HDOT design procedures for new flexible pavements (the ESALC are based on the axle weight distributions).

3.4.1 Tools used to analyze the WIM data

As described in reference [14], there are several primary causes for obtaining invalid data from WIM stations, including: system component malfunctions, loop timeouts, weight sensor thresholds, classification algorithms, calibration factors, rough pavement, roadway geometry, congestion, lane closeure and alignment shift, lane changing while crossing sensors, and weather related factors. Consequently, several data quality check procedures are recommened to be followed by an agency's WIM Office Data Analyst [14].

This section is limited to the processing of the data obtained from the WIM stations in Hawaii as obtained from files of type "wgt" defined in the TMG [15]. The files were provided by HDOT's Plannning Branch. The analyses in the following sections pertain to issues observed from the data provided and do not include other aspects that may have been performed prior to the generation of the "wgt" files.

Given the voluminous amount of information generated by WIM stations, it is imperative to use software to process the data. For this purpose, three different tools were used throughout the project: TrafLoad [16], PrepME, and a third tool developed by the PI.

3.4.2 TrafLoad

TrafLoad is a product of NCHRP Project 1-39, "Traffic Data Collection, Analysis, and Forecasting for Mechanistic Pavement Design" [16]. It was the first tool selected for analysis of the WIM data because its output could be used directly with the MEPDG and because of its use of rigorous data quality control checks. The program uses a rational approach to weigh observations based on well documented procedures [16] and the software is free. TrafLoad assumes that all input data have already been quality checked.

Unfortunately, while working on an interim report for this project, it was found that its use was quite cumbersome. Often, one would obtain non-informative error messages such as the one depicted in Figure 3-4, which even for someone with familiarity Structured Query Language (SQL) queries may be too cryptic to find out what the problem is and how to resolve it.

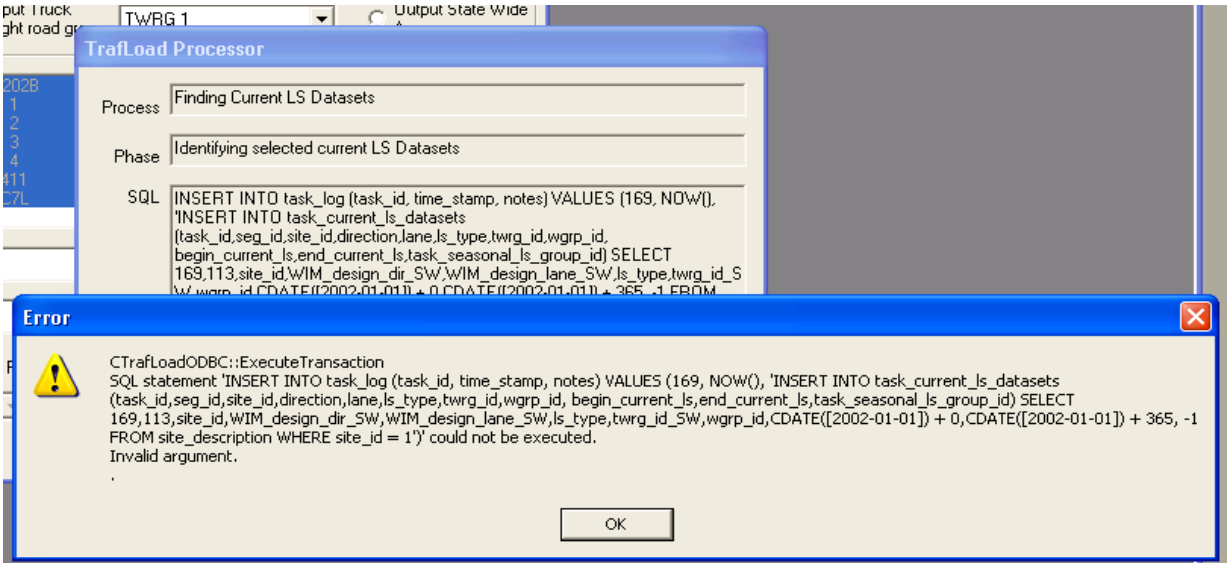

Figure 3-4. Non-informative TrafLoad error message.

Although with effort many of these issues were overcome, it was also found that on some occasions some of the output was questionable, thus also making suspicious the use of other outputs from TrafLoad. Figure 3-5 illustrates one of these problems. The figure shows an example of TrafLoad output with the estimated average number of single, tandem, tridem, and quad axles for each vehicle class. Three shaded rectangles have been added to highlight the problem. The rectangle closest to the top of the figure highlights the problems that were found with the estimation of the number of axles per vehicle for vehicle classes 4 and 5. By definition (see Figure 3-1), vehicle class 5 must have two single axles. Also, most class 4 vehicles (buses) have two single axles although some may have one single axle and one tandem axle (and some other combinations are possible for articulated buses.) Nevertheless, the average number of single axles is typically close but lower than 2. As can be seen, the predicted average of single axles for vehicle classes 4 and 5 were 3.78 and 3.99 in this example (which are essentially twice what was expected.) Similarly, for vehicle class 6, the estimated values of 2 singles and 2 tandems were double of what is correct for this class of truck (this is highlighted by the second shaded rectangle). A similar observation can be made for vehicle class 9, whose averages should be close to 1 single and 2 tandems. As can be seen in the last rectangle, once again the values were twice as expected. The most puzzling aspect of this error is that it occurred for only some

stations. It is recognized that some of these problems may have originated by lack of familiarity with the program and questionable input data. However, in that case, the program should have generated appropriate warnings instead of producing unreasonable output.

```
; ================================================================================
; MODULE, WIM
; LOAD GROUP AGPV OUTPUT
; id, description,direction, vc_id,single_ratio,tandem_ratio,tridem_ratio,quad_ratio
8,"site -    C7L",3,4,3.78,0.22,0.00,0.00
8,"site -    C7L",3,5,3.99,0.00,0.00,0.00
8,"site -    C7L",3,6,2.00,2.00,0.00,0.00
8,"site -    C7L",3,7,1.79,0.71,1.39,0.19
8,"site -    C7L",3,8,5.00,0.96,0.01,0.00
8,"site -    C7L",3,9,2.31,3.84,0.00,0.00
8,"site -    C7L",3,10,2.15,2.15,1.84,0.00
8,"site -    C7L",3,11,4.89,1.19,0.87,0.03
8,"site -    C7L",3,12,3.11,1.40,0.89,0.85
8,"site -    C7L",3,13,3.32,2.01,0.37,1.30
```

Figure 3-5. TrafLoad problematic output.

As mentioned before, TrafLoad uses rigorous quality controls. While this is a strength, at the time the analysis with this program was performed some of the requirements appeared too restrictive. Specifically, in order to be able to derive axle load spectra, TrafLoad requires a minimum of 1 week of classification counts for 12 consecutive months. This requirement meant that some stations with almost continuous data for 11 months could not be used. At that time, most stations had one month (typically December) without data. Therefore, even though for most months there were data for most of the days in the month (and typically in more than one year), that data could not be used to derive the axle load spectra.

At the time the first analysis was performed, it was considered that a better alternative was needed instead of using standard axle loadings from some other locations, thus discarding some substantial local traffic loading information with potentially acceptable quality. The rationale was that it was better to derive the axle load spectra for those months with good data and interpolate from them for the other months than using data from other locations. Any potential biases in the months with interpolated values are probably smaller than what one would get from using values from other locations. As will be seen later, the data collected during the last few years has confirmed the similarities between the different monthly axle load spectra.

3.4.3 Analysis with the customized traffic loading analysis tool and Prep-ME

Because of the issues described in the previous paragraphs, the PI developed a program to estimate the axle load spectra for each axle configuration, the average number of axles by axle type for each vehicle category, and the percentage of trucks on each lane (by vehicle class). Since the program logic is relatively simple, it is important to feed it with information from months with balanced numbers of the different days of the week to avoid biasing the distributions. Considering that most of the data selected contained information for almost the complete month, day of the week effects in the generated distributions should be minor.

More recently, the PI was also asked to represent HDOT in a pool fund study led by Dr. Kelvin Wang at the University of Oklahoma, which is developing a program named Prep-ME to prepare data for use with the MEPDG. Fortunately, the PI was able to use a beta version of Prep-ME to perform some quality checks, discard months with problematic data, and visually check that there were no significant differences between the distributions generated by the two programs. This was important as the axle load spectra used in the calibration efforts of the MEPDG were generated by the author's program in part for convenience and in part because Prep-ME could not generate the axle load spectra by direction at the time it was used (the latest release of PrepME also permits the analysis by direction.) The following paragraphs describe some of the analyses performed with the beta version of Prep-ME and the in-house traffic loading analysis tool and discuss some characteristics of the axle load spectra for the HDOT's WIM stations.

3.4.3.1 Analyses with Prep-ME

Prep-ME uses data checks from the Traffic Monitoring Guide [15]. First, it checks the front and drive axle weights of Class 9 trucks. The peaks of the distributions are expected to be between 8,000 and 12,000 lb. for the front axles and between 30,000 and 36,000 lb. for the drive tandem axles. Second, Prep-ME also checks gross vehicle weights (GVW). The GVW check is based on the observation that most sites have two peaks in the GVW distribution. The first peak typically occurs between 28,000 and 36,000 lb., representing unloaded tractor semitrailers [15]. The second peak in the GVW distribution corresponds to the most commonly loaded vehicle

condition and it falls somewhere between 72,000 lb. and 80,000 lb., although it may vary with the type of commodities transported.

In Prep-ME, the tolerable ranges on which the above peaks are expected to fall can be increased with a relaxation multiplier that ranges between 1 and 2. As shown in the box labeled "Not accepted" in Figure 3-6, most of the Hawaii WIM stations did not pass all the initial checks. Only station C202B passed all the checks[2]. However, after using the relaxation multiplier for some of the requirements, some other stations could also be considered acceptable. Notice also that the user can mark a station as "accepted" even though it did not passed all the quality checks. This is important as the quality checks flag potential problems but they do not necessarily indicate that the data are bad. Instead, they indicate that a more detailed analysis is needed.

Figure 3-7 illustrates that after further analysis other stations could be moved into the "Accepted" category. Notice that station 438 in Ala Moana Blvd. shown in Figure 3-8 is in the accepted category in Figure 3-7 even though the same figure shows that this station failed to pass the drive tandem axle weight check and the GVW check. It is important to note that the drive tandem axle check in Prep-ME analyzes the relationship of the drive tandem axle weights as a function of the GVW. This is illustrated in Figure 3-9. As can be seen in that figure, apparently the reason why Station 438 did not pass the drive tandem axle check is that for loaded trucks (> 72 kips GVW) the axle weights were slightly higher than the limit resulting from application of the relaxation multiplier to the normal range. As for the GVW, apparently the program does not identify the 2nd peak for some months of the year for this station. However, stations displaying no loaded GVW peak or a very mild one like in this case are not uncommon. This is apparently the case for several of the Hawaiian Stations. A possible explanation for this phenomenon is that given the generally shorter trip lengths in Hawaii, there may be a higher than normal proportion of trips with trucks not fully loaded and with trucks carrying very heavy loads (a justification of why the latter is believed to be observed, as opposed to having a WIM calibration problem, is

[2] In the figure, station C202B is listed as 92029 since at the time of the analysis Prep-ME only accepted numeric station identifications.

provided shortly). Both, a higher proportion of partially loaded and very heavily loaded trucks would have the effect of flattening or even eliminating the second peak. Furthermore, trucks with intermediate loading may also explain some of the shifting of the first peak to the right. Of course, it may also be the case the WIM station is out of calibration.

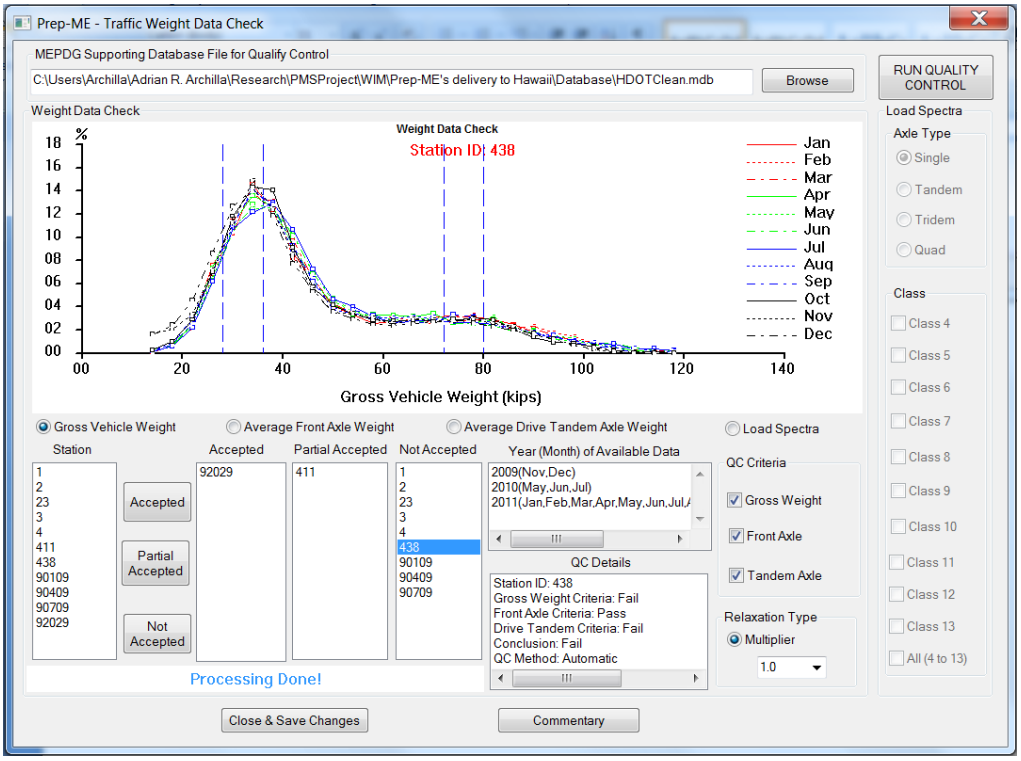

Figure 3-6. Initial quality checks with Prep-ME.

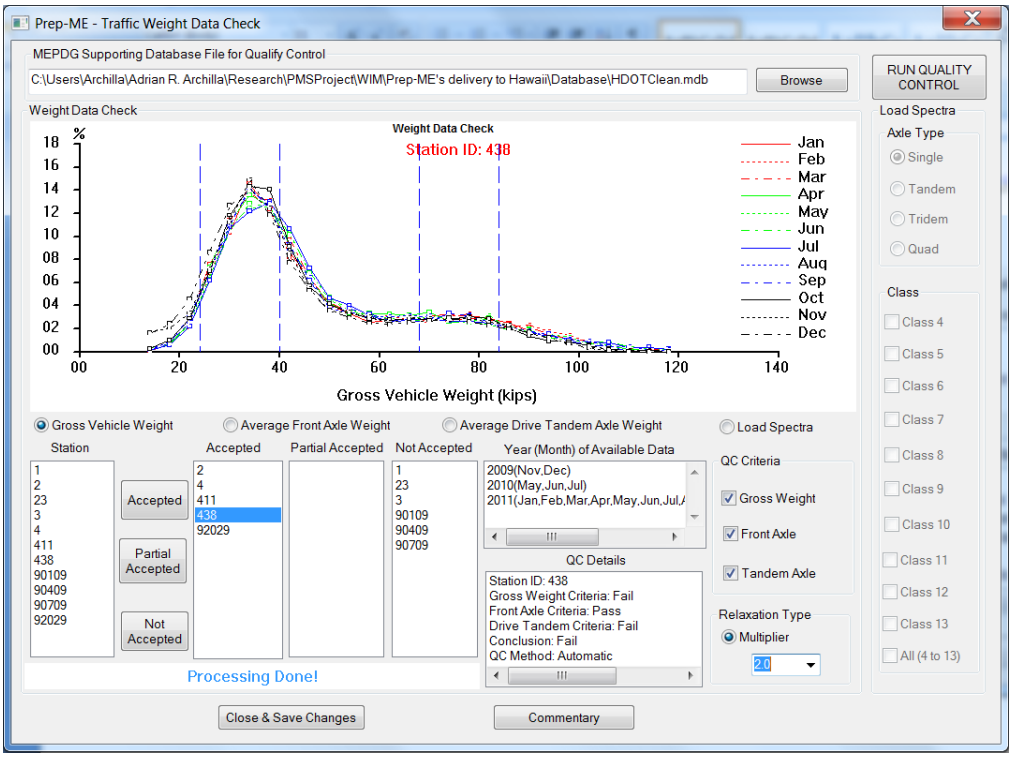

Figure 3-7. Increasing the relaxation multiplier moves more stations into the accepted category.

Figure 3-8. Location of sensors at Station 438 in Ala Moana Blvd.

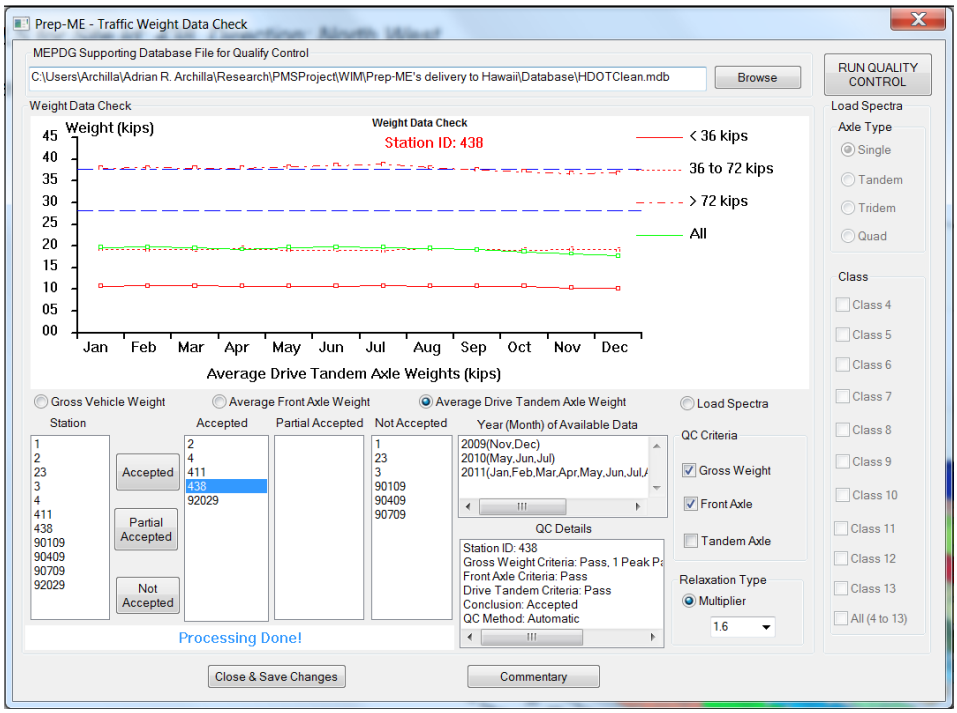

Figure 3-9. Drive Tandem Axle Check as a function of GVW.

Since Prep-ME was available for evaluation during a relatively short interval of time and there was a need to further analyze some issues that were detected for vehicle classes other 9, the rest of the analysis was performed with the PI customized program.[3]

3.4.3.2 Analyses with a customized traffic loading analysis tool

Although Prep-ME was extremely useful to analyze the State WIM data, its evaluation was limited to a relative short period of time. For this project, it was not possible to wait for a newer version with several improvements to obtain Axle Load Spectra (ALS). At the time the analyses were performed, Prep-ME did not have the capability to produce axle load spectra by direction. However, previous analyses with TrafLoad and a first version of a customized program developed by the PI showed that some of the Hawaiian stations had significantly different loading patterns for each direction of travel. Furthermore, as explained below, several

[3] A new release of Prep-ME is already available for evaluation but there was no time for testing it before completing this report.

other issues, particular for other vehicle classes were also discovered in the data. Therefore, the program initially developed by the PI was further modified and used for the analyses presented in this section. Basically, the customized program (in reality, three programs with different capabilities were used although they are referred here as a single program) obtains the axle load spectra on a monthly basis from the raw "wgt" data files. The program also allows the calculation of the distributions of GVW by vehicle class and month, the distributions of the front axle by vehicle class and month, the distribution of the drive tandem axle by vehicle class (for those with such axles) and month, and the percentages of vehicle class by lane for each WIM Station. The customized program essentially counts the number of axles in each axle weight bin for each combination of station, direction, year, month, vehicle class, and axle type. The criteria used for discriminating between single, tandem, tridem, and quad axles are:

- Single axle: single axle spaced at least 2.4 meters (8 ft.) from another axle (steering axles are also counted as single axles even if their spacing to the next axle is less than 2.4 meters).
- Tandem axle: two axles spanning no more than 2.4 meters (8 ft.).
- Tridem axle: three axles spanning no more than 3 meters (10 ft.).
- Quad axle: four axles spanning no more than 3.8 meters (12.5 ft.).

The program also allows the visualization of the axle load distributions for each axle type and vehicle class combination by plotting the corresponding histograms in three dimensional charts (with month of the year as the third dimension). Figure 3-10 shows an example of such a chart for Station 438, vehicle class 9, and tandem axles. A rotation capability and the ability to select which months the user wants displayed further help in the visualization of the distributions and the analysis of problems in the data. Moreover, tooltips are provided for each bar of the histogram when the user hovers the mouse arrow over it so that it is clear what load range and what percentage the bar represents

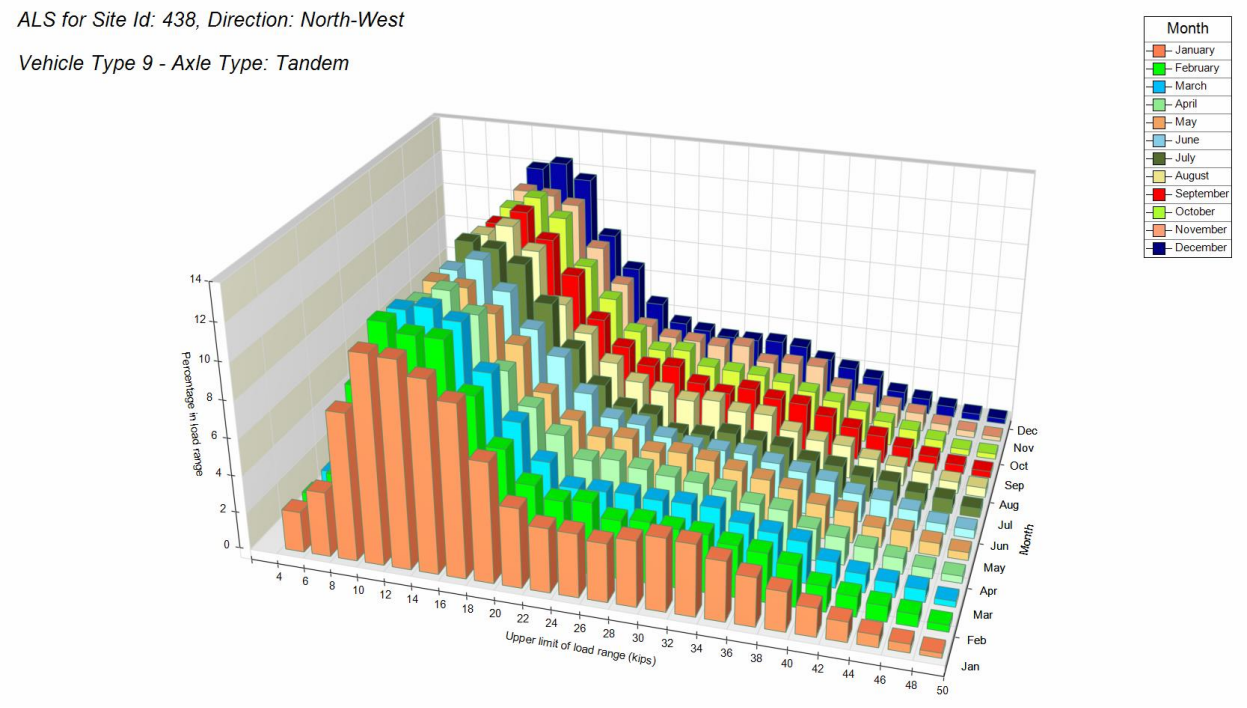

Figure 3-10. ALS for tandem axles of vehicle class 9 traveling in the North-West direction on Station 438 on Ala Moana Blvd.

Since no weighing of the data to account for day of week effects was performed, it has been imperative to use only months with substantial data (typically, at least two weeks of data for each month/year combination included in the sample) so as to minimize the possibility of introducing day of the week biases.

3.4.3.2.1 Data issues encountered

To arrive at sensible axle load spectra (ALS) or distributions; first, several data issues had to be overcome. Figure 3-11 shows a problem found with the data from Station S8R in the Big Island. The figure shows the ALS found over several years for tandem axles of vehicle class 9, supposedly in the North direction. As it is apparent by comparing the charts for the different years, two different patterns are observed for years 2006, 2008, 2009, and 2010 and for years

2007, 2011, and 2012[4]. Aside from other data issues, it is clear that the patterns between the two sets of years are strikingly different. A similar set of charts for the opposite direction showed that the same patterns displayed for each year are reversed. This implies that some coding error was intruced into the "wgt" files. The problem is relatively easy to visualize graphically but one needs to be looking for the differences across years. Blind automatic processing of the data may result in a totally unrealistic distribution for either direction. Also, notice how the histograms for 2008 exhibit peaks at higher load ranges when compared to the similar distributions in 2006 and 2009. In fact, both peaks for the first seven months in 2008 (around 36,000 to 40,000 lb for the unloaded peak and 80,000 to 84,000 lb for the loaded peak) are higher than normal, which may indicate that the WIM station may have been out of calibration for those months. This case is known as the "Two Peaks Shifted" case.

The previous example shows that with the use of the ALS charts or GVW distribution charts, it is relatively simple to spot years with invalid or problematic data. This is further illustrated in Figure 3-12, which shows inconsistent distributions throughout the year unlikely to be attributed to seasonal changes. The main challenge in these cases was to decide whether there were any valid data or whether all data should be discarded for that particular year. This was typically performed by several means, including observing the distributions for GVW, front and drive tandem axles on each year, observing if there were shifts of the distributions for a given axle/vehicle class combination or GVW across years, and observing whether any shifts in the distributions within a given year for a given axle/vehicle class combination or GVW were repeated for different vehicle classes and axle types on the same year. After all, the purpose of summarizing the information monthly is to capture any seasonal changes in the axle weight distributions. Thus, differences across months do not necessarily mean there are problems in the

[4] The chart for 2010 is not shown since it only had three months of valid data. However, the pattern for those three month was similar to those of years 2006, 2008, and 2009. After this problem was brought up to the attention of HDOT personnel, the information for the additional months was also provided after downloading it with FHWA's software TMAS 2.0. At some point, the directions had been corrected for years 2008, 2009, and 2010 although it is not known to the PI when and where those coding changes occur. Now the data from 2007 to 2012 and the first five months of 2013 are all consistent. The heavier loading for this station occurs in the South direction.

data. It may well be due to changes in the type/volumes of commodities being transported on a given roadway. The reason for looking for shiftings that are common across vehicle classes on a given year is that seasonal changes in commodity volumes more likely affect some vehicle classes more than others. In particular, there may not be many reasons for changes in bus weights and vehicle class 9 weights to be highly correlated. For the Hawaii data, when shiftings in the distributions in a given year and for a given vehicle class were observed, similar shifts were observed in the distributions for other vehicle classes as well, indicating a likely calibration problem with the WIM station.

Figure 3-13 illustrates the above problem with GVW data for station 10W in 2006. From the months with usable data, it can be seen that in June of that year the GVW distributions for vehicle class 9 shifted to the left slightly. The same shift can also be observed for buses (vehicle class 4) as shown in Figure 3-14. Thus, one is led to believe that this is more likely a consequence of a small adjustment in the WIM calibration parameters than any real change in the distributions. Whether some data should be retained or discarded in a case like this one is not always easy to determine. In this case, the before and after distributions show parameters within normal ranges. In many other situations, however, such changes pointed out to cases where the peaks of the distributions were unreasonable.

As indicated earlier, the customized program was modified to derive front and drive tandem axle distributions. These were useful to assess the location of the peaks of the distributions. For many of the stations, the peaks were located slightly higher than normal. However, considering also that for many of those stations there were several years of data available and that the stations are regularly calibrated, it could not be always concluded that the corresponding data were erroneous. A thorough freight study is required to determine if and why the loads are higher than normal for some of these stations. Nevertheless, as discussed in the following paragraphs, a significant effort was made to differentiate situations with higher than normal loading from those with calibration problems.

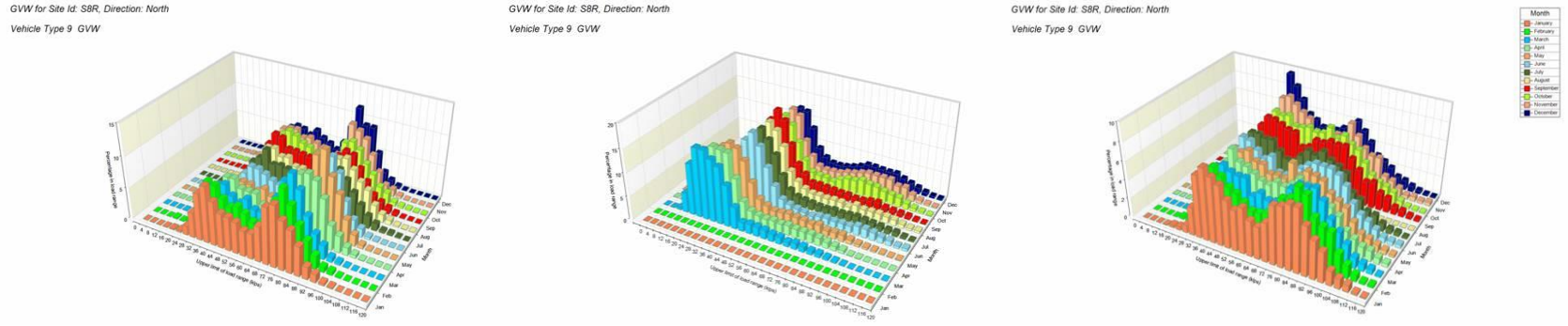

a) Year 2006 b) Year 2007 c) Year 2008

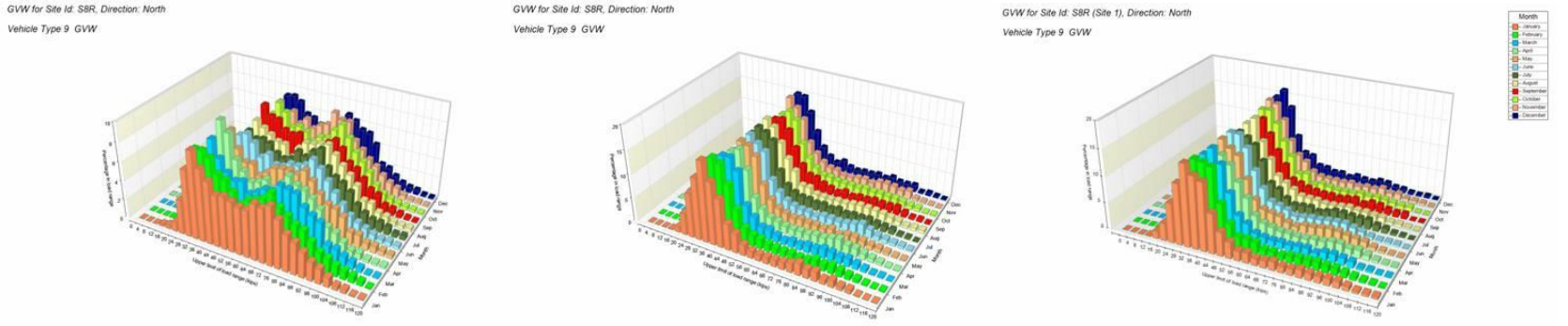

d) Year 2009 e) Year 2011 f) Year 2012

Figure 3-11. Potential data coding errors in the direction field for station S8R.

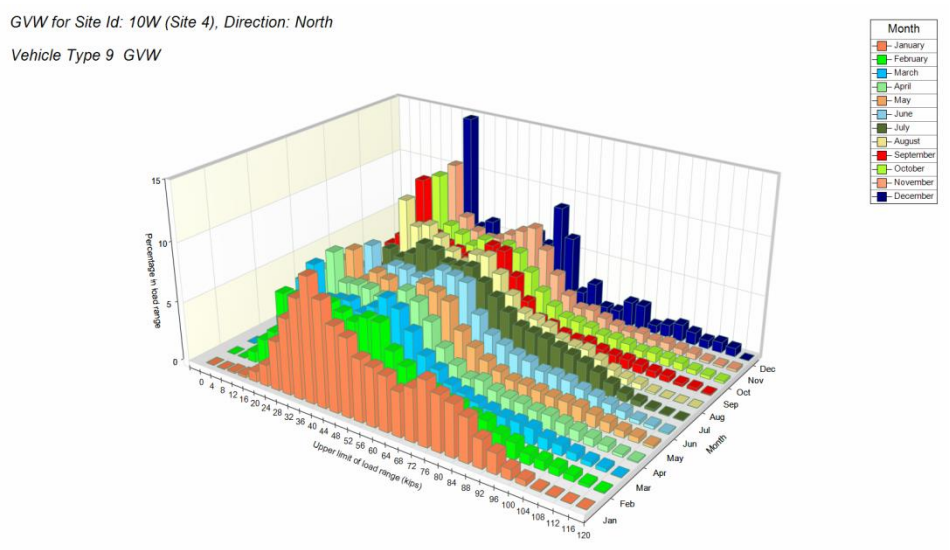

Figure 3-12. Example where identification of problematic data was relatively simple.

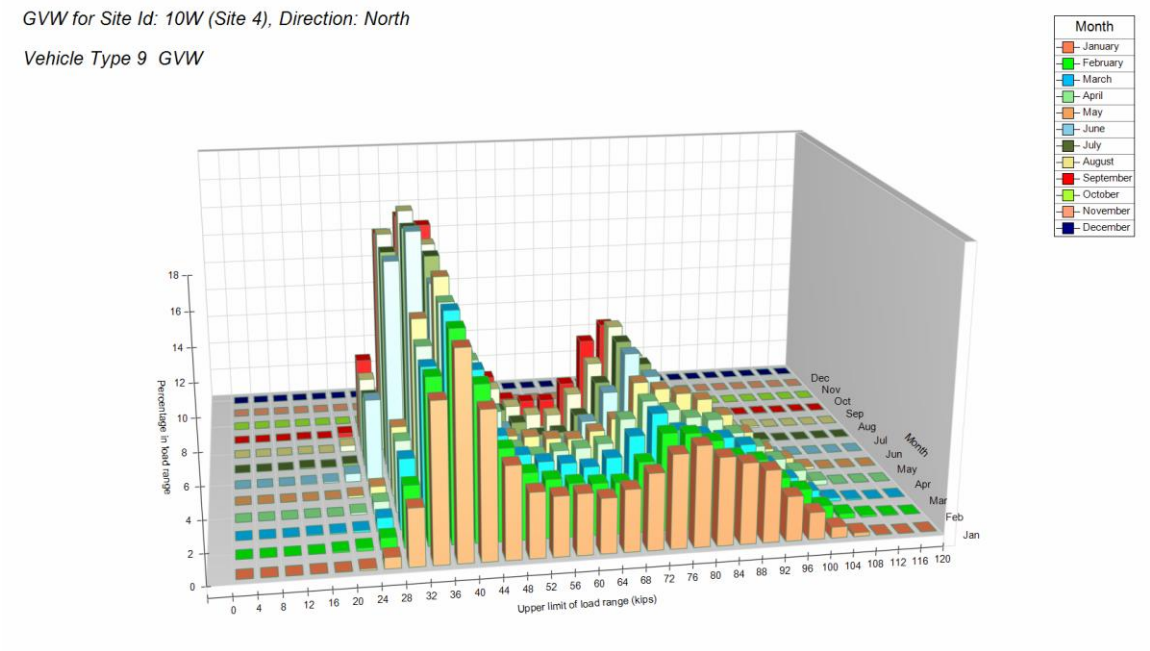

Figure 3-13. Example of a shift to the left in the GVW distributions due to a possible calibration adjustment.

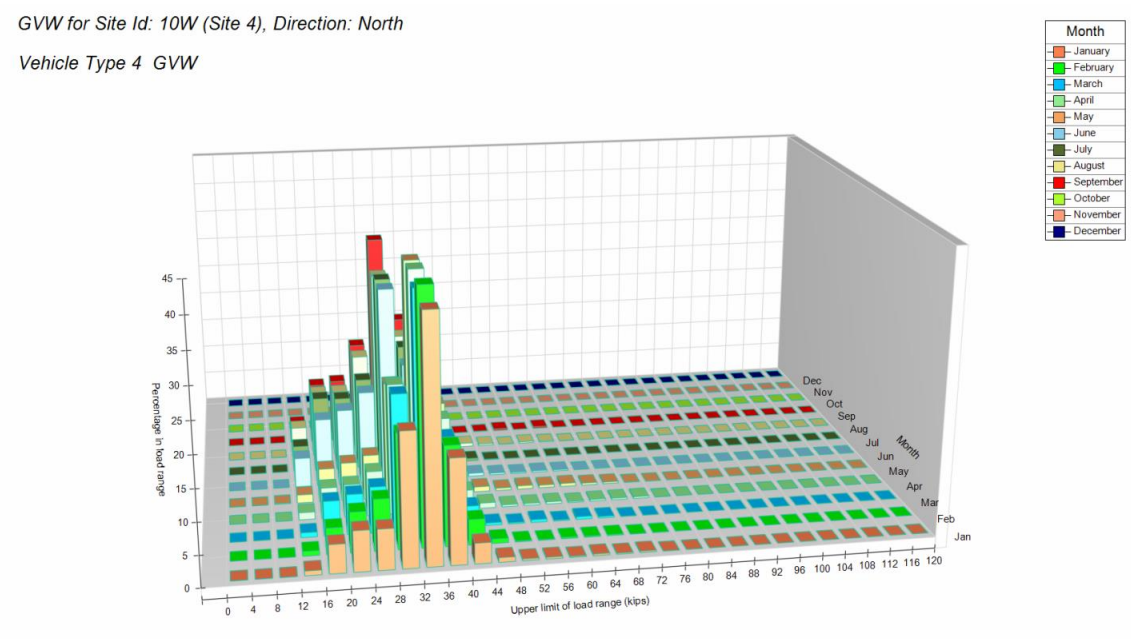

Figure 3-14. Shift in the GVW distributions for buses mimicking the shift observed for vehicle class 9 trucks of Figure 3-13.

The capability of deriving the front axle load distributions for a given vehicle class, as opposed to the distribution of all single axles, was useful because as expected it shows narrower distributions with better defined peaks and less noisy tails. Figure 3-15 provides an example. The same advantage can be noted for the difference in the distributions between drive tandem axles and all tandem axles for a given vehicle class with such axles.

As expected, the differences between the distributions for front and all single axles for vehicle class 9 are generally minor since this vehicle class generally has a single front axle and two tandems. The additional singles are generally the result of tandem configurations with separation between axles in excess of the limit to be classified as tandem. Thus, those axles will be recorded as two singles instead of one tandem. A corollary of this is that if only vehicles of class 9 are being analyzed, similar inferences can be obtained with both distributions (front or all singles).

The discrimination of the front axle distribution is much more useful for buses than for class 9 vehicles as the former have a substantial number of non-frontal single axles with different loading patterns. Figure 3-16 illustrates this for Station 438 in Ala Moana Blvd. In this example, the front axle distribution has a single peak in the 11,000 lb. to 12,000 lb. range whereas the all-singles distribution has an additional second peak in 25,000 lb. to 26,000 lb. range.

Parenthetically, that the second peak exceeds the Hawaii limit for single axles of 22,500 lb. [17] is not surprising. First, the two most common city buses, Gillig Phantom 40' (374 vehicles) and the 60' articulated bus New Flyer D60LF (111 vehicles) [18] have rear gross axle weight ratings of 25,600 lb. and 26,000 lb., respectively ([19], [20], [21])[5] and second, this Station is located in an area of Honolulu with a combination of high volume of buses and ridership. Thus, it would be erroneous to consider the data from this station invalid because of the higher than normal peaks on these distributions.

The above paragraphs point out many of the issues encountered when the WIM data are analyzed carefully. Inevitably, although the literature presents extremely valuable suggestions for verifying the quality of the data, the application of the rules are sometimes subjective and based on judgment on the analyst helped with knowledge of local conditions. All quality controls need to be applied carefully as there appear to be many loading situations that do not conform to what is considered "normal".

It is important to point out that a few other quality control checks were imposed to the data including the separation between the front and the first loading axle and the consistency between the number of axles counted for a given vehicle and the class it was assigned to. For many stations, there was a non-negligible number of separations between the front axle and the first loading axle that were too small. It is not known the cause of the problem though for some stations, lane changing may be a contributing factor. The information for axles with the above problem were discarded. In other situations, based on the number of axles and their separations, some vehicles needed to be reclassified.

---

[5] The values reported above were obtained from public records from other agencies and are just a bit higher than the values of 23,350 lb and 25,000 lb reported by The Bus in a survey performed for this project in 2006.

The following section presents the best estimates of the axle load spectra (ALS) for the different stations across the State after applying the quality controls described in this section. Although the quality of the data was looked at for several vehicle classes (mostly classes 4, 6, and 9), the actual selection of the month/year combinations to include were based mostly on vehicle class 9. As will be shown, for the most part, this resulted in acceptable ALS for other vehicle classes as well. However, unexpectedly, in a few cases the loading distributions for other vehicle classes showed a disproportionate number of unloaded axles. This is illustrated in Figure 3-17. The left chart in the figure shows that for the North direction of Station 10W on Kalaeloa, the percentage of single axles with less than 3,000 lb. for the month of August (the series shown on light yellow color) is more than 10% (actually 10.44%). For the other months, the same weight interval had percentages varying from about 0.2% to 0.8%. Clearly, something happened on this Station on at least one of the months of August used as input that caused that single axles on buses were not weighed properly. This is despite the fact that the single and tandem axle distributions for class 9 vehicles did not show any problem for any of the input months (remember the months selected were deemed to be months with good quality data) and of course for the resulting ALS for vehicle class 9. The ALS for vehicle class 9 for this station are presented in the following section. Furthermore, what is even more puzzling is that the resulting distribution for *tandem* axles of buses did not show the same problem whereas the distributions for both single and tandem axles on vehicles class 6 did show the problem. In other words, the problem may be axle/vehicle dependent. There are a few options to fix this problem. One is to find the month contributing the problematic data, eliminate it as input and regenerate the distribution. This of course, may have the effect of eliminating valuable data for vehicle class 9 and other vehicle classes. A second viable option for this particular case in which the monthly distributions are so similar to each other is to simply substitute the distribution for the month of August with the distribution of one of the other months (or an average). With the similarities of the distributions in this example and the Hawaiian climate, this should have no practical consequence. The last option is to eliminate or reduce the percentage for the weight category and prorate the difference among all the other weight categories according to their percentages such that the sum of all categories adds up to 100. This is what was actually done to correct the

problem. As shown in part b) of Figure 3-17, the corrected series looks practically the same as for the other months.

3.4.3.2.2 ALS for Hawaiian WIM stations

This section briefly discusses some salient features of the ALS obtained following the quality control checks described in the previous section. Most of the discussion is based on the distributions of tandem axles on vehicles of class 9 although for station 438 some relevant distributions for other vehicle classes are also presented.

As a result of the quality control process, only the data corresponding to the number of days for each month/year shown in Table 3-1 were used to obtain the ALS for the two directions at each WIM station. The corresponding number of weighed vehicles are provided in Table 3-2. Providing this number is important as it helps to understand why for some vehicle classes the distributions are not very well defined. Since there are 38 weight intervals for each month of the year, a relatively large sample size is needed for each vehicle class to reliably define the value of each interval, particularly those with lower frequencies. Distributions with less than 15,000 vehicles weighed in a year should be looked at with caution, particularly for those axles with lower frequencies. For those vehicle classes that are relatively rare in the State (namely, mostly vehicle classes 7, 11 and 12 and to a lesser degree vehicle classes 8 and 10) the distributions are simply less well defined than those observed for vehicle classes 4, 5, 6, and 9. Of course, since they are relatively rare, they also play a minor role in the design of any particular pavement. The values in Table 3-2 also help in the interpretation of the reliability of the average number of axles per vehicle class presented in the following section. Unfortunately, for Stations C12E in Maui and Station 023 on the Likelike highway the data were not of enough quality to obtain reliable distributions and so these stations are not used in the analysis.

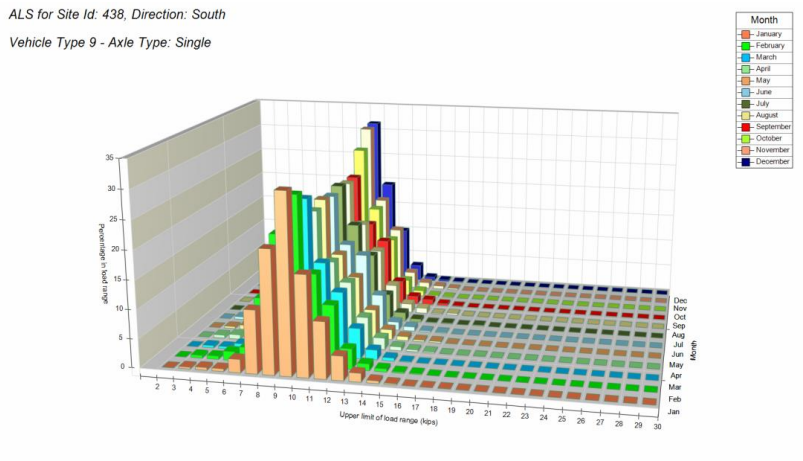

a) Front Axles

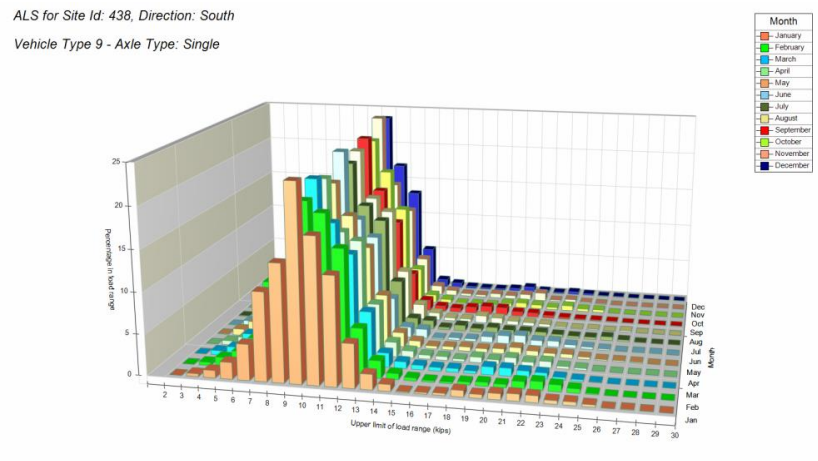

b) All single axles

Figure 3-15. Example of the differences between a Front Axle Distribution and All Single Axles Distribution for vehicle class 9.

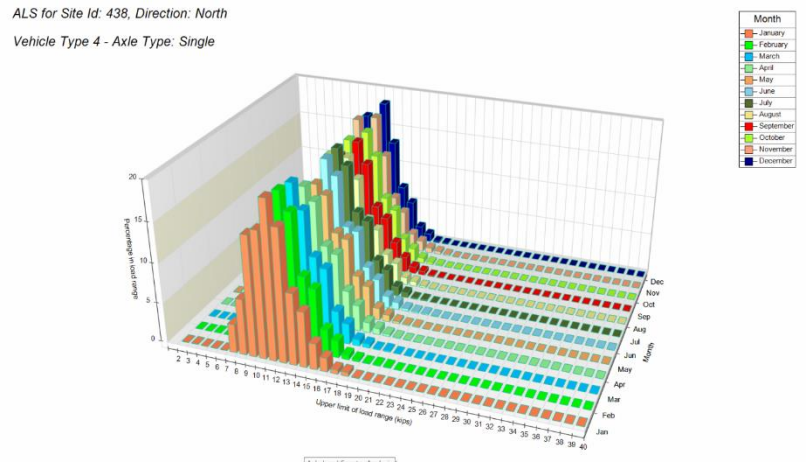

a) Front Axles

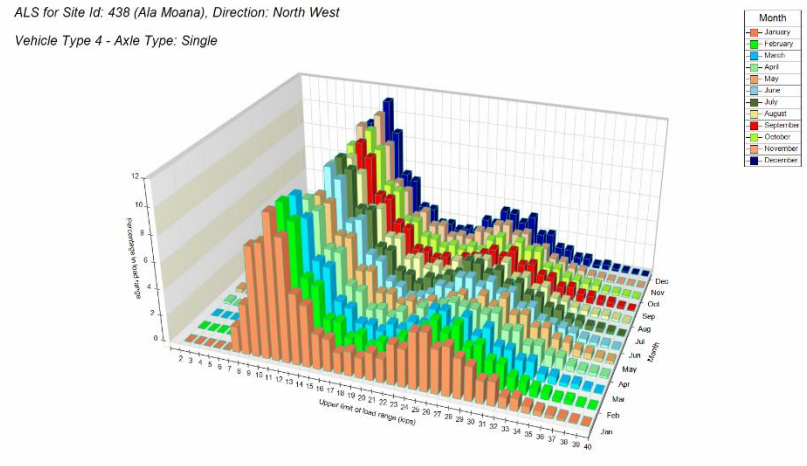

b) All single axles

Figure 3-16. Example of the differences between a Front Axle Distribution and All Single Axles Distribution for vehicle class 4.

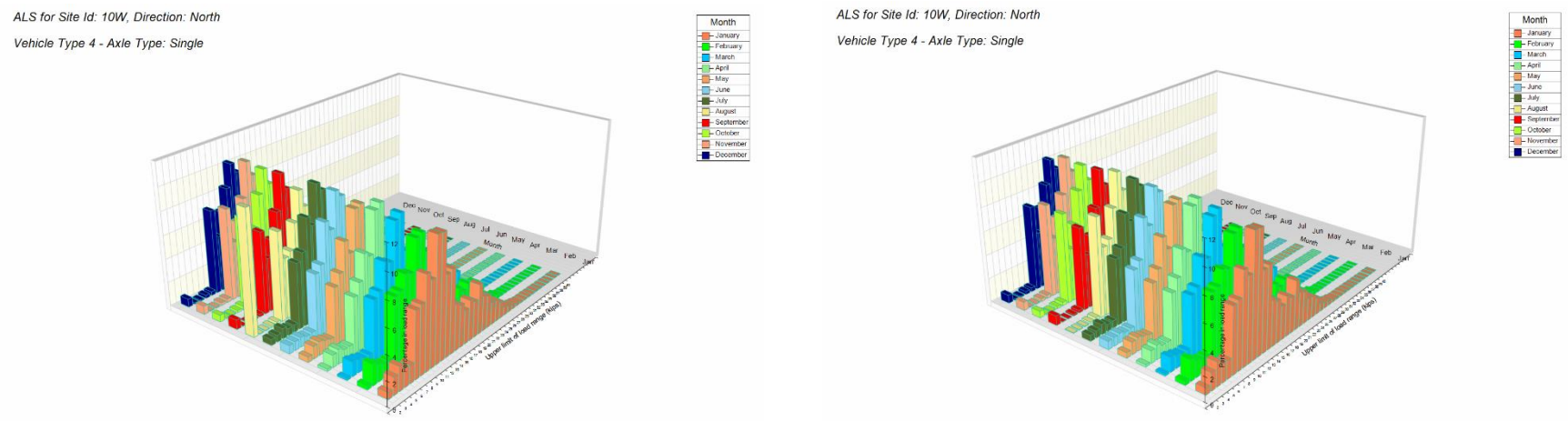

Figure 3-17. Correction of erroneous number of unloaded axles for buses.

Table 3-1. Number of days on each month and year for which information was available for each station and direction.

Station	Year	Direction	Number of Days in Year	Number of Days with Useful Data in Month											
				1	2	3	4	5	6	7	8	9	10	11	12
438	2011	1	353	31	28	31	30	31	30	31	31	30	30	24	26
		5	292	31	28	31	30	31			31	30	30	24	26
	2012	1	356	31	28	31	28	29	30	31	31	30	31	28	28
		5	356	31	28	31	28	29	30	31	31	30	31	28	28
S8R	2007	1	300			31	30	30	26	31	30	30	31	30	31
		5	300			31	30	30	26	31	30	30	31	30	31
	2008	1	362	31	28	30	30	31	30	30	31	30	31	29	31
		5	362	31	28	30	30	31	30	30	31	30	31	29	31
	2009	1	359	31	28	30	30	30	30	31	31	28	31	29	30
		5	359	31	28	30	30	30	30	31	31	28	31	29	30
	2010	1	361	31	28	31	30	31	30	31	28	30	30	30	31
		5	361	31	28	31	30	31	30	31	28	30	30	30	31
	2011	1	360	31	28	31	30	31	30	31	29	30	30	28	31
		5	360	31	28	31	30	31	30	31	29	30	30	28	31
SS9	2008	1	120				30	31	30	29					
		5													
	2011	1	351	27	26	31	30	30	28	31	30	30	30	29	29
		5	263		26	31	30	30	28			30	30	29	29
	2012	1	359	31	29	31	29	31	30	31	31	30	28	29	29
		5	359	31	29	31	29	31	30	31	31	30	28	29	29
C202B	2006	1	180	31	27	31	25	28	25						13
	2007	1	349	27	26	31	30	31	29	28	30	29	31	30	27
	2008	1	139			26	27	27	28	31					
	2009	1	357	30	28	30	30	31	27	30	31	28	31	30	31
	2010	1	87					31	26	30					
	2011	1	320	31	26	31	26	28	29	25	26	24	25	25	24
	2012	1	329	23	28	27	21	27	29	24	31	30	31	29	29

Direction codes are consistent with the FHWA Traffic Monitoring Guide (1-North, 2-Northeast, 3-East, 4-Southeast, 5-South, 6-Southwest, 7-West, 8-Northwest, 9-N/S or NE/SW combined, 0-E/W or SE/NW combined).

Table 3-1 (continued): Number of days on each month and year for which information was available for each station and direction.

Station	Year	Direction	Number of Days in Year	Number of Days with Useful Data in Month											
				1	2	3	4	5	6	7	8	9	10	11	12
10W	2006	1	75							31	31	13			
		5	142	27	28	31	30	26							
	2007	1													
		5	120				30	30	30	30					
	2010	1													
		5	91					31	29	31					
	2011	1													
		5	352	31	28	31	30	31	30	31	25	29	30	28	28
	2012	1	362	28	29	31	30	31	30	31	31	30	31	30	30
		5	28	28											
H41W	2006	2	227	31	28		30	31	30		31		16	30	
		6	227	31	28		30	31	30		31		16	30	
	2007	2	323	31	26	29	30	31	30	31		30	31	30	24
		6	323	31	26	29	30	31	30	31		30	31	30	24
	2008	2	178	30	29	28	30	31	30						
		6	178	30	29	28	30	31	30						
C4K	2011	3	355	31	28	31	30	31	29	31	31	30	30	23	30
		7	355	31	28	31	30	31	29	31	31	30	30	23	30
	2012	3	359	31	28	31	30	29	30	31	31	30	30	29	29
		7	359	31	28	31	30	29	30	31	31	30	30	29	29
C10K	2011	1	264	31	28	31	30				31	30	30	26	27
		5	264	31	28	31	30				31	30	30	26	27
	2012	1	360	31	28	31	30	31	30	31	31	30	31	28	28
		5	360	31	28	31	30	31	30	31	31	30	31	28	28
CC7L	2006	3	162			31		28	30	28	24	21			
		7	147			28		27	30	31	31				
	2007	3	153			31	30	31	30	31					
		7	153			31	30	31	30	31					
	2011	3	350	30	28	31	30	31	29	31	31	30	30	23	26
		7	350	30	28	31	30	31	29	31	31	30	30	23	26
	2012	3	351	31	26	29	28	30	30	30	31	29	30	29	28
		7	351	31	26	29	28	30	30	30	31	29	30	29	28

Direction codes are consistent with the FHWA Traffic Monitoring Guide (1-North, 2-Northeast, 3-East, 4-Southeast, 5-South, 6-Southwest, 7-West, 8-Northwest, 9-N/S or NE/SW combined, 0-E/W or SE/NW combined).

Table 3-2. Sample sizes (number of vehicles weighed) use to obtain the ALS at each station.

Station	Direction	Vehicle Class									
		4	**5**	**6**	**7**	**8**	**9**	**10**	**11**	**12**	**13**
488	North-West	174,842	758,493	135,379	2,255	10,260	62,162	8,536	26	50	269
	South-East	93,873	780,915	152,345	1,093	11,793	58,068	8,242	36	840	229
S8R	North	47,101	408,105	73,841	6,776	11,682	194,988	4,859	146	268	257
	South	43,844	419,997	82,054	495	11,621	209,922	5,164	1,693	1,349	222
S9	North	12,266	242,521	15,709	278	5,869	14,194	1,032	25	26	20
	South	10,627	205,475	12,570	288	6,506	13,180	697	16	30	9
C202B	North	11,616	544,186	449,364	4,361	27,316	485,362	20,011	1	21	6,200
	South	-	-	-	-	-	-	-	-	-	-
10W	North	68,285	439,505	155,476	6,691	29,475	211,860	18,108	553	2030	810
	South	89,572	989,532	255,751	7,538	34,129	330,507	28,786	265	849	846
H41W	North-East	25,153	425,803	85,072	2,812	31,046	118,561	4,562	2,245	57	488
	South-West	20,760	535,369	73,984	4,595	21,018	120,343	4,475	2,672	1,015	1,385
C4K	East	74,421	408,118	49,753	2,918	29,345	25,126	2,042	101	31	58
	West	147,617	673,988	96,687	5,033	23,343	40,097	2,415	163	226	337
C10K	North	92,489	603,211	225,562	9,563	36,050	257,953	15,865	400	2,739	1,111
	South	111,062	832,137	240,514	15,569	48,853	264,850	25,457	5,522	1,322	1,430
C7L	East	428,397	2,498,424	520,240	20,952	143,875	649,643	34,851	1,104	4,537	3,007
	West	97,894	738,279	139,246	4,747	67,037	214,211	17,575	296	755	1,506

Figure 3-18 to Figure 3-28 show the resulting ALS for the stations with enough data to obtain representative distributions. Notice that to make the comparisons simpler, most of the figures are for tandem axle distributions on vehicles of class 9 although as discussed later, the effects of other vehicle classes may be more important for some stations. The distributions for tandem axles of vehicle class 9 on Station 438 (Figure 3-18) show a pattern in both directions that is common to several stations. They have a very well defined unloaded peak in the 12,000 lb. to 14,000 lb. range in one direction (10,000 lb. to 12,000 lb. range in the opposite direction) and a very mild loaded peak located, depending on the month, on either the 30,000 lb. to 32,000 lb. range or 32,000 lb. to 34,000 lb. range in one direction and almost a non-existent peak in the opposite direction. It must be noted that even for the North-West direction, on which the soft second peak can be observed for some months, the peaks are very mild and any minor changes in the data can affect their location. As noted earlier, this type of distribution would not pass the

drive tandem check. Furthermore, their peaks are also both slightly out of what is considered acceptable. However, with so many trucks with intermediate loading, it is reasonable to expect that some of those could help shifting the unloaded peak to the right.

As for the flat second peak and its location or non-existence, it can be argued that both trucks with intermediate loading and overweight trucks would tend to flatten the peak. For this and other stations, it is also notable the long tails to the right. These may indicate a relatively high proportion of overloaded trucks are crossing this station, which in addition to flattening the peak would tend to shift it to the right. Of course, the difficult question to answer is whether these tails are realistic or are the results of a calibration problem with the WIM station. This is one of the situations in which looking at the distributions of axles for other vehicle classes and of the distributions of the drive tandem axles can be very useful. As shown in Figure 3-19, the ALS for tandem axles of buses at Station 438 do not exhibit long right tails. Consequently, it is logical to infer that the long tails observed for tandem axles of vehicle class 9 are representative of the actual loading conditions instead of being a calibration problem artifact. In fact, by observing the distributions for **drive-tandem** axles (not shown) it can be further inferred that the highest loads usually occur on the non-drive tandem axles, perhaps as a result of imbalanced loading (at this station, the tails taper off faster for the drive tandem axles distributions than for the all tandem distributions.)

It is also interesting to note that at this location, tandem axles on other vehicle classes can be more damaging compared to those for vehicle class 9. As seen in Figure 3-19 for tandem axles on buses and Figure 3-20 for tandem axles on vehicle class 6, the distributions for these vehicle classes are concentrated on the higher side. Of course, it has to be remembered that with each passage of a vehicle class 9 there are two tandem axle load applications but there is only one tandem axle load application for each passage of the other vehicle classes. Thus, the relative damaging effects cannot be inferred solely from these distributions but together with the information about the number of axles per vehicle as well as the other axle types on each vehicle class.

The distributions for tandem axles on vehicle class 9 at station 10W shown in Figure 3-21 exhibit a similar pattern but with better defined loaded peaks. This is not surprising as one would

expect a higher proportion of loaded trucks coming from and going to Campbell industrial park. Notice, however, that for this station a detailed analysis of all the available data (2005-2012) had to be performed to obtain these distributions. Without filtering of the data, the same type of long right tails, as shown for station 438, were initially obtained. However, for WIM station 10W, in many cases the distributions for the tandem axles of buses also displayed suspiciously long right tails, indicating that much of those data may have been collected during periods with some calibration issues. For the above reasons, as shown in Table 3-1, only some of the available data were used to develop the ALS.

The distributions for station C4K shown in Figure 3-22 exhibit again the pattern of a very marked unloaded peak and a very mild or non-existent loaded peak. The distributions for station C10K shown in Figure 3-23 are more triangular as a result of a somewhat lower percentage for the unloaded peak and a higher proportion of intermediate loads. Again, no upper peaks can be identified. Station S9 on the big island also display a similar pattern (Figure 3-26). For the three WIM stations mentioned, with the exception of the South direction on station C10K, the long tails can be justified when the comparison with the tandem axles on buses explained in the previous paragraphs are used.

The distributions for stations C7L (Figure 3-24), H41W (Figure 3-25), and S8R (Figure 3-27) have the distinctive feature of being quite different in each direction. In these cases, the loaded and unloaded peaks of the most heavily loaded direction are about the same height with differing degrees of intermediate loading for each of the three stations. Although differences per direction could be noted for all WIM stations, for most, averaging the directional distributions would have only a modest effect on designs. However, for the latter three stations the differences are so significant that separate consideration of the heavier loaded direction is warranted. Of the three stations, at present, the distributions derived for stations H41W and S8R are considered reliable. Again, with reference to Table 3-1, it can be seen that only parts of three years out of the seven year period of available data (2005-2012) were used to develop the distributions for station H41W. Information for other years at this station produced distributions that appear to be biased upward by about 4,000 to 6,000 lb. for the higher load ranges.

It must be noted that the loading for tandem axles of vehicle class 9 in the south direction at station S8R appears high. However, the maximum loading on tandem axles of buses was below 36,000 lb. and consistent with the 34,000 lb. limit. Thus, since no overestimation appears to be happening for buses, it may well be that the heavy loading in this station is real.

At present the information for station C7L is considered suspect since the distributions (Figure 3-24) present long tails that cannot be justified using the comparative approach with tandem axles on buses described earlier. Furthermore, the distributions of tandem axles on buses exhibited a unimodal (single peak) distribution with the peak located around 24,000 lb. to 25,000 lb. and a non-negligible percentage of loads around 50,000 lb. At this point, it cannot be established if these are realistic loadings or that they are the result of a calibration error.

Finally, Figure 3-28 shows the distribution on Station C202B. This is the WIM station with the longest record of good data. The pattern of loading on this station is markedly different from all others with a very high loaded peak, which indicates, as is logical for town-bound traffic from a port, that most trucks crossing this station are fully or intermediately loaded. Also, the consistency of the distributions from month to month is remarkable, which is probably a result of the enforcement efforts at this location. Despite this being the only station exhibiting a pattern with a single identifiable peak for loaded trucks and a high proportion of intermediately loaded trucks, traffic loading at this station is not the most damaging in the State. One of the reasons is that the distributions for semitrailer truck, by far the most common truck at this station, do not exhibit a long right tail seen for other stations, which again is probably attributed to the enforcement efforts at this site. In addition, bus loads at this site are very light compared to many other locations.

As can be seen from most figures, there seem to be little if any seasonal effects for any of the stations. Any minor seasonal trends are probably hidden by the precision with which the data are collected. Lastly, one of the challenges in applying the quality control checks is the risk of eliminating valid results because they do not conform to what is expected. Although an attempt was made to avoid this, there is always the risk of eliminating data to obtain the result that one is expecting a priori.

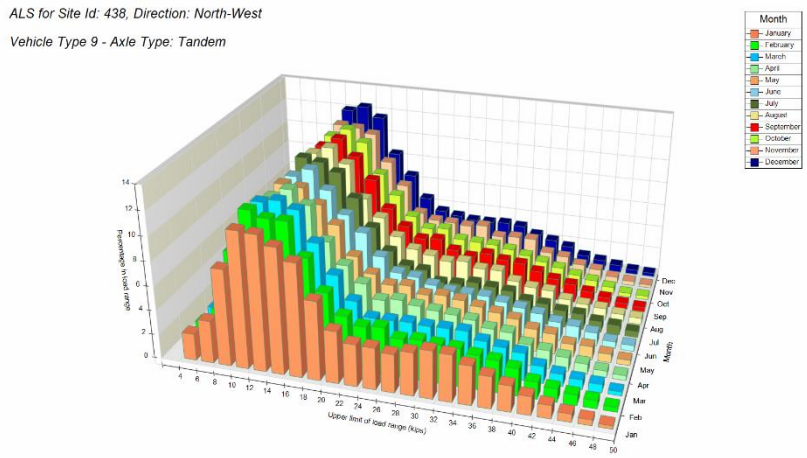

a) North-West

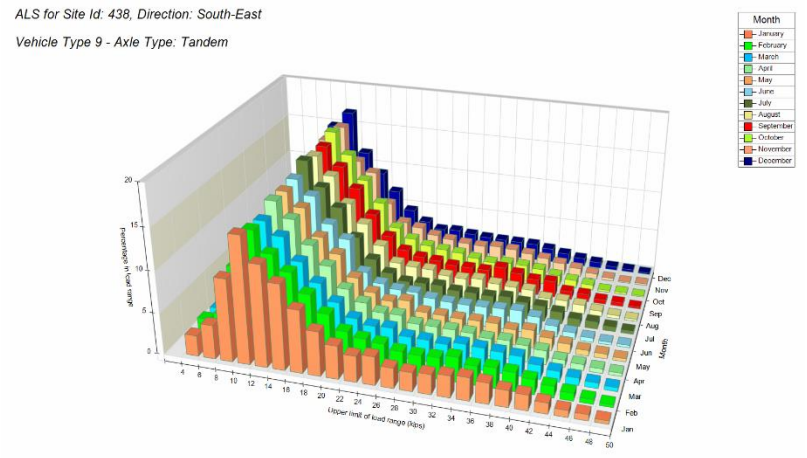

b) South-East

Figure 3-18. ALS for tandem axles of vehicle class 9 on Station 438.

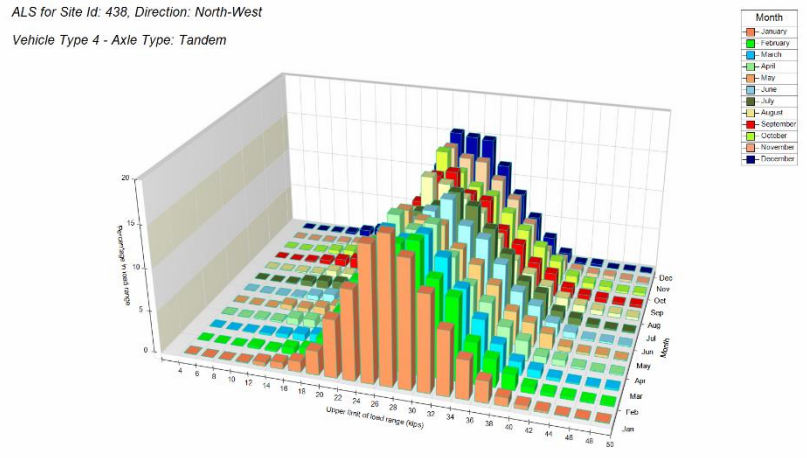

a) North-West

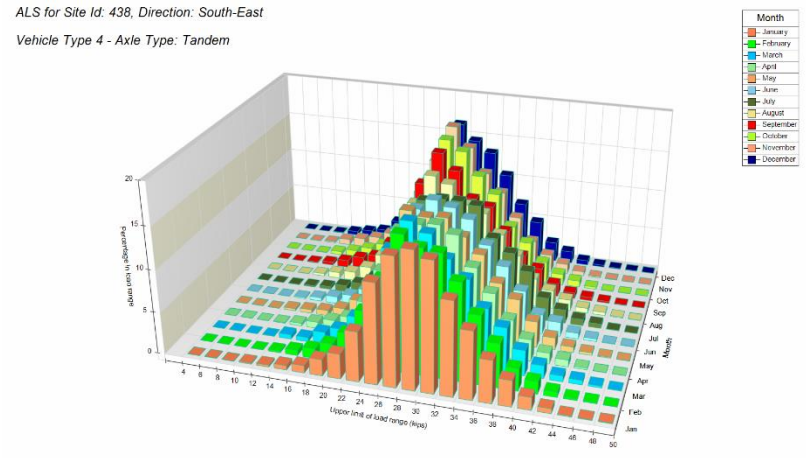

b) South-East

Figure 3-19. ALS for tandem axles of vehicle class 4 on Station 438.

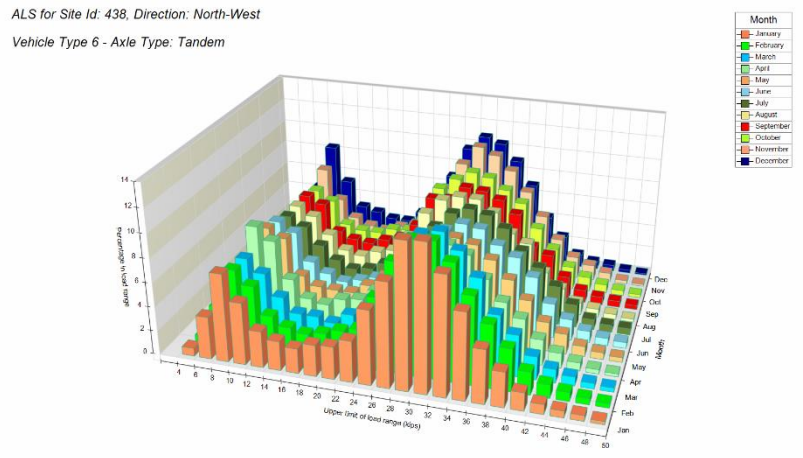

a) North-West

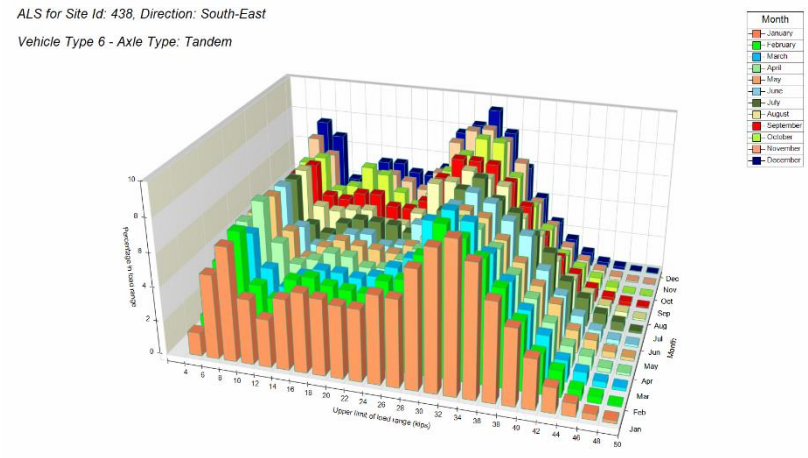

b) South-East

Figure 3-20. ALS for tandem axles of vehicle class 6 on Station 438.

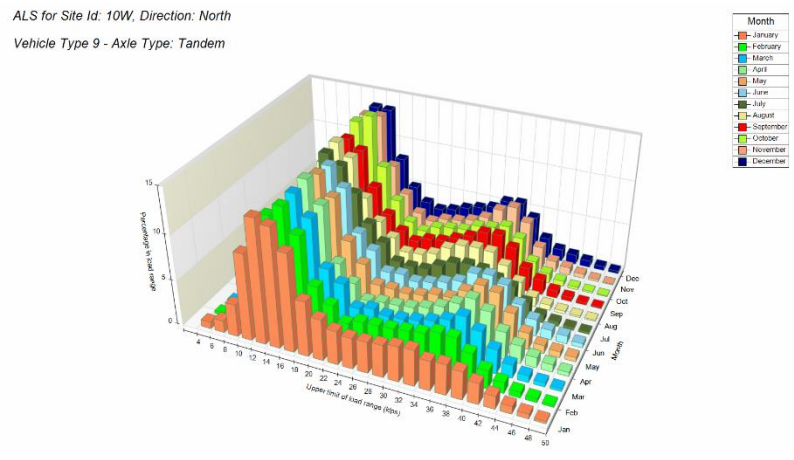

a) North

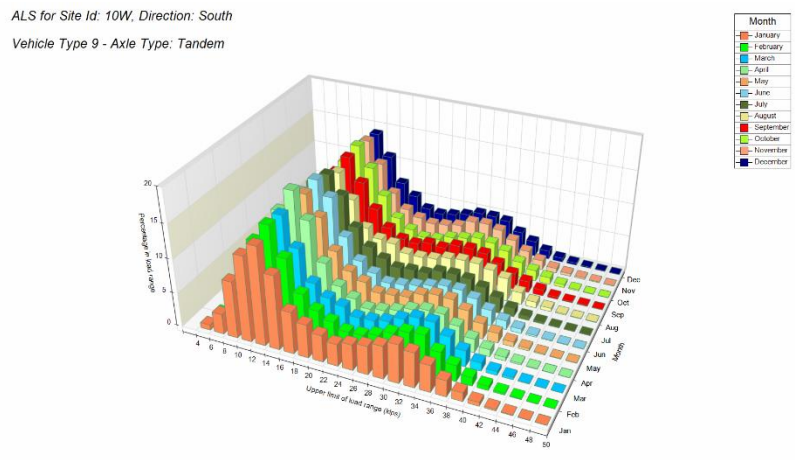

b) South

Figure 3-21. ALS for tandem axles of vehicle class 9 on Station 10W.

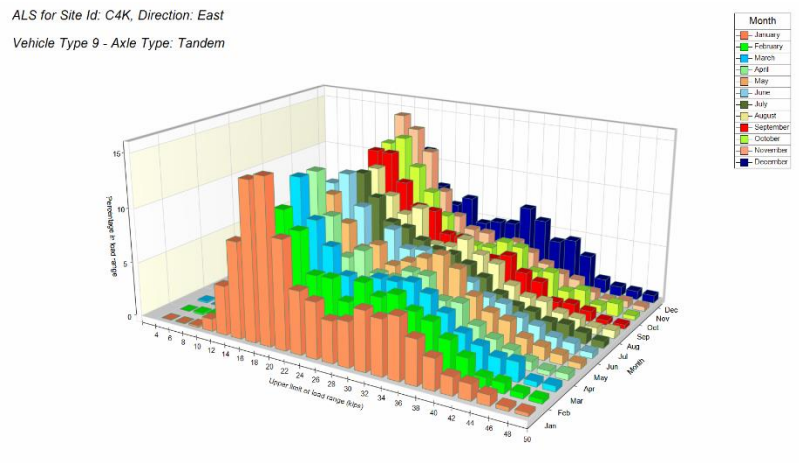

a) East

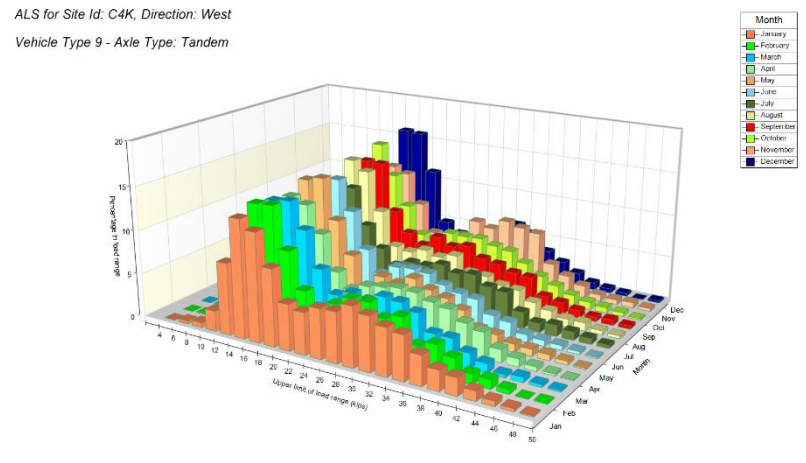

b) West

Figure 3-22. ALS for tandem axles of vehicle class 9 on Station C4K.

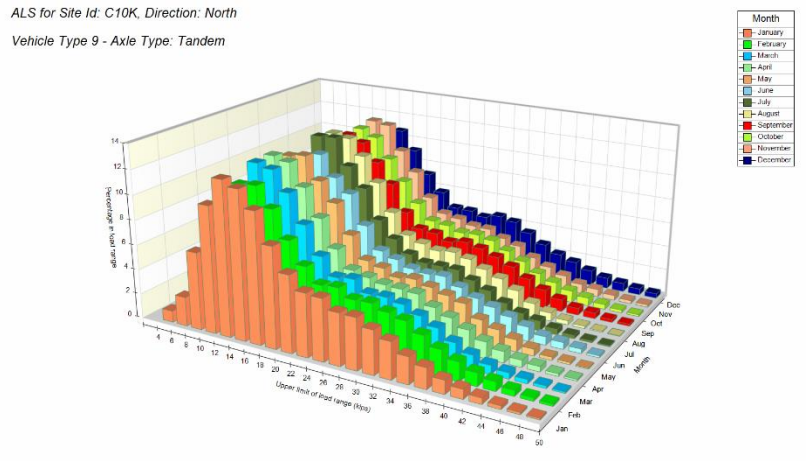

a) North

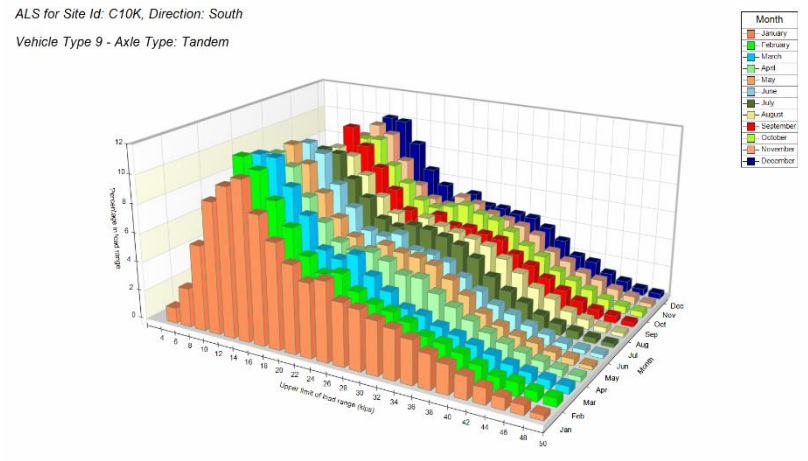

b) South

Figure 3-23. ALS for tandem axles of vehicle class 9 on Station C10K.

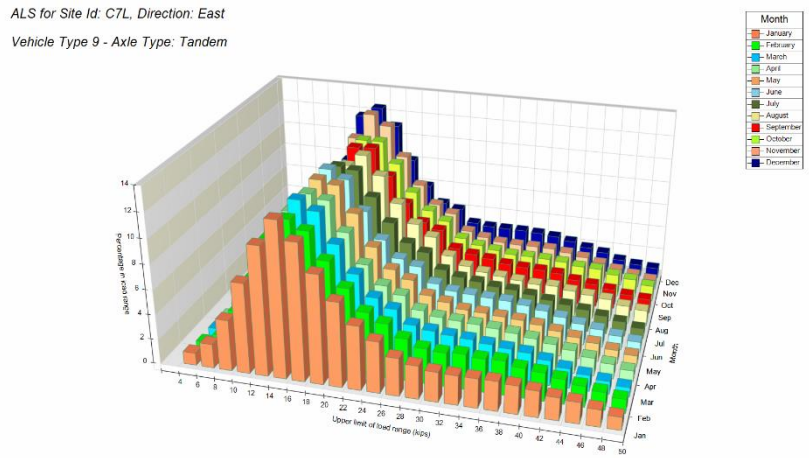

a) East

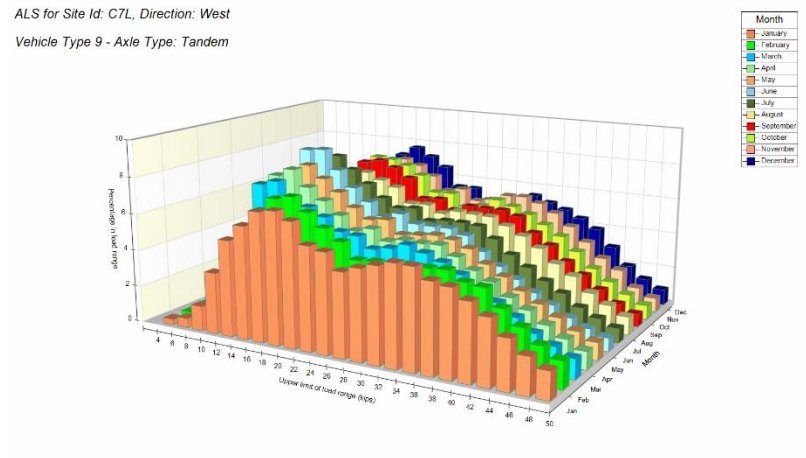

b) West

Figure 3-24. ALS for tandem axles of vehicle class 9 on Station C7L.

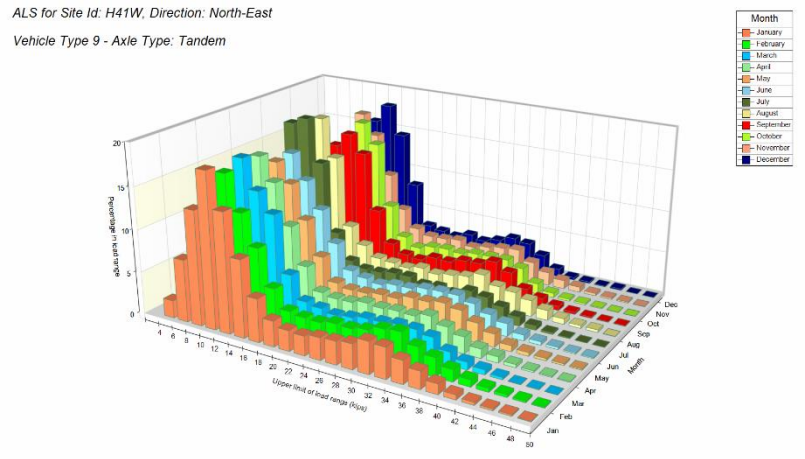

a) North-East

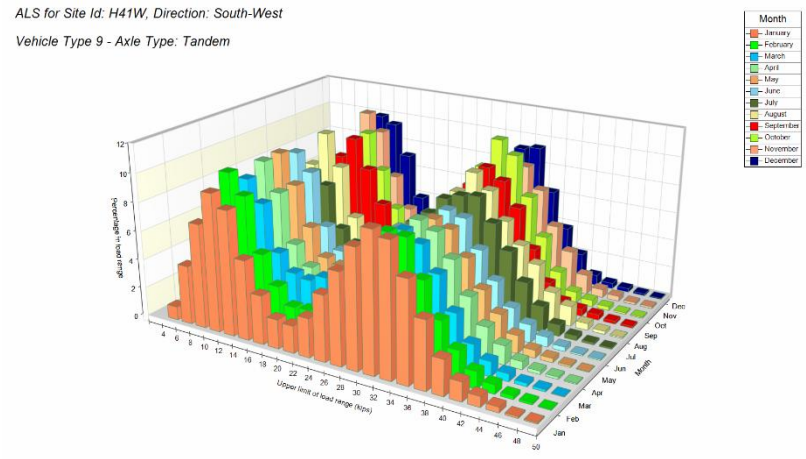

b) South-West

Figure 3-25. ALS for tandem axles of vehicle class 9 on Station H41W.

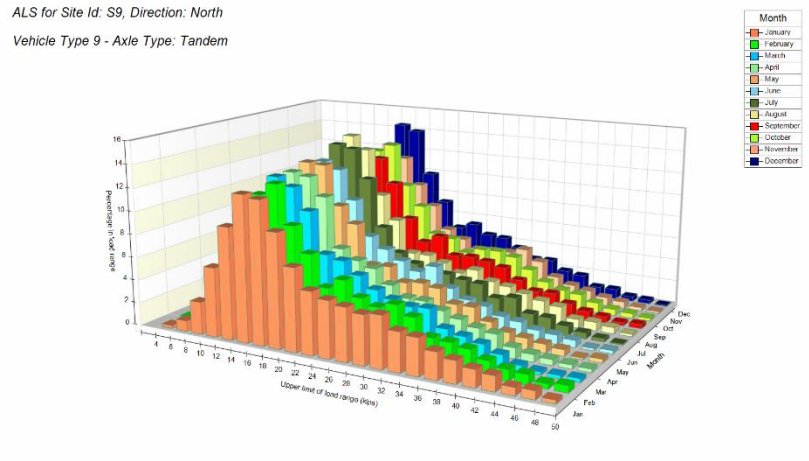

a) North

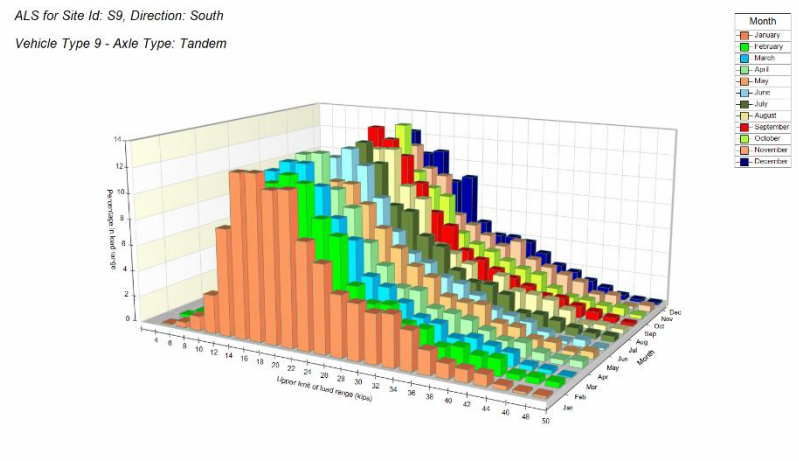

b) South

Figure 3-26. ALS for tandem axles of vehicle class 9 on Station S9.

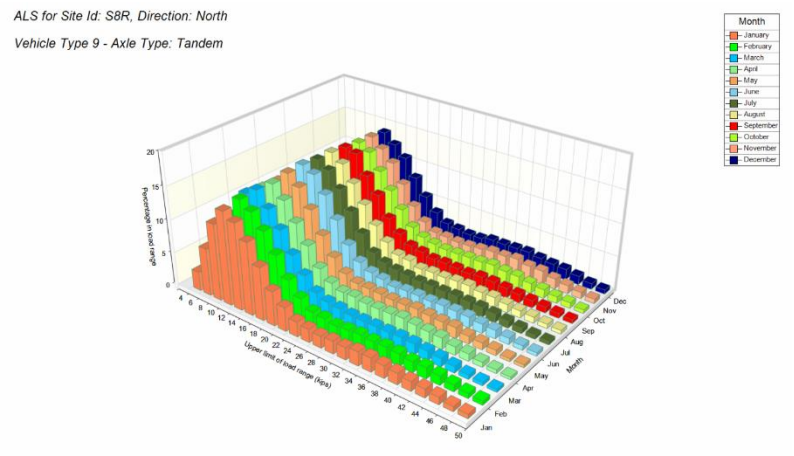

a) North

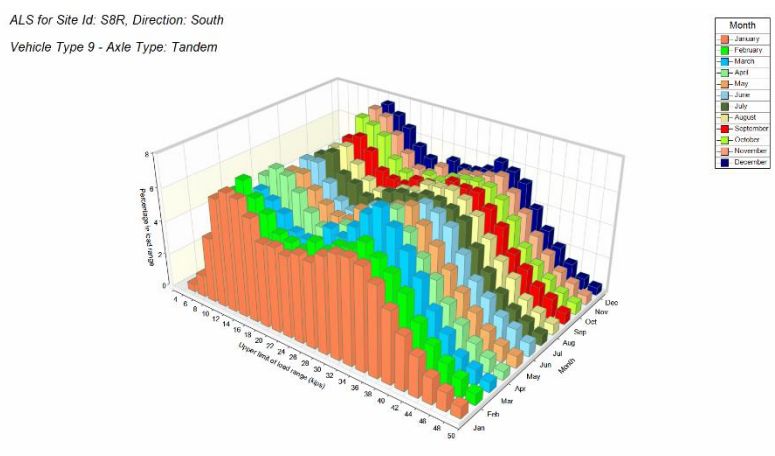

b) South

Figure 3-27. ALS for tandem axles of vehicle class 9 on Station S8R.

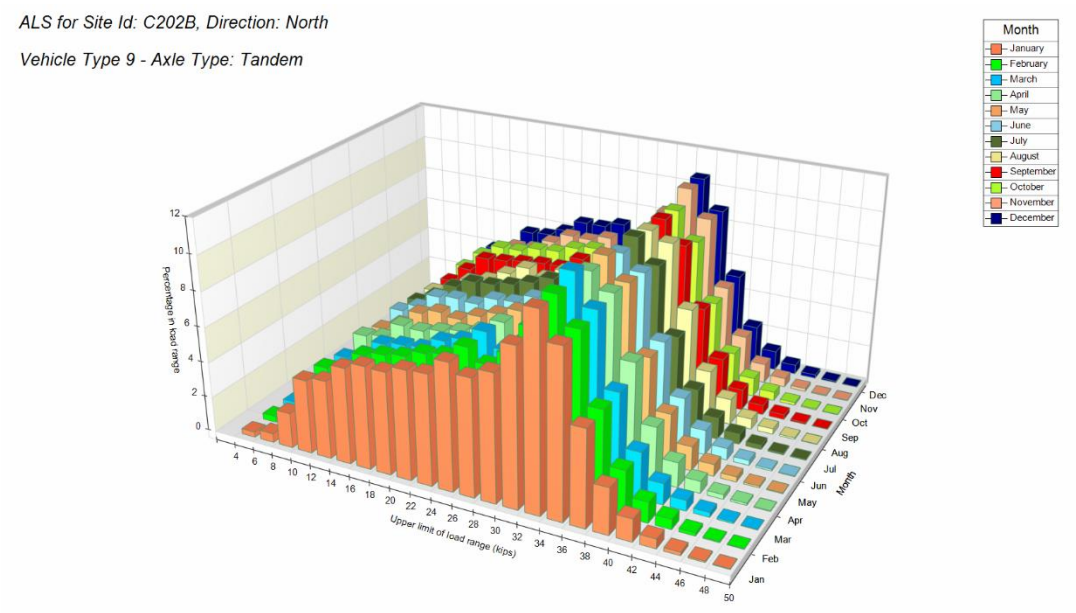

Figure 3-28. ALS for tandem axles of vehicle class 9 on Station C202B.

3.4.3.2.3 Average Number of Axle Types per Truck Class

The average number of axles of each type per vehicle is an essential complement to the ALS. In the MEPDG, these two inputs are used along with vehicle classification, AADTT, directional distribution, lane distribution, monthly adjustment factors, and traffic growth to estimate over time the number of repetitions of loads on different load ranges applied by the different axle types.

This input represents the average number of axles for each truck class (classes 4 to 13) for each axle type (single, tandem, tridem, and quad). For an example of its meaning, consider a hypothetical situation in which the different axle types on three buses are counted. Suppose that the first bus has two single axles (a steering axle, which is counted as single axle, and a rear single axle), the second bus has one single and one tandem, and the third bus has three singles (say, an articulated bus.) Therefore, if these three buses were representative of the bus loading at the location of interest (i.e., if the proportions observed for each of these buses with respect to the total number of buses were about 1/3), then the average number of single axles per bus would be (2+1+3)/3 =2 and the average number of tandem axles would be (0+1+0)/3 = 0.33. On the other hand, if at another location one observes for every articulated bus with three single axles

two buses with one single axle and a tandem axle and three with two single axles, then the average number of single axles per bus at this other location would be (3×2+2×1+1×3)/6 = 1.83 and the average number of tandem axles would be (3×0+2×1+1×0)/6 = 0.33. Notice how the average number of single axles changed. Although for this simple example the average number of tandem axles did not change with the bus proportions with different configurations, in general, the average number of axles for all axle types would change with changes in those proportions. The main point of the above example is to show that the average number of axles per vehicle class are related to the characteristics of the traffic stream observed at each location. Therefore, slightly different number of axles per vehicle class should be expected for each WIM station.

As with most other MEPDG inputs, the number of axles types per truck class can be input at different levels as follows:

- Level 1 – values determined through direct analysis of site-specific traffic data (AVC, WIM, or traffic counts).
- Level 2 – values determined through direct analysis of regional/statewide traffic data (AVC, WIM, or traffic counts).
- Level 3 – default values based on analysis of national databases such as the LTPP database.

Table 3-3 provides level 3 estimates of the number of axle types per truck class estimated using LTPP data presented in NCHRP 1-37A (2004).

For locations around WIM sites, it is better to use estimates of these values from the data for those sites. In order to obtain the average number of axles per vehicle class at each of the WIM sites in Hawaii, the customized program to compute ALS develop by the PI was enhanced to provide the estimates. The input data consisted of exactly the same information used to develop the ALS (Table 3-1). Table 3-4 through Table 3-12 provide the estimates of the average number axles per vehicle by axle type and for each direction at each of the WIM sites with useful information in Hawaii. In general, the values obtained are within expectations. Notice that the small sample sizes for some vehicle classes such as vehicle classes 7, 11, 12, and 13 coupled with the fact that some of these may exhibit a wide variety of configurations resulted in wide variations between sites for some of the axle of these truck classes.

Table 3-3. MEPDG default values for the average number of single, tandem, and tridem axles per truck class.

Truck Classification	Number of Single Axles per Truck	Number of Tandem Axles per Truck	Number of Tridem Axles per Truck	Number of Quad Axles per Truck
4	1.62	0.39	0.00	0.00
5	2.00	0.00	0.00	0.00
6	1.02	0.00	0.00	0.00
7	1.00	0.26	0.83	0.00
8	2.38	0.67	0.00	0.00
9	1.13	1.93	0.00	0.00
10	1.19	1.09	0.89	0.00
11	4.29	0.26	0.06	0.00
12	3.52	1.14	0.06	0.00
13	2.15	2.13	0.35	0.00

Note: The number of quad axles per truck class is 0.00, because there were too few counted in the LTPP traffic.

The grayed cells in the following tables correspond to values estimated with samples of less than 500, which was considered as a minimum to obtain reliable estimates of the average for those axles that are relatively uncommon.

Table 3-4. Average number of single, tandem, tridem, and quad axles per vehicle class estimated from WIM Station 438.

Vehicle Class	Direction							
	North-West				South-East			
	Average number per truck of:				Average number per truck of:			
	Single Axles	Tandem Axles	Tridem Axles	Quad Axles	Single Axles	Tandem Axles	Tridem Axles	Quad Axles
4	1.903	0.230	0.000	0.000	1.524	0.521	0.000	0.000
5	2.000	0.000	0.000	0.000	2.000	0.000	0.000	0.000
6	1.000	1.000	0.000	0.000	1.000	1.000	0.000	0.000
7	1.004	0.043	0.836	0.121	1.027	0.080	0.711	0.210
8	2.260	0.729	0.000	0.000	2.118	0.873	0.000	0.000
9	1.035	1.980	0.002	0.000	1.061	1.965	0.003	0.000
10	1.003	1.041	0.958	0.000	1.006	1.037	0.961	0.001
11	1.731	0.077	0.923	0.000	1.944	0.111	0.889	0.000
12	1.160	0.880	0.980	0.000	1.033	0.996	0.985	0.005
13	1.026	0.784	1.260	0.019	1.039	0.847	1.144	0.035

Table 3-5. Average number of single, tandem, tridem, and quad axles per vehicle class estimated from WIM Station S8R.

Vehicle Class	Direction							
	North				South			
	Average number per truck of:				Average number per truck of:			
	Single Axles	Tandem Axles	Tridem Axles	Quad Axles	Single Axles	Tandem Axles	Tridem Axles	Quad Axles
4	1.498	0.502	0.000	0.000	1.503	0.498	0.000	0.000
5	2.000	0.000	0.000	0.000	2.000	0.000	0.000	0.000
6	1.000	1.000	0.000	0.000	1.000	1.000	0.000	0.000
7	1.002	0.003	0.996	0.002	1.000	0.002	0.996	0.002
8	2.259	0.740	0.000	0.000	2.234	0.764	0.000	0.000
9	1.208	1.895	0.000	0.000	1.248	1.876	0.000	0.000
10	1.002	1.021	0.976	0.001	1.002	1.021	0.977	0.001
11	4.123	0.171	0.178	0.000	4.711	0.119	0.017	0.000
12	2.907	0.910	0.239	0.101	3.623	1.084	0.041	0.135
13	1.031	0.837	1.794	0.000	1.000	0.734	1.797	0.023

Table 3-6. Average number of single, tandem, tridem, and quad axles per vehicle class estimated from WIM Station S9.

Vehicle Class	Direction							
	North				South			
	Average number per truck of:				Average number per truck of:			
	Single Axles	Tandem Axles	Tridem Axles	Quad Axles	Single Axles	Tandem Axles	Tridem Axles	Quad Axles
4	1.727	0.279	0.000	0.000	1.732	0.269	0.000	0.000
5	2.000	0.000	0.000	0.000	2.000	0.000	0.000	0.000
6	1.000	1.000	0.000	0.000	1.000	1.000	0.000	0.000
7	1.004	0.007	0.993	0.000	1.000	0.003	0.812	0.184
8	2.517	0.481	0.000	0.000	2.302	0.698	0.000	0.000
9	1.298	1.849	0.001	0.000	1.277	1.860	0.001	0.000
10	1.000	1.030	0.967	0.000	1.003	1.030	0.970	0.000
11	3.960	0.160	0.240	0.000	2.375	0.000	0.875	0.000
12	2.846	1.077	0.192	0.000	1.767	0.633	0.567	0.167
13	3.750	0.600	0.700	0.000	1.444	0.222	1.55	0.111

Table 3-7. Average number of single, tandem, tridem, and quad axles per vehicle class estimated from WIM Station C202B.

Vehicle Class	Direction							
	North				South			
	Average number per truck of:				Average number per truck of:			
	Single Axles	Tandem Axles	Tridem Axles	Quad Axles	Single Axles	Tandem Axles	Tridem Axles	Quad Axles
4	1.848	0.152	0.000	0.000	-	-	-	-
5	2.000	0.000	0.000	0.000	-	-	-	-
6	1.000	1.000	0.00	0.00	-	-	-	-
7	1.001	0.082	0.916	0.002	-	-	-	-
8	2.000	0.995	0.000	0.000	-	-	-	-
9	1.037	1.981	0.000	0.000	-	-	-	-
10	1.007	1.051	0.947	0.001	-	-	-	-
11	2.000	0.000	1.000	0.000	-	-	-	-
12	1.238	1.857	0.095	0.000	-	-	-	-
13	1.481	0.913	0.448	0.615	-	-	-	-

Table 3-8. Average number of single, tandem, tridem, and quad axles per vehicle class estimated from WIM Station 10W.

Vehicle Class	Direction							
	North-West				South-East			
	Average number per truck of:				Average number per truck of:			
	Single Axles	Tandem Axles	Tridem Axles	Quad Axles	Single Axles	Tandem Axles	Tridem Axles	Quad Axles
4	1.908	0.268	0.000	0.000	1.932	0.268	0.000	0.000
5	2.000	0.000	0.000	0.000	2.000	0.000	0.000	0.000
6	1.000	1.000	0.000	0.000	1.000	1.000	0.000	0.000
7	1.009	0.131	0.469	0.400	1.005	0.069	0.762	0.169
8	2.207	0.785	0.000	0.000	2.295	0.686	0.000	0.000
9	1.169	1.912	0.002	0.000	1.171	1.910	0.003	0.000
10	1.016	1.019	0.976	0.004	1.014	1.028	0.968	0.002
11	3.603	0.260	0.246	0.000	2.260	0.498	0.543	0.000
12	1.086	0.989	0.936	0.026	1.334	0.908	0.735	0.118
13	1.400	0.522	0.785	0.383	1.226	0.907	0.859	0.223

Table 3-9. Average number of single, tandem, tridem, and quad axles per vehicle class estimated from WIM Station H41W.

Vehicle Class	Direction							
	North				South			
	Average number per truck of:				Average number per truck of:			
	Single Axles	Tandem Axles	Tridem Axles	Quad Axles	Single Axles	Tandem Axles	Tridem Axles	Quad Axles
4	1.778	0.223	0.000	0.000	1.824	0.179	0.000	0.000
5	2.000	0.000	0.000	0.000	2.000	0.000	0.000	0.000
6	1.000	1.000	0.00	0.00	1.000	1.000	0.000	0.000
7	1.627	0.659	0.310	0.031	1.107	0.190	0.492	0.317
8	2.292	0.710	0.000	0.000	2.409	0.564	0.012	0.000
9	1.227	1.884	0.001	0.000	1.219	1.884	0.003	0.001
10	1.070	1.082	0.917	0.000	1.061	1.041	0.928	0.015
11	4.514	0.229	0.011	0.000	4.509	0.210	0.019	0.002
12	1.158	1.035	0.877	0.018	1.387	0.627	0.690	0.291
13	1.522	1.596	0.662	0.064	1.279	0.866	0.526	0.516

Table 3-10. Average number of single, tandem, tridem, and quad axles per vehicle class estimated from WIM Station C4K.

Vehicle Class	Direction							
	East				West			
	Average number per truck of:				Average number per truck of:			
	Single Axles	Tandem Axles	Tridem Axles	Quad Axles	Single Axles	Tandem Axles	Tridem Axles	Quad Axles
4	1.892	0.184	0.000	0.000	2.045	0.092	0.000	0.000
5	2.000	0.000	0.000	0.000	2.000	0.000	0.000	0.000
6	1.000	1.000	0.00	0.000	1.000	1.000	0.000	0.000
7	1.010	0.104	0.436	0.461	1.020	0.094	0.494	0.412
8	2.009	0.785	0.000	0.000	2.348	0.641	0.000	0.000
9	1.205	1.880	0.011	0.000	1.167	1.904	0.008	0.000
10	1.427	1.434	0.563	0.001	1.214	1.222	0.777	0.001
11	1.644	0.139	0.861	0.000	1.939	0.344	0.650	0.000
12	1.452	1.355	0.548	0.032	1.168	0.951	0.872	0.071
13	1.500	0.672	0.707	0.345	1.828	0.866	0.845	0.160

Table 3-11. Average number of single, tandem, tridem, and quad axles per vehicle class estimated from WIM Station C10K.

Vehicle Class	Direction							
	North				South			
	Average number per truck of:				Average number per truck of:			
	Single Axles	Tandem Axles	Tridem Axles	Quad Axles	Single Axles	Tandem Axles	Tridem Axles	Quad Axles
4	1.926	0.278	0.000	0.000	1.874	0.282	0.000	0.000
5	2.000	0.000	0.000	0.000	2.000	0.000	0.000	0.000
6	1.000	1.000	0.000	0.000	1.000	1.000	0.000	0.000
7	1.017	0.113	0.531	0.356	1.011	0.075	0.665	0.260
8	2.153	0.829	0.001	0.000	2.196	0.754	0.001	0.000
9	1.162	1.914	0.003	0.000	1.182	1.891	0.011	0.000
10	1.124	1.083	0.895	0.021	1.056	1.086	0.909	0.003
11	3.073	0.423	0.283	0.000	2.472	0.448	0.501	0.000
12	1.057	0.970	0.963	0.028	1.408	1.063	0.753	0.029
13	1.139	0.758	1.012	0.219	1.464	1.064	1.003	0.046

Table 3-12. Average number of single, tandem, tridem, and quad axles per vehicle class estimated from WIM Station C7L.

Vehicle Class	Direction							
	East				West			
	Average number per truck of:				Average number per truck of:			
	Single Axles	Tandem Axles	Tridem Axles	Quad Axles	Single Axles	Tandem Axles	Tridem Axles	Quad Axles
4	2.054	0.133	0.000	0.000	2.016	0.122	0.000	0.000
5	2.000	0.000	0.000	0.000	2.000	0.000	0.000	0.000
6	1.000	1.000	0.000	0.000	1.000	1.000	0.000	0.000
7	1.022	0.097	0.496	0.407	1.006	0.122	0.734	0.145
8	2.309	0.682	0.000	0.000	2.282	0.710	0.000	0.000
9	1.117	1.937	0.003	0.000	1.113	1.940	0.002	0.000
10	1.089	1.105	0.891	0.002	1.039	1.061	0.938	0.000
11	2.836	0.173	0.516	0.000	1.966	0.544	0.632	0.000
12	1.060	0.998	0.958	0.015	1.362	0.864	0.768	0.117
13	1.377	1.533	0.725	0.049	1.504	1.261	0.919	0.013

3.4.3.2.4 Monthly Adjustment Factors (MAF)

The MEPDG ([1], [2]) uses monthly adjustment factors (MAF) to account for seasonal traffic fluctuations. The MAF, as used in the MEPDG [1], is simply 12 times the proportion of the annual truck traffic for a given truck class that occurs in a specific month. Thus, for uniform traffic throughout the year, the factor for each month is equal to 1. A factor greater than 1 implies that traffic for that month is higher than average and a factor less than 1 implies that traffic is lower than average. Naturally, the sum the MAF for the 12 months of the year must equal 12.

The importance of accurate estimation of these factors is that the effects of traffic loading is dependent on climatic conditions that affect material characteristics, and in turn, the strains in the pavement. Thus, the same traffic loading can have very different damaging effects depending of the month of year on which it is applied. For States with wide variarions in temperature or precipation, the effects can be substantial. Large changes in temperature significantly affect the moduli of bound materials, thus affecting the overall pavement stiffness and the load induced strains. Furthermore, in colder climates, prolonged freezing conditions substantially increase the moduli of unbound layers for some time and when above freezing temperatures return, the water in those bound layers melt and significantly reduce the moduli of unboud layers and the subgrade. These freeze/thaw cycles can have a substantial detrimental effect on the pavement performance. Precipitation causes moisture changes in the materials of unbound layers and the subgrade, also affecting their moduli.

In Hawaii, the temperature differentials between summer and winter are relatively minor and freezing conditions are practically non-existent. The most likely adverse factor is that of changes in moisture conditions throughout the year. Althoguh in Hawaii there are indeed differences in precipitation throughout the year, signigicant monthly precipitation can occur almost all year round. The weather stations in the state report more than 200 wets days per year. Thus, for Hawaiian conditions use of the default MAF (= 1 for each month and each vehicle class) is expected to have only a relatively minor effect on the predictions of the pavement deterioration process.

A study of the MAF conducted in 2007 as part of this project using classification and weight data from the available WIM stations at that time showed that there were generally no substantial variations of the factors. Furthermore, the factors did not appear to follow a seasonal

pattern clearly identifiable. Although the study had some limitations in terms of data quality, its resutls, together with the relatively minor seasonal climatic differences in the State, lead to the conclusion that derivation of the factors was not of first priority and thus the MAF were not studied further. With the new version of Prep-ME soon to be realeased, the factors should be relatively simple to compute with the data that pass the quality checks.

The following paragraphs present the derivation of the MAF previously performed with data from 2002 to 2006.

As mentioned before, the information available at the time did not lend itself to the derivation of reliable estimates of the MAF for all stations. Despite the limitations in the data, the AVC (Automatic Vehicle Classification) data were used to derive monthly adjustment factors for the same locations as the WIM stations. Although as indicated before the estimates may not have been entirely reliable, they did provide an indication of the variability around the default value and provided a basis to study their potential effects on the predictions. Based on the type of AVC information available, the stations could be classified according to NCHRP 1-39 [16] as:

LEVEL 1

- Station C12E – Hoonapiilani, Maui
- Station S8R – Queen Kaahumanu, Big Island
- Station S9 – Queen Kaahumanu, Big Island

LEVEL 2

- Station 10W – Kalaeloa @ Palailai Interchange, Oahu
- Station C202B – Sand Island @ Bascule Bridge, Oahu
- Station H41W – H-3 @ MP 1.28, Oahu
- Station C7L – H-1, Waimalu Viaduct, Oahu

Level 1 stations are required to have at least one week of data for at least 12 consecutive months. Since this requirement was imposed by TrafLoad, it was not possible to use that software to derive MAF for Level 2 stations. TrafLoad was then used to derive MAF only for the Level 1 stations.

Table 3-13 and

Table 3-14 present the monthly adjustment factors (MAF) obtained with TrafLoad for stations S8R and S9, respectively. A similar table was also derived for station C12E. Although the latter passed the quality checks, there was less confidence on its results due to the lower traffic volumes and therefore they are not presented.

The results for vehicle class 9 at station S8R show relatively minor variations around 1 of the MFA (maximum variation of about 13 %.) The same can be noted for station S9. From these two tables, it can be noted that for other vehicle classes such as classes 4 and 6, the variations are in some cases larger. However, the higher MAF do not occur when more rain is to be expected (around December and January). Other vehicle classes play only a minor role either because they represent a small percentage of the traffic stream (vehicle classes 7, 8, and 10-13) or because they impose relatively small loads (vehicle class 5).

Consequently, using default MAFs is not expected to have significant effects on pavement design for Hawaii.

Table 3-13. MAF for Station S8R – Queen Kaahumanu, Big Island.

Month	Vehicle Class									
	4	**5**	**6**	**7**	**8**	**9**	**10**	**11**	**12**	**13***
1	1.105	1.004	0.946	0.793	0.953	0.940	0.961	1.298	0.895	1.000
2	1.227	1.133	0.977	0.956	0.919	0.952	0.851	1.481	1.000	1.000
3	1.053	1.183	1.061	1.011	0.924	1.040	0.916	1.351	1.000	1.000
4	1.203	1.288	0.994	0.902	1.081	1.134	0.916	1.376	1.052	1.000
5	1.245	1.326	0.977	1.039	1.081	1.129	1.061	1.559	1.264	1.000
6	0.911	0.793	0.961	1.093	1.182	1.126	1.012	0.312	1.264	1.000
7	0.773	0.770	1.019	1.011	1.062	0.956	0.723	0.598	0.737	1.000
8	0.869	0.817	1.084	0.793	1.025	0.983	0.948	0.649	1.105	1.000
9	0.842	0.770	1.030	0.902	0.991	0.953	1.077	0.649	0.790	1.000
10	1.185	1.242	0.966	1.011	1.025	0.924	1.334	1.325	1.052	1.000
11	1.001	0.926	0.985	1.176	0.929	0.918	1.077	0.832	1.052	1.000
12	0.585	0.746	1.002	1.311	0.829	0.946	1.124	0.571	0.790	1.000

* MAF set equal to 1 because estimates were unreliable.

Table 3-14. MAF for Station S9 – Queen Kaahumanu, Big Island.

Month	Vehicle Class									
	4	**5**	**6**	**7**	**8**	**9**	**10**	**11***	**12**	**13***
1	1.076	1.051	1.035	1.049	1.015	0.977	0.989	1.000	1.112	1.000
2	1.288	1.254	1.011	1.312	1.203	1.064	0.954	1.000	1.033	1.000
3	1.272	1.182	1.008	0.655	1.287	1.007	0.954	1.000	0.794	1.000
4	1.380	1.164	0.990	1.115	1.235	1.144	0.818	1.000	0.636	1.000
5	1.206	1.037	0.909	0.918	1.110	0.996	0.920	1.000	1.113	1.000
6	0.768	0.961	0.969	1.246	1.020	1.072	1.091	1.000	0.954	1.000
7	0.666	0.943	1.036	0.787	0.957	0.952	1.057	1.000	1.192	1.000
8	0.936	0.868	1.055	0.984	0.957	0.941	0.954	1.000	1.033	1.000
9	0.774	0.923	0.980	0.852	0.602	0.880	0.750	1.000	0.874	1.000
10	0.811	1.039	1.103	1.902	0.592	1.065	1.261	1.000	0.954	1.000
11	0.833	0.731	0.864	0.460	0.796	0.865	0.887	1.000	1.112	1.000
12	0.990	0.846	1.039	0.721	1.225	1.038	1.363	1.000	1.192	1.000

* MAF set equal to 1 because estimates were unreliable.

The above results were based on stations located on the Big Island but it was also desirable to estimate the MAF for Oahu.

Even though the information from the Level 2 stations could not be used to derive MAF with TrafLoad, two of those stations, namely stations “10W” and “C202B”, contained a significant amount of information. Consequently, the information from stations “10W” and “C202B” was used to derive the factors. The analysis was performed manually using Microsoft Excel. The following paragraphs explain the process.

Traffic typically exhibits hourly and day of week variations that if not accounted for when using data for less than the whole month could bias the estimates of the MAF.

The following procedure works well if all the days of the week have a relatively similar volume or if the ratio between the number of hours of weekdays, number of hours on Saturdays, and number of hours on Sundays is about 5:1:1. In this case, one can simply average the hourly volumes for each vehicle class and for each hour of the day and then add these averages to obtain an estimate of the average daily traffic (ADT) in the month for that vehicle class. Then, the month ADT divided by AADT for the vehicle class in question provides an estimate of the MAF for that vehicle class. For example, for a given vehicle class, say Class 4, average daily traffic = average number of class 4 vehicles in hour 0 (0:01 A.M. to 1:00 A.M.) + average number of

class 4 vehicles in hour 1 (1:01 A.M. to 2:00 A.M.) + … + average number of class 4 vehicles in hour 23 (11:01 P.M. to 12:00 P.M.).

When the conditions for the above procedure are not met, the estimates would be biased. For example, suppose that for a given hour of the day the average weekday traffic volume is 100, whereas the Saturday and Sunday traffic volumes for the same hour of the day are both 50. In this case the average hourly volume is $(5 \times 100 + 2 \times 50)/7 = 86$ vehicle/h. However, if for the given hour there are 2 weekday observations, 1 Saturday observation and 1 Sunday observation and one simply average these observations, the estimated hourly volume would be $(100 + 100 + 50 + 50)/4 = 75$, which in this case is biased towards the weekend volumes. The solution in such cases is to calculate the average weekday and the average weekend separately and then calculate a weighted average of these two values (with a weight of 5 for weekdays and a weight of 2 for weekends).

In the case of station "10W", the processing of the data was not very complicated since there were data for most of the days on each month. The only problem found was the lack of data for hour "0" for many of the months in the southwest direction, second lane. However, since traffic volume for hour "0" is very low, just about 0.33% of the total in the day, a proportionality rule was adopted to estimate that hourly volume for this particular situation. In addition, since data were available for most of the days on each month with data (i.e. in general a fair representation of weekday and weekend traffic was available for each month) both procedures described above produced similar results. The MAF presented below were obtained without separating between weekday and weekend traffic.

In the case of station "C200B" a few more complications were found.

- For many months a separation of weekend and weekday traffic was required. Also, it was not possible to discriminate between Saturday and Sunday traffic since there were many months without data for one of those days.
- In some cases there were missing data for one or two hours (usually "0" or "23"). Since the hours missing represent hours with low volumes, the volumes for those hours were estimated based on proportions from the other days with 24 hours of data.

- For some months there were days with many consecutive hours with zero volume. These hours were not taken into account as it appears they are the result of problems during the data collection.
- Finally, results that appear to be highly suspect were also eliminated. For example, the average number of Class 7 vehicles in March 2002 was 79.1 while from April 2002 to December 2002 the monthly average for that vehicle class oscillated between 0 and 4.9.

For the analysis, the classes were grouped as follows:

- Class 4
- Class 5
- Class 6
- Classes 7 and 8
- Classes 9 and 11
- Classes 10, 12, and 13

Table 3-15 through Table 3-18 present the monthly adjustment factors (MAF) obtained with the manual procedures outlined above for each direction at stations 10W and C202B. Again, for vehicle class 9, with the exception of two values for the North direction at Station C202B, the factors do not deviate too much from 1. The maximum values were again observed in the summer months. Thus, use of a value of 1 for the winter months would result in slightly conservative designs. Nevertheless, for some of the reasons exposed and other that will be discussed later, the use of default MAF is not expected to be of much consequence. Therefore, until newer MAF are derived with the more recent data it is recommended to use the defaults.

Table 3-15. MAF for Station C202B – Sand Island @ Bascule Bridge, North, Oahu.

Month	Vehicle Class									
	4	**5**	**6**	**7***	**8***	**9***	**10***	**11***	**12***	**13***
1	1.073	1.020	0.872	1.148	1.148	0.798	1.054	0.798	1.054	1.054
2	1.330	1.103	0.854	1.307	1.307	0.740	1.062	0.740	1.062	1.062
3	0.554	0.941	0.793	0.660	0.660	0.536	0.578	0.536	0.578	0.578
4	0.642	1.066	0.881	0.857	0.857	0.926	1.031	0.926	1.031	1.031
5	0.704	1.037	0.864	0.880	0.880	0.865	0.890	0.865	0.890	0.890
6	1.236	1.103	1.166	1.088	1.088	1.273	1.199	1.273	1.199	1.199
7	1.242	1.099	1.208	1.043	1.043	1.233	1.139	1.233	1.139	1.139
8	1.081	0.985	1.103	1.024	1.024	1.111	1.001	1.111	1.001	1.001
9	0.895	0.868	0.995	0.967	0.967	0.979	0.954	0.979	0.954	0.954
10	1.241	1.029	1.224	1.082	1.082	1.336	1.115	1.336	1.115	1.115
11	1.088	0.929	1.034	0.910	0.910	1.127	0.964	1.127	0.964	0.964
12	0.913	0.820	1.005	1.034	1.034	1.074	1.014	1.074	1.014	1.014

* MAF were combined for vehicle classes 7 and 8, 9 and 11, and 10, 12, and 13.

Table 3-16. MAF for Station C202B – Sand Island @ Bascule Bridge, South, Oahu.

Month	Vehicle Class									
	4	**5**	**6**	**7***	**8***	**9***	**10***	**11***	**12***	**13***
1	1.190	1.023	0.913	1.144	1.144	0.955	0.985	0.955	0.985	0.985
2	1.253	1.033	0.970	1.207	1.207	0.953	0.973	0.953	0.973	0.973
3	1.084	1.415	1.162	1.086	1.086	1.091	1.077	1.091	1.077	1.077
4	1.128	1.177	1.026	1.103	1.103	1.098	1.124	1.098	1.124	1.124
5	0.871	1.142	1.027	1.051	1.051	1.049	1.051	1.049	1.051	1.051
6	0.923	0.887	0.901	0.950	0.950	0.973	0.971	0.973	0.971	0.971
7	0.664	0.898	0.956	1.006	1.006	1.034	1.091	1.034	1.091	1.091
8	0.818	0.851	0.964	0.908	0.908	0.934	0.832	0.934	0.832	0.832
9	1.079	1.110	1.108	0.985	0.985	1.099	1.064	1.099	1.064	1.064
10	0.614	0.714	0.922	0.871	0.871	0.890	0.869	0.890	0.869	0.869
11	1.075	0.858	1.040	0.860	0.860	0.948	0.908	0.948	0.908	0.908
12	1.301	0.893	1.012	0.828	0.828	0.977	1.055	0.977	1.055	1.055

* MAF were combined for vehicle classes 7 and 8, 9 and 11, and 10, 12, and 13.

Table 3-17. MAF for Station 411 – H-3 @ MP 1.28, North-East, Oahu.

Month	Vehicle Class									
	4	**5**	**6**	**7***	**8***	**9***	**10***	**11***	**12***	**13***
1	0.916	0.974	0.972	1.018	1.018	0.930	0.769	0.930	0.769	0.769
2	0.928	0.954	0.935	0.961	0.961	0.937	0.857	0.937	0.857	0.857
3	0.941	0.959	1.123	1.069	1.069	1.010	0.938	1.010	0.938	0.938
4	0.889	0.993	1.048	1.054	1.054	1.031	1.061	1.031	1.061	1.061
5	1.020	1.086	1.087	1.134	1.134	1.162	1.427	1.162	1.427	1.427
6	0.876	1.027	0.940	1.037	1.037	1.040	1.187	1.040	1.187	1.187
7	1.015	1.069	1.026	1.086	1.086	1.162	1.146	1.162	1.146	1.146
8	1.044	0.985	1.025	1.048	1.048	1.026	0.947	1.026	0.947	0.947
9	1.070	0.980	1.042	1.021	1.021	0.982	1.041	0.982	1.041	1.041
10	1.184	0.966	0.916	0.818	0.818	0.816	0.767	0.816	0.767	0.767
11	1.118	0.985	0.948	0.827	0.827	0.864	0.961	0.864	0.961	0.961
12	0.998	1.022	0.940	0.926	0.926	1.040	0.900	1.040	0.900	0.900

* MAF were combined for vehicle classes 7 and 8, 9 and 11, and 10, 12, and 13.

Table 3-18. MAF for Station 411 – H-3 @ MP 1.28, South-West, Oahu.

Month	Vehicle Class									
	4	**5**	**6**	**7***	**8***	**9***	**10***	**11***	**12***	**13***
1	0.997	0.945	0.959	0.893	0.893	0.970	0.901	0.970	0.901	0.901
2	1.018	0.984	0.934	0.883	0.883	0.947	0.859	0.947	0.859	0.859
3	1.133	0.941	1.064	0.977	0.977	1.004	1.322	1.004	1.322	1.322
4	0.982	0.959	1.025	0.989	0.989	1.033	1.343	1.033	1.343	1.343
5	0.990	1.082	1.080	1.063	1.063	1.163	1.159	1.163	1.159	1.159
6	0.846	0.996	1.004	1.054	1.054	1.049	0.882	1.049	0.882	0.882
7	1.064	1.022	1.071	1.139	1.139	1.177	0.901	1.177	0.901	0.901
8	0.977	0.986	1.062	1.066	1.066	1.031	0.954	1.031	0.954	0.954
9	0.972	1.055	1.061	1.066	1.066	0.967	0.942	0.967	0.942	0.942
10	1.181	1.205	0.938	1.008	1.008	0.779	0.799	0.779	0.799	0.799
11	0.982	0.985	0.876	0.966	0.966	0.835	1.083	0.835	1.083	1.083
12	0.859	0.841	0.926	0.898	0.898	1.046	0.854	1.046	0.854	0.854

* MAF were combined for vehicle classes 7 and 8, 9 and 11, and 10, 12, and 13.

3.5 DERIVATION OF ESALC

Although one of the main goals of this project is advancing towards implementation of the MEPDG, it is recognized that the current procedure used by HDOT to design pavements will continue to be used for some time. Therefore, an update of some pavement design parameters with newer information is desirable. In particular, relating to traffic loading, HDOT's design procedure utilizes *Equivalent Single Axle Load Constants* (ESALC) to convert the traffic

information into equivalent repetitions of a standard single axle of 18,000 lb. (80 kN). This section presents the development of updated values of those ESALC from the WIM information presented earlier. The current ESALC values were derived from data obtained from 1972 to 1974. The derivation of updated values with more current information (2006 - 2012) is important for several reasons. As mentioned above, even though the use of mechanistic-empirical (M-E) procedures will eventually replace the old procedures, the transition will take effect over several years and therefore updated values more representative of current conditions are still needed. Moreover, in many occasions, the starting point for an M-E analysis will be the result of a design with old procedures using ESALC. Finally, the values will also be useful for the counties when using other design procedures (ESALC can be easily converted to truck factors (TF) as used in other design procedures such as the Asphalt Institute by simply dividing them by 365.)

The ESALC are derived separately for each vehicle class. The addition of ESALC for buses is considered an important improvement to the procedures since in many situations this vehicle class produces a substantial amount of the damage to the pavement structure. This may be particularly significant for some city and county roads. In past analyses, it appears that buses were pooled together with class 5 vehicles for which the ESALC value was relatively low. As shown below, the new ESALC for buses are significantly higher than for vehicle class 5 trucks. Other differences are noted in the values for other vehicles classes as well.

3.5.1 HDOT Method for Calculating ESAL Constants

The procedure used by HDOT for calculating the ESALC was documented by Scott Kauai, which in turn was reproduced from an HDOT's internal document. Basically, the same procedure is documented here but with a slight modification because the input data is provided in terms of a distribution of loads instead of an actual count for each vehicle class and axle type.

The procedure is explained with reference to Figure 3-29, which shows the ESALC derivation for vehicle class 9 at station 438, direction 2 (Northeast). In the table, the columns for each axle type are labeled a, b, etc. just above the numeric information. The nomenclature is given in Table 3-19.

Table 3-19. Nomenclature for the ESALC calculation table.

Column	Description
A	Lower limit of axle load range (lb.)
B	Upper limit of axle load range (lb.)
C	Average axle load in range adjusted for axle type (lb.)
D	ESAL for the average single axle load
e	Frequency of axles in the axle load range (the sum of values in this column must be 1).
f	Frequency (column e) times the average number of axles of the axle type in question for the truck (the values of average number of single, tandem, tridem, and quad axles per truck are shown at the top right of the table)
G	ESAL contribution by axle type in load range.

The values in each column are calculated as follows:

1. *Column c*: Determine the average single axle loads for each axle load range adjusted for axle type. The adjustment factor is 1.0 for single axles, 1.1 for tandem axles, 1.2 for tridem, and 1.2 for quad axles[6]. The calculation is accomplished with the following equation:

[6] A possible justification for the adjustment factors is that the loading on multi-axle configurations may not be evenly distributed. For example, a tandem axle with a 32 kip load may have a load configuration of 16/16 kip loading or 14/18 kip loading. When calculating the load equivalency factor (LEF), these different load configurations produce different values:

LEF 1: $2 * (16/18)^{4.2} = 2.44$

LEF 2: $(14/18)^{4.2} + (18/18)^{4.2} = 2.70$

$$(\text{Column c}) = \frac{\text{Average axle load}}{\text{Number of axles in axle type}} (\text{Adjustment factor})$$

which for each axle configuration specializes as follows:

Single axles:

$$(\text{Column c}) = \frac{[(\text{Column a}) + (\text{Column b})] / 2}{1} \times (1.0)$$

Tandem axles:

$$(\text{Column c}) = \frac{[(\text{Column a}) + (\text{Column b})] / 2}{2} \times (1.1)$$

Tridem axles:

$$(\text{Column c}) = \frac{[(\text{Column a}) + (\text{Column b})] / 2}{3} \times (1.2)$$

Quad axles:

$$(\text{Column c}) = \frac{[(\text{Column a}) + (\text{Column b})] / 2}{4} \times (1.2)$$

2. *Column d*: Determine the ESAL of one axle *of the axle type* (single, tandem, tridem, or quad) for each axle load range, column d:

$$(\text{Column d}) = (\text{Number of axles in axle type}) \times \left[\frac{(\text{Column c, kips})}{(18\,\text{kips})} \right]^{4.2}$$

For example for a tridem axle this equation is:

$$(\text{Column d}) = (3) \times \left[\frac{(\text{Column c, kips})}{(18\,\text{kips})} \right]^{4.2}$$

The example shows that the LEF values are higher when the load is not distributed evenly between the axles in the axle configuration. Some of the evidence from the WIM data indeed indicates unevenness of the load on multi-axle configurations.

3. *Column f*: Multiply the frequency in column *e* by the average number of axle types per vehicle (for the vehicle class in question):
   The value in column *e* provides the frequency with which the load range appears for the given axle type. For example, the value in Figure 3-29 for the load range 40,000-42,000 lb. in column *e* for tandem axles is 0.0142. This means that for every 1,000 applications of tandem axles of vehicle class 9, about 14 applications will be in the 40,000 lb-42,000 lb. load range.

   Now consider 1,000 passages of vehicle class 9. Based on the average number of tandem axles per truck passage shown at the top right of the table, *on average*, each passage of a truck will contribute with 1.980 applications of tandem axles and thus for 1,000 vehicles the number of tandem axle load applications will be 1,980. Out of these, (0.0142) (1,980) ≈ 28 will be in the load range of 40,000-42,000 lb. The computation was presented in terms of 1,000 vehicles just to make it easier its understanding. However, in column *f* of the table number of applications of the axle type in question is computed for one truck instead of 1,000. Thus, the value appearing on the table is basically the value computed above divided by 1,000, which gives the normalized number of applications in the load range for the axle type per vehicle passage. The explanations for other axle types are entirely analogous.

   Notice that the sum of the values in columns *f* is approximately equal to the average number of axles (as defined by the axle types) per truck shown on the top right corner of the worksheet. In the example of Figure 3-29, the sum is about 3.02, which agrees well with what is normally expected for vehicle class 9, whose most common configurations consists of 1 single and 2 tandem axles (that is about 3 axle types)[7].

[7] The fact that vehicle class 9 shows in general a number of single axles greater than 1 and of tandem axle less than 2 appear to be related to the definition of single and tandem axles. Many axles are being classified as single simply because their measured axle separation to adjacent axles is slightly more 2.4 m.

4. *Column g*: Determine the ESAL contribution for the axle in the load range. This is accomplished by simply multiplying the values in columns *d* and *f*.

5. *Truck factor (TF)*: add up the values in all columns *g*. This value provides the average effect of a single vehicle passage in terms of equivalent single axle loads of 18,000 lb. This is known as the truck factor (TF) in other design procedures.[8]

6. *ESALC*: Determine the ESALC for use in the Traffic Index (TI) calculation by multiplying the *TF* obtained in the previous step by 365. The ESAL constant essentially provides the ESAL/truck in a whole year. Recall that for the TI calculation in the HDOT pavement design procedure the number of trucks is given in trucks per day and the design life is given in years. The transformation from daily to yearly effects is already incorporated in the ESALC.

The procedure described above was used with the data from each WIM station that passed the quality checks described in section 3.4.3 (This was done for each direction and for each vehicle class.) Table 3-20 summarizes the results for the most prevalent vehicle classes 4, 5, 6, and 9.

The values in this table show substantial differences from location to location or even for both directions at the same location. For example, the ESALC value for buses in the North-West direction at station 438 is almost three times the value for the opposite direction. The same type of unbalance by direction can be noted for example for vehicle class 9 at Station H41W. Notice that identifying the reasons for such unbalances is not simple since they can be related to generally higher loads being transported in one direction than in the other, or even with the same loading per direction having the loading concentrated on fewer vehicles (e.g., buses with a well-defined peak period and another peak that is more spread out during the day), or a combination of these.

[8] This value could be useful for those wishing to use other design procedures. It must be noted however that the truck factors presented here are based on a 4.2 exponent for the calculation of the load equivalency factors instead of the 4.0 exponent or load equivalency tables used in some other procedures (e.g., AASHTO, 1993).

ESALC Calculation

											Veh. Weighed							Average number of axles of each type per truck							
Distributions based on valid data from years 2006 - 2012											62,162												Singles:	1.035
																							Tandems:	1.980
Site 438					**Direction of Travel:**		**8**																Tridems:	0.002
																							Quads:	0.000
FHWA Vehicle Type 9: Single trailer trucks 5 axles																								

Single Axles							Tandem Axle							Tridem Axle						
Axle load range – lower limit	Axle load range – upper limit	Average single axle load	ESALs per single axle	Freq.	Freq. * avg. No. of singles per truck	ESAL contr. from axle in load range	Axle load range – lower limit	Axle load range – upper limit	Average single axle load	ESALs per tandem axle	Freq.	Freq. * avg No. of tandems per truck	ESAL contr. from axle in load range	Axle load range – lower limit	Axle load range – upper limit	Average single axle load	ESALs per tridem axle	Freq.	Freq. * avg No. of tridems per truck	ESAL contr. from axle in load range
a	b	c	d	e	f	g	a	b	c	d	e	f	g	a	b	c	d	e	f	g
	3,000	3,000	0.0005	0.002	0.002	0.00000		6,000	3300	0.0016	0.0239	0.0473	0.00008		12,000	4800	0.0116	0.6422	0.0012	0.00001
3,000	4,000	3,500	0.0010	0.011	0.011	0.00001	6,000	8,000	3850	0.0031	0.0390	0.0772	0.00024	12,000	15,000	5400	0.0191	0.1297	0.0002	0.00000
4,000	5,000	4,500	0.0030	0.013	0.013	0.00004	8,000	10,000	4350	0.0088	0.0829	0.1640	0.00145	15,000	18,000	6600	0.0444	0.0499	0.0001	0.00000
5,000	6,000	5,500	0.0069	0.020	0.020	0.00014	10,000	12,000	6050	0.0205	0.1137	0.2252	0.00462	18,000	21,000	7800	0.0895	0.0056	0.0000	0.00000
6,000	7,000	6,500	0.0139	0.034	0.035	0.00048	12,000	14,000	7150	0.0414	0.1165	0.2307	0.00955	21,000	24,000	9000	0.1632	0.0180	0.0000	0.00001
7,000	8,000	7,500	0.0253	0.132	0.136	0.00345	14,000	16,000	8250	0.0755	0.1075	0.2129	0.01608	24,000	27,000	10200	0.2761	0.0000	0.0000	0.00000
8,000	9,000	8,500	0.0428	0.198	0.205	0.00878	16,000	18,000	9350	0.1277	0.0849	0.1680	0.02146	27,000	30,000	11400	0.4405	0.0000	0.0000	0.00000
9,000	10,000	9,500	0.0683	0.257	0.266	0.01815	18,000	20,000	10450	0.2038	0.0639	0.1265	0.02579	30,000	33,000	12600	0.6707	0.0098	0.0000	0.00001
10,000	11,000	10,500	0.1040	0.157	0.163	0.01689	20,000	22,000	11550	0.3103	0.0462	0.0915	0.02840	33,000	36,000	13800	0.9828	0.0270	0.0000	0.00005
11,000	12,000	11,500	0.1523	0.108	0.112	0.01706	22,000	24,000	12650	0.4546	0.0369	0.0731	0.03325	36,000	39,000	15000	1.3950	0.0098	0.0000	0.00003
12,000	13,000	12,500	0.2162	0.043	0.045	0.00969	24,000	26,000	13750	0.6453	0.0368	0.0729	0.04704	39,000	42,000	16200	1.9273	0.0105	0.0000	0.00004
13,000	14,000	13,500	0.2987	0.014	0.014	0.00425	26,000	28,000	14850	0.8915	0.0323	0.0640	0.05706	42,000	45,000	17400	2.6019	0.0287	0.0001	0.00014
14,000	15,000	14,500	0.4033	0.007	0.007	0.00274	28,000	30,000	15950	1.2036	0.0324	0.0642	0.07727	45,000	48,000	18600	3.4430	0.0000	0.0000	0.00000
15,000	16,000	15,500	0.5336	0.002	0.002	0.00127	30,000	32,000	17050	1.5927	0.0320	0.0634	0.10094	48,000	51,000	19800	4.4768	0.0069	0.0000	0.00006
16,000	17,000	16,500	0.6939	0.001	0.001	0.00095	32,000	34,000	18150	2.0709	0.0309	0.0611	0.12657	51,000	54,000	21000	5.7319	0.0000	0.0000	0.00000
17,000	18,000	17,500	0.8884	0.001	0.001	0.00055	34,000	36,000	19250	2.6515	0.0270	0.0535	0.14187	54,000	57,000	22200	7.2387	0.0111	0.0000	0.00015
18,000	19,000	18,500	1.1220	0.000	0.000	0.00049	36,000	38,000	20350	3.3485	0.0229	0.0454	0.15191	57,000	60,000	23400	9.0299	0.0139	0.0000	0.00023
19,000	20,000	19,500	1.3996	0.000	0.000	0.00038	38,000	40,000	21450	4.1772	0.0192	0.0381	0.15912	60,000	63,000	24600	11.1405	0.0056	0.0000	0.00011
20,000	21,000	20,500	1.7267	0.000	0.000	0.00027	40,000	42,000	22550	5.1535	0.0142	0.0281	0.14476	63,000	66,000	25800	13.6075	0.0000	0.0000	0.00000
21,000	22,000	21,500	2.1091	0.000	0.000	0.00014	42,000	44,000	23650	6.2947	0.0111	0.0219	0.13777	66,000	69,000	27000	16.4704	0.0000	0.0000	0.00000
22,000	23,000	22,500	2.5528	0.000	0.000	0.00044	44,000	46,000	24750	7.6191	0.0082	0.0162	0.12369	69,000	72,000	28200	19.7707	0.0000	0.0000	0.00000
23,000	24,000	23,500	3.0644	0.000	0.000	0.00029	46,000	48,000	25850	9.1458	0.0055	0.0109	0.09972	72,000	75,000	29400	23.5524	0.0000	0.0000	0.00000
24,000	25,000	24,500	3.6505	0.000	0.000	0.00030	48,000	50,000	26950	10.8951	0.0037	0.0074	0.08076	75,000	78,000	30600	27.8616	0.0148	0.0000	0.00076
25,000	26,000	25,500	4.3184	0.000	0.000	0.00042	50,000	52,000	28050	12.8885	0.0029	0.0057	0.07395	78,000	81,000	31800	32.7469	0.0167	0.0000	0.00101
26,000	27,000	26,500	5.0756	0.000	0.000	0.00008	52,000	54,000	29150	15.1484	0.0015	0.0031	0.04639	81,000	84,000	33000	38.2591	0.0000	0.0000	0.00000
27,000	28,000	27,500	5.9300	0.000	0.000	0.00027	54,000	56,000	30250	17.6983	0.0011	0.0022	0.03318	84,000	87,000	34200	44.4515	0.0000	0.0000	0.00000
28,000	29,000	28,500	6.8898	0.000	0.000	0.00000	56,000	58,000	31350	20.5628	0.0007	0.0015	0.03052	87,000	90,000	35400	51.3796	0.0000	0.0000	0.00000
29,000	30,000	29,500	7.9636	0.000	0.000	0.00012	58,000	60,000	32450	23.7677	0.0006	0.0012	0.02892	90,000	93,000	36600	59.1013	0.0000	0.0000	0.00000
30,000	31,000	30,500	9.1604	0.000	0.000	0.00014	60,000	62,000	33550	27.3397	0.0003	0.0007	0.01869	93,000	96,000	37800	67.6772	0.0000	0.0000	0.00000
31,000	32,000	31,500	10.4896	0.000	0.000	0.00000	62,000	64,000	34650	31.3068	0.0002	0.0005	0.01523	96,000	99,000	39000	77.1699	0.0000	0.0000	0.00000
32,000	33,000	32,500	11.9609	0.000	0.000	0.00000	64,000	66,000	35750	35.6381	0.0002	0.0003	0.01171	99,000	#####	40200	87.6448	0.0000	0.0000	0.00000
33,000	34,000	33,500	13.5845	0.000	0.000	0.00000	66,000	68,000	36850	40.5437	0.0001	0.0002	0.00931	#####	#####	41400	99.1695	0.0000	0.0000	0.00000
34,000	35,000	34,500	15.3708	0.000	0.000	0.00000	68,000	70,000	37950	45.8749	0.0001	0.0002	0.00712	#####	#####	42600	111.8142	0.0000	0.0000	0.00000
35,000	36,000	35,500	17.3306	0.000	0.000	0.00000	70,000	72,000	39050	51.7242	0.0001	0.0001	0.00555	#####	111,000	43800	125.6516	0.0000	0.0000	0.00000
36,000	37,000	36,500	19.4754	0.000	0.000	0.00000	72,000	74,000	40150	58.1252	0.0001	0.0001	0.00642	111,000	#####	45000	########	0.0000	0.0000	0.00000
37,000	38,000	37,500	21.8166	0.000	0.000	0.00000	74,000	76,000	41250	65.1128	0.0000	0.0001	0.00403	#####	#####	46200	########	0.0000	0.0000	0.00000
38,000	39,000	38,500	24.3664	0.000	0.000	0.00000	76,000	78,000	42350	72.7227	0.0000	0.0000	0.00226	#####	#####	47400	########	0.0000	0.0000	0.00000
39,000	40,000	39,500	27.1371	0.000	0.000	0.00000	78,000	80,000	43450	80.9321	0.0001	0.0001	0.01155	#####	#####	48600	########	0.0000	0.0000	0.00000
40,000	41,000	40,500	30.1416	0.000	0.000	0.00000	80,000	82,000	44550	89.9593	0.0000	0.0000	0.00294	#####	#####	49800	########	0.0000	0.0000	0.00000
		Single Axle ESAL contribution =				**0.088**			**Tandem Axle ESAL contribution =**				**1.903**			**Tridem Axle ESAL contribution =**				**0.003**
											VT9 Truck Factor =		**1.994**							
											VT9 ESALC =		**727.7**							

Figure 3-29. Example of worksheet used to calculate ESALC.

Table 3-20. ESAL Constants derived from the WIM sites.

Station	Direction	Vehicle Class			
		4	5	6	9
C202B	North	178	51	218	978
10W	North	808	58	406	867
	South	439	31	401	501
438	North West	1,904	50	687	728
	South East	705	49	560	610
C7L	East	1,497	103	710	1,213
	West	1,181	83	842	1,418
C4K	East	1,463	184	920	1,280
	West	951	91	728	1,127
C10K	North	772	40	288	557
	South	647	88	854	899
H41W	North East	359	46	334	454
	South West	340	30	480	1233
S9	North	455	18	391	656
	South	508	25	931	793
S8R	North	446	32	735	648
	South	359	29	435	1,324
Interpolated 10W, S9, & C10K North		591	34	488	674

The values at station C4K for vehicle class 9 are about twice those at station 438 for the same vehicle class. In this case, the difference appears to be mostly related to the long right tails of the distributions observed on some of the freeway stations such as C4K. Notice that some of the values for the stations C4K, C7L, and H41W located on Oahu freeways are even higher than those at station C202B, for which the proportion of loaded trucks is higher than at any other station. This illustrates that, barring errors in the data used to develop the distributions, changes in weight limit enforcement or special overweight heavy loading permitting could have important benefits in extending the life of pavements. As discussed in section 3.4.3.2.2, out of these three stations only the data for station C7L had suspiciously long right tails for several vehicle classes. However, that did not appear to be the case for the other two stations and therefore it is believed the above observations are valid.

It can also be observed that for most locations, the ESALC derived for buses are much higher than 65, which is the ESALC used in the last HDOT pavement design manual (HDOT, 2002) for class 5 vehicles (the class that was typically used to account for bus effects). On the other hand, the derived values for class 5 vehicles are generally lower than 65. The net change thus depends on the proportions of vehicles on every particular project under consideration but in general it is expected to result in higher values of ESALs.

3.6 RECOMMENDATIONS FOR USING LOCAL WIM INFORMATION

An important aspect in the analysis of WIM data is to form truck weight road groups based on a combination of known geographic, industrial, agricultural, and commercial patterns along with knowledge of trucking patterns that occur on specific roads [15] so that designers can select the appropriate group for each particular situation. The Traffic Monitoring Guide [15] specifies criteria to test the quality of selected truck weight groups and determine the precision of estimates from those groups. Obviously, the quality and precision estimates are based on statistical analysis. Typically, at least six stations are needed per group. Thus, with only 9 WIM sites with usable data across the State, it is not possible to perform a rigorous statistical evaluation of groupings since it is clear that at least two or three groups are needed to represent loading conditions within the State.

As was shown in Figure 3-2, the WIM stations in the State are located on either freeways, principal arterials, or port/industrial roads. Thus, it is difficult to know solely from WIM data what the loading is on other roads, particularly those on the Windward side of the island of Oahu and Hawaii. Furthermore, since station C12E in Maui did not provide reliable data and there is no WIM station in Kauai, axle load spectra for those islands are not yet well defined. Yet, pavements still need to be designed in those locations. Therefore, based on the observations provided in the previous section, the following recommendations for using the information from the local WIM data are proposed.

First, recommendations are provided for use of the WIM data with the MEPDG and then with the HDOT design procedure.

3.6.1 Use of the WIM data with the MEPDG

Obviously, for locations around the WIM sites, the corresponding distributions for those sites should be used unless a dramatic change in loading conditions at some nearby intersection or interchange is possible. Table 3-21 shows the suggested assignment of stations to routes. For simplicity, except for station C4K, only the direction with heavier traffic is suggested for design.

For all other pavement segments, the data from stations C202B, 10W, S9, S8R, H41W, 438, and the North direction of station C10K were averaged. The reason for choosing these stations is that they do not include the unreliable data of station C7L and the south direction of station C10K (unreliable in the sense that they had long right tails that could not be justified from the quality control checks and thus they were not considered representative of normal conditions.) Station C4K was not included in the average as it does not appear that such high loads are observed in other locations.

It is believed that the distributions selected to compute the average are more representative of the likely loading conditions to be found on most roads throughout the State. Although the data from stations C12E and 023 were questionable, they nevertheless provided some indication that the loading at those sites are less severe than the average from the other stations.

As an exception to the assignment in Table 3-21, it is recommended that for those roadway sections with known heavily unbalanced loading (such access roads to quarries), the loading corresponding to the heavy direction at station S8R (the north direction) be used. This would provide heavy vehicle class 9 loading and moderate bus loading.

In order to simplify the use of these guidelines, Table 3-21 provides the name of the file containing axle load spectra information corresponding to each case. Thus, to follow these recommendations when using the MEPDG, the designer would only need to decide which file to use based on Table 3-21 and then import the corresponding file into the Pavement ME Design software, which is a relatively simple process. Note that the average number of axles per truck should be selected consistently from the appropriate table in Section 3.4.3.2.3 (page 74) (i.e., corresponding to the site selected for the ALS input.) Table 3-22 provides the number of axles per vehicle corresponding to the interpolated ALS.

Table 3-21. Suggested assignment of WIM station data to routes.

Station	Routes	ALS file name
C202B North	64 11 MP 0.00-10.00 19 MP 0.00-10.00	C202B_North_ALS_MEPDG.alf
10W North	95	10W_North_ALS_MEPDG.alf
438 North-West	92, 7412, 7413 MP 0.00-0.35	438_North-West_ALS_MEPDG.alf
C4K East	H-1 East MP 8.00-22.00, H-201 East, 7310	C4K_East_ALS_MEPDG.alf
C4K West	H-1 West MP. 8.00-22.00, H-201 West	C4K_West_ALS_MEPDG.alf
C10K North	H-1 MP 0.00-8.00 H-1 MP 22.00-27.16	C10K_North_MEPDG.alf
H41W South-West	H-3, H-2	H41W_South-West_ALS_MEPDG.alf
S9 South	11 10.00-121.98	S9_South_ALS_MEPDG.alf
S8R North	19 MP.66.5-99.52	S8R_North_ALS_MEPDG.alf
Interpolated	All other roads	Interpolated_All_ALS_MEPDG.alf

Table 3-22. Values for the average number of single, tandem, and tridem axles per truck class corresponding to the interpolated ALS.

Truck Classification	Number of Single Axles per Truck	Number of Tandem Axles per Truck	Number of Tridem Axles per Truck	Number of Quad Axles per Truck
4	1.85	0.27	0.00	0.00
5	2.00	0.00	0.00	0.00
6	1.00	1.00	0.00	0.00
7	1.01	0.06	0.71	0.22
8	2.30	0.70	0.00	0.00
9	1.22	1.89	0.00	0.00
10	1.03	1.04	0.96	0.00
11	3.05	0.27	0.44	0.00
12	1.62	0.92	0.68	0.07
13	1.79	0.60	0.98	0.19

Figure 3-30 shows the interpolated ALS for tandem axles on vehicle class 9 and Figure 3-31 illustrates the interpolated ALS for tridem axles on vehicle class 10. Notice that given the relative low frequency of occurrence of this axle/vehicle class combination, the ALS are not defined too well for the individual WIM stations but for the interpolated ALS a clearly defined patterns start to emerge. Finally, the samples for vehicle classes 7, 11, 12, and 13 were often too small to obtain a reliable ALS for every month. Therefore their monthly distributions were further averaged to obtain a single distribution to be used for every month of the year. Given the Hawaiian climatic conditions, this should have no significant effect on pavement design but it has the advantage of elucidating how the distributions actually look like. Figure 3-32 shows the interpolated ALS for tandem axles of vehicle class 11.

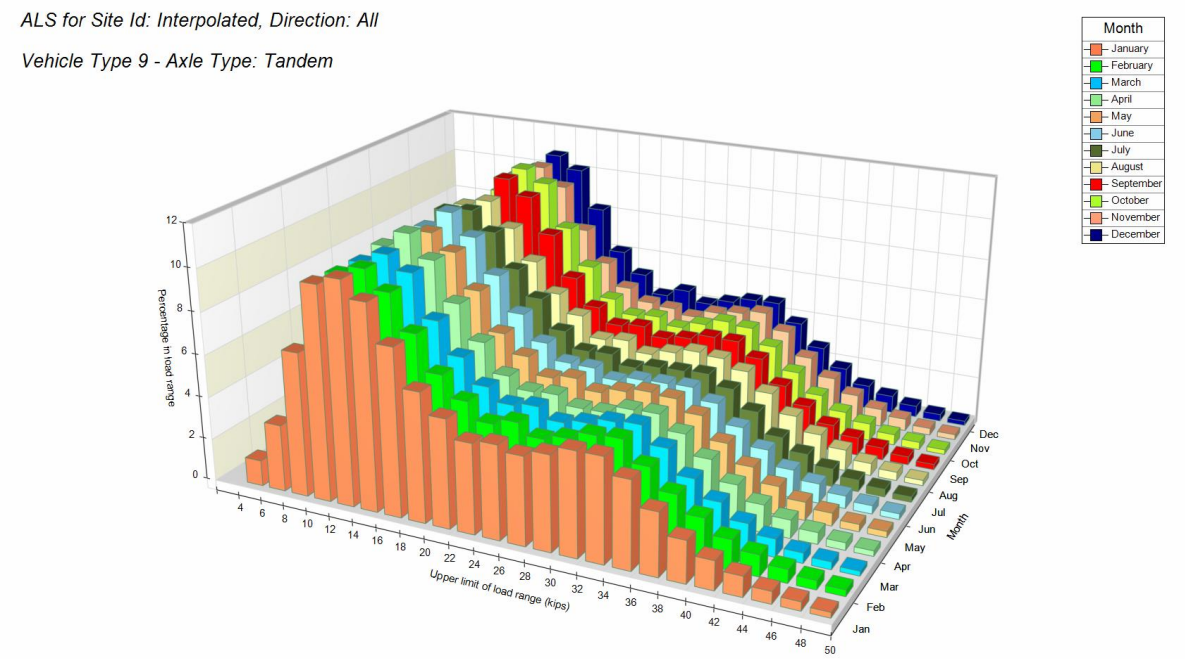

Figure 3-30. Interpolated ALS for tandem axles on vehicle class 9.

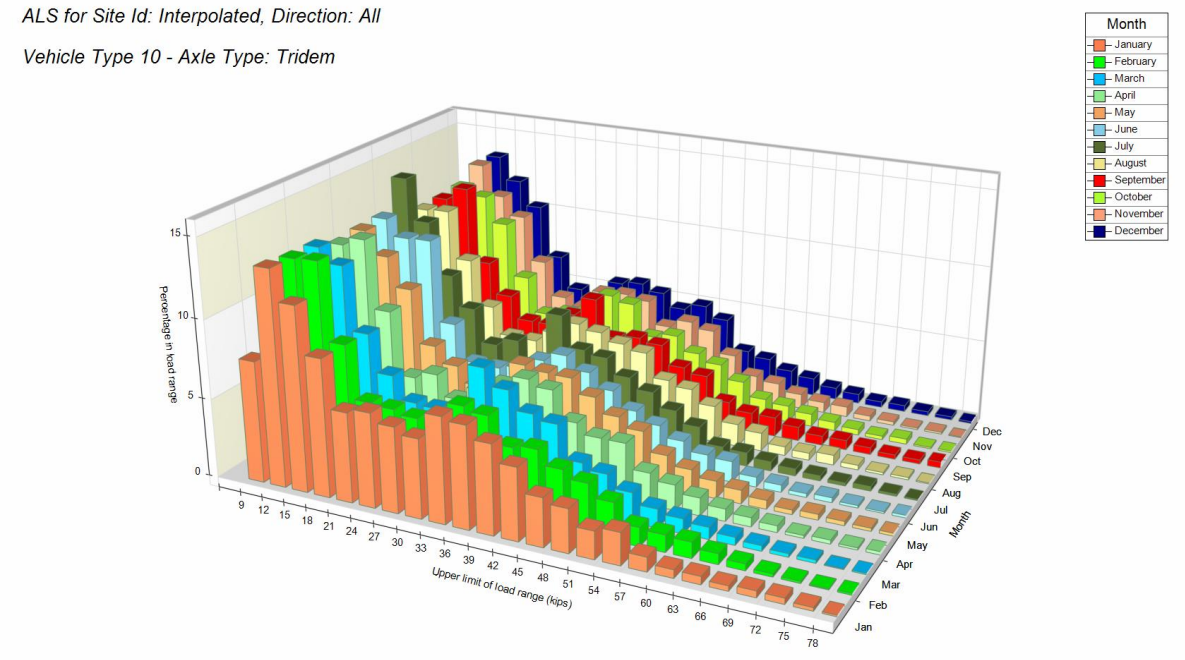

Figure 3-31. Interpolated distribution for tridem axles on vehicle class 10.

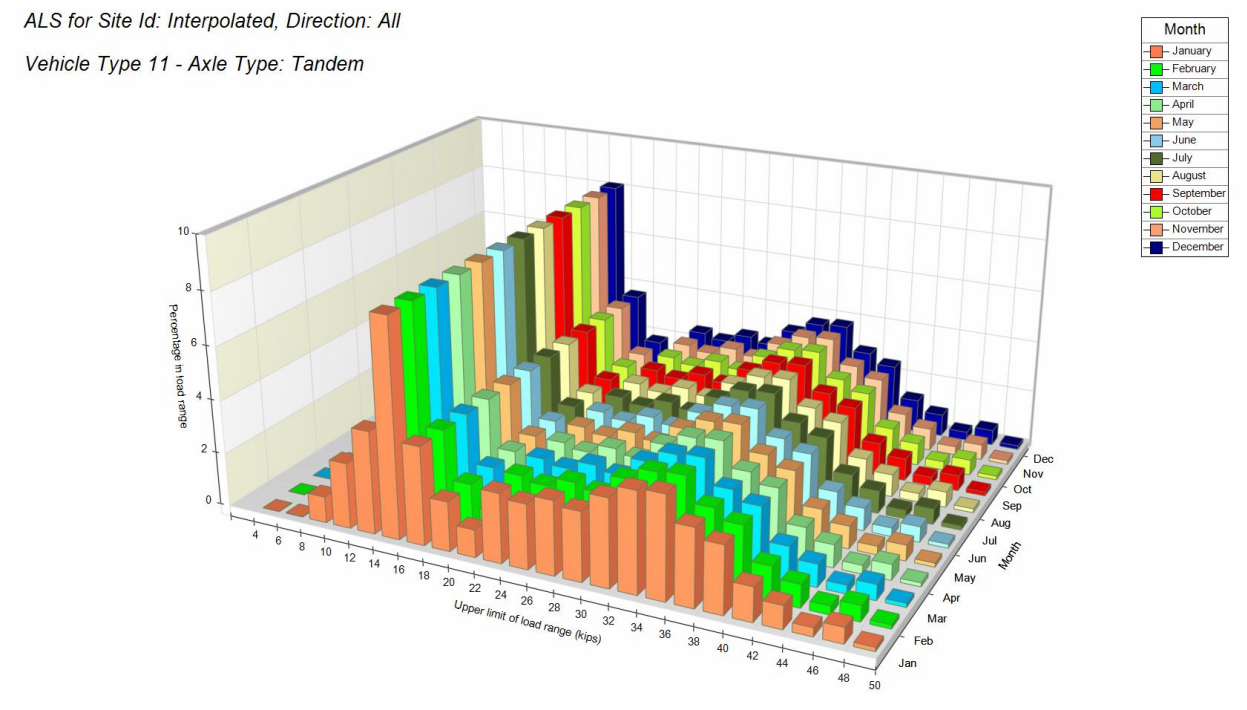

Figure 3-32. Interpolated distribution on tandem axles of vehicle class 11.

It is interesting to note that only about 2.4% of traffic on non-freeway (primary) roads is heavy or commercial vehicles, and Classes 4 and 5 comprise 87% of the heavy vehicles. About 3.3% of traffic on freeways is heavy or commercial vehicles, and Classes 4, 5, 6 and 9 comprise 94% of the heavy vehicles. These statistics support the emphasis put on these vehicle classes and the simplifications performed for vehicle classes 7, 11, 12, and 13, though as discussed earlier, it is not just the frequency of loading but also the magnitude that affects pavement design. Nevertheless, from the derived distributions, most of the damage on most state roads is most likely caused by vehicle class 4, 5, 6, and 9.

3.6.2 Use of the WIM information with the HDOT design procedure

In principle, the same ideas described for the use of the WIM data with the MEPDG are applicable to designs with the HDOT design procedure. That is, one could use the ESALC most appropriate for each site as presented in Table 3-23. However, the HDOT design procedure is rather conservative and relatively insensitive to traffic loading since the latter is converted into a traffic index (TI) using the following equation:

$$TI = 9\left(\frac{ESAL}{1,000,000}\right)^{0.119} \quad (3\text{-}1)$$

Given the very low exponent on equation (3-1), a doubling of traffic results in an increase of *TI* of only 8.6%. Even if traffic is tripled, the *TI* is increased by only 14%. In the HDOT design procedure, the final thicknesses of the different layers would be directly proportional to the value of the *TI* were it not for the rounding that is generally performed during layer thicknesses selection, the application of a safety factor, and the use of a factor known as the "gravel factor" to determine the layer thicknesses (which is not constant for asphalt concrete). The reason is that the *TI* enters in a multiplicative form in the equation to compute a gravel equivalent (*GE*) needed to protect each layer. The *GE*s are in turn used to compute the layer thicknesses. The point of the discussion is that layer thicknesses would increase approximately proportional to the *TI*, though not exactly. Thus, a 10% increase in *TI* would represent an approximate 10% increase of layer thickness. As mentioned before, some of the rounding of layer thicknesses, the application of a safety factor that increases the thickness of asphalt concrete, or even the requirement of determining the *TI* to the nearest 0.5, can have a similar or in many cases a larger effect than the inaccuracies in the *ESAL* computations.

In order to evaluate the potential impact of consolidating the sets of *ESALC* in Table 3-23 into two or three groups, the number *ESAL*s were computed with the average *ESALC* values corresponding to different trial groupings. For this, several different traffic streams with varying vehicle class distributions were used. The vehicle class distributions were selected from those used during the calibration efforts of the MEPDG (explained in chapter 7). The ratios of the number of *ESAL*s for different load groupings were then evaluated to estimate the potential effect

on thickness design (remember that a factor of 2 translate in about 8% change in total pavement thickness in terms of gravel equivalent.)

Based on the above analysis, three different groups were created as presented in Table 3-24. The first group is recommended for the design of freeways. The second group is recommended for the design of roads with moderately heavy truck loading and heavy bus loading such as routes 92 (Ala Moana Blvd./Nimitz Hwy), 95, parts of 99, and 19 in the Kona area on the Big Island. The third group is recommended for all other roads. These groupings permit some differentiation based on some known characteristics of the roads. It must be noted that the ratio of *ESAL*s computed with the *ESALC* from group 1 to that computed with the *ESALC* from group 3 varied from about 1.40 to 2.35. Therefore, the differences in thicknesses between designs with these two groups are expected to be at most 10%. The *ESALC* from group 2 would in general result in an intermediate design. Notice that the actual variations in the resulting thicknesses depends on the heavy traffic loading composition.

Table 3-23. ESALC corresponding to the traffic loadings in Table 3-21.

Station	Vehicle Class									
	4	**5**	**6**	**7**	**8**	**9**	**10**	**11**	**12**	**13**
C202B North	178	51	218	824	241	976	863	1,375	245	793
10W North	808	58	406	964	728	867	1,452	556	2,068	4,235
438 North-West	1,904	50	687	1,391	170	728	2,145	145	2,587	4,429
C4K East	1,461	184	920	1,717	1,490	1,280	1,142	1,054	3,110	2,333
C4K West	951	91	728	1,255	308	1,127	1,290	810	2,657	1,597
C10K North	772	40	288	829	318	557	754	738	1,081	2120
H41W South-West	340	30	480	1,136	154	1,233	870	1,596	1,571	1,021
S9 South	508	25	931	1,119	781	793	1,267	61	1,362	3,849
S8R South	359	29	435	1,223	677	1,324	2,141	2,179	2,415	9,359

Table 3-24. Updated ESALC values for Hawaii.

ESALC Groups	Vehicle Class									
	4	**5**	**6**	**7**	**8**	**9**	**10**	**11**	**12**	**13**
1: Freeways	1,206	138	824	1,486	899	1,204	1,216	932	2,884	1,965
2: Intermediate loading (92, 95, 19, 99 MP 16.00-23.83)	1,024	46	509	1,193	525	973	1,913	960	2,357	6007
3: All other roads	343	38	575	972	511	885	1,065	718	804	2,321

3.7 PECENT TRUCKS IN THE DESIGN LANE

This section presents the analysis of the percent trucks in the design lane, which is also commonly known as the lane distribution factor. This factor accounts for the distribution of truck traffic between lanes in one direction [1]. It is usually computed as the percentage of trucks in the design lane relative to all truck traffic in the design direction.

In the MEPDG, a slightly different definition is used [22]; it is defined by the primary truck class for the roadway, where the primary truck class is defined in [22] as "the truck class with the majority of applications using the roadway." The MEPDG Manual of Practice [22] further states "In other words, the percentage of trucks in the design lane is estimated for each truck class, and the predominant truck class is used to estimate this value."

Unfortunately, the above statements in quotes contain some vague language. It is probably safe to assume that by "applications" the MEPDG Manual of Practice means "number of trucks"; but depending on lane usage by different vehicle classes, it may be more problematic to know what is meant by "predominat truck class". Interpreting it as the truck class with the highest volume could result in an underestimation of traffic loading effects. The reason is that for Hawaiian conditions the "predominant truck" would most often be a class 5 truck which has relatively minor damaging power compared to the other truck classes. Thus, for example, for a section with 30% class 5 trucks, 20% buses (class 4) and 20% of class 9 trucks the latter two are likely to have much more damaging power than that of class 5 trucks.

For Hawaii, it is recommended to estimate what truck class has the most damaging power and use it as the predominant truck class. A simple way proposed here to estimate which vehicle class has the most damaging power is to simply multiply the percentage of vehicles in each class by the corresponding ESALC appropriate for the section and selecting the class with the largest product. In cases where the numbers for the two top classes are close (say, withing 20% of each other), an average of the lane distribution factors for those two classes could be used instead of simply selecting the one for the largest.

The lane distribition factor (LDF) (or *design lane factor* in HDOT's procedure) has not received much attention in the recent past for pavement design in Hawaii probably because its value is specified in the design procedure. However, use of unrealistic LDF's or Design Lane Factors could have almost as much of an adverse effect (over or under design of a pavement) as any other traffic loading input. As discussed in the previous sections, the use of the different sets of ESALC could affect the calculations of ESALs by a factor of about 2. An effect of almost the same order of magnitude would be produced by using a factor of 0.8 if a factor of 0.5 were more representative of actual conditions (a 60% overestimation of the loading in this example.)

A motivation for studying this factor in some detail is that while collecting cracking information from HDOT's video logs over several years for calibration of the MEPDG, it was noted that on multilane highways, cracking often started earlier and/or was present on a larger extent on the inside rather than the outside lanes even though these were constructed at the same time. No apparent reason other than perhaps different loading on each lane could be found. In addition, the LDF specified in the current HDOT pavement design procedure [13] (LDF = 1.00 or 100% for 1 and 2 lanes, 0.80 or 80% for 3 lanes, and 0.75 or 75% for 4 lanes in one direction) were in some cases quite different from those suggested in the MEPDG [1] (LDF=1.00 for 1 lane, LDF = 0.90 for 2 lanes, LDF = 0.60 for 3 lanes, and LDF = 0.45 for 4 lanes.) Notice that for the four lanes case, traffic estimated with HDOT's recommendation would be 1.67 times the one obtained following the MEPDG recommendations. Neither document provided guidance about cases with more than four lanes.

Actually, the MEPDG Manual of Practice [22] states that the percent trucks in the design lane may be estimated from AVC (automated vehicle classification) data or manual vehicle count data. The same recommendation is provided here since AVC data can be obtained for

design from HDOT's Planning Branch. Although it would be desirable that for every pavement design on existing facilities the LDF were based on traffic information at the site, it is recognized that this may not always be the case. Furthermore, for widening cases, some guidance is still needed.

In order to gain some understanding of the lane usage by heavy vehicles in the State, the information from the WIM stations on multilane highways was analyzed. For this purpose, the PI's program discussed in previous sections was enhanced to compute the percentages by lane for each vehicle class at the different stations. Figure 3-33 shows the layout of the sensors at two of the WIM sites. As can be observed, one of the sections in Oahu have a large number of lanes in each direction. Notice that lane 1 at all WIM sites is the leftmost lane, which differs from the numbering used in the TMG [15].

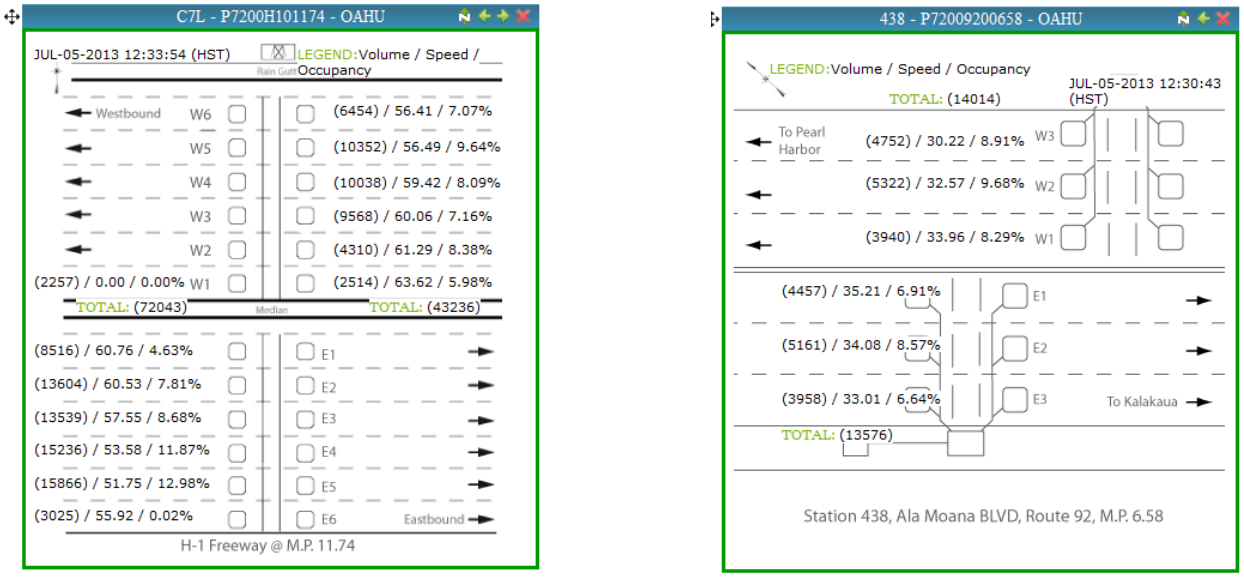

Figure 3-33. Layout of sensors at two of the WIM Stations in Oahu.

Table 3-25 shows the lane distribution by vehicle class on each direction at the WIM stations on multi-lane highways. The first three stations in the table have two lanes in each direction, the following three have three lanes and the last one, station C7L, has six lanes in each direction. In this table, the values provided for vehicle classes 7, 11, 12, and 13 should be look at with caution since they are generally based on a much smaller number of observations than for the other vehicle classes.

For the cases with two lanes in one direction, it can be observed that the percentage by lane can be quite variable from station to station, but at least for this limited number of sites, it never goes much higher than 80% for the vehicle classes most likely to represent the primary trucks in Hawaii (4, 5, 6, 8, 9, or 10). It is important to note that when traveling north at station 10W, the station is located just after an important intersection on which some heavy traffic may be diverted and just before an interchange. Therefore, the higher LDF value at this site, as compared to the values at the other sites, appears to be more related to the trip destination than to lane selection. This, however, is always a possibility that should be accounted for.

It is also interesting to note that lane 1 (the inside lane) at these stations often carries a higher percentage of trucks than the outside lane, which is contrary what is often expected.

On the facilities with three lanes in one direction, it can be observed that the LDF is highly variable and that the lane with the largest percentage varies by location. The LFD varies from 42.5 to 76%. It is interesting to note that three locations have different characteristics. Station C10K is located just before or after a ramp entry/exit from an interchange. Thus, some effect from the interchange may be expected (although at this location, existing pavement condition may have also been a factor). Station C4K is further away from ramp entries and exits. Station 438 is on an arterial with piers to the right of the Southeast bound traffic and with other important truck destinations on the left for the Northbound traffic, which in part may explain why the LDF is the highest for outside lane for traffic traveling in the Southeast direction and the highest in the inside lane for traffic traveling in the opposite direction. The above discussion highlights the need to use actual traffic observations whenever possible.

Finally the values for station C7L suggest that heavy traffic tends to be concentrated on the center lanes when several lanes are available. For six lanes, the maximum percentage observed is 33%.

Given all the above observations, it is suggested to use the values in Table 3-26 (page 109) for design when field data collection is not possible or when AVC data are not available. These LDF or Design Lane Factor values represent a compromise between the highly conservative values in the current HDOT design procedure [13] and the values in the MEPDG.

Table 3-25. Lane distributions at WIM stations on multilane highway.

Station	Direction	Lane	Vehicle Class									
			4	**5**	**6**	**7**	**8**	**9**	**10**	**11**	**12**	**13**
10W	North	1	45.8	74.7	79.8	80.9	76.6	80.7	57.1	90.0	95.6	87.0
		2	54.2	25.3	20.2	19.1	23.4	19.3	42.9	10.0	4.4	13.0
	South	1	76.7	68.1	52.1	42.7	62.1	53.7	60.0	43.2	55.0	56.9
		2	23.3	31.9	47.9	57.3	37.9	46.3	40.0	56.8	45.0	43.1
H41W	North-East	1	56.1	60.0	56.5	70.1	52.8	55.0	55.5	67.3	55.8	66.0
		2	43.9	40.0	43.5	29.9	47.2	44.0	44.5	32.7	44.2	34.0
	South-West	1	51.2	52.7	56.1	54.2	46.2	49.2	51.5	53.8	33.7	34.9
		2	48.8	47.3	43.9	45.8	53.8	50.8	48.5	46.2	66.3	65.1
C202B	North	1	58.7	48.4	68.9	60.6	64.3	74.9	75.8	92.6	76.4	76.4
		2	40.9	51.2	30.7	36.2	34.7	20.2	18.5	7.4	23.6	22.1
C4K	East	1	33.4	31.2	25.1	24.5	41.6	42.5	24.1	36.6	45.2	36.2
		2	43.5	42.3	46.6	56.2	45.7	40.7	53.1	53.5	35.5	53.5
		3	23.1	26.5	28.3	19.3	12.7	16.8	22.8	9.9	19.3	10.3
	West	1	55.3	39.9	51.1	39.1	49.3	49.7	46.0	36.8	42.5	21.7
		2	30.3	37.7	36.2	46.1	35.4	38.9	45.5	33.7	50.4	69.4
		3	14.4	22.4	12.7	14.8	15.3	11.4	8.5	29.5	7.1	8.9
438	South-East	1	26.8	24.3	17.8	33.0	31.8	11.4	4.3	8.3	0.8	1.8
		2	39.8	36.2	37.4	30.1	33.4	12.6	9.2	41.7	1.9	27.5
		3	33.4	39.5	44.8	36.9	34.8	76.0	86.5	50.0	97.3	70.7
	North-West	1	16.1	47.8	59.3	58.9	34.4	55.7	60.6	57.7	40.0	75.1
		2	12.7	31.8	28.3	37.9	43.7	30.8	31.8	38.5	46.0	20.8
		3	71.2	20.4	12.4	3.2	21.9	13.5	7.6	3.8	14.0	4.1
C10K	North	1	37.0	36.8	29.7	40.2	18.6	26.8	28.1	21.5	6.4	32.9
		2	53.0	55.6	64.6	55.7	69.7	68.9	68.3	56.3	91.2	61.7
		3	10.0	7.6	5.7	4.1	11.7	4.3	3.6	22.2	2.4	5.4
	South	1	23.4	26.3	18.4	21.9	12.0	20.0	16.8	6.7	18.8	23.6
		2	38.4	39.6	48.8	53.4	37.4	48.3	58.6	25.9	53.3	54.0
		3	38.2	34.1	32.8	24.7	50.6	31.7	24.6	67.4	27.9	22.4
C7L	East	1	14.6	6.0	1.8	2.2	2.8	2.1	0.9	0.2	0.2	0.6
		2	16.4	17.2	13.9	15.8	9.0	14.7	12.7	5.3	4.9	13.1
		3	18.5	21.7	30.6	26.2	21.4	33.2	35.8	14.7	58.4	41.6
		4	16.3	25.6	33.1	28.0	32.6	33.4	34.3	25.3	30.2	35.7
		5	20.5	27.7	20.4	27.8	33.3	16.6	16.3	54.5	6.3	9.0
		6	13.7	1.8	0.2	0.0	1.0	0.00	0.00	0.00	0.00	0.00
	West	1	13.1	8.8	7.5	5.9	3.1	6.7	5.1	9.7	2.5	2.2
		2	12.7	15.5	24.1	24.7	13.9	24.9	29.2	31.0	26.7	21.7
		3	23.8	22.6	28.7	27.7	30.6	31.4	37.2	25.0	36.2	41.4
		4	16.2	20.3	19.7	20.5	22.4	18.2	16.7	15.3	18.4	24.6
		5	17.0	20.1	13.0	14.1	19.3	13.9	9.0	12.6	13.5	8.2
		6	17.2	12.7	7.0	7.1	10.7	4.9	2.8	6.4	2.7	1.9

Table 3-26. Suggested Lane Distribution Factors.

Number of Lanes in One Direction	Lane Distribution Factor
1	100
2	90
3	75
4	60
5	50
6 or more	45

CHAPTER 4. PAVEMENT CONDITION

4.1 INTRODUCTION

As indicated by Haas, Hudson, & Zaniewski [3], four types of pavement outputs are periodically used by highway agencies for pavement evaluation. These include measures of structurally adequacy (e.g., structural number and deflection with a Falling Weight Deflectometer (FWD), Benkelman beam, etc.), rideability or serviceability (e.g., international roughness index (IRI)), surface distress (cracking, rutting, raveling…), and surface friction. These measures provide the means for assessing and updating if necessary design predictions, scheduling rehabilitation measures, improving design models, construction and maintenance practices, and updating network programs [3].

This chapter describes the pavement outputs currently collected by HDOT, the efforts to visualize, transform, and interpret them, and areas of potential improvement.

4.2 INTERNATIONAL ROUGHNESS INDEX – IRI

Pavement roughness contributes significantly to the perceived serviceability of road users. The most widely used measure of pavement roughness is the International Roughness Index (IRI) developed by Sayers, Gillespie, & Queiroz [23] in a study conducted for the World Bank. In order to measure it, road profilers equipped with laser sensors and accelerometers are used to measure the vertical profile of the road. Then, the IRI is estimated using a mathematical algorithm that simulates the up and down movement per unit distance traveled by a quarter of car with certain characteristics while travelling the road at 80 km/h.

A main advantage of IRI is that its value has the same scale[9] and meaning anywhere in the world. This is because the quarter car characteristics (tire spring constant, suspension spring constant, suspension damper/dashpot constant, mass of the suspension and mass of the car) and

[9] Of course, different units are used in different parts of the world. In the US, IRI is expressed in inches/mi whereas in countries using the SI system of units it is expressed in m/km or mm/m (1 mm/m = 1 m/km = 63.35 in/mi).

the vehicle speed (80 km/h) are all specified. Thus, no matter how a profile is obtained, as long as it provides an accurate representation of the road, then IRI can be computed accurately too.

IRI has now been collected by HDOT for several years. For this project, data for 2003, 2004, 2005, 2007, 2009, and 2010 were used. The 2003, 2004, and 2005 data were collected with an ARAN van by HDOT personnel. The rest of the data were collected by Mandli, Inc. for HDOT's Planning Branch. There were also some data available for 2001 collected by Roadware and for 2003 by Mandli but due to some difficulties, these data were not analyzed. All the data are reported every 0.01 mi (52.8 ft.). Therefore, the amount of information is voluminous, particularly for those years on which every lane of multi-lane highways were surveyed.

Early on, it was realized that visualization of such vast amount of information was desirable. HDOT's has the capability in its Road Information System (RIS) web portal of displaying the IRI information in color coded maps (Figure 4-1), which is very useful.

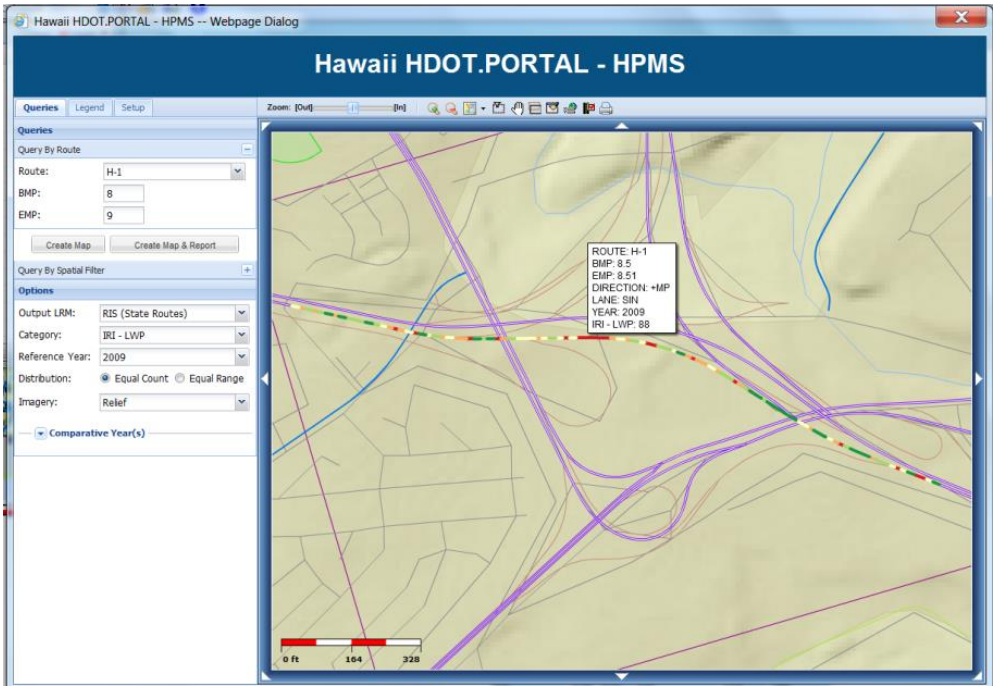

Figure 4-1. Display of IRI in maps in HDOT's web portal.

Other software such as ProVAL (Profile Viewing and Analysis Software) [24] is an excellent and free software tool for visualization and analysis of road profiles but it is geared more towards project level analysis than network level analysis. In addition, the available data

sets contained only IRI values instead of road profiles, which is reasonable at the network level considering the substantially larger storage capacity needed for storing profiles.

A tool was created to store and visualize the roughness information in charts. The tool is intended to complement the mapping in the web portal. The purpose was to be able to observe the IRI trends for a road for several years all at once and to be able to see the trends for each road and easily zoom in to (or zoom out from) sections of interest. Although such types of analyses can be done with a spreadsheet program, zooming in or our can quickly become tedious and time consuming. As the analysis progressed, several capabilities were added including zooming and scrolling in charts, correction of data series (shifting and or compression/expansion of series), segmentation of roads into statistically homogeneous sections, user editing of the automatically generated segment change-points, and reporting of the segmented information into comma delimited files. In addition, the tool allows the visual comparison of series by lanes for a given year or by year for a given lane and provides visual cues for data obtained at low speeds or with IRI above user specified thresholds, which are excluded from the reported averages. The following section provides more details of the program and, more importantly, about some of the issues identified with the data.

4.2.1 IRI Data Processing Tool

At present, the tool developed for processing the IRI data has a very basic menu. Essentially, it has three options for data analysis and three for database utilities as shown in Figure 4-2.

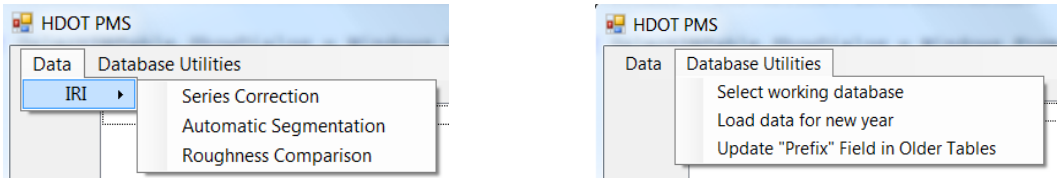

Figure 4-2. IRI Processing Tool Menu.

Selecting the "Series Correction" option under "Data➔IRI**"** takes the user to the screen shown on Figure 4-3. Notice that the screen has been configured specifically for Hawaii.[10] As shown in the figure, a list box is already populated with the routes with available information for the selected island and source of data. Note that the first route is selected by default and for this route the list box labeled "Lanes" lists all the lanes for which information is available for that route and in the direction selected.

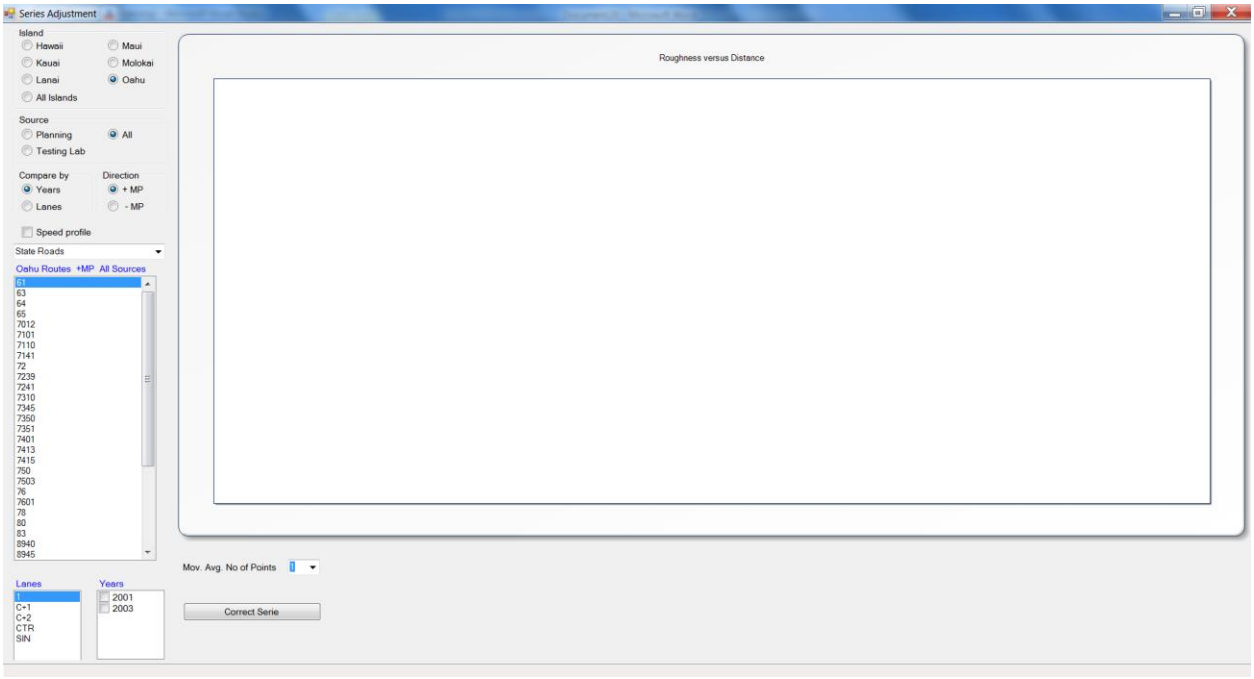

Figure 4-3. IRI data Processing Tool – Series Adjustment Screen.

The details of the interface above already help to illustrate some of the challenges found when automatically processing information from different sources without following a particular standard. First, notice that the direction is labeled as either "+MP" or "-MP". This was adopted from the convention used in the data collected for the Planning Branch. However, even for that data source, the direction field for one of the years had a "+" or a "-" instead. For the data collected by the Materials and Testing Research Branch (MT&R), the lanes were designated left

[10] In retrospect, using radio buttons and check boxes on this interface is not the best option. If the program is improved in the future, other controls that allow a more easy customization should be considered.

and right instead. Thus, some processing of the data was needed before performing the import operation into the database.

A more difficult problem to address is the convention used for lane designation. The testing branch uses CTR for the center lane, C+1 for the lane adjacent to the right of the center lane, C+2 for the next lane to the right, and so on. It also uses SIN (shoulder in) for the rightmost lane before the shoulder and a few other designations that address other particular situations that are not described here. Unless there is some problem with the collected data, the series for the CTR lane is continuous and of the same length as the route. For roads with at least some portion with two lanes in one direction, there will be data for a lane designated as SIN. In contrast, the data collected by the MT&R branch used the convention of designating the lanes as 1, 2, 3, etc., starting from the leftmost lane. Data for lane 1 were collected continuously. That is, the series for lane 1 has the same length as the route. Notice that conversion of the data is then not always as simple as changing the lane designation for a whole series since the data for the SIN lane in the Planning Branch designation could be stored in lane 2, lane 3, etc. in the MT&R branch database depending on the number of lanes on different portions of the highway. Since these conversions were needed to be done only once, they were performed manually with all the risk for introducing errors that this operation carries. Therefore, it is highly recommended that all branches use the same lane designation. Use of the RIS web portal should be make adoption of the planning branch designation relatively simple[11].

Now, returning to the processing and visualization of the data, as soon as the user selects a year among those available for the selected route/lane/direction combination, the corresponding series is plotted on the chart. The user can select to display more than one year if so desired. Figure 4-4 shows a typical situation. In this example, the series corresponding to the CTR lane of H-1 is shown for the slightly more than the 27-mi length of the route.

Although the noise in the series is very high (which is the most typical situation), long segments with high IRIs are easily identifiable. Note also that the changes in the background colors indicate sections with different number of lanes. The user can easily observe the number

[11] Of course, conversion of other older sources for data (not necessarily for roughness or distresses) could still be challenging.

of lanes on a given section by simply hovering the mouse over one of the background areas and waiting for a tooltip like the one shown in the figure to appear. Similar, tooltips containing the mile point and the IRI value for each point of the series are provided when the user hovers the mouse over them.

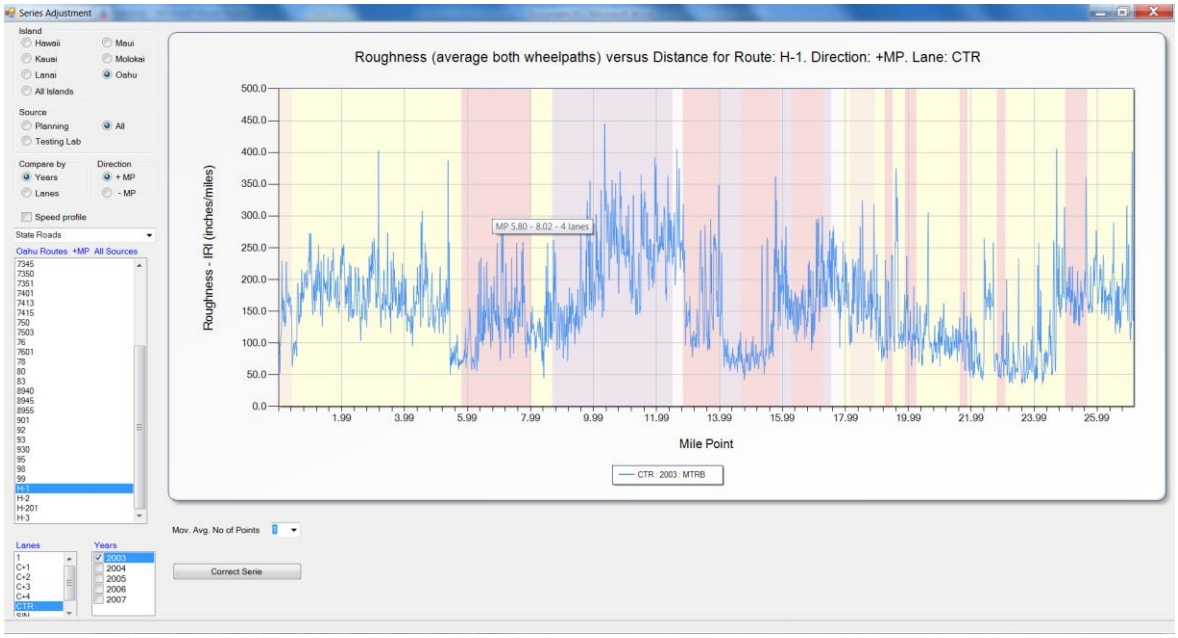

Figure 4-4. Visualization of a single series in the IRI Data Processing Tool.

4.2.1.1 Series Smoothing

When additional years are selected, the corresponding series are shown and the vertical scale is changed to accomodate the range of the new series, if needed. If the range increases significantly, details of interest may be more difficult to visualize, as illustrated in Figure 4-5. The series in this figure now overlap considerably and it is very difficult to visually assess if IRI is inceasing or not or by how much. As shown by a shaded area on the right side of Figure 4-5, the program has the capability for zooming in an area of interest. The result of the zooming operation is shown in Figure 4-6. A comparison of the series over this area is now easier. Nevertheless, depending on the noise in the data, their quality, and number of series in the chart such comparisons may still be challenging in some situations. Therefore, the capability to smooth the data by applying a moving average to each series was added. The moving average is applied by selecting the number of points to use in its calculation in the list box below the chart.

For example, for an 11 point moving average instead of diplaying the IRI value correspoding a given location, the series contains the average of that value, the five points before, and the five points after.

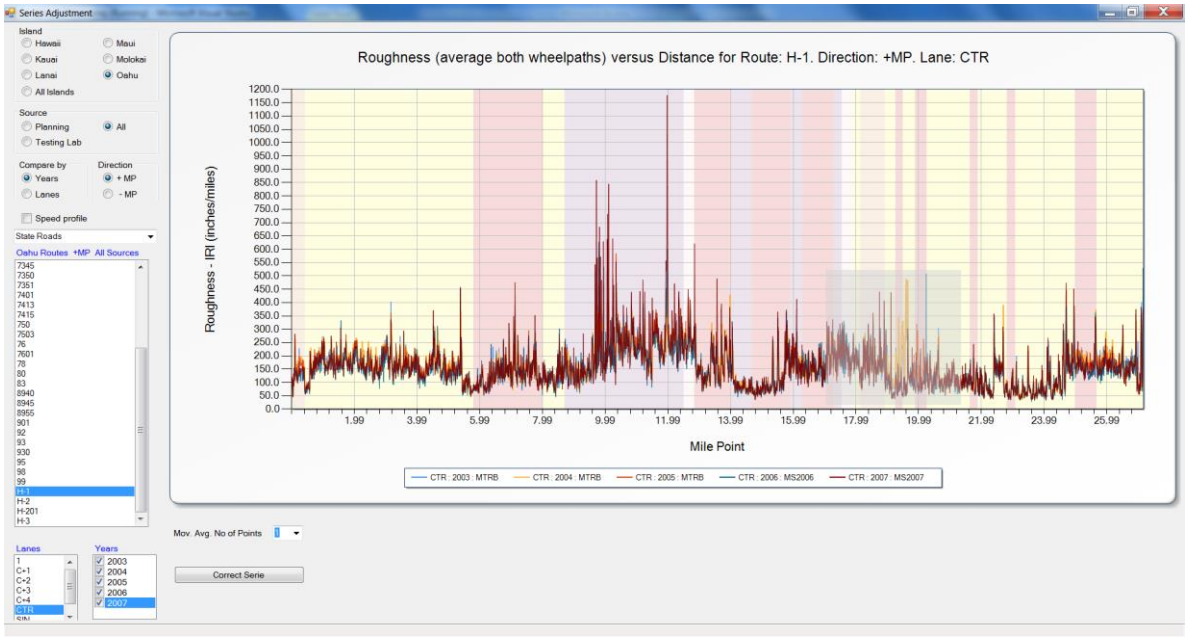

Figure 4-5. Visualization of two or more series in the IRI Data Processing Tool.

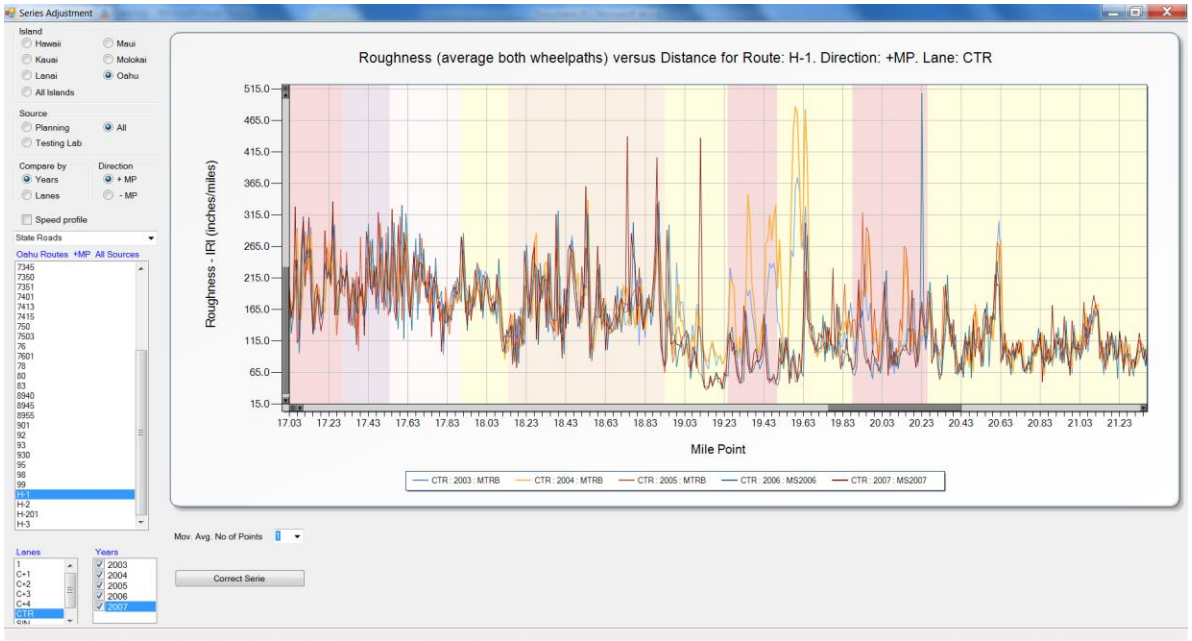

Figure 4-6. Visualization of several series in the IRI Processing Tool after zooming in.

Figure 4-7 shows how the smoothing with a moving average allows for a much more clear comparison between series. Now, for the example in the figure, the fast deterioration occurring approximately between mile points 19.2 and 19.7 in the years 2003 and 2004 is evident and it is also apparent that by 2005 the section had been rehabilitated. Rehabilitation after mile point 19.7 does not appear to have occurred until 2006.

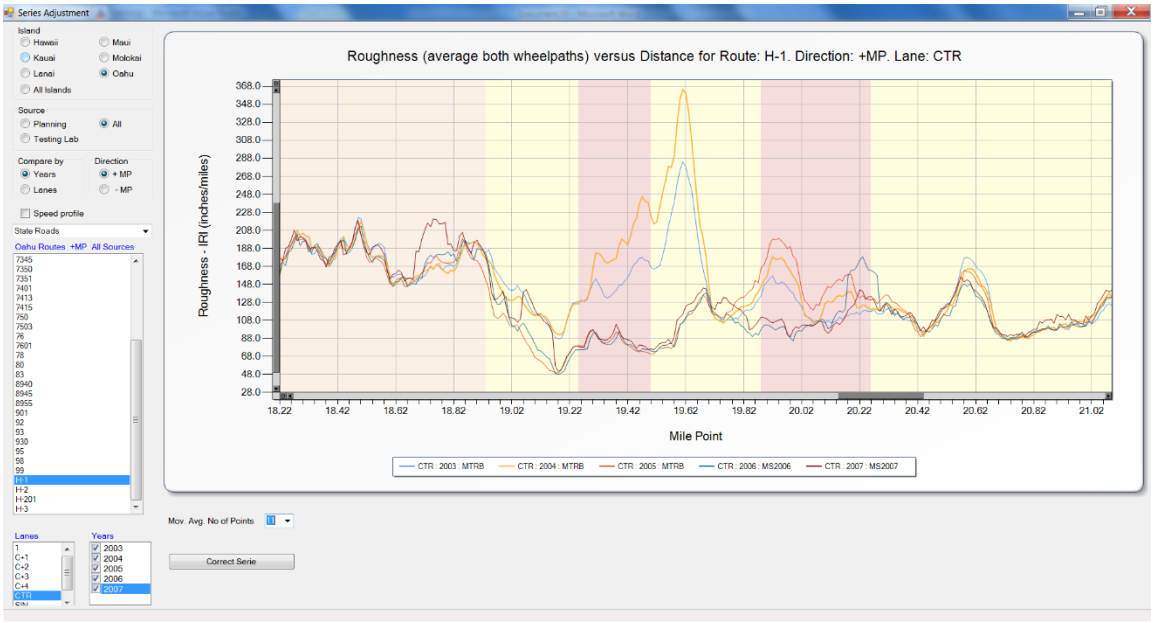

Figure 4-7. Use of moving averages to smooth out the series.

4.2.1.2 Series correction

Figure 4-8 also illustrates how consistent the series can be from year to year. This is actually quite remarkable considering that the measurements were performed with equipment from two different vendors and by different personnel. However, it is important to point out that although the consistency between series is real, the original data contained some shifting that needed to be corrected as shown in Figure 4-9. The shifting can occur in some cases simply because of the start of the data collection is shifted slightly longitudinally. In other cases, however, it was evident that the series, although exhibiting almost the same pattern than in other years, was either compressed or stretched. This was perhaps the result of inaccurate calibration of the distance measuring instrument. It is important to note that for roads of length in the order

of 100 mi such as routes 11 and 19 in the Big Island, the differences at the end of the road were as much as 0.5 mi.

The problem described above is a more difficult problem to deal with because a simple shifting cannot solve it. One possible correction is to shift parts of the series by different amounts on different locations. If the series is being stretched, this would result in holes being introduced to the series. On the other hand, if a series needs to be compressed, some information where the different sections overlap would need to be either discarded or averaged.

It is interesting to note that the series for 2006 in Figure 4-8 presented holes or small distances without IRI information as illustrated by the breaks in the corresponding line. This was observed for many routes on that year and was noted mainly because it created some programming challenges. It is not known what caused these breaks, but these breaks are consistent with a need for stretching the series. Another potential reason is that the data on those locations were collected at low speeds and therefore eliminated from the database.

In order to overcome the shifting, the capability of compressing or stretching a data series was implemented. Obviously, without the original road profile, a new IRI computation cannot be run. However, an approximation can be obtained under the assumption that the total up and down movement would be approximately the same before and after the correction but that this movement would occur over a longer or shorter distance resulting in slightly smaller or larger IRI values. The actual computations are as follows. For simplicity, and without loss of generality, the explanation is made assuming that the origin of the series is not moved; however the algorithm is implemented so that it works when both end points are moved.

The *cumulative area* under the curve of IRI is computed for each point of the original series. After this, the end point is moved to its estimated correct new location, thus stretching or compressing the original series. Therefore, the x-coordinates of each point of the new series would now be separated by less or more than 0.01 mi. Now, the corrected series is generated by assigning x-coordinates to its points that are separated exactly 0.01 mi. For each of these new points, a cumulative area under the curve is assigned by interpolating from the cumulative area under the curve of the original series after the stretching/compressing. Finally, the IRI for each point is obtained by reversing the cumulative operation. That is, for the first point, its IRI is the cumulative IRI divided by the 0.01 mi interval; for the second point, the IRI is computed by first

subtracting from its cumulative IRI the cumulative IRI of the first point and then diving the difference by 0.01 mi; and similarly for the third and the rest of the points.

As shown in Figure 4-8, to perform the series correction the user needs to select the series to be corrected (which is grayed out) and then enter the values of the before and after begin mile points (BMP) and end mile points (EMP). The tooltips of the series are useful to determine appropriate values. Figure 4-9 shows the result of applying the above algorithm to the series in Figure 4-8. Again, the patterns on the left part of the figure are remarkable similar. The algorithm can also be applied to only part of a series.

It must be noted that for about the last three miles, this facility has either concrete pavement (which at the time had a rough ride because of faulting) or a viaduct, which explains the lower consistency of the trends between years.

It is also important to note that simply moving the points of the original series horizontally and interpolating the new points from them typically results in a highly smoothed series. That is, the high and low values are significantly compressed as a result of the interpolation. Therefore, use of such approach is not recommended.

Although the method presented above still produces a slight smoothing, it is usually very minor and the series retains most of its original features. Also, when the series is stretched, the resulting IRI values are reduced slightly and when the series is compressed they are increased slightly.

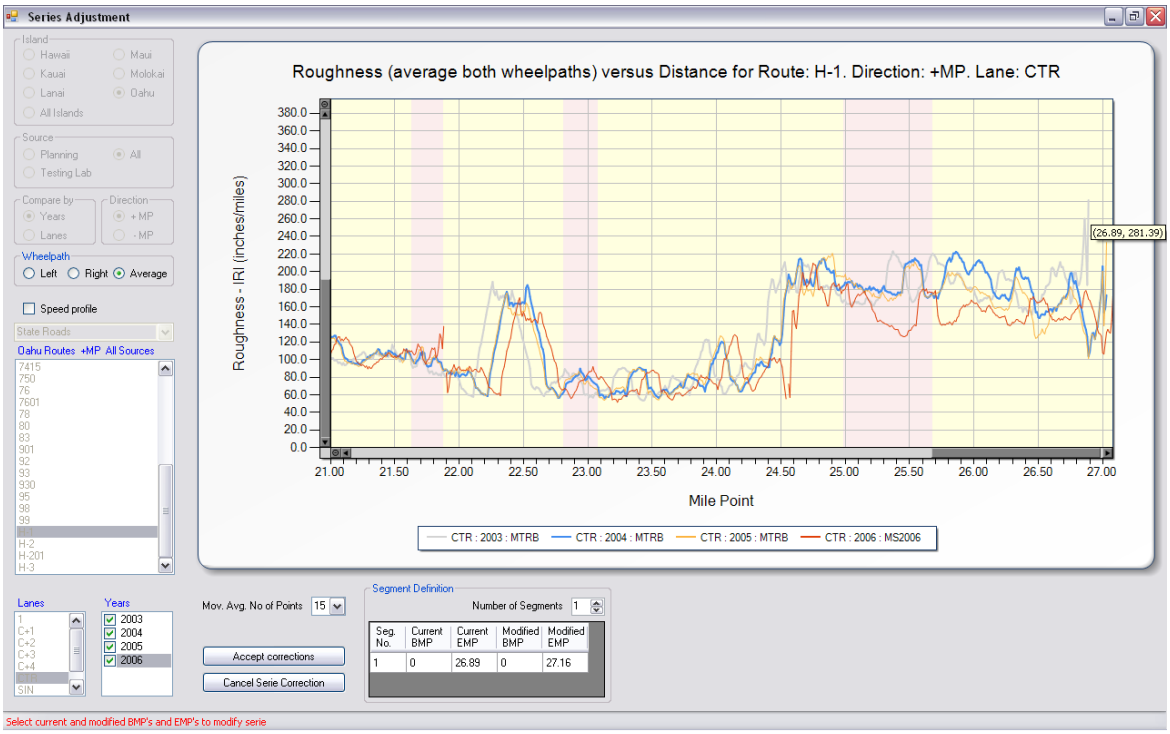

Figure 4-8. Similar patterns for different years that are shifted longitudinally.

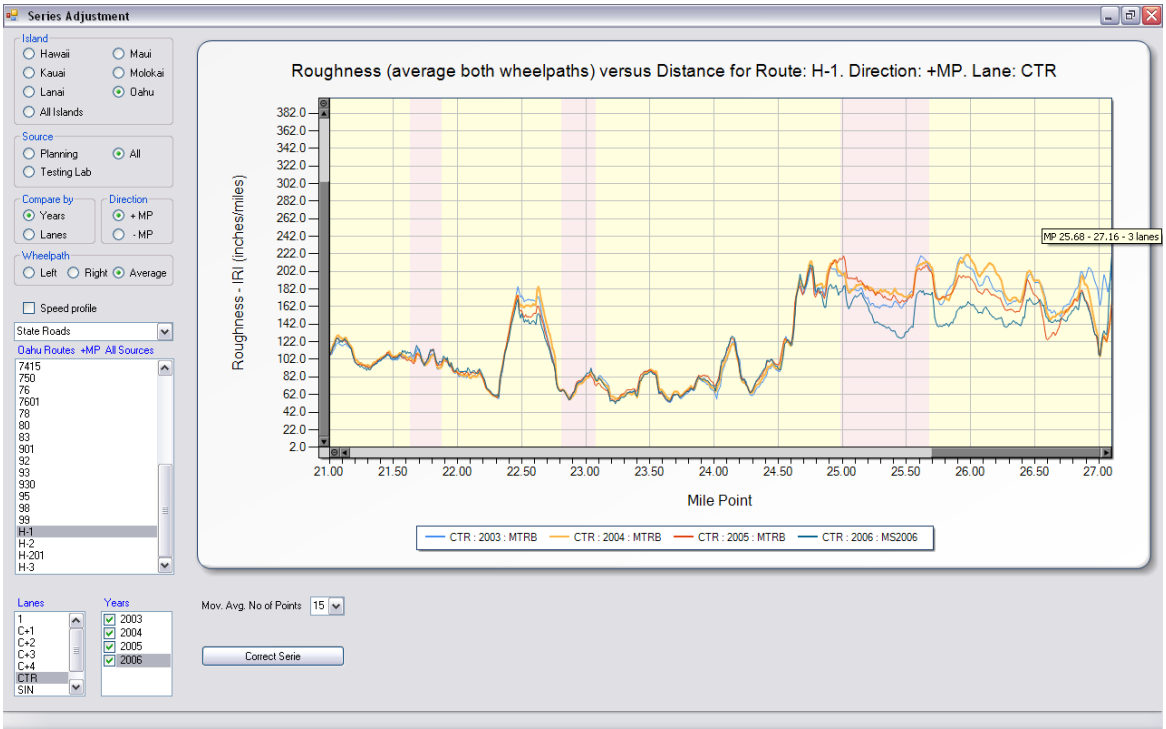

Figure 4-9. Patterns after correcting the series.

4.2.1.3 Segmentation into homogeneous sections

A recurrent issue in pavement management is the segmentation of the network into homogeneous pavement segments. Many different pieces of information can be used to accomplish this, including pavement structural information, FWD deflections, number of lanes, traffic, etc. coupled with engineering judgment to avoid sections that are too long or too short. Roughness can also be used to help define homogeneous pavement sections.

For this purpose, an algorithm developed by Dr. Fridtjof Thomas ([25], [26], [27]) that combines a Bayesian identification of transitions (change–points) between two homogeneous road sections with a heuristic approach to find multiple homogeneous sections was implemented in the program. The segmentation algorithm identifies changes in the level, in the variance, or in the autocorrelation of the series of measurements. Therefore, the homogenous segments identified need not have a constant level of IRI.

To create a segmentation, the user needs to select the Automatic Segmentation option in the main menu (Figure 4-2) and then select the route/lane/direction/year combination of interest. The series to be segment needs to be selected by clicking on it as shown in Figure 4-10. The selected series is highlighted with small circular dots. The segmentation is simply performed by pressing the “Automatic Segmentation” button. After only a few seconds a segmentation such as that shown in Figure 4-11 is displayed.

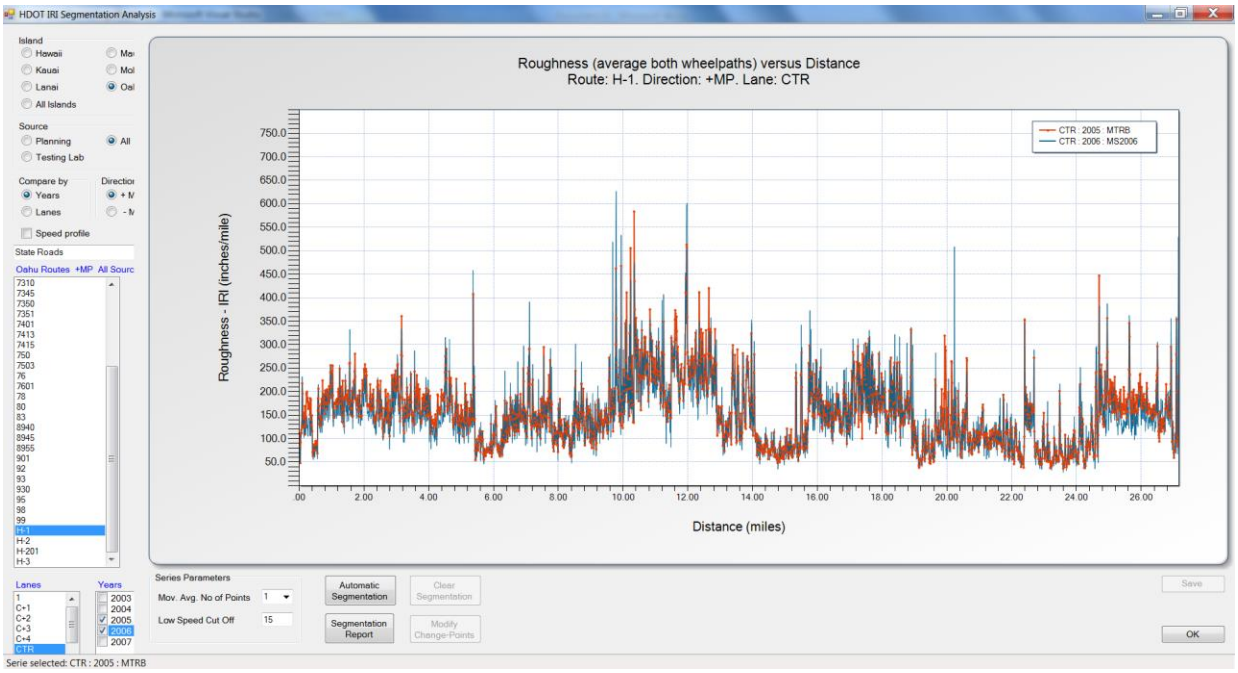

Figure 4-10. Selecting a series to perform an automatic segmentation.

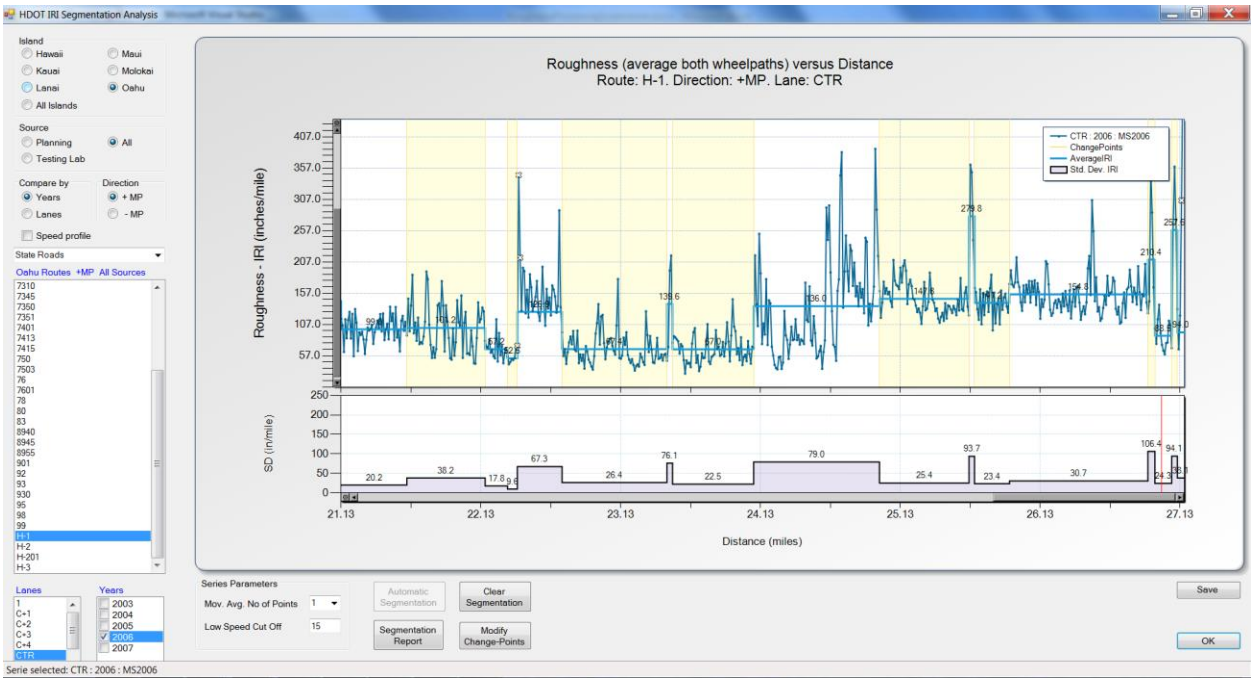

Figure 4-11. Automatic segmentation into homogeneous segments.

As mentioned before, change-points between segments can be generated not only by differences in the mean values but also by changes in the variability of the data as illustrated for

the change point close to MP 25 in Figure 4-11. Notice that the average values before and after this change-point are very similar but the standard deviations is more than double before the change-point than after the change-point.

A segmentation report can be easily generated by simply pressing the "Segmentation Report" button, which brings up the window shown in Figure 4-12. If an automatic segmentation was generated before pressing the button the BMP and EMP on the report will correspond to the change points of the segmentation. Otherwise, the program selects a default interval and reports the associated values. For each interval, the average, standard deviation, and number of points used to compute them are reported for each of the series selected in the segmentation screen. All the information can be exported into comma delimited files for further analysis or report generation with spreadsheet software. The number of intervals as well as their end points can also be changed easily by the user. Notice that unlike other fields, the background of the BMP field is white, which indicates that the field can be edited by the user. When the user changes a given BMP, the software automatically changes the EMP of the previous segment and recalculates the appropriate statistics for affected segments.

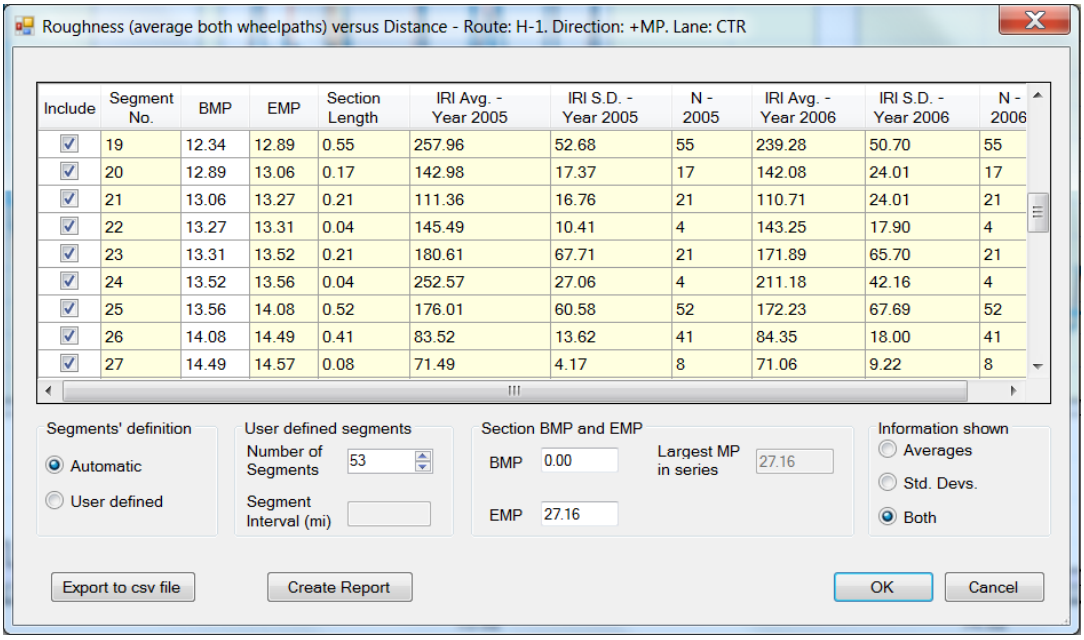

Figure 4-12. Segmentation report.

Occasionally, the user may find the location of some change-points unsatisfactory. In such situations, selecting the "Modify Change-Points" button in Figure 4-11 allows dragging change-points to more desirable locations. Change-points can also be inserted or deleted. Figure 4-13 illustrates an interval (from MP 14.07 to MP 15.32) where the user may desire to change the locations of its change-points. As shown in Figure 4-14, the statistics for the affected intervals are automatically updated after each change point is moved, inserted or deleted.

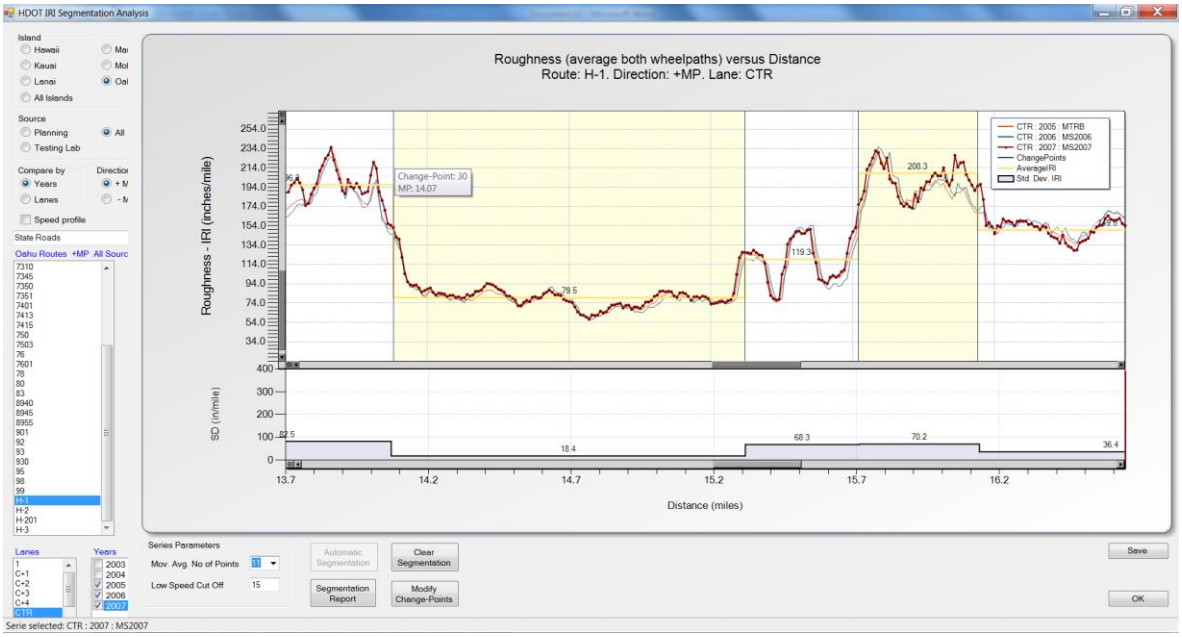

Figure 4-13. Change-points needing modification.

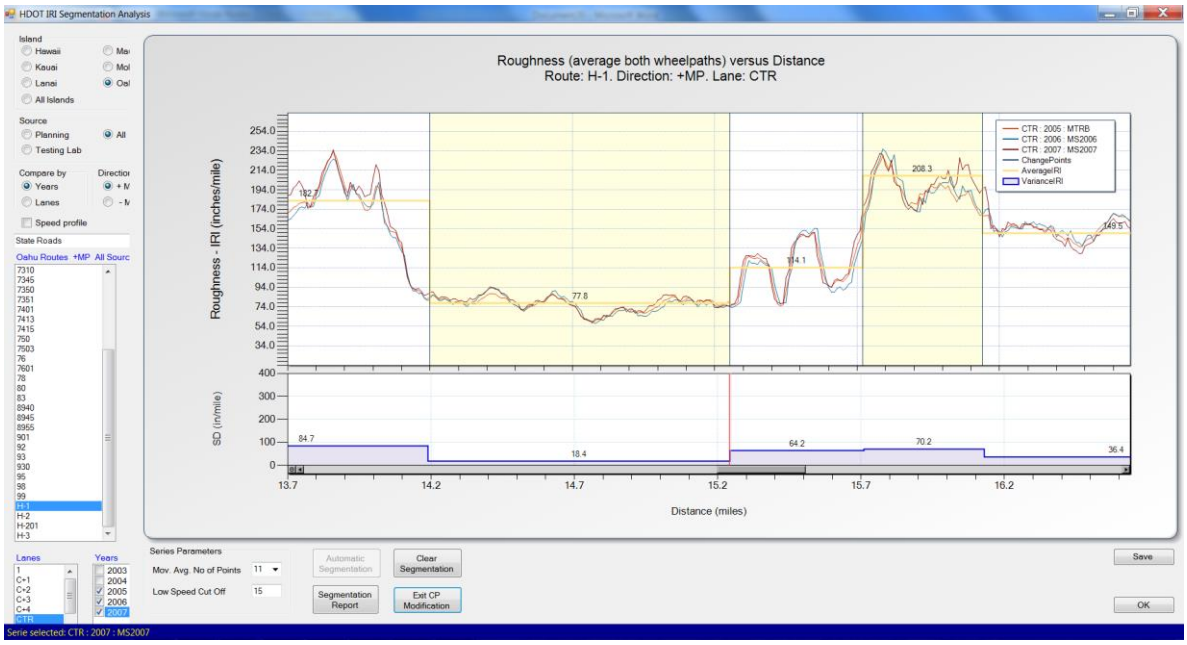

Figure 4-14. Result of dragging change-points to different locations.

4.2.1.4 Additional IRI Data Processing Tool features

A common need when analyzing pavement performance is the comparison of IRI levels (or other indicators) for a given section of interest over time. Although this can be done with a spreadsheet by using the export option in a segmentation report described in the previous section, it is convenient to have an option within the program to do this. Such option is accessed by selecting “Roughness Comparison” in the main menu (Figure 4-15). This bring up a window where the end points of the analysis interval can be selected. Figure 4-15 shows a bar chart that is generated once the analysis interval is selected and the “Update” button is clicked. Notice that the analysis interval is marked with a yellow background in the top chart. The bar chart provides a very quick way to visualize the trends on different segments of a route.

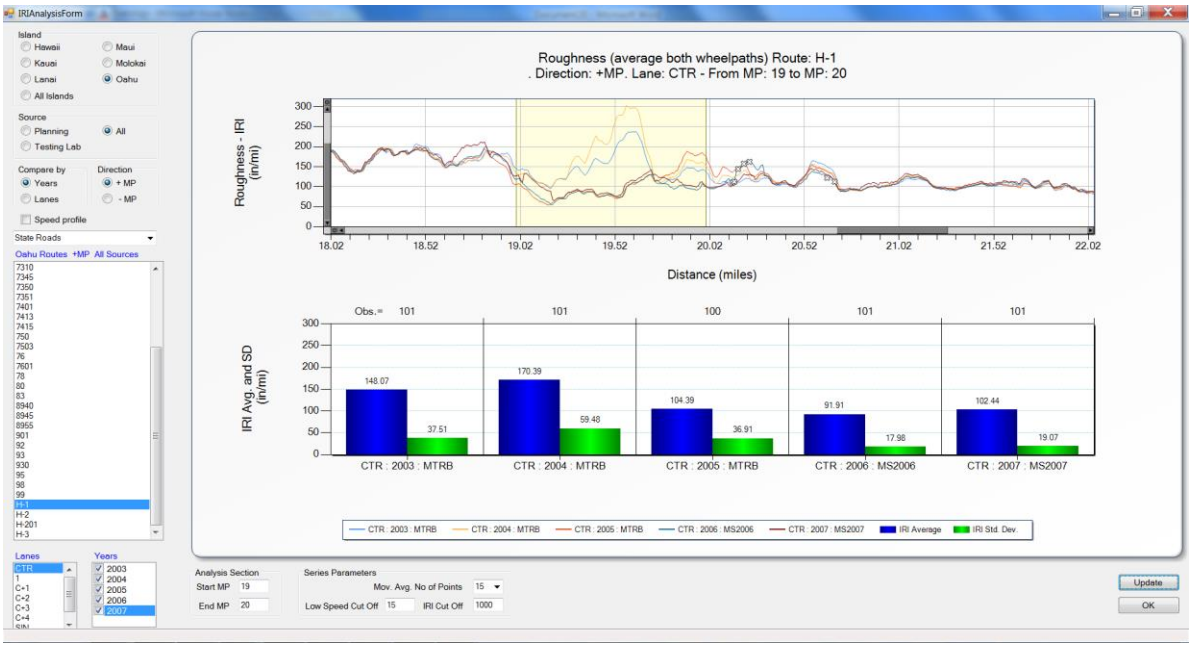

Figure 4-15. Comparison of IRI averages and standard deviations across years.

The figure also illustrates that a "Low Speed Cut Off" value and an "IRI Cut Off" value can be defined. The low speed cut off is used to exclude in the computation the values that were collected at very low speeds, which tend to be problematic. The IRI cut off is used to exclude very high values of IRI.

The rest of the menu options not yet described (Figure 4-2) are related to database utilities. The first of these options is self-explanatory. It simply allows the user to select which data base to work with. At this point, the database is an Access database and because of the speed limitations with large tables in Access, the information is spread out in different tables so that the interface is responsive. This requires that the data be imported following certain rules, which the second option under "Database Utilities" enforces by formatting the tables appropriately.

Note that in all examples provided in the previous sections, series were available only up year 2007. The reason for this is related to a problem that has been recurrent in dealing with data for this project; namely, that the formats on which the data are provided have not been consistent over time. In order to import data, a common format also needs to be used. The program was originally created to read comma delimited files but it soon became evident that using a database was more efficient for dealing with the whole network. Thus, a format based on the database

used for the 2006 data was created and the data from years 2003, 2004, 2005 was reconfigured into that same format. When the 2007 data were received, a new "Prefix" field had been added, which created problems for importing the data. Since the "Prefix" field indicates whether a road is a state road, county road, etc., it was felt necessary to include it. In order to deal with this, the input format was changed again and an option was added to change the old formats.

After 2007, the data were delivered in yet a slightly different format and since the PI had to devote time to other project activities, there was no time to modify the program once again. If HDOT desires to use this program, future work should specify either the format in which vendors should provide the data or the format of an ASCII or comma delimited file that should be followed to facilitate the import operation. The data for 2007 and 2009 were used for calibration of the guide but the 2009 data were not processed with this program.

In addition to the above, the program still needs some improvements to avoid a few known bugs that may halt its use and make the chart scrolling more responsive.

4.2.2 Notes about the observed IRI trends

The figures presented in the previous sections illustrate some features that are representative of many other situations in the State. In general, IRI increases with time as the pavement ages but it tends to do so at a relatively slow rate with very consistent trends in time. A notable exception is for significantly deteriorated pavements on which IRI may increase quite rapidly. Typically, once that condition is reached, application of a preventive maintenance treatment is no longer cost-effective. In addition, this typically results in difficulties during calibration of IRI predictions models, as predicted changes in cracking and rutting, which are used to predict IRI, are usually gradual.

Therefore, use of roughness *alone* may not be conducive to obtaining cost effective maintenance strategies at the network level.

Note also that it is common to observe changes in the averages that jump from less than 100 in/mi to more than 200 in/mi and that in many situations such dramatic changes cannot be attributed solely to changes in the surface condition of the pavement. Sections on high fills and embankments before or after bridges typically display much higher IRI's than other sections. Notice that the previous statement does not refer just to the short transition between a bridge and

its approach/exit but to longer sections sometimes as long as 0.1 mi to 0.3 mi. Confirming this observation may be important to determine whether specifications for embankments need to be updated. As discussed in the chapter of calibration of the MEPDG, for new sections, the IRI on sections on high fills is about 50 in/mi higher than on other sections.

Finally, referring back to Figure 4-15, it can be seen that the average IRI reported for 2006 is smaller than that reported for 2005[12]. Typically, unless it is known that some maintenance activity was conducted on the section, such a reduction would be attributed to noise in the data. However, in this particular situation, it is important to point out that systematic reductions occur for too many sections from 2005 to 2006. The reason is that, despite the consistency of the IRI trends, different equipment and personnel were used to perform the survey on these years. Thus, the reduction is apparently in big part due to biases of one equipment versus the other. Thus, it is important to remember that whenever changes are made on equipment and/or technology such differences are to be expected. The point here is that although changes are needed as technology evolves, performing them too often also involves additional risks.

4.3 PAVEMENT CONDITION

As pointed out by Shahin [7], an important feature of a pavement management system (PMS) is the ability to determine both the current condition of the pavement network and predict its future condition. According to Haas, Hudson, & Zaniewski [3], surface distress surveys are directed in large part towards assesing the maintenace needs to prevent accelerated future distress or the rehabilitation measures needed to improve the pavement.

This section describes the analysis of the surface pavement condition data available at HDOT. Reliable distress information is essential for implementation of a PMS and for calibration of the mechansitic-empirical pavement design procedures.

As dicussed below, at HDOT several different procedures have been used by different people following different distress definition protocols to collect pavement surface distress

[12] The IRI's in previous years are higher. However, this section was rehabilitated before the 2005 data collection cycle.

information over time. Furthermore, the lengths used for sampling are also quite different between the different surveys. The end result is that despite that a significant amount of information was collected over time, its use at present is limited. The following list provides some general descriptions of the different pavement distress surveys (as best undertood by the PI):

- 1986 – 2004: Visual (winshield) survey of pavement condition by raters from the Materials Testing & Research Branch (MT&R) sitting in a van traveling at about 30 mph down the road. Sampling sections were generally one mile long. Low, medium and high severity of the following distress types were recorded on each lane: alligator cracking, block cracking, transverse cracking, longitudinal cracking, reveling, and potholes. In addition, a field for percent of rutting was also included in the data. Portland Cement Concrete (PCC) pavements sections were not surveyed.
- 2005-2006: Basically, it was the same type of winshield survey as the previous one but conducted by different personnel from the MT&R branch. The same of type of distresses were collected but over pavement segments of variable length. Segment lengths were as short as 0.03 mi and as long as 9 mi. The criteria used to define the segments are unknown, though it appears that at least in part they were based on easily identifiable features such as number of lanes and the location of intersections and interchanges. Oddly, on PCC segments, "equivalent" asphalt concrete distresses were recorded. Again, it is not known how that "equivalence" was defined. Nevertheless, even if it were known, use of such an approach is discouraged as there is no such thing as an equivalence of distresses between these types of pavements.
- 2006, 2009, 2010: Distresses measured by Mandli Communications, Inc. (Mandli) from forward videolog images on 0.1 mi long segments. The 2006 and the 2009/2010 data correspond to two different data collection cycles. The 2010 data collection was limited in some respects discussed later. The following details corresponds to the 2009 data collection cycle. The sampling rate was 500 frames per mile, or one frame every 0.002 mi (10.6 ft) at speeds between 0 and 60 mph. The camera resolution was 2048 x 1152 pixels. The measuring vehicle was equipped with a distance measuring instrument (DMI) capable of measuring distance accurate to within +/- one thousand

(0.001) mile per mile and an Applanix POS LV 220 Position Orientation System. Latitude, longitude, and elevation with an accuracy level of (+/-) 1-5 meters were also recorded. Rut depths and roughness (IRI) were measured with a Dynatest RSP Mark-III 5-point laser road surface profiler and were reported every 0.01 mi. Both were included on a Roughness table within the delivery database. For IRI, data collected at speeds below 13 mi/h were flagged and not included. Rutting was reported for the left and right wheel paths as well as their average. Other distresses were collected following the Strategic Highway Research Program (SHRP) distress identification manual as a guide. These were summarized and reported every tenth of a mile (0.1 mi). Two different tables were delivered for Asphalt and Concrete pavements. Data were collected also in 2007 but for Oahu they included only ramps, service roads and frontage roads.

- 2010: Visual survey performed by MT&R branch personnel. In this case, an attempt to simplify the data collection was made. Essentially, data were collected again visually. The MT&R brach personnel made an attempt to improve the data collection effort by obtaining a video with audio at the same time the survey was performed. Unfortunately, an all or nothing criterion for each distress was used for each 0.1 mi segment. In other words, the distresses were recorded as either being present or not (0 or 100%). Except perhaps for very long homogeneous segments (for which aggregation of these data could be performed), they are not useful for predicting pavement deterioration, computing an agregate index or for calibration of deterioration models.

Clearly, effective use of such disparate information is challanging. Some of the data were more difficult to analyze than others. In particular, the data for 2010 had less information content. In addition, the 2010 information was available in paper forms instead of electronically. Although some effort was made to save the information in computer files; in the end, it was considered that such effort was not worthwhile to be continued.

4.3.1 Analysis of the Historical Winshield Pavement Condition Data

An effort was made to evaluate the potential of the historical pavement distress data for suitability to develop deterioration models and for use with PMS software. Given some concerns

with the nature of the data, the calculation of a condition index combining all the distress information for a section into a single index was considered. Although many decisions may need to be taken based on individual distresses, the summary of the pavement condition in an index is also beneficial as it allows the rapid visualization of the condition over time and summarizing information for upper management and the public. Several different indexes have been used for PMS, but here, particular attention was paid to the Pavement Condition Index (PCI) as defined in ASTM D6433. This is the only index that has an ASTM standard. Also, it is used by PAVER™, which is one of the PMS programs that was evaluated. Furthermore, in 2006, HDOT personnel started reporting pavement condition in terms of PCI.

Unfortunately, the computation of the PCI's used in 2006 did not strictly follow the ASTM D6433 procedure. Thus, substantially different values from those using the ASTM procedure were reported, as shown in Figure 4-16 for a sample of sections. When Figure 4-16 was created, it was not clear whether the interpretation, by the PI, of the reported distress values was incorrect or whether the problem was in the calculation procedure. Later on it was determined that it was the latter. A procedure unknown to the PI and certainly unrelated to ASTM D6433 had been used but not documented[13]. The use of the different procedure led to such different results. What this example demonstrates is the importance of clearly defining how data are collected, what the values in the different data fields mean, and how they are being processed so that evaluation of condition over time is consistent. Misinterpretations of any of these factors may be problematic. As seen in Figure 4-16, another person using the same exact data could have reached very different conclusions about the network condition and its evolution.

[13] The assertion that the problem was in the calculation procedure is based on the equation used on spreadsheet with the calculations. The ASTM PCI computation uses deduct values and in the spreadsheet these appeared to be correct. The only difference was found in the actual computation of the PCI from the deduct values.

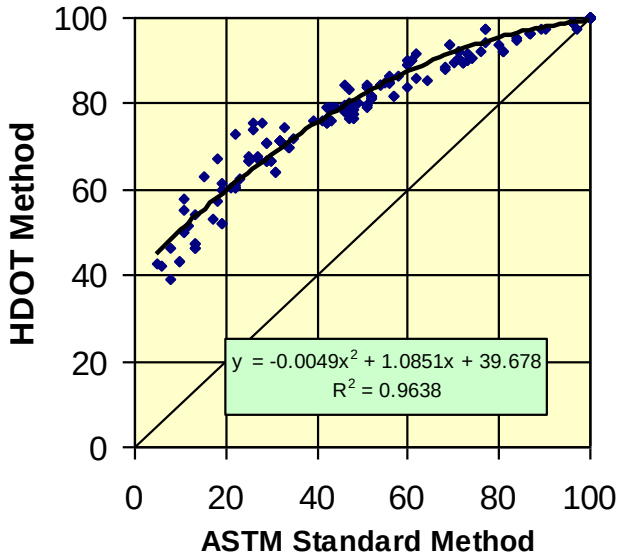

Figure 4-16. Differences between PCI calculated according to ASTM D6433 and 2006 HDOT's approach.

It is speculated that the reason why a simplified approach had been used is that the actual PCI calculation, although not mathematically difficult, is somewhat involved. As mentioned before, PAVER™ and other PMS programs can calculate the PCI. However, manual input of the data into PAVER™ with the only purpose of visualization would have been tedious and extremely time consuming. Furthermore, since the PCI sampling requirements were not met[14], some additional tweaking of the data would have been needed, making the data input process even more time consuming and prone to error. Since it was not clear whether these data would be used, it was preferred to implement the PCI computation procedure in a computer algorithm.

As with many of the software tools developed during this project, what started as a program to simply compute PCI with the historical data was later improved to create charts to visualize the data, and then it was enhanced to read the Mandli data, make appropriate transformations, and save the data into an appropriate format to import into PAVER™. The

[14] The recommended sample unit size is 2,500±1,000 ft^2. In contrast, HDOT data were usually available for 1 lane-mi = 63,360 ft^2 (assuming 12 ft lanes).

following section briefly discusses the PCI visualization capabilities originally develop to visualize the historical information.

4.3.1.1 PCI Calculation and Visualization

This section provides a very brief description of the efforts to calculate and visualize the Pavement Condition Index (PCI) according to ASTM D6433.

4.3.1.1.1 Pavement Condition Index (PCI)

ASTM D6433 defines the pavement condition index as a numerical rating of the pavement condition that ranges from 0 to 100 with 0 being the worst possible condition and 100 being the best possible condition. Furthermore, ASTM D6433 indicates that the PCI provides a measure of the present condition of the pavement based on the distresses observed on the surface of the pavement, which also indicates the structural integrity and surface operational condition. The PCI cannot measure structural capacity.

The PCI calculation involves the subdivision of the network into branches (routes for HDOT), the branches into sections, and the sections into sampling units. According to ASTM D6433, the calculation of PCI is done at the sampling unit level. Each sampling unit should be 2,500 ft^2 ± 1,000 ft^2. This requirement is problematic for the interpretation of HDOT historical information since the data has been collected visually mostly for every one lane-mile (1 lane-mi = 63,360 ft^2 for 12 ft. lanes). Shahin [7] has investigated the effect of the sampling unit size and from his results it can be inferred that samples much larger than the recommended size would lead to an underestimation of the PCI. Unfortunately, the magnitude of the underestimation for such big sample sizes cannot be inferred from his results. Nevertheless, considering that the information is obtained at highway speeds, this type of error is likely less important than the error incurred during the actual evaluation.

The PCI can be computed following these simple steps: 1) calculate deduct values corresponding to each of the distresses observed in a pavement sampling section, 2) obtain a total

deduct value from the individual deducts[15], 3) compute a corrected total deduct, and 4) subtract the corrected total deduct value from 100.

The calculation of the deduct value is based on the "density" of each distress type[16]. ASTM provides charts for the calculation of the deduct values for each distress type and severity such as the one shown Figure 4-17 for fatigue cracking. As mentioned above, the calculation of PCI requires computing a *corrected total deduct* from the *total deduct*. The corrected total deduct value depends on the number of distresses used in its computation[17]. Figure 4-18 shows the correction curves as a function of the number of deduct values (q).

[15] The total deduct is not necessarily the sum of the individual deducts. The PCI calculation recognizes that a distress may not have the same effect in combination with other distresses. An iterative procedure must be followed in which distresses are ordered in decreasing order of deducts and only some of these are used to compute the total deduct. This is the only real involved and somewhat confusing step in the PCI calculation.

[16] Depending on the type of distress, density refers to 100 multiplied by either: the area with the distress (e.g., area of fatigue cracking) divided by the sampling area, linear feet with the distress (e.g., length of longitudinal cracking) divided by the sampling area, or number of occurrences (e.g., number of potholes) divided by the sampling area. Notice the peculiar use of the word density, since it conforms to the usual meaning only for distresses for which an area is measured.

[17] What makes things a bit more confusing is that to determine the number of deducts, an iterative procedure must be followed. Thus, the number of deducts is not necessarily the same as the number of distresses.

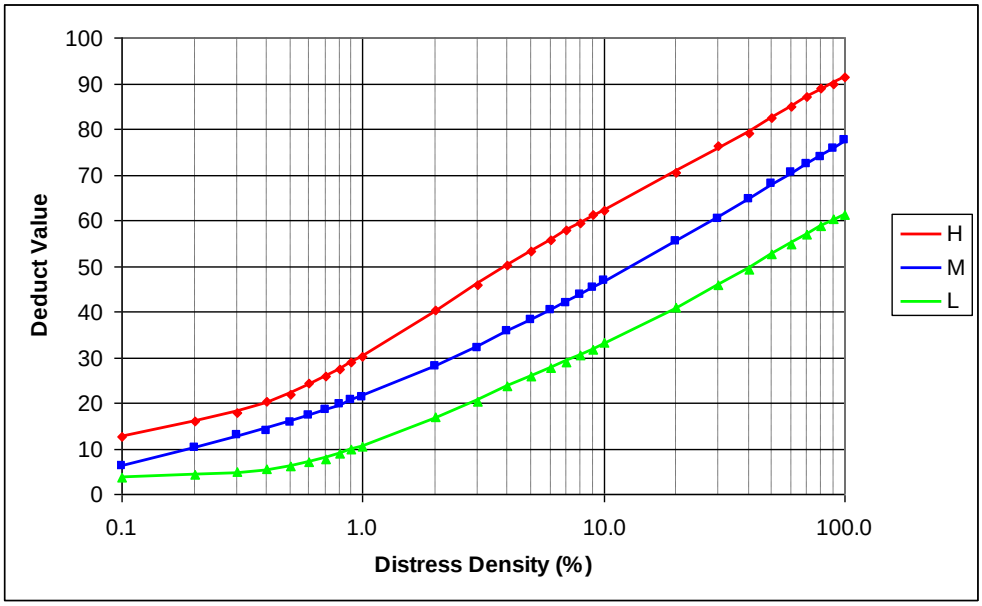

Figure 4-17. Deduct value curves for low, medium, and high severities of fatigue cracking in asphalt concrete pavements (the lines represent the polynomial fits to the digitized data points).

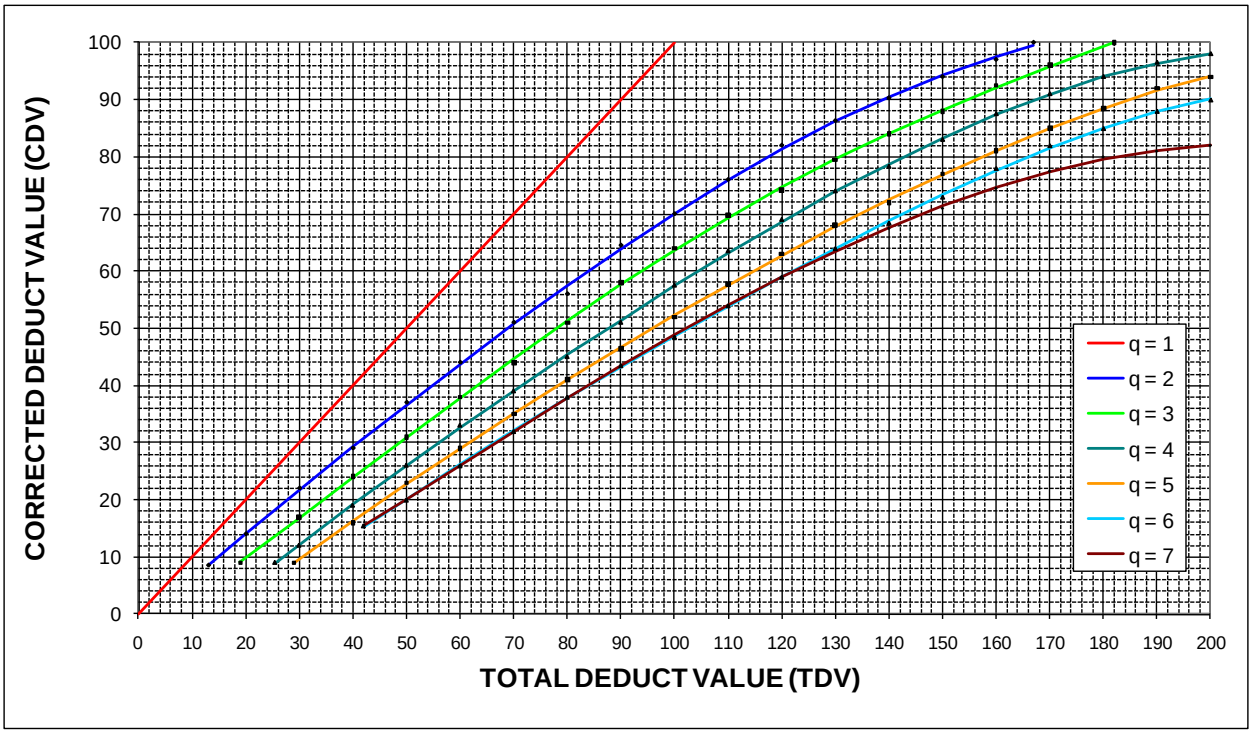

Figure 4-18. Determination of corrected deduct values for asphalt concrete pavements.

4.3.1.1.2 Visualization of Historical PCI

A customized program was created to visualize the PCI computed from the historical data. The program simply reads a comma delimited file (essentially as provided by HDOT in the 1986-2004 data file) and proceeds to compute the Pavement Condition Index for each section and year available. The information is sorted by section and then by year.

For each section and year, the PCI is computed by first calculating the deduct value corresponding to each distress type-severity-extent combination and then following the procedures recommended in ASTM D6433 for computing the appropriate number of deducts and in turn, the total deduct value and PCI.

In order to compute the deduct values; ASTM D6433 deduct curves had to be incorporated into the program. To do this, the curves were first digitized and then polynomials were fitted to the data. In Figure 4-17 and Figure 4-18, the lines correspond to the polynomial fits and the points represent the digitized data. Once the parameters of the equations for calculating deduct values and corrected deduct values in the aforementioned charts (the polynomial fits) were estimated, the implementation of the algorithm for computing PCI was relatively simple. The algorithm was implemented in Visual Basic.

Although the program follows the ASTM D6433 standard in most respects, due to the type of data available, it was not possible to follow the sample size recommendations. Furthermore, given the very approximate nature of the data, the potential effect of severity level definitions (discussed in more detail in the next section) were not considered since while driving at 30 mph, these are very approximate anyway.

Several charting capabilities were provided to visualize the data either at the route level (over distance and time) or at the network level. Figure 4-19 to Figure 4-21 provide examples of the type of charts that can be generated.

The trends in Figure 4-19 allow a quick comparison of the evolution of the average condition on the islands. As with any chart displaying aggregate data, one must be careful in the analysis as there may be some artificial differences caused by some of the characteristics of the data instead of the real condition of the network. For example, notice the big drop in average condition for Oahu in 2003. It is not clear whether on that year there was a real big drop in the

average network condition or that only a subset of the network was surveyed. As shown Figure 4-19 for one of the points, the program provides tooltips indicating the lane-miles on which the average for each point is based. Interestingly, the average on Oahu for 2001 was based on 807.52 lane-miles while the average for 2003 was based on only 205.62 lane-miles.

In addition to averages, it is also important to know the distributions of pavement condition for each island and for the whole state. Histograms such as the one in Figure 4-20 are useful to evaluate the overall condition of the network on a particular year.

Finally, charts such as the one in Figure 4-21 allow a quick review of the condition of a route over distance and time. Notice that areas with no PCI reported in the chart are areas with either concrete pavements or in viaducts.

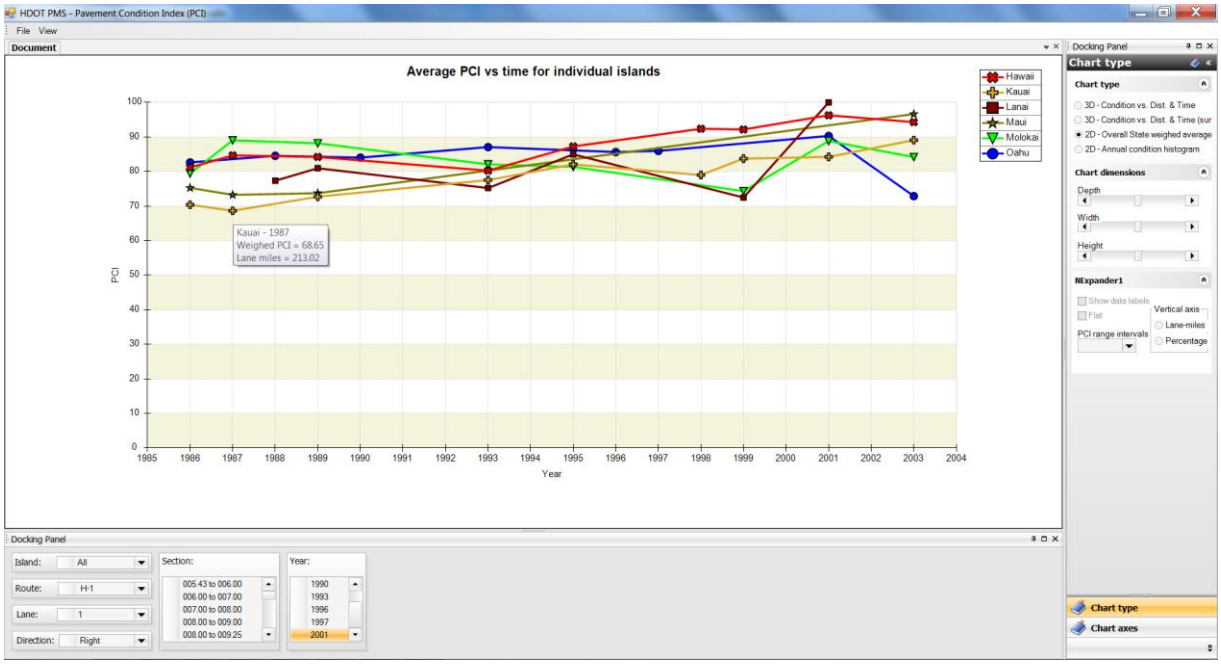

Figure 4-19. Trends of average PCI vs. time for each island.

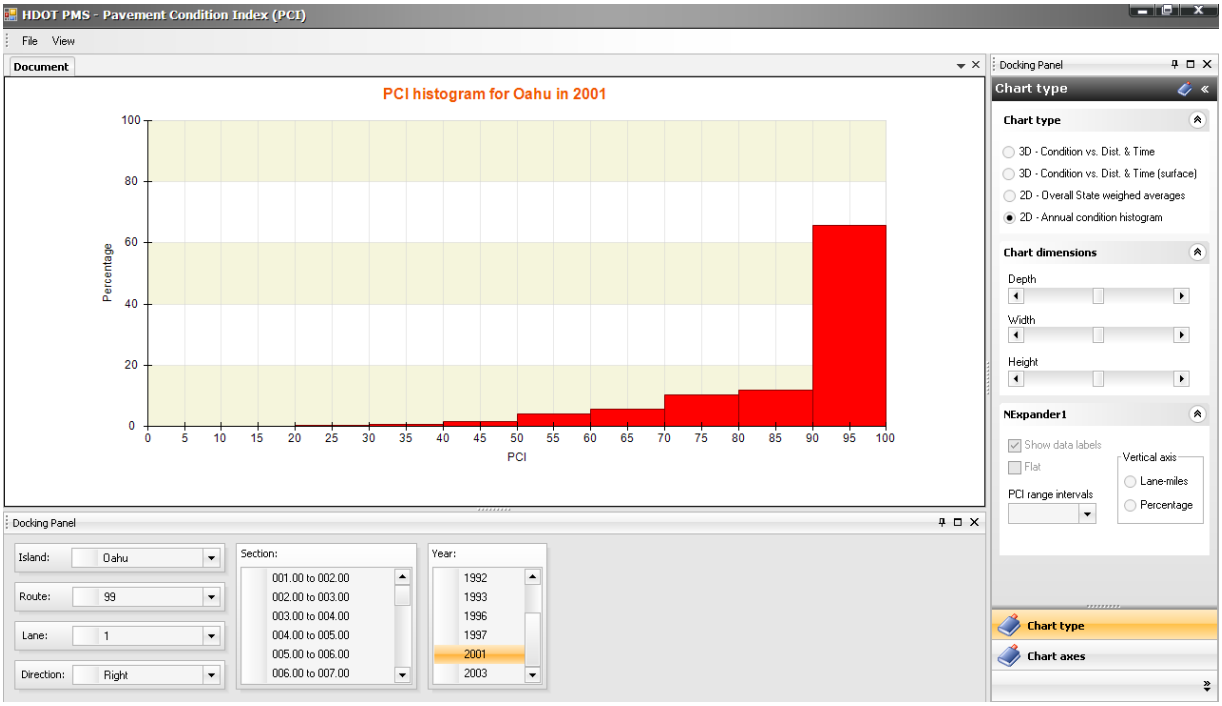

Figure 4-20. PCI histogram for an island in a particular year.

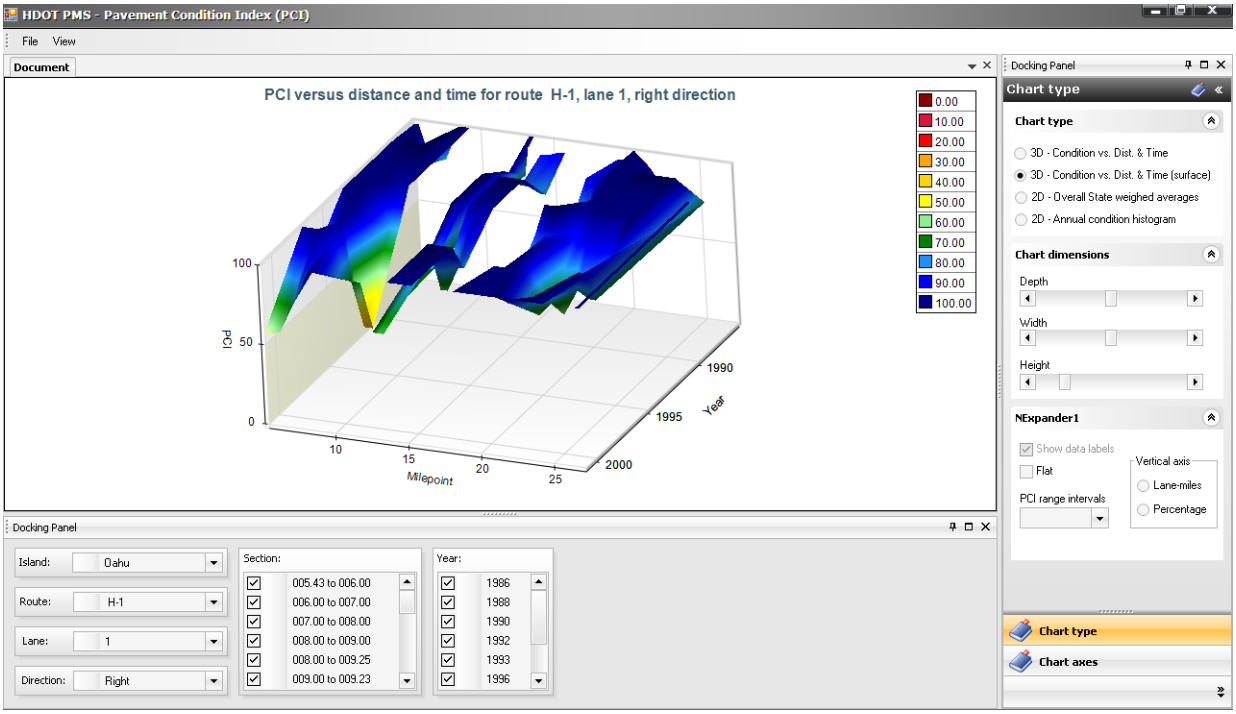

Figure 4-21. PCI vs. distance and time for a given route.

A capability has been added to select begin and end mile points for the charts as well as the periods to be displayed. Figure 4-22 shows an example in which the end points have been changed to focus on a given section of the road. In addition, as illustrated in Figure 4-23, the user can interactively rotate the chart by clicking and dragging it and also can control its dimensions with the three scrollbars shown on the right of the figure.

4.3.1.1.3 Observations about the historical data

Except for issues such as the one discussed for Oahu's average pavement condition in 2003, the historical data appears to have been collected quite consistently. The main concern with these data are the coarseness with which they were collected (length of sampling sections) which may not be useful for dealing with localized problems and the level at which some distresses can be observed.

Because of either the nature of the data collection or the nature of the actual pavement deterioration, it may be difficult to use PCIs from the distress data collected in the same way to proactively find appropriate timing of maintenance activities. To illustrate this, consider again Figure 4-22. Notice that there is a relatively sudden drop in condition from 100 to nearly 40. After that, the condition increases again. The structural data mining information indicates that this section was overlaid with 3.5" of AC Mix IV in 1997, which is consistent with the improvement observed after that year. Before that, between MP 8.07 and 8.68, it had been overlaid with 2.5 of AC Mix V in 1981 over a pavement originally constructed on 1968. After MP 8.81, it had been overlaid with 2.5" of AC Mix V in 1986 over the pavement built also in 1968. Finally, from MP 8.68 to 8.81, the 1997 overlay of 3.5" of AC Mix IV had been laid on top of a 2.5" ACB (Asphalt Concrete Base) course constructed in 1997 directly on top of the 1968 pavement.

According to the figure, the pavement condition was nearly 100 until about 1990. That is, depending on the section within the mile, it stayed in excellent condition between 4 or 9 years (or 22 for the short segment from 8.68 to 8.81). After that, the condition dropped to slightly more than 80 in 3 years and then it dropped dramatically to about 40 in a period of just 3 years. This behavior may well be consequence of the cracking of the old pavement reflecting through the overlay. However, it may also be partly a consequence of missing some of the initial stages of cracking while surveying visually at 30 mph.

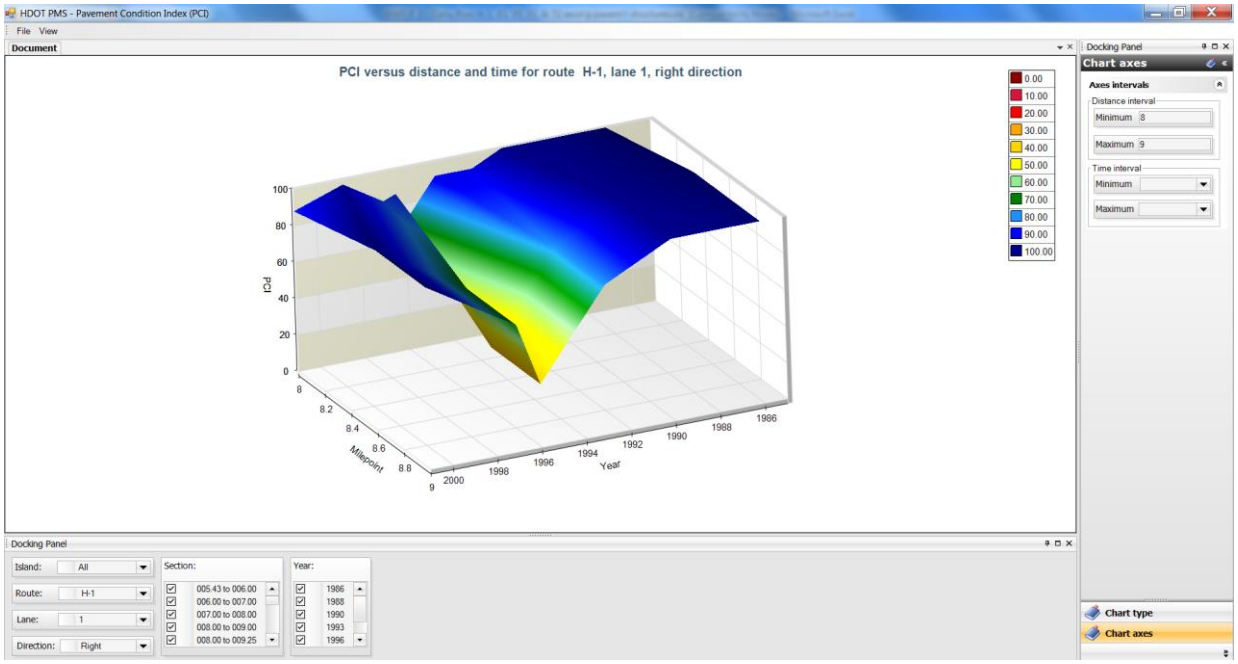

Figure 4-22. Identifying triggers may be difficult.

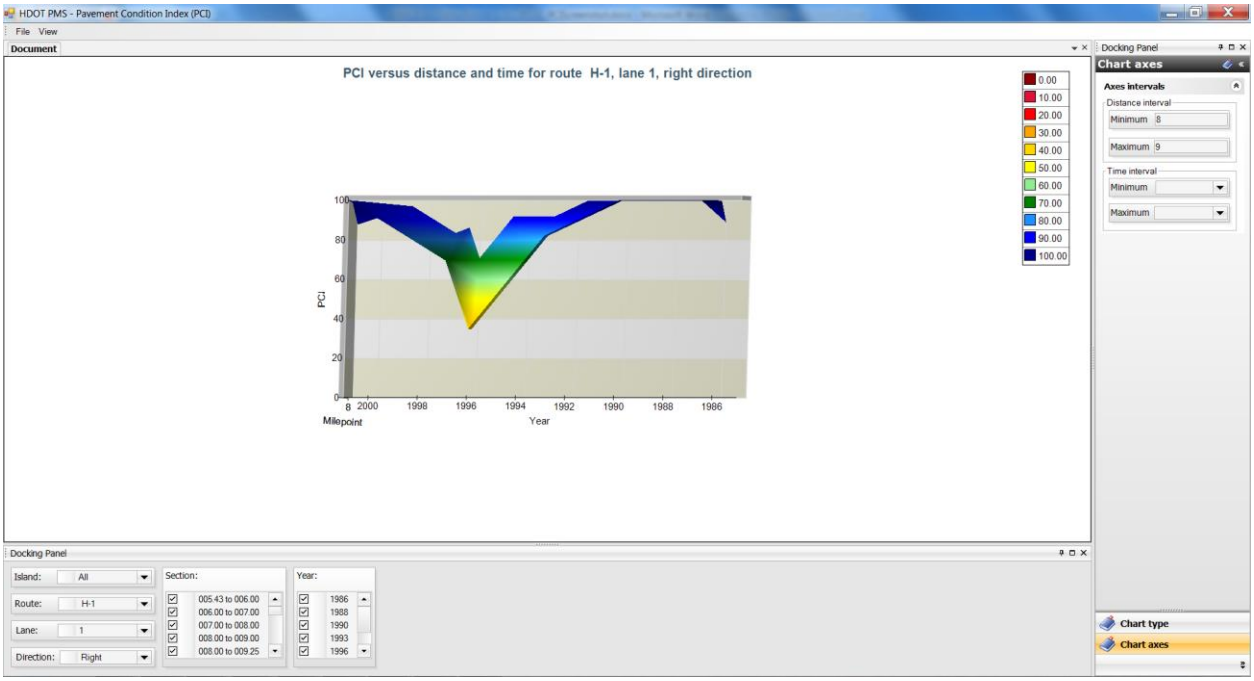

Figure 4-23. Rotation of the chart facilitates visualization of the timing of different conditions.

There is at least some evidence that some early stages of cracking may not be captured during the visual surveys. Consider the situation shown on Figure 4-24 on route 7101. This highway was rehab in 2006 and the picture was obtained from the 2009 photo log. In 2010, no distresses had been reported for this route. If early stages of cracking are unreported, once cracking becomes evident, the rate of decreased in PCI may be artificially increased.

The above observation notwithstanding, it is also quite likely that the drop in PCI for overlays over cracked pavements is quite sudden. Figure 4-25 was taken also on route 7101 on the day it was being overlaid. It is not surprising that such wide cracks would reflect through the overlay relatively quickly (however, it must be noted the two photos were not taken at the same spot.)

In summary, the historical distress information was collected consistently throughout the years and, in combination with the pavement structural information, can then be useful for assessing the effectiveness of past pavement rehabilitation/maintenance strategies because pavements in excellent condition will be rated as such and pavements in poor condition will be rated as poor. However, given the observed sudden drops in condition, there are concerns about whether the surveys conducted at 30 mph can really identify appropriately the timing for preventive maintenance activities. Also, data collection on mostly 1-mile long segments does not lend itself to using the data with a more refined network.

Figure 4-24. Unreported cracking in visual surveys.

Figure 4-25. Existing cracking over which the overlay was applied on a section of route 7101.

4.3.2 Planning Branch Pavement Distress Survey

The data collected by Mandli Communications, Inc. (Mandli) for the Planning Branch presents the advantage of being collected over 0.1-mi long segments. Thus, these data are much more adaptable to whatever sectioning is chosen in the end for the PMS network. In addition, the 0.1 mi segments are about twice the size recommended for PCI calculation, which limits the potential bias in PCI to about 5% based on Shahin's evaluation of the sample size effects [7]. Furthermore, distresses are collected for both asphalt concrete and PCC pavements. Therefore, the whole network can be considered when selecting maintenance strategies.

Figure 4-26 and Figure 4-27 show the distress types collected by Mandli and their rating method. These are supposed to be collected according to the SHRP or LTPP Stress Identification Manual [28], which is probably the most commonly used rating protocol in the US. However, the crack width of ½-in used to differentiate medium from high severity cracking is different from the ¾-in criteron in LTPP.

It is also important to note that some distress and severity level definitions in the LTPP Stress Identification Manual are different from those in ASTM D6433. Therefore, calculation of

the PCI according to ASTM D6433 with distresses collected according to LTPP requires making data transformations which involve assumptions and create some challenges.

4.3.2.1 Some differences between LTPP and ASTM D6433 distress definitions

Although the LTPP and ASTM D6433 protocols generally deal with similar distresses, there are some important differences. For example, in LTPP, the lengths of longitudinal and transverse cracking are measured separately. Furthermore, two types of longitudinal cracking are considered: wheel path and non-wheel path longitudinal cracking. Wheel path longitudinal cracking is typically a load associated distress whereas non-wheel path longitudinal cracking is not typically considered to be associated with traffic loading (although as it will be discussed later, loading may also be a factor in non-wheel path longitudinal cracking in Hawaii.) In contrast, in ASTM D6433, the length of longitudinal and transverse cracking are combined into a single measure, presumably because they are associated with either poorly constructed joints; shrinkage of the Hot Mix Asphalt (HMA) layer due to low temperatures or hardening of the asphalt and/or daily temperature cycling; or reflective cracks from cracking beneath the the surface course (but not from PCC joints.) In ASTM D6433, fatigue cracking is considered to start as a series of parallel longitudinal cracks, which, is similar to the recommendation in LTPP of rating as fatigue cracking any wheel path longitudinal cracks with associated random cracking or meandering with a quantifyable area.[18]

The difference in the treatment of longitudinal cracking in ASTM D6433 and the LTPP Distress Identification Manual would not be too problematic if data collected according to LTPP were used to compute PCI according to ASTM D6433 (and if cracking extent were the only thing to be considered). The reason is that Longitudinal and Transverse cracking can be easily combined.

[18] The relevance of the discussion of fatigue cracking here is that with both methods, ***longitudinal*** cracks in the wheel path are likely to be classified as fatigue cracking. However, there is a higher chance for raters using ASTM D6433 to classify these as longitudinal.

Distress Type	Distress Description	Severity			Method of Measurement	
		Low	Medium	High	LTPP-SHRP Rating Method	* Mandli's Rating Methods
LTTP-SHRP	LTTP-SHRP	S1	S2	S3		Dristress Writer
Longitudinal Non-Wheel Path Cracking	Cracks predominantly parallel to pavement centerline and outside the wheel path.	Cracks with a mean width <= 1/8 in.; or a sealed crack with sealant material in good condition.	Cracks with a mean width > 1/8 in. and <= 1/2 in.; or any crack with a mean width <= 1/2 in. and adjacent low severity random cracking.	Cracks with a mean width > 1/2 in.; or any crack with a mean width <= 1/2 in. and adjacent moderate to high severity random cracking.	Record the length in feet of longitudinal cracking outside the defined wheel path at each severity level.	1 click = one crack covering 25% of the image frame length. 2 clicks = the crack goes 1/2 of the frame length. 3 clicks = the crack goes 3/4 of the frame length. 4 clicks = the crack goes the entire frame length. 5 clicks = a second crack is started covering 1/4 of the frame length. 6 clicks = the second crack covers 1/2 of the frame length. 7 click = the second crack covers 3/4 of the frame length. 8 clicks = the second crack covers 100% of the frame length....*(2)
Fatigue Cracking	Occurs in areas subject to repeated traffic loadings (wheel paths). Can be a series of interconnected cracks. Develops into-many-sided, sharp-angled pieces with chicken wire/alligator pattern, in later stages. Cracks occur in a continuous pattern less than 1 sq. ft. in area.	An area of cracks with no or only a few connecting cracks; cracks are not spalled.	An area of interconnected cracks forming a complete pattern; cracks may be slightly spalled.	An area of moderately to severely spalled interconnected cracks forming a complete pattern.	Record square feet of affected area at each severity level. If different severity levels existing within an area cannot be distinguished, rate the entire area at the highest severity present.	1 click = 1/4 of one wheelpath is covered. 2 clicks = 1/2 of one wheelpath is covered. 3 clicks = 3/4 of one wheel path is covered 4 clicks = One wheel path is covered. 5 clicks = 1/4 of the second wheel path is covered 6 clicks = 1/2 of the second wheel path is covered 7 clicks = 3/4 of the second wheel path is covered 8 clicks = Both wheel pahts are covered.....*(2)
Longitudinal Wheel Path Cracking	Cracks predominantly parallel to pavement centerline and within the wheel path. Cracks with associated random cracking are rated as fatigue.	Cracks with a mean width <= 1/8 in.; or a sealed crack with sealant material in good condition.	Cracks with a mean width > 1/8 in. and <= 1/2 in.; or any crack with a mean width <= 1/2 in.	Cracks with a mean width > 1/2 in.; or any crack with a mean width <= 1/2 in.	Record the length in feet of longitudinal cracking within the defined wheel path at each severity level.	1 click = 1/4 of one wheelpath is covered. 2 clicks = 1/2 of one wheelpath is covered. 3 clicks = 3/4 of one wheel path is covered 4 clicks = One wheel path is covered. 5 clicks = 1/4 of the second wheel path is covered 6 clicks = 1/2 of the second wheel path is covered 7 clicks = 3/4 of the second wheel path is covered 8 clicks = Both wheel pahts are covered.....*(2)
Edge Cracking	Cracks predominantly longitudunal and within one foot of right edge of pavement edge. ON UNPAVED SHOULDERS ONLY.	Cracks with a mean width <= 1/8 in.; or a sealed crack with sealant material in good condition.	Cracks with a mean width > 1/8 in. and <= 1/2 in.; or any crack with a mean width <= 1/2 in. and adjacent low severity random cracking.	Cracks with a mean width > 1/2 in.; or any crack with a mean width <= 1/2 in. and adjacent moderate to high severity random cracking.	Record the length in feet of longitudinal cracking within the defined wheel path at each severity level.	1 click per 25% of the image frame. 2 clicks means the crack goes 50% of the image frame. 3 clicks means 75% of the image frame. 4 clicks means 100% of the image frame. *(3)
Patching	Portion of pavement surface greater that 1 sq. ft. that has been removed and replaced or additional material applied to the pavement after original construction.	Patch has, at most, low severity distress of any type.	Patch has, at most, moderate severity distress of any type. Any Potholes documented are rated as a Medium severity Patch.	Patch has, at most, high severity distress of any type; or the patch has additional different patch material within it.	Record number of patches and square feet of affected surface area at each severity level. Only record the patch if it is greater than 1 sq. ft. Note: Any distress in the boundary of the patch is included in rating the patch. Rutting (settlement) may be at the perimeter or interior of the patch.	One click per 25% or less of the image area. 1 click = 1-25% of the section is covered. 2 clicks = 26%-50% of the section is covered. 3 clicks = 51-75% of the section is covered. 4 clicks = 76-100% of the section is covered....*(3)
Transverse Cracking	Cracks that are predominantly perpendicular to pavement centerline.	An unsealed crack with mean width <= 1/8 in.; or a sealed crack with sealant material in good condition and with a width that cannot be determined.	Cracks with a mean width > 1/8 in. and <= 1/2 in.; or any crack with a mean width <= 1/2 in. and adjacent low severity random cracking.	Cracks with a mean width > 1/2 in.; or any crack with a mean width <= 1/2 in. and adjacent moderate to high severity random cracking.	Record number of transverse cracks at each severity level. Rate the entire transverse crack at the highest severity level present for at lease 10% of the total length of the crack. Cracks less than 1 ft. in length are not recorded.	One click per occurrence. *(1)
Block Cracking	A pattern of cracks that divides the pavement into approximately rectangular pieces. Rectangular blocks range in size from approximately 1 sq. ft. to 100 sq. ft.	Cracks with a mean width <= 1/8 in.; or a sealed crack with sealant material in good condition.	Cracks with a mean width > 1/8 in. and <= 1/2 in.; or any crack with a mean width <= 1/2 in. and adjacent low severity random cracking.	Cracks with a mean width > 1/2 in.; or any crack with a mean width <= 1/2 in. and adjacent moderate to high severity random cracking.	Record square feet of affected area at each severity level. If fatigue cracking exists within the block cracking area, the area of block cracking is reduced by the area of fatigue cracking.	One click per 25% or less of the image area. 1 click = 1-25% of the section is covered. 2 clicks = 26%-50% of the section is covered. 3 clicks = 51-75% of the section is covered. 4 clicks = 76-100% of the section is covered....*(3)

Figure 4-26. Distresses collected by Mandli for asphalt concrete pavements.

Distress Type	Distress Description	Severity			Method of Measurement	
		Low	Medium	High	LTPP-SHRP Rating Method	* Mandli's Rating Methods
LTTP-SHRP	LTTP-SHRP	S1	S2	S3		Dristress Writer
Lane Shoulder Drop Off	Dropoff in Shoulder Height compared to Lane	< 1/2"	>1/2 but less than 1"	> 1 "	Record the lengths	One click per 25% or less of the image frame length. 1 click = 1-25% of the image frame length. 2 clicks = 26%-50% of the image frame length. 3 clicks = 51-75% of the image frame length. 4 clicks = 76-100% of the image frame length....*(3)
Raveling	Wearing away of the pavement surface caused by the dislodging of aggregate particles and loss of asphalt binder. Raveling ranges from loss of fine particles to loss of some coarse aggregate and ultimately to a very rough and pitted surface with obvious loss of aggregate.	Low Eroison	Med Erosion	High Erosion	Record square feet of affected surface. Raveling should not be rated on chip seals.	One click per 25% or less of the image area. 1 click = 1-25% of the section is covered. 2 clicks = 26%-50% of the section is covered. 3 clicks = 51-75% of the section is covered. 4 clicks = 76-100% of the section is covered....*(3)
Potholes	Physical segment missing from surface usually hole or crater appearance.	Exists	na	na		see *(4)
Reflection Cracking	joints visible on asphalt over concrete	Exists	na	na		see *(4)
Shoving	Pile up of asphalt in waves	Exists	na	na		see *(4)
Bleeding	Or Flushing. Oil appearance from Asphalt	Exists	na	na		see *(4)
Polished Aggregate	Polished appearance of aggregate from wearing.	Exists	na	na		see *(4)
Rutting	A rut is a longitudinal surface depression in the wheel path. It may have associated transverse displacement.	Not applicable - see Roughness Table -Direct Input	Not applicable - see Roughness Table -Direct Input	Not applicable - see Roughness Table -Direct Input	Not applicable - see Roughness Table - Direct Input	Not applicable - see Roughness Table -Direct Input

Calculations used in Output Table.

* Mandli's DIGILOG/PHOTOLOG images are taken at 500 frames per mile or 10.56 foot intervals. Routes are rated using the Distress Writer. Distress that is seen within the bottom of the image is recorded with a "click".

* The database tables contain distress data reported in 528 ft. (0.1 mi.) increments.
There are 50 frames for every 0.1 mile and each of these frames are broken into four quadrants.

Distresses are transferred into percents (OF THE 528 FT SECTION) by multiplying by a given factor.

*(1) **Transverse Cracking** data is equal to the sum of all cracks observed over the 50 frames, but the ceiling value will not exceed 100 (meaning that there are at least 100 transverse cracks of that severity in those 50 frames).

*(2) The values of **LWP, LNWP & Fatigue** are totaled over 50 frames, multiplied by a scaling number, and rounded to the nearest integer. (this converts 8 clicks to 100%)

*(3) The values of **Block, Patching, Raveling & Lane-Shoulder Drop off** are totalled over 50 frames, multiplied by a scaling number, and rounded to the nearest integer. (this converts 4 clicks to 100%)

*(4) The value of Potholes, Reflection Cracking, Shoving, Bleeding, and Polished Aggregate is a 1 (exists) for each frame that has an occurence of this distress.

Figure 4-26 (Continued) Distresses collected by Mandli for asphalt concrete pavements

Distress Type	Distress Description	Severity			Method of Measurement	
		Low	Medium	High	LTPP-SHRP Rating Method	* Mandli's Rating Methods
LTTP-SHRP	LTTP-SHRP	S1	S2	S3		Distress Writer
Number of Slabs	Count the number of slabs in the concrete section being rated					One click for each slab
Corner Breaks	A portion of the slab separated by a crak, which intersects the adjacent transverse and logitudinal joints, describing approximately a 45-degree angle with the direction of traffic. The of the sides is from 0.3 m to one-half the width of the slab on eaach side of the corner.	Crack is not spalled for more than 10 percent of the length of the crack; there is no measurable faulting; and the corner pice is not broken into two or more pieces and has no loss of material and no patching.	Crack is spalled at low severity for more than 10 percent of its total length; or faulting of crack or joint is <13mm; and the corner piece is not broken into two or more pieces.	Crack is spalled at moderate to high severity for more than 10 percent of its total length; or faulting of the crack or joint is >=13mm; or the corner piece is broken into two or more pieces or contains patch material.	Record number of corner breaks at each severity level. Corner breaks that have been repaired by completely removing all broken pieces and replacing them with patching material should be rated as a patch. If the boundaries of the corner break are visible, then also rate as a high severity corner break.	One click for each slab affected.
Durability Cracking	Closely spaced crescent-shaped hairline cracking pattern. Occurse adjacent to joints, cracks, or free edges; initiating in slab corners. Dark coloring of the cracking pattern and surrounding area.	"D" cracks are tight, with no loose or missing pieces, and no patching is in the affected area.	"D" cracks are well-defined, and some small pieces are loose or have been displaced.	"D" cracking has a well-developed pattern, with a significant amount of loose or missing material. Displaced pieces, up to 0.1m^2, may have been patched.	Record number of slabs with "D" cracking and square meters of area affected at each severity level. The slab and affected area severity rating is based on the highest severity level present for at least 10 percent of the area affected.	One click for each slab affected.
Longitudinal Cracking	Cracks that are predominantly parallel to the pavement centerline.	Crack widths <3mm, no spalling and no measurable faulting; or well-sealed and with a width that cannot be determined.	Crack widths >=3mm and <13mm; or with spalling <75mm; or faulting up to 13mm.	Crack widths >=13mm; or with spalling >=75mm or faulting >=13mm.	Record length in meters of longitudinal cracking at each severity level. Also record length in meters of longitudinal cracking with sealant in good condition at each severity level.	1 click = one crack covering 25% of the image frame length. 2 clicks = the crack goes 1/2 of the frame length. 3 clicks = the crack goes 3/4 of the frame length. 4 clicks = the crack goes the entire frame length. 5 clicks = a second crack is started covering 1/4 of the frame length. 6 clicks = the second crack covers 1/2 of the frame length. 7 click = the second crack covers 3/4 of the frame length. 8 clicks = the second crack covers 100% of the frame length...."(2)
Transverse Cracking	Cracks that are predominantly perpendicular to the pavement centerline.	Crack widths <3mm, no spalling and no measurable faulting; or well-sealed and the width cannot determined.	Crack widths >=3mm and <6mm; or with spalling <75mm; or faulting up to 6mm.	Crack widths >=6mm; or with spalling >=75mm or faulting >=6mm.	Record number and length of transverse cracks at each severity level. Rate the entire transverse crack at the highest severity level present for at least 10 percent of the total length of the crack.	One click per occurance. "(1)
Transverse Joint Seal Damage	Joint seal damage is any condition which enables incompressible materials or water to infiltrate the joint from the surface.	Joint seal damage exists over less than 10 percent of the joint.	Joint seal damage exists over 10-50 percent of the joint.	Joint seal damage as described above exists over more than 50 percent of the joint.	Indicate whether the transverse joints have been sealed (yes or no). If yes, record number of sealed transverse joints at each severity level. Any joint seal with no apparent damage is considered to be low severity.	One click for each slab affected.
Spalling of Transverse Joints	Cracking, breaking, chipping, or fraying of slab edges within 0.3m from the face of the transverse joint.	Spalls <75mm wide, measured to the face of the joint, with loss of material, or spalls with no loss of material and no patching.	Spalls 75mm to 150mm wide, measured to the face of the joint, with loss of material.	Spalls >150mm wide, measured to the face of the joint, with loss of material, or broken into two or more pieces, or contains patch material.	Record number of affected transverse joints at each severity level. A joint is affected only if the total length of spalling is 10 percent or more of the length of the joint. Rate the entire transverse joint at the highest severity level present for at least 10 present for at least 10 percent of the total length of the spalling.	One click for each slab affected.
Spalling of Longitudinal Joints	Cracking, breaking, chipping, or fraying of slab edges within 0.3m from the face of the longitudinal joint.	Spalls <75mm wide, measured to the face of the joint, with loss of material, or spalls with no loss of material and no patching.	Spalls 75mm to 150mm wide, measured to the face of the joint, with loss of material.	Spalls >150mm wide, measured to the face of the joint, with loss of material, or broken into two or more pieces, or contains patch material.	Record length in meters of longitudinal joint affected at each severity level. Only record spalls that have a length of 0.1m or more. Spalls that have been repaired by completely removing all broken pieces and replacing them with patching material should be rated as a patch. If the boundaries of the spall are visible, then also rate as a high severity spall.	One click for each slab affected.
Longitudinal Joint Seal Damage	Joint seal damage is any condition which enables incompressible materials or water to infiltrate the joint from the surface.	Exists	N/A	N/A	Record number of longitudinal joints that are sealed (0, 1, 2). Record total length of sealed longitudinal joints with joint seal damage. Individual occurrences are recorded when at least 1m in length	One click for each slab affected.
Patching	A portion, greater than 0.1m^2, or all of the original concrete slab that has been removed and replaced, or additional material applied to the pavement after original construction.	Patch has low severity distress of any type; and no measurable faulting or settlement; pumping is not evident.	Patch has moderate severity distress of any type; or faulting or settlement up to 6mm; pumping is not evident.	Patch has a high severity distress of any type; or faulting or settlement >=6mm; pumping may be evident.	Record number of patches and square meters of affected surface area at each severity level, recorded separately by material type - rigid versus flexible. For slab replacement, rate each slab as a separate patch and continue to rate joints.	One click per 25% or less of the image area. 1 click = 1-25% of the section is covered. 2 clicks = 26%-50% of the section is covered. 3 clicks = 51-75% of the section is covered. 4 clicks = 76-100% of the section is covered...."(3)

Figure 4-27. Distresses collected by Mandli for PCC pavements.

Distress Type	Distress Description	Severity			Method of Measurement	
		Low	Medium	High	LTPP-SHRP Rating Method	* Mandli's Rating Methods
LTTP-SHRP	LTTP-SHRP	S1	S2	S3		Distress Writer
Map Cracking	A series of cracks that extend only into the upper surface of the slab. Larger cracks frequently are oriented in the longitudinal direction of the pavement and are interconnected by finer transverse or random cracks.	Exists	N/A	N/A	Record the number of occurrences and the square meters of affected area.	One click per 25% or less of the image area. 1 click = 1-25% of the section is covered. 2 clicks = 26%-50% of the section is covered. 3 clicks = 51-75% of the section is covered. 4 clicks = 76-100% of the section is covered....*(3)
Scaling	The deterioration of the upper concrete slab surface, normally 3mm to 13mm, and may occur anywhere over the pavement.	Exists	N/A	N/A	Record the number of occurrences and the square meters of affected area.	One click for each slab affected.
Polished Aggregate	Surface mortar and texturing worn away to expose coarse aggregate.	Exists	N/A	N/A	Record square meters of affected surface area.	One click for each slab affected.
Pop-Outs	Small pieces of pavement broken loose from the surface, normally ranging in diameter from 25mm to 100mm, and depth from 13mm to 50mm	Exists	N/A	N/A	Not Recorded	
Blow-ups	Localized upward movement of the pavement surface at transverse joints or cracks, often accompanied by shattering of the concrete in that area.	Exists	N/A	N/A	Record the number of blow-ups	One click for each slab affected.
Lane-to-Shoulder Drop-off	Difference in elevation between the edge of slab and outside shoulder; typically occurse when the outside shoulder settles.	Exists	N/A	N/A	Measure at the longitudinal construction joint between the lane edge and the shoulder. Record to the nearest millimeter at 15.25m intervals; if the traveled surface is lower than the shoulder, record ad a negative value.	One click for each slab affected. *(4)
Lane-to-Shoulder Separation	Widening of the joint between the edge of the slab and the shoulder	Exists	N/A	N/A	Record to the nearest millimeter at intervals of 15.25m along the lane-to-shoulder joint. Indicate whether the joint is well-seald (yes or no) at each location.	One click for each slab affected. *(4)
Water Bleeding	Seeping or ejection of water from beneath the pavement through cracks. In some cases, detectable by deposits of fine material left on the pavement surface, which were eroded (pumped) from the support layers and have stained the surface.	Exists	N/A	N/A	Record the number of occurrences of water bleeding and pumping and the length in meteres of affected pavement with a minimum length of 1m.	One click for each slab affected.

Calculations used in Output Table.

* Mandli's DIGILOG/PHOTOLOG images are taken at 500 frames per mile or 10.56 foot intervals. Routes are rated using the Distress Writer. Distress that is seen within the bottom of the image is recorded with a "click".

* The database tables contain distress data reported in 528 ft. (0.1 mi.) increments. There are 50 frames for every 0.1 mile and each of these frames are broken into four quadrants.

Distresses are **transferred into percents (OF THE 528 FT SECTION) by multiplying by a given factor.**

*(1) The sum of all cracks observed over the 50 frames, but the ceiling value will not exceed 100 (meaning that there are at least 100 transverse cracks of that severity in those 50 frames).

*(2) The values of **Longitudinal Cracking** are totaled over 50 frames, multiplied by a scaling number, and rounded to the nearest integer. (this converts 8 clicks to 100%)

*(3) The values of **Patching and Map-Cracking** are totalled over 50 frames, multiplied by a scaling number and rounded to the nearest integer. (this converts 4 clicks to 100%)

*(4) The values of **Lane-to-Shoulder Separation and Lane-to-Shoulder Drop-off** are the sum of all occurences. If rated, severity is at least medium severity.

Figure 4-27 (Continued) Distresses collected by Mandli for PCC pavements.

However, a difficulty to translate the distresses arises from the different definitions of severity levels in each protocol. In LTPP, the severity levels for longitudinal cracks are:

- Low severity: A crack with a mean width ≤ 6 mm (1/4 in); or a sealed crack with sealant material in good condition and with a width that cannot be determined.
- Moderate severity: Any crack with a mean width > 6 mm (1/4 in) and ≤ 19 mm (3/4 in); or any crack with mean width ≤ 19 mm (3/4 in) and adjacent low severity random cracking.
- High severity: Any crack with a mean width > 19 mm; or any crack with a mean width ≤ 19 mm and adjacent moderate to high severity random cracking.

In contrast, the severerity levels in ASTM D6433 are defined as:

- Low severity: One of the following conditions exists:
    - Non-filled crack with less than 3/8 in (100 mm).
    - Filled crack of any with (filler in satisfactory condition.
- Medium severity: One of the following conditions exists:
    - Non-filled crack width is 3/8 in to 3 in. (10 to 76 mm).
    - Non-filled is up to 3 in (76 mm) sorrounded by light and random cracking.
    - Filled crack is of any width sorrounded by light random cracking.
- High severity: One of the following conditions exists:
    - Any crack filled or non-filled sorounded by medium or high severity random cracking.
    - Non-filled crack over 3 in. (76 mm).
    - A crack of any width where a few inches of pavement around the is severely broken.

Clearly, there is no single one-to-one equivalence between these disparate definitions of severity. Some differences for other distresses could also be noted. Therefore, when data are

collected according to LTPP, different PCI values will be obtained depending on how the translations from LTPP distresses to ASTM D6433 distresses are made. If the data are translated differently by different people on different years (or worse yet, if the distress identification protocol is changed) then PCI values would also change.

A 1999 LTPP distress data variability study ([29], [30]) investigated, among other things, the effects of the variability within distress types and severity levels on the PCI. When comparing the variability on PCI vs. the variability in individual distresses, the authors of the study found that there was a general improvement in the agreement among individual raters, the means of different groups of raters evaluated on different workshops, and a reference value. This was an expected result as the PCI computational procedure tends to supress the sensitivity of the PCI to variability in individual distress ratings. The authors acknowledged that distress types had to be combined and that a few minor assumptions had to be made (e.g., severity levels were assumed to be the same for a few distress types.)

Thus, it is apparent that as long as the same set of assumptions for data translation are used, one would get relatively consistent PCI values over time. Now, this says nothing about how the computed PCI would differ from a PCI computed collecting the distresses according to the ASTM D6433 procedure instead of the LTPP procedure. For the example of longitudinal/transverse cracking mentioned earlier, the deduct value for a given distress density of high severity cracking is about twice the corresponding value for medium severity. For a more specific example, consider a situation with 2,000 ft/mile of longitudinal cracking. According to the ASTM distress density definition for a 12 ft lane, this corresponds to a density of $2000/(5280\times12)\times100 = 3.2\%$, which in turn corresponds to deduct values of about 18 and 36 for medium and high severity cracking, respectively. Since more than one distress would typically be present and some proportion of each distress severity would be correctly classified, the differences are not expected to be as large as in the above example. Nevertheless, what the example demonstrates is that the differences can be substantial in some situations. Many factors are involved so there is no single rule to estimate the effect on PCI. However, the PCI obtained with distresses measured with a different protocols would generally be different from the PCI computed with distresses measured according to ASTM D6433. Also, the relative weighing of the different distresses could also change.

In conclusion, for PCI calculation and use in PMS, it is desirable to measure distresses according to ASTM D6433. This would result in "true" PCI values in the spirit of the developers of the index. However, an important consideration for selecting a particular method for the distress survey is its intended use. The distress information at HDOT has at least two other potential uses for which the SHRP method is more compatible. One is the calibration of the MEPDG and the other is reporting for the Highway Performance Monotoring System (HMPS). In both of these cases, distresses collected with the SHRP protocol are easier to use. Thus, if ASTM D6433 is adopted, minor adaptations would have to made to measure the information needed for HPMS and calibration of the MEPDG.

If HDOT continues the use of the LTPP protocol, it must do so consistenly over time so that PCI from different years can be used to study trends without introducing artificial noise[19]. It must also document any adaptation of the protocol and the reasons for it (for example, use of a ½ in instead of a ¾ in criterion to discriminate between medium and high severity cracks. It must also specify how to convert distresses in one protocol to the other for the calculation of PCI. Finally, it may also be necessary to adjust threshold values used in PMS decisions to account for the fact that the values computed are not "true" PCI values. It must be recognized that once translation of distresses are performed the resulting index is really a modified index. This report later describes how the conversions were made with the 2006/2009 Planning Branch data.

In summary, collecting data according to ASTM D6433 is recommended for PCI calculations but using the SHRP or LTPP Distress Identification Manual would still be acceptable as long as the same method is used in all future surveys and the use of data transformations and other assumptions are consistently used over time. It is also extremly important that all transformations and assumptions are well documented.

4.3.2.2 Analysis of 2006, 2009, and 2010 Planning Branch Data

The data collected by Mandli for the Planning Branch in 2006 and 2009 were also used to assess PCI. The data for 2006 and 2009 were available for practically the whole network. Data were collected also in 2010 but they were more limited because only distresses required for

[19] This is, of course, if HDOT decides that using a condition index to summarize the distresses is desirable.

HPMS reporting were collected. Therefore, the 2010 data by themselves could not be used to compute PCI. Assuming little changes from 2009 to 2010 in the other distresses, a PCI could be computed but given that this procedure is questionable, some results are only mentioned briefly in the next section. The following paragraphs describe the characteristics of the 2006 and 2009 data.

As explained earlier, Mandli delivered distress data collected from forward videolog images mostly in 0.1 mi long segments[20]. The actual data were collected for each frame, every 0.002 mi (10.56 ft). Although much more voluminous, use of these data would have been more convenient for the assignment of distresses to pavement management sections. Assignment of the data collected in 0.1 mi segments to pavement management sections of varying lengths and with beginning and end points not necessarily located in 0.1 mi multiples still poses some challenges, particularly for relatively short sections. Although the database delivered by Mandli contains a table with the raw data for each frame, there was no information to link the records in this table with the appropriate milepoint. Therefore, only the processed 0.1 mi segment information was used. Each 0.1 lane-mile segment can be considered a sampling unit.

The program created to visualize the historical HDOT pavement condition data was adapted to process the information from Mandli with two purposes. One was the computation of PCI outside any PMS program for variance reporting and the second was to feed distress information to PAVER™ (one of the PMS programs being evaluated) in an appropriate format. Once the data were translated into distress densities for PCI calculation, computing distress quantities to input in PAVER™ was straightforward (for those distresses not already in the appropriate format).

[20] At route ends, there are sections smaller than 0.1 mi long. In other situations, some sections were longer than 0.1 mi. As in any large data collection effort, some errors (mostly human errors) can be expected. In a few cases, some sections were clearly miscoded, as the section lengths were much larger than 0.1 mi (sometimes these were tenths or hundredths of miles long) and overlapped the normal 0.1 mile segments. Detecting these problem was essential for proper interpretation of the data and importing it into PMS software.

4.3.2.2.1 Computation of PCI

4.3.2.2.1.1 Asphalt Concrete Pavements

To compute PCI using the data collected by Mandli for the planning branch, translation of the reported distresses into those in ASTM D6433 was required. To accomplish this, several assumptions were needed and they are documented in this section. In the rest of this subsection, ASTM D6433 will be referred to simple as ASTM for short. Several equations are developed to compute the distress densities required to calculate the corresponding deduct values. Many of these equations are unit dependent so care should be taken to use the indicated units.

Distresses for which an area is required to be measured such as fatigue cracking, patching, and raveling required no transformation. The percentages reported in the database for all these correspond directly to their corresponding distress densities.

Both, LTPP and ASTM, require reporting the *length* of longitudinal cracking. However, as discussed before, LTPP differentiates between wheel path (load associated) and non-wheel path (non-load associated) longitudinal cracking. In contrast, in ASTM, longitudinal cracking is combined with transverse cracking because they are both presumed to be non-load associated. In the database provided by Mandli, longitudinal cracking (both wheel path and non-wheel path) was given as percentage, with 100% representing twice the length of the section. Thus, for longitudinal wheel path cracking, 100% is equivalent to both wheel paths being cracked in their full length and 50% is equivalent one wheel path being cracked entirely. These percentages can be easily converted into length for sections of known dimensions.

To compute the PCI, it was assumed that wheel path longitudinal cracking was caused by loading (which is the typical cause) and thus longitudinal wheel path cracking was considered as fatigue cracking. Since the extent of fatigue cracking in ASTM is measured by the area affected, a conversion from length (or percentage as given in the database) to area was required. For the conversion, the recommendation in the guide for local calibration of the MEPDG [31] of multiplying the cracking lengh by 1 ft was used. Then, the area of wheel path longitudinal cracking so computed was added to the area of fatigue cracking for each segment (equivalently, the distress densities were added.)

Since the wheel path longitudinal cracking was expressed in percentage with 100% representing both wheel paths entirely cracked, its contribution to the distress density of fatigue cracking (identified with the subscript AC for Alligator Cracking) was computed for standard 12 ft lanes as:

$$\begin{aligned} DD_{AC\_from\_LWPC} &= \frac{2 \times Segment\,Length \times 1\ ft \times Percentage}{Segment\,Area} \\ &= \frac{2 \times Segment\,Length \times 1\ ft \times Percentage}{Segment\,Length \times Lane\,Width} \\ &= \frac{2 \times Percentage}{12} \\ &= \frac{Percentage}{6} \end{aligned} \qquad (4\text{-}1)$$

In the above equation, the part of the subscript *LWPC* stands for Longitudinal Wheel Path Cracking. Notice that the same equation is valid when using SI units since the 1 ft. in the numerator and the lane width in the denominator would both be affected by exactly the same factor. The value obtained with equation (4-1) was added to the reported percentage for fatigue cracking to obtain the total distress density from which the corresponding deduct value was obtained for fatigue cracking.

The above transformation was done for each severity level. Since the definitions of severity levels in LTPP and ASTM are different, consideration was given to converting the part of the reported values from one severity level into other severity levels. For example, the value reported for high severity cracks in LTPP (crack width > 19 mm or any crack width < 19 mm and adjacent moderate to high severity random cracking) would typically include some moderate cracking (say 70%) and some high severity cracking (say, 30%) as defined in ASTM. However, any such proportioning of the distress would have been arbitrary and debatable without data to back it up. Furthermore, since the distresses are collected visually, judgment of severity levels is quite approximate anyway. Therefore, it was decided to calculate the index with the severity definitions in LTPP recognizing that the resulting PCI does not conform to the ASTM standard. This is important because if HDOT changes to ASTM or some other distress survey protocol, the computed PCI value would also be affected. The same assumption was made for all distresses on

which severity levels were identified. For a few distresses, no severity was identified. The assumption made in each of those cases is discussed for each particular situation.

Edge cracking was reported as a percentage with 100% representing the section length. Since the distress density (DD) definition in ASTM for distresses that are measured in length is DD = length/area × 100, the value corresponding to edge cracking was computed as:

$$\begin{aligned} DD_{EC} &= \frac{Segment\,Length \times Percentage}{Segment\,Area} \\ &= \frac{Segment\,Length \times Percentage}{Segment\,Length \times LaneWidth} \\ &= \frac{Percentage}{12}\frac{1}{ft} \end{aligned} \tag{4-2}$$

Unlike the equation for computing the distress density contributed by longitudinal cracking, equation (4-2) is only valid for US units (notice that the resulting value has units of 1/ft.). A different equation and resulting values must be used for SI units. Nevertheless, the computed deduct values are the same no matter the system of units used because different charts (deduct value curves) are applicable for US and SI units. In this report, US customary units have been used, but it is important to have this fact in mind if other units are used.

Essentially the same conversion, Equation (4-2), was needed for computing the distress density for Lane/Shoulder Drop-Off.

The distress density for longitudinal non-wheel path cracking was computed as:

$$\begin{aligned} DD_{LNWPC} &= \frac{2 \times Segment\,Length \times Percentage}{Segment\,Area} \\ &= \frac{2 \times Segment\,Length \times Percentage}{Segment\,Length \times LaneWidth} \\ &= \frac{Percentage}{6}\frac{1}{ft} \end{aligned} \tag{4-3}$$

Although the result in equation (4-3) appears identical to that in equation (4-1), this is only because in equation (4-1) a width of 1 ft. was assumed to convert linear cracking into area. For a different width, the numerical values provided by the equations would not be same. In

addition, as for equation (4-2), equation (4-3) is unit dependent, so the results should be used only with charts or deduct value curves in US units.

Transverse cracking was reported by Mandli as the number of occurrences in a segment. In order to convert these into a distress density as defined in ASTM, each transverse crack was assumed to be as long as the lane width, which was further assumed to be 12 ft. With this assumption, the distress density for transverse cracking (TC) can be computed as:

$$\begin{aligned} DD_{TC} &= \frac{Occurrences \times 12\ ft}{Segment\ Area} \times 100 \\ &= \frac{100 \times 12\ ft \times Occurences}{Segment\ Length(\ ft) \times 12\ ft} \\ &= \frac{100 \times Occurrences}{Section\ Length(\ ft)} \end{aligned} \qquad (4\text{-}4)$$

Notice that the assumption of 12 ft. lane widths is immaterial since the value appears in the numerator and the denominator. Equation (4-4) (as any of the equations for computing distress densities for distresses measured in length) is once again unit dependent. Furthermore, to use the deduct values from the charts in US customary units in ASTM, the section length must be expressed in ft. With the results from equations (4-3) and (4-4), the distress density for longitudinal and transverse cracking was computed as $DD_{L\&T} = DD_{LNWPC} + DD_{TC}$.

Joint reflection cracking is also measured as the number of occurrences in a segment. Again, assuming that these cracks go across the whole lane width (assumed to be 12 ft.), then equation (4-4) can also be used to compute their distress density (DD_{JRC}).

The distress density for Potholes (DD_{PH}), which is measured in number of occurrences was computed as:

$$
\begin{aligned}
DD_{PH} &= \frac{Occurrences}{Segment\,Area} \times 100 \\
&= \frac{100 \times Occurences}{Segment\,Length(\,ft) \times 12\ ft} \\
&= \frac{8.33 \times Occurrences}{Section\,Length(\,ft)}
\end{aligned}
\tag{4-5}
$$

Shoving was also measured in terms of number of occurrences. However, ASTM requires the *area* with shoving. Thus, it was assumed that each occurrence of shoving had an area of 12 sq. ft. Furthermore, since no severity level was identified, it was further assumed that all shoving had medium severity. Therefore, the distress density for shoving (DD_{Shove}) was computed as:

$$
\begin{aligned}
DD_{Shove} &= \frac{Occurrences \times 12\ ft^2}{Segment\,Area} \times 100 \\
&= \frac{100 \times 12\ ft^2 \times Occurences}{Segment\,Length(\,ft) \times 12\ ft} \\
&= \frac{100 \times Occurrences}{Section\,Length(\,ft)}\ ft
\end{aligned}
\tag{4-6}
$$

Bleeding presents yet another situation. Again, no severity was identified so for this distress a low severity was assumed in each case. Further, for each occurrence it was assumed that the area of bleeding was equal to the area covered by the corresponding frame, i.e., 10.56 ft. x 12 ft. With this assumption, the distress density for bleeding is computed as:

$$
\begin{aligned}
DD_{Bleed} &= \frac{Occurrences \times 10.56 \times 12\ ft^2}{Segment\,Area} \times 100 \\
&= \frac{100 \times 10.56 \times 12\ ft^2 \times Occurences}{Segment\,Length(\,ft) \times 12\ ft} \\
&= \frac{1056 \times Occurrences}{Section\,Length(\,ft)}\ ft
\end{aligned}
\tag{4-7}
$$

The distress density for Polished Aggregate (PA) was also computed using equation (4-7) with DD_{PA} instead of DD_{Bleed}. A medium severity was assumed for this distress.

To include rutting in the PCI calculations, additional processing of the data was needed. Unlike the other asphalt concrete distresses, rutting was provided in a different table with different data intervals. Rutting was reported every 0.01 mi instead of every 0.10 mi. Thus, the data needed to be consolidated. In addition, ASTM indicates that for each severity level, rutting should be measured in squared feet of surface area. Low severity ruts are defined as those with a mean rut depth between 1/3 in. and ½ in., medium severity ruts are greater than ½ in. and up to 1 in., and high severity ruts are greater than 1 in. The ASTM D6433 standard is silent about how the area should be measured.

In order to include rutting in the computation of PCI, the following transformations of the data were performed. The rut depth for each wheel path for every 0.01 mile data interval was analyzed to determine its severity level based on the mean rut depth. Whenever a rut at a given severity level was detected, a width of 2 ft. was assigned to it. Then for each segment, the sum of the areas of rutting at each severity level were obtained (2ft × 10.56ft for one wheel path or twice this product for both wheel paths with rutting at the given severity level.) With these areas on hand, computing the distress densities is straightforward. Unlike the previous transformations, which were done with a Visual Basic program, these were performed with a query in Access. One last data manipulation step involved creating another query to join the rutting information with the other distress information.

Although the descriptions are probably quite tedious to follow, it was considered important to document the assumptions made to interpret the data. It is very common to find very loose definitions of how data are obtained and processed. That alone can introduce significant noise and/or biases in trends. Although technological advances are making data collection at the network level more practical, these changes also create challenges and keep the documentation of details as relevant as ever.

4.3.2.2.1.2 PCC Pavements

The analysis of the PCC distress survey data was similar to that used for HMA pavements. Again, to conform to the requirements for PCI calculation, several transformations of the data and assumptions were required. The following paragraphs described the transformations and assumptions used for individual distresses.

In ASTM, blow-ups are rated as low, medium, or high severity depending on the effect they have on ride quality. In contrast, in LTPP only the number of blow-ups are recorded. Since this distress is almost non-existent in Hawaiian PCC pavements, for the few cases in which they were observed they were assumed to be of low severity. The information for this distress type is already provided in the appropriate format so no translation is required. ASTM requires counting the number of slabs affected by blow-ups, which is what is reported in the database created by Mandli.

Corner breaks, divided slabs, longitudinal cracks, durability cracking, polished aggregates, and pumping are also counted by the number of slabs affected by them. For example, if a slab has two or more corner breaks it is still quantified as one slab affected. A joint with pumping affects the two adjacent slabs[21]. The distress density is then computed by dividing this number by the number of slabs in the sampling unit.

From the information provided in the database by Mandli and assuming an average slab length of 15 ft., the computation of the distress density for blow-ups (DD_{BU}), corner breaks (DD_{CB}), and durability cracks (DD_{DC}) can be performed with the following equation:

$$\begin{aligned} DD &= \frac{Slabs affected}{Number of\ Slabs in Sampling Area} \times 100 \\ &= \frac{100 \times Slabs affected}{Segment Length(ft)/15\ ft} \\ &= \frac{6.67 \times Slabs affected}{Section Length(ft)}\ ft \end{aligned} \tag{4-8}$$

A divided slab is one divided by cracks into four or more pieces due to overloading and/or inadequate support. LTTP does not include divided slab as distress and thus it is not available in the database. However, the database contains the number of slabs affected by transverse cracking, which has been used here as proxy for divided slabs. Equation (4-8) can be used to compute its distress density. Actually, a more appropriate assignment of transverse cracks would be to the linear cracking discussed next since it includes longitudinal, transverse

[21] It is assumed that the proper number of slabs is provided. Notice that two transverse joints with pumping do not necessarily mean that four slabs were affected. If the joins are consecutive, only three slabs are affected.

and diagonal cracks. However, since for a given distress density the deduct values for divided slab are higher than for linear cracking, the assignment as divided slabs is a bit more severe.

As mentioned before, linear cracking includes longitudinal, transverse, and diagonal cracks. The number of slabs affected by these should be counted. Again, once a slab has one or more of these cracks, it is counted as one slab affected (unless they divide the slab into four or more pieces, in which case it is counted as a divided slab). Since the number of transverse cracks were conservatively counted as divided slabs, only slabs with longitudinal and diagonal cracks should be included as slabs with linear cracks. The database contains information for only longitudinal cracking and apparently, the same approach used to quantify longitudinal cracks in asphalt concrete pavements was used. It is not known what the logic for that decision was but it would have been desirable to count slabs with the distress instead. *This is indeed recommended for future surveys*. In order to use the longitudinal cracking information, the percentage of linear cracking in the database was assumed to give directly the percentage of slabs in the section with longitudinal cracks or the distress density. As discussed in chapter 8, to enter the information into PAVER^{TM}, the distress density was converted into a number of slabs with longitudinal cracks.

The number of slabs with joint seal damage were used to compute deduct values for joint seal damage. This is the only distress in which ASTM does not require computing a density of distress. Instead, the deduct values are computed directly from the severity level, which is based on the overall sealant's condition for a particular sample unit. Deduct values of 8, 4 or 2 are assigned for high, medium, and low severity levels, respectively. Since overall sealant's condition cannot be determined from the information provided, the following approximation was used. For segments with some seal damage reported, the severity level with the largest reported number of transverse joints with seal damage was used as the overall sealant's condition.

The percentage of patching in the database provided by Mandli gives an indication of the sample area patched. This is not necessarily the same as the percentage of slabs cracked, which is what ASTM computes as the distress density. Nevertheless, for lack of a better indicator, it was assumed the percent area cracked was the same as the percentage of slabs cracked. This value was used to estimate the distress density of the ASTM distress "Patching, Large (More Than 5 sq. ft.) and Utility Cuts".

Faulting was not collected until the 2010 survey, thus it could not be included in the PCI computation from the 2006 and 2009 surveys. This is a very important distress that should continue to be included in future surveys of PCC pavements. Its consideration in the 2010 survey was a welcomed addition. In the 2010 survey, faulting was reported for each 0.01 mi interval. Therefore, calculation at 0.1 mi intervals would require data manipulations to aggregate the data similar to those described for rutting in asphalt concrete pavements.

Similarly to what was done for asphalt concrete pavements, every 0.1 lane-mi segment was considered a sampling unit for PCI calculation.

4.3.2.3 PCI Histograms

After carrying out the data translations explained in the previous section, the PCIs were computed using the procedure described in ASTM D6433. This section presents a few observations about the histograms created with these data.

First, consider a general comparison between the 2006 and 2009 data. Figure 4-28 shows the histogram of PCI for all islands in 2006 and all types of roads: state roads (SR), ramps (RMP), service roads (SVR), frontage (FRO), and intermodal connectors (IMC). Figure 4-29 presents the same histogram but for 2009.

The left tails of the distributions are almost identical below a PCI of 50 but there are significant differences in the distributions for PCI values above 50. The mode, which in both cases is in the range of 90 to 100, is much higher for 2006 than for 2009. Correspondingly, the heights of the intermediate bars are higher for 2009. The magnitude of the change for the whole network in only three years appear quite substantial. Without information for the maintenance and rehabilitation work performed during those years[22], it is difficult to ascertain whether this is due to a lack of consistency of the data collected on these two years or whether it represents a real change in the network condition. The magnitude of the change appears too severe to be due solely to the latter. Nevertheless, the differences could have been caused, at least in part, by an

[22] The mining data available for the project contained information only until about 2006. Since several issues were detected with the reliability of original information, the data are currently been verified and updated. This will hopefully shed some light into the reasons for the substantial change from 2006 to 2009.

asphalt shortage that started on the islands in 2006 because one of the two local refineries stopped producing asphalt and by the significant economic slowdown during that period. The shortage affected asphalt paving in Hawaii until Asphalt Hawaii opened its Kalaeloa asphalt terminal in 2009. Therefore, at least partly, the above factor may have played a role in the substantial change between the two data collection surveys. In addition, as shown in the chart titles, the histograms are based on different mileages of the network; however, it is also unlikely that the additional mileage surveyed in 2009 could have caused such an important effect.

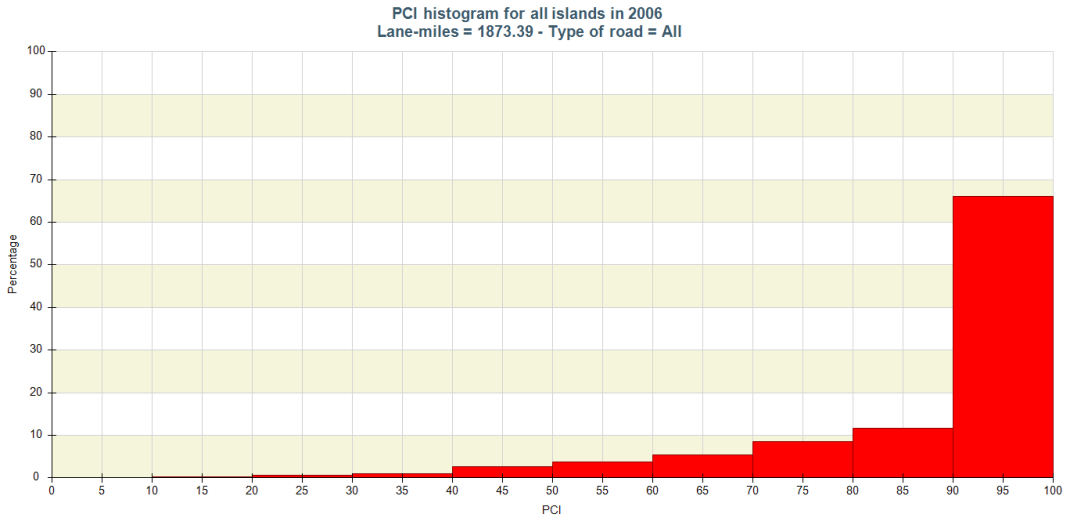

Figure 4-28. Histogram of the PCI observed on all islands in 2006.

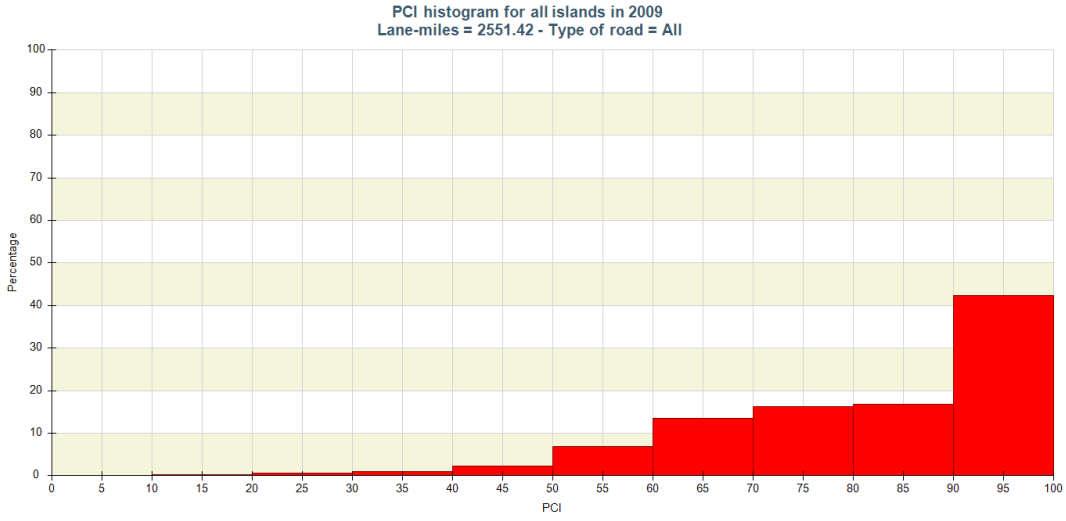

Figure 4-29. Histogram of the PCI observed on all islands in 2009.

As indicated earlier, pavement condition data were also obtained in 2010. However, only the distresses required for HPMS reporting were collected (longitudinal cracking, transverse cracking, fatigue cracking and rutting for asphalt concrete pavements and fatigue cracking (percent slabs cracked) and faulting for PCC pavements) [9].

The above distresses have in general an important effect on the calculation of PCI. Thus, they were merged with the rest of the distresses measured in 2009 to obtain a gross estimate of the PCI distribution in 2010. Since preservation type treatments have not been used much in the past in Hawaii, the resulting PCIs would provide an upper bound of the pavement condition, except for roads rehabilitated between 2009 and 2010, for which the computed PCI value would represent a lower bound. Figure 4-30 shows the resulting distribution. Despite the fact that many of the same (non-load-associated) distresses were used from 2009, this distribution looks a lot closer to the 2006 distribution than the one for 2009, which would indicate that substantial rehabilitation work was performed in 2009. This would need to be confirmed by HDOT records with updated pavement structural information from data mining activities.

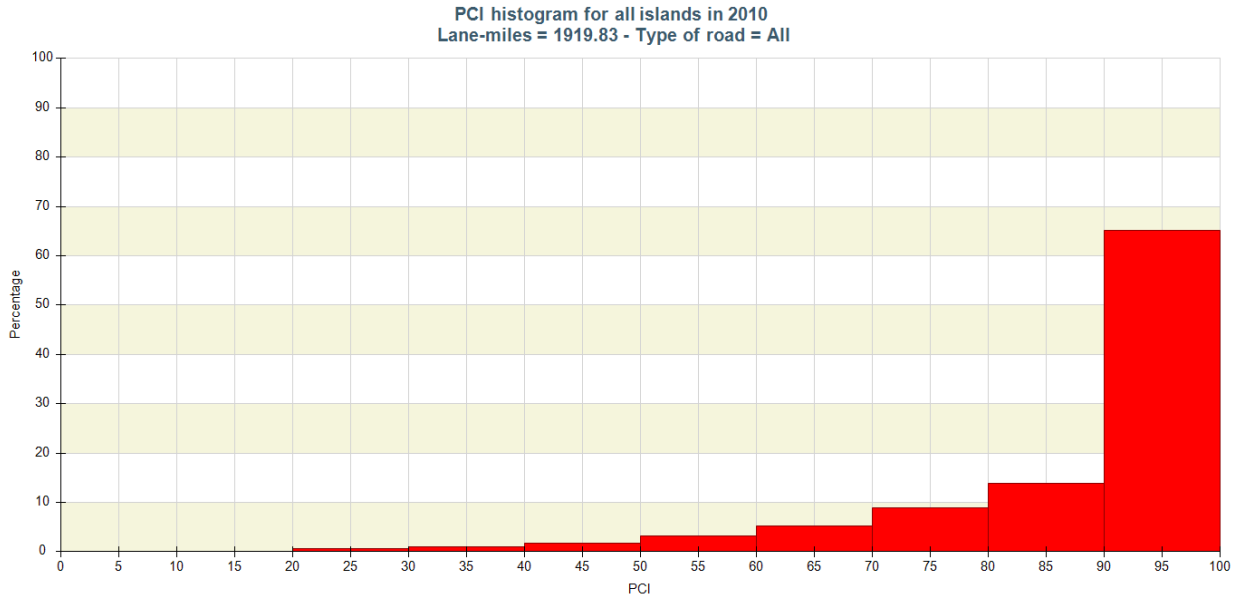

Figure 4-30. PCI distribution obtained by merging the distresses measured in 2010 with the rest of the distresses measured in 2009.

As shown Figure 4-31 for the 2009 data, the histogram can also be presented in terms of lane-miles in the vertical axis, which for some purposes may be more useful. Notice that except for the vertical scale, this is the same chart presented in Figure 4-29.

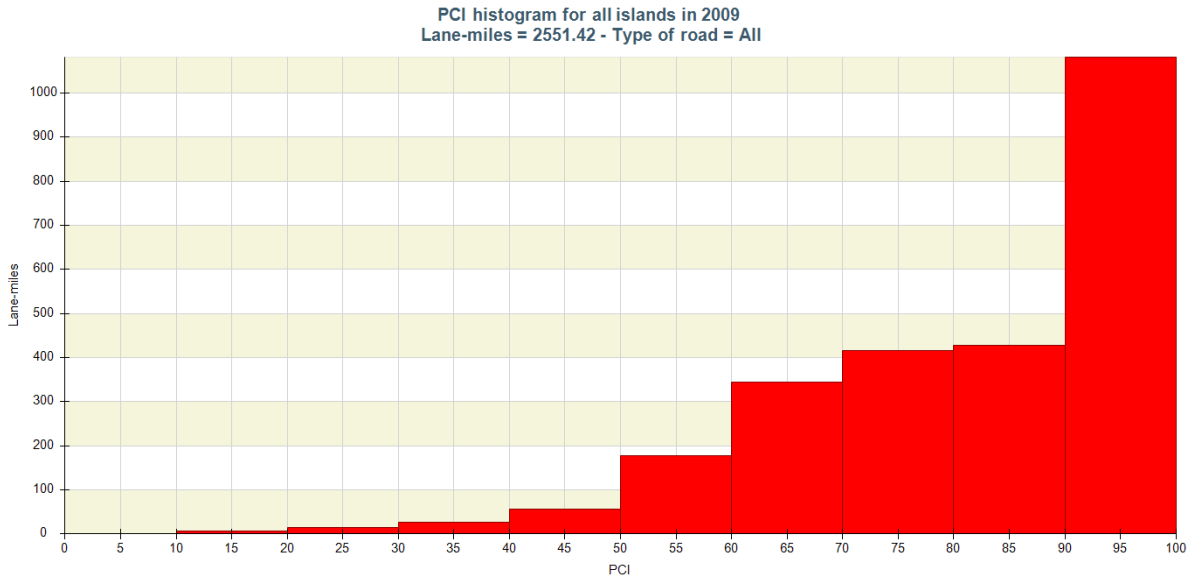

Figure 4-31. Presenting the PCI results in terms of lane-miles.

It is also convenient to be able to compare the histograms for the different islands and for the different road types. Figure 4-32 through Figure 4-35 show the histograms for all roads in 2009 obtained for the islands of Oahu, Hawaii, Kauai, and Maui, respectively. The figures are presented in the order of improving conditions in the highest PCI range. Clearly, the 2009 data indicate that the average condition in Maui is better than that in Oahu.

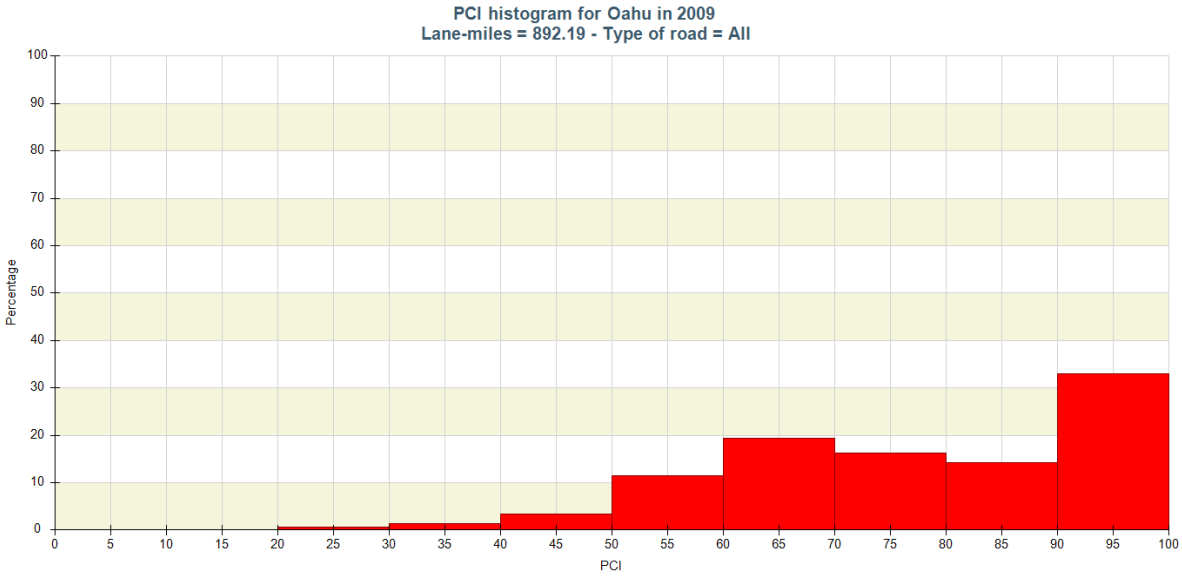

Figure 4-32. PCI distribution for all roads in Oahu in 2009.

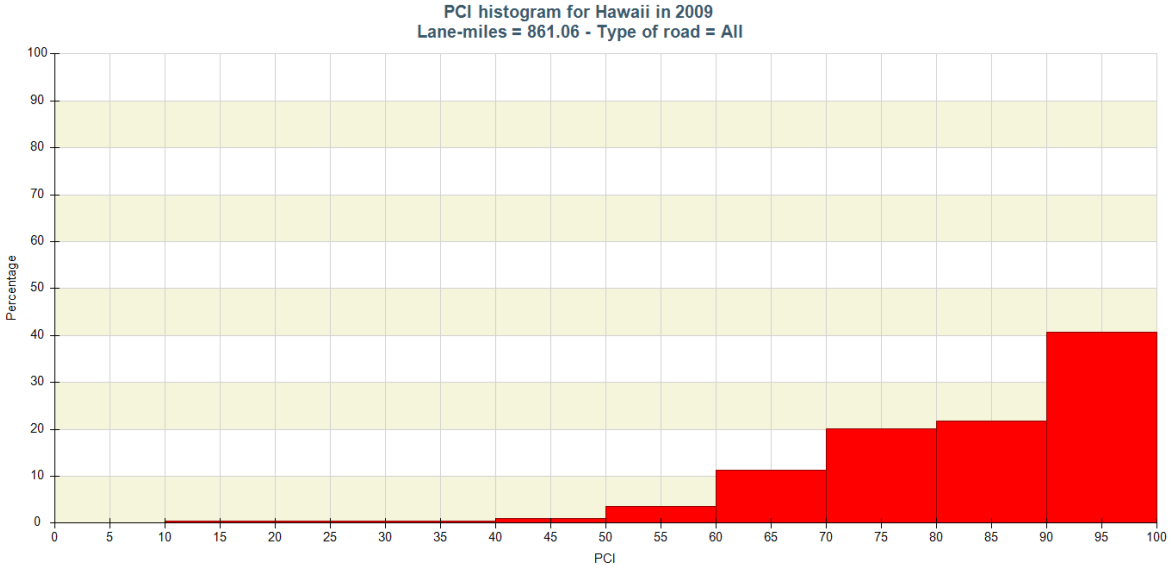

Figure 4-33. PCI distribution for all roads in Hawaii in 2009.

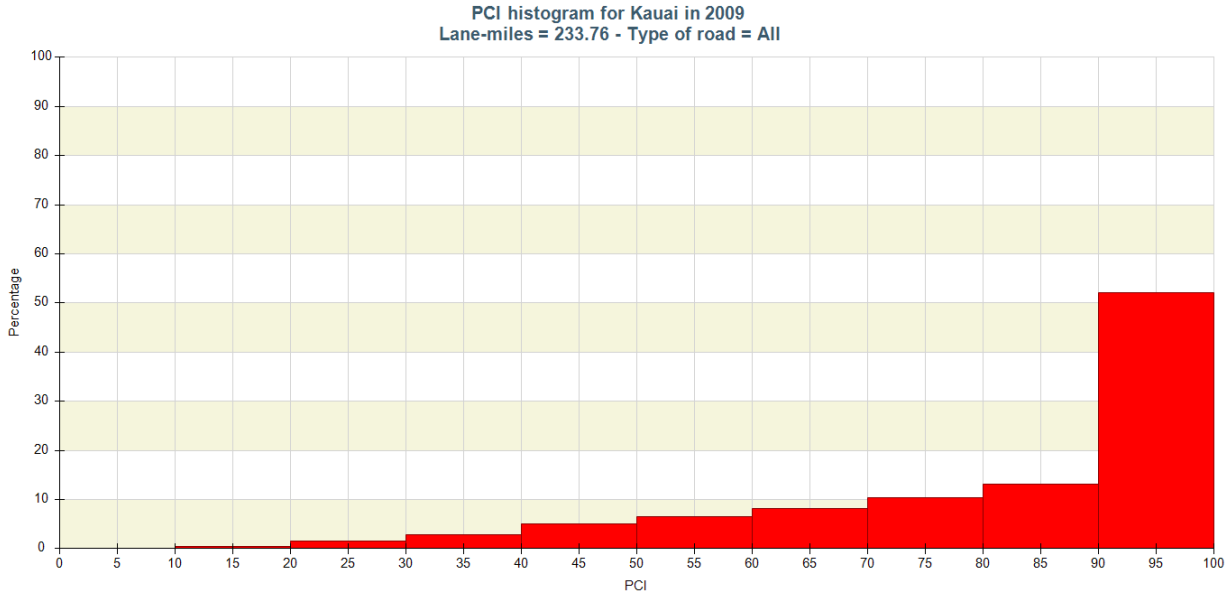

Figure 4-34. PCI distribution for all roads in Kauai in 2009.

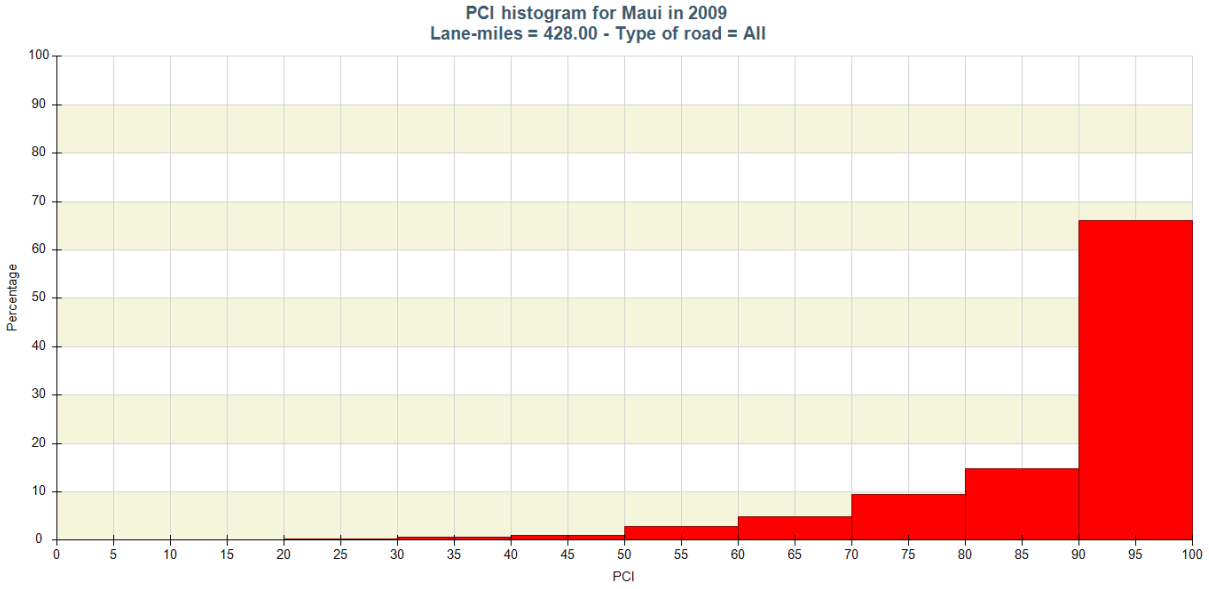

Figure 4-35. PCI distribution for all roads in Maui in 2009.

This type of analysis combined with reliable and up-to-date maintenance and rehabilitation records, if repeated in time, can be useful for reviewing budget allocations to

different districts as well as for reviewing the effectiveness of maintenace and rehabilitation practices.

Another convenient way of displaying information is by road types. For Oahu in 2009, Figure 4-36 through Figure 4-39, show the distributions of the PCI on state roads (SR), ramps (RMP), service road (SRV) and frontage roads (FRO), respectively. IMC roads are not displayed as the data for these added up to less than 5 miles. As most of the mileage in Oahu is contributed by state roads, not surprisingly, the PCI distribution for this type of roads look similar to that obtained for all roads (Figure 4-32.) The distribution for ramps also looks very similar but with a lower percentage in the top PCI range. Service and frontage roads exhibit generally lower conditions.

Finally, Figure 4-40 and Figure 4-41 show the distributions of PCI for PCC pavements in Oahu in 2009 for all roads and for ramps, respectively. It can be seen that PCC ramps are in generally worse condition than other PCC roads.

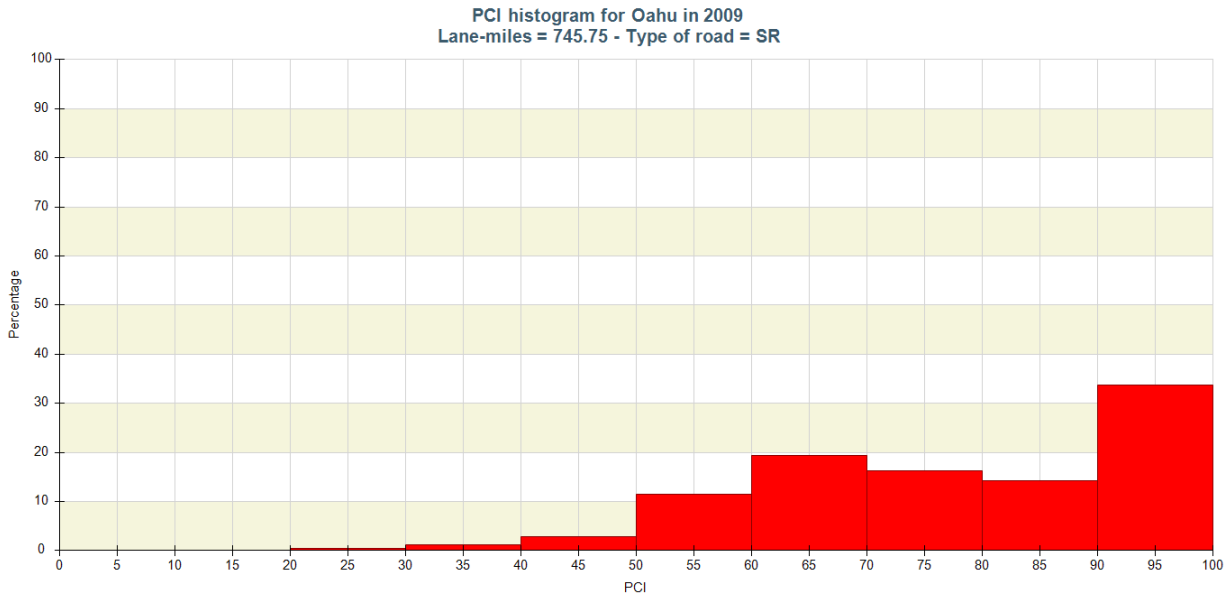

Figure 4-36. PCI distribution for state roads in Oahu in 2009.

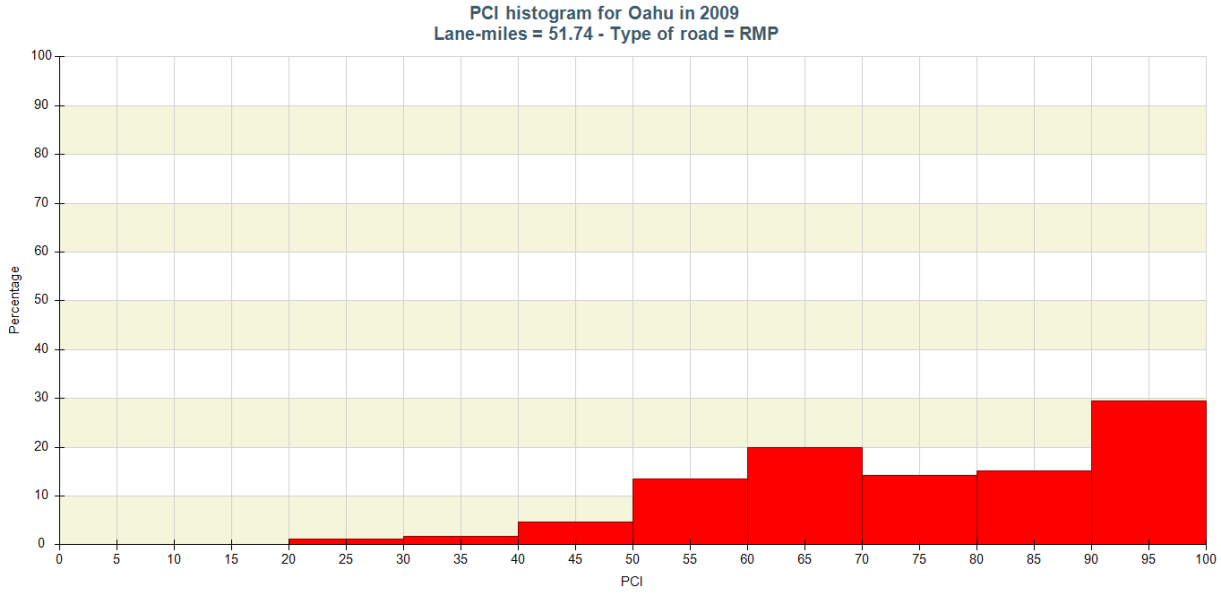

Figure 4-37. PCI distribution for ramps in Oahu in 2009.

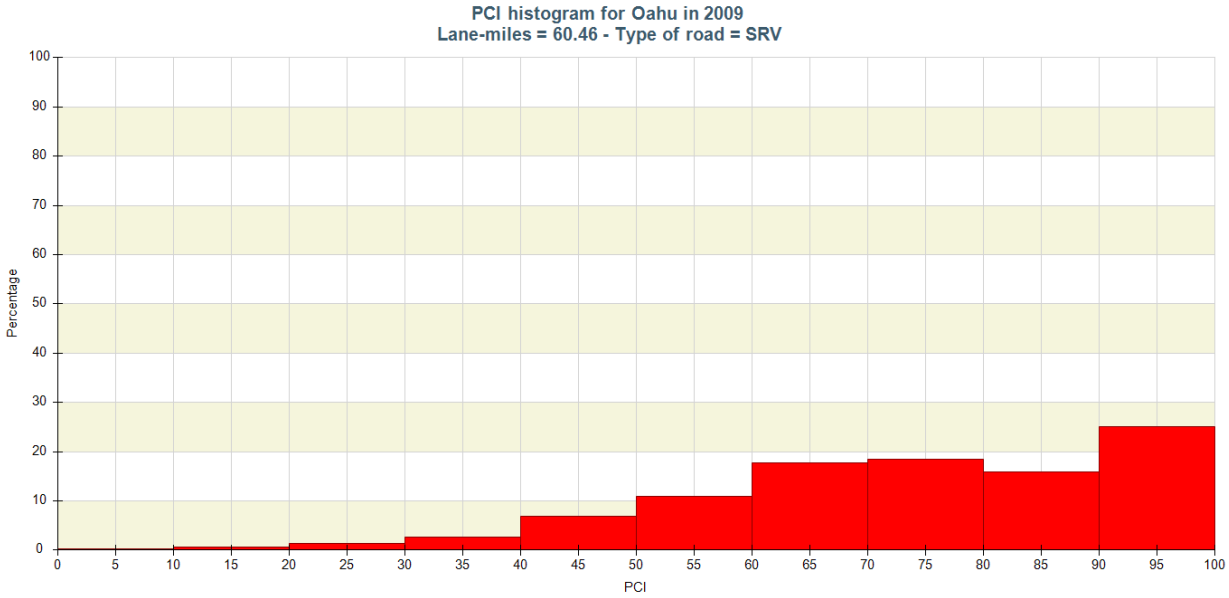

Figure 4-38. PCI distribution for service roads in Oahu in 2009.

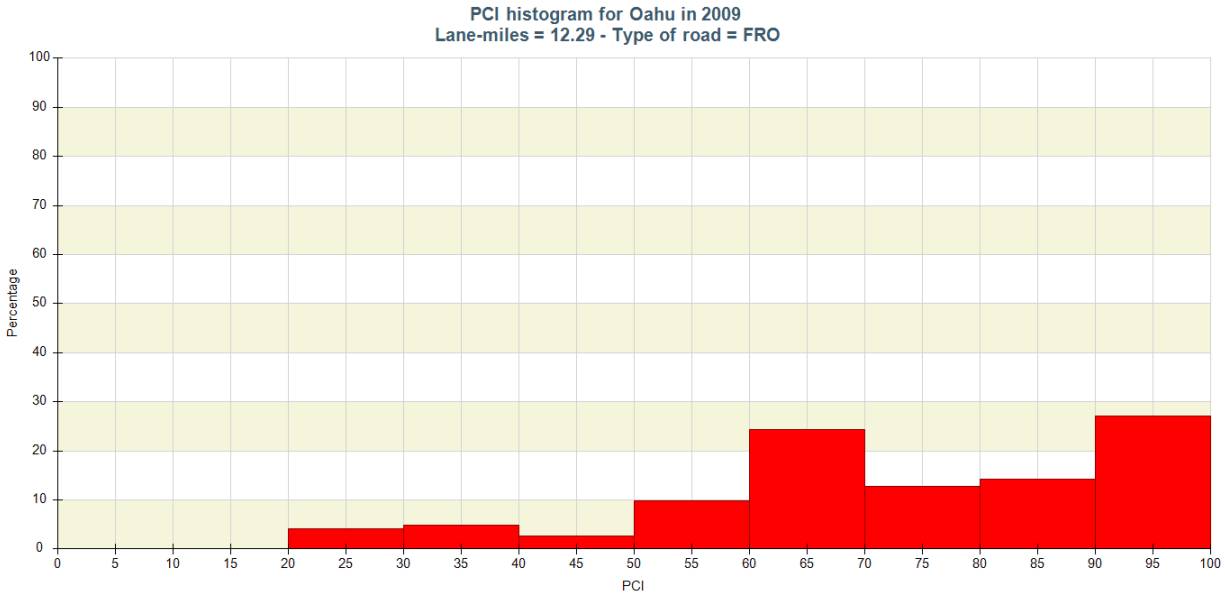

Figure 4-39. PCI distribution for frontage roads in Oahu in 2009.

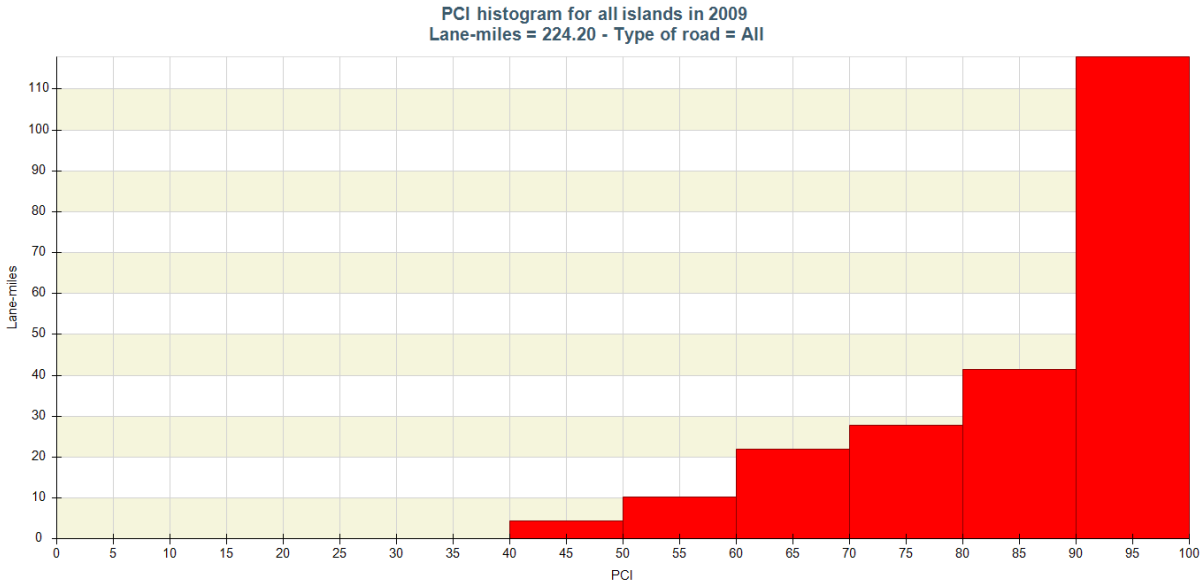

Figure 4-40. PCI distribution for PCC pavements (all road types) on all islands in 2009.

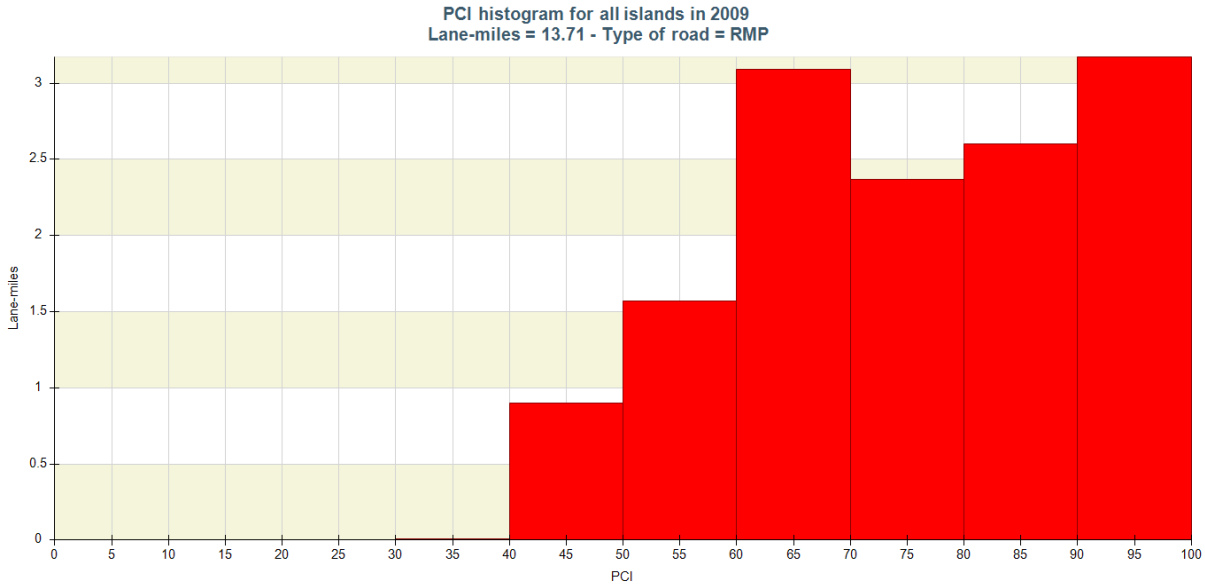

Figure 4-41. PCI distribution for PCC ramps on all islands in 2009.

4.3.3 General distress survey observations

The detailed study of the survey information available from previous years has helped identify a few issues that should be considered in future surveys. These are described in this section.

A distress type that is suspected to be under reported is raveling and weathering. At least for several roads in Oahu, raveling seems to be a common distress. Regardless of the PMS procedure finally adopted by HDOT, raveling can be an important factor in determining candidate sections for preservation treatments, which are most effective for climate/aging related distresses. Yet, in the 2009 data survey, out of 25,331 records for state roads, there were only 86 records with 1% or more low severity raveling reported, 12 records with 1% or more medium severity raveling reported (2 of which are included in the previous 86), and only 2 records with 1% or more high severity raveling reported. In other words, less than 0.35% of the network is reported as having some raveling. Furthermore, the percentages reported in those records are generally low.

Figure 4-42 shows a condition found on many roads in Hawaii. A substantial loss of aggregate can be noted on the surface of the road. In the most severe spots, the surface is disintegrating as illustrated in Figure 4-43. When this distress is present, oftentimes it appears on

many places on the same road, indicating either mix compaction problems, segregation of the mix, or simply that is a relatively old pavement surface for which it would have been desirable to apply a preservation treatment before getting to the current condition. Figure 4-44 shows a similar problem on a location close to the one in Figure 4-42.

Figure 4-42. Substantial loss of aggregate (Kalanianaole Highway).

Figure 4-43. Close up illustrating the disintegration of the pavement surface and the loose aggregate.

Figure 4-44. Another example of severe raveling on Kalanianaole Highway.

Identification of raveling from forward pictures may be challenging, as it may be difficult to discern whether one is observing raveling or a coarse pavement texture. Furthermore, as illustrated in Figure 4-45, in those ocassions that raveling is observed, delimiting the affected area can be subjective and also difficult in locations further away from the point of view of a particular frame or when it appears mixed with other distresses. Moreover, often only some parts of an area are affected and their limits are not well defined. Finally, as shown in Figure 4-46, for some sections raveling manifests over small areas pehaps as a result of segregation and/or poor mix compaction. On large data collection efforts, it may be tempting to neglect such small areas.

On occasions, some raveling may be confused with cracking, as on forward pictures the lost aggregates may look as cracks. Oftentimes, raveling will be combined with some cracking. Figure 4-47 shows a section for which cracking appears to be significantly over reported. Apparently, the longitudinal joint and raveling were considered as fatigue cracking.

Figure 4-45. Challenges when attempting to quantify areas with raveling.

Figure 4-46. Small raveled areas.

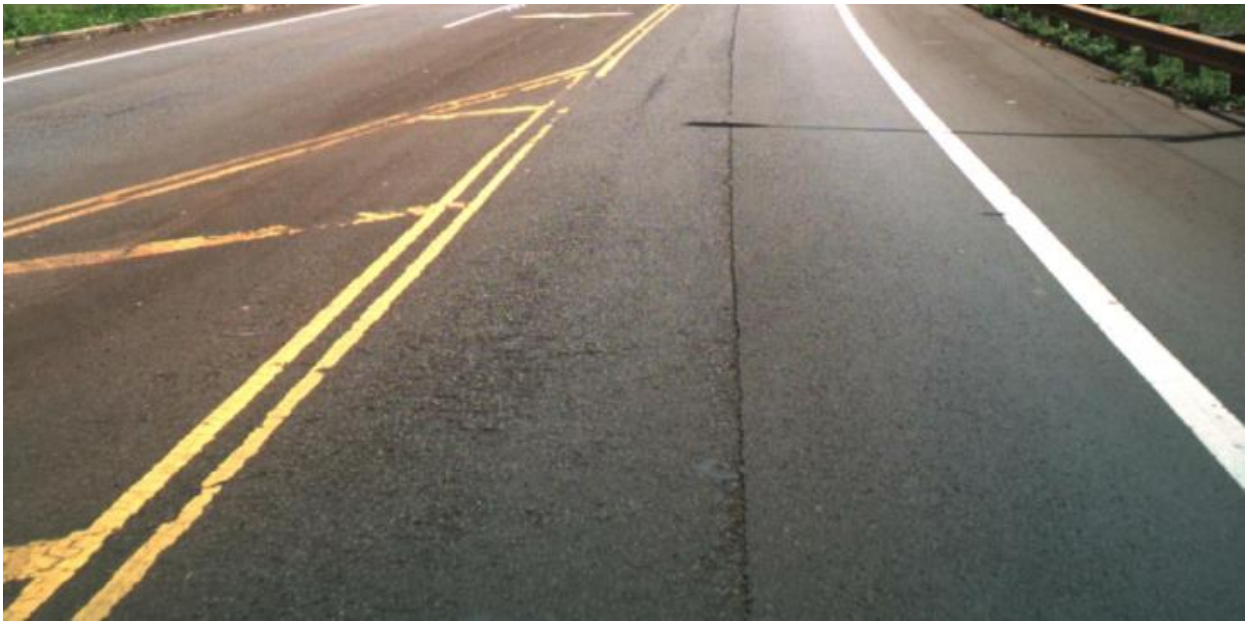

Figure 4-47. Longitudinal joint and raveling misclassified as fatigue cracking. (Route 99 – MP 7.70).

The following paragraphs describe a few other issues that were detected in the data that should be checked as part of a quality asssurance process. Many of these are relatively easy to solve but it is still worth pointing them out for future reference.

On the 2010 roughness table delivered by Mandli, both rutting and faulting are reported on every 0.01 mi data intervals. Unless one of these intervals straddles a change in pavement type, only one of these two distresses can be present. Thus, for most sections only one of these distresses would be different from zero. However, several 0.01 mi long intervals were found where both rutting and faulting were different from zero even though there was no pavement type change within the interval. This is a relatively minor problem but it can also be solved relatively easily.

On ocassions, there seem to be a potential for double counting of cracking. For example, a few segments were found for which the sum of percentages of fatigue cracking at the different severity levels were much high than 100%. Something similar was noted when adding the percentages of say, fatigue cracking and block cracking.

Although the data is supposedly reported every 0.1 mi (except for smaller segments), there are some fields with much larger differences between the begin mile point (BMP) and the end mile point (EMP) (larger than 100 mi in one case.) The data should be QA for this kind of problem, flagging any overlapping of intervals for review. As described in a later chapter, when preparing the data to be imported into PAVER^{TM}, these overlapping sections created several problems and thus, the problematic intervals were ignored. However, ignoring them is not the best solution as the problem most of the time appears to be caused by mistyping of one of the end points, which is also an easy problem to fix if the proper interval can be identified.

Several cells with distress information have negative numbers that appear to be result of some error. These should also be detected and fixed or eliminated.

Also, as indicated before, it may be easier to aggregate the data given in the raw data file (the file that contains the information collected for each frame on 0.002 mi intervals) as this will help avoid having to prorate the data for 0.1-mi segments when they straddle a PMS section. However, for this, a key should be provided in the raw distress data table that allows linking the frame information with mile points (or if enough information is already available in the delivered database, instructions about how to perform the linking should be provided).

It is suggested to continue collecting longitudinal and transverse cracking separately to facilitate HPMS reporting (i.e., longitudinal non-wheel path cracking as one distress and

transverse cracking (HPMS item 53) as the other). They can be combined later on for PCI calculations or for other purposes.

4.3.4 Future distress surveys

It is important to pause here to analyze what would be appropriate for the future distress surveys. From a consistency point of view, the first thought would be to maintain the method currently used. However, as far as the PI knows, the next distress data collection cycle would be performed by Mandli using an automated analysis of downward pictures (at least for cracking distresses). Thus, even if the same protocols are followed, some important differences should be expected, particularly in the levels of cracking. Thus, the data will not be entirely consistent for one more cycle. However, it is highly recommended that if succesful, the technology used in the next cycle be continued in the future with as few changes as possible. It is also important to follow the protocol selected for performing the distress survey with as few changes as possible. If for any reason there is a need to change some aspect of the protocol, this should be well documented and highlighted.

It is expected that some of the cracking that before went undetected will be caught earlier with the downward imaging. It is also expected that the lengths and areas of cracking (depending on the type being measured) will be more repeatable. Finally, some differences should also be expected in the classification of cracks into the different categories. Raters tend to classify some cracks differently from those obtained by a computer algorithm.

It is also important for HDOT to decide and maintain the protocol used to perform the distress surveys. A careful study of the distress definitions in the two most widely used distress identification protocols, SHRP/LTPP [28] and ASTM D6433, reveals several differences that would translate into differences on the computed PCI values.

The above paragraphs nonwithstanding, it is important to point that some highway agencies are starting to change the methodologies for classifying and quantifying cracking of flexible pavements. This is because the LTPP and ASTM D6433 survey methodologies were developed mostly for field walking surveys, which are not practical at the network level.

A good example is provided by California. As reported by [32], the California Department of Transportation (Caltrans) is considering a method in which cracks are classified

into one of four categories: transverse cracking (non-load-associated), longitudinal cracking (non-load-associated outside the wheel path), wheel path cracking (load-associated), and XF cracking (intended to identify cracking caused by reflection of underlying cracks and joints). Each of these are related to broad but distinct cracking mechnisms. These authors have proposed a protocol to quantify them from automated distress surveys. A main advantage of their method is that it relies only on cracking length, which is determined relatively accurately by automated procedures instead of relying on crack widths, which are not easy to determine. The procedure is intended to eliminate as much as possible subjective ratings. In addition, these authors also define wheel path areas that are wider than those defined in AASHTO R55-10. The wider areas appear to be more realistic given the typical heavy vehicle wheel widths and wander. If HDOT starts using downward imaging continuously to perform the distress surveys, consideration should be given to these procedures as they have the potential to significantly reduce subjective ratings.

Finally, as mentioned earlier, raveling is a difficult distress to quantify from photographs and appears to be currently under-reported. However, significant technological advances have been made in recent years that may help measuring indicators of raveling at the network level. Specifically, a Raveling Index (RI) indicator has been proposed to detect and quantify raveling conditions [33]. RI is obtained by measuring the volume of aggregate loss (holes due to missing aggregates) per unit of surface area. HDOT should consider testing the use of 3D Laser technology to quantify RI, particularly since 3D Laser technology is already been used by HDOT. It is important to note that Mandli Communications, Inc., the vendor currently providing the distress survey services, will be using 3D Laser technology from Pavemetrics Systems, Inc. for automated cracking detection. Pavemetric Systems, Inc. has been involved in developing the RI index. Thus, except perhaps for cost considerations, evaluation of the technology locally appears feasible. Furthermore, the same technology can also provide measurements of a Road Porosity Index, which is a pavement macro-texture indicator similar to what is obtained with the sand patch method typically used to evaluate pavement macro-texture. Among other things, pavement macrotexture affects safety (tire/road friction level, water runoff and aquaplanning conditions) and noise.

CHAPTER 5. PAVEMENT ME DESIGN

Introduction to Mechanistic-Empirical Design

5.1 INTRODUCTION

A main objective of this study is to advance in the calibration of the MEPDG or, as it is now known, the AASHTO Pavement ME Design. As indicated in Chapter 1, a main advantage of a mechanistic-empirical approach over entirely empirical approaches is that, in addition to being a more rational and scientifically substantiated approach, it provides mechanisms for calibration to local conditions. The mechanistic-empirical (ME) approach has been used in different forms for pavement design for decades and thus its principles are well known.

This chapter gives an overview of some of the main ME principles to provide a framework for some of the discussions about material characterization and traffic and climate inputs that follow as well as for the discussion of calibration of the design guide. Emphasis is given to issues that are more relevant to the most prevalent Hawaiian conditions. Thus, for example, subjects such as creep compliance used for thermal cracking calculations are not discussed. For a detailed and general introduction to the ME approach, reference is made to the book of Huang [34]. Other general references providing good introductory concepts to the subject are those of Mallick & El-Korchi [35] and Papagiannakis & Masad [36].

The best source for detailed discussion of the concepts used in the MEPDG is the report from the National Cooperative Highway Research Program (NCHRP) research study 1-37A that resulted in its creation [1]. A shorter description of inputs and issues with the MEPDG is provided in the MEPDG Manual of Practice [22]. For those already with some familiarity with the ME pavement design approach, the MEPDG Manual of Practice should probably be the first reference to be consulted for further details.

The MEPDG documentation [1] is voluminous and intimidating for those without background on mechanistic-empirical procedures. On the other hand, although the

MEPDG Manual of Practice [22] provides an excellent overview, it may leave some readers without familiarity on ME design hanging on some details. Thus, the purpose of this chapter is to provide a very basic introduction to the ME approach to pavement design as well as the importance of the design inputs and interpretation of its outputs so that the basic ideas can be understood. The goal is to complement the MEPDG documentation referenced above.

In this chapter, an effort has been made to avoid as much as possible duplication with the MEPDG documentation. *Nevertheless, some duplication is unavoidable and therefore some sections have been paraphrased and others reproduced from it.* This is made clear at the outset so that lengthy sections within quotation marks are avoided.

The mechanistic-empirical design and analysis procedure calculates pavement responses (stresses, strains, and deflections) and uses those responses to compute incremental damage over time. The procedure empirically relates the cumulative damage to observed pavement distresses. This ME based procedure is shown in flowchart form in Figure 5-1 [1]. "MEPDG", as is used in this report, refers to the documentation and software package" ([1], [2]).

As with any other design procedure, the first design stage consists in evaluating the conditions for the new or existing pavement. The evaluation portion provides inputs required for design. These consist of environmental conditions, material characteristics, and traffic loading. As part of the design, levels of reliability for each distress type analyzed also need to be chosen. The second stage involves the selection of a trial design, which is analyzed for adequacy against the user input performance criteria and reliability values through the prediction of distresses and smoothness. If the design does not meet the desired performance criteria at the specified reliability level, it is revised and the evaluation process repeated as necessary. If inadequate, other trial designs (involving design features such as layer thicknesses and materials) are analyzed until one is found meeting all the design criteria. This approach differs with traditional design procedures that resulted in a set of thicknesses for the given material characteristics. As shown in Figure 5-1, the ME approach is iterative in nature. After one or more competing alternatives are selected, the third stage (which is beyond the scope of this introduction)

proceeds to the selection of a strategy by considering life cycle costs and other considerations.

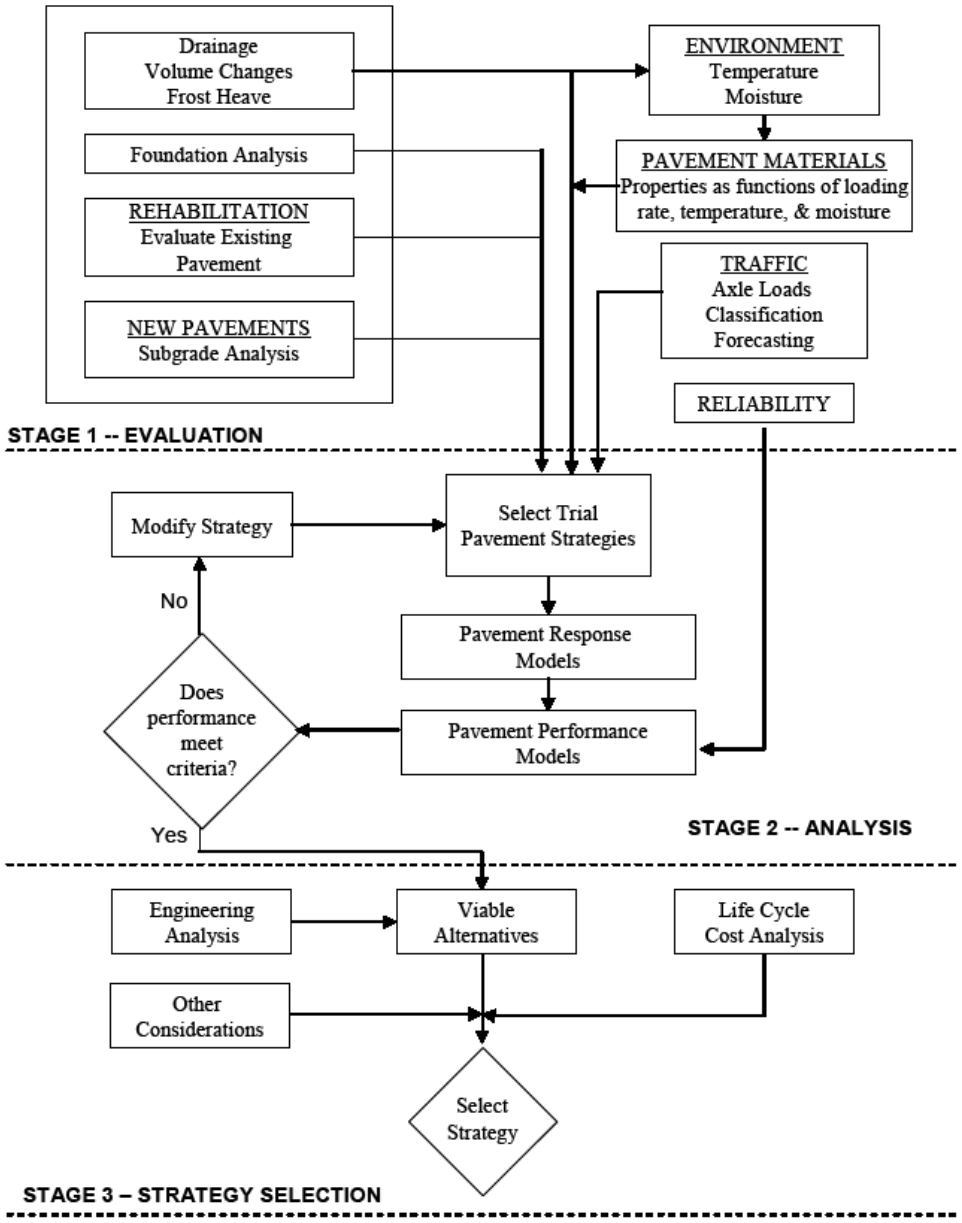

Figure 5-1. Conceptual schematic of the three-stage design approach. Source: **[1]**.

It is important to note at the outset that the basic premise of the mechanistic-empirical approach for pavement design is conceptually simple. The difficulties lie in

understanding how things are integrated and in feeding the procedures with adequate information. Most of the rest of this chapter focuses on these two aspects.

5.2 Hierarchical Input Levels

The MEPDG uses a hierarchical input level scheme to categorize the designer's knowledge of the input parameters. This hierarchical input structure allows users with minimal experience in ME based procedures to use the method with little initial investment. Three levels are available for determining the input values for most of the material and traffic parameters:

- **Input Level 1** – Input parameter is measured directly; it is site- or project specific. This level represents the greatest knowledge about the input parameter for a specific project but has the highest testing and data collection costs to determine the input value. Level 1 should be used for pavement designs having unusual site features, materials, or traffic conditions that are outside the inference space used to develop the correlations and defaults included for input levels 2 and 3.
- **Input Level 2** – Input parameter is estimated from correlations or regression equations. In other words, the input value is calculated from other site-specific data or parameters that are less costly to measure. Input level 2 may also represent measured regional values that are not project-specific.
- **Input Level 3** – Input parameter is based on "best-estimated" or default values. Level three inputs are based on global or regional default values – the median value from a group of data with similar characteristics. This input level has the least knowledge about the input parameter for the specific project but has the lowest testing and data collection costs.

5.3 Purpose of the Hierarchical Input Levels

With the exception of the HMA transverse or thermal cracking prediction methodology, input level has no effect other than knowledge of the input parameter (which is important for critical inputs). This approach provides the designer with a lot of

flexibility in obtaining the inputs for a design project based on the criticality of the project and the available resources. The hierarchical input structure allows the user with limited experience in ME based design procedures and only standard test equipment for measuring material properties to use the MEPDG. On the other extreme, it allows an experienced user to measure many inputs for a design-build type of project, or for the forensic evaluation of an existing pavement.

5.3.1 Selecting the Input Level

For a given design project, inputs can be obtained using a mix of levels, such as dynamic modulus from level 1, traffic load spectra from level 2, and subgrade resilient modulus from level 3. No matter what input design levels are used, the computational algorithms for damage and distress are the same. The same models and procedures are used to predict distresses and smoothness. Of course, the highest the level the more reliable the predictions are expected to be.

The MEPDG recommends that the designer use the highest level of inputs available at the time of design.

5.4 MECHANISTIC-EMPIRICAL ANALYSIS

As the name implies, the mechanistic-empirical design procedure involves both mechanistic and empirical components. The mechanistic component determines the pavement responses in terms of *stresses, strains, and deflections* on some points within the pavement structure caused by a *given traffic loading condition* and for the *material characteristics* prevailing under the *environmental conditions* at the time the loading is applied.

The highlighted words in the above descriptions are important. Traffic loading always consists of a distribution of traffic load magnitudes on different heavy vehicle's axle load configurations (single, tandem, tridem, and quad axles). The environment and in turn the characteristics of the materials in the different layers of the pavement structure are constantly changing and thus, the effect of a given load depends on when it is applied.

The empirical component relates empirically the pavement responses computed in the mechanistic analysis to different pavement distresses such as cracking and rutting.

This is the weakest link of the methodology. A brief explanation of the mechanistic component is given in the following section followed by a section on the empirical components for bottom up fatigue cracking and rutting, which are the two traditionally considered mechanisms in ME design of flexible pavements. The MEPDG also calculates top-down fatigue cracking, thermal cracking, reflection cracking, and smoothness. More discussion about the consideration of these distresses for Hawaii is provided later in the sequel.

5.4.1 Mechanistic Analysis

The structural response model is a mechanistic model based on fundamental engineering principles. It is used to calculate critical pavement responses (deflections, stresses, and strains). The MEPDG uses internally the JULEA program as the structural response model used for flexible pavements. JULEA is one of many computer programs that are available for computing the state of stresses, strains and deflections caused by loads on pavement systems. The linear layer elastic theory assumes that each layer *i* is homogeneous, isotropic, and linear elastic with elastic modulus (E_i) and Poisson ratio (ν_i), that the material is weightless and infinite in areal extent and that each layer has a finite thickness h_i, except for the lowest layer, which is infinite in thickness [34]. Other assumptions include continuity conditions at layer interfaces (including friction between layers) and that the load is applied with uniform pressure over circular areas. A stress dependent finite element program was also available in the MEPDG for flexible pavement analyses using input level 1 for unbound materials, but it was not included in the global calibration effort [1]. The use of the finite element program for flexible pavements was intended for research purposes only. This option is disabled in the current version of Pavement ME Design [2].

To fix ideas about the mechanistic analysis, consider a pavement structure such as the one shown in Figure 5-2. The pavement structure is a layered system and is typically modeled using linear layered elastic analysis. In the example of Figure 5-2, the structure is loaded by a single load of magnitude P over a circular area with radius *a.* Since the materials are assumed linear elastic, the superposition principle can be used to determine the pavement responses for any number of loads applied with uniform pressure over

circular areas. In particular, the loading configurations usually applied by vehicular traffic are easily accommodated. Most computer programs available allow the analysis of multiple-wheel loading configurations.

Clearly, some of the above assumptions are not applicable in practice. For example, most geomaterials are non-linear (i.e., the modulus of each layer is not constant but depends on the state of stresses) and the load is not really applied over a circular area. Nevertheless, the theory has served well for many years for its simplicity and ease of use. As indicated before, to date, the more advanced modeling techniques such as finite element analysis that can cope with nonlinearities, dynamic effects, anisotropy, etc., are used mostly for research purposes.

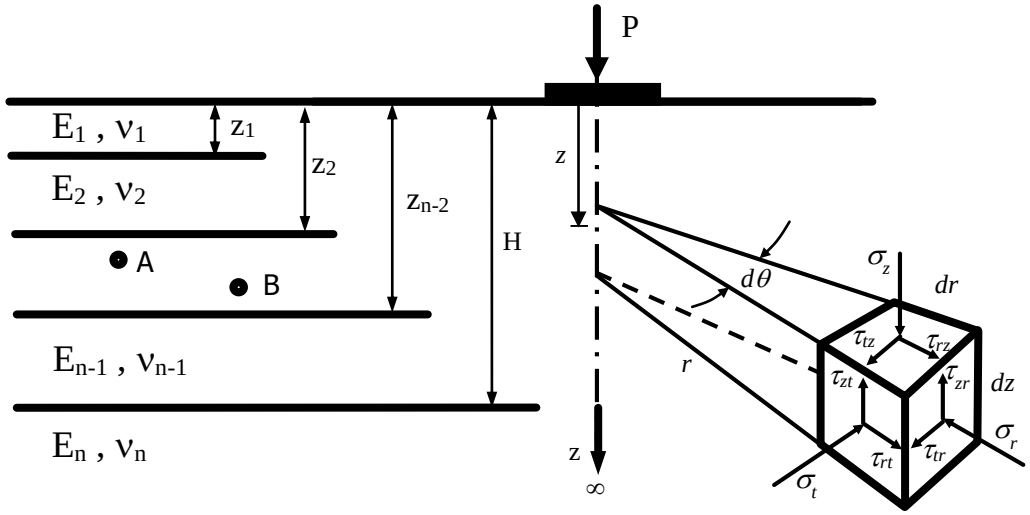

Figure 5-2. State of stresses at a point within a linear elastic layered pavement structure [34].

Now, with reference to Figure 5-2, consider a differential element located at a depth *z* below the pavement surface, at a distance *r* from the center of the load and of dimensions *dz*, *dr*, and *r dθ*. The state of stresses at such point will be defined by the six components σ_z, σ_r, σ_t, τ_{rz} (=τ_{zr}), τ_{tz} (=τ_{zt}), and τ_{zr} (τ_{rz}). Most linear layer elastic analysis programs report these stresses along with the associated (normal) principal stresses σ_1,

σ_2, and σ_3[23]. In addition, these programs also report the state of *strains* at the point either in the normal, tangential and vertical directions (ε_z, ε_r, ε_z, ε_{rz}, ε_{tz}, and ε_{zr}) or in the principal directions ε_1, ε_2, and ε_3 or both. Deflections at any selected point within the pavement structure can also be computed. The differential element can be located anywhere within the pavement structure such as points A or B in Figure 5-2.

In order to illustrate how different pavement properties affect the distribution of stresses and strains, the following paragraphs describe the changes with the help of several figures. The figures illustrate some of the distribution of stresses and strains that can be computed for a pavement structure. They were all created for a 9,000-lb load applied over a circular area with a 5.91-in radius (a typical loading configuration used with the Falling Weight Deflectometer (FWD) to simulate the loading of a standard single axle load). In each figure, two different scenarios are analyzed for comparison. Part a) of each figure considers that a load is applied on a pavement structure consisting of 6 inches of Hot Mix Asphalt (HMA) with a modulus of 500,000 psi, an unbound granular base layer 12 inches thick with modulus of 30,000 psi, and a fine grained subgrade with a modulus of 10,000 psi. The Poisson ratios were assumed to be 0.30, 0.4, and 0.45 for the HMA, base, and subbase layers, respectively. The value of 0.30 for HMA is approximately the value that the MEPDG would calculate based on the modulus of the HMA. In part b) of each Figure, either the thickness of HMA is maintained at 6 inches and its modulus is changed 2,500,000 psi to simulate a lower temperature of the HMA or the modulus is maintained at 500,000 psi and the thickness of the HMA layer is changed to 12" to compare the distributions with a thicker pavement structure. For the 2,500,000 psi case, the Poisson ratio of the HMA is changed to 0.15, which is the value that would be estimated by the MEPDG. In order to interpret the figures, it is important to point out that the *center* of the load is always located on the left side of each chart and the edge of the load is located at a distance from the center of 5.91 inches. Only the first 30

[23] Recall the principal stresses for the differential element are those located at the same point but with a different orientation of the element such that σ_1 is the maximum normal stress, σ_3 is the minimum normal stress and there are no shear stresses acting on the faces of the element.

inches of the pavement structure are shown in depth and laterally. In all cases, axial stresses/strains with positive signs are compressive and those with negative signs are tensile. Finally, since the color pallets are the same for the different scenarios in a given stress or strain distribution chart, it is important to look carefully at the legend of each figure as in most situations a similar color would represent different stress/strain levels on different charts.

Figure 5-3 illustrates how the distribution of vertical stresses for the base case (6 inches of HMA and 500,000 psi HMA modulus) compares with that obtained when the modulus of the HMA is changed to 2.500.000 psi. As one would expect, the vertical stresses dissipate faster with depth for the stiffer HMA layer. Of course, the faster dissipation of vertical stresses comes at the cost of much higher tensile stresses in the HMA layer, as can be observed in the distributions of radial stresses in Figure 5-4. Note that although the coloring in the two parts of Figure 5-4 is similar, the stresses are much higher in part (b). As an aside, Figure 5-4 also helps to illustrate a somewhat vexing issue with the use of linear layer elastic analysis, which is the prediction of tensile stresses in granular base layers. Unless some cementation occurs in these layers, these tensile stresses are typically not realistic. However, this problem is not significant for thicker bound layers.

Figure 5-5 shows the corresponding principal stress distributions. Although not as easy visualize, the figure shows how that the stiffer layer spreads the stresses over a wider area. In this figure, the short segments indicate the direction in which the principal stresses act. As can be seen, these lines are generally more horizontal in part (b) than in part (a), which illustrates the slab action effect typically associated with concrete pavements (the modulus of concrete is higher than that assumed for part (b)). It may also be surprising to see that immediately below the load; the stresses are higher in the horizontal direction than in the vertical direction. Nevertheless, this a perfectly valid outcome.

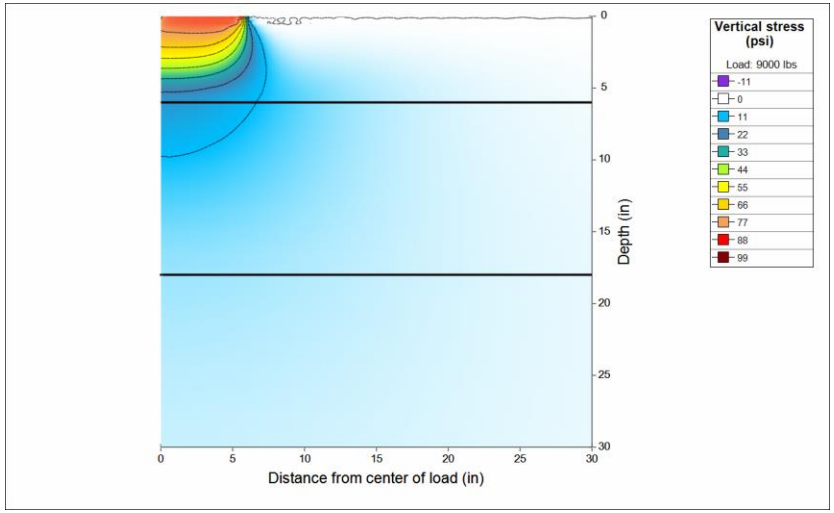

(a)

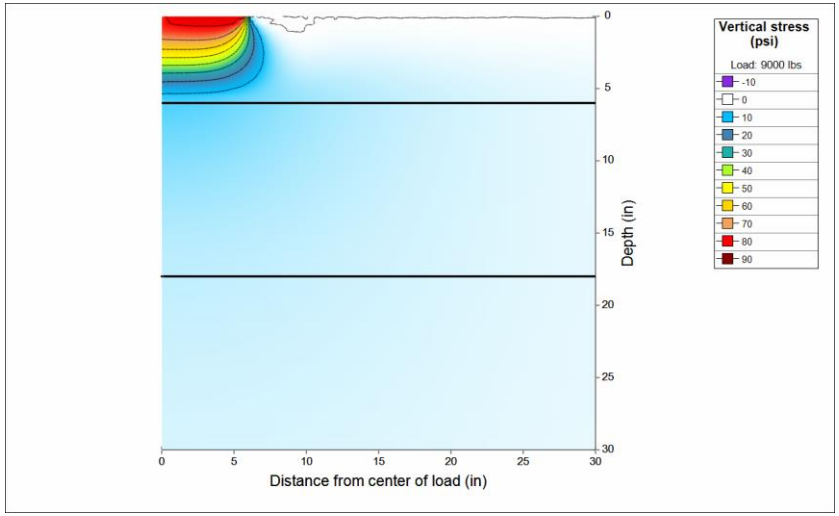

(b)

Figure 5-3. Vertical stress distribution for a 9,000 lb. circular load on a pavement structure with a 6" HMA layer, 12" granular base with 30,000 psi modulus (ν = 0.40), and a fine-grained subgrade with 10,000 psi modulus (ν = 0.45)

(a) E_{HMA} = 500,000 psi and ν = 0.30 and (b) E_{HMA} = 2,500,000 psi and ν = 0.15.

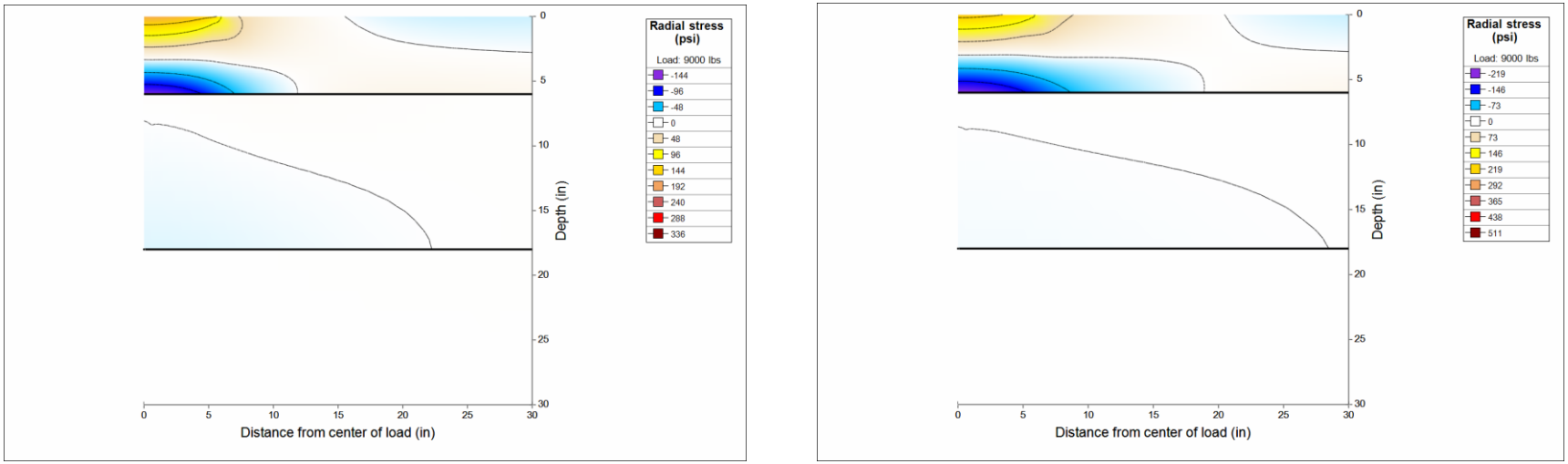

(a) (b)

Figure 5-4. Radial (horizontal) stress distribution for a 9,000 lb. circular load on a pavement structure with a 6" HMA layer (ν = 0.35), 12" granular base with 30,000 psi modulus (ν = 0.40), and a fine-grained subgrade with 10,000 psi modulus (ν = 0.45)

(a) E_{HMA} = 500,000 psi and (b) E_{HMA} = 2,500,000 psi.

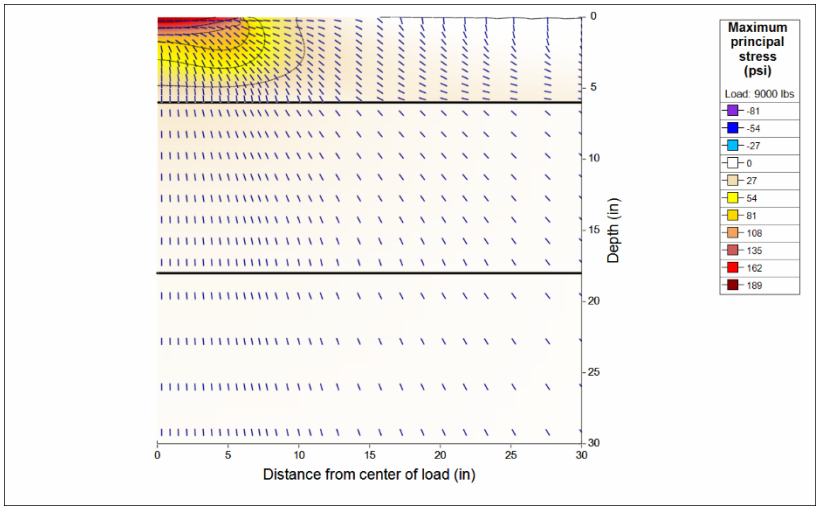

(a)

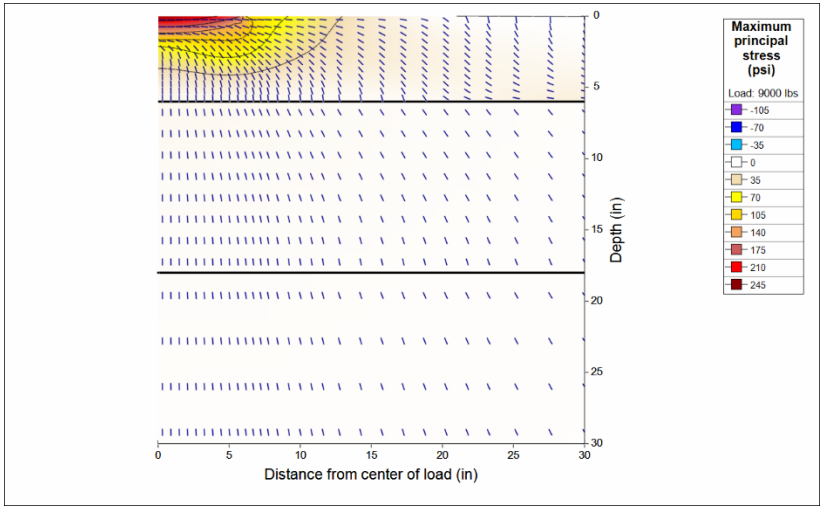

(b)

Figure 5-5. Maximum principal stress distribution for a 9,000 lb. circular load on a pavement structure with a 6" HMA layer (ν = 0.35), 12" granular base with 30,000 psi modulus (ν = 0.40), and a fine-grained subgrade with 10,000 psi modulus (ν = 0.45)

(a) EHMA = 500,000 psi and (b) EHMA = 2,500,000 psi.

Since the distress transfer functions used in ME analyses typically involve strains, it is also illustrative to compare their distributions. Figure 5-6 shows the distribution of vertical strains for the same two scenarios discussed before. Notice how the strains are more than halved for the stiffer 2,500,000 psi HMA layer with respect to the 500,000 psi HMA layer. On the other hand, it is interesting to note that the predicted vertical strains immediately below the load are tensile instead of compressive for the lower HMA modulus! Although this may appear counterintuitive, it is related in part to the effect of the Poisson ratio for the HMA layer.

The results in Figure 5-7, which show the distributions of radial strains, clearly illustrate why fatigue cracking is typically associated with the maximum horizontal tensile strain at the bottom of the asphalt concrete layer. It is typically at this location where tensile strains are a maximum. Once again, it is important to look at the chart legends to see that the tensile strains are significantly lower for the stiffer HMA layer.

Finally, it is also illustrative to see the distribution of the minimum principal strains. These are shown in Figure 5-8 for the same two scenarios. Consistent with the results in Figure 5-4, the minimum tensile principal stains occur at the bottom of the HMA and the stiffer layer reduces them substantially. However, note that for the scenario with the E_{HMA} = 500,000 psi, there is a significant area where tensile strains near the surface are not negligible. This effect is accentuated for even lower moduli (higher temperatures) and may be a relevant factor in the explanation why the typical cracking occurring on Hawaii State Roads appear to be top-down longitudinal cracking. A more thorough discussion of this issue is presented later in the report.

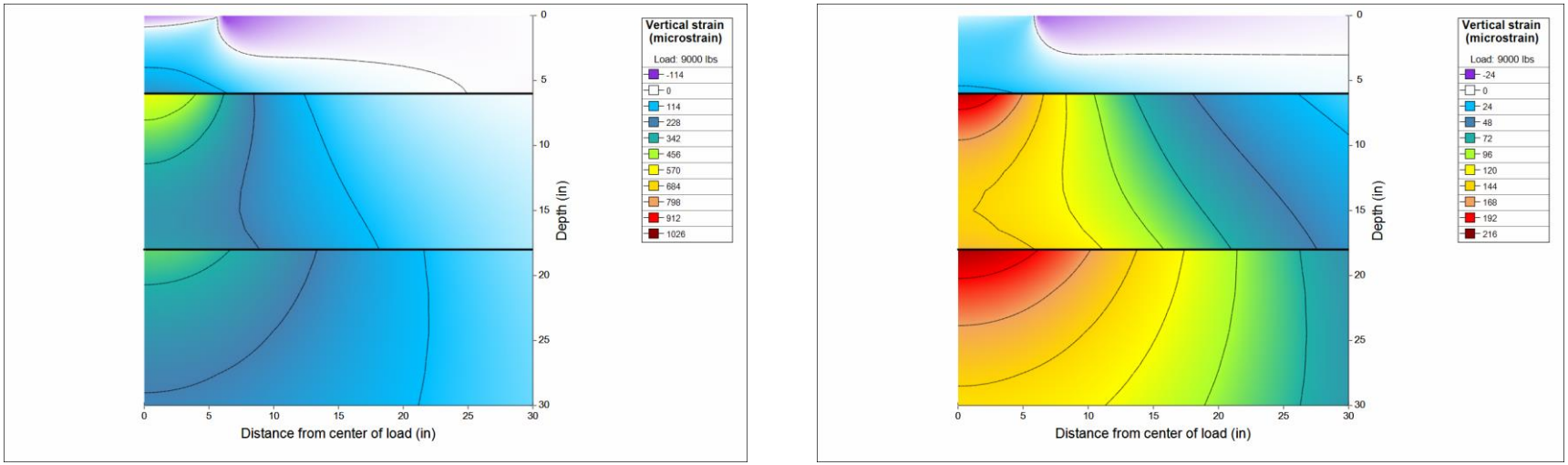

(a)

(b)

Figure 5-6. Vertical strain distribution for a 9,000 lb. circular load on a pavement structure with a 6" HMA layer, 12" granular base with 30,000 psi modulus ($\nu = 0.40$), and a fine-grained subgrade with 10,000 psi modulus ($\nu = 0.45$)

(a) E_{HMA} = 500,000 psi and $\nu = 0.30$ and (b) E_{HMA} = 2,500,000 psi and $\nu = 0.15$.

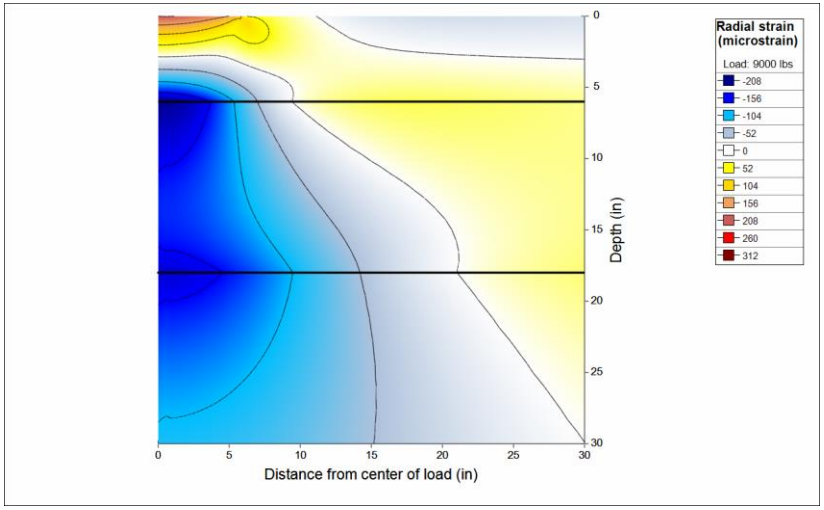

(a)

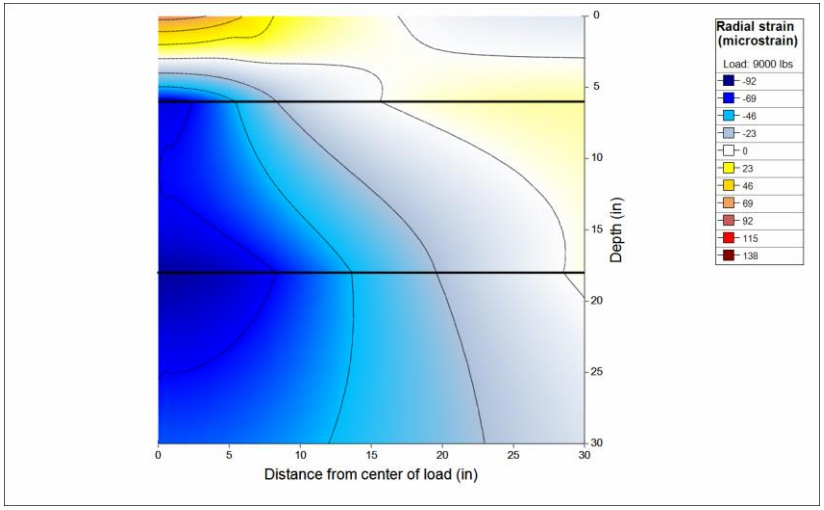

(b)

Figure 5-7. Radial (horizontal) strain distribution for a 9,000 lb. circular load on a pavement structure with a 6" HMA layer (ν = 0.35), 12" granular base with 30,000 psi modulus (ν = 0.40), and a fine-grained subgrade with 10,000 psi modulus (ν = 0.45)

(a) E_{HMA} = 500,000 psi and ν = 0.30 and (b) E_{HMA} = 2,500,000 psi and ν = 0.15.

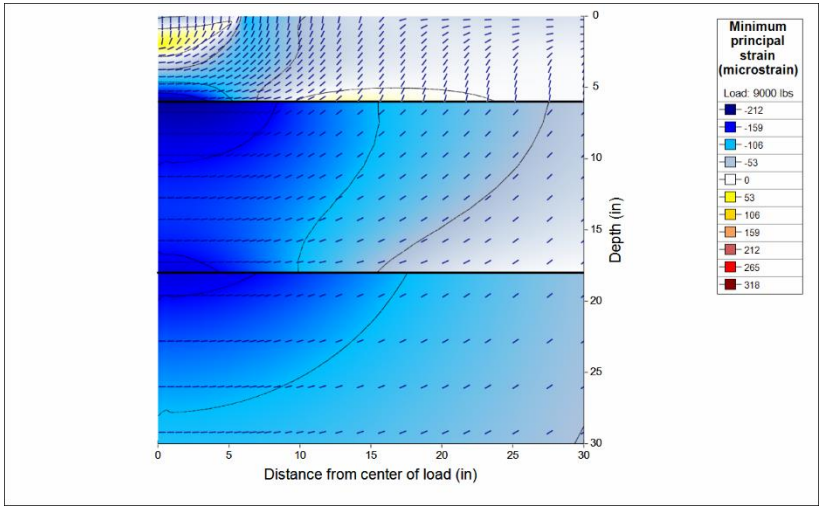

(a)

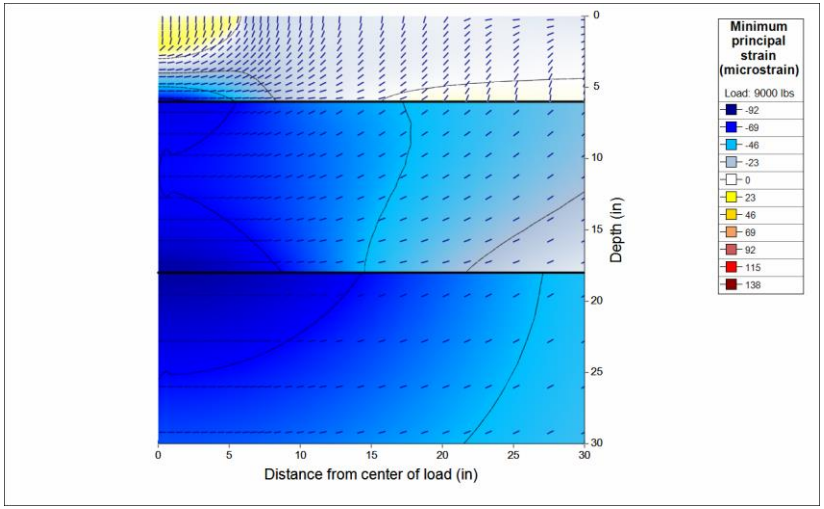

(b)

Figure 5-8. Minimum principal strain distribution for a 9,000 lb. circular load on a pavement structure with a 6" HMA layer (ν = 0.35), 12" granular base with 30,000 psi modulus (ν = 0.40), and a fine-grained subgrade with 10,000 psi modulus (ν = 0.45)

(a) E_{HMA} = 500,000 psi and ν = 0.30 and (b) E_{HMA} = 2,500,000 psi and ν = 0.15.

The following figures illustrate the effect of layer thickness on the distribution of stresses and strains. In each of the following six figures, scenario (a) is the same as scenario (a) in Figure 5-3 to Figure 5-8. In other words, the left sides of the new figures are the same as those presented in those figures. The difference is presented for scenario (b), which considers an HMA layer thickness of 12 inches but with a modulus of 500,000 psi and $\nu = 0.3$. That is, except for the HMA layer thickness, there is no other difference between the two scenarios.

Figure 5-9 shows how a thicker layer of HMA helps the reduction of compressive vertical stresses in the base and subbase. Although, it may not be obvious, the reductions are substantial (a factor of about two.)

The same applies to the radial (horizontal) stresses illustrated in Figure 5-10. Again, attention must be paid to the legend of each chart to appreciate the significant reduction in horizontal stresses for the thicker HMA layer. Figure 5-11 shows the distribution of principal stresses for which the same observations as for the two previous figures can be made.

Figure 5-12 to Figure 5-14 show the comparison of the distributions of vertical, horizontal, and minimum principal strains, respectively. Again, by paying attention to the chart legends, it can be noted the substantial reduction of strains caused by the thicker layer. Figure 5-14 shows that for the thicker HMA layer (scenario b), there exists tensile strains near the surface of the layer that are similar in magnitude to the maximum of the maximum tensile strain at the bottom of the HMA (in this particular example they are about 60% of the maximum). With a lower modulus of the HMA layer, the tensile strain near the surface can become equal or higher than that at the bottom of the HMA. This again may provide an explanation for the prevalent longitudinal cracking observed on state roads. These typically consists of thick structures and the top is subjected to high temperatures throughout the year, which are the two factors that may results in higher tensile strains at the top relative to those at the bottom. Section 7.6 (page 408) provides a more detailed discussion of the load induced tensile strains near the surface.

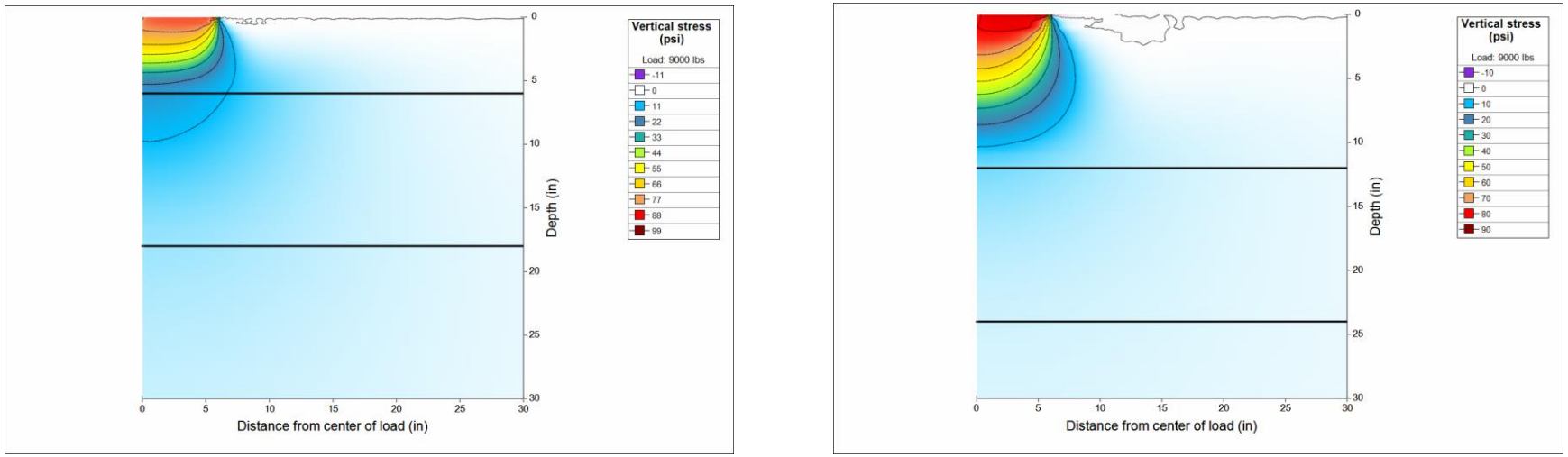

(a)

(b)

Figure 5-9. Vertical stress distribution for a 9,000 lb. circular load on a pavement structure HMA layer (E_{HMA} = 500,000 psi, ν = 0.30), 12" granular base with 30,000 psi modulus (ν = 0.40), and a fine-grained subgrade with 10,000 psi modulus (ν = 0.45)

(a) h_{HMA} = 6 inches and (b) h_{HMA} = 12 inches.

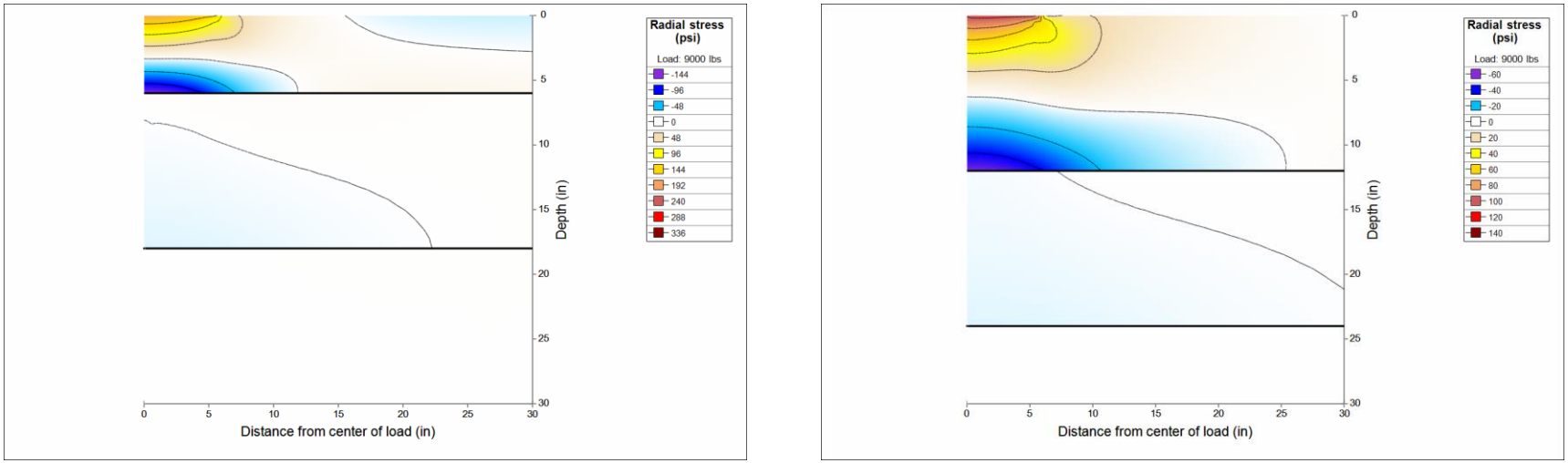

(a) (b)

Figure 5-10. Radial (horizontal) stress distribution for a 9,000 lb. circular load on a pavement structure HMA layer (EHMA = 500,000 psi, ν = 0.30), 12" granular base with 30,000 psi modulus (ν = 0.40), and a fine-grained subgrade with 10,000 psi modulus (ν = 0.45)

(a) h_{HMA} = 6 inches and (b) h_{HMA} = 12 inches.

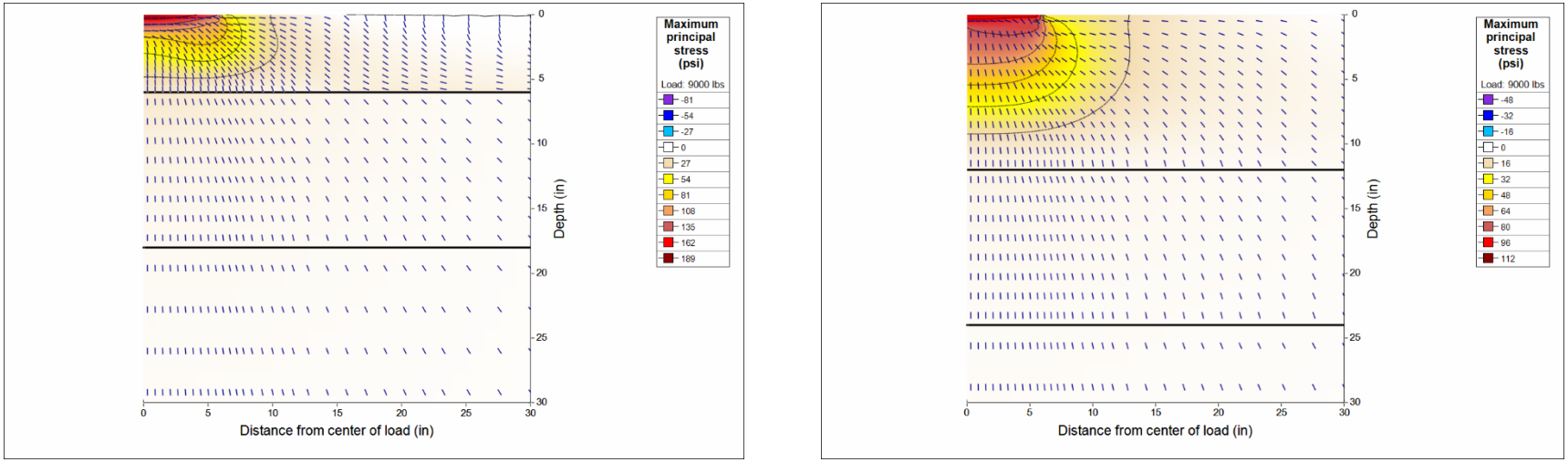

(a) (b)

Figure 5-11. Maximum principal stress distribution for a 9,000 lb. circular load on a pavement structure HMA layer (E_{HMA} = 500,000 psi, ν = 0.30), 12" granular base with 30,000 psi modulus (ν = 0.40), and a fine-grained subgrade with 10,000 psi modulus (ν = 0.45)

(a) h_{HMA} = 6 inches and (b) h_{HMA} = 12 inches.

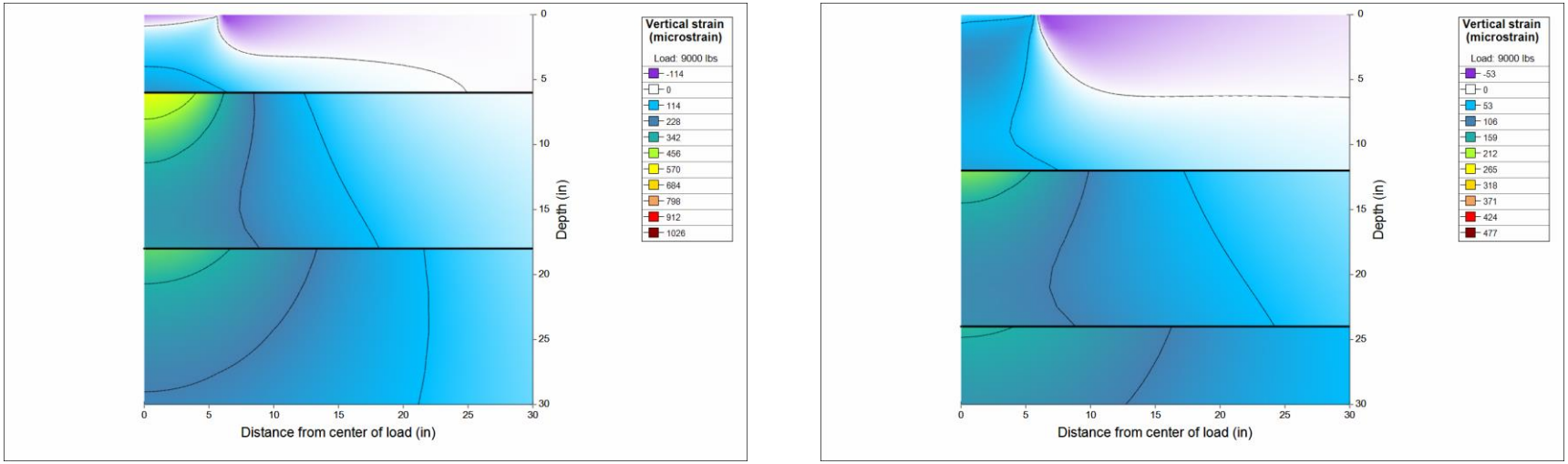

(a)

(b)

Figure 5-12. Vertical strain distribution for a 9,000 lb. circular load on a pavement structure HMA layer (E_{HMA} = 500,000 psi, ν = 0.30), 12" granular base with 30,000 psi modulus (ν = 0.40), and a fine-grained subgrade with 10,000 psi modulus (ν = 0.45)

(a) h_{HMA} = 6 inches and (b) h_{HMA} = 12 inches.

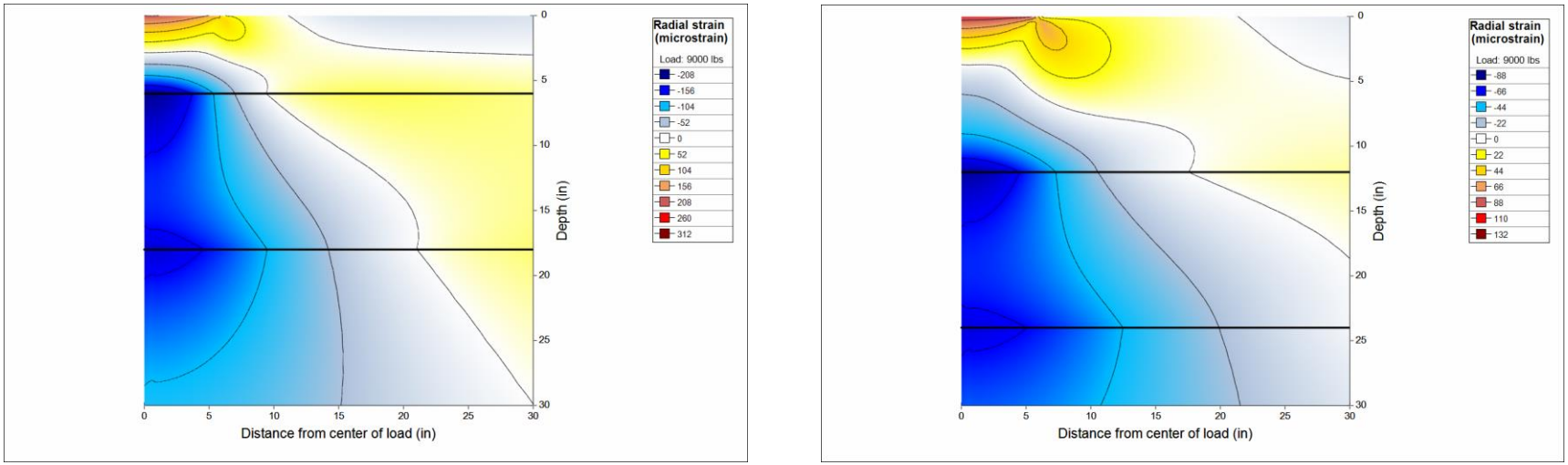

(a) (b)

Figure 5-13. Radial (horizontal) strain distribution for a 9,000 lb. circular load on a pavement structure HMA layer (E_{HMA} = 500,000 psi, ν = 0.30), 12" granular base with 30,000 psi modulus (ν = 0.40), and a fine-grained subgrade with 10,000 psi modulus (ν = 0.45)

(a) h_{HMA} = 6 inches and (b) h_{HMA} = 12 inches.

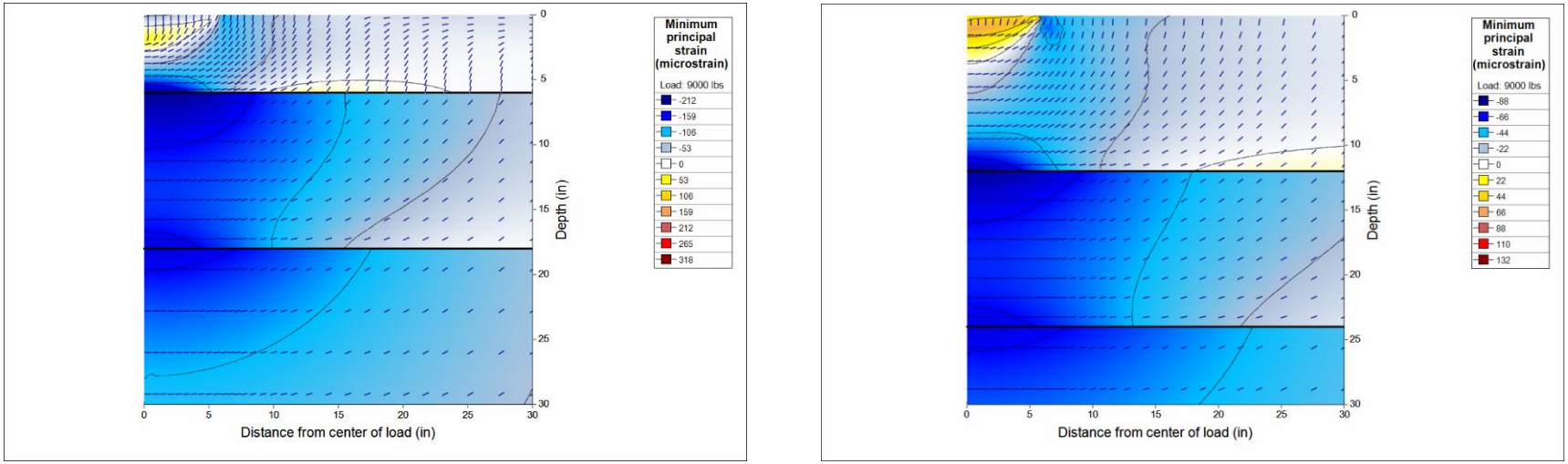

(a) (b)

Figure 5-14. Minimum principal strain distribution for a 9,000 lb. circular load on a pavement structure HMA layer (E_{HMA} = 500,000 psi, ν = 0.30), 12" granular base with 30,000 psi modulus (ν = 0.40), and a fine-grained subgrade with 10,000 psi modulus (ν = 0.45)

(a) hHMA = 6 inches and (b) hHMA = 12 inches.

The theory behind linear layered elastic analysis is beyond the scope of this report. For those interested in learning more about it [34] provides an excellent introduction. In any case, to use a linear elastic analysis program one does not need to know the details of the theory but only the main assumptions and limitations. The computer programs can be used in the same way geotechnical engineers typically use charts or equations for determining state of stresses based on Boussinesq theory. In fact, the MEPDG does all the pavement response calculations in the background and the designer never even sees these intermediate results. Nevertheless, an understanding of the main concepts is important to appreciate the ME design approach and avoid its use as a black box.

Different pavement responses have been used for different distress types. In what follows most of the discussion will be centered on bottom up fatigue cracking (i.e., cracking initiating at the bottom of the asphalt concrete layer) and rutting (the longitudinal depressions in the wheel path of the pavement). Therefore, only the responses associated with these distresses are discussed.

Fatigue cracking is typically associated with the maximum horizontal tensile *strain* at the bottom of the asphalt concrete layer whereas rutting is associated in the MEPDG to the maximum vertical compressive *strain* at the midpoint of each *sublayer* (for rutting analysis, the pavement structural layers are subdivided more finely). Other pavement responses are used in mechanistic-empirical analysis for other purposes. Specifically, deflections are used for back-calculation of layer moduli on rehabilitation projects. In addition, in the research release of the MEPDG stresses were used for non-linear materials whose moduli depend on them.

In summary, the pavement response results of the mechanistic analysis for a given load and environmental condition that are used to predict distresses are:

- Bottom-up fatigue cracking: the maximum tensile strain at the bottom of the asphalt concrete layer.
- Rutting: the maximum vertical compressive strains at the mid-depth of each sublayer.

These pavement responses are then related to the distresses as explained in the following section.

5.4.2 Empirical Analysis

In the empirical part of the analysis, the pavement responses are related empirically to the different distresses.

5.4.2.1 Bottom-up fatigue cracking

For bottom-up fatigue cracking, the *allowable* number of repetitions *of the load under consideration* is related to the *maximum tensile strain* at the bottom of the asphalt concrete layer and the modulus of the asphalt concrete by:

$$N = K_1 \ \varepsilon_t^{-k_2} \ |E^*|^{-k_3} \tag{5-1}$$

where

N = allowable number of load repetitions,

$|E^*|$ = dynamic complex modulus of the asphalt concrete mixture (psi),

ε_t = tensile strain at the bottom of the asphalt concrete layer (microstrain = $\mu\varepsilon = 10^{-6}$ in/in), and

K_1, k_2, and k_3 = empirically derived parameters[24].

This equation is derived from laboratory fatigue cracking experiments. Figure 5-15 shows a beam fatigue apparatus (BFA), one of the pieces of equipment used to carry out this type of experiments. In order to predict cracking in the field, the parameters K_1, k_2, and k_3 are adjusted for a given level of cracking (i.e., the model is calibrated for field conditions). The MEPDG has been calibrated for a level of cracking of 50% of total lane area when N loads are applied. The values of K_1, k_2 and k_3 used in the MEPDG for 7% air voids and 11% asphalt content *by volume* are 1.793×10^{-3}, 3.949, and 1.281 respectively. These values are used in the examples below. Figure 5-16 illustrates a case of a section exhibiting significant fatigue cracking.

[24] The value of K_1 is provided in the guide as function of air voids, volumetric asphalt content and another parameter k_1, which explains why a capital letter was used for this first parameter.

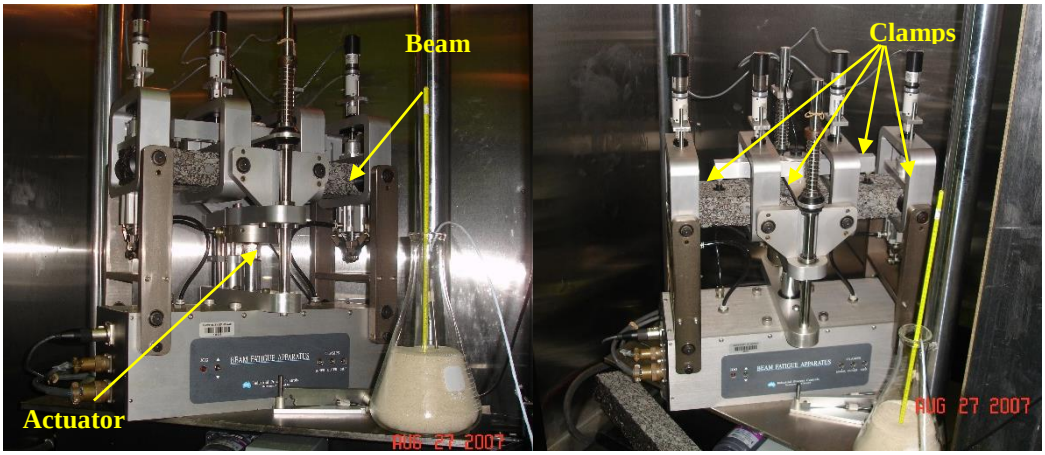

Figure 5-15. Beam Fatigue Apparatus used for fatigue testing.

Figure 5-16. Example of section exhibiting fatigue cracking.

If all the traffic loads were identical and the environmental conditions were constant over time (i.e., constant material characteristics over time), equation (5-1) could be used directly for verification of the adequacy of a trial pavement structure. To illustrate this, consider the following simple example. Let *n* be the predicted (expected) number of repetitions of the constant load magnitude over the design or performance period. The value of *n* is derived from traffic loading information. For example, consider the evaluation of a pavement for a section with constant traffic of *two* identical heavy vehicles per day. Further, assume that all heavy vehicles have two axles with exactly the same loads. For those conditions, the predicted value of *n* for a design period of say, 20 years, would be

n = (20 years) × (365 days/year) × (2 repetitions/veh) × (2 veh/day) = 29,200 repetitions. Thus, if N (the allowable number of repetitions corresponding to the strain level caused by the load in question) were greater than 29,200 repetitions then the design would be adequate from a bottom-up fatigue cracking perspective because the pavement would be able to withstand this number of repetitions without reaching the threshold of unacceptable level of fatigue cracking[25]. On the other hand, if N were lower than 29,200, the design would be inadequate since the cracking would become unacceptably high before reaching the end of the design period.

To illustrate the use of equation (5-1), suppose that the modulus of the mix is 1,000,000 psi (and for now assume this is constant throughout the year) and that the load produces a 150×10^{-6} (150 με) tensile strain at the bottom of the asphalt concrete layer. Then, the allowable number of repetitions is

$$N = 1.793\times10^{-3}\ (0.00015)^{-3.949}\ (1{,}000{,}000)^{-1.281} = 46{,}580$$

Therefore, in this case the pavement would reach the end of the design period with an acceptable level of cracking[26]. Had the computed allowable number of repetitions being much higher, say 2,000,000, the pavement would have been grossly over designed and then a weaker (and more economical) pavement structure should have been tried for the loading conditions under consideration.

For a larger load producing a 180×10^{-6} tensile strain the allowable number of repetitions is

$$N = 1.793\times10^{-3}\ (0.00018)^{-3.949}\ (1{,}000{,}000)^{-1.281} = 22{,}673$$

In this case, the pavement structure is clearly inadequate to withstand the predicted traffic loading of 29,200 repetitions over the design period.

As indicated before, many linear elastic layered analysis programs would make calculation of the tensile strains and in turn this type analysis very simple. The problem is that the assumptions made in the above examples are clearly unrealistic. Traffic loading is

---

[25] For simplicity, the example assumes that 50% of the total lane area cracking is an acceptable threshold criterion. In reality, 50% of the total lane area cracked is too high a value.

[26] Again 50% of the total lane area is a very high value, but it is used here to simplify the exposition.

always variable (with different vehicle classes, different axle configurations, and different axle loads as illustrated in chapter 3) and the environmental conditions are never constant, even for Hawaii that has relatively stable whether conditions compared to other parts of the country. In fact, near the pavement surface, variations of the HMA modulus of an intact layer of more than 500,000 psi could be expected from winter to summer in Hawaii.

5.4.2.1.1 Consideration of different traffic loads

When conditions are not constant, how should one evaluate the adequacy of the pavement? To illustrate the answer to this question, consider another simple (and still unrealistic) example. Suppose again the design period is 20 years and that the two axles of the heavy vehicles have different load levels L_1 and L_2. Let ε_{t1} and ε_{t2} be the maximum tensile strains at the bottom of the asphalt concrete layer caused by loads L_1 and L_2, respectively. Then, equation (5-1) could be used to compute N_{f1} and N_{f2} for load levels L_1 and L_2, respectively. Each of these values represents the number of repetitions of the respective load that the pavement could withstand if each of the loads were applied without the presence of the other. However, the loads are actually intermingled. In this particular example, an application of load L_1 is followed by an application of load L_2, then L_1 again, L_2 again and so on. Obviously, because of the presence of the two different loads, the pavement would reach an unacceptable level of cracking before N_{f1} or N_{f2} repetitions of load magnitudes L_1 and L_2 are applied. An important question is whether the pavement would survive the application of the loading predicted over the design period. Using again the simplified example of constant traffic consisting of two identical heavy vehicles per day, the predicted number of repetitions of loads L_1 and L_2 would be $n_1 = n_2$ = (20 years) × (365 days/year) × (1 repetition of load L_i/veh) × (2 veh/day) = 14,600 repetitions ($L_i = L_1$ or L_2 for n_1 or n_2, respectively).

Now suppose that (using a linear layer elastic computer program) the predicted tensile strains for loads L_1 and L_2 are 150×10^{-6} and 180×10^{-6} respectively. The corresponding allowable number of repetitions would then be

$$N_1 = 1.793\times10^{-3}\ (0.00015)^{-3.949}\ (1{,}000{,}000)^{-1.281} = 46{,}580$$

and

$$N_2 = 1.793\times10^{-3}\ (0.00018)^{-3.949}\ (1{,}000{,}000)^{-1.281} = 22{,}673$$

The answer to put all these pieces of information together is given by what is known as Miner's hypothesis or Miner's law [1], which states that fatigue *damage* of the asphalt concrete layer is given by the following relationship.

$$D = \sum_{i=1}^{M} \frac{n_i}{N_i} \tag{5-2}$$

where:

D = damage,

M = total number of load magnitudes,

n_i = actual predicted load repetitions for load magnitude L_i, and

N_i = load repetitions allowed under conditions prevailing in i.

Miner's hypothesis is simply a practical relationship that provides a mechanism to combine the effects of different traffic loads, though some question their validity.

As indicated before, the MEPDG has been calibrated so that when the damage is 100% (D=1) the predicted cracking is 50% of the total lane area (which in turn approximates 100% of the wheel path areas).

Thus returning to the example, the application of Miner's law in this case indicates that at the end of the design period the damage would be:

$$D = \frac{14{,}600}{46{,}580} + \frac{14{,}600}{22{,}673} = 0.313 + 0.644 = 0.957$$

Since D < 1, then the pavement would not have reached the 50% of the total lane area cracked, although it would be very close to doing so.

It is important to reiterate that 50% of the total lane area is a very high value of cracking. Typically a smaller threshold value is used. The equation used to translate damage into the percentage cracking used in the MEPDG for bottom-up fatigue cracking is[27]:

[27] A more complicated equation equivalent to equation (5-3) is presented in the MEPDG. However, knowledge of the more complicated equation is needed mostly for those involved in the calibration of the MEPDG cracking model. The complete expression is presented in section 7.5.2.

$$FC_{Bottom} = \frac{100}{1 + e^{\left[C_2'\left(-2 + \log 10\left(D \times 100\right)\right)\right]}} \quad (5\text{-}3)$$

where

FC_{bottom} = bottom-up fatigue cracking, percent lane area,

D = bottom-up fatigue damage, and

$$C'_2 = -2.40874 - 39.748 \times \left(1 + h_{AC}\right)^{-2.856}$$

and where:

h_{AC} = total thickness of the asphalt layers, in.

In the above example, the predicted level of cracking (assuming h_{AC} = 5 inches) is

$$FC_{Bottom} = \frac{100}{1 + e^{\left[\left(-2.647\right)\left(-2 + log 10\left(0.957 \times 100\right)\right)\right]}} = 48.7\ \%$$

The thickness of the asphalt concrete layer is included to account for the longer time it takes for a crack to propagate on a thick layer than on a thin layer.

With a cracking criterion of 50%, the pavement design would be acceptable[28].

5.4.2.1.2 Consideration of changing environmental conditions

In the ME approach, the effects of changes in environmental conditions can be taken into account in the same way as changes in load magnitudes; that is, using Miner's law. In the case of a single load magnitude but different environmental conditions, the law takes the form:

[28] Once again, in reality, a lower criterion (of about 20%) is more reasonable; 50% represents an excessive level. Reconstruction would is typically warranted before reaching such a high level.

$$D = \sum_{i=1}^{T} \frac{n_i}{N_i} \tag{5-4}$$

where:

D = damage,

T = total number of periods with different environmental conditions.

n_i = actual predicted load repetitions for period i.

N_i = load repetitions allowed under conditions prevailing in period i.

The reason why the predicted N changes from period to period is that the environmental conditions affect the moduli of the different pavement layers and as illustrated earlier this in turn changes the state of stresses and strains within the pavement structure. Thus, there are changes in both the strain and the modulus in equation (5-1). Temperature changes significantly affect the moduli of hot mix asphalt layers (as well as the moduli of unbound materials under freezing conditions) and changes in moisture affect the moduli of unbound materials. Consequently, even under identical loading conditions, the strains produced within the pavement structure are different on different periods and this in turn yields different values of N (see again equation (5-1)). Even the daily temperature changes affect the moduli of HMA.

For illustration, consider once again an example of a design for a 20-year period with traffic consisting of heavy vehicles with two axles with exactly the same loads. Assume the year has two distinct seasons (e.g., a dry, hotter season and a rainy, colder season) such that the pavement structure is overall stronger in the first season which last nine months (~ 274 days) than during the second season that last three months (~ 91 days). Suppose that the main reason for the pavement structure being stronger in the first season than in the second season is that during the second season moisture severely weakens the subgrade material. Nonetheless, during the first season (which is hotter), the HMA modulus is 900,000 psi and during the second season (colder) is 1,100,000 psi. Further, suppose that using the corresponding moduli, the computed maximum tensile strains at the bottom of the asphalt concrete layer are 120×10^{-6} and 170×10^{-6} for seasons 1 and 2 respectively. Under these conditions, the calculation of damage proceeds as follows:

Season 1:

n_1 = (20 years) × (274 days/year) × (2 repetitions/veh) × (2 veh/day) = 21,920

$$N_1 = 1.793 \times 10^{-3} \left(0.00012\right)^{-3.949} \left(900{,}000\right)^{-1.281} = 128{,}679$$

Season 2:

n_2 = (20 years) × (91 days/year) × (2 repetitions/veh) × (2 veh/day) = 7,280

$$N_2 = 1.793 \times 10^{-3} \left(0.00017\right)^{-3.949} \left(1{,}100{,}000\right)^{-1.281} = 25{,}148$$

Application of Miner's law then results in:

$$D = \frac{21{,}920}{128{,}679} + \frac{7{,}280}{25{,}148} = 0.170 + 0.289 = 0.459$$

Using equation (2.3) (again assuming an asphalt concrete layer thickness of 5 in) the computed damage results in the following percentage of bottom-up fatigue cracking in the total lane area:

$$FC_{Bottom} = \frac{100}{1 + e^{\left[\left(-2.647\right)\left(-2 + \log 10\left(0.459 \times 100\right)\right)\right]}} = 29.0\ \%$$

This value can then be directly compared against the agency threshold to assess whether the trial pavement structure is adequate. If a 20% threshold is used, then the trial pavement structure needs strengthening.

5.4.2.1.3 Consideration of different traffic loads and environmental conditions simultaneously

Different loads and environmental conditions are accommodated simultaneously in the ME approach with the following form of Miner's law:

$$D = \sum_{j}^{T} \sum_{i=1}^{M} \frac{n_{ij}}{N_{ij}} \tag{5-5}$$

where:

D = damage,

M = total number of load magnitudes,

T = total number of periods with different environmental conditions,

n_{ij} = actual predicted load repetitions for load magnitude L_i during period j, and

N_{ij} = load repetitions allowed for load L_i under conditions prevailing in j.

To illustrate the use of equation (5-5), assume as in the previous example that the year has two distinct seasons (e.g., a dry, hotter season and a rainy, colder season) such that the pavement structure is overall stronger in the first season which last nine months (~ 274 days) than during the second season that last three months (~ 91 days). Suppose again that during the first season (which is hotter) the HMA modulus is 900,000 psi and during the second season (which is colder) is 1,100,000 psi. Further, assume traffic loading consisting *on average* of 1.4 veh/day of a vehicle class with two axles (say, a local bus operating with low frequency on weekdays only) and 0.6 veh/days of another vehicle class with two axles (e.g., a 2-axle garbage truck). Assume the axle loads on the bus are L_1 and L_2 and those on the truck are L_3 and L_4 and that they produce tensile strains at the bottom of the HMA of 80×10^{-6}, 105×10^{-6}, 65×10^{-6} and 115×10^{-6}, respectively during season 1 and 100×10^{-6}, 120×10^{-6}, 80×10^{-6} and 140×10^{-6} respectively during season 2.

Under these conditions, application of Miner's law proceeds as follows:

Season 1:

n_{11} = (20 years) (274 days/year) (1 repetition/veh) (1.4 veh/day) = 7,672

$N_{11} = 1.793\times10^{-3}\ (0.00008)^{-3.949}\ (900{,}000)^{-1.281}$ = 638,107

n_{21} = (20 years) (274 days/year) (1 repetition/veh) (1.4 veh/day) = 7,672

$N_{21} = 1.793\times10^{-3}\ (0.000105)^{-3.949}\ (900{,}000)^{-1.281}$ = 218,031

n_{31} = (20 years) (274 days/year) (1 repetition/veh) (0.6 veh/day) = 3,288

$N_{31} = 1.793\times10^{-3}\ (0.000065)^{-3.949}\ (900{,}000)^{-1.281}$ = 1,448,774

n_{41} = (20 years) (274 days/year) (1 repetition/veh) (0.6 veh/day) = 3,288

$N_{41} = 1.793\times10^{-3}\ (0.000115)^{-3.949}\ (900{,}000)^{-1.281}$ = 152,230

Season 2:

n_{12} = (20 years) (91 days/year) (1 repetition/veh) (1.4 veh/day) = 2,548

$N_{12} = 1.793\times10^{-3}\ (0.0001)^{-3.949}\ (1{,}100{,}000)^{-1.281}$ = 204,435

n_{22} = (20 years) (91 days/year) (1 repetition/veh) (1.4 veh/day) = 2,548

$N_{22} = 1.793 \times 10^{-3} \left(0.00012\right)^{-3.949} \left(1{,}100{,}000\right)^{-1.281}$ = 99,511

n_{32} = (20 years) (91 days/year) (1 repetition/veh) (0.6 veh/day) = 1,092

$N_{32} = 1.793 \times 10^{-3} \left(0.00008\right)^{-3.949} \left(1{,}100{,}000\right)^{-1.281}$ = 493,462

n_{42} = (20 years) (91 days/year) (1 repetition/veh) (0.6 veh/day) = 1,092

$N_{42} = 1.793 \times 10^{-3} \left(0.00014\right)^{-3.949} \left(1{,}100{,}000\right)^{-1.281}$ = 54,137

Damage:

$$D = \frac{7{,}672}{638{,}107} + \frac{7{,}672}{218{,}031} + \frac{3{,}288}{1{,}448{,}774} + \frac{3{,}288}{152{,}230} + \frac{2{,}548}{204{,}435} + \frac{2{,}548}{99{,}511} + \frac{1{,}092}{493{,}462} + \frac{1{,}092}{54{,}137}$$

= 0.0120 + 0.0352 + 0.0023 + 0.0216 + 0.0124 + 0.0256 + 0.0022 + 0.0202

= 0.1315

Bottom-up fatigue cracking (for h_{AC} = 5 in.):

$$FC_{Bottom} = \frac{100}{1 + e^{\left[\left(-2.647\right)\left(-2 + \log 10\left(0.1315 \times 100\right)\right)\right]}} = 8.8\ \%$$

5.4.2.1.4 Summary for bottom-up fatigue cracking and consideration of other issues

Careful reading of the previous sections should provide those readers not familiar with ME procedures with a good idea of how different loading and environmental conditions are integrated in the bottom-up fatigue cracking procedures through Miner's law. As indicated at the beginning, the ideas and calculations are relatively simple. However, actual axle loads are typically different for different vehicle classes and vary over a wide range of magnitudes even for a single vehicle class. Furthermore the loads are applied through different axle configurations (single, tandem, tridem, and quad axles), which complicates matters further.

In all cases, the procedure involves the same computations for a given axle load magnitude and axle configuration and environmental conditions:

- Prediction of the expected number of repetitions of the axle in question under the given set of environmental conditions over the design period;

- Prediction of the maximum horizontal tensile strain at the bottom of the asphalt concrete layer produced by the axle in question under the given set of environmental conditions;
- Prediction of the corresponding allowable number of repetitions; and
- Computation of the damage (ratio of n/N) for the axle in question under the given set of environmental conditions.

The addition of the damage induced by each axle load magnitude and configuration for all different environmental conditions yields the total damage over the design period, which in turn is converted to a percentage of cracking over the total lane area.

Although the procedure in concept is simple, the bookkeeping of all these calculations becomes unmanageable with a large number of loads and environmental conditions. All these repetitive tasks are ideal for implementation in digital computers and fortunately, all the calculations are performed transparently to the user by the MEPDG, allowing the user to concentrate on the inputs to the problem and on the analysis of the outputs from the program. In fact, the MEPDG considers two more issues not yet discussed for fatigue cracking that make the bookkeeping even more complicated. The two issues are the environmental variations occurring within a period and the effects of traffic wander. Detailed discussion of these is beyond the scope of this report. Only a brief discussion is presented in subsequent text.

5.4.2.1.5 Changes of environmental conditions within a season

All the examples presented above assume that environmental conditions within a season were constant. In reality, there are always monthly and even daily variations. Seasonal effects within the MEPDG are considered on a monthly basis[29]. In order to reduce the number of computations, the MEPDG subdivides the distribution of temperatures expected during the month into five quintiles and computes the corresponding damage for each assuming that traffic is distributed equally during each quintile. The subdivision of the temperature distribution is illustrated in Figure 5-17 in terms of the normalized variable $z = (t - \mu)/\sigma$,

[29] Under freezing and thawing conditions, the MEPDG uses half-month periods but this is not applicable for most of Hawaii.

where t = temperature, μ = mean temperature during the season and σ = standard deviation of temperature during the season.

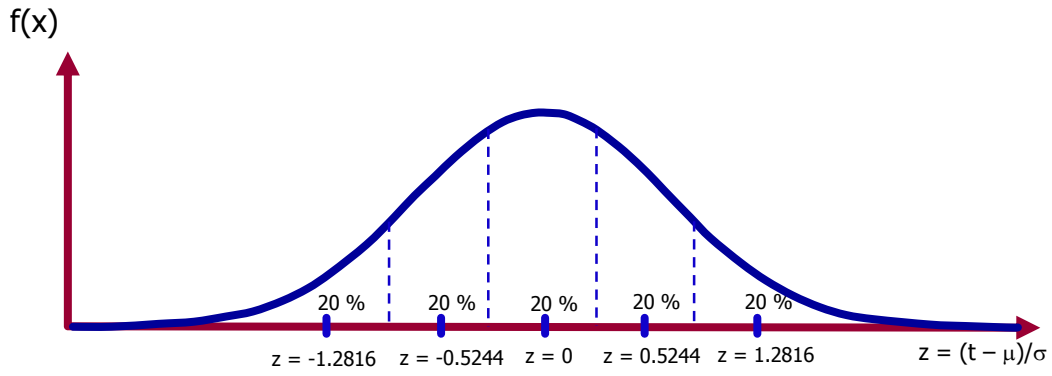

Figure 5-17. Consideration of temperature distributions within a season in the MEPDG.

5.4.2.1.6 Traffic wander

The discussions in the previous sections assumed that each traffic load is located in the same position within the transverse pavement section. Actual traffic loading, however, typically exhibits a distribution of lateral positions known as wander as illustrated in part C of Figure 5-18 below. A normal distribution is typically assumed for traffic wander.

In all the previous examples, the damage was estimated using the maximum tensile strain at the bottom of the asphalt concrete layer and the location of the point where that maximum occurs was assumed to be the same for each load repetition. However, the maximum damage does not occur always at the same point for consecutive load applications. As indicated in part B of the figure, *a single passage* of a load produces variable damage laterally. For the dual wheel configuration shown in the figure, the maximum damage appears to be close to the center of each wheel. The shape of this damage curve actually depends on the thickness of the asphalt concrete layer among other things, so this is not always the case.

Wander makes the determination of the location with maximum damage difficult. In order to solve the problem, the MEPDG evaluates the damage at different points at the bottom of the asphalt concrete layer as shown by points 1 through 5 in part A of the figure (actually, a larger number of points is analyzed by the MEPDG). As with the temperature effects described in the previous section and in order to simplify the analysis, the wander distribution (assumed to be normally distributed) is split into five quintiles and the loads are located at a representative point of the quintile to evaluate the damage. For example, consider

the damage D_1 caused at point 3 by a load located as shown in part D of the figure. In this case the damage at point 3 is practically zero. When the load is located as in part E, the damage at point 3 is D_2. Similar observations can be made for the other three quintiles. Then the total damage caused on average at point 3 is simply $D = 0.2\ D_1 + 0.2\ D_2 + 0.2\ D_3 + 0.2\ D_4 + 0.2\ D_5$ since there is an equal chance of 20% of the load being located on any of these positions.

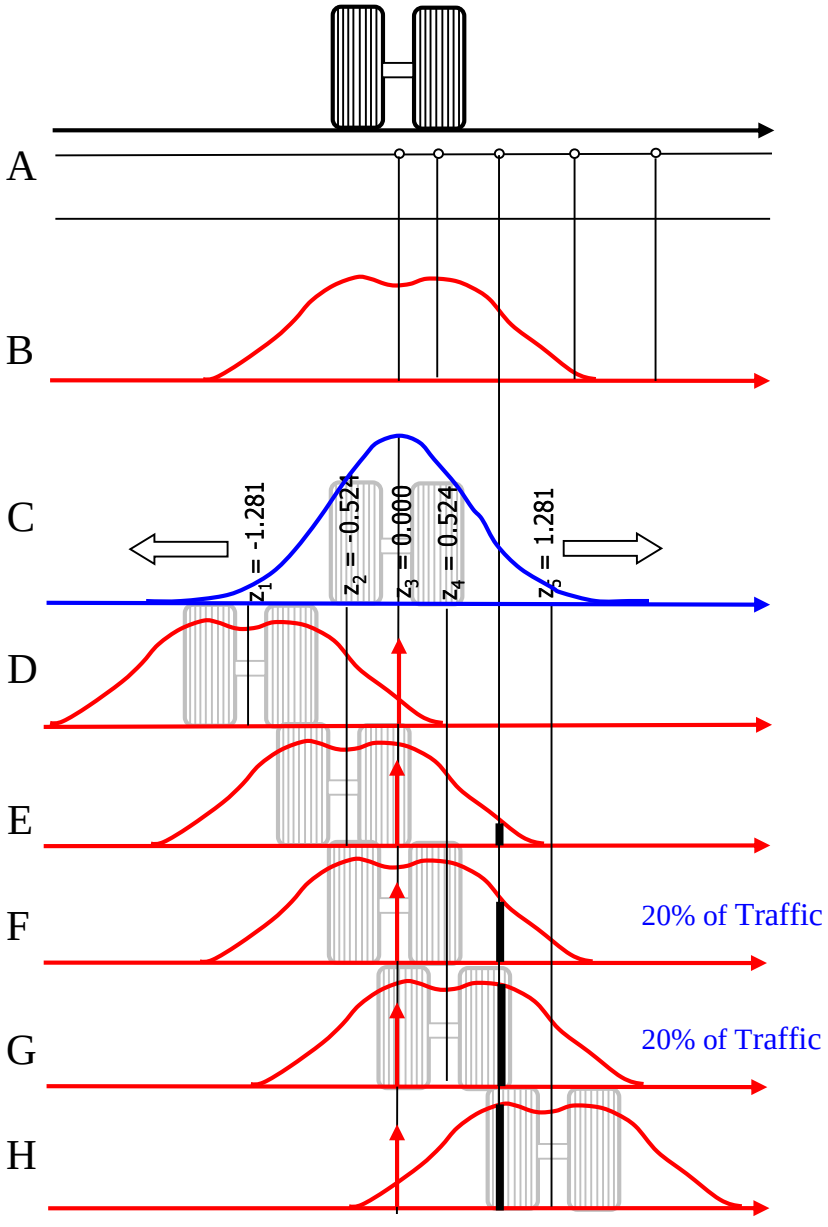

Figure 5-18. Treatment of Wander in the MEPDG.

The analysis is a bit more complex for tandem, tridem, and quad axles since the search of the point with the highest damage also needs to be performed longitudinally. The details are beyond the scope of this introduction.

Again, this description is provided only so that the designer is aware of the effects of wander and understands the importance of the related input in the MEPDG, which consists of a single value. All the calculations are done transparently by the MEPDG.

5.4.2.2 Rutting or permanent deformation

Rutting is a surface depression in the wheel paths normally accompanied by small upheavals to the sides. It is caused by inelastic or plastic deformations in any or all of the pavement layers and subgrade. As indicated in the MEPDG, these plastic deformations are typically the result of:

- Densification or one-dimensional compression and consolidation, and
- Lateral movements or plastic flow of materials (HMA, aggregate base, and subgrade soils) from wheel loads.

Figure 5-19 illustrates rutting apparently originating mostly in the asphalt concrete by plastic flow in the HMA.

Figure 5-19. Section with center and right lanes exhibiting noticeable rutting in the mix.

As indicated in [1], “The width and depth of the rutting profile is highly dependent upon the pavement structure (layer thickness and quality), traffic loading and the environment at the design site. In the transverse profile, rutting along the wheel path modifies

drainage characteristics and reduces runoff capability. Water can accumulate in traffic lanes, creating conditions for aquaplaning of vehicles, reduced skid resistance of the surface course, and unsafe traffic conditions. In the longitudinal profile, differential permanent deformations due to variability of materials and/or construction increase roughness and reduce the overall serviceability of the road."

A major objective of the MEPDG is to ensure that asphalt mix design is definitely linked to the structural design process. The MEPDG evaluates the permanent deformation within all rut susceptible layers (generally asphaltic and all unbound material layers) in the pavement within the analysis period. The contribution to the total rut depths from each layer are predicted as a function of time and traffic repetition. As for fatigue cracking, the approach presented in the MEPDG for permanent deformation is based upon calculating incremental distortion or rutting within each sublayer. First, for the mechanistic analysis the pavement structure is subdivided in sublayers as shown in Figure 5-20:

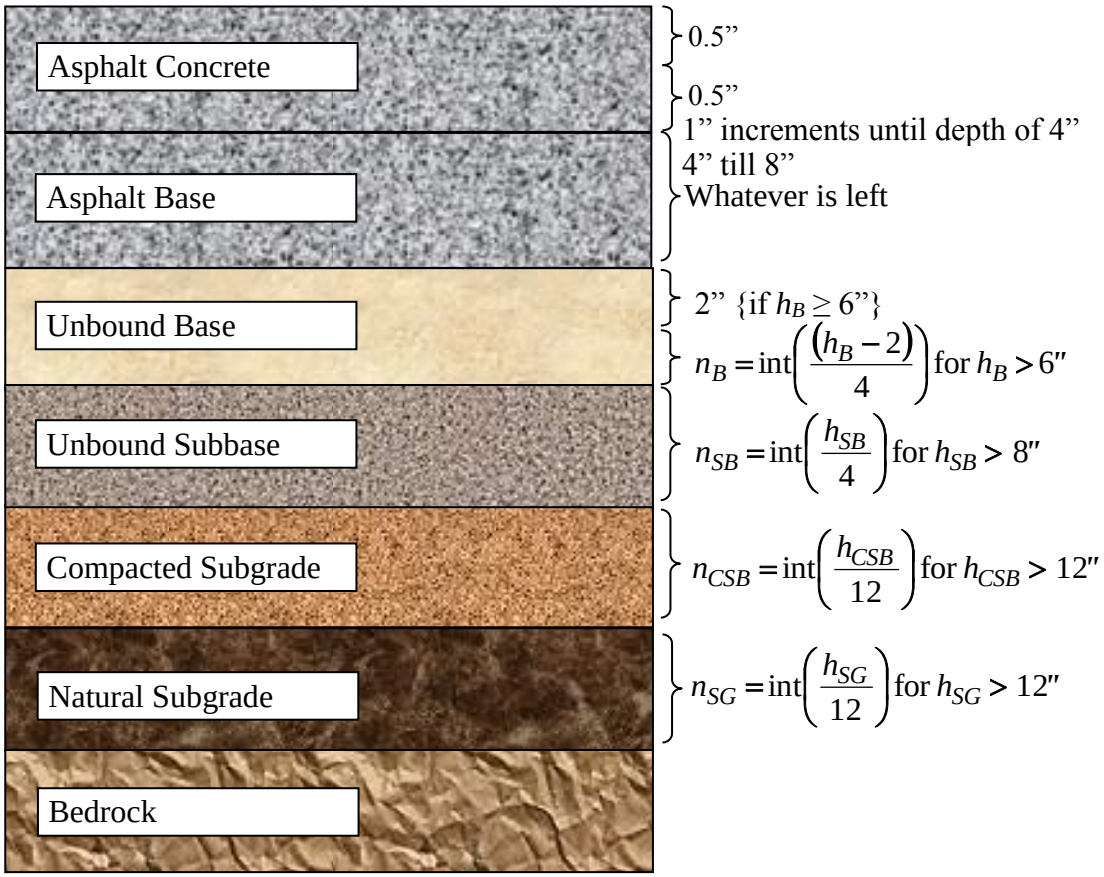

Figure 5-20. Sublayering used by the MEPDG **[1]**.

During the mechanistic analysis, the MEPDG computes the maximum vertical compressive strains at mid-depth of each sublayer. These strains are termed ε_r since they are based on elastic assumptions and thus represent recoverable or resilient deformation[30]. These are the mechanistic responses that are linked empirically to the permanent deformation.

The function linking the mechanistic response to the permanent deformation is derived from laboratory experiments adjusted to represent field conditions. Unlike cracking, which occurs on the bound layers only[31], the permanent deformation generally occurs in all layers and therefore permanent deformation models are needed for the different materials of each layer. Specifically, for asphalt concrete mixes, the function (explained in detail below) is derived from laboratory repeated load permanent deformation triaxial tests. The result of one such test is presented in Figure 5-21, which shows the total permanent deformation as a function of the number of repetitions of a certain load magnitude under certain confinement conditions. The results in the figure were obtained with the Simple Performance Tester (SPT) or as is now known the Asphalt Mix Performance Tester (AMPT) of the University of Hawaii at Manoa shown in Figure 5-22.

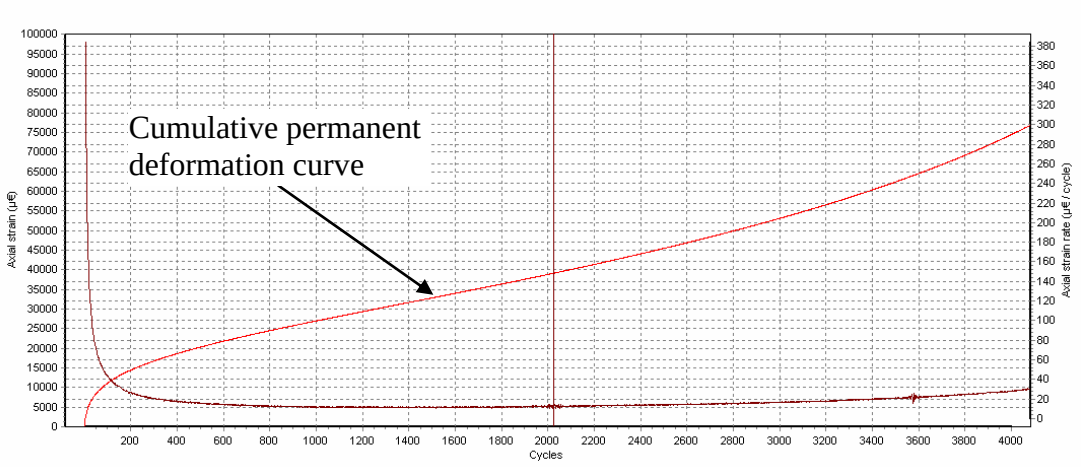

Figure 5-21. Example of the output from permanent deformation test results.

[30] For unbound materials the MEPDG uses the symbol ε_v instead of ε_r since ε_r is reserved for the resilient strain obtained *during the laboratory tests* used to determine the permanent deformation model parameters.

[31] The MEPDG also models cracking originating in cement treated bases.

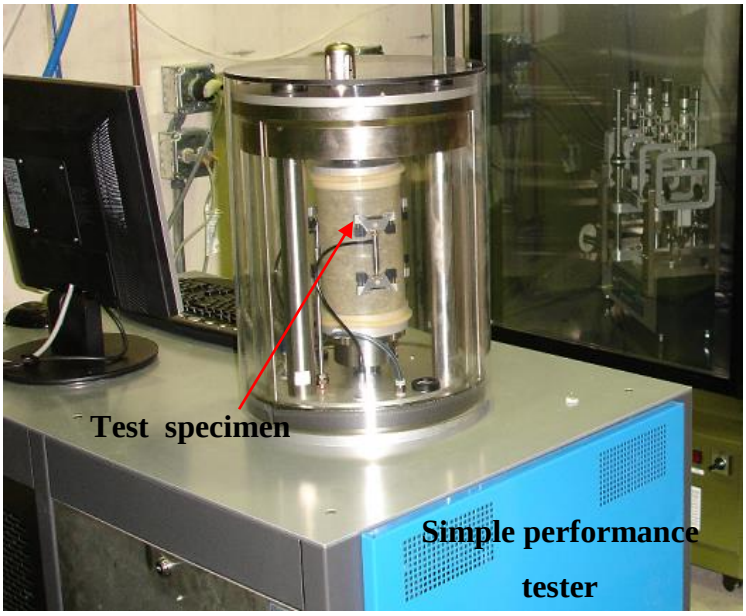

Figure 5-22. Simple performance tester.

The test results shown in Figure 5-21 exhibit the three stages typically observed under axial repeated loading permanent deformation tests. These are illustrated schematically in Figure 5-23. The first stage exhibits high rates of deformation mostly due to rearrangement of the structure of the mix under the new loading conditions. During the second stage, the deformation rate is approximately constant. Finally, the third stage is where the rate of deformation increases with each load repetition until complete failure occurs.

The total permanent deformation in Figure 5-23 after *N* loading cycles is the accumulation of the permanent deformation that occurs during each loading cycle. Figure 5-24 illustrates schematically the permanent (plastic) and resilient strains occurring in a mix during one cycle.

The MEPDG models only the first two stages of permanent deformation with the first stage being considered only as an extrapolation of the secondary stage. Specifically, the *laboratory*-derived model in the MEPDG for asphalt concrete mixes is:

$$\frac{\varepsilon_p}{\varepsilon_r} = 10^{-3.15552} T^{1.734} N^{0.39937} \qquad (5\text{-}6)$$

In this equation, ε_p is the total permanent deformation accumulated up to cycle *N*, *T* is the temperature of the mix during the test in °F and ε_r is the resilient strain corresponding to

the state of stresses applied during the test. It has been found experimentally that during the permanent deformation test the resilient strain is approximately constant.

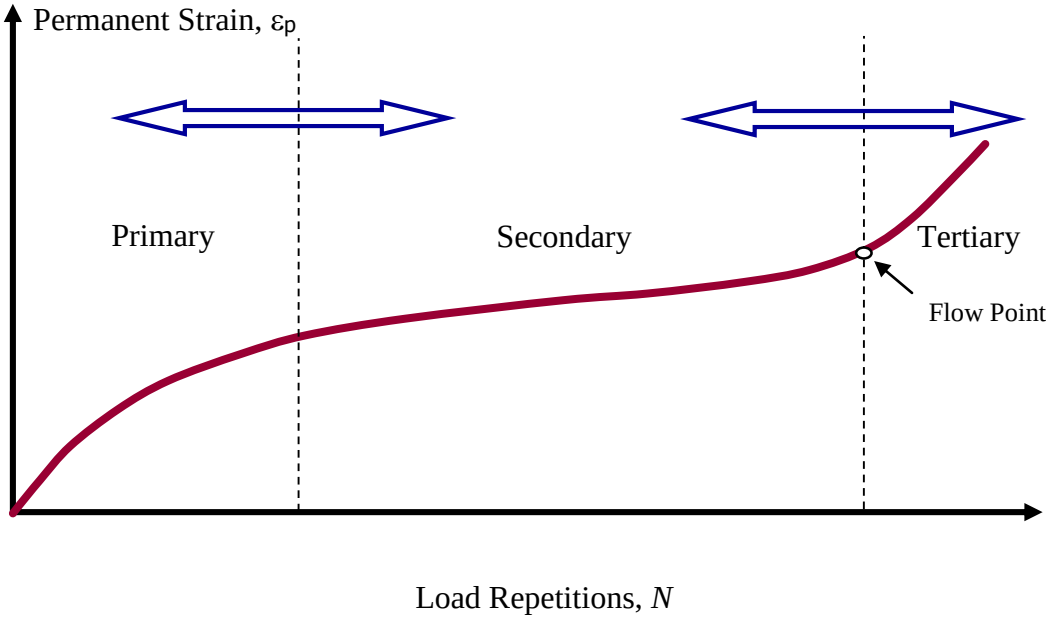

Figure 5-23. Three stages of permanent deformation **[1]**.

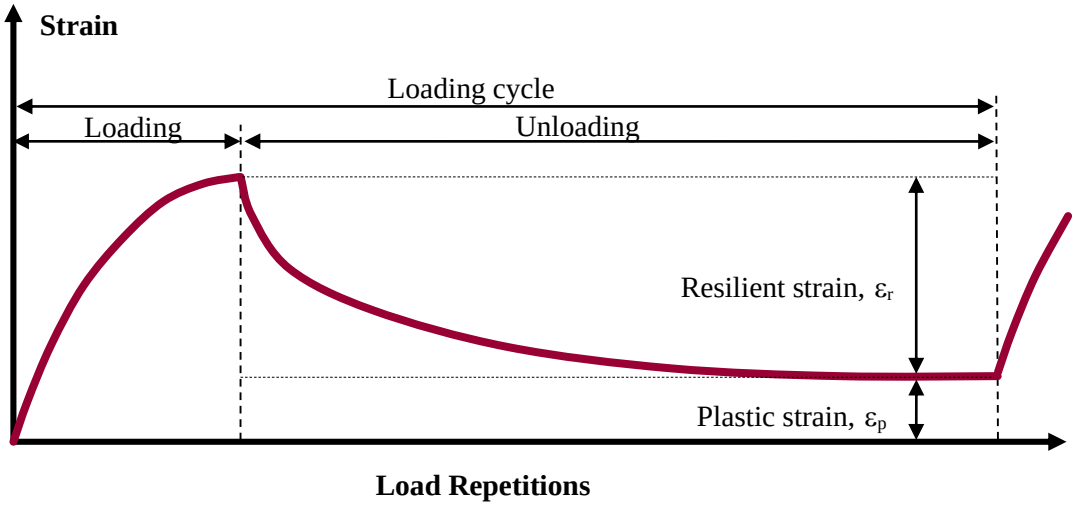

Figure 5-24. Schematic of the permanent (plastic) and resilient strains occurring in a mix during one loading cycle.

The above equation was calibrated for field conditions by the MEPDG research team. The final expression used to compute permanent deformation within an HMA sublayer is

essentially equation (5-6) calibrated for field conditions multiplied by the thickness of the sublayer in question. Specifically[32],

$$\Delta_{p(HMA)} = \varepsilon_{p(HMA)} h_{HMA} = k_z \beta_{r1} 10^{k_1} T^{k_2 \beta_{r2}} n^{k_3 \beta_{r3}} \varepsilon_r h_{HMA} \quad (5\text{-}7)$$

where

$\Delta_{p\,(HMA)}$ = Accumulated permanent or plastic vertical deformation in the HMA layer/sublayer, in.

$\varepsilon_{p\,(HMA)}$ = accumulated permanent or plastic axial strain in the HMA layer/sublayer, in/in.

$\varepsilon_{r\,(HMA)}$ = resilient or elastic calculated by the structural response model at the mid-depth of each HMA sublayer, in/in.

h_{HMA} = thickness of the HMA layer/sublayer, in.

n = number of axle load repetitions.

T = mix or pavement temperature, °F.

k_z = depth confinement factor.

k_1, k_2, k_3 = global field calibration parameters[33] (from the NCHRP 1-40D recalibration; $k_{1r} = -3.35412$, $k_{2r} = 1.5606$, $k_{3r} = 0.4791$)

$$k_z = (C_1 + C_2\ depth)\ 0.328196^{depth}$$

$$C_1 = -0.1039\ h_{ac}^2 + 2.4868\ h_{ac} - 17.342$$

$$C_2 = 0.0172\ h_{ac}^2 - 1.7331\ h_{ac} + 27.428$$

$\beta_{r1}, \beta_{r2}, \beta_{r3}$ = local calibration factors

Note that the factor k_z was incorporated to correct for confining pressure at different depths. The parameters β_{r1}, β_{r2}, and β_{r3} can be used to calibrate the rutting model for local

---

[32] In [22], h_{HMA} is missing from the term on the right of the second equal sign.

[33] There is an inconsistency in the treatment of the parameters k_{2r} and k_{3r} between the Interim MEPDG Manual of Practice documentation [22] and the MEPDG software help and Pavement ME software. The notation above agrees with the software.

conditions provided a historical PMS database is available with rutting information as well pavement structural (including rehabilitation), loading, and mix characteristics information.

For unbound materials, the following field-calibrated mathematical equation is used to calculate plastic vertical deformation within all unbound sublayers and the foundation or embankment soil:

$$\Delta_{p(soil)} = \beta_{s1} k_{s1} \left(\frac{\varepsilon_0}{\varepsilon_r} \right) e^{-\left(\frac{\rho}{n}\right)^{\beta}} \varepsilon_v h_{soil} \tag{5-8}$$

where

$\Delta_{p(soil)}$ = permanent or plastic deformation for the layer/sublayer, in.

n = number of axle load applications.

ε_0 = intercept determined from laboratory repeated load permanent deformation tests, in/in.

ε_r = resilient strain imposed in laboratory test to obtain material properties ε_0, b, and r, in/in.

ε_v = average vertical resilient or elastic strain in the layer/sublayer and calculated by the structural response model, in/in.

h_{soil} = thickness of the unbound layer/sublayer, in.

k_{sl} = global calibration coefficients; k_{sl} = 1.673 for granular materials and 1.35 for fine grained materials.

β_{s1} = local calibration constant for the rutting in the unbound layers; the local calibration constant was set to 1.0 for the global calibration effort.

$\log \beta$ = -0.61119 – 0.017638 (W_c)

$$\rho = 10^9 \left(\frac{C_0}{\left(1 - \left(10^9\right)^{\beta}\right)} \right)^{\frac{1}{\beta}} \tag{2.9}$$

$$C_0 = \ln\left(\frac{a_1 M_r^{b_1}}{a_9 M_r^{b_9}}\right) \quad (2.10)$$

W_c = water content, percent.

M_r = resilient modulus of the unbound layer or sublayer, psi.

$a_{1,9}$ = regression constants; a_1 = 0.15 and a_9 = 20.0.

$b_{1,9}$ = regression constants; b_1 = 0.0 and b_9 = 0.0[34].

As indicated before, the relevant result of the mechanistic analysis for rutting is the resilient strain ε_r (or ε_v for unbound materials). With the value of ε_r (ε_v) computed at different depths within the pavement structure, the plastic deformations for each layer/sublayer can be estimated using equations (5-7) or (5-8) and these, in turn, can be used to estimate the total permanent deformation in the pavement structure (rutting) as follows:

$$RD = \sum_i \Delta_{p(HMA)}^i + \sum_j \delta_{aGran}^j + \sum_m \delta_{aSub}^m \quad (5\text{-}9)$$

where

RD = pavement permanent deformation (in the sub-season).

Δ_p^i = total plastic deformation in HMA sublayer *i*.

$\delta_d{}^j{}_{Gran}$ = total plastic deformation in granular base sublayer *j*.

$\delta_a{}^m{}_{Sub}$ = total plastic deformation in subgrade sublayer *m*.

The above process is repeated and accumulated for each sub season therefore providing an estimate of rut depth progression.

5.4.2.3 Other distress types considered by the MEPDG for flexible pavements

As indicated earlier, the MEPDG can calculate other distress types. In fact, the user can decide which distress types considered by the MEPDG should be included in the analysis. For asphalt concrete pavements, the additional distresses are thermal cracking, top-

[34] Since both β_1 and β_9 are zero, C_0 could be simplified to $C_0 = \ln(a_1/a_9) = \ln(0.15/20) = -4.893$, which is a constant. It is not clear why the MEPDG researchers chose to present the equation in this more complicated form. The same equation is presented in the MEPDG Manual of Practice [22].

down fatigue cracking, and reflection cracking. In addition, the MEPDG can also calculate smoothness (roughness) as a function of the distresses.

5.4.2.3.1 Thermal cracking

Because of the narrow range of relatively high temperatures prevalent in Hawaii, thermal cracking is not a major concern on the State's roads. As expected, when performing the calibration it was found that no thermal cracking is predicted for state roads regardless of how much the corresponding calibration parameter was changed. This is not surprising since the thermal cracking model is based on temperatures below freezing. Therefore, its consideration for pavement design in Hawaii is not recommended. This simplifies somewhat the number of inputs that must be considered in detail.

5.4.2.3.2 Top down fatigue cracking

The approach used by the MEPDG for top-down fatigue cracking is almost identical to the one presented above for bottom-up fatigue cracking. The main differences are that the location of the critical strain is at the surface of the asphalt concrete layer instead of at the bottom and that there are some differences in the empirical equations and the measurement of cracking (top-down fatigue cracking is calibrated with longitudinal cracking, which is measured in ft./mile).

As described later in the calibration portion of this report (section 7.5, page 388), this is probably the main mechanism by which cracking starts on state roads with thick pavement structures.

As stated in the MEPDG "the engineer should recognize that given a choice between surface longitudinal [top-down] cracking and alligator [bottom-up] cracking, it will normally be advisable to select the longitudinal surface cracking distress over alligator cracking. The reason for this is due to the fact that the eventual presence of surface (top down) cracks as well as permanent deformation in the upper HMA layers, can always be milled in future rehabilitations strategies. However, if alligator cracking is present, the chances of full "slab-layer" damage for the total HMA layer(s) are quite high. If this is the case, it is apparent that complete removals of the HMA layer or very thick overlays are the only preferred rehabilitation option."

At this point it is recommended to limit longitudinal cracking to 2000 ft./mi as recommended in the MEPDG. More research is needed to find out if 1) most of the observed

longitudinal cracking really corresponds to top-down cracking and 2) if so, at what level the cracks start to propagate through the whole layer thickness (if they do). If cracking is allowed to reach this point, then whether it started from the top or the bottom does not make much difference since the structural integrity is lost anyway.

5.4.2.3.3 Reflection cracking

Despite the limitations for modeling reflection cracking in the current MEPDG procedures, its consideration for overlay design represents a move in the right direction since this is a major distress mode in HMA overlays of both flexible and PCC pavements. The rest of this section is mostly reproduced from the MEPDG documentation.

Reflection cracking refers to the propagation of cracks through the overlay due to movements near cracks and joints in the existing pavement. This movement may be vertical due to loading, horizontal due to temperature changes, or more probably a combination of both. Load-induced movements are influenced by the thickness of the overlay and the thickness, modulus, and load transfer in the existing pavement. Temperature induced movements are influenced by daily and seasonal temperature variations, the coefficient of thermal expansion of the existing HMA and PCC layers and the spacing of cracks.

The complex combination of tensile and shear strains at the bottom of the overlay cause cracks to initiate at the bottom of the HMA layer. With time, the cracks propagate upward through the HMA overlay. As the process continues, multiple reflection cracks will form and eventually portions of the HMA overlay will spall and dislodge from the pavement surface. Even with periodic or routine maintenance (crack sealing), reflection cracks eventually lead to a reduction of pavement smoothness and shorten the life of the overlay. The overlay design procedure allows the designer to consider two types of reflection cracks: reflection of cracks that exist on the surface prior to overlay placement and those that develop in the existing surface after overlay placement.

5.4.2.3.3.1 Existing Cracks in Pavement Surface – Prior to Overlay Placement.

The MEPDG uses a simplified empirical model to predict the percentage of cracks in the overlaid pavement that propagate through the overlay. Specifically, it considers the percentage of cracks as a function of time using a sigmoidal function:

$$RC = \frac{100}{1 + e^{a+bt}} \quad (5\text{-}10)$$

where:

RC = Percent of cracks reflected, %.

t = Time, years.

a and b = Fitting parameters.

The parameters a and b for HMA overlays of flexible pavements are given by

$a = 3.5 + 0.75\ h_{AC}$

and

$b = -0.688584 - 3.37302\ h_{AC}^{(-0..915469)}$

where

h_{AC} = thickness of the overlay, in.

Clearly, this model is very limited as it does not consider the influence of traffic loading or environment (although this could be achieved by making the parameters a and b to vary with these variables). Furthermore, it requires further local calibration. For this, however, a database will be required containing at a minimum information on cracking condition before placement (and if applicable after milling), cracking after overlay placement (preferable at several points in time), overlay thickness and mix type, and traffic loading.

The empirical model for reflective cracking is used for estimating the amount of cracking from a non-surface layer that has reflected to the surface after a certain period of time. Although the model is limited, it represents a first effort to include this important distress type in rehabilitation designs.

5.4.2.3.3.2 Cracks Occurring in Existing Pavement Layers after Overlay Placement

Even after overlay placement, the underlying bound layers (including all asphalt bound and chemically stabilized layers) undergo additional fatigue damage with continued traffic loading, and eventually crack. The continual fatigue damage accumulation of these layers is considered in the MEPDG overlay analysis procedures.

For any given month *m*, the total fatigue damage is estimated by the following equation:

$$D_m = \sum_{i=1}^{m} \Delta D_i \tag{2.13}$$

where:

D_m = Damage for month *m*.

ΔD_i = Increment of damage in month *i*.

The area of fatigue cracking for the underlying layer at month *m* (CA_m) is given by equation (2.14).

$$CA_m = \frac{100}{1 + e^{6 - 6D_m}} \tag{5-11}$$

For each month *i*, there will be an increment of damage ΔD_i (calculated using similar procedures to the ones explained earlier) which will cause an increment of cracking area ΔCA_i to the stabilized layer. To estimate the amount of cracking reflected from the stabilized layer to the surface of the pavement for month *m*, the reflective cracking model is applied incrementally, as follows:

$$TRA_m = \sum_{i=1}^{m} RC_{m-i} \times \Delta CA_i \tag{5-12}$$

where:

TRA = Total reflected area for month *m*.

RC_{m-i} = Percent cracking reflected for Age = $m - i$; (Age in years).

ΔCA_i = Increment of fatigue cracking for month *i*.

The reflective cracking model is applied to each increment of fatigue cracking area because the time elapsed for each of these increments is different. The model included in the MEPDG is based on engineering judgment and a limited amount of published data from Georgia [1].

5.4.2.3.3.3 Smoothness (Roughness)

Functional adequacy is quantified in the MEPDG by pavement smoothness. The parameter used to define pavement smoothness (or roughness which is the lack of smoothness) in the MEPDG is the International Roughness Index (IRI). Rough roads lead to user discomfort and higher vehicle operating costs.

In the MEPDG, IRI is predicted empirically as a function of pavement distresses, site factors that represent the foundation's shrink/swell and frost heave potential, and an estimate of the IRI at the time of construction. The design premise included in the MEPDG for predicting smoothness degradation is that the occurrence of surface distress will result in increased roughness (increasing IRI value), or in other words, a reduction in smoothness. The unit of smoothness calculated by the MEPDG is inches per mile (meters per kilometer).

The MEPDG uses equation (5-13) to predict IRI development on new HMA pavements and HMA overlays:

$$IRI = IRI_0 + 0.0150(SF) + 0.400(FC_{Total}) + 0.080(TC) + 40.0(RD) \quad (5\text{-}13)$$

where

IRI_0 = initial IRI after construction, in/mi.

SF = site factor, refer to equation (5-14) below.

FC_{Total} = area of fatigue cracking (combined alligator, longitudinal, and reflection cracking in the wheel path), percent of total lane area. All load related cracks are combined on an area basis – length of cracks is multiplied by 1 foot to convert length into an area basis.

TC = length of transverse cracking (includes the reflection of transverse cracks in existing HMA pavements), ft./mi.

RD = average rut depth, in.

The site factor (SF) is calculated by:

$$SF = Age(0.02003(PI + 1) + 0.007947(\text{Precip} + 1) + 0.000636(FI + 1)) \quad (5\text{-}14)$$

where

Age = pavement age, years.

PI = percent plasticity index of the soil.

FI = average annual freezing index, degree F days.

Precip = average annual precipitation or rainfall, in.

These equations are used by the MEPDG to predict IRI over time (as the predictions of cracking and rutting also change over time).

CHAPTER 6. MATERIAL CHARACTERIZATION

6.1 INTRODUCTION

As discussed in chapter 5, material properties such as modulus and Poisson ratio play a fundamental role in the prediction of pavement responses. In addition, some of the parameters of the fatigue and permanent deformation models also depend on material characteristics. Other material properties such as the coefficient of thermal expansion (COE) and flexural strength of concrete are fundamental for PCC pavement design. Binder viscosity and dynamic shear modulus, thermal conductivity and heat capacity of different materials, soil characteristic curves (which affect the water content variations over time), unbound material gradations, and permeability are other properties playing a role in pavement performance.

A major challenge to the use of a mechanistic-empirical (ME) pavement design procedure is obtaining reliable inputs. The hierarchical input level scheme in the MEPDG provides the user a lot of flexibility for obtaining the inputs based on the criticality of the project and the available resources [22]. For practical reasons, material testing for most projects is limited to some properties that are relatively easy to measure. Furthermore, it is common to measure properties, such as CBR or R-value of unbound materials that are related to the properties of interest only through correlations.

Even for very important projects, some properties would need to be estimated. Clearly, accurate estimates of actual material properties would result in designs that are more representative of the actual pavement performance. Consequently, it is desirable to have a library of local material properties, at least for those properties that may affect the designs the most.

This chapter describes available information on material properties as well as the efforts that as part of this and other related projects were performed to characterize them. The material properties discussed include dynamic modulus, permanent deformation, and fatigue cracking of HMA mixtures, viscosity and dynamic shear modulus of asphalt binders, resilient modulus of granular materials, resilient modulus of soils, and coefficient of thermal expansion of concrete. The permeability of a coarse-grained base material considered as an alternative to the untreated permeable base material currently used is also presented. In order

to limit the length of the chapter, only the most relevant aspects are described on it. A lengthy discussion is provided on layer moduli (dynamic modulus of asphalt concrete mixes and resilient modulus of unbound materials) as these are essential for the computation of stresses and strains. Several assumptions are needed for estimation of these properties. Other details are relegated to appendices.

6.2 DYNAMIC (COMPLEX) MODULUS

The description of the ME approach in the preceding chapter highlights the importance of the determination of the moduli of the different layers. These are used for the computation of the resilient strains by the structural response model (mechanistic analysis, Figure 5-2). Then, the resilient strains are used for calculating distresses and roughness using empirical functions (section 5.4.2).

The Mechanistic-Empirical Pavement Design Guide (MEPDG) uses the dynamic modulus (|E*|) as the design stiffness parameter of Hot Mix Asphalt (HMA) and the resilient modulus as the stiffness parameter of granular bases, subbases, and subgrades. The following paragraphs describe the information available about the dynamic modulus. Resilient modulus of unbound materials and soils is discussed in section 6.3.

6.2.1 Dynamic Modulus - |E*| Definition

Dynamic modulus (|E*|) is the *absolute value* of another quantity known as the complex modulus, E*. The complex modulus E* is used in the theory of viscoelasticity to predict time dependent (but recoverable deformations). The MEPDG does not use viscoelastic calculations to predict stresses and strains caused by loads. Nevertheless, |E*| has been adopted as the elastic modulus of HMA for stress and strain computations.

Before presenting their formal definitions, it is convenient to describe briefly the equipment and procedure used to measure them.

Several pieces of equipment capable of applying cyclic compressive loading with or without confinement could be used for dynamic modulus determination. However, because of some complexities with these pieces of equipment, a major component of NCHRP Project 9-29, *Simple Performance Tester for Superpave Mix Design* [37], was the design and manufacture of a simple performance tester capable of performing among others, the dynamic modulus test. As a result, what is now known as the Asphalt Mixture Performance

Tester (AMPT) was developed[35]. Details on the development of the AMPT can be found in Chapter 3 of [38]. The final equipment specification for the AMPT is included as Appendix E in [39].

6.2.1.1 Description of the AMPT

The AMPT is a bottom loading dynamic testing machine with a triaxial cell that doubles as environmental conditioning chamber due to a fully integrated refrigeration and heating unit, a hydraulic dynamic actuator with its associated hydraulic power supply, and a high response control and data acquisition system (Figure 6-1).

Figure 6-1. Asphalt Mixture Performance Tester.

The loading frame, consisting of three vertical columns and two heavy-duty circular crossheads, is specifically designed to limit deflection and vibrations which might influence the accuracy of measurements during dynamic testing of Hot Mix Asphalt (HMA). The internal dimensions of the system allow the evaluation of 150 mm tall specimens with a

[35] The original name of the AMPT was Simple Performance Tester (SPT) and much of the literature refers to it as such.

diameter of 100 mm. The AMPT test specimens are usually obtained after coring and sawing mixes compacted with the Superpave Gyratory Compactor (SGC), although specimens obtained from field coring activities can also be used, provided the HMA is thick enough.

Figure 6-2 shows the test set up with the Asphalt Mixture Performance Tester (AMPT) with a sample inside. The dynamic loading is applied to the HMA specimen by means of a low friction, double acting, high-speed hydraulic force actuator, which also includes a co-axial displacement transducer. For dynamic modulus testing, axial deformations are measured by means of specimen-mounted LVDTs.

Considering the particular characteristics of asphalt mixtures, the AMPT features an environmental chamber with temperature control of ± 0.5 °C between 4 °C and 60 °C that doubles as a confining cell if triaxial testing of the specimens is required. Dynamic modulus tests are typically performed under unconfined conditions. Nevertheless, the ability to apply confinement to the specimens with the AMPT is particularly useful for permanent deformation testing, where stress levels that more closely replicate those observed in the field are required. There is also evidence that confinement affects dynamic modulus, particularly at high temperatures and low frequencies [40].

As required by the AASHTO TP79 specification [41], control of the systems and data acquisition and processing of all the relevant signals before and during the tests are performed electronically by means of fully automated pre-programmed routines. Although many variations of the test procedure to determine |E*| can be found worldwide, arguably the most common methods are the recently released AASHTO T342 [42] (which is based on the formerly known AASHTO TP62) and AASHTO TP79, which is the standard test procedure established specifically to determine the dynamic modulus of HMA with the AMPT [41].

The two test protocols are used to determine the dynamic modulus of asphalt mixtures in axial loading mode at various combinations of temperature and loading frequency. In both methods a dynamic compressive axial stress is applied perpendicular to the parallel flat faces of a cylindrical HMA specimen, producing a deformation small enough to ensure that the asphalt material behaves elastically. From a testing point of view, the two procedures are very similar, except that a reduced number of temperatures and an expanded range of frequencies are prescribed in AASHTO TP79 (specifically, testing at temperatures of 4.4, 21.1, and 46.1°C and at loading frequencies of 10, 1.0, 0.1, and 0.01 Hz). As reported by Bonaquist in

[38], the use of a reduced number of temperatures and frequencies in developing a dynamic modulus master curve for asphalt mixtures was found to be appropriate.

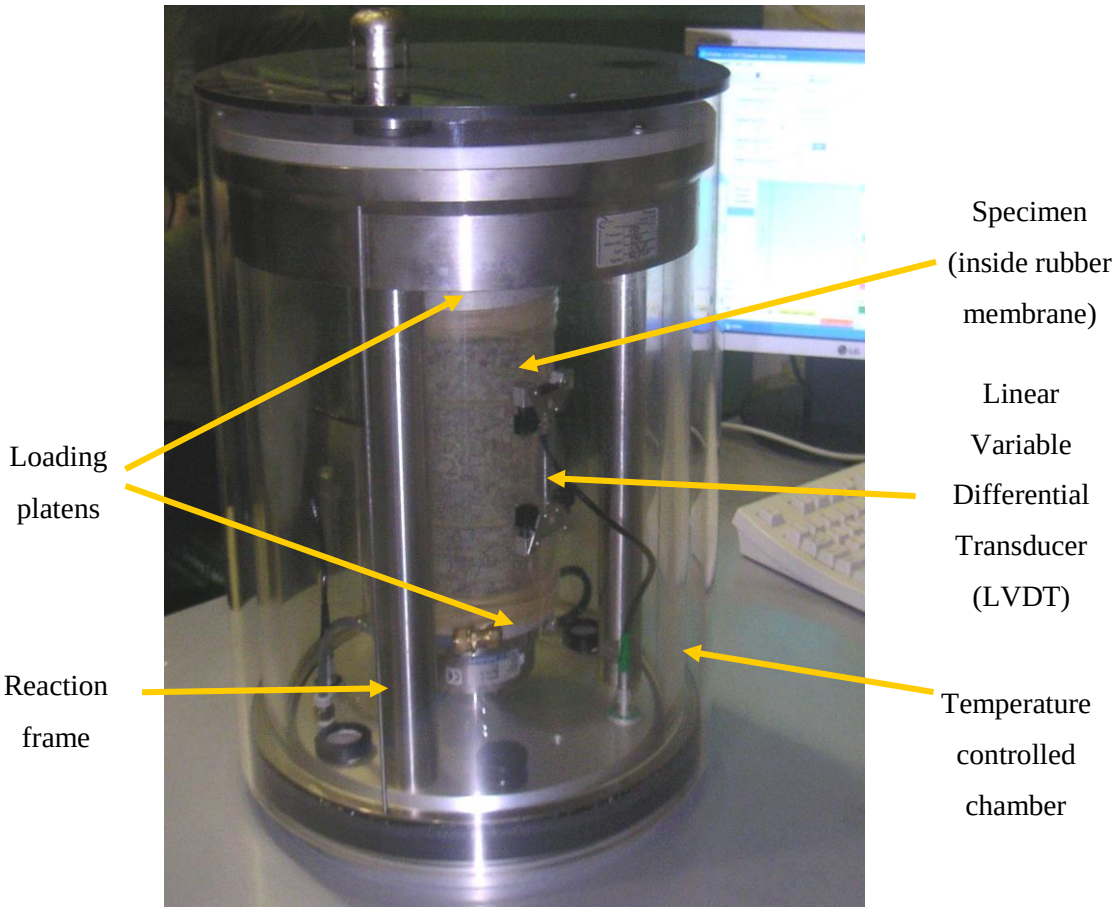

Figure 6-2. Dynamic modulus test set up in the AMPT.

6.2.1.2 E* and |E*| definitions

The complex modulus (E*) and dynamic modulus (|E*|) are some of the parameters that can be used to predict the time dependent behavior of viscoelastic materials. The details of how that is accomplished is beyond the scope of this report. However, it is important to provide a brief description and interpretation of |E*|, as this is used as the elastic modulus of HMA in the MEPDG.

In order to unambiguously define E* and |E*|, it is convenient to explain how σ and ε are varied with time during the test.

In the AMPT, after application of a contact stress of around 5% of the maximum axial stress ($\sigma_{contact}$), a bottom ram transmits through the bottom platen a cyclic sinusoidal axial

load while Linear Variable Differential Transducers (LVDTs) simultaneously measure the resulting vertical deformations. In the configuration shown in Figure 6-2, three LVDTs located 120° apart on the cylindrical specimen are used.

The application of a sinusoidal stress results in strains that also follow an approximate sinusoidal pattern. Figure 6-3 shows the applied sinusoidal axial stress and the corresponding strain response of a typical bituminous mixture. In this figure, scales have been chosen so that the two curves have the same vertical separation between peaks. The figure also illustrates a characteristic time shift (Δt) of viscoelastic materials between the loading curve and the deformation curve.

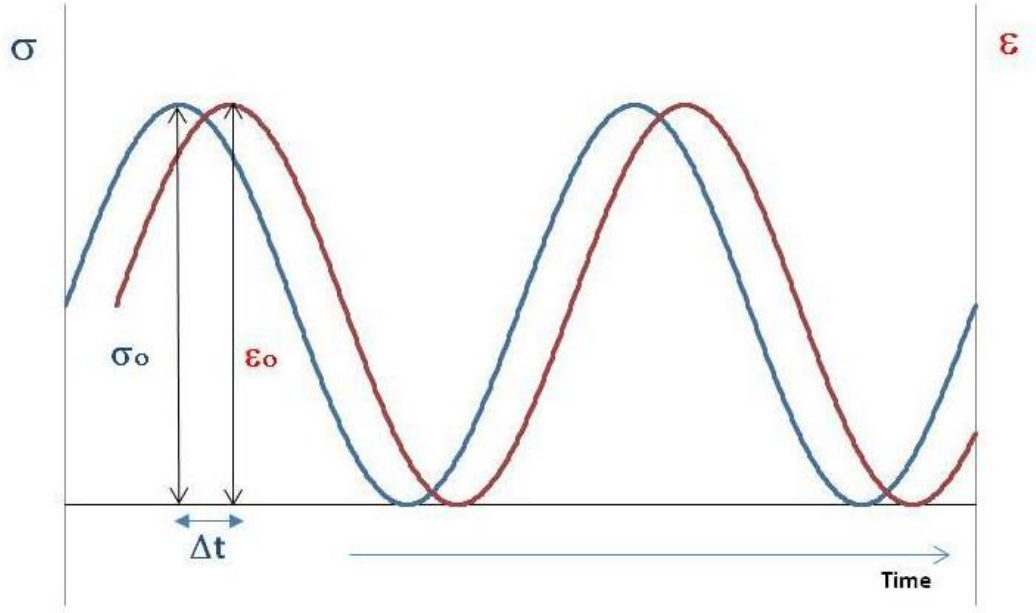

Figure 6-3. Typical Applied Stress and Associated Strain Response of HMA during |E*| Test.

The time dependency of the stress (σ) (the sinusoidal load) is conveniently described by a complex number that provides the deviation Δσ around the mean stress value over the cycle.

$$\Delta\sigma = \frac{\sigma_0}{2} e^{i\omega t} = \frac{\sigma_0}{2}\cos(\omega t) + i\frac{\sigma_0}{2}\sin(\omega t) \qquad (6\text{-}1)$$

where σ_0 is the peak-to-peak stress difference in Δσ, ω is the angular velocity and *t* is time.

Similarly, the time dependency of the resulting strain ε is conveniently described by a complex number that provides the deviation Δε around the mean strain value over the cycle.

$$\Delta\varepsilon = \frac{\varepsilon_0}{2} e^{i(\omega t - \phi)} = \frac{\varepsilon_0}{2}\cos(\omega t - \phi) + i\frac{\varepsilon_0}{2}\sin(\omega t - \phi) \quad (6\text{-}2)$$

where ε_0 is the peak-to-peak strain difference in $\Delta\varepsilon$, ϕ is the phase angle, and the other variables are as defined before. An interpretation of the phase angle ϕ is provided shortly. Actually, with the mechanical models typically used to model viscoelastic materials (spring and dashpots connected in series and parallel), it can be shown that the strain follows equation (6-2) when the stress is given by equation (6-1).

The sinusoids in both cases are represented by the real parts of the complex numbers in equations (6-1) and (6-2).

With the above stress and strain quantities defined, it is now relatively simple to define the complex modulus E*. As any other modulus, it is given by a ratio of stress to strain. More specifically, with the notation above, it is given by:

$$E^* = \frac{\Delta\sigma}{\Delta\varepsilon} = \frac{\frac{\sigma_0}{2}}{\frac{\varepsilon_0}{2}} \times \frac{e^{i\omega t}}{e^{i(\omega t - \phi)}} = \frac{\sigma_0}{\varepsilon_0} \times e^{i\phi} = \frac{\sigma_0}{\varepsilon_0}\cos(\phi) + i\frac{\sigma_0}{\varepsilon_0}\sin(\phi) \quad (6\text{-}3)$$

In equation (6-3), the real component of E*, typically denoted E', is known as the storage modulus. In contrast, the imaginary part, denoted E", is called the loss modulus. The ratio of the loss modulus to the storage modulus, E"/E' is equal to tan ϕ.

It is important to note that under viscoelastic theory all deformations are recoverable. There are no permanent deformations.

At low temperatures and high frequencies of loading, HMA tends to behave more elastically and therefore its storage modulus tends to zero and consequently the phase angle also tends to zero ($\tan\phi \rightarrow 0$). On the other hand, at high temperatures and low frequencies of loading, HMA is more viscous (higher loss modulus) and thus the phase angle increases ($\tan\phi \rightarrow \infty$). The phase angle is always a quantity between 0 and 90°.

Now, it can be seen that E*, being the ratio of two complex quantities, is itself a complex quantity. Remembering that the magnitude of a complex number is given by the square root of the Cartesian coordinates of the real and imaginary components, the dynamic modulus |E*| is then given by:

$$|E^*| = \sqrt{\left(\frac{\sigma_0}{\varepsilon_0}\right)^2 \cos^2(\phi) + \left(\frac{\sigma_0}{\varepsilon_0}\right)^2 \sin^2(\phi)} = \frac{\sigma_0}{\varepsilon_0} \qquad (6\text{-}4)$$

Since concepts involving complex numbers are somewhat abstract, it is useful to visualize how the stress and strain quantities are related to a complex number. The explanation is done with reference to Figure 6-4, which also helps to illustrate the relationship between the phase angle and the time lag between the curves.

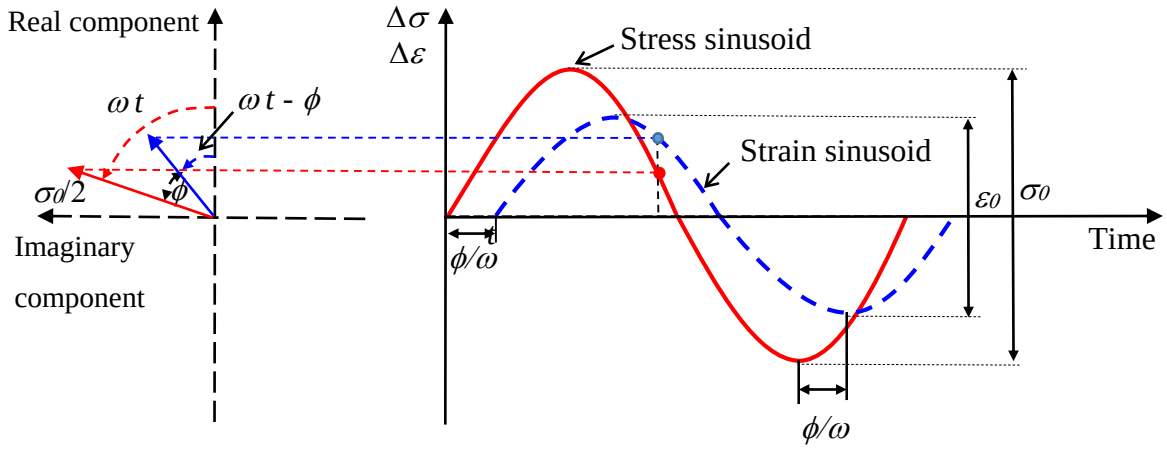

Figure 6-4. Phase angle between stress and strain curves in viscoelastic materials.

The left side of the figure illustrates the position at time *t* of two vectors, one for stress and one for strain, rotating counterclockwise in a complex space at an angular velocity ω. The vectors have magnitudes of $\sigma_0/2$ and $\varepsilon_0/2$ for stress and strain, respectively. For convenience, the real part of the vector is oriented up in the vertical direction and the imaginary part is oriented in the horizontal direction to the left. At time *t*, the real part of the location of the tip of the stress vector is the same as the stress at time *t*, as shown by the dot on the stress curve. Now, imagine that as the vector rotates counterclockwise at angular velocity ω (i.e., as time *t* increases), other points on the stress curve are generated such that the abscissa is the time *t* and the ordinate is equal to the real part of the stress vector. In other words, the location of the tip of the vector provides the vertical position of the sinusoid at any time *t*. The strain sinusoid is generated in exactly the same way by the strain vector which is rotating at the same angular velocity ω but behind the stress vector by the angle ϕ.

Hopefully, the visualization of the sinusoids being generated by the trace of the tips of two rotating vectors helps to understand the usefulness of using complex numbers to

represent the stresses and strains in this test. More importantly, the Euler (exponential) representation of complex numbers make the calculation of the ratio of the complex stress and strain quite simple.

Finally, the visualization above is also useful for explaining the relationship between the time shift between the curves (see Δt in Figure 6-3) and the phase angle ϕ. Note that both rotating vectors in the complex plane are separated angularly by ϕ. Since both vectors rotate at the same speed, if the peak stress is reached at a time T (which implies $\cos(\omega T) = 1$ for the stress sinusoid), then the peak strain will be reached at a later time $T+\Delta t$ (which implies that $\cos(\omega (T+\Delta t)- \phi) = 1$ for the strain sinusoid.) In both cases, since the sinusoids are at their peaks, the argument of the cosine function must be 0 (or 2π, 4π, etc.). If, without loss of generality, $\omega T = 0$ in the stress sinusoid, then $\omega \Delta t - \phi$ must also be 0 in the strain sinusoid for $\cos(\omega (T+\Delta t)- \phi) = 1$ to be true. Thus, the peak of the strain sinusoid will happen with a time lag of $\Delta t = \phi / \omega$ with respect to the peak of the stress sinusoid, as illustrated in Figure 6-4. Thus, the phase lag is directly related to the phase angle and it is inversely related to the angular velocity.

The AMPT software requires entering a frequency of loading (cycles/sec or Hz) instead of angular velocity. The frequency *f* is related to the angular velocity ω by: $\omega = 2 \pi f$.

Unlike in Figure 6-3, the vertical scales of stress and strain curves were not selected in Figure 6-4 so that the sinusoids have the same height. This makes the discussion more general.

It is important to note that with a stress amplitude of σ_0 as depicted in Figure 6-3, the average stress during the test, σ_{avg}, is $\sigma_{avg} = \sigma_{contact} + \sigma_0/2$. Therefore, the total time dependent stress is given by $\sigma = \sigma_{avg} + \Delta\sigma$. Similarly, with a strain amplitude of ε_0 as depicted in Figure 6-3, the average strain during the test, ε_{avg}, is $\varepsilon_{avg} = \varepsilon_{contact} + \varepsilon_0/2$ (where $\varepsilon_{contact}$ is the strain corresponding to $\sigma_{contact}$). Therefore, the total time dependent strain is given by $\varepsilon = \varepsilon_{avg} + \Delta\varepsilon$. For materials tested in the linear viscoelastic range, the contact stress has little influence in the determination of $|E^*|$.

The theory of the complex modulus can be derived from mechanical models (combinations of spring and dashpots) that provide justification for some of the assumptions. Huang [34] provides a good introduction to the subject.

6.2.2 Determination of |E*|

Dynamic modulus depends on mix characteristics, which is why testing of particular mixes or the use of models that include mix characteristics are needed for modelling HMA responses to loading. However, even for a single mix, dynamic modulus is substantially affected by several factors. The two single most important factors that are currently considered in the MEPDG are frequency (or its inverse, time of loading) and temperature. Variations in any of these two factors can result in dynamic modulus changes of orders of magnitude. Consequently, the results of dynamic modulus testing typically consist of a set of dynamic modulus values obtained at different temperatures and time of loading (or equivalently frequency of loading).

In order to perform a test, test frequencies, conditioning time, target temperature, target confining stress, initial modulus, axial gauge length, and specimen dimensions need to be defined in the software setup menu[36]. Some of these inputs, such as frequencies, are used directly for control of the test while others, such as the conditioning time, are included only for informational purposes. The conditioning time is the time allowed for the sample to reach the target test temperature uniformly within the specimen.

Initial modulus is important for the machine to select an appropriate initial load for testing. Although the load is automatically controlled, an initial modulus that is too different from the actual modulus can cause control problems. The initial modulus can be easily estimated with the tuning feature of the software before performing the test.

Figure 6-5 shows the AMPT software output after applying a cyclic stress to a given sample at a temperature of 70°F (21.1°C) for a load frequency of 1 Hz along with the resulting cyclic strains. A careful look at the figure reveals the characteristic phase shift of viscoelastic materials between the loading curve and the deformation curves described earlier.

The applied stress, confining pressure (if any), temperature and resulting axial strain from the three on-specimen displacement transducers are measured as a function of time and then used to calculate the dynamic modulus and other required values, such as phase angle,

[36] These descriptions, of course, are for the equipment currently available at UH.

average temperature, average confining pressure and a number of data quality measurements, as illustrated in Figure 6-5.

The values of dynamic modulus shown in the first row of the table within the Figure 6-5 illustrate the substantial effect that frequency, *f* (or equivalently time of loading, $t = 1/f$) has on the dynamic modulus. The higher the frequency (the shorter the time of loading) the higher is the measured dynamic modulus. Since temperature also has a substantial effect on the measured dynamic modulus, the test is performed at several temperatures to cover the range of pavement temperatures expected in the field.

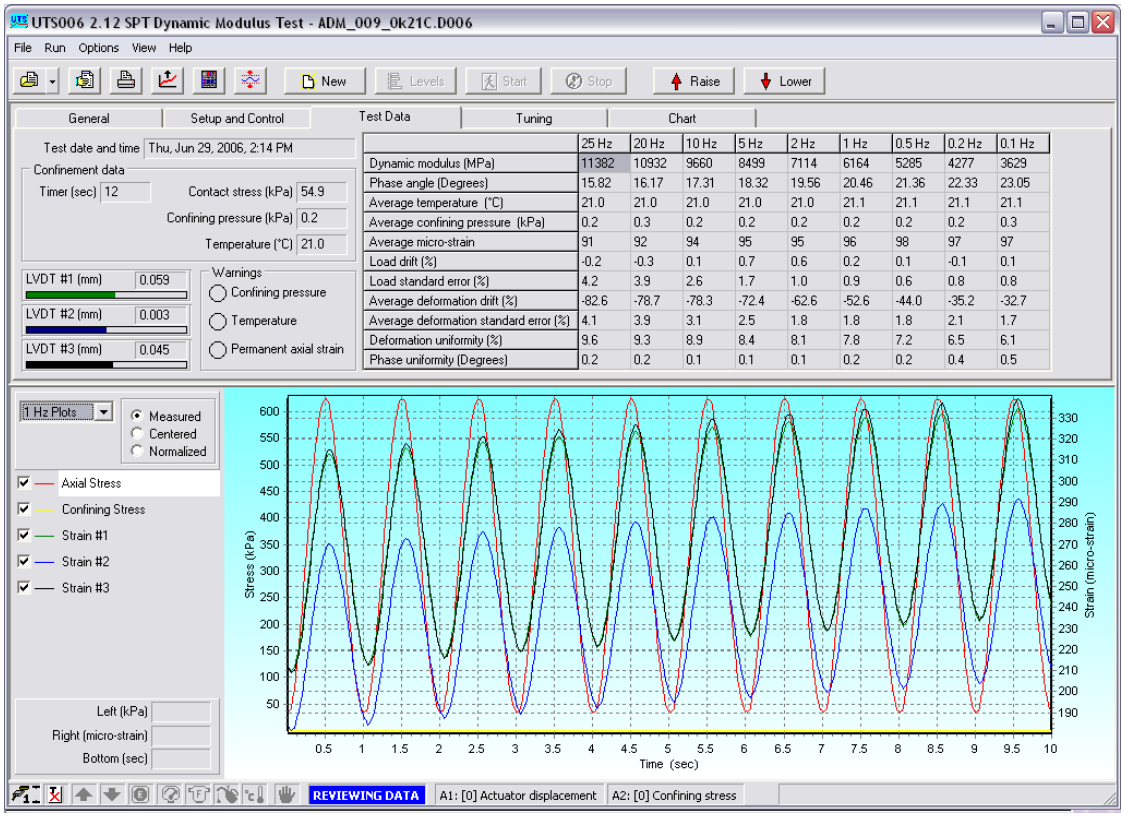

	25 Hz	20 Hz	10 Hz	5 Hz	2 Hz	1 Hz	0.5 Hz	0.2 Hz	0.1 Hz
Dynamic modulus (MPa)	11382	10932	9660	8499	7114	6164	5285	4277	3629
Phase angle (Degrees)	15.82	16.17	17.31	18.32	19.56	20.46	21.36	22.33	23.05
Average temperature (°C)	21.0	21.0	21.0	21.0	21.0	21.1	21.1	21.1	21.1
Average confining pressure (kPa)	0.2	0.3	0.2	0.2	0.2	0.2	0.2	0.2	0.3
Average micro-strain	91	92	94	95	95	96	98	97	97
Load drift (%)	-0.2	-0.3	0.1	0.7	0.6	0.2	0.1	-0.1	0.1
Load standard error (%)	4.2	3.9	2.6	1.7	1.0	0.9	0.6	0.8	0.8
Average deformation drift (%)	-82.6	-78.7	-78.3	-72.4	-62.6	-52.6	-44.0	-35.2	-32.7
Average deformation standard error (%)	4.1	3.9	3.1	2.5	1.8	1.8	1.8	2.1	1.7
Deformation uniformity (%)	9.6	9.3	8.9	8.4	8.1	7.8	7.2	6.5	6.1
Phase uniformity (Degrees)	0.2	0.2	0.1	0.1	0.1	0.2	0.2	0.4	0.5

Figure 6-5. Dynamic Modulus Test Output from the AMPT.

Figure 6-6 illustrates the results from a complete set of measurements on an HMA specimen for temperatures ranging from 39.9F (4C) to 129.2F (54C) and time of loading ranging from 0.04 s to 10 s (or equivalently frequencies ranging from 25 Hz to 0.1 Hz). As illustrated in this figure, the dynamic modulus is affected substantially by both temperature and time of loading (note that both chart scales are logarithmic so the differences are indeed significant; in this example the modulus varied from about 526,000 psi (3,629 MPa) to about 1,650,000 psi (11,382 MPa)!)

6.2.3 Dynamic Modulus Master Curve

For mechanistic-empirical pavement design, the dynamic modulus |E*| is needed for any given temperature and time of loading. Therefore, an interpolation model is required to predict |E*| for any condition. Such interpolation is achieved with the use of the time-temperature superposition principle, which allows superposition of a series of curves (each for a constant value of temperature and varying frequencies of loading) by horizontal shifts in the frequency domain to form what is known as a "Master Curve".

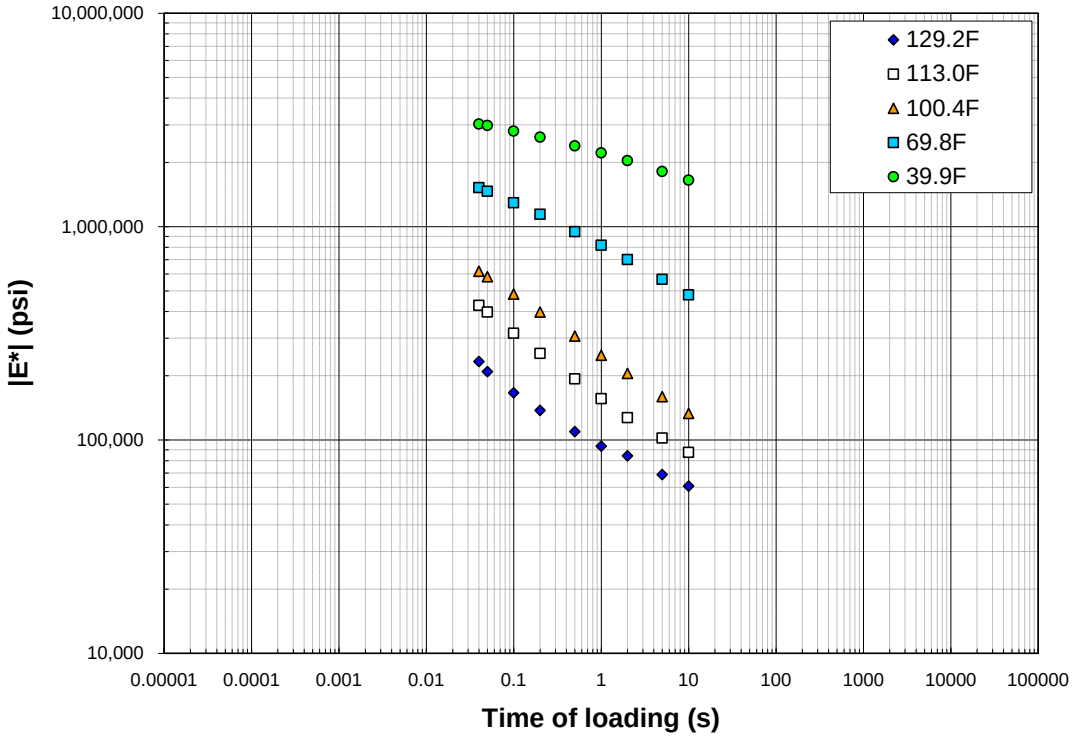

Figure 6-6. Example of dynamic modulus test results.

The time-temperature superposition principle assumes that the effect of time of loading (or frequency) on the material properties can be replaced by the effect of temperature, and vice versa. In this way, the master curve can be defined as a function that describes simultaneously the dependency of |E*| on both the temperature and the time of loading.

Although estimation of the master curve model parameters can be accomplished in a single step, it is easier to explain it and visualize it as a two-step process in which first, the curves obtained by varying loading time (or frequency) at each temperature are shifted horizontally until a smooth curve is obtained and second, a smooth function is fitted to the resulting data points. Figure 6-7 illustrates the shifting and the resulting fitted |E*| master curve for a particular mix (reference temperature of 21.1 ºC = 70.0 ºF).

The amount of shifting along the time of loading axis (i.e., horizontal) is related to what is known as the *shift factor*, which is defined, in logarithmic terms by the equation:

$$\log(t_r) = \log(t) - \log(a(T)) \tag{6-5}$$

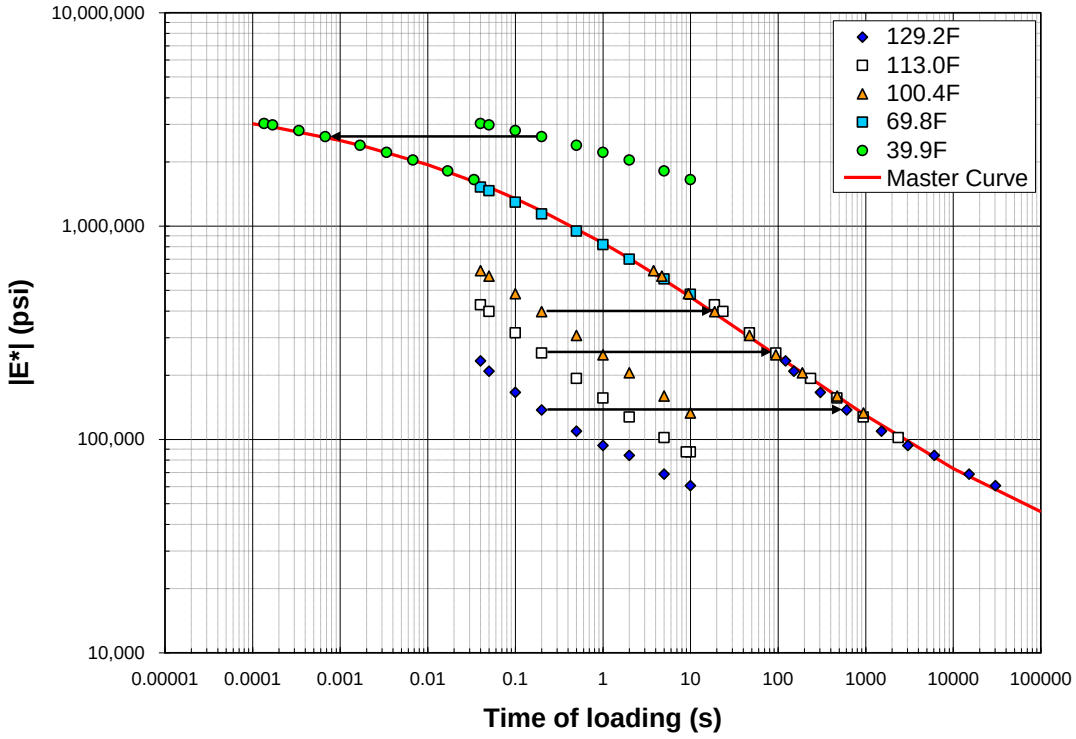

Figure 6-7. Example of shifting and curve fitting during the development of master curve (T_{ref} =69.8 ºF=21.0ºC).

In equation (6-5), *a(T)* is the shift factor (which is a function of temperature, as illustrated in Figure 6-8), *t* is the time of loading at the desired temperature, t_r is the reduced time of loading at a reference temperature, and *T* is the temperature of interest[37]. As can be deduced from equation (6-5), the shifts shown in Figure 6-7 are equal to the negative of the log(a(*T*)) (note that the time of loading is given in logarithmic scale in Figure 6-7). For example, as shown in Figure 6-8 the shift factor for 100 ºF is about -2. Correspondingly, the

[37] t_r, the reduced time of loading, is a fictitious time of loading. Its interpretation is as follows. The same modulus |E*| would be measured whether a sample is tested at any given temperature *T* and time of loading *t* or whether it is tested at the reference temperature (typically 70 ºF) and time of loading t_r.

points for the 100 ºF temperature are shifted about two log cycles to the right in Figure 6-7. These shifted points are the ones used to fit the master curve.

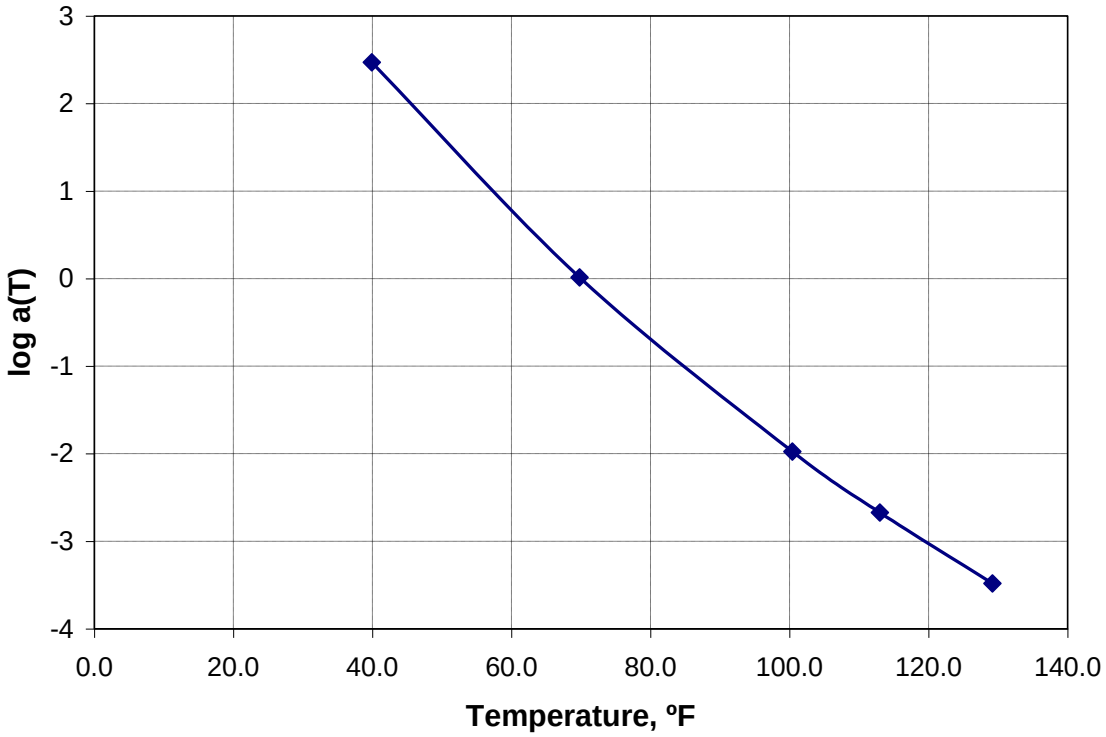

Figure 6-8. Example of the Shift Factor as a function of temperature.

Although different continuous functions could be used for the |E*| master curve, the sigmoidal function presented in equation (6-6) is perhaps one of the most commonly used these days, as it is the form used by the Pavement ME Design software [2].

$$\log_{10}|E^*| = \delta + \frac{\alpha}{1+e^{\beta+\gamma(\log t_r)}} \tag{6-6}$$

In equation (6-6), t_r is the reduced time of loading at the reference temperature, α is the minimum value of log |E*|, $\delta+\alpha$ corresponds to the maximum value of log |E*|, and β and γ are parameters describing the shape of the sigmoidal function. This equation describes the time dependency of the modulus at the reference temperature whereas the shift factors describe the temperature dependency of the modulus; both are essential ingredients of the master curve.

6.2.3.1 Shift factor models

Different approaches are available to establish the relationship between the shift factors and temperature. Some of these are discussed next.

6.2.3.1.1 Shift Factor Modeled only as Function of Temperature

The parameters of the master curve can be estimated using equation (6-6) along with the following equation to model the shift factor as a function of temperature:

$$\log(a(T)) = AT_i^2 + BT_i + C \tag{6-7}$$

where *A*, *B* and *C* are model parameters and T_i is the temperature in °F. All seven parameters (*A*, *B*, *C* and the parameters of the sigmoid) are estimated simultaneously by the MEPDG. The only information required for their estimation is the dynamic modulus test results.

Since the computations are done internally by the MEPDG, there is generally no need for users to determine the parameters of these equations. The master curve and shift factors are part of the output in the MEPDG.

Still, if so desired, different computer applications are available at the moment to process data from AMPT |E*| tests and generate master curves. Advanced dedicated software that can perform this task include the licensed Rheology Analysis Software (RHEA) from Abatech [43]. Other software that can be used towards this end include Matlab and Excel, although it is important to note that users need accessibility to the software and possess a basic understanding of programming macros within these particular applications. In addition, interested users can obtain the MasterSolver Excel worksheet, which was prepared as part of NCHRP Report 9-29, and is available for free from the Transportation Research Board website [37].

In addition, the PI has also developed a software application to automatically generate the mixture's modulus master curve using the output files generated by IPC Global's AMPT. This tool can potentially facilitate the use of perceived complex results from asphalt dynamic modulus tests into routine pavement engineering practice. It allows, among other things, direct reading of the summary files generated by the AMPT in SI units and compute the master curve parameters using US customary units, thus avoiding unit conversions. The details of the tool are presented in [44]. This software is also available for free to HDOT.

6.2.3.1.2 Shift Factor Modeled as Function of Temperature through Binder Viscosity

As the asphalt binder ages, the binder and the mix become stiffer. In order to account for the stiffening of the mix with time, the MEPDG currently uses two different procedures: one developed under project NCHRP 1-37A [1] and the other under NCHRP 1-40D . Only the first one is explained in detail in this report since the second procedure has not yet been nationally calibrated.

In the procedure developed under project NCHRP 1-37A, the MEPDG uses equation (6-8) below to compute the shift factor instead of equation (6-7).

$$\log(a(T)) = c\left(\log\eta - \log\eta_{T_R}\right) \tag{6-8}$$

where

η = binder viscosity, cP (centipoise)[38],

η_{T_R} = binder viscosity at reference temperature, cP

c = model parameter estimated simultaneously with α, β, γ, and δ of equation (6-6) for given mix |E*| values and binder viscosity data.

Equation (6-8) appears to require two less parameters than equation (6-7). However, it also requires prediction of the binder viscosity as function of temperature. This is achieved in the MEPDG through the following two-parameter equation:

$$\log\log\eta = A + VTS\log T_R \tag{6-9}$$

where

η = binder viscosity, cP (centipoises),

T_R = temperature, Rankine (= temperature in °F + 459.67)

---

[38] For this particular equation use of any unit of viscosity is acceptable as long as the same units are used for both viscosity values. Recall that $\log\eta - \log\eta_{T_R} = \log\frac{\eta}{\eta_{T_R}}$, which does not depends on the units. This is not true however for most other equations in the MEPDG, so analysts need to be careful with units when making calculations using MEPDG equations outside the MEPDG.

A = regression intercept;

VTS = regression slope of viscosity temperature susceptibility.

Parameters A and VTS are estimated by the guide based on the binder characterization data required as input by the MEDPG for levels 1 and 2 or are provided based on the binder grade for level 3.

6.2.3.2 Example of Dynamic Modulus Computations

As indicated before, for pavement design the dynamic modulus |E*| is needed for any given temperature and time of loading. Equations (6-5), (6-6), and (6-7) are now used along with a specific set of parameters α, β, γ, δ, A, B, and C to illustrate how this is accomplished. Note that there is no need for users of the guide to perform computations like the ones presented here. Nevertheless, understanding of these promotes a more informed use of the procedure.

Suppose that $\delta = 4.186$, $\alpha = 2.465$, $\beta = -0.871$, $\gamma = 0.457$, $A = 0.000204$, $B = -0.100$, and $C = 6.00$. First notice that for the reference temperature of 70°F equation (6-7) yields

$$\log(a(T)) = 0.000204\,(70)^2 - 0.100\,(70) + 6.00 \approx 0 \text{ or } a(T) = 1$$

as it should be for the reference temperature (this restriction is imposed during estimation of the parameters of the equation).

If an estimate of the dynamic modulus is required for a temperature of say, 85°F, and a time of loading of 8 seconds, then the calculations proceed as follows. From equation (6-7):

$$\log(a(T)) = 0.000204\,(85)^2 - 0.100\,(85) + 6.00 = -1.025 \text{ or } a(T) = 0.0942$$

Therefore from equation (6-5), the reduced time (i.e., the time of loading that would yield the same modulus at the reference temperature as the modulus obtained at the given temperature of 85°F and loading time of 8s) is:

$$t_r = t/a(T) = (8\text{ s})/(0.0942) = 84.96\text{ s}$$

Then, using equation (6-6), the |E*| is calculated as:

$$\log_{10}|E^*| = 4.186 + \frac{2.465}{1+e^{-0.871+0.457\log_{10}(84.96)}} = 5.412$$

or

$$|E^*| = 258{,}188\text{ psi.}$$

which agrees with the value of |E*| obtained for $t_r \approx 85$ s in Figure 6-8. The same procedure can be used for any other temperature and time of loading.

6.2.3.3 MEPDG Use of the Master Curve

Seven parameters are required to completely characterize the mix master curve whether equation (6-7) is used (in which case the parameters are $\alpha, \beta, \gamma, \delta$ of equation (6-6) and *A*, *B*, and *C* of equation (6-7)) or whether equations (6-8) and (6-9) are used (in which case the parameters are $\alpha, \beta, \gamma, \delta$ of equation (6-6), *c* of equation (6-8) and *A* and *VTS* of equation (6-9)[39]). Both approaches are used within the MEPDG [1].

The estimation of these parameters is done by the MEPDG from the appropriate inputs for each case. Then, the MEPDG can use the master curve to estimate the dynamic modulus of HMA layers for any pavement temperature and frequency of loading.

The main advantage of the use of equations (6-8) and (6-9) over the use of equation (6-7) is that binder aging can be taken directly into account by changing the binder viscosity with age.

Binder aging is modeled internally in the MEPDG by a system known as Global Aging System, which includes four sub-models for binder aging occurring on different stages:

- Original to mix/lay-down model to account for short term aging occurring during mixing and lay-down.
- Surface aging model to predict the viscosity of the binder at the surface of the pavement after any period of time using the viscosity at mix/lay-down.
- Air voids adjustment to adjust for different air voids in the mix.
- Viscosity-depth model.

The details of the Global Aging System are beyond the scope of this report. It is important to realize, however, that binder characterization inputs required by the MEPDG are used to obtain binder viscosity with equation (6-9) at any temperature and that these are used

[39] The parameter *A* of the quadratic equation (6-7) should not be confused with the binder parameter *A* used in equation (6-9).

(after being modified by the Global Aging System to account for aging) in equation (6-8) to predict the dynamic modulus at any temperature and age.

Figure 6-9 illustrates the effects of the seasonal variations and aging on HMA sublayers of a 10-in thick HMA combination of layers for the Honolulu environment as reported by the MEPDG[40]. The yearly fluctuations in temperature (from winter to summer) are apparent in the figure. Notice also that the modulus increases in the first few years and then stabilizes. This last effect is more pronounced for those layers closer to the surface (more exposed to aging) than deeper in the pavement structure (in this particular example the order of the lines in the graph correspond exactly with their position from top to bottom in the pavement structure). The differences of modulus between sublayers is caused by the different loading times experienced by the HMA at different depths[41].

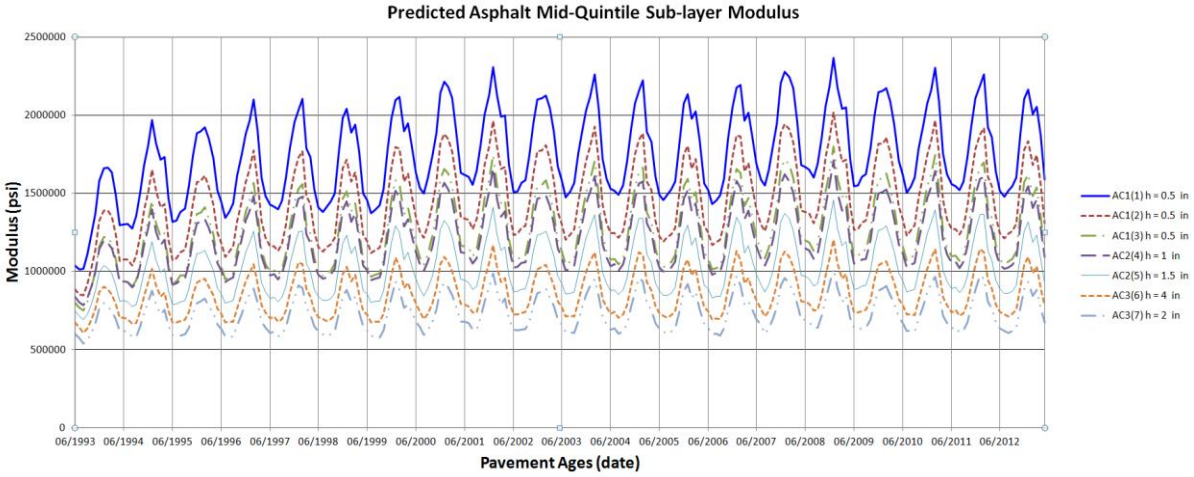

Figure 6-9. Simulated variations of HMA modulus over time (including the temperature variations over time and aging) and depth.

[40] In the example, there are three layers AC1 (AC Mix IV), AC2 (AC Mix III), and AC3 (ACB) of thicknesses of 1.5, 2.5, and 6 inches, respectively. Each of these, are subdivided into sublayers with the thicknesses shown in the figure legend. The software numbers these sublayers automatically with the numbers shown in parenthesis in the legend.

[41] Since very early after the release of the MEPDG, there were concerns about the possibility of the loading time/frequency effect overriding the temperature effect [53]. Although the MEPDG research team agreed with this concern, the latest version of the Pavement ME Design software (used to generate Figure 6-9) has not addressed this issue yet. As discussed later, this may indeed be an important consideration for Hawaii.

6.2.4 MEPDG Dynamic Modulus Predictions

Different models are used in the MEPDG to estimate the master curve for new HMA layers depending on the inputs level. For input level 1, the MEPDG derives the master curve parameters directly from values of |E*| obtained by testing with the AMPT the mix expected to be used in the project.

For input levels 2 and 3, the MEPDG makes use of either Witczak's model adopted in project NCHRP 1-37A [1] or the enhanced Witczak's model adopted in project NCHRP 1-40D [22].

The next section evaluates the adequacy of the level 2 and 3 predictions of |E*| for some Hawaiian mixes. It is shown that although the predictions are generally reasonable, they are somewhat biased for the mixes tested locally. Therefore, Section 6.2.4.2 considers the use of pseudo-level 1 data generated from a model developed with Superpave 12.5 mm mixes prepared with local materials. Most of the concepts in these two sections are from [45], [46] and [47].

6.2.4.1 MEPDG Levels 2 and 3 Dynamic Modulus Predictions

The two Witczak's models used by the MEPDG were developed with extensive databases and provide a good fit to the data used in their development. They use information about gradation, mixture volumetrics, and binder characteristics. The only difference in the use of the models for levels 2 and 3 is that specific laboratory test data are required for binder characteristics for level 2 but only the grade of the binder (Superpave, conventional viscosity or conventional penetration) is required for level 3.

6.2.4.1.1 |E| Master Curves Models Used in the MEPDG*

Bari and Witczak [48] provide a summary of the models developed over the last 50 years as well as the two models used by the MEPDG. These last two models are now briefly described.

For levels 2 and 3, the parameters of the |E*| model adopted in the NCHRP 1-37A study [1] were obtained by fitting the model to a data set containing 2,750 test data points from 205 Hot Mix Asphalt (HMA) un-aged laboratory blended mixtures. This version of the Witczak |E*| predictive model is as follows:

$$\log_{10}|E^*| = -1.25 + 0.029\rho_{200} - 0.0018(\rho_{200})^2 - 0.0028\rho_4 - 0.0048V_a - 0.822\frac{V_{beff}}{V_{beff}+V_a} + \frac{3.872 - 0.0021\rho_4 + 0.004\rho_{38} - 0.000017(\rho_{38})^2 + 0.0055\rho_{34}}{1+e^{(-0.6033-0.3133\log(f)-0.3935\log(\eta))}} \quad (6\text{-}10)$$

where

|E*| = dynamic modulus of the mix, 10^5 psi

η = viscosity of the binder, 10^6 Poise

f = loading frequency, Hz

ρ_{200} = % passing No. 200 (0.075 mm) sieve

ρ_4 = cumulative % retained on No. 4 (4.76 mm) sieve

ρ_{38} = cumulative % retained on 3/8 in (9.5 mm) sieve

ρ_{34} = air voids, % by volume

V_{beff} = effective binder content, % by volume

The model adopted in project NCHRP 1-40D, developed also by Bari and Witczak [48], expresses the dynamic modulus |E*| as:

$$\log_{10}|E^*| = -0.349 + 0.754\left(|G^*|^{-0.0052}\right) \times \left(\begin{array}{l} 6.65 - 0.32\rho_{200} + 0.0027(\rho_{200})^2 + 0.011\rho_4 - 0.0001\rho_4^2 \\ +0.006\rho_{38} - 0.00014\rho_{38}^2 - 0.08V_a - 1.06\left(\frac{V_{b_{eff}}}{V_{b_{eff}}+V_a}\right) \end{array}\right) + \frac{2.56 + 0.03V_a + 0.71\left(\frac{V_{b_{eff}}}{V_{b_{eff}}+V_a}\right) + 0.012\rho_{38} - 0.0001\rho_{38}^2 - 0.001\rho_{34}}{1+e^{(-0.7814-0.5785\log(|G_b^*|)+0.8834\log\delta_b)}} \quad (6\text{-}11)$$

where

|E*| = dynamic modulus, psi

ρ_{200} = aggregates (by aggregates weight) passing through No. 200 sieve, %

ρ_4 = cumulative aggregates (by aggregates weight) retained on the No. 4 sieve, %

ρ_{38} = cumulative aggregates (by aggregates weight) retained on the 3/8 in. sieve, %

ρ_{34} = cumulative aggregates (by aggregates weight) retained on the ¾ in. sieve, %

V_a = air voids (by volume of the mix), %

V_{beff} = effective binder content (by volume of the mix), %

$|G_b^*|$ = dynamic shear modulus of binder, psi

δ_b = phase angle of binder associated with |Gb*|, degree

This model was fitted by Bari and Witczak to 7,400 dynamic modulus data points with an $R^2 = 0.80$ and Se/Sy = 0.45 in arithmetic scale and $R^2 = 0.90$ and Se/Sy = 0.32 in log scale. R^2 and Se/Sy are statistical measures of goodness of fit such that the closer are the R^2 to 1 and the Se/Sy ratio to 0 the better the fit. Based on these measures, the model provides an excellent fit to their data though unfortunately, no information is provided for either model about the significance of each individual model parameter.

6.2.4.1.1.1 Hawaii's Experimental |E*| Database

A data set was created at UH with HMA dynamic modulus (|E*|) test results for 79 laboratory-mixed/laboratory compacted specimens. The specimens were prepared with two different gradations, three binder types, and varying asphalt contents and air voids. All these mixes were prepared with aggregate from the Makakilo quarry in Oahu.

Figure 6-10 illustrates in a 0.45-power gradation chart the two Superpave 12.5 mm Nominal Maximum Aggregate Size (NMAS) gradations included in the database. Gradation B was selected as representative of gradations that had been used in actual paving projects whereas gradation A was selected to represent a gradation that could result from gradation B due to changes in the stockpiles or feeding of aggregates at the plant. Based on a later analysis of quality assurance records in the island of Oahu, it was found that these gradations are representative not only of Superpave gradations but also of many State Mix Type 4 gradations, which fall between gradations A and B or slightly outside, and that are commonly used throughout the island. This is illustrated in Figure 6-11, which shows a sample of State Mix IV gradations from different projects along with gradations A and B.

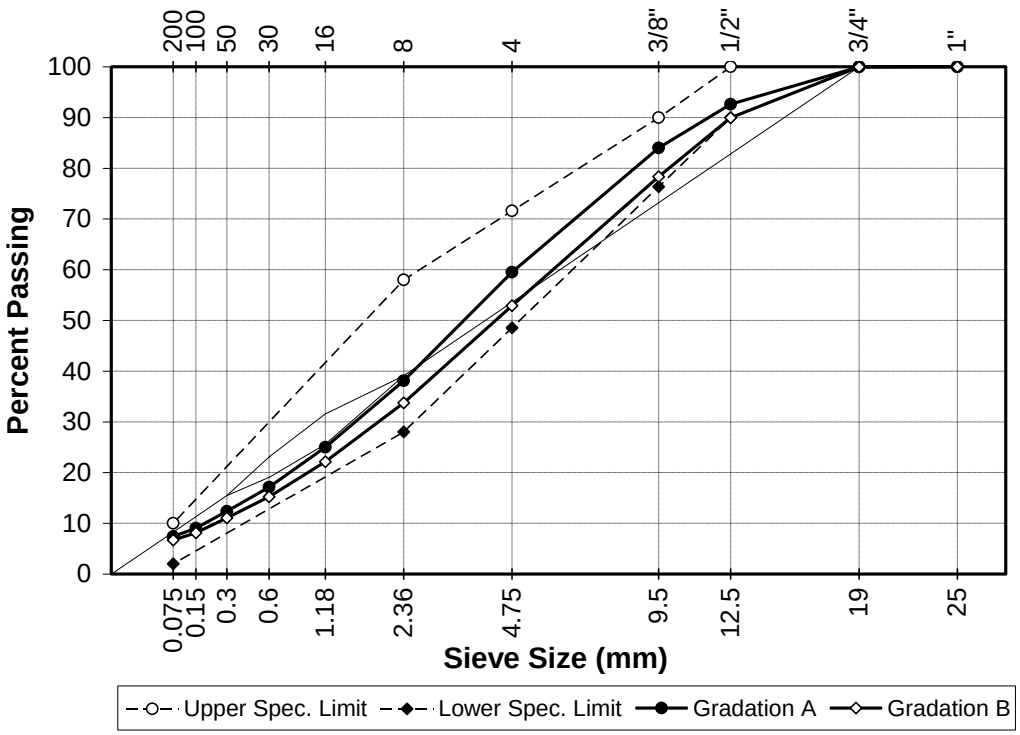

Figure 6-10. Gradations A and B.

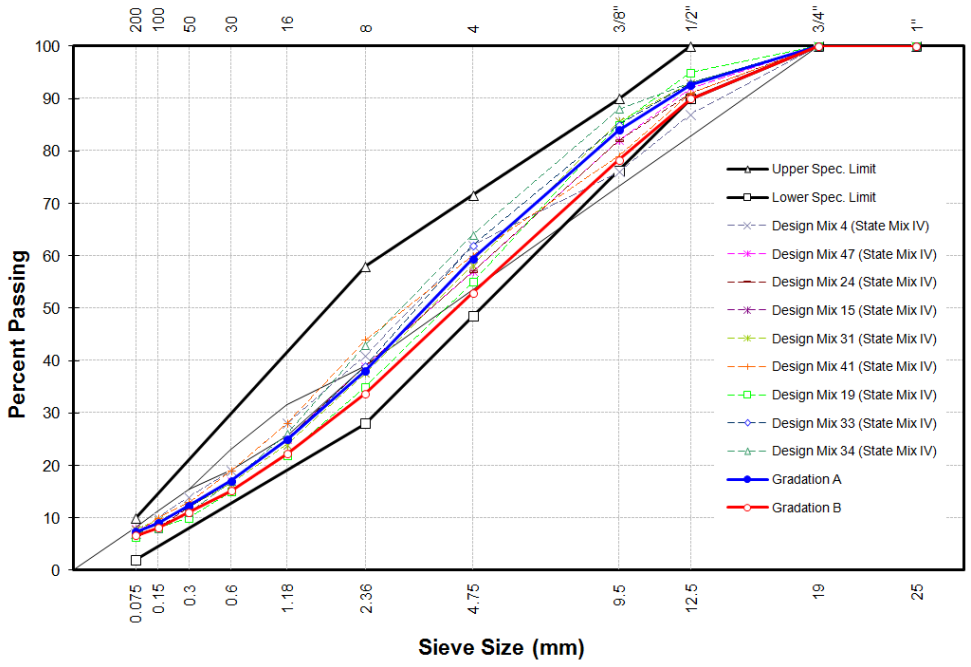

Figure 6-11. Examples of gradations of State IV mixes used in different projects.

Of the three binders used in the preparation of the specimens, one is a virgin (unmodified) PG64-16 and the other two are polymer modified binders. Of the modified

binders, one was a commercially available SBS modified PG70-22[42], whereas the other, labeled PG70-XX, was obtained by modifying a PG64-16 binder with a commercially available reactive elastomeric terpolymer mixed with polyphosphoric acid as catalyst.

The specimens were prepared with varying air voids and asphalt contents to study the potential differences with the binders not only under optimum conditions but under the conditions that can be expected in the field as well. Asphalt contents at the estimated optimum and at 0.5% below and 0.5% above the estimated optimum were selected for each gradation. In addition, the air voids in the samples varied from slightly below 3% to almost 10%. From an analysis of quality assurance records for Oahu, it was found that these values were in fact quite representative of the range of air voids found for Type IV and Superpave 12.5 mm NMAS mixes. Figure 6-12 shows the cumulative distribution of air voids for these types of mixes based on 512 observations from the quality assurance records mentioned above along with a Weibull distribution fitted to the data.

Incidentally, it must be noted that the hypothesis that the distribution of air voids is *Normal*, which is the most common assumption used in practice, had to be rejected at a 5% significance level when using a Chi-squared goodness of fit test. However, the hypothesis that the distribution follows a Weibull distribution could not be rejected at the same significance level.

[42] The PG70-22 binder modified with SBS is the same used in a section of the Moanalua Freeway in 2004.

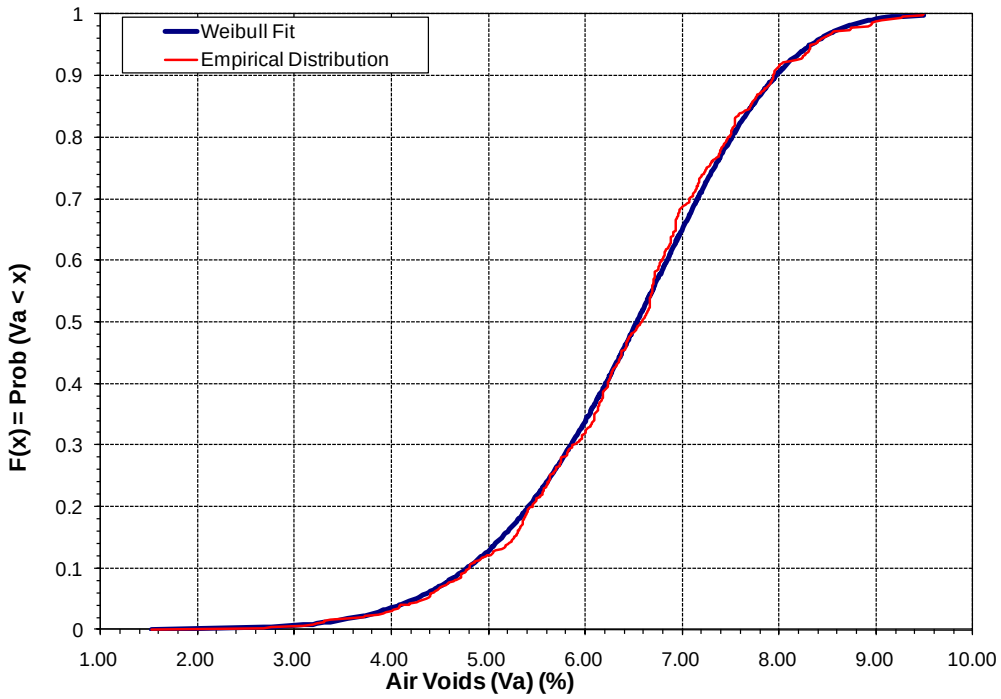

Figure 6-12. Air voids distribution from quality assurance records.

The laboratory mixes were aged for four hours before compaction. Table 6-1 shows the volumetric characteristics of the laboratory prepared specimens.

The dataset also contains |E*| information for five more specimens corresponding to three different mixes. The mix for two of these specimens is a Superpave 12.5 NMAS collected from a pavement preventive maintenance project on the H-3 freeway in Oahu. This mix was prepared with PG64-16 binder and aggregate from the Kappa quarry also in Oahu. The mix for two other specimens is a State Mix Type IV collected from another rehabilitation project on the Farrington Highway in Oahu. This is a warm mix asphalt (WMA) project that was prepared with aggregate from the Makakilo quarry, PG64-16 binder, and Sasobit™. A final specimen was compacted with a 12.5 mm NMAS Superpave mix collected at an asphalt plant also with a PG64-16 binder and aggregates from the Kappa quarry in Oahu (retained in 4.75 mm) and Ameron Maui (passing 4.75 mm) in Maui. Table 6-2 provides the volumetric characteristics of these mixes.

In total, 2,447 valid |E*| measurements were obtained for the 84 specimens. It is important to notice that despite the large number of observations, there is very limited variability in gradations for a statistical analysis of the type required for local calibration of either of the Witczak equations. In fact, there are only five different gradations. Similarly,

there are only three binders in the database, which also restricts the types of analysis that can be performed with this information.

In addition to volumetric and |E*| testing, some limited binder testing was performed on unaged binder and on binder aged in the Rolling Thin Film Oven (RTFO). The binders were tested at several temperatures for viscosity with a Brookfield rotational viscometer and for dynamic shear modulus and phase angle with a Dynamic Shear Rheometer.

Values of *A* and *VTS* were estimated from both sets of measurements. In the following analyses, only the *A* and *VTS* values from the DSR measurements are used. These are presented in Table 6-3.

Table 6-1. Characteristics of the laboratory mixed/laboratory compacted HMA specimens.

Aggregate Gradation	Binder	Specimen ID	Va (%)	Pb (%)	Pbe, % (vol.)	Unit Weight (pcf)	G_{mm}	G_{mb}	VMA	VFA
A	PG64-16	ADM001B	3.4	5.7	10.22	162.6	2.696	2.605	13.6	75.2
		ADM001C	2.7	5.7	10.29	163.7	2.696	2.623	13.0	79.2
		ADM001D	3.3	5.7	10.22	162.6	2.696	2.606	13.6	75.4
		ADM002	5.5	5.7	10.00	159.1	2.696	2.549	15.5	64.7
		ADM002B	4.6	5.7	10.09	160.4	2.696	2.571	14.7	68.5
		ADM002C	5.2	5.7	10.03	159.5	2.696	2.556	15.2	65.9
		ADM003	5.1	5.7	10.04	159.7	2.696	2.559	15.1	66.4
		ADM003B	7.4	5.7	9.80	155.8	2.696	2.497	17.2	57.0
		ADM003C	6.8	5.7	9.86	156.9	2.696	2.514	16.6	59.4
		ADM004	10.1	5.7	9.51	151.3	2.696	2.425	19.6	48.6
		ADM004B	9.3	5.7	9.60	152.6	2.696	2.446	18.9	50.9
		ADM005	9.3	5.7	9.60	152.6	2.696	2.446	18.9	50.9
		ADM006	4.3	5.7	10.12	161.1	2.696	2.581	14.4	70.4
		ADM007	2.7	6.2	11.49	162.2	2.673	2.6	14.2	80.8
		ADM008	2.2	6.2	11.55	163.1	2.673	2.614	13.8	84.0
		ADM025	7.4	5.2	8.61	157.1	2.72	2.518	16.0	53.7
		ADM026	7.4	5.2	8.61	157.2	2.72	2.519	16.0	53.8
		ADM027	9.1	5.2	8.45	154.3	2.72	2.472	17.6	48.1
		ADM028	9.4	5.2	8.42	153.7	2.72	2.463	17.9	47.1
	PG70-XX	ADM009	3.0	5.7	10.39	163.0	2.692	2.612	13.4	77.8
		ADM010	3.3	5.7	10.36	162.5	2.692	2.604	13.6	76.0
		ADM011	7.4	5.7	9.91	155.5	2.692	2.492	17.3	57.2
		ADM012	7.1	5.7	9.94	156.0	2.692	2.5	17.1	58.2
		ADM013	9.7	5.7	9.67	151.8	2.692	2.432	19.3	50.0
		ADM014	9.7	5.7	9.67	151.6	2.692	2.43	19.4	49.8
		ADM015	7.3	5.2	8.75	157.2	2.716	2.519	16.0	54.7
		ADM016	7.0	5.2	8.77	157.6	2.716	2.525	15.8	55.5
		ADM017	7.0	6.2	11.10	154.9	2.669	2.482	18.1	61.3
		ADM018	5.7	6.2	11.26	157.0	2.669	2.516	17.0	66.3
	PG70-22	ADM019	2.7	5.7	11.13	162.1	2.67	2.597	13.9	80.3
		ADM020	2.4	5.7	11.17	162.7	2.67	2.607	13.5	82.6
		ADM021	6.9	5.7	10.65	155.1	2.67	2.486	17.5	60.7
		ADM022	6.9	5.7	10.65	155.1	2.67	2.485	17.6	60.6
		ADM023	9.1	5.7	10.40	151.4	2.67	2.427	19.5	53.3
		ADM024	9.6	5.7	10.35	150.7	2.67	2.415	19.9	52.0

Table 6-1 (continued) Characteristics of the laboratory mixed/laboratory compacted HMA specimens.

Aggregate Gradation	Binder	Specimen ID	Va (%)	Pb (%)	Pbe, % (vol.)	Unit Weight (pcf)	G_{mm}	G_{mb}	VMA	VFA
B	PG64-16	BDM001	3.2	5.3	10.11	162.7	2.695	2.608	13.3	75.8
		BDM001B	2.3	5.3	10.21	164.2	2.695	2.632	12.5	81.4
		11CH53	2.5	5.3	10.19	163.9	2.695	2.627	12.7	80.1
		BDM002	5.7	5.3	9.86	158.6	2.695	2.542	15.5	63.5
		BDM002B	5.3	5.3	9.90	159.2	2.695	2.552	15.2	65.1
		BDM002C	5.2	5.3	9.91	159.5	2.695	2.556	15.1	65.8
		BDM003	5.1	5.3	9.92	159.6	2.695	2.557	15.0	65.9
		BDM004	9.6	5.3	9.45	152.1	2.695	2.437	19.0	49.7
		BDM005	10.1	5.3	9.40	151.2	2.695	2.423	19.5	48.2
		BDM006	3.6	5.3	10.08	162.2	2.695	2.599	13.6	73.9
		BDM007	2.8	5.8	11.36	162.1	2.672	2.597	14.2	80.2
		BDM007B	2.1	5.8	11.44	163.2	2.672	2.616	13.5	84.5
		BDM008	2.4	5.8	11.40	162.7	2.672	2.607	13.8	82.4
		BDM009	7.8	4.8	8.49	156.3	2.718	2.505	16.3	52.0
		BDM010	7.8	4.8	8.49	156.4	2.718	2.507	16.3	52.2
		BDM011	9.9	5.8	10.53	150.3	2.672	2.408	20.4	51.6
		BDM011B	5.5	5.8	11.04	157.5	2.672	2.524	16.6	66.6
		BDM012	9.7	5.8	10.56	150.6	2.672	2.414	20.2	52.2
		BDM012B	6.1	5.8	10.97	156.6	2.672	2.509	17.1	64.3
		BDM013	9.5	5.3	9.46	152.3	2.695	2.44	18.9	50.0
		BDM013B	10.1	4.8	8.25	152.6	2.719	2.445	18.3	45.0
		BDM014	9.3	5.3	9.48	152.6	2.695	2.445	18.8	50.5
		BDM014B	10.2	4.8	8.24	152.4	2.719	2.442	18.4	44.7
	PG70-XX	BDM015	10.4	5.8	10.79	148.7	2.661	2.383	21.2	50.8
		BDM015B	5.2	5.8	11.42	157.4	2.661	2.522	16.6	68.6
		BDM016	6.7	5.8	11.25	155.0	2.661	2.484	17.9	62.8
		BDM017	8.8	5.3	9.87	152.8	2.684	2.449	18.6	53.0
		BDM018	7.9	5.3	9.97	154.3	2.684	2.473	17.8	55.9
		BDM019	7.2	4.8	8.89	156.7	2.707	2.512	16.1	55.2
		BDM020	6.8	4.8	8.93	157.4	2.707	2.523	15.7	56.8
		BDM021	8.6	4.8	8.75	154.3	2.707	2.473	17.4	50.3
		BDM022	8.3	4.8	8.78	154.9	2.707	2.482	17.1	51.4
		BDM023	5.4	5.3	10.23	158.4	2.684	2.538	15.7	65.3
		BDM024	5.5	5.3	10.22	158.3	2.684	2.537	15.7	65.1
		BDM025	2.1	5.3	10.59	163.9	2.684	2.627	12.7	83.3
		BDM026	2.2	5.8	11.78	162.4	2.661	2.603	14.0	84.4
		BDM027	2.5	5.3	10.55	163.4	2.684	2.618	13.0	81.1
		11EL53	2.3	5.3	10.57	163.7	2.684	2.623	12.8	82.3
		BDM028	2.3	5.8	11.78	162.3	2.661	2.601	14.0	83.9
	PG70-22	BDM029	5.1	4.8	8.93	160.7	2.712	2.575	14.0	63.9
		BDM030	5.2	5.3	10.13	159.1	2.688	2.549	15.3	66.2
		BDM031	8.3	4.8	8.63	155.2	2.712	2.487	16.9	51.0
		BDM033	2.1	5.8	11.67	162.9	2.665	2.610	13.7	85.0

Table 6-2. Characteristics of additional HMA specimens

Mix Type	Binder	Specimen ID	Va (%)	Pb (%)	Pbe, % (vol.)	Unit Weight (pcf)	G_{mm}	G_{mb}	VMA	VFA
SP 12.5 mm	PG64-16	H3-E1	4.3	6.1	11.41	149.4	2.501	2.394	15.7	72.7
SP 12.5 mm	PG64-16	H3-E2	4.5	6.1	11.38	149.0	2.501	2.388	15.9	71.6
MT IV	Warm Mix	FARE41	0.9	5.9	12.47	153.2	2.476	2.455	13.3	93.6
MT IV	Warm Mix	FARE51	2.3	5.9	12.29	151.0	2.476	2.420	14.6	84.5
SP 12.5 mm	PG64-16	GL1S71	5.8	5.2	10.88	152.0	2.587	2.436	16.7	65.1

Table 6-3. A and VTS values for the binders inferred from DSR measurements after RTFO aging.

Short Term Aged Asphalt	A	VTS
PG 64-16	10.706	-3.574
PG70-XX	9.634	-3.169
PG70-22	9.504	-3.124

6.2.4.1.1.2 Predicted vs. Observed |E*| using the MEPDG models

As described earlier, the models adopted in the MEPDG for estimation of |E*| at levels 2 or 3 have been successfully fitted to data from comprehensive databases. Nevertheless, it is important to verify their applicability to Hawaiian mixes.

Figure 6-13 and Figure 6-14 show the observed vs. predicted values obtained with the model adopted in NCHRP 1-37A (equation (6-10)) in linear and logarithmic scales respectively. The data have been differentiated by each gradation-binder combination. From Figure 6-13, it can be seen that the line of equality is also almost a separation line for the predictions for the unmodified and polymer modified binders. In general, from Figure 6-13, for medium to high observed |E*| values, the NCHRP 1-37A model tends to under predict |E*| for the unmodified mixes used in this study and over predict it for the modified mixes studied. On the other hand, for low observed |E*| values, the inference from Figure 6-14 (which highlights the differences for smaller values of |E*|) is that the model tends to over predict the modulus for all the mixes. Nevertheless, it can also be concluded that if no other information is available, the use of this model for levels 2 and 3 provides reasonable modulus values (at least within the order of magnitude).

In order to compare the observed values with the predictions of the model adopted in project NCHRP 1-40D (equation (6-11)), values of |G*| and δ are needed at several frequencies. Thus, instead of directly using the DSR measurements of |G*| and δ (which were obtained at a single frequency of 1.59 Hz (10 rad/s)), these were used to determine *A* and *VTS*, and then the estimated *A* and *VTS* values were used to compute estimates of |G*| and δ using the equations developed by Bari and Witczak [49]. Figure 6-15 and Figure 6-16 show the observed vs. predicted values in linear and logarithmic scales respectively.

Although for a given observed |E*| value the range of predictions is about the same as or smaller than the range of predictions with the NCHRP 1-37A model, contrary to a priori expectations, the enhanced model shows a bias for all types of mixes analyzed in this study for high values of |E*|. It tends to always over predict the |E*| values.

The above observation could be a consequence of the fact that several conversions are required to predict |G*| and δ for any frequency and temperature. Recall that although some values of |G*| and δ were available at a single frequency, they were used to predict *A* and *VTS* and from these, the |G*| and δ were predicted for any frequency and temperature. In any case, for level 3 analyses, these are the types of predictions that would be needed to use the model. Both models are quite sensitive to the binder characteristics.

In summary, the models adopted in the MEPDG for estimation of |E*| produce reasonable but apparently somewhat biased results for some of the mixes in this study. For those cases in which level 2 or 3 must be used, the models in the MEPDG would give reasonable modulus estimates, provided reasonably accurate volumetric properties are used.

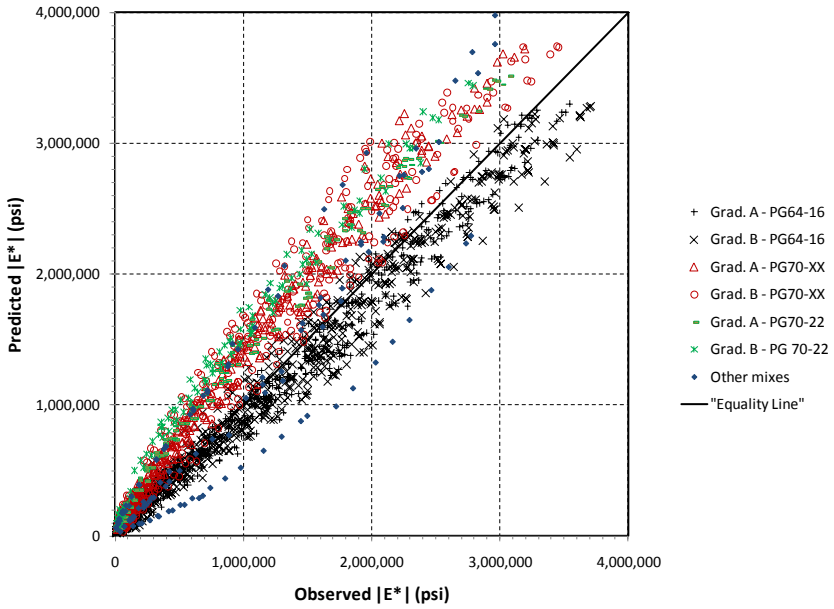

Figure 6-13. Observed vs. Predicted |E*| in linear scale - NCHRP 1-37A model.

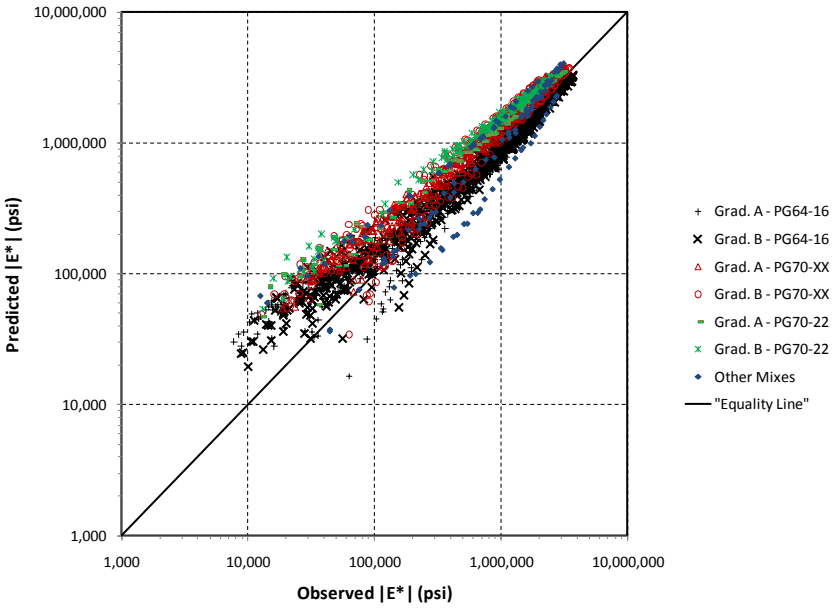

Figure 6-14. Observed vs. Predicted |E*| in logarithmic scale - NCHRP 1-37A model.

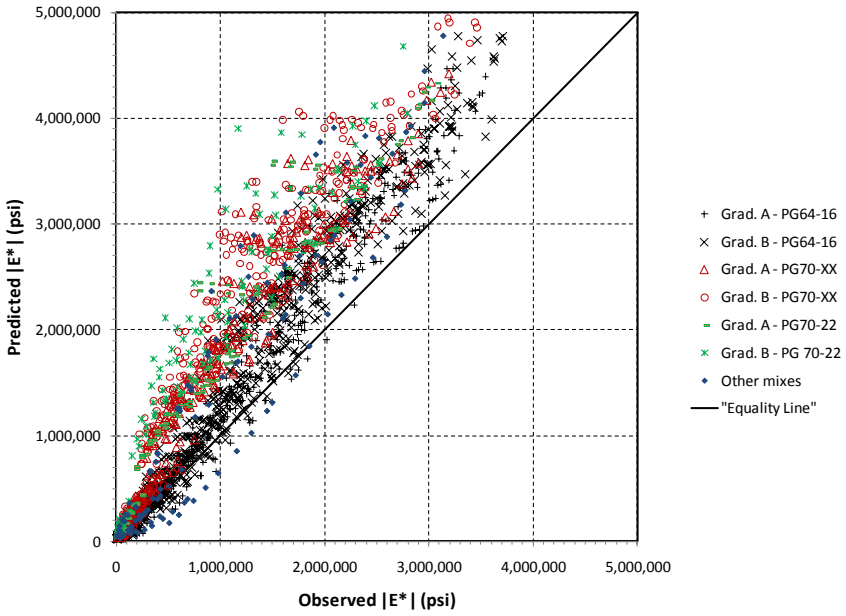

Figure 6-15. Observed vs. Predicted |E*| in linear scale - NCHRP 1-40D model.

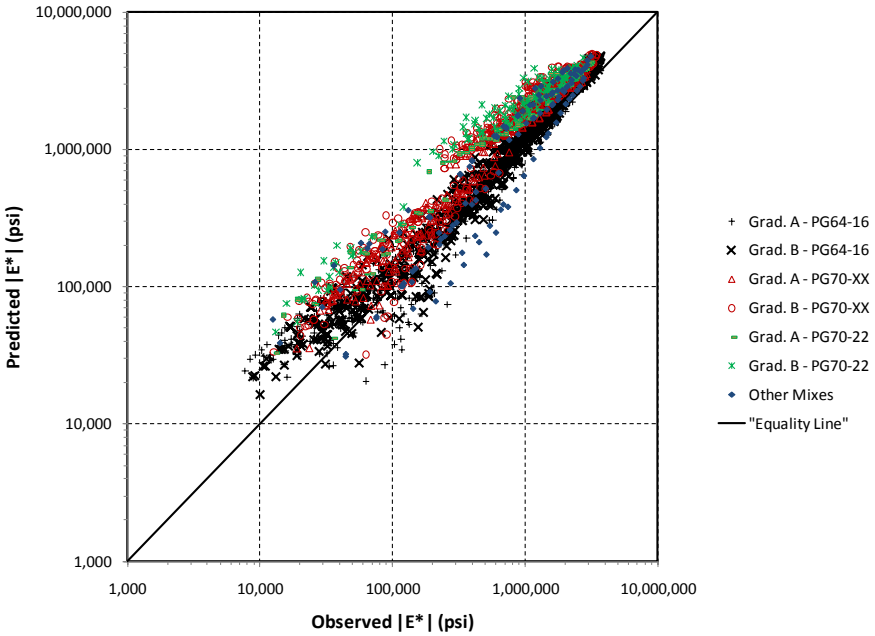

Figure 6-16. Observed vs. Predicted |E*| in logarithmic scale - NCHRP 1-40D model.

6.2.4.2 Development of a local |E*| model

6.2.4.2.1 Model specification

As described earlier, the models adopted in the MEPDG for estimation of |E*| produce reasonable but apparently biased results for some of the local mixes. This section

describes the development of a model similar to those used in the MEPDG that uses local mix information.

Similarly to the approach used by Witczak, the point of departure for the formulation of the model is equation (6-6) but making the parameters of this equation functions of mix characteristics.

As discussed earlier, equations (6-5) (page 240) through (6-7) (page 242) can be used to describe the changes in dynamic modulus with changes in frequency of loading and temperature. For this, a total of seven parameters (δ, α, β, γ, *A*, *B*, and *C*) are needed.

A comparison of equations (6-6) (page 241) and (6-11) (page 248) shows that the first three lines in equation (6-11) are equivalent to δ in equation (6-6), that the numerator in the fourth line of equation (6-11) is equivalent to α in equation (6-6), and that the exponent of *e* in equation (6-11) ($-0.7814 - 0.5785 \log |G_b^*| + 0.8834 \log \delta_b$) is equivalent to ($\beta + \gamma \log_{10} t_r$) in equation (6-6).

At first, the last comparison may not appear entirely clear since there is no such thing as a reduced time in equation (6-11) as there is for equation (6-6). In reality, t_r appears implicitly in (6-11) as well given that similar master curves can be derived for $|G^*|$ and δ_b as it was done here for $|E^*|$. What is important to notice is that δ and α were considered both functions of mixture volumetrics and aggregate structure. Furthermore, based on the comparisons of the exponents of *e*; β and γ are in essence considered functions of binder characteristics.

The estimation of the model presented below is based on these observations plus some experimenting. The model finally selected is one that provided the largest number of statistical significant parameter estimates at a 95% confidence level. The following equation shows the model finally selected:

$$\log_{10}|E^*| = \delta_1 + \delta_2 V_a + \delta_3 \left(\frac{V_{b_{eff}}}{V_{b_{eff}} + V_a} \right) + \delta_4 D_E + \delta_5 D_W + \delta_6 D_{H3} + \delta_7 D_F + \frac{\alpha_1 + \alpha_2 \left(\frac{V_{b_{eff}}}{V_{b_{eff}} + V_a} \right) + \alpha_3 D_E + \alpha_4 D_W + \alpha_5 D_{H3} + \alpha_6 D_F}{1 + e^{\left(\beta_1 + \beta_2 V_a + \beta_3 \left(\frac{V_{beff}}{V_{beff} + V_a} \right) + \beta_4 D_E + \beta_5 D_W + \beta_6 D_B + (\gamma_1 + \gamma_2 D_E) \log_{10}(t_r) \right)}} \quad (6\text{-}12)$$

where

$$\log(a(T)) = \log\left(\frac{t}{t_r} \right) = AT^2 + BT + C \quad (6\text{-}13)$$

$$A = A_1 + A_2 D_E \quad (6\text{-}14)$$

$$B = B_1 + B_2 D_E \quad (6\text{-}15)$$

$$C = -T_{ref}(T_{ref} A + B) \quad (6\text{-}16)$$

and where

T = temperature, ºF

T_{ref} = reference temperature, ºF (usually 70 ºF),

V_a = air voids (by volume of the mix), %

V_{beff} = effective binder content (by volume of the mix), %

D_E = 1 if mix prepared with PG70-XX binder and 0 otherwise

D_W = 1 if mix prepared with PG70-22 binder and 0 otherwise

D_{H3} = 1 if Superpave Mix used in H3 project and 0 otherwise

D_F = 1 if Mix Type IV used in Project 7101 A -01-04M and 0 otherwise

D_B = 1 if mix prepared with gradation B and 0 otherwise

At first, equations (6-12) through (6-16) may appear to be complex. However, they are simple extensions of equations (6-10) and (6-11). The following text explains the differences followed by a presentation of the estimation results.

First, notice that the first two lines of equation (6-12) are equivalent to δ in equation (6-6).The difference is that the term is made a function of air voids (V_a), voids filled with asphalt expressed in decimal (VFA/100 = $V_{beff}/(V_{beff}+V_a)$), and other variables that indicate whether the mix is modified and the type of modifier or if the mix is one of the additional mixes presented above. The new δ term is:

$$\delta = \delta_1 + \delta_2 V_a + \delta_3 \left(\frac{V_{b_{eff}}}{V_{b_{eff}} + V_a} \right) + \delta_4 D_E + \delta_5 D_W + \delta_6 D_{H3} + \delta_7 D_F \quad (6\text{-}17)$$

Notice that these indicator variables D_E, D_W, D_{H3} and D_F are useful to determine differences in mixes when limited information is available. For example, if a mix was prepared with PG70-XX, the δ value would be given by

$$\delta = \delta_1 + \delta_2 V_a + \delta_3 \left(\frac{V_{b_{eff}}}{V_{b_{eff}} + V_a} \right) + \delta_4 \quad (6\text{-}18)$$

since $D_E = 1$, $D_W = 0$ (the mix is not prepared with PG70-22), $D_{H3} = 0$, and $D_F = 0$. Thus, the assumption is that the δ term will change depending on type of binder or mixture but that the effects of air voids and VFA are the same for all types of mixes. This is similar to the more detailed use of gradation information in the MEPDG default models.

Similarly, the numerator of the third line of equation (6-12) provides the value of α as a function of mix characteristics, i.e.

$$\alpha = \alpha_1 + \alpha_2 \left(\frac{V_{b_{eff}}}{V_{b_{eff}} + V_a} \right) + \alpha_3 D_E + \alpha_4 D_W + \alpha_5 D_{H3} + \alpha_6 D_F \quad (6\text{-}19)$$

The only difference between this expression and the one for δ is that air voids is not included in equation (6-19) since it was not found significant. As for the β term, it becomes:

$$\beta = \beta_1 + \beta_2 V_a + \beta_3 \left(\frac{V_{beff}}{V_{beff} + V_a} \right) + \beta_4 D_E + \beta_5 D_W + \beta_6 D_B \quad (6\text{-}20)$$

This is again a very similar expression to the ones for δ and α. The main difference is that it contains an indicator variable (D_B) that differentiates specimens with gradation B from other specimens. As described later, this is the only place where an effect of gradation was specifically detected. This function further differs from the one adopted in the MEPDG in that it is a function of volumetric characteristics. Thus, in this model, not only the maximum and minimum values of the sigmoidal function depend on mixture volumetrics but the shape as well.

The γ term is the simplest one and has the following form:

$$\gamma = \gamma_1 + \gamma_2 D_E \quad (6\text{-}21)$$

This term is considered to be different for the mixes with PG70-XX, as are the expressions (6-14) and (6-15) for the *A* and *B* terms, respectively, in equation (6-13). Notice that the term *C* is made a function of *A*, *B*, the reference temperature (70 ºF) such that the shift factor is equal to 1 at the reference temperature of 70ºF. In other words, no new parameters are needed to compute *C*.

6.2.4.2.2 Estimation of model parameters and evaluation of results

As indicated before, the variables included in the model are the ones that produced statistical significant results. The parameters of these equations were estimated using the non-linear mixed effects approach available in S-Plus. Table 6-4 shows the estimation results (parameter estimates are shown with three significant figures). Based on the t-statistics and the p-values for the individual parameters, it can be observed that most parameter estimates are statistically significant at a 95% confidence level.

The R^2 for the fit is 0.985 in linear scale, which indicates an excellent fit. Figure 6-17 presents a comparison of the observed versus fitted values in linear scale and Figure 6-18 shows the comparison in logarithmic scales.

It can be observed that the predictions are now clearly unbiased for all the mixes. Also, by comparing Figure 6-18 with Figure 6-14 and Figure 6-16, it can be seen that the variation for low |E*| conditions is reduced greatly.

An important consideration in the estimation of parameters of statistical models is not only the overall goodness of fit and the achievement of overall unbiased results but also the statistical significance of individual parameters or set of parameters and the analysis of the reasonableness of the results in terms of the signs of the parameters. However, for non-linear regression models this latter task is more difficult than for linear models, particularly when some of the variables may be correlated and appear in more than one term. This is exactly the case with this model since V_a and VFA are negatively correlated and many of the indicator variables (such D_E) appear in many terms. Nevertheless, an attempt is made here to analyze some of the most important aspects of the model.

First, notice that the parameter estimate for D_E (δ_4) in the term δ (equation (6-18)) is positive, which indicates that other things being equal, the mixes prepared with PG70-XX binder have a higher lower bound for |E*| than mixes prepared with PG64-16 unmodified binders. On the other hand, the parameter for D_E (α_3) in the α term is negative (equation (6-19)), which indicates that other things being equal, the mixes prepared with PG70-XX binder have a lower range for |E*| than mixes prepared with PG64-16 unmodified binders. From the fact that the estimate of $|\alpha_3| > \delta_4$, it can be inferred that the modified mix will be softer than the unmodified mix at low temperatures and high frequencies. Thus, the use of the PG70-XX binder results in stiffer mixes at high temperatures and low frequencies of loading, which is beneficial for resisting rutting, and results in slightly softer mixes at low temperatures and high frequencies of loading, which is beneficial for cracking.

The analysis for the corresponding parameters (δ_5 and α_4) for the modified PG70-22 binder leads to exactly the same conclusion. The only difference is that the absolute values of the parameters for the PG70-22 binder are smaller than those for the PG70-XX binder. This indicates that both modified binders reduce the range of variation of |E*| with temperature and frequency, but that the PG70-XX does it a little bit more than the PG70-22. This is illustrated in Figure 6-19 which shows the estimated master curves for gradation A and for specimens with air voids V_a = 5% and binder content P_b = 5.8% (the VFA is computed based on P_b and the G_{se} determined in the laboratory for each mix). Notice that the figure shows |E*| as function of the reduced frequency in Hz, which in the MEPDG is computed as the inverse of the reduced time in s ($f_r = 1/t_r$). The effect of binder type is evident.

Table 6-4. Dynamic Modulus Parameter Estimation Results

Parameter Name	Variable	Parameter Estimate	Standard Error	t-value	p-value
δ_1	--	1.32	0.225	5.86	<.0001
δ_2	V_a	-0.0474	0.0077	-6.15	<.0001
δ_3	VFA	0.0252	0.0028	9.07	<.0001
δ_4	D_E	0.573	0.0807	7.10	<.0001
δ_5	D_W	0.449	0.0758	5.92	<.0001
δ_6	D_{H3}	-0.753	0.160	-4.71	<.0001
δ_7	D_F	0.568	0.104	5.47	<.0001
α_1	--	5.936	0.170	34.93	<.0001
α_2	VFA	-3.04	0.0023	-13.50	<.0001
α_3	D_E	-0.600	0.0880	-6.82	<.0001
α_4	D_W	-0.492	0.0748	-6.58	<.0001
α_5	D_{H3}	0.543	0.170	3.19	0.0014
α_6	D_F	-0.644	0.102	-6.32	<.0001
β_1	--	-3.12	0.200	-15.6	<.0001
β_2	V_a	0.0613	0.0101	6.05	<.0001
β_3	VFA	2.06	0.0022	9.43	<.0001
β_4	D_E	0.196	0.0211	9.31	<.0001
β_5	D_W	0.356	0.0240	14.8	<.0001
β_6	D_B	0.0464	0.0103	4.50	<.0001
γ_1	--	0.431	0.0067	64.3	<.0001
γ_2	D_E	-0.0473	0.0127	-3.71	0.0002
A_1	--	0.000207	1.56E-05	13.2	<.0001
A_2	D_E	0.0000690	2.83E-05	2.44	0.015
B_1	--	-0.103	0.0028	-36.5	<.0001
B_2	D_E	-0.0128	0.0051	-2.49	0.0129

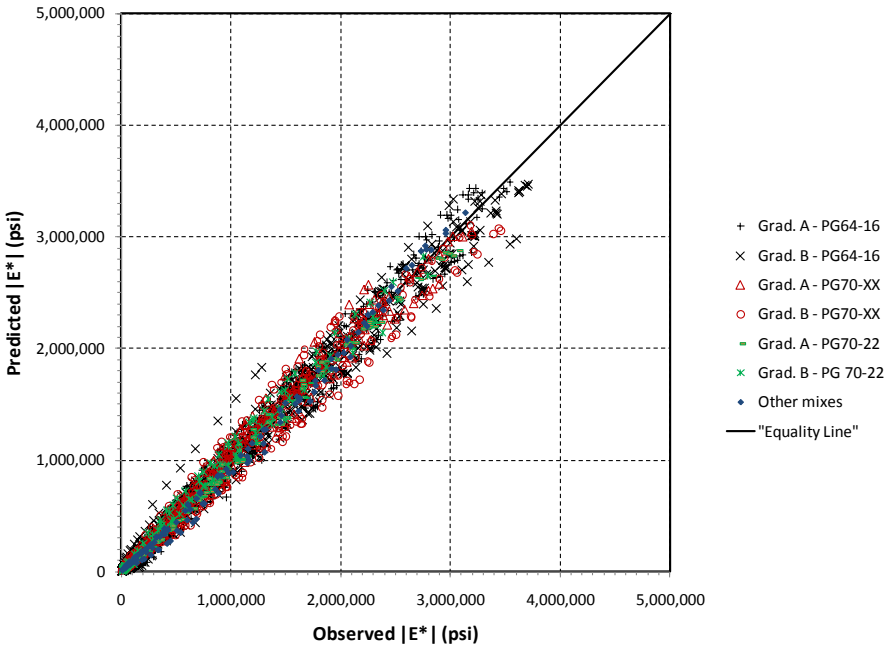

Figure 6-17. Observed versus fitted dynamic modulus values – linear scale.

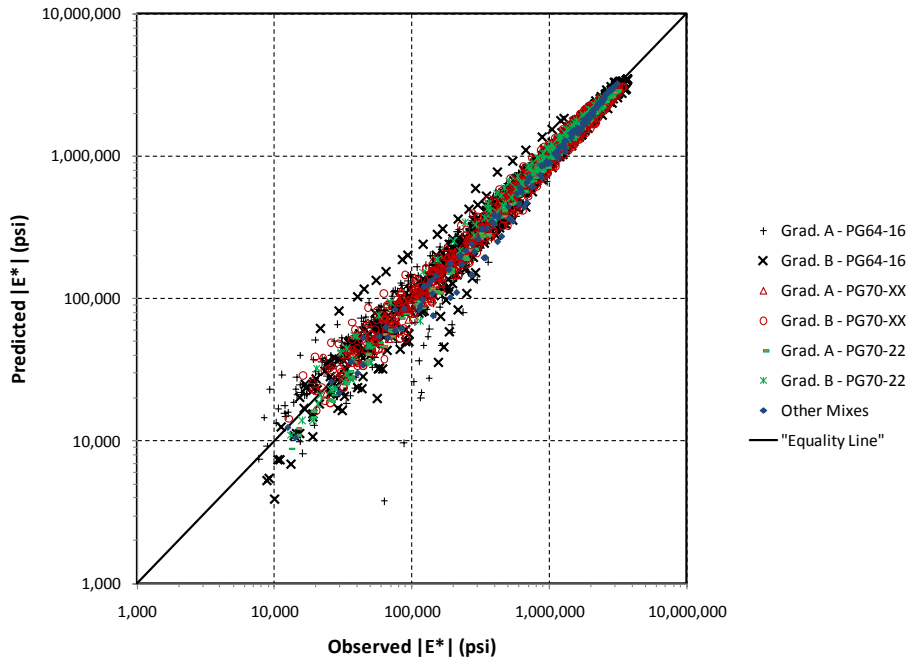

Figure 6-18. Observed versus fitted dynamic modulus values – logarithmic scale.

It should be clear that the shape of the master curves presented in Figure 6-19 are also affected by parameters related to binder type, namely, β_4, β_5, γ_2, A_2, and B_2.

Other parameter estimates with similar interpretations to the δs and αs described above that were found to be statistically significant are δ_6, δ_7, α_5, and α_6.

δ_6 and α_5 are parameters related to a field mix used in a particular pavement preservation project on the H-3 freeway. In this case, the signs are reversed, which indicates that this mix (other things being equal) is softer at high temperatures and low frequencies and stiffer at low temperatures and high frequencies. This mix appears to perform much poorer than other mixes analyzed in this study. It should be noted however that although the model accounts for air voids and voids filled with asphalt, the H-3 mixes were compacted in the lab with too low air voids and too high VFA, which may have affected to some degree the results. Further information is required to ascertain whether the results from those two specimens are just outliers or whether there is some other type of problems with those mixes.

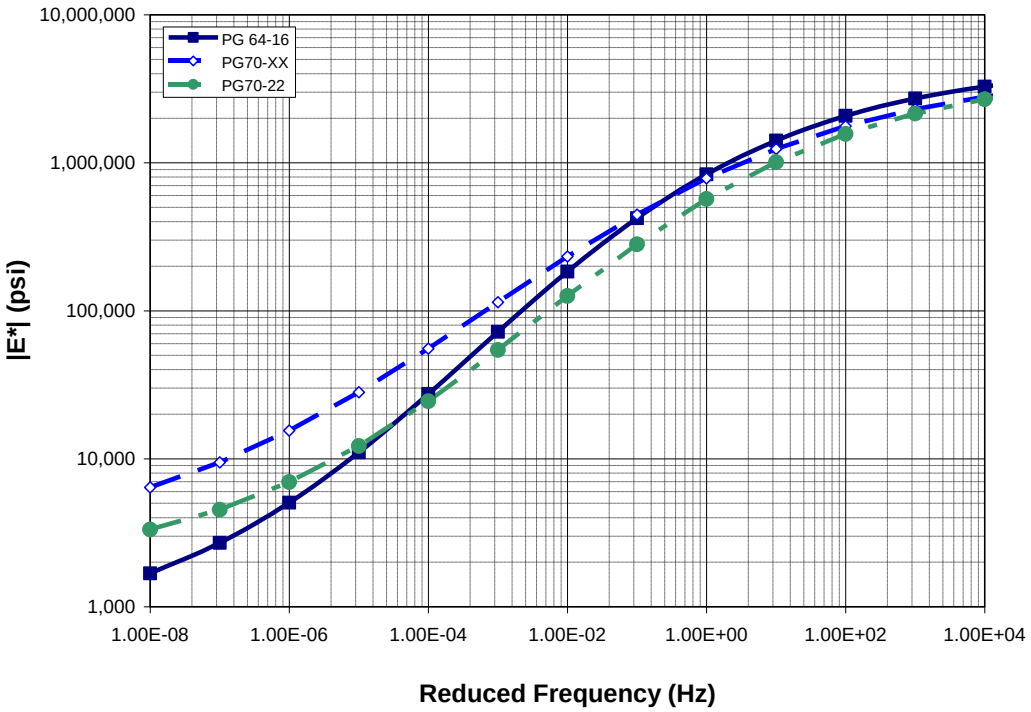

Figure 6-19. Comparison of predicted master curves for mixes with gradation "A" for three different binders (T_{ref} = 70ºC, V_a = 5% and P_b = 5.8%).

The parameters for the Farrington Highway preservation project, δ_7 and α_6, are similar to those for the PG70-XX. Thus, the performance of this mix (in terms of its |E*| value) appears to be similar to that of the polymer modified mix. Interestingly, despite this apparently good response, this project showed some early signs of distress after only 1½ years. The picture in Figure 4-24 (page 141) is from the same highway section. As mentioned in Section 4.3.1.1.2 (page 136), some of the paving was performed on a section that still showed severe fatigue cracking after milling, which may explain the poor field performance.

This example stresses the point that to achieve the benefits of good mixes not only the mix characteristics but also the structural integrity of the pavement need to be adequate.

No variable differentiating between the behavior of gradations A and B were found to be significant in the δ and α terms. Apparently, the two gradations perform similarly when the volumetric variables V_a and VFA are the same. Parameter β_6 is the only one that captures some difference between the two gradations. Figure 6-20 illustrates the effect of this parameter for mixes with and without modified binder. In general, although statistically significant, the differences between the two gradations are relatively minor when compared to the effects of other variables.

The effects of air voids and voids filled with asphalt are intricately related; thus, the end effects are analyzed instead of analyzing the individual parameters. Figure 6-21 shows the effect of air voids for a mix with asphalt content P_b = 5.8% and the PG70-XX binder. The effect of air voids is quite apparent, with higher air voids resulting in lower dynamic moduli. Notice also that keeping the binder content constant while varying the air voids (as assumed in this figure) requires varying the VFA as well.

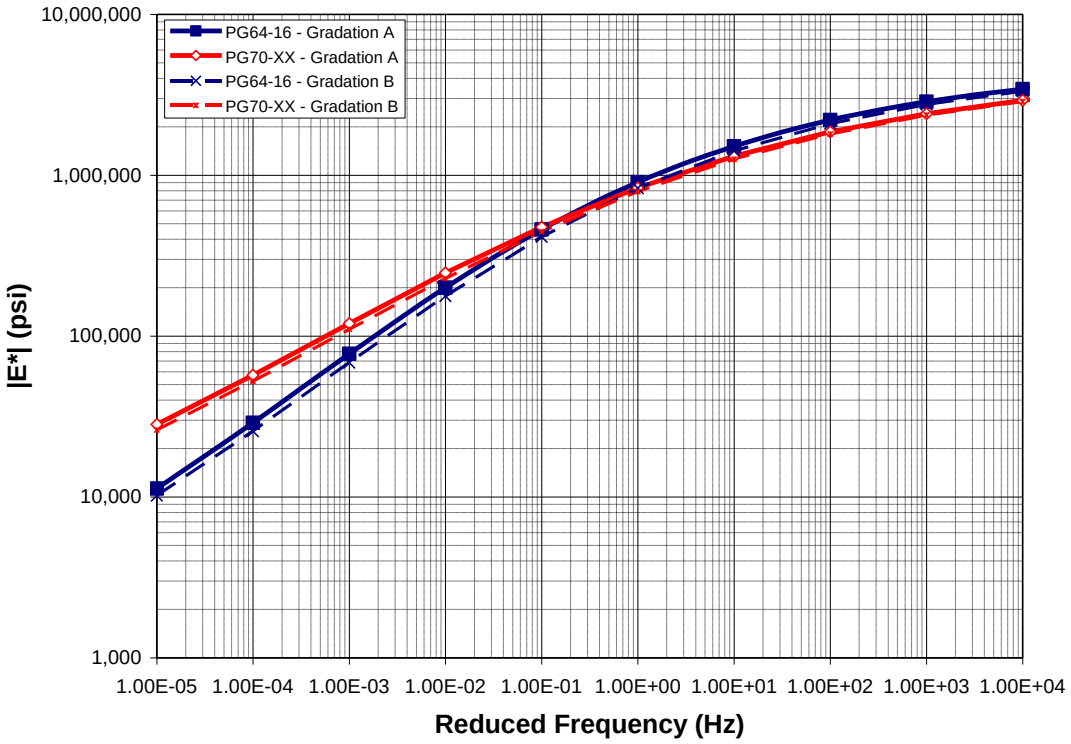

Figure 6-20. Comparison of predicted master curves for gradations A and B (T_{ref} = 70ºC, V_a = 5% and P_b = 5.3%)

Figure 6-22 shows the effect of binder content for a mix with V_a = 5% and the PG70-XX binder. Again, keeping the air voids constant while varying the binder content (as assumed in the figure) requires varying the VFA as well. Unlike the effects of air voids, the effects on the dynamic modulus of varying binder content do not appear to be so substantial. It should be noted that this may be partly a consequence of the fact that there is not as much variation of binder contents in the sample as there is in air voids, which may have precluded a better identification of its effect.

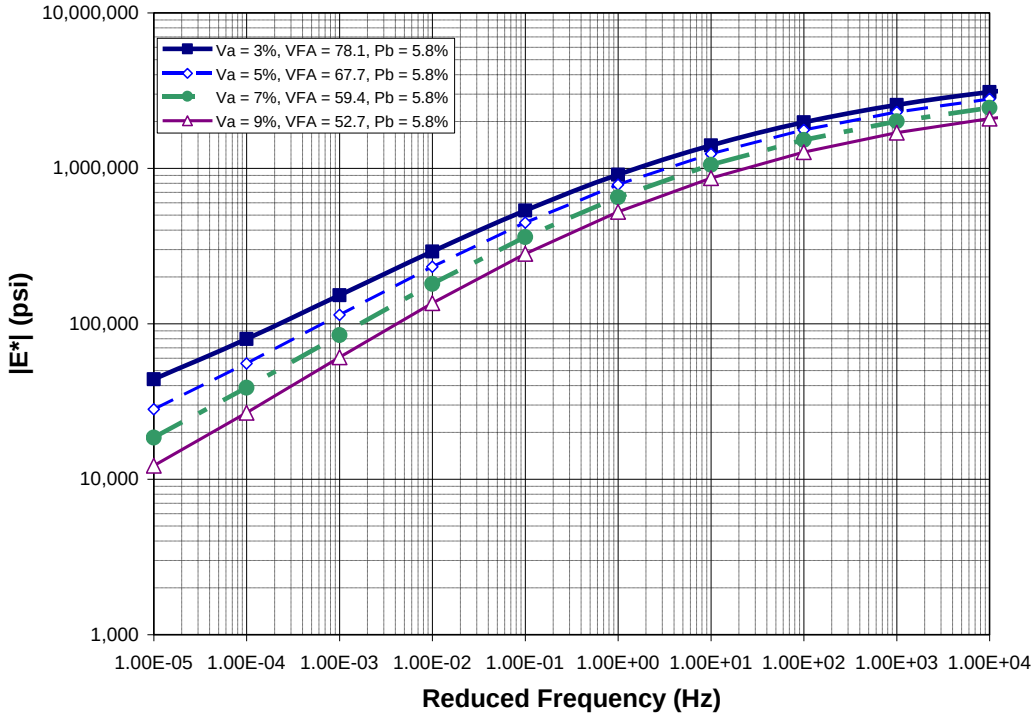

Figure 6-21. Comparison of predicted master curves for mixes with different air voids levels (gradation "A", PG70-XX, T_{ref} = 70ºC, and P_b = 5.8%).

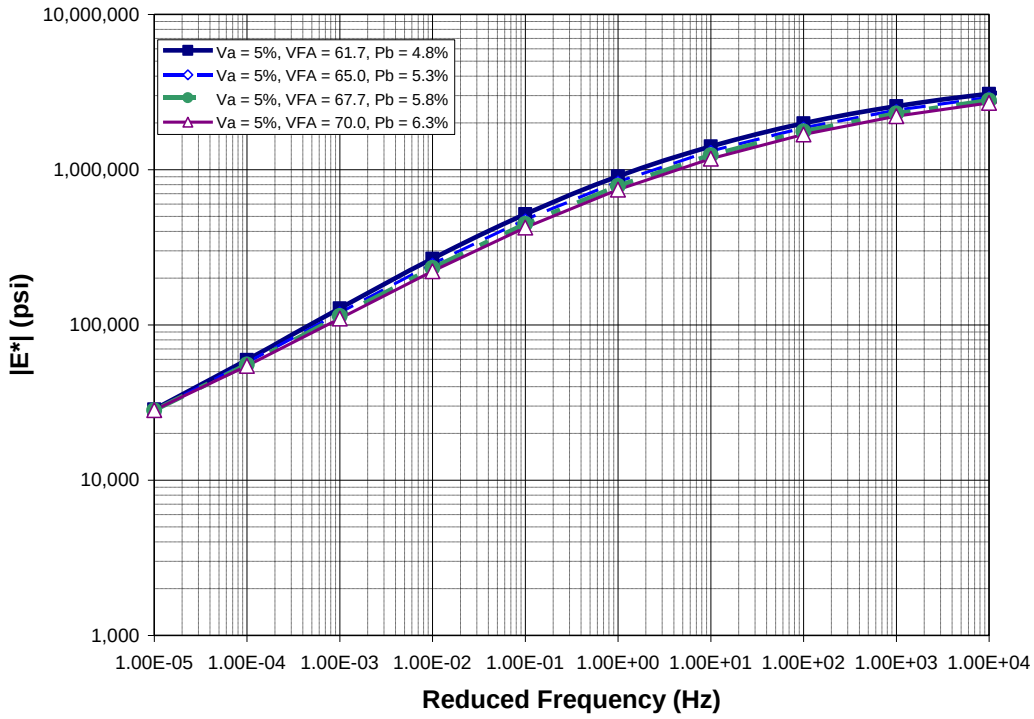

Figure 6-22. Comparison of predicted master curves for mixes with different binder contents (gradation "A", PG70-XX, T_{ref} = 70ºC, and V_a = 5%).

6.2.4.2.3 Discussion of suggested use of the local model

As the use of the MEPDG progresses, ideally, the best option for individual states should be the calibration of one of Witczak's equations or similar equations for their particular conditions. However, this may demand a substantial database with very detailed information, which may be difficult to obtain locally.

The results of the locally calibrated model can be used to generate |E*| values for selected temperature and frequencies for input into the MEPDG as pseudo-level 1 data. This is the approach used in this study for calibration of the guide for State Type IV and Superpave 12.5 mm NMAS mixes. Since a similar model has not yet been developed for State Type III and Type V mixes, the inputs for those mixes was performed at a level 2.

As the previous sections have shown, relatively accurate results can be achieved with this approach because although the data may be less detailed, the model is still based on observations of local materials and thus may account for unobserved factors that cannot possibly be included or that may be difficult to include in a universal model. Thus, although the values generated by the model are not really level 1 data, they provide an alternative to the use of level 2 or 3 inputs, which are based solely on gradation and binder characteristics.

It is also important to point out that the sole prediction of |E*| is not enough to predict accurately distresses such as permanent deformation. As illustrated in [50] and [51] (the results in [50] were based on a subsample of the sample used in this report), the predictions with the MEPDG without any adjustments in the calibration parameters of the permanent deformation model for modified mixes do not appear to give enough credit to polymer modified mixes and under some conditions, the MEPDG may even indicate that the modified mixes perform worse than the unmodified mixes. Additional permanent deformation testing and modeling together with the model presented in this section tend to confirm those findings [52]. Permanent deformation of HMA is discussed in section 6.5 (page 333) of this report.

6.2.4.2.4 Model Validation

As part of a more limited study, additional HMA specimens were compacted and tested for dynamic modulus and permanent deformation. Testing was performed on two sets of six specimens of a control unmodified mix, a polymer modified mix, and a fiber reinforced mix. For each mix, two specimens were compacted at three different target air voids. The mix design adopted had been used by Grace Pacific Corporation (GPC) in a paving project performed around the time of the study. GPC provided the samples of the same aggregates and the same asphalt binder used in that project, which were used in the preparation of specimens in the laboratory. In addition, testing was performed on six specimens (2 replicates at three target air voids) of another unmodified mix produced at a local asphalt plant.

Figure 6-23 shows the gradations of the mixes used by Rayapeddi Kumar [47]. For lack of a better name, they were designated C and D. The figure also shows for comparison gradations A and B used in the development of the local model. In addition, for limits of 12.5 mm NMAS are also shown. Gradation C meets the gradation Superpave (SP) 12.5 mm NMAS mix. It also meets the State Mix IV gradation On the other hand, Gradation D meets the SP 19.0 mm NMAS requirements.

Figure 6-24 shows gradation D along with the SP 19 mm gradation limits.

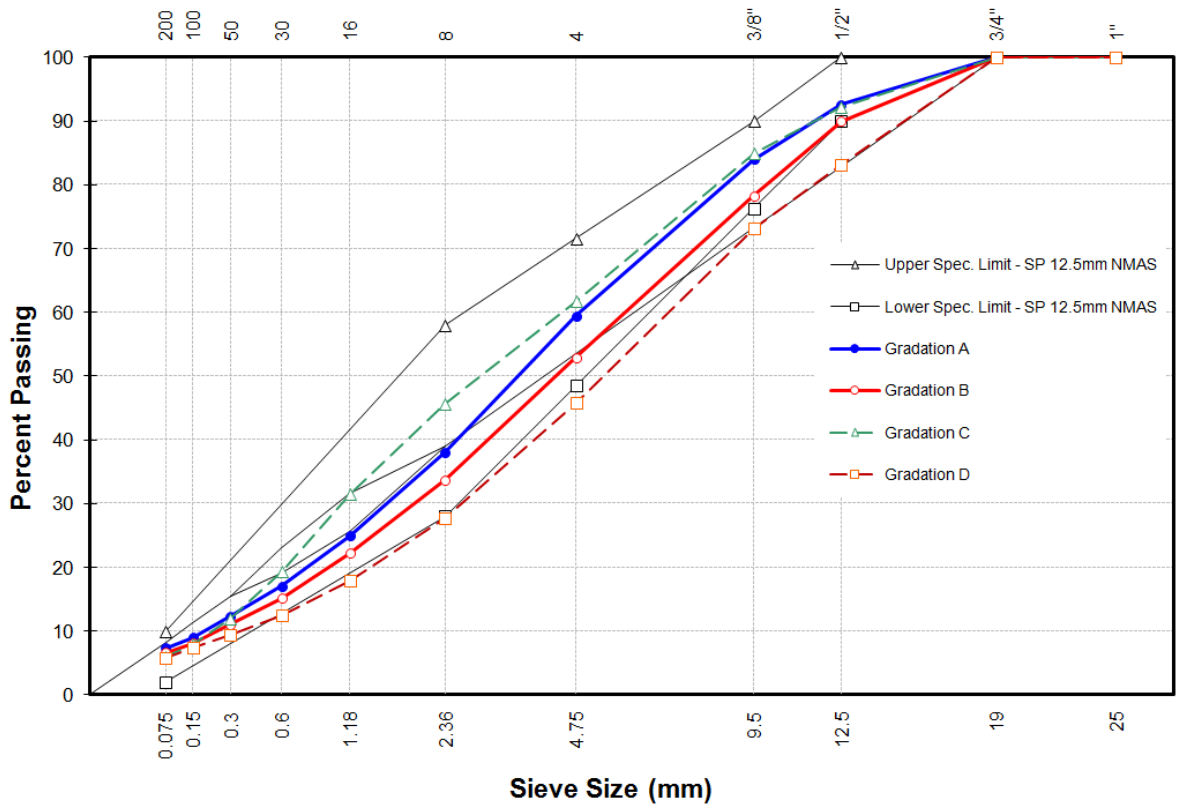

Figure 6-23. Comparison of C and D gradations with gradations A and B.

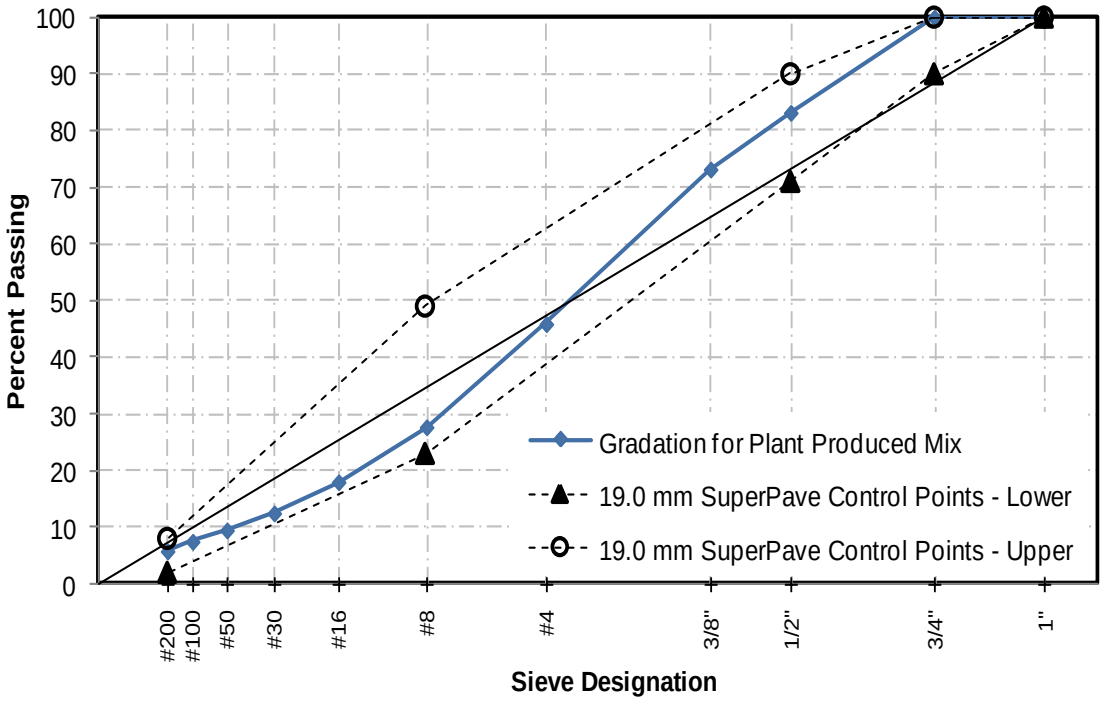

Figure 6-24. Gradation D.

The aggregates used in the preparation of HMA samples in the laboratory were from the Ameron Kapa'a quarry in the island of Oahu, Hawaii. For the plant produced mixes, the coarse aggregates were also from the Ameron Kapa'a quarry in Oahu, Hawaii but the fine aggregates were from Ameron Puunene quarry from the island of Maui, Hawaii.

The control, PMA, and fiber reinforced mixes were prepared with gradation C. The other unmodified mix was prepared with gradation D.

The unmodified binder was a PG64-22 now supplied by Asphalt Hawaii. Although the high temperature grade is the same as that used in the previous study, the source of the binder is different. Therefore, differences in some binder characteristics may be expected. From informal conversations with for some people in the field, there seems to be a feeling that the new binder (source: Saudi Arabia) is a bit softer.

Similarly to the previous study, to prepare the polymer modified asphalt (PMA) specimens, the unmodified binder from Asphalt Hawaii was modified with 1% of DuPont's Elvaloy®RET and mixed with 0.3% (by weight of binder) polyphosphoric acid. The latter is added to act as a catalyst of the reaction between Elvaloy RET and the binder. An additional set of specimens were prepared with the unmodified binder but introducing into the mix HMA Forta-FI Fibers® in a proportion of 1 lb/ton.

In summary, the four types of mixtures tested in this study and the notation used by Rayapeddi Kumar [47] to identify them were:

1. Laboratory produced mixtures with gradation C prepared using virgin asphalt binder (VLPM).
2. Laboratory produced mixtures using gradation C prepared using polymer modified asphalt binder (PMALPM).
3. Laboratory produced mixtures with gradation C prepared using unmodified binder and fibers (FRACLPM).
4. Plant produced mixtures with gradation D prepared using virgin asphalt binder (VPPM).

Other details on the preparation of the specimens and their characteristics are described in [47]. Before discussing the |E*| model validation, the next subsection provides some additional information about the procedure used by Rayapeddi Kumar [47] to disperse the fibers in the mix.

6.2.4.2.4.1 Fibers Used in the Study

FORTA-FI® HMA blend fibers were used in this study. In its manufactured condition, the fibers are clasped together. The fibers were fluffed using a makeshift procedure prior to mixing them with hot aggregates. This is done to enhance the effect of fibers and improve the distribution of fibers in the HMA mixture. The procedure involved placing packaged fibers inside a hollow cylinder, the top of which was then covered using a perforated disc. Next, compressed air was blown from the top to achieve the desired result. Figure 6-25 through Figure 6-27 show the fibers in its manufactured condition, the fluffing setup, and the resulting fluffed fibers. The fluffed fibers were then weighed as required and mixed with hot aggregates before asphalt was introduced into the mixing bowl.

Figure 6-25. FORTA-FI HMA Fibers in its manufactured condition.

Figure 6-26. Setup used to fluff the fibers.

Figure 6-27. FORTA-FI® HMA fibers after fluffing.

6.2.4.2.4.2 |E*| model validation

From Rayapeddi Kumar's study [47], 451 additional |E*| valid observations were obtained and used to evaluate the local model and the NCHRP 1-37A model. A summary of the volumetric characteristics of all the HMA specimens is presented in Table 6-5. As can be seen from the table, the actual air voids (V_a) and target air voids (V_a) did not always match. The result is particularly troublesome for the specimens prepared with the plant produced mix (VPPM). It is suspected that the big differences for this mix are due to some error in its maximum theoretical specific gravity (G_{mm}) determination.

The volumetric properties in Table 6-5 were used with the local model (equations (6-12) to (6-20)) to estimate the values of |E*| for each frequency/temperature combination with valid data points for each specimen. Figure 6-28 shows the observed vs. predicted values in linear scales and Figure 6-29 shows the same results with logarithmic scales to better observe the low |E*| predictions. Since the gradations are different from the ones used to develop the model, the following assumptions were made. The plant mix (VPPM) was assumed to have gradation B, since its gradation was closer to this gradation than to gradation A. The other mixes were assumed to have gradation A. Note that above the #4 sieve, gradations A and C are practically the same but below that sieve there are differences that could be significant. In any case, this was the best assumption that could be made. Furthermore, no fibers were used in the estimation of the model. For the fiber reinforced mixes, it was assumed that the binder was unmodified. The rationale for the last assumptions is that the beneficial effect of the fibers occur at relatively large strains. Since small strains are applied to determine |E*|, then the fibers are expected to have only a minor effect on the computed mix stiffness.

Table 6-5. Characteristics of HMA specimens tested by Rayapeddi Kumar **[47]**.

Specimen ID	Mix Type	P_b (%)	Target V_a (%)	G_{mm}	G_{mb}	Actual V_a (%)	VMA (%)	VFA (%)
VPPM1	Virgin	5.5%	3.0%	2.560	2.539	0.8%	9.8	91.8
VPPM2	Virgin	5.5%	3.0%	2.560	2.543	0.7%	9.6	93.1
VPPM3	Virgin	5.5%	5.0%	2.560	2.498	2.4%	11.2	78.4
VPPM4	Virgin	5.5%	5.0%	2.560	2.496	2.5%	11.3	77.8
VPPM5	Virgin	5.5%	7.0%	2.560	2.419	5.5%	14.0	60.7
VPPM6	Virgin	5.5%	7.0%	2.560	2.420	5.5%	14.0	60.9
VLPM1	Virgin	6.7%	3.0%	2.460	2.408	2.1%	13.5	84.2
VLPM2	Virgin	6.7%	3.0%	2.460	2.418	1.7%	13.1	86.9
VLPM3	Virgin	6.7%	5.0%	2.460	2.349	4.5%	15.6	71.1
VLPM3B	Virgin	6.7%	5.0%	2.460	2.337	5.0%	16.0	68.7
VLPM4	Virgin	6.7%	5.0%	2.460	2.341	4.8%	15.8	69.6
VLPM5	Virgin	6.7%	7.0%	2.460	2.282	7.2%	18.0	59.7
VLPM6	Virgin	6.7%	7.0%	2.460	2.264	8.0%	18.6	57.2
PMALPM1	Polymer Modified	6.7%	3.0%	2.452	2.413	1.6%	13.3	88.0
PMALPM2	Polymer Modified	6.7%	3.0%	2.452	2.417	1.7%	13.1	86.8
PMALPM3	Polymer Modified	6.7%	5.0%	2.452	2.346	4.6%	15.7	70.5
PMALPM4	Polymer Modified	6.7%	5.0%	2.452	2.351	4.4%	15.5	71.5
PMALPM5	Polymer Modified	6.7%	7.0%	2.452	2.286	7.1%	17.8	60.4
PMALPM6	Polymer Modified	6.7%	7.0%	2.452	2.296	6.7%	17.5	61.8
FRACLPM1	Fiber Reinforced	6.7%	3.0%	2.460	2.404	2.3%	13.6	83.2
FRACLPM2	Fiber Reinforced	6.7%	3.0%	2.460	2.403	2.3%	13.6	83.1
FRACLPM3	Fiber Reinforced	6.7%	5.0%	2.460	2.338	5.0%	16.0	69.0
FRACLPM4	Fiber Reinforced	6.7%	5.0%	2.460	2.351	4.4%	15.5	71.4
FRACLPM5	Fiber Reinforced	6.7%	7.0%	2.460	2.271	7.7%	18.4	58.2
FRACLPM6	Fiber Reinforced	6.7%	7.0%	2.460	2.268	7.8%	18.5	57.8

Figure 6-28 shows a close clustering of points similar to the one observed during the development of the model. This is an indication that for the most part, the model captures the volumetric, temperature, and frequency effects quite well. However, it is now evident that the predictions are biased slightly upward. This is consistent for all the mixes. Figure 6-29 presents a different view of the same bias. A clear shift upward is observed in this figure. It is difficult to ascertain whether the bias is caused by the different gradations or the different binder used. However, considering the relative positions of the plant produced mix gradation (gradation D) and the laboratory produced mixes (gradation C) with respect to the model gradations A and B (Figure 6-23), it is most likely that the aggregate gradation would have a different effect for the plant produced mixes than for the laboratory produced mixes.

Therefore, it is suspected that the difference is caused mainly by the binder. Note that if the above *speculation* is correct, it implies that the reason why the model over-predicts the values of |E*| is because the binder currently supplied is somewhat softer than before. It is important to note, however, that the differences are relatively minor and that |E*| alone is not a good indicator of mix performance.

The bias above can be easily corrected for these mixes by subtracting 0.3 from δ (equation (6-17)) and adding 0.22 to α (equation (6-19)). These two factors are not the result of a re-estimation of the model. Instead, they were simply derived by trial and error. The fit in Figure 6-30 resulting from these corrections is acceptable for all practical purposes.

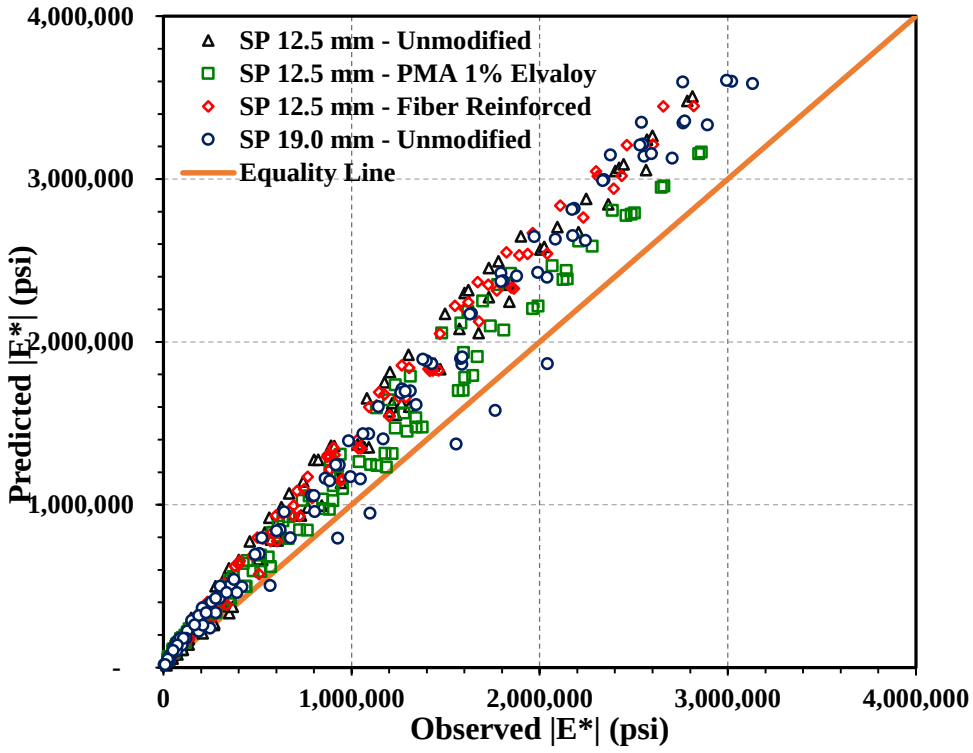

Figure 6-28. Observed vs. Predicted |E*| using Rayapeddi Kumar's data and the local |E*| model (linear scale).

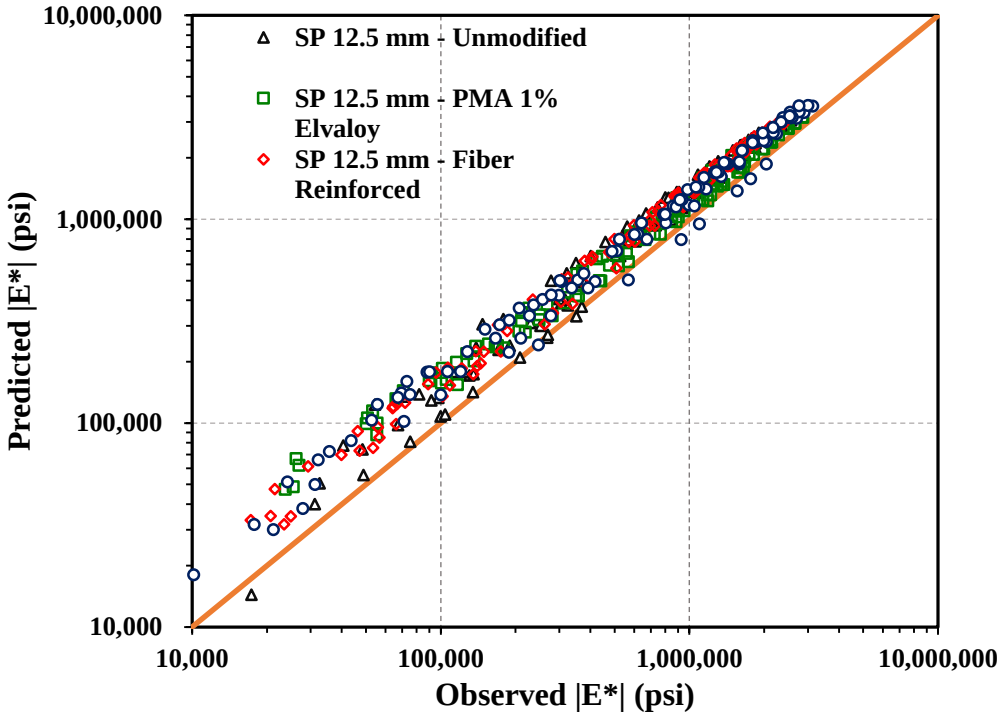

Figure 6-29. Observed vs. Predicted |E*| using Rayapeddi Kumar's data and the local |E*| model (logarithmic scale).

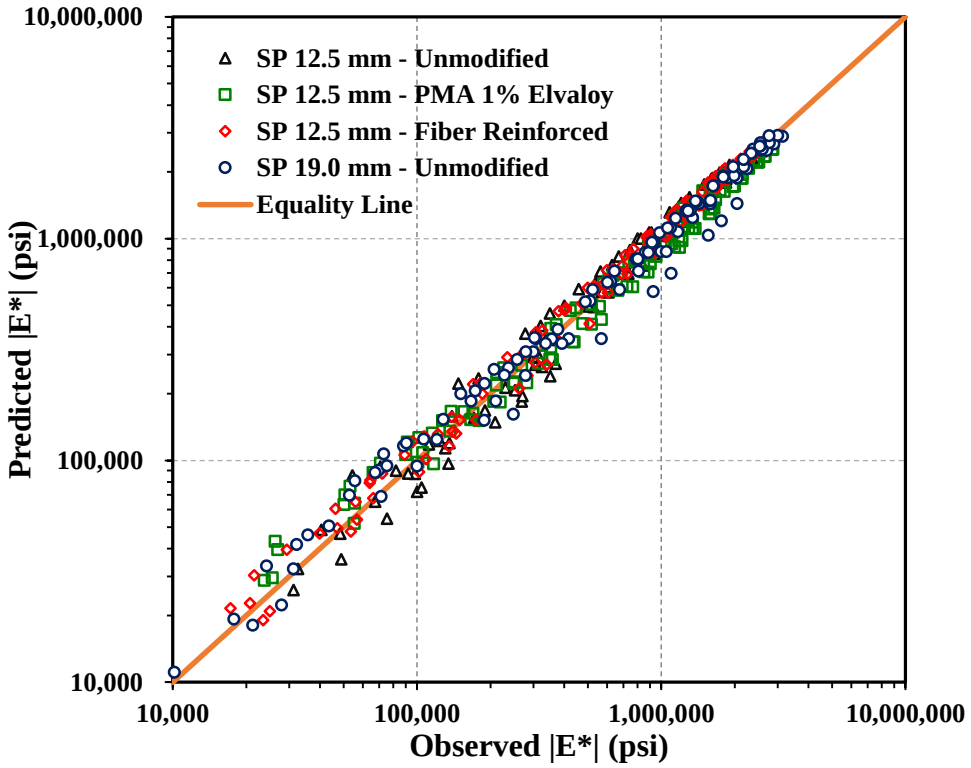

Figure 6-30. Observed vs. Predicted |E*| using Rayapeddi Kumar's data and the local |E*| model after bias correction (logarithmic scale).

Rayapeddi Kumar's data were also used to evaluate the NCHRP 1-37A model. Figure 6-31 and Figure 6-32 show the results in linear and logarithmic scales, respectively. The predictions for the unmodified control mix are acceptable but they deviate more for the other mixes. Still, if no other information is available, the model provides reasonable values with some minimal information.

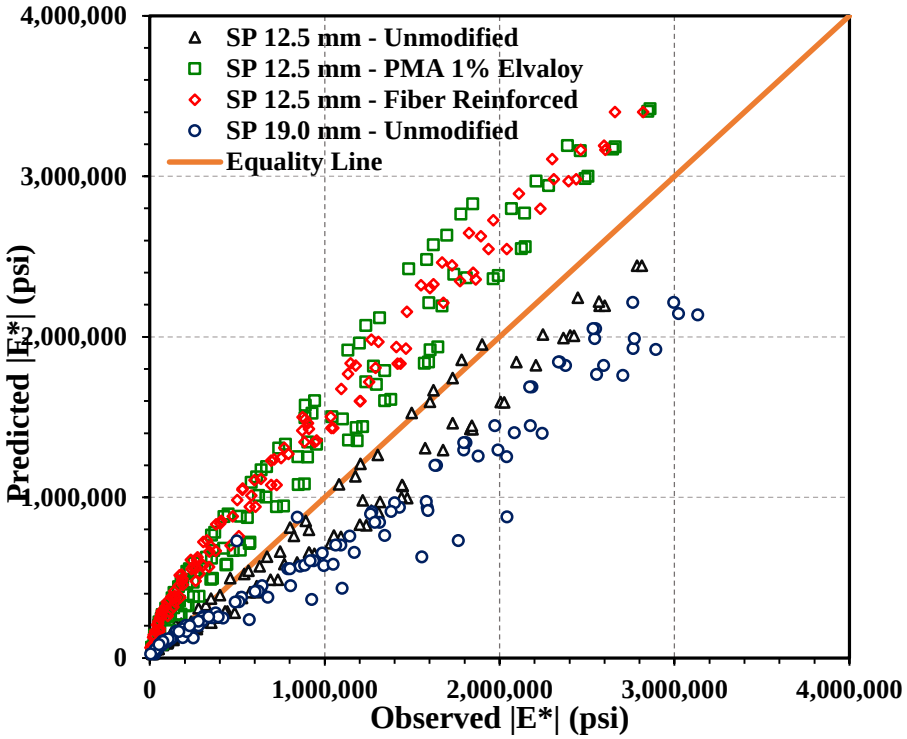

Figure 6-31. Observed vs. Predicted |E*| using Rayapeddi Kumar's data and NCHRP 1-37A |E*| model (linear scale).

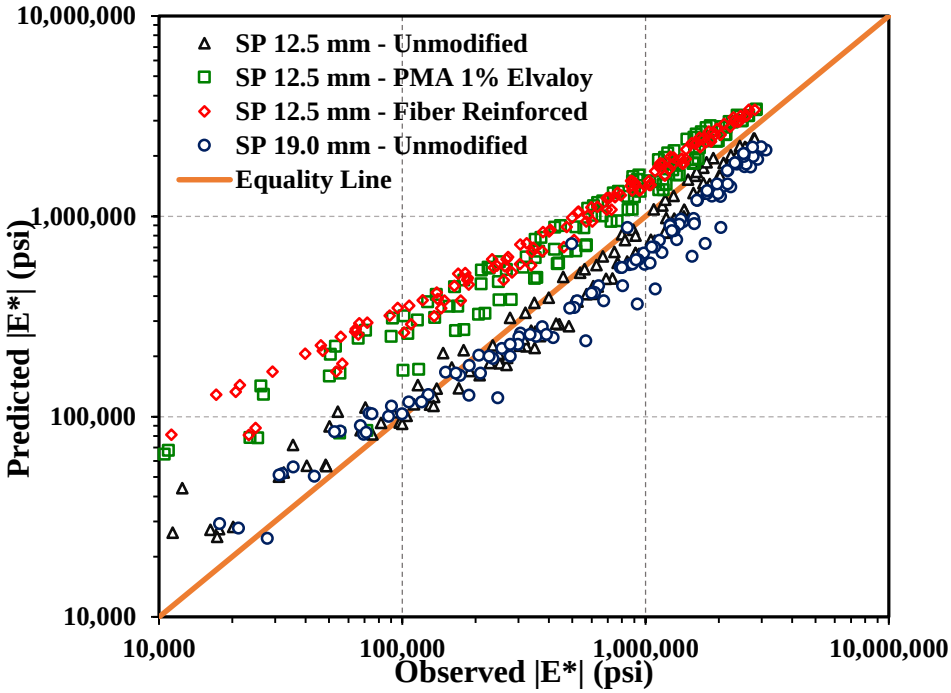

Figure 6-32. Observed vs. Predicted |E*| using Rayapeddi Kumar's data and the NCHRP 1-37A |E*| model (logarithmic scale).

6.2.4.2.5 Additional Issues

Despite the significant understanding about HMA dynamic modulus that has been developed over decades, there are still a few issues that need further study. As mentioned in section 6.2.1.1 (page 230), there is evidence that confinement affects dynamic modulus, particularly at high temperatures and low frequencies [40] but more research is needed to develop models that determine |E*| as a function of confinement level. Without confinement, the |E*| values at high temperatures and low frequencies of loading appear to be conspicuously low for some mixes. Another related issue is that all the |E*| testing is performed in compression, where the aggregate and the binder contribute to the modulus. However, in tension, the modulus would depend mostly on the binder. Thus, constitutive models that account for the state of stresses should be developed. A possible reason that these issues have not been studied in more detail is that their modeling requires the use of non-linear finite element analysis.

Despite the widely use of |E*|, there are still controversies about the frequency determination in the field [53]. As discussed in the next chapter (section 7.6.1), solving this issue may be of particular interest to Hawaii since it seems that in the MEPDG the effect of frequency is always dominating the effect of temperature.

6.2.4.2.6 Summary and Conclusions

The main objectives of this section were to evaluate the adequacy of the |E*| models used in the MEPDG for levels 2 and 3 designs, and to estimate a simplified version of those models to provide more accurate data as pseudo-level 1 data. The following conclusions are provided based on the finding:

1) The two models currently used in the MEPDG for levels 2 and 3 provide in general reasonable estimates of |E*| for those levels of analysis, although for the mixes analyzed, the results appear to be biased.
2) The NCHRP 1-37A model tends to under predict the |E*| of the Hawaii unmodified mixes and over predict the |E*| of the polymer modified mixes.
3) The NCHRP 1-40D model tends to over predict the |E*| for both the unmodified and polymer modified mixes analyzed.
4) An alternative model using the same sigmoidal function of the MEPDG model but using indicator variables to account for some of the differences between mixes for which no detailed information is available was developed and estimated. The developed model shows excellent statistical results even though the number of observations in the database is substantial. Thus it is believed to capture the behavior of the mixes studied quite well.
5) A limited validation of the model with mixes prepared with new binder supplied on the state indicates that the local model produces reasonable but somewhat bias estimates. A small correction to two of the terms of the model corrects the bias. If mixes that are too different from the ones analyzed here are considered, the NCHRP 1-37A model still provides reasonably estimates of |E*|.

6.3 RESILIENT MODULUS OF UNBOUND MATERIALS AND SOILS

The moduli of unbound bases, subbases, and subgrade soils are essential inputs for mechanistic-empirical pavement design.

For these materials, time of loading is not as important as for HMA. However, their moduli are significantly affected by many other factors that make their determination non-trivial. Among these are the stress level, which depends on the position of the element within the pavement structure, the load magnitude, material conditions such as moisture content, etc. Furthermore, since moisture content can vary throughout the year, so does the modulus. A

basic understanding of the interaction of these terms becomes important to select reasonable input values.

This section, after a brief introduction to the models used to predict modulus of unbound materials and soils, provides a summary of the information locally available. Although the Pavement ME Design software [2] currently uses a single modulus value for each layer for a given set of environmental conditions, the discussions in this section about the modulus dependence on stress provide the background to make informed decision when selecting M_r values.

6.3.1 Resilient Modulus

For unbound base and subbase materials and soils, the elastic modulus used in the mechanistic analysis is the resilient modulus.

The resilient modulus test for fine-grained materials is typically performed on cylindrical specimens of a height h = 8 in. and a diameter ϕ = 4 in. For coarse-grained materials, due to their larger maximum aggregate sizes, the diameter of the test specimen is increased to ϕ = 6 in. and correspondingly the height is increased to h = 12 in. to maintain the height to diameter ratio to a minimum of 2 (Figure 6-33).

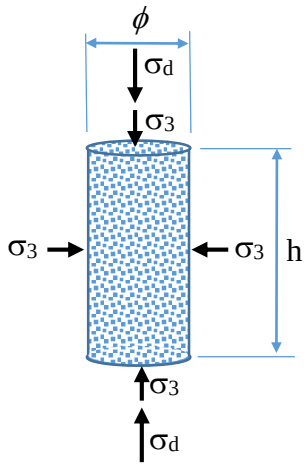

Figure 6-33. Resilient modulus test specimen.

The resilient modulus test is basically a "confined uniaxial"[43] repeated loaded test in which a haversine deviator stress pulse (σ_d) followed by a rest period is applied repeatedly to a sample already subjected to an all-around confinement stress (σ_3). During the test, the resilient (recoverable) strains are also measured. Figure 6-34 illustrates the stress pulse and Figure 6-35 the resulting resilient strains.

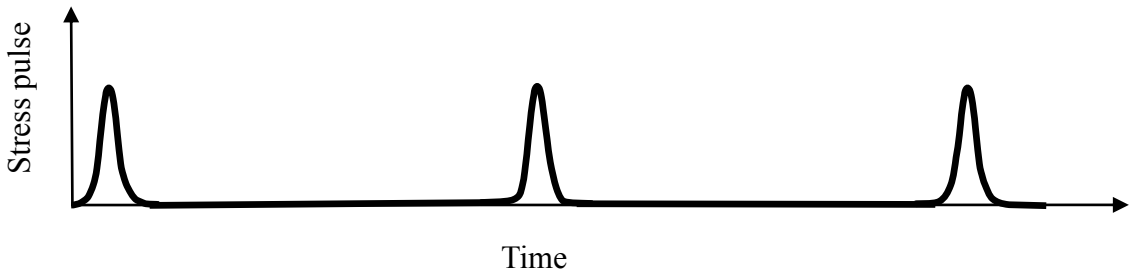

Figure 6-34. Stress pulse and rest period in a resilient modulus test.

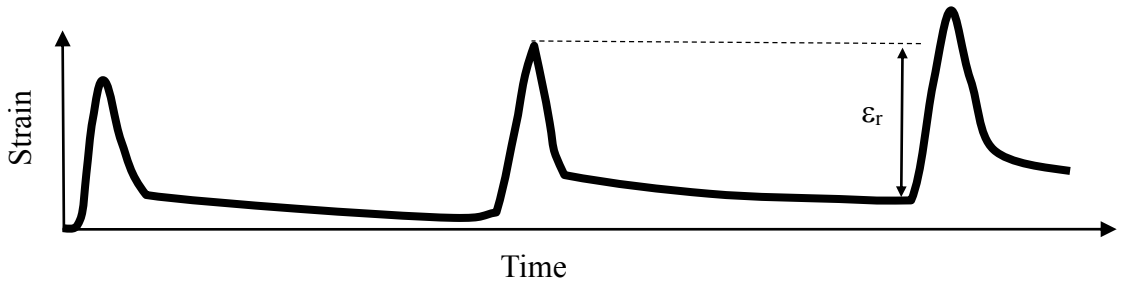

Figure 6-35. Resilient strain (ε_r).

Since unbound materials are stress-dependent, the test is performed at different stress levels (different combination of confinement and deviator stresses.) Figure 6-35 also illustrates that with each cycle some permanent deformation is typically accumulated. At relatively small stress levels and after several repetitions of the load pulse, as shown in Figure 6-36, the permanent deformation accumulated per cycle becomes smaller and the slope of the σ_d-ε_r curve relatively constant. All resilient modulus test protocols require the measurement

[43] As stated by Muir Wood [156]: "The most widely used apparatus for investigating the stress:strain behaviour of soils is, in origin, a 'confined uniaxial' testing device known (misleadingly) as the triaxial apparatus."

of M_r after a certain number of repetitions at each stress level to capture this mostly elastic response.

The slope of the σ_d-ε_r curve after a large number of cycles is by definition the resilient modulus:

$$M_r = \frac{\sigma_d}{\varepsilon_r} \tag{6-22}$$

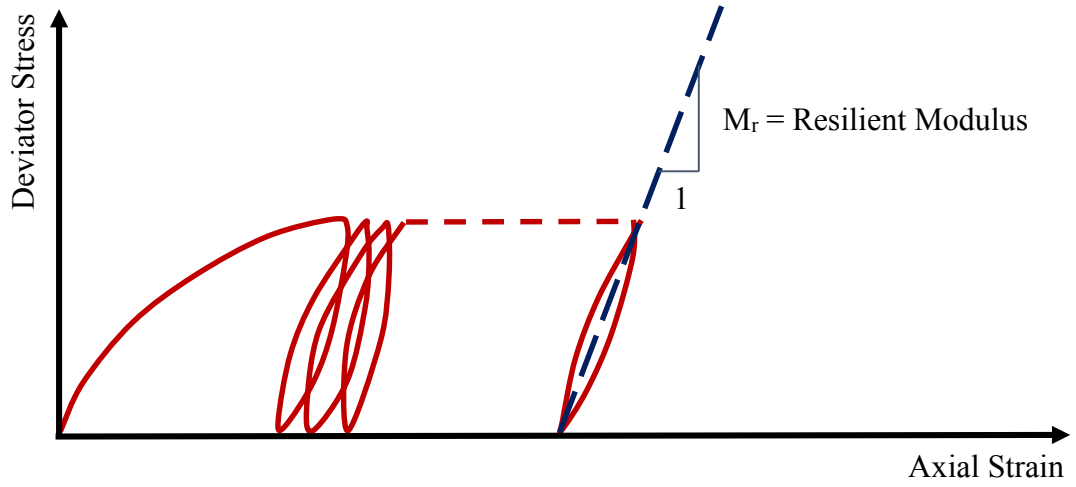

Figure 6-36. Deviator stress vs. axial strain in the resilient modulus test.

It is important to recognize that a resilient modulus test does not result in a single modulus for the material tested but instead in a set of several resilient modulus values at the different stress levels. The influence of stress state is significant on the resilient moduli of both cohesive and cohesionless soils.

Li and Selig [54] identified three factors that influence the resilient modulus: (1) loading condition or stress state, (2) soil type and structure, and (3) soil physical state (combination of molding water content and dry unit weight). For a specific sample tested in the lab, the last two factors are fixed but the effect of stress state still needs to be modeled. This is considered in the next section. For designs on which testing is not performed or when changes in M_r over time are required, models that incorporate the last two factors in addition to state stress are needed. These are covered in Section 6.3.1.2.3.

6.3.1.1 Modeling the effect of stress state

Several models have been proposed to predict the stress dependency of M_r. A description, as well as some limitations of some of the models, is found in Ooi et al. [55]. The list of models described in that reference is not exhaustive but it provides a good description of some of some important modeling issues. In the following, only the model adopted in the MEPDG [1] is described in detail.

The MEPDG uses a generalized constitutive model for resilient modulus. The generalized model used in the design procedure is as follows:

$$M_{r\,opt} = k_1\, p_a \left(\frac{\theta}{p_a}\right)^{k_2} \left(1+\frac{\tau_{oct}}{p_a}\right)^{k_3} \tag{6-23}$$

where

$M_{r\,opt}$ = resilient modulus at optimum water content, psi,

θ = bulk stress = $\sigma_1 + \sigma_2 + \sigma_3$,

σ_1 = major principal stress,

σ_2 = intermediate principal stress = σ_3 for M_r tests on cylindrical specimens,

σ_3 = minor principal stress/confining pressure,

τ_{oct} = octahedral shear stress,

$$= \frac{1}{3}\sqrt{(\sigma_1-\sigma_2)^2+(\sigma_1-\sigma_3)^2+(\sigma_2-\sigma_3)^2}$$

p_a = normalizing stress (atmospheric pressure) (14.7 psi),

k_1, k_2, k_3 = regression parameters (obtained by fitting resilient modulus test data to equation).

The constitutive model coefficients (the parameters k_1, k_2, and k_3) are estimated from data through linear or non-linear regression (they can be estimated very easily using linear regression by taking logarithms of both sides of the equation). A typical requirement is that the values determined for each test specimen should be such that the multiple correlation coefficient, R^2, exceeds 0.90.

Regarding the signs of the parameters k_1, k_2, and k_3, the MEPDG documentation [1] states:

> "Coefficient k_1 is proportional to Young's modulus. Thus, the values of k_1 should be positive since M_r can never be negative. Increasing the bulk stress, θ, should produce stiffening or hardening of the material, which results in a higher M_r. Therefore, the exponent k_2, of the bulk stress term for the above constitutive equation should also be positive. Coefficient k_3 is the exponent of the octahedral shear stress term. The values for k_3 should be negative since increasing the shear stress will produce a softening of the material (i.e., a lower M_r)."

Witczak and Uzan (1988) found that for granular materials tested in a triaxial stress state, the deviator stress has two contrary effects on the stiffness of the material; they argue that an increase in deviator stress will result in an increase in bulk stress ($\theta=3\sigma_3+\sigma_d$), which leads to increase in the stiffness of the material and that an increase in deviator stress also increases the octahedral shear stress, which tends to decrease the modulus. Hicks and Monismith (1971) on the other hand reported a "slight softening of the granular material at low deviator stress levels and a slight stiffening behavior at higher levels of deviator stress."

There is a widely held belief that, for unbound materials, the coefficient k_3 should be negative ([1], [56], [57], and [58]). However, the sign of k_3 has been reported to be positive by other researchers including references [59] and [60]. Furthermore, a study by Song ([61] and [62]) conducted at the UH pavement laboratory with virgin and recycled granular materials tested using the AASHTO T307 procedure also revealed positive k_3 values for the octahedral shear stress term in the MEPDG model (equation (6-23)). Song obtained k_3 values as high as 0.82, which is uncommon. Nevertheless, values as high as 1.595 have been reported [63]. Unfortunately, the last two references misreported the value of k_1, which appears to be smaller than usual by a factor of 1,000. This is a common occurrence because the state of stresses are commonly expressed in kPa whereas the modulus is expressed in MPa.

In the MEPDG, once M_{ropt} is obtained, the resilient modulus at any moisture content (M_r) is then estimated internally as follows:

$$M_r = 10^{a+\frac{b-a}{1+\exp\left[\beta+k_s\left(S-S_{opt}\right)\right]}} M_{ropt} \qquad (6\text{-}24)$$

where M_{ropt} is the resilient modulus of the soil at optimum water content, S is the degree of saturation, S_{opt} is the degree of saturation at optimum, *a* and *b* are constants representing the

minimum and maximum values, respectively, of $\log(M_r/M_{ropt})$, β is a location parameter defined as $\ln(-b/a)$ so that the ratio M_r/M_{ropt} is equal to one at optimum, and k_s is a regression parameter. The exponent of the number 10 in equation (6-24) represents a sigmoidal function that approximates a linear relationship between $\log(M_r/M_{ropt})$ and $S - S_{opt}$ within a narrow range of saturation values, beyond which, $\log(M_r/ M_{ropt})$ approaches *a* or *b*. M_{ropt} is estimated using equation (6-23).

6.3.1.2 Predicting M_r for Pavement Design

With the above background on resilient modulus, attention is now turned to the prediction of resilient modulus for pavement design. This is again a challenging task because for unbound materials the theory used to model pavement performance does not match the actual material response but it is instead a useful compromise to make the calculations practical. This is in addition to all the uncertainties typically associated with sampling and testing. More specifically, in the current version of the Pavement ME design software [2], unbound materials are assumed to be linear elastic, homogeneous and isotropic, when in fact neither of these assumptions are generally satisfied.

This section first describes the options for obtaining M_r values in Hawaii and provides a discussion of how to use them to derive inputs for the MEPDG. In addition to providing background for selecting M_r values for design, this section provides a framework for later discussion of some important issues, including correction factors for back-calculated layer moduli, effects of non-linearities, changes of M_r with layer thickness/depth, and consideration of environmental effects.

6.3.1.2.1 Input Level 1 – Laboratory testing

The current version of the Pavement ME Design software [2] does not allow to input information at level 1, as the option to use Finite Element analysis to account for unbound materials non-linearities is disabled. Nevertheless, as indicated and illustrated later, it is important for pavement analysts to understand the stress dependency of M_r when selecting appropriate input moduli. Thus, the level 1 testing is discussed next.

Level 1 resilient modulus values for unbound granular materials, subgrade and bedrock are determined from cyclic triaxial tests on prepared representative samples. The MEPDG recommended standard methods for modulus testing are:

- NCHRP 1-28A, “Harmonized Test Methods for Laboratory Determination of Resilient Modulus for Flexible Pavement Design.”
- AASHTO T307, “Determining the Resilient Modulus of Soil and Aggregate Materials.”

These test methods describe the laboratory preparation, testing, and computation of test results. As described earlier, the state of stresses substantially affects the resilient modulus measurements. Therefore, stress states used for modulus testing are based upon the depth at which the material will be located within the pavement structure. Consequently, the test protocols specify different stress levels depending on whether the material will be used as a base/subbase or as a subgrade.

There are some differences between the two test protocols. One difference is that AASHTO T-307 uses LVDT’s that measure the deformation between end platens whereas NCHRP 1-28A utilizes on-specimen clamp mounted LVDT’s. Another major difference is in the state of stress testing sequences. In this respect, the NCHRP 1-28A testing sequences are considered superior because they try to avoid shear failure of the specimen early in the sequence, which is a more likely possibility under AASHTO T-307 sequences.

Figure 6-37 illustrates the resilient modulus test set up for coarse-grained materials available in the pavement laboratory at UH. Since the measurement of vertical strains is performed through Linear Variable Differential Transducers (LVDT) located outside the triaxial cell, the test set-up matches better the requirements of AASHTO T307. The testing sequence can be configured to match either protocol. Equipment for performing resilient modulus of fine-grained materials with clamp mounted internal LVDTs is available at the geotechnical laboratory at UH.

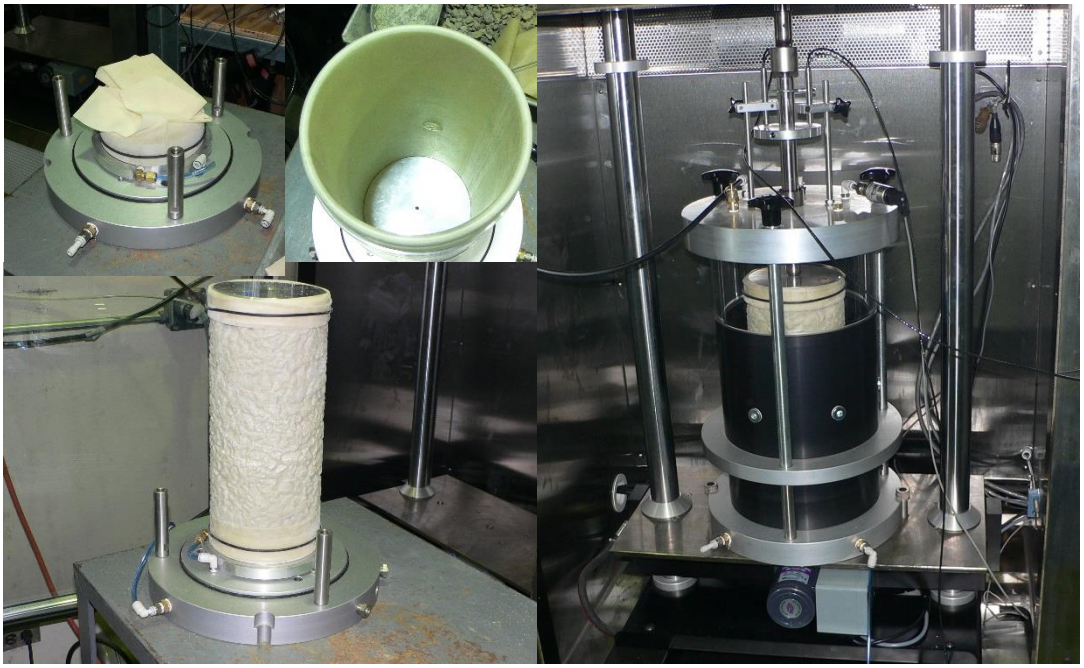

Figure 6-37. Resilient Modulus Test Set-up for granular materials at UH.

The results obtained to date for granular materials in this research were obtained with the equipment set up shown in Figure 6-37.

6.3.1.2.2 Input Levels 2 & 3

At input level 2, the Pavement ME Design software [2] allows entering the resilient modulus directly or values that allow its computation from correlations. Other inputs accepted include CBR, R-Value, Layer coefficient [12], DCP Penetration, and plasticity and gradation information. At level 3, only resilient modulus can be input. Regardless of the input level, the user can allow the program to modify the input values by temperature and moisture or enter a single resilient modulus value to use throughout the year. In addition, at level 2, the user also has the option to enter monthly representative values.

Although the correlations with CBR, R-Value, etc. are widely used, it must be remembered that these are very approximate at best and that they do not account for potential different behavior of local materials. This is particularly relevant for fine-grained tropical residual soils, which are known to exhibit characteristics that are different from those of soils of temperate regions on the U.S. continent. According to Mitchell and Sitar [64], tropical residual soils including those in Hawaii are likely to be less dense, less plastic, less compressible, stronger, and more permeable than temperate soils of comparable liquid limit. Therefore, estimating the resilient modulus from models developed locally should be

preferred to relying on correlations developed elsewhere. Notice that this is not judgment on the reliability of the measurements of CBR, R-Value, etc. but on the applicability of the correlations to local conditions.

6.3.1.2.3 Local Models of M_r

In this subsection, information that may be useful to estimate local resilient modulus values is presented.

6.3.1.2.3.1 Fine-Grained Soils

Sandefur [65] developed an extensive database of resilient modulus values for several Hawaiian fine-grained soils in the island of Oahu, tested at different density levels and moisture conditions. Index properties of these soils are summarized in [65]. All these soils plot below the A-line and are classified as silts. M_r tests were performed in accordance with Long-Term Pavement Performance (LTPP) Protocol P46 [66]. Testing was performed at six target dry densities and molding water contents or physical states: 100% and 95% relative compaction (ASTM D 698 Procedure C) and at each relative compaction, samples were compacted at approximately three different water contents: $w_{opt} - 2\%$, w_{opt} and $w_{opt} + 2\%$, where w_{opt} = the optimum water content.

A total of 78 M_r tests were performed. Each soil was tested at three confining stresses (2, 4 and 6 psi) and five deviator stresses (2, 4, 6, 8 and 10 psi) giving more than 1,100 M_r values.

Using these data, the parameters of several models were estimated by Ooi et al. [55]. All the models in this reference had functional forms similar to that of equation (6-23). Unfortunately, equation (6-23) itself was not included among those estimated in that paper. Archilla et al. [67] used the same database together with LTPP resilient modulus data for fine-grained soils to estimate a model using two advanced statistical techniques known as joint estimation and mixed effects. Although the model form was a bit more involved, it can be used directly to estimate the parameters k_1, k_2, and k_3 of equation (6-23). In addition, since the model was estimated jointly with LTPP data (continental US data), bias parameters were also derived. These bias parameters allow the estimation of the differences in behavior of continental fine-grained soils vis-à-vis the tropical Hawaiian fine-grained soils. This may allow correcting the values reported in a database developed at the national level [68] for

local use when no other information is available. The data from the aforementioned database is available at: http://nchrp923b.lab.asu.edu/index.html. (last accessed: July 2013).

For the joint estimation with Hawaiian soils, sections with M_r information on fine-grained soils (more than 50% percent passing the #200 sieve) were extracted from the LTPP database. The M_r and soil information from 31 different sections (yielding 465 M_r observations) were extracted from the database.

Using the two databases, the following model was estimated[44]:

$$M_r = K_1\ 10^{\left[\left(a\left(1+\beta_{a\_LTPP}\ LTPP\right)\right)\left(1-\frac{1+\exp(\beta_L)}{1+\exp\left[\beta_L+k_s(S-S_{opt})+k_e(e-e_{opt})+k_{se}(S-S_{opt})(e-e_{opt})\right]}\right)\right]} p_a \times\left(\frac{\theta}{p_a}\right)^{K_2}\left(1+\frac{\tau_{oct}}{p_a}\right)^{K_3} \quad (6\text{-}25)$$

$$K_1 = 1{,}000\times\left(\beta_{k_1}+\beta_{k_1\_LTPP}\ LTPP+\left(\beta_{k_1\_w_{opt}}+\beta_{k_1\_LTPP\_w_{opt}}\ LTPP\right)w_{opt} + \left(\beta_{k_1\_P_{Silt}}+\beta_{k_1\_LTPP\_P_{Silt}}\ LTPP\right)P_{Silt}\right) \quad (6\text{-}26)$$

$$K_2 = \beta_{k_2}+\beta_{k_2\_LTPP}\ LTPP+\beta_{k_2\_w_{opt}}\ w_{opt} \quad (6\text{-}27)$$

$$K_3 = \beta_{k_3}+\beta_{k_3\_LTPP}\ LTPP+\left(\beta_{k_3\_e}+\beta_{k_3\_LTPP\_e}\ LTPP\right)(e-e_{opt}) + \left(\beta_{k_3\_w}+\beta_{k_3\_LTPP\_w}\ LTPP\right)(w-w_{opt}) \quad (6\text{-}28)$$

where LTPP is an indicator variable = 1 for LTPP observations and = 0 for observations for the Hawaiian soils, w_{opt} is the percent optimum water content of the soil, P_{Silt} is the percent silt, w is the as-compacted water content of the sample, e is the voids ratio of the sample, e_{opt} is the voids ratio corresponding to w_{opt}, S is the saturation of the sample, S_{opt} is the saturation corresponding to w_{opt} and the βs are model parameters. The parameter estimates of the model are given in Table 6-6.

Figure 6-38 shows the observed vs. predicted values for both data sources.

[44] Unfortunately, the 1,000 factor in the equation for K_1, which is essential to obtain reasonable answers, was missing in [67].

Essentially the same model was used for both databases with β_{a_LTPP}, $\beta_{k_1\_LTPP}$, $\beta_{k_1\_LTPP\_w_{opt}}$, $\beta_{k_1\_LTPP\_P_{Silt}}$, $\beta_{K_2\_LTPP}$, $\beta_{K_3\_LTPP}$, $\beta_{K_3\_LTPP\_e}$ and $\beta_{K_3\_LTPP\_w}$ representing bias parameters of the joint estimation to account for the different behavior between Hawaiian and mainland soils. These parameters were not arbitrarily added. Rather, they were included when they were statistically significant based on log-likelihood ratio tests.

Note that the MEPDG model only accounts for the effects of saturation levels (moisture content) but not for the effect of compaction (voids ratio). Instead, equation (6-25) also permits to account for compaction level and the interaction with saturation. Figure 6-39 shows the variation of the first term multiplying K_1 in equation (6-25), which has an important influence in the computed resilient modulus. It can be observed that high saturation and/or high void ratios lead to low M_r values. Conversely, at low saturation and low void ratios, the term is at its maximum and is insensitive to small changes in *e* and *S*. At conditions in between, M_r is very sensitive to changes in saturation and void ratio. These results appear reasonable for the ranges of *e* and *S* analyzed and are intuitively correct.

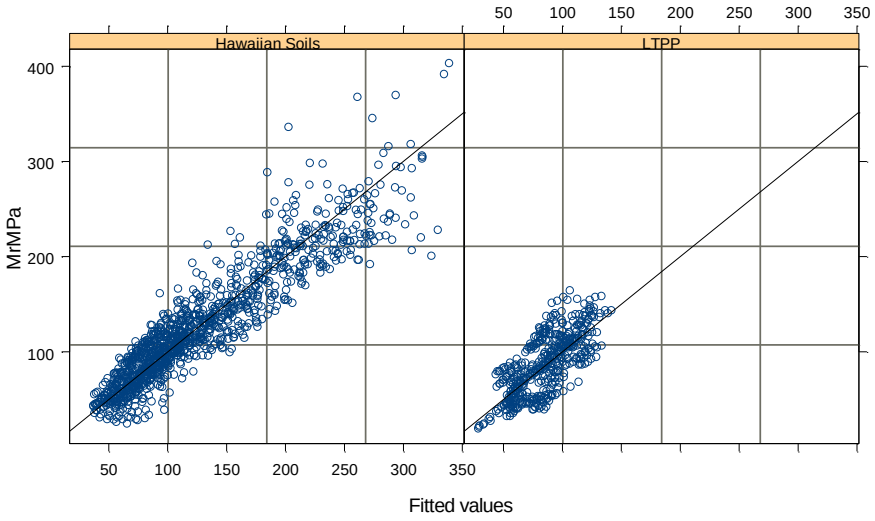

I

Figure 6-38. Observed vs. predicted M_r values with Archilla et al. model **[67]**.

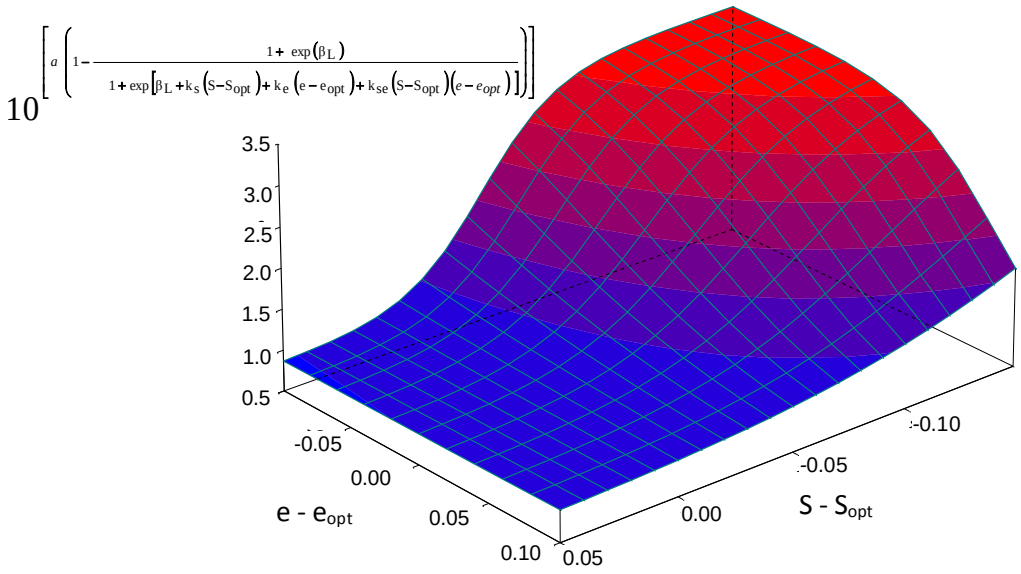

Figure 6-39. Estimated variation of multiplicative term in equation (6-25) with ($e-e_{opt}$) and ($S-S_{opt}$) for Hawaiian fine-grained soils.

Table 6-6. Parameter Estimates for equation (6-25) M_r model.

Parameter No.	Parameter	Parameter Estimate	Standard Error	t-value	p-value	Parameter Combination	
						Hawaiian	LTPP
1	a	-0.0687	0.0379	-1.81319	0.0700	a	$a(1+\beta_{a\_LTPP})$
	β_{a_LTPP}	0.0218	0.0263	0.82753	0.4081		
2	β_L	2.0256	0.4986	4.06286	<.0001	β_L	β_L
3	k_s	37.8543	16.6835	2.26895	0.0228	k_s	k_s
4	k_e	5.5869	4.4645	1.25140	0.2187	k_e	k_e
5	k_{se}	-203.6267	114.0792	-1.78496	0.0728	k_{se}	k_{se}
6	β_{k_1}	7.8761	1.2586	6.25774	<.0001	β_{k_1}	$\beta_{k_1}+\beta_{k_1\_LTPP}$
	$\beta_{k_1\_LTPP}$	-5.6831	1.2931	-4.40257	<.0001		
7	$\beta_{k_1\_w_{opt}}$	-0.0993	0.0191	-5.18755	<.0001	$\beta_{k_1\_w_{opt}}$	$\beta_{k_1\_w_{opt}}+\beta_{k_1\_LTPP\_w_{opt}}$
	$\beta_{k_1\_LTPP\_w_{opt}}$	0.0575	0.0213	2.70175	0.0071		
8	$\beta_{k_1\_P_{Silt}}$	-0.0741	0.0153	-4.85167	<.0001	$\beta_{k_1\_P_{Silt}}$	$\beta_{k_1\_P_{Silt}}+\beta_{k_1\_LTPP\_P_{Silt}}$
	$\beta_{k_1\_LTPP\_P_{Silt}}$	0.0623	0.0163	3.82767	0.0001		
9	β_{K_2}	0.8573	0.0884	9.70100	<.0001	β_{K_2}	$\beta_{K_2}+\beta_{K_2\_LTPP}$
	$\beta_{K_2\_LTPP}$	-0.3577	0.0571	-6.25244	<.0001		
10	$\beta_{K_2\_w_{opt}}$	-0.0158	0.0025	-6.42980	<.0001	$\beta_{K_2\_w_{opt}}$	$\beta_{K_2\_w_{opt}}$
11	β_{K_3}	-2.9856	0.0937	-31.86498	<.0001	β_{K_3}	$\beta_{K_3}+\beta_{K_3\_LTPP}$
	$\beta_{K_3\_LTPP}$	2.1325	0.1715	12.43443	<.0001		
12	$\beta_{K_3\_e}$	-3.7825	1.1623	-3.25429	0.0012	$\beta_{K_3\_e}$	$\beta_{K_3\_e}+\beta_{K_3\_LTPP\_e}$
	$\beta_{K_3\_LTPP\_e}$	-3.2473	1.9301	-1.68251	0.0927		
13	$\beta_{K_3\_w}$	-0.5488	0.0426	-12.8794	<.0001	$\beta_{K_3\_w}$	$\beta_{K_3\_w}+\beta_{K_3\_LTPP\_w}$
	$\beta_{K_3\_LTPP\_w}$	0.5304	0.0997	5.3192	<.0001		

In general, the parameters of the model have intuitively correct signs. For example, a higher w_{opt} in a fine-grained soil is typically associated with a more plastic soil. The higher the plasticity, the lower will be the value of M_r, and the lesser will be the effect of confinement. The negative signs for $\beta_{k_1\_w_{opt}}$ and $\beta_{K_2\_w_{opt}}$ produce exactly these effects since K_1 and K_2 are positive.

The negative sign of $\beta_{k_1\_LTPP}$ indicates that the LTPP soils generally have lower M_r than Hawaiian soils, which agrees with the observations of Mitchell and Sitar [64] as previously discussed. Since $\beta_{k_1\_w_{opt}}$ is negative, the positive sign of $\beta_{k_1\_LTPP\_w_{opt}}$ makes the sum $\beta_{k_1\_w_{opt}} + \beta_{k_1\_LTPP\_w_{opt}}$ closer to 0, implying that the LTPP soils are less affected by changes in w_{opt}.

$\beta_{K_2\_LTPP}$ has a negative sign, indicating that M_r of LTPP soils are less affected by confinement than Hawaiian soils. This trend is expected in more clayey and more plastic soils. Since most of the LTPP soils are classified as clays compared to all silts with the Hawaiian soils, this parameter has a reasonable sign.

The negative signs of $\beta_{K_3\_e}$ and $\beta_{K_3\_w}$ also lend themselves to intuitive interpretations. Since K_3 is typically negative for fine-grained soils, the model predicts that larger void ratios and water contents lead to a more negative K_3. The more negative K_3 becomes, the faster M_r decreases with τ_{oct} indicating that shearing has a larger effect on poorly compacted and wetter soils than in well compacted and drier soils. $\beta_{K_3\_LTPP\_e}$ is also negative making $\beta_{K_3\_e} + \beta_{K_3\_LTPP\_e}$ even more negative, indicating that void ratio has a greater effect on M_r for LTPP soils than Hawaiian soils. On the other hand, $\beta_{K_3\_LTPP\_w}$ is positive making $\beta_{K_3\_w} + \beta_{K_3\_LTPP\_w}$ closer to zero, suggesting that M_r of LTPP soils is less sensitive to deviations in water content compared to Hawaiian soils. This is consistent with the fact that M_r of coarser soils (silts) are more affected by deviator stress than finer (clayey) soils.

The parameters $\beta_{k_1\_PSilt}$ (Hawaiian soils) and $\beta_{k_1\_PSilt} + \beta_{k_1\_LTPP\_PSilt}$ (LTPP soils) were both negative, implying a decrease in M_r with a higher proportion of silt-size particles. Although this result seems at first surprising, the parameters are highly statistically significant (Table 6-6). Yau and Von Quintus [69] found similar results for fine-grained LTPP soils since their K_1 term included percent clay as a covariate and their estimate of this parameter was positive in their models. For a given % fines, a decreasing percent clay implies

an increasing P_{Silt}, which explains the consistency with the Yau and Von Quintus study but not the rationale. In reality, when P_{Silt} increases, the soil plasticity decreases and therefore, w_{opt} also decreases. The net effect is typically an increase in M_r. However, the parameter for P_{Silt} governs the change caused by changing the percent silt *maintaining all else constant* (including w_{opt}), which as mentioned before is practically impossible. It may well be the case that if such a change in P_{Silt} with *all else constant* were possible the net effect would be a reduction in M_r.

6.3.1.2.3.2 Potential application of the model in practice

In practice, Equation (6-25) could be easily utilized in a spreadsheet program. One just needs to specify the values of the 13 model parameters associated with one of the two databases and the seven soil parameters (e_{opt}, w_{opt}, S_{opt}, e, w, S and P_{silt}). To obtain the soil parameters, results from three common geotechnical tests are required: (1) Proctor test ($e_{opt} = G_s\gamma_w/\gamma_{dmax} - 1$, w_{opt}); (2) specific gravity (to obtain e_{opt} and $S_{opt} = G_s w_{opt}/e_{opt}$); and (3) grain size analyses (P_{silt}). The design void ratio, e, is related to the relative compaction (RC) as provided in the specifications ($e = G_s\gamma_w/[RC*\gamma_{dmax}] - 1$). The design water content, w, is specified by the designer in relation to the compaction curve and climatic factors. The degree of saturation is $S = G_s w/e$.

The calculations can then be performed for any state stresses as discussed in the following example. Perhaps the most challenging aspect of the calculation is the estimation of the state of stresses, and more importantly, which among the many state of stresses that could be selected is the most representative. An explanation of this issue is presented after the examples.

Example 1

As an example, consider a Hawaiian soil with w_{opt} = 27.4%, w = 29.0%, P_{Silt} = 45.0%, e_{opt} = 0.93, e = 0.93, S_{opt} = 0.85, S = 0.90, and G_s = 2.90. Also, recall that in US units, p_a = 14.7 psi. For a Hawaiian soil the LTPP variable is zero. Therefore, the parameters with LTPP in their subscripts disappear from equations (6-25) through (6-28). Therefore, with the parameters provided in Table 6-6, K_1, K_2, and K_3 are:

$$K_1 = 1{,}000 \times (7.8761 - 0.0993 \times 27.4 - 0.0741 \times 45.0) = 1{,}821$$

$$K_2 = 0.8573 - 0.0158 \times 27.4 = 0.424$$

$$K_3 = -2.9856 - 3.7825 \times (0.93 - 0.93) - 0.5488 \times (29.0 - 27.4) = -3.864$$

The factor multiplying K_1 is:

$$10^{\left[(-0.0687)\left(1 - \frac{1+\exp(2.0256)}{1+\exp[2.0256+37.854(0.90-0.85)+k_e(0.93-0.93)-203.627(0.90-0.85)(0.93-0.93)]}\right)\right]} = 10^{(-0.0687)(0.8523)} = 0.874$$

With the above values in hand, it is now easy to compute the resilient modulus for any state of stress. Consider for example a case where σ_3 = 2 psi and σ_d = 8 psi, which implies that σ_1 = 10 psi, θ = (2 + 2 + 10) psi = 14 psi, and $\tau_{oct} = \frac{1}{3}\sqrt{(2-2)^2 + (10-2)^2 + (2-10)^2} = 3.77$ psi. Then, from equation (6-25), the resilient modulus for this state of stress is:

$$M_r = 1{,}821 \times 0.874 \times 14.7\ psi \times \left(\frac{14.0}{14.7}\right)^{0.424}\left(1 + \frac{3.77}{14.7}\right)^{-3.864} \approx 9{,}500 \text{ psi}$$

Example 2

Consider the same information as in example 1, but now estimate the resilient modulus for a mainland soil. As before, w_{opt} = 27.4%, w = 29.0%, P_{Silt} = 45.0%, e_{opt} = 0.93, e = 0.93, S_{opt} = 0.85, S = 0.90, and G_s = 2.90. Now the LTPP variable is one. Therefore, with the parameters provided in Table 6-6, K_1, K_2, and K_3 are:

$$K_1 = 1{,}000 \times [(7.8761 - 5.6831) + (-0.0993 + 0.0575) \times 27.4 + (-0.0741 + 0.0623) \times 45.0] = 517$$

$$K_2 = (0.8573 - 0.3577) - 0.0158 \times 27.4 = 0.067$$

$$K_3 = (-2.9856 + 2.1325) + (-3.7825 - 3.2473) \times (0.93 - 0.93) + (-0.5488 + 0.5304) \times (29.0 - 27.4) = -0.883$$

Notice that based on these results, a soil on the US continent is generally less stiff (lower K_1 value) and is less sensitive to changes in θ and τ_{oct} than a Hawaiian soil of similar characteristics. The factor multiplying K_1 is now:

$$10^{\left[(-0.0687+0.0218)\left(1 - \frac{1+\exp(2.0256)}{1+\exp[2.0256+37.854(0.90-0.85)+k_e(0.93-0.93)-203.627(0.90-0.85)(0.93-0.93)]}\right)\right]} = 10^{(-0.0469)(0.8523)} = 0.912$$

Again, for σ_3 = 2 psi and σ_d = 8 psi (σ_1 = 10 psi, θ = 14 psi, and τ_{oct} = 3.77 psi), equation (6-25) now yields:

$$M_r = 517 \times 0.912 \times 14.7\ psi \times \left(\frac{14.0}{14.7}\right)^{0.067} \left(1 + \frac{3.77}{14.7}\right)^{-0.883} \approx 5{,}650 \text{ psi}$$

Comparing the result in example 2 with that in example 1, it can be seen that for the particular soil characteristics considered, the estimated resilient modulus for the Hawaiian soil is (9,500-5,650)/5,650 × 100 = 68% higher than the M_r for the soil with the same characteristics in the continental US. In fact, considering all the state of stresses at which the Hawaiian soils were tested, this difference ranges from about 50% to 210% higher!

This provides a good illustration of the dangers of using models and correlations developed in other places without much scrutiny. When there are no other options, analysts will often have to resort to such correlations. However, for cases like this one, where a local model has been estimated, preference should be given to the use of the local model provided that data to use it are available.

Although correlations between M_r and other soils characteristics (CBR, R-Value, DCP penetration, etc.) may provide in some situations acceptable inputs, these correlations are typically valid under specific conditions that are not always well specified (moisture content, compaction level, exudation pressure, etc.). To date, it is not known to what extent the commonly used correlation equations are applicable for Hawaiian conditions. It is important to note however that two relationships between CBR and M_r and between R-Value and M_r have been implicitly used in the HDOT procedure for years. Equation 1.1a in the current HDOT manual [13] is nothing more than the combination of the two well know equations $M_r(psi) = 1{,}500$ CBR and $M_r(psi) = 555$ R-Value + 1,155. For the reasons discussed below, unless there is no other choice the use of such relationships is discouraged.

6.3.1.2.3.3 Practical considerations

For input level 3, the analyst still needs to estimate the resilient modulus M_r. Although such estimate of M_r could be obtained from the website http://nchrp923b.lab.asu.edu/ developed under NCHRP project 9-23B [68]; for the same reasons discussed before, this may result in a gross underestimation of M_r.

Table 6-7 is an example of the type of information that can be obtained from the website. To simplify the exposition, the rows for some additional layers were deleted from the table. Clearly, when information for more than one layer is available, some judgment will be needed to select which one would be more representative of the likely subgrade.

Table 6-7. Type of information that can be obtained from the NCHRP 9-23b webpage.

Map Character	Map Unit Key	Map Unit Name	Component Name
3B7	677310	Pulehu-Mokuleia-Kawaihapai-Haleiwa (s9464)	Kawaihapai

AASHTO Classification	AASHTO Group Index	Top Depth (in)	Bottom Depth (in)	Thickness (in)	% Component	Water Table Depth Annual Min (ft)	Depth to Bedrock (ft)
A-6	14	0	22	22	29	N/A	N/A

CBR from Index Properties	Resilient Modulus from Index Properties (psi)	Passing #4 (%)	Passing #10 (%)	Passing #40 (%)	Passing #200 (%)	Passing 0.002 mm (%)	Liquid Limit (%)
6.3	8291	95	95	95	75	40	40

Plasticity Index (%)	Saturated Volumetric Water Content (%)	Saturated Hydraulic Conductivity (ft/hr)	Parameter af (psi)	Parameter bf	Parameter cf	Parameter hr (psi)
20	48	0.10836	2.5641	0.918	0.3949	3000.05

Suppose that the information is as given in Table 6-7. Note that the table already contains an estimate of the resilient modulus and CBR. Unfortunately, the resilient modulus estimate is based on data from the continental US, which as seen earlier results in estimates that are biased downward for Hawaiian fined-grained soils. Parenthetically, notice that the estimate is provided irrespective of the actual pavement structure or traffic load. Clearly, both the pavement structure and magnitude of the load influence the state of stresses and thus the resilient modulus. However, incorporating the effect of the load magnitude is considered impractical since a single representative M_r value for the whole load spectrum has to be selected anyway in the current MEPDG implementation. As a simplification, one could obtain an estimate of the state of stresses at the subgrade level for a standard axle load (i.e., a single load of 9,000 lb on one side of the axle) using one of the several linear layer elastic analysis programs available and perform the same type of analysis of the previous two examples. A difficulty with this approach is that Table 6-7 does not contain all the information needed to perform the analysis.

One alternative is to complement the information in Table 6-7 with additional information from the National Cooperative Soil Survey, National Cooperative Soil Characterization Database, available online at http://ncsslabdatamart.sc.egov.usda.gov. This is an excellent resource but this would add to the workload.

A perhaps more practical alternative is to enter the information in Table 6-7 into the MEPDG which, based on regression models, can estimate some of the missing information (other than entering the data into the MEPDG, no real additional work is needed). Then, an analysis similar to that presented in the previous two examples could be carried out.

Still, given all the simplifications, it is not worth to devote this much effort into the determination of M_r. Instead, a reasonable value is needed. At this time, for those projects on which no other information can be obtained (either through sampling or FWD) *it is recommended as a practical alternative to use the NCHRP 9-23B website to obtain a first estimate of the resilient modulus and increase it by 100% (i.e., multiply by 2).* As shown in example 2 above, a 100% increase is a reasonably good compromise value.

6.3.1.2.3.4 Resilient Modulus of Bases/Subbases

This section presents the results of resilient modulus tests performed on coarse-grained materials at UH.

Testing has been performed on a limited number of samples of different materials. No particular plan was followed to sample the materials. Instead, they were obtained as samples of convenience. For example, samples from a full depth reclamation project were requested when the PI had the opportunity to visit one such project in the island of Kauai. Also, significant testing was performed on foamed asphalt base material to evaluate its potential for local use. Although eventually the equipment used to prepare this material was shipped out of the state, significant understanding of the material has been gained should interest to use it arises in the future. More importantly, testing was performed simultaneously on an unbound subbase material from the Hawaiian Cement Halawa quarry for comparison. Finally, some testing was also performed on 3-Fine aggregates from the Makakilo quarry, which are typically used as one of the components in HMA. Interest in the resilient modulus of 3-Fine materials arose because this aggregate meets the widely used Wisconsin OGBC gradation (see Table A-2 in Appendix A) and may provide an alternative for permeable base material. Unless stated otherwise, the test were performed for 100% relative compaction (AASHTO T-180) and optimum moisture content.

The discussion about the stress dependency of the resilient modulus for fine-grained soils is also applicable to coarse-grained materials. In fact, since these are typically subjected to higher state of stresses, the stress dependency has a larger effect. Thus, this issue will be revisited later in the chapter.

6.3.1.2.3.5 Test results for a few base/subbase materials

As for fine-grained soils, the test results consist of a series of resilient modulus values for different state of stresses.

Table 6-8 presents the result for the 3-Fine Aggregates from the Makakilo quarry following the AASHTO T-307 loading sequence. These results correspond to the specimen shown in Figure 6-37. The specimen was prepared with material with a gradation with 99.9% passing the 3/4" (19 mm) sieve, 66.4% passing the 1/2" (12.5 mm) sieve, 27.7% passing the 3/8" (9.5 mm) sieve, and only 1.7% passing the No. 4 sieve (4.75 mm). The material is so open graded and permeable that compaction moisture content has a negligible effect on the resulting density for a given compaction level.[45]

It is well known that for some coarse grained materials, the following simplified constitutive equation provides a good fit:

$$M_r = k_1\, p_a \left(\frac{\theta}{p_a} \right)^{k_2} \tag{6-29}$$

As shown in Figure 6-40, the 3-Fine material is a good example where this equation provides an excellent fit with estimated parameters k_1 = 1,230 and k_2 = 0.495.

The simplification of equation (6-29) does not always provide the desired results. Consider the data presented in Table 6-9 for a specimen from a coral base material used sometimes as base. Fitting equation (6-29) to these data produces a moderate fit with k_1 = 1,998, k_2 = 0.426, and an R^2 of only 0.845. When the full model is used, repeated for convenience below as equation (6-30), a much better fit is obtained with an R^2 of 0.967.

$$M_r = k_1\, p_a \left(\frac{\theta}{p_a} \right)^{k_2} \left(1 + \frac{\tau_{oct}}{p_a} \right)^{k_3} \tag{6-30}$$

[45] Note that the table includes values for the contact stress and the cyclic stress. Their sum is the deviator stress, which is used for computing the θ and τ_{oct}. However, the resilient strain measured during the test is due only to the cyclic stress. Therefore, the resilient modulus must be computed as $Mr = \sigma_{cyclic}/\varepsilon_r$.

Table 6-8. Test results for the 3-Fine Aggregates.

Confining Stress (psi)	Contact Stress (psi)	Cyclic Stress (psi)	Bulk Stress (psi)	Octahedral Stress (psi)	Resilient Modulus (psi)
3.0	0.4	2.7	12.1	1.4	17,143
3.0	0.7	5.4	15.1	2.9	17,748
3.0	1.0	8.1	18.1	4.3	19,679
5.0	0.6	4.5	20.1	2.4	21,203
5.0	1.1	9.0	25.1	4.8	23,543
5.0	1.6	13.5	30.1	7.1	25,289
10.0	1.3	9.0	40.2	4.8	30,196
10.0	2.3	18.0	50.2	9.5	33,706
10.0	3.3	26.9	60.1	14.2	35,154
15.0	1.4	9.0	55.3	4.9	34,358
15.0	1.9	13.5	60.3	7.2	37,237
15.0	3.4	26.9	75.3	14.3	40,942
20.0	2.0	13.5	75.4	7.3	40,148
20.0	2.5	18.0	80.4	9.7	42,925
20.0	4.5	35.9	100.4	19.1	46,790

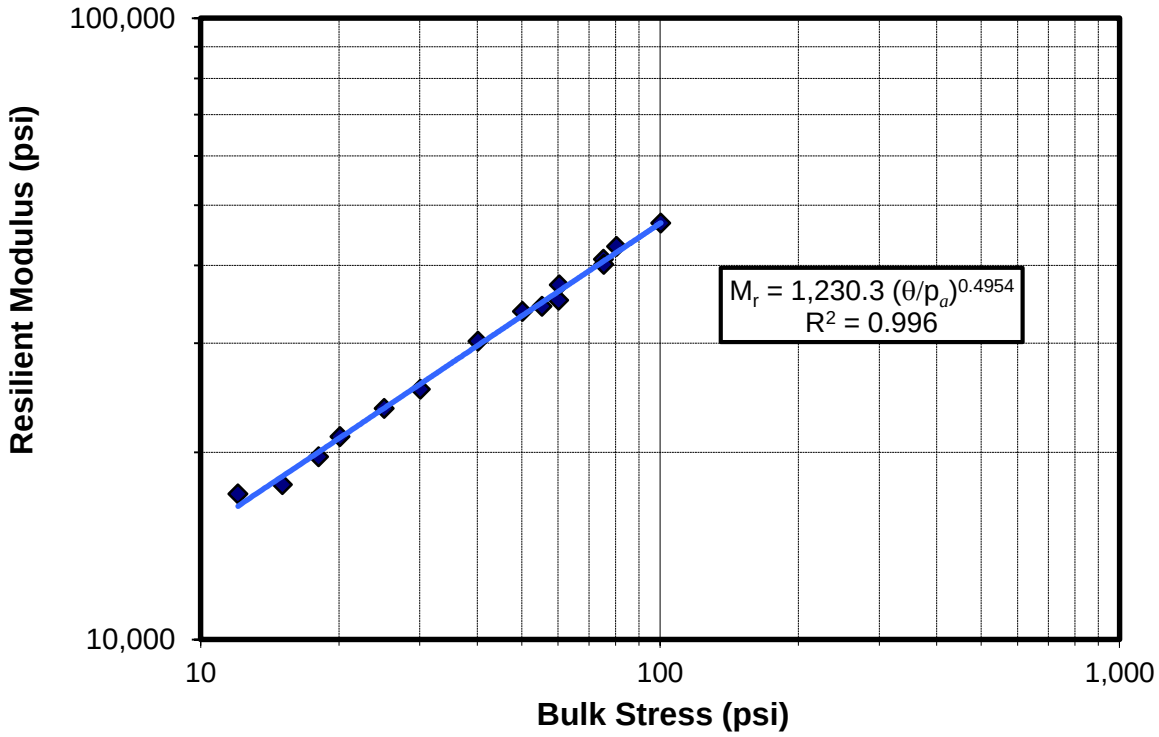

Figure 6-40. Resilient modulus vs. bulk stress (θ) for 3-Fine material.

The parameter estimates of equation (6-30) for the coral base material are k_1 = 1,760, k_2 = 0.181, and k_3 = 0.932. The t-statistics of the log(k_1), k_2, and k_3 are 215, 4.13, and 6.63 respectively[46], which indicate that they are all statistical significantly different from zero at a significance level less than 1% (all p-values are almost zero). This material provides an example in which restricting k_3 to be negative would have clearly produced an inferior fit. The comparison of observed vs. fitted values for both models in Figure 6-41 provides a clearer picture of how much better the fit is with the 3-parameter model than with the 2-parameter model for the coral base material.

In general, it can be seen that for similar stress levels, the coral material is stiffer than the 3-Fine material.

The results for a specimen from a reclamation project, the Ala Kinoiki reclamation project in Kauai, also resulted in a positive k_3 and a slightly negative but statistically insignificant k_2. Specifically, the parameter estimates are: k_1 = 1,187.2, k_2 = -0.008, and k_3 = 1.557. The R^2 is 0.978. The corresponding t-statistics are 264, -0.23, and 13.3. Therefore, parameters k_1 and k_3 are statistically significantly different from zero but k_2 is not. Thus, re-estimation of the model with k_2 set equal to zero should produce a similar fit. The R^2 of the regression after re-estimation with k_2 = 0 is 0.978[47], which is essentially the same fit. From a statistical point of view, this fit is excellent. The estimates of the parameters changed slightly to k_1 = 1187.4 and k_3 = 1.535. Notice again the very high value of k_3, which is somewhat unusual and needs to be analyzed further.

Forcing k_3 to be non-positive and k_2 to be non-negative for the Ala Kinoidi sample resulted in a much lower fit with an R^2 of only 0.655. As mentioned before, other researchers have estimated positive values for k_3 and there does not appear to be a good justification of why it should always be negative but the high values of k_3 above were a bit concerning at first.

---

[46] Since logs are taken to perform the regression, the parameter estimated in the regression is not k_1 but the log(k_1) from which k_1 can be computed easily. This is the reason why the t-statistic correspond to log(k_1).

[47] A difference in R^2 was noticed only in the fourth decimal.

Table 6-9. Test results for the Coral Base at optimum water content.

Confining Stress (psi)	Contact Stress (psi)	Cyclic Stress (psi)	Bulk Stress (psi)	Octahedral Stress (psi)	Resilient Modulus (psi)
3.0	0.4	2.7	12.1	1.4	31,541
3.0	0.7	5.4	15.1	2.9	29,963
3.0	1.0	8.1	18.1	4.3	31,937
5.0	0.6	4.5	20.1	2.4	31,805
5.0	1.1	9.0	25.1	4.8	35,661
5.0	1.6	13.5	30.1	7.1	40,618
10.0	1.3	9.0	40.2	4.8	38,812
10.0	2.3	18.0	50.2	9.6	52,444
10.0	3.3	27.0	60.2	14.3	60,430
15.0	1.4	9.0	55.4	4.9	40,691
15.0	1.9	13.5	60.4	7.3	48,401
15.0	3.4	26.9	75.3	14.3	68,135
20.0	2.0	13.5	75.5	7.3	51,967
20.0	2.5	18.0	80.5	9.7	61,172
20.0	4.7	36.0	100.6	19.2	81,279

6.3.1.2.3.1 Additional Tests of Base Materials

This subsection focuses on additional resilient modulus laboratory tests performed on base materials by Rayapeddi Kumar [47] as part of this project and Song [61] as part of a project on recycled materials. First, the results by Rayapeddi Kumar are explained in some detail followed by a summary of Song's results.

The laboratory tests performed on base course materials by Rayapeddi Kumar [47] include: (a) Gradation analysis, (b) Modified Proctor test, and (c) Resilient Modulus test.

Material Source

A small experimental plan for base course materials included 2 different types of aggregates namely, (a) virgin and (b) recycled. Virgin aggregates (Type B) were collected from the Hawaiian Cement – Halawa Quarry in Aiea, Honolulu, Hawaii. A limited amount of recycled material (foamed asphalt mixture) (~300 lbs) was delivered to the University of Hawaii at Manoa pavement engineering laboratory by Alakona Corporation, Honolulu, Hawaii.

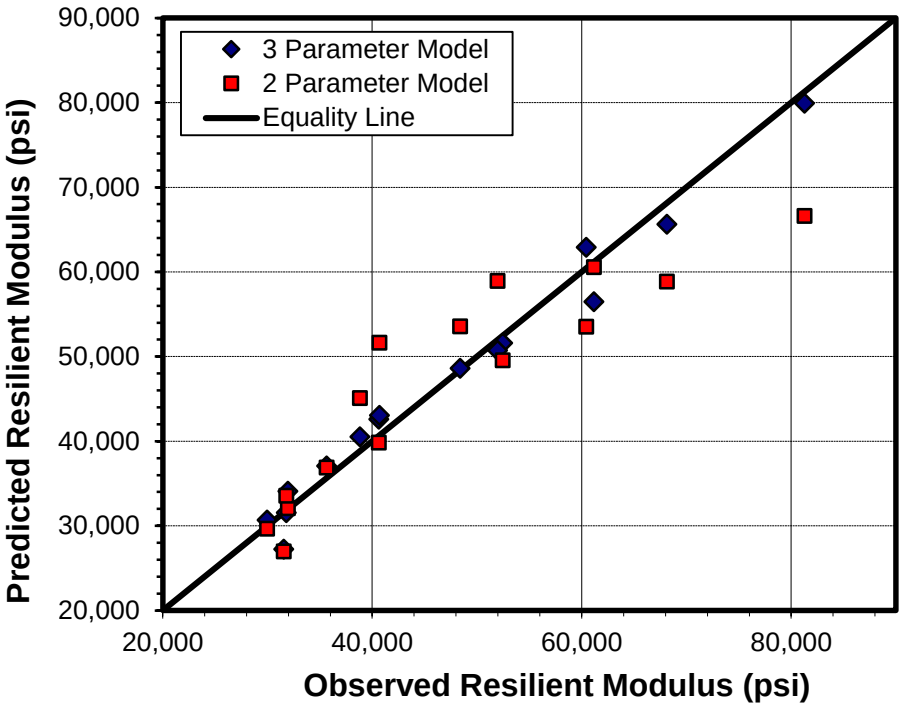

Figure 6-41. Comparison of Observed vs. Predicted Resilient Moduli for the 3- and 2-parameter models with the Coral Base.

The foamed asphalt (FA) base mixture used in this study was produced using 100% RAP, stabilized using 2% of foamed (expanded) asphalt, and 1% of Portland cement as filler.

Base Course Material Information

In this section, the details of two tests performed on base course materials are provided. First, the gradation analysis of aggregates is presented. Next, the Modified Proctor test performed to determine the optimum moisture content and maximum dry density is explained.

Gradation Analysis of Aggregates

The gradation analysis of RAP was performed using the AASHTO T27 procedure. According to AASHTO T27, the aggregate sample used for sieve analysis is dried at 110 °C. However, the RAP sample used for gradation analysis in this study was oven dried at only 60 °C for 48 hours prior to sieving. The reason for using a lower temperature to dry the RAP material is because it contains asphalt binder, which could soften and help create lumps. The presence of lumps could result in misrepresentation of actual gradation if the lumps are not broken during sieving. For virgin aggregates, the gradation analysis provided by Hawaiian

Cement Halawa – Quarry was used. The gradation analysis results for RAP along with the minimum and maximum requirements for 3/4" maximum nominal aggregate size allowed by the HDOT for untreated base course materials is presented in Figure 6-42.

The gradation provided by Hawaiian Cement – Halawa (HCH) quarry along with the minimum and maximum requirements for 1-1/2" maximum nominal aggregate size allowed by the HDOT for untreated base course materials is presented in Figure 6-43. This figure also includes the results of a gradation analysis performed using the AASHTO T11 procedure (wet sieve analysis) to determine the actual percentage of virgin material passing the #200 sieve. Based on the dry sieve analysis results, both virgin material and RAP gradation fall within the HDOT requirements for untreated base course material. However, for the virgin material, the wet sieve analysis results indicate that the material is out of specifications.

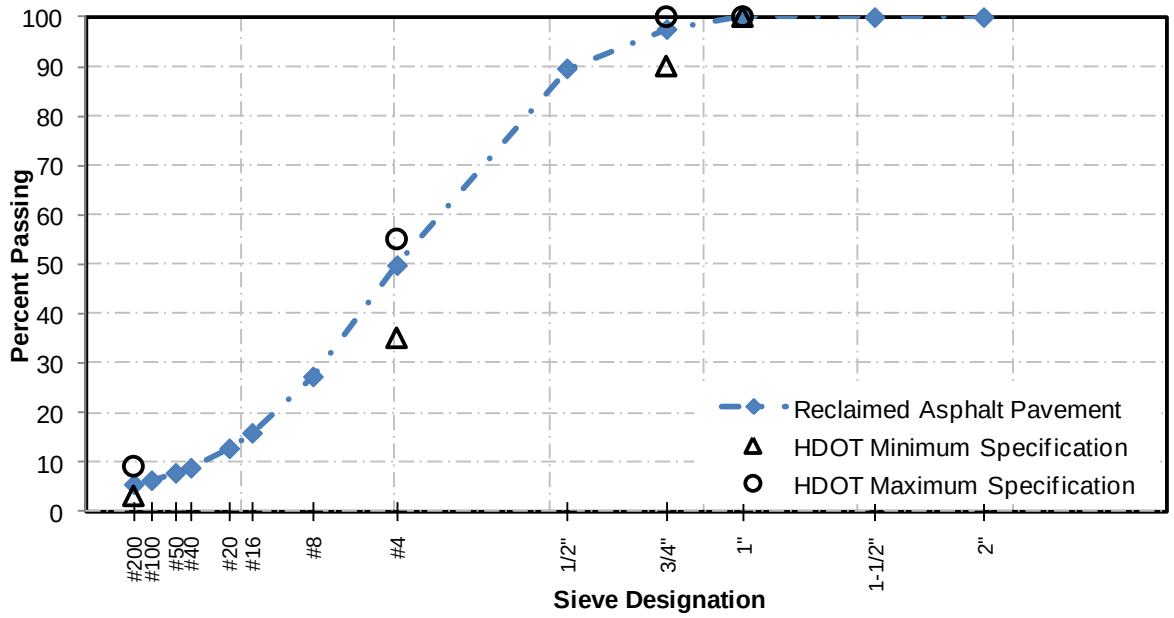

Figure 6-42. Gradation analysis of RAP compared with HDOT requirements for ¾" maximum nominal untreated base.

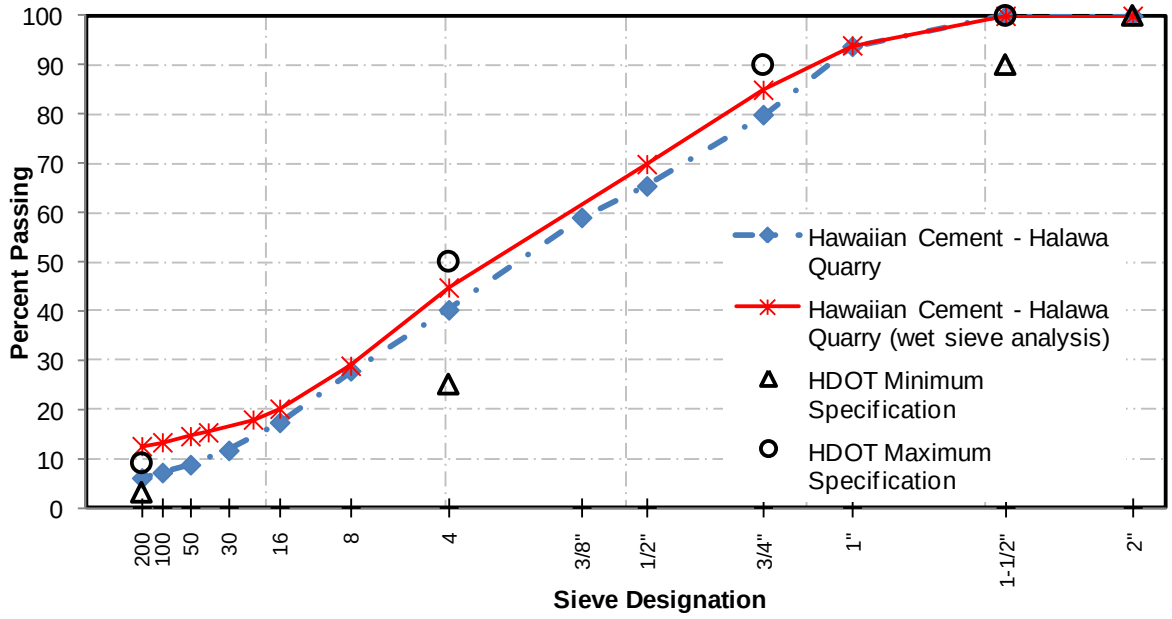

Figure 6-43. Gradation analysis of virgin aggregates from Hawaiian Cement – Halawa Quarry compared with HDOT requirements for 1-1/2" maximum nominal untreated base.

The RAP material used in this study is also compared with the gradation requirements recommended by Akeroyd and Hicks [70], which is widely considered by several researchers to provide the limits of desired gradation of RAP for producing foamed asphalt mixtures. Figure 6-44 illustrates the gradation analysis of RAP superimposed on the grading requirements recommended by Akeroyd and Hicks. As can be seen from the figure, the material falls within Zone A, which indicates the material is in the "ideal" grading limits for foamed asphalt stabilization.

Maximum Dry Density and Optimum Moisture Content

The maximum dry density (γ_{dmax}) and optimum moisture content (OMC) of both materials were determined using the standard AASHTO T180 – Method D procedure. The OMC and maximum dry density values are presented in Figure 6-45. Table 6-10 summarizes the test results.

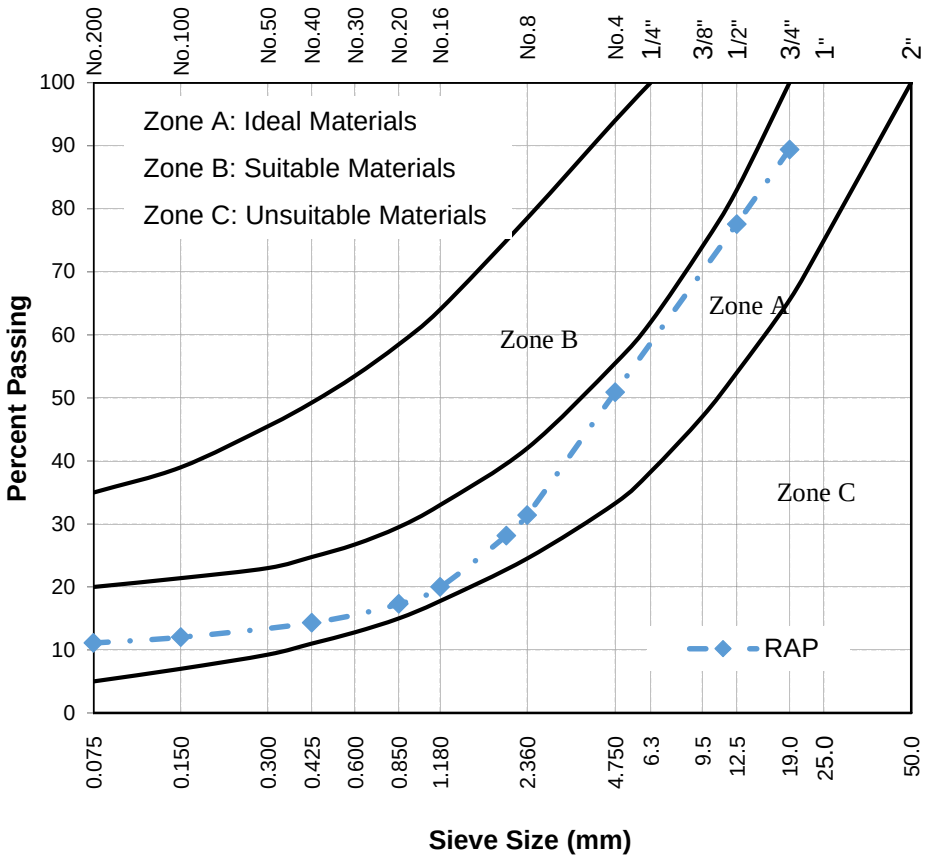

Figure 6-44. RAP Gradation and desired aggregate grading for FA (Redrawn after Akeroyd and Hicks, 1988)

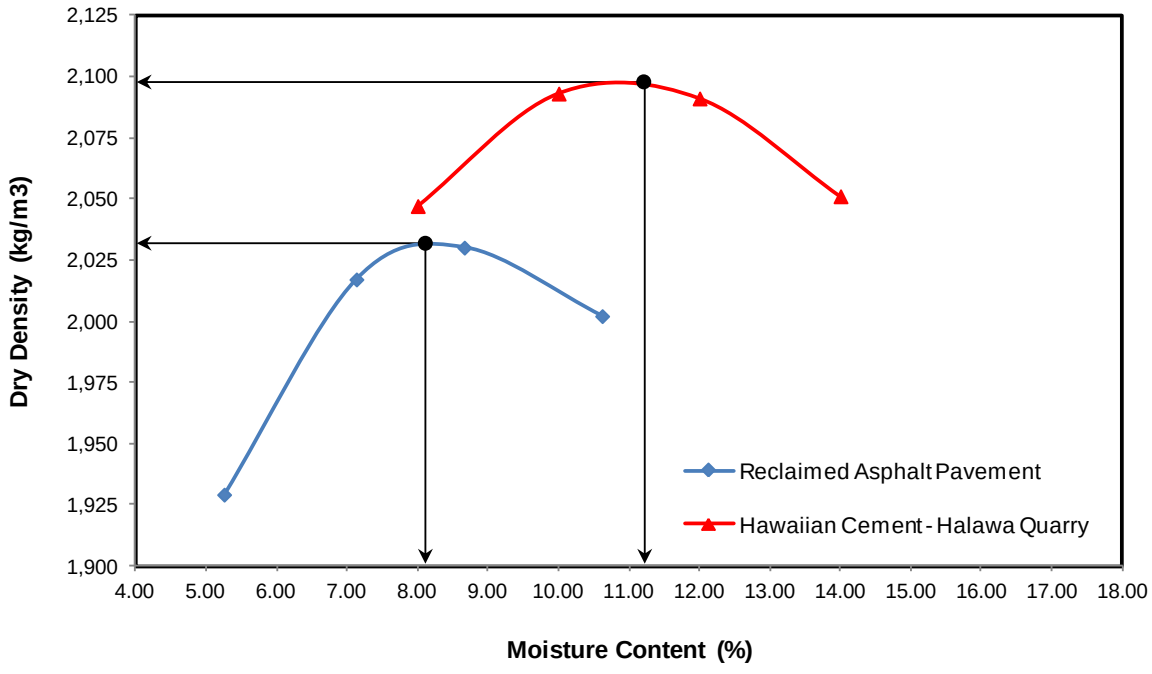

Figure 6-45. Moisture-density relationship of base course materials.

Table 6-10. Maximum Dry Density and Optimum Moisture Content values.

Material	Maximum Dry Density (kg/m^3)	Maximum Dry Density (lb/f^3)	Optimum Moisture Content (%)
Hawaiian Cement – Halawa	2098	131.0	11.2
Reclaimed Asphalt Pavement (RAP)	2032	126.9	8.1

Test Specimen Preparation for Resilient Modulus Testing

Resilient modulus testing included compaction and testing the materials at three different densities; 98%, 100%, and 102% of the maximum dry density. The specimens were tested using the repeated load triaxial resilient modulus in accordance with AASHTO T307; except that the number of load repetitions applied during each testing sequence was reduced. The nominal maximum size of the virgin aggregates and RAP, which is used to produce foamed asphalt mixtures, was found to be 50 mm and 19.0 mm respectively. Based on AASHTO T307, the dimensions of the cylindrical test specimen for testing the virgin material and FA base was required to be compacted using a vibratory hammer in a split mold with a target diameter of a 150 mm and a height between 305 mm and 318 mm.

Further, since there was no prior experience with the characterization of foamed asphalt mixtures, and because of limited availability of FA, it was decided to reduce the size of the test specimens so as to compact two replicates at three target densities. Accordingly, each specimen using FA base was compacted using a vibratory hammer in a split mold with a target diameter of 100 mm and a height of 203.2 mm. All the specimens compacted using FA mixtures were cured at 40 °C for 2 days. They were compacted in accordance with the AASHTO T307 procedure prior to testing.

Resilient Modulus Testing

The resilient modulus testing was performed using the IPC Global Universal Testing System (UTS) consisting of a hydraulic axial stress and a pneumatic confining stress loading system, and a computer-controlled data acquisition system (CDAS) connected to a personal computer. The machine is capable of applying repeated cycles of a haversine-shaped load pulse of 0.1 seconds with a 0.9 seconds rest period. The deformation produced in the sample

during testing is captured by two external sample Linear Variable Differential Transducers (LVDTs) and a system LVDT that is attached to the actuator that provides the system deformation. A test specimen placed inside the testing chamber along with sample LVDTs is shown in Figure 6-37.

The stress state testing sequence of the AASHTO T307 procedure was used. A total of 15 combinations (from Table 2 of AASHTO T307) of deviator and confining stresses were applied to the compacted sample. The two stages of the resilient modulus test are: (a) Conditioning and (b) Measuring stress and strains to calculate M_r.

Conditioning: AASHTO T307 requires between 500 and 1000 repetitions of the conditioning deviator stress. The reason for applying the conditioning sequence is to eliminate the effects of the initial loading versus reloading. Further, the conditioning also helps in reducing the effects of any imperfect contact between the top platen, base plate, and the test specimen.

Measuring stress and strains to calculate Mr: Following the conditioning cycles, the resilient modulus testing was performed by applying 50 cycles at each combination of confining stress and deviator stress. Repeated cycles of haversine-shaped load pulse of 0.1s with a rest period of 0.9s were applied for both conditioning and testing. M_r was calculated as the average of the ratios of the deviator stress to resilient strain for the last five cycles (46-50).

The repeated load triaxial resilient modulus tests were performed to evaluate the behavior of virgin aggregates and FA base mixtures when compacted at three different density levels. The effect of bulk stress at each combination of the loading sequence on the resilient modulus of virgin aggregates and FA base specimens compacted at three different densities was observed. For brevity, the results of one specimen from each of the three densities are presented in Figure 6-46 and Figure 6-47. The figures show resilient modulus of three specimens plotted against the bulk stress ($\theta = 3\sigma_3 + \sigma_d$) on a log-log graph, where σ_3 = the confining pressure and σ_d = the deviator stress. As can be seen from the figure, M_r increases with increase in density.

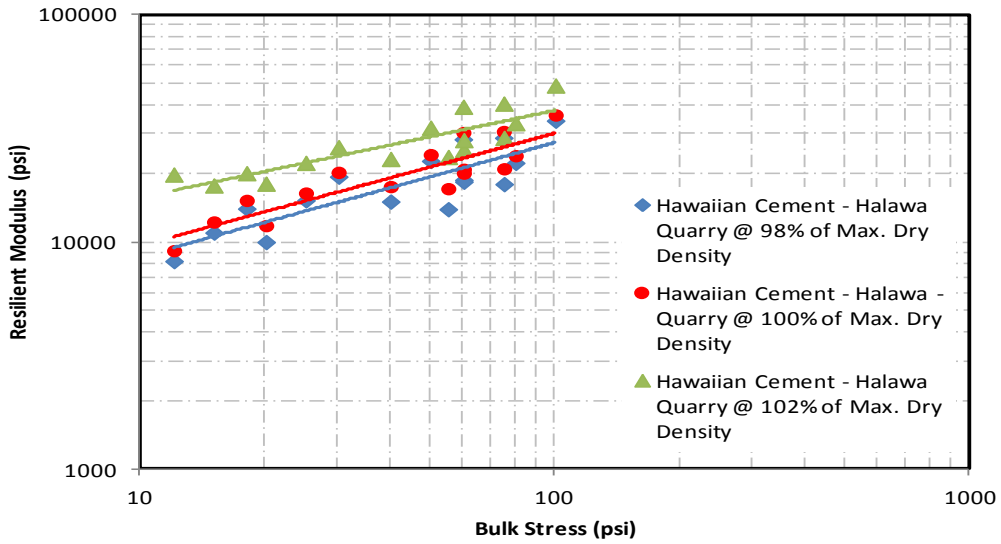

Figure 6-46. Effect of bulk stress on resilient modulus for virgin aggregates compacted at three different densities.

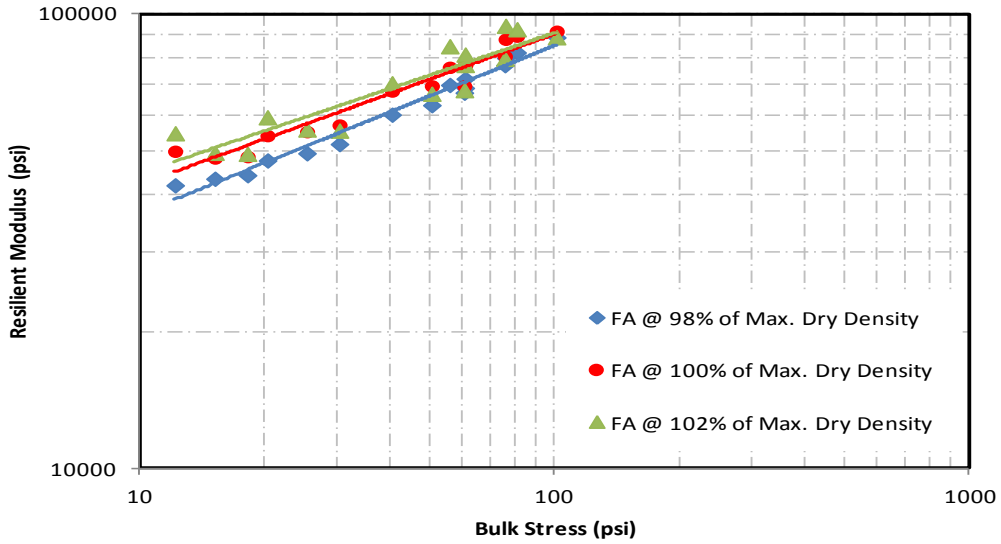

Figure 6-47. Effect of bulk stress on resilient modulus of FA base mixtures compacted at three different densities.

Figure 6-48 shows the effect that deviator stress has on the resilient modulus of specimens compacted at 98%, 100%, and 102% of the maximum dry density using virgin aggregates. The figure was constructed using the average values of M_r and deviator stress from two replicate specimens. For these specimens, regardless of the level of confinement, it

is clear that a higher compaction level translates into a higher resilient modulus for the same deviator stress level. The effect of deviator stress on M_r for each specimen of virgin aggregates is presented individually in Appendix A of [47], where the same trends observed in Figure 6-48 are present.

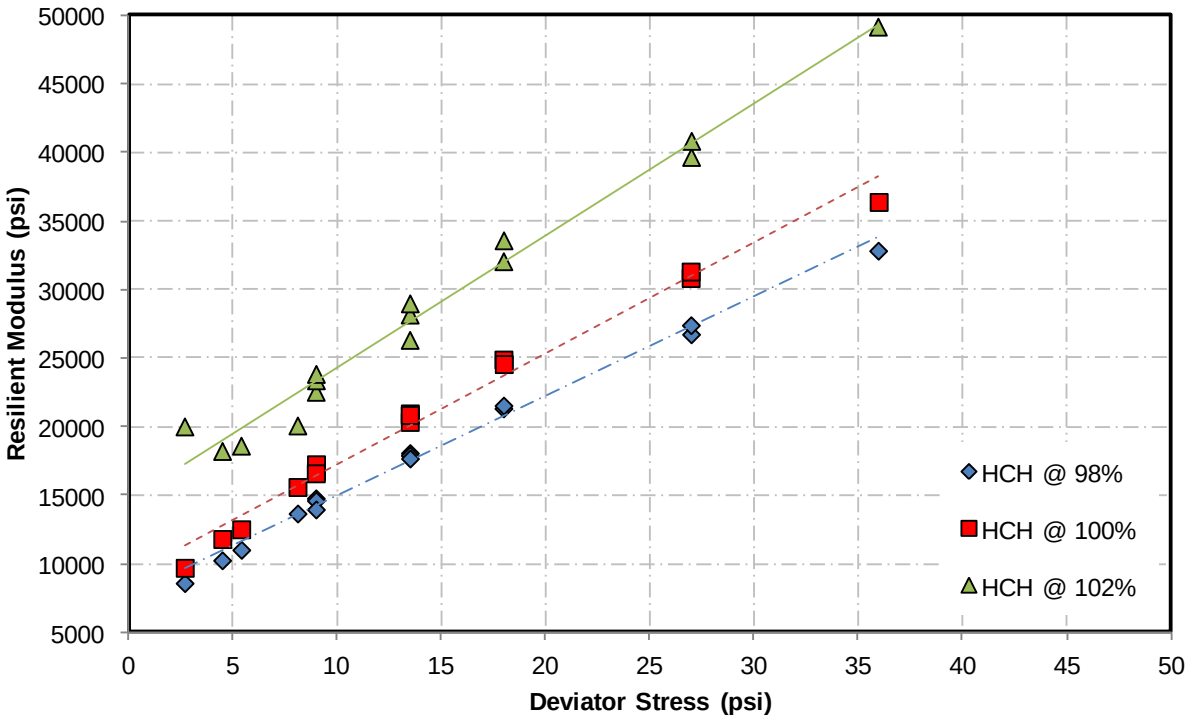

Figure 6-48. Mr vs. deviator stress for specimens compacted at different densities using virgin aggregates.

Figure 6-49 shows the same information as Figure 6-48 except that data for two of the confining stresses are not included. This figure is presented to illustrate why the estimation results for this material indicate that confining stress has little effect on the modulus of virgin aggregates. As can be observed in Figure 6-49, the points corresponding to a given density level follow a similar trend regardless of level of confinement. This is not obvious from Figure 6-48. As for the effect of shear, note that except at the low level of confining stress (3 psi) for specimens compacted at 102% of maximum dry density, where the modulus shows a "slight" softening behavior, the M_r values increase with deviator stress for specimens compacted at all densities.

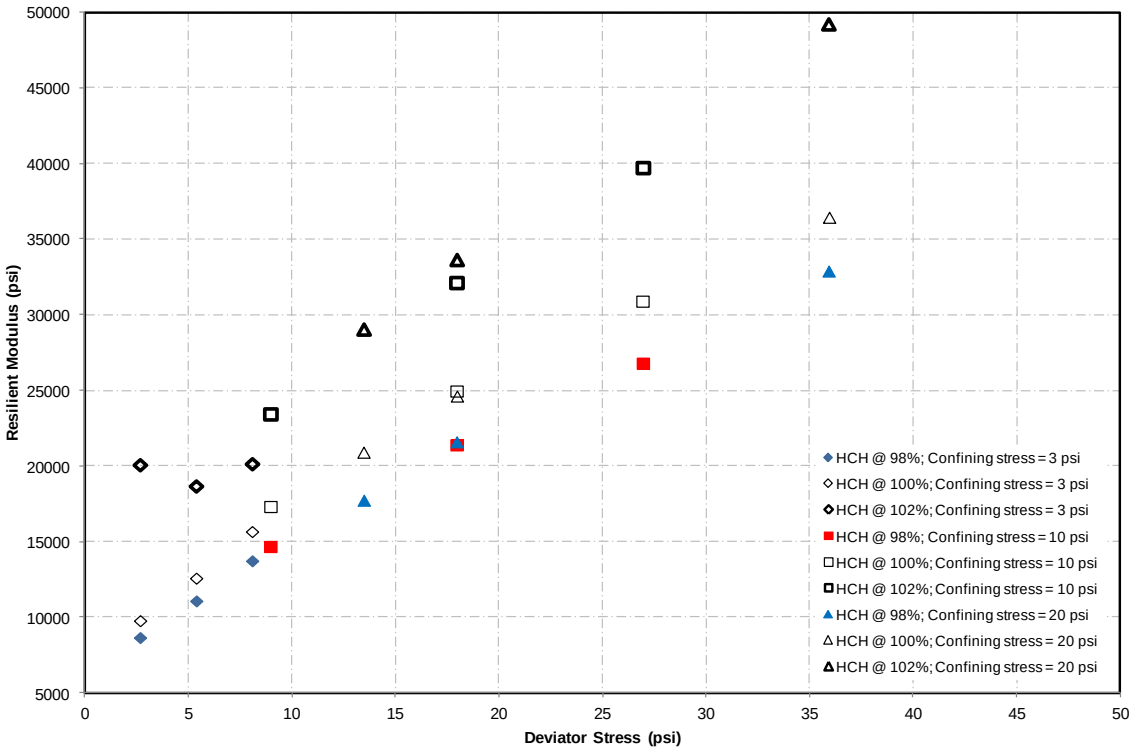

Figure 6-49. M_r vs. deviator stress for specimens compacted at different densities using virgin aggregates at low (3 psi), intermediate (5 psi), and high (20 psi) confining stress level.

Figure 6-50 shows the variation of resilient modulus with deviator stress at each confining stress level for foamed asphalt mixture specimens compacted at 98, 100, and 102% percent of maximum dry density. This figure is again constructed using the average values of M_r and deviator stress from two replicate specimens. For these specimens, an increase in the modulus is observed with increase in deviator stress at all confining stress levels for specimens compacted at 98% of maximum dry density. For the specimens compacted at 100% of maximum dry density, a slight increase in modulus with deviator stress is observed. Furthermore, for the specimens compacted at 102% of maximum dry density, it is observed that the resilient modulus decreases with increase in deviator stress at all confining levels.

For the specimens compacted at 102% of maximum dry density, at low and intermediate level of confining stress (σ_3 = 3, 5, and 10 psi), the modulus values show a "slight" softening behavior and subsequently increase marginally with increase in deviator stress. It is also observed from the figure that at the higher confining stresses (10, 15 and 20 psi) the trend lines with deviator stress tend to cross for the 100% and 102% compaction levels. The relative position of the crossing point also appears to depend on the confining stress.

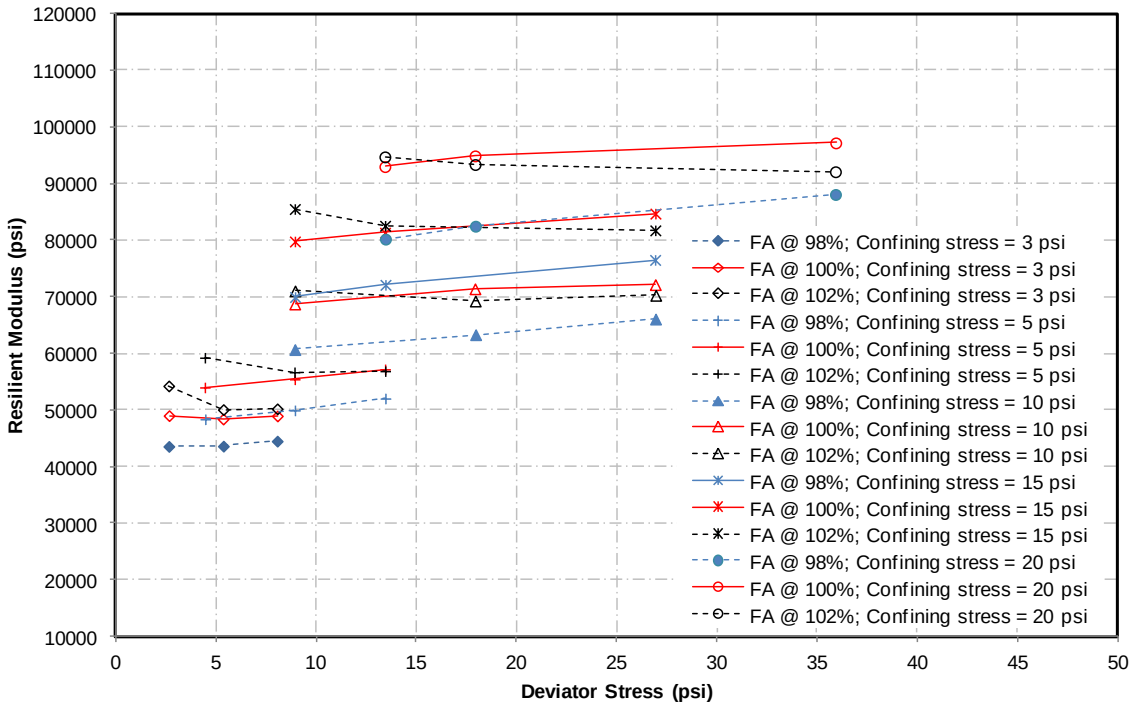

Figure 6-50. Mr vs. deviator stress for specimens compacted at different densities using FA mixtures.

To evaluate the effects of deviator stress and octahedral shear stress on M_r of virgin aggregates and FA based mixtures, the coefficients of the three-parameter model of equation (6-30) was estimated using linear regression with the data from each specimen. Table 6-11 presents the statistical estimation results.

From the summary of regression coefficients presented in Table 6-11, Rayapeddi Kumar [47] made several observations (for readability of this document, the last observation is slightly modified in the following list):

1. The resilient modulus of virgin aggregates and FA mixtures show an increasing trend with increase in bulk stress at increasing levels of compaction.

Table 6-11. NCHRP 1-37A M_r model parameter estimates in Rayapeddi Kumar's study **[47]**.

Specimen ID	k_1	p-value (k_1)	k_2	p-value (k_2)	k_3	p-value (k_3)	R^2
FA1 @ 98	2887.61	2.03E-27	0.39	2.04E-09	-0.09	3.42E-01	0.97
FA2 @ 98	3022.21	1.25E-26	0.39	1.31E-08	-0.18	1.14E-01	0.96
Average FA @ 98	**2954.91**		**0.39**		**-0.14**		
FA1 @100	3312.90	3.22E-26	0.47	3.67E-09	-0.29	2.79E-02	0.97
FA2 @ 100	3362.65	8.75E-27	0.39	1.01E-08	-0.26	3.14E-02	0.96
Average FA @ 100	**3337.77**		**0.43**		**-0.27**		
FA1 @ 102	3662.43	1.14E-24	0.44	2.20E-07	-0.57	2.94E-03	0.91
FA2 @ 102	3645.89	5.15E-26	0.43	1.96E-08	-0.43	4.08E-03	0.95
Average FA @ 102	**3654.16**		**0.44**		**-0.50**		
HCH1 @ 98	575.57	8.46E-22	0.09	1.34E-01	1.75	9.81E-07	0.95
HCH2 @ 98	595.97	2.54E-25	0.08	2.57E-02	1.54	2.91E-09	0.98
Average HCH @ 98	**585.77**		**0.09**		**1.65**		
HCH1 @ 100	667.78	4.90E-23	0.16	5.03E-03	1.42	1.10E-06	0.96
HCH2 @ 100	694.08	6.36E-23	0.09	1.05E-01	1.62	3.46E-07	0.96
Average HCH @ 100	**680.93**		**0.13**		**1.52**		
HCH1 @ 102	1051.43	1.70E-24	0.07	9.67E-02	1.34	2.53E-07	0.96
HCH2 @ 102	1091.80	6.28E-25	0.06	1.34E-01	1.33	1.18E-07	0.96
Average HCH @ 102	**1071.6**		**0.07**		**1.34**		

2. For virgin aggregates, a higher compaction level translates into a higher resilient modulus for the same deviator stress. However, for FA base mixture specimens, an increase in the modulus is observed with increase in deviator stress at all confining stress levels for specimens compacted at 98% of maximum dry density. For the specimens compacted at 100% of maximum dry density, a slight increase in modulus with deviator stress is observed. Furthermore, for the specimens compacted at 102% of maximum dry density, it is observed that the resilient modulus decreases with increase in deviator stress at all confining levels.
3. The parameter k_2 in the NCHRP 1-37A equation, which is the exponent for the bulk stress term, is positive. This indicates increase in bulk stress increases the stiffness of virgin aggregates and FA base mixtures.
4. The parameter k_3 in the NCHRP 1-37A equation, which is the exponent for the octahedral shear stress term, is negative for FA base mixtures, suggesting the stiffness of FA base mixtures decreases with increase in octahedral shear stress. This behavior is analogous to the observations made by Witczak and Uzan (1988) as explained earlier. Further, it can be seen from the *p*-values of parameter k_3 that the octahedral shear stress is not statistically significant for FA base specimens compacted at 98% of maximum dry density.
5. The sign of the parameter k_3 in the NCHRP 1-37A equation is positive for specimens compacted using virgin aggregates, which means an increase in octahedral shear stress increases the resilient modulus of the material.

The positive sign for k_3 is contrary to the widely held belief that, for unbound materials, the coefficient k_3 should be negative ([1], [56], [57], and [58]). Nevertheless, as indicated before, the sign of parameter k_3 has been reported to be positive by several researchers including Heydinger et al. [59] and Bennert and Maher [60]. There is really no fundamental reason why k_3 should always be negative. However, the estimated values of k_3 described above are higher than those in [59] and [60], which is somewhat unique. As mentioned before, Stolle et al. [63] reported values as high as 1.595, which is comparable to those values obtained by Rayapeddi Kumar. Note that since Rayapeddi Kumar used a smaller number of repetitions at each stress

level, there may be some concern about whether that affected the results. Interestingly, the foamed asphalt specimens, which were also tested with the smaller number of repetitions did not exhibit the same behavior.

Fortunately, Song [61], also performed resilient modulus tests on virgin aggregates meeting HDOT specifications for base requirements according to AASHTO T-307. In this case, the recommended number of repetitions were used. The gradations were similar to those used by Rayapeddi Kumar but the source of the aggregates was the Makakilo quarry. Table 6-12 shows the parameters estimated by Song [61][48].

Table 6-12. Parameter estimation results for equation (6-30) obtained by Song **[61]** with virgin untreated base material.

w **(%)**	**Density (kg/m3)**	**Density (lb/ft3)**	k_1	k_2	k_3	R^2
8.7	1,743	107.65	980	0.68	0.02	0.99
9.0	1,798	111.04	1,120	0.29	0.79	0.98
9.5	1,821	112.46	640	0.69	0.52	0.99
9.3	1,825	112.71	1,240	0.46	0.32	1.00
12.6	1,713	105.79	550	0.76	0.32	0.99
11.5	1,822	112.53	870	0.40	0.82	0.99
14.0	1,723	106.41	620	0.68	0.30	1.00
14.2	1,800	111.17	640	0.73	0.35	1.00
13.2	1,827	112.84	680	0.75	0.19	1.00

Although the values are not as high as those of Rayapeddi Kumar, they are still higher than those reported in much of the literature. Note, however, that the trends with density for virgin aggregates are more consistent in Rayapeddi Kumar's result. For example, it is clear that increasing density result in lower k_3. Further research is needed to ascertain whether this is a phenomenon attributable to these combinations of source of aggregate and gradations.

[48] In Table 6-12 the parameter k_1 was corrected by a factor of 1,000 since they were originally misreported.

Nevertheless, as indicated earlier, values almost as high as those of Rayapeddi Kumar have been reported by other researchers [63]. In particular, these authors state[49]:

> "The parameter k_3, similar to K_3, can be negative or positive, ranging from -0.432 to 1.595." … "As described by Eqs. (2) and (4), the resilient moduli of base/subbase aggregates are generally affected by both the bulk and the deviatoric (or the octahedral) stresses. The resilient moduli data, however, clearly show that the M_r values of most materials are dominated by the bulk stress θ, with the effect of deviatoric stress being negligible." … "On the other hand, for materials that are less pressure sensitive and consequently have smaller K_2 (or k_2) values, the application of shear stress within the range in this study appears to cause an increase in resilient modulus."

In summary, the resilient modulus of some local base materials appear to increase with deviator stress.

6.3.1.2.3.2 Developing inputs for Level 2 and Level 3 Analyses

For input level 3, the Pavement ME Design software (MEPDG) [2] requires the input of a single value of M_r. The user has the option of allowing the program to modify the value according to the temperature and moisture predictions or to use the value entered as an annual representative value. For input level 2, the software adds an option of entering monthly representative values instead of a single value. Furthermore, for level 2, the user can select whether to input resilient modulus or another property that is correlated with M_r. In addition to resilient modulus, the properties accepted are CBR, R-Value, AASHTO Layer coefficient a_i, DCP Penetration, and Plasticity Index (PI) and gradation. As discussed in previous sections, using some of these options can be dangerous and it is discouraged. In particular, the use of gradation and PI, as shown earlier, can grossly underestimate the value of M_r.

Note that the gradation and PI information is not used only when the user selects the option to compute M_r from them. When the program is allowed to modify the M_r values according to the temperature and moisture predictions at levels 2 and 3, it utilizes equation (6-24) together with moisture predictions with the Enhanced Integrated Climatic Model (EICM) to

[49] The parameters with uppercase *K* in their statement are related to another model.

modify the M_r values with changes in moisture[50]. During the local calibration efforts, it was noted that regardless of the resilient modulus values input, the program very quickly converged to a modulus corresponding to an "equilibrium". The reason is that, as just mentioned, the program uses the EICM to compute moisture and temperature changes throughout the design life. This is one of the attractive features of the MEPDG over other design procedures.

For levels 2 and 3, the MEPDG Manual of Practice [22] recommends using the values shown in Table 6-13 for new designs. For rehabilitation or reconstruction designs, the same reference indicates that the resilient modulus of each unbound layer and embankment may be back-calculated from deflection basin data. The MEPDG Manual of Practice also indicates that the back-calculated values need to be adjusted to laboratory conditions with the correction factors listed in Table 6-14. For reasons that will be discussed in Section 7.4 (page 369), this practice is discouraged in this report.

With respect to new pavement sections, the values for resilient modulus at optimum water content in Table 6-13 should be used with caution. Notice that they depend on the soil type, location within the pavement (base/subbase or embankment), and pavement type (flexible or rigid). The location within the pavement accounts to some extent for the state of stresses. However, it must be recognized that the state of stresses on a given unbound material element can vary widely depending on other factors not considered in this table such as the thickness of the HMA layer, stiffness of the HMA layer, stiffness parameters of other layers in the pavement, and thicknesses of other layers in the pavement. A more thorough discussion of this topic is presented in section 7.4.

[50] In locations with freezing conditions, the MEPDG further modifies the values based on computations of the freezing zone within the pavement structure. Since for most of the State freezing is inexistent, the issue is not discussed further here.

Table 6-13. Recommended Levels 2 and 3 Resilient Moduli at Optimum Moisture for Unbound Aggregate Base, Subbase, Embankment, and Subgrade Soil (Source: [22]).

AASHTO Soil Classification	Recommended Resilient Modulus at Optimum Moisture (AASHTO T 180), psi		
	Base/Subbase for Flexible and Rigid Pavements	Embankment and Subgrade for Flexible Pavements	Embankment and Subgrade for Rigid Pavements
A-1-a	40,000	29,500	18,000
A-1-b	38,000	26,500	18,000
A-2-4	32,000	24,500	16,500
A-2-5	28,000	21,500	16,000
A-2-6	26,000	21,000	16,000
A-2-7	24,000	20,500	16,000
A-3	29,000	16,500	16,000
A-4	24,000	16,500	15,000
A-5	20,000	15,500	8,000
A-6	17,000	14,500	14,000
A-7-5	12,000	13,000	10,000
A-7-6	8,000	11,500	13,000

Table 6-14. MEPDG Recommended Correction Values to Convert Calculated Layer Modulus Values to an Equivalent Resilient Modulus Measured in the Laboratory (Source: [22]).

Layer Type	Location	C-Value or Mr/E_{FWD} Ratio
Aggregate Base/Subbase	Between a Stabilized and HMA Layer	1.43
	Below a PCC Layer	1.32
	Below an HMA Layer	0.62
Subgrade-Embankment	Below a Stabilized Subgrade/Embankment	0.75
	Below an HMA or PCC Layer	0.52
	Below an Unbound Aggregate Base	0.35

6.4 FATIGUE CRACKING

A limited study on fatigue cracking of local mixes was performed by Munar-Castaneda [71]. Munar-Castaneda tested thirty (30) unmodified-mix specimens and forty two (42) Elvaloy-modified-mix specimens at 1% concentration by mass of binder under *stress-controlled conditions*. Most of the specimens had air voids close to 7%.

These results are useful as they provide an estimate of how much additional fatigue life can be obtained from polymer modification. It is important to mention, however, that the results are limited in terms of the number of conditions tested (only one temperature) and the compaction conditions of the specimens. It is suspected that on some occasions the aggregates in the mix may have been crushed during compaction, thus adding some noise to the data.

6.4.1 UH Flexural Fatigue Performance Tests

Under stress-controlled conditions, the stress is maintained constant and the resulting strain and flexural stiffness are continuously monitored. A report was created for each test that shows the variation of flexural stiffness and tensile strain as the load repetitions increase as well as the initial and final values of the test variables (Figure 6-51).

Flexural stiffness followed the expected 90°-rotated S shape of typical fatigue performance in stress-controlled tests. The rate of decrease of stiffness is initially very high, then it reaches an approximate constant value and finally it increases again until the specimen fails. The stiffness value decreases dramatically due to the continuous increase in tensile strain and the accumulation of permanent strain (creep). This creep is caused by the presence of higher stiffness in compression than in tension, and by the hysteretic heating due to the viscoelasticity of the asphalt mix during cyclic loading [72].

In the fatigue flexural test, each specimen was tested with a sinusoidal load at one controlled stress in the range of 1,000 kPa to 1,850 kPa, peak to peak. The frequency of the test is 10 Hz (i.e. loading pulse width 100 msec) and the temperature of the tests was targeted at 20°C. The initial tensile strain was measured at the 50^{th} cycle of the test, and the failure by fatigue was defined to occur when the stiffness of the beam presented a reduction of 80% of the initial value measured at the 50^{th} load repetition. The samples included in the analysis have an air void content close to 7% and an asphalt content of 5.3%.

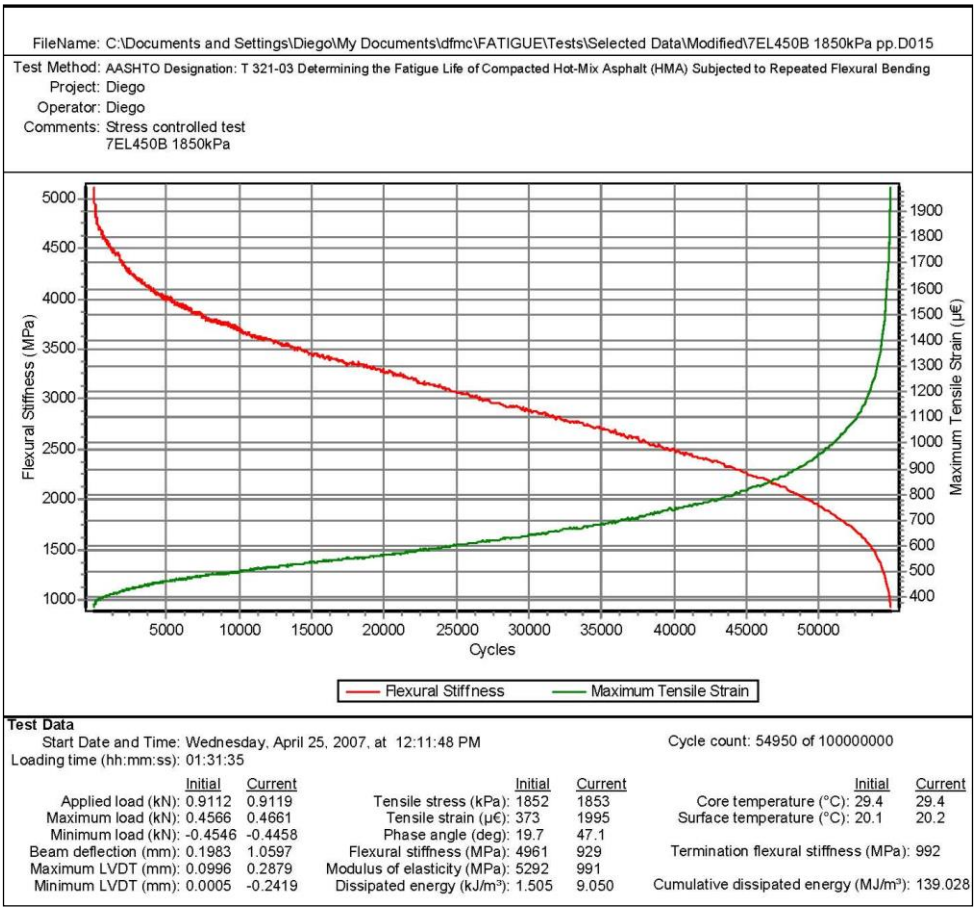

Figure 6-51. Example of fatigue test report given by UTS015 software used to perform the test.

From all the beams tested, seventeen (17) unmodified and thirty (30) Elvaloy-modified were included in the analysis after removing specimens due to problems during the testing, not compliance with air void content in the allowable range (6% - 8%), or fatigue life greater than 1,000,000 cycles (to avoid large errors associated with high fatigue performances). The complete database with the fatigue tests results is presented reference [71]. Table 6-15 shows for each type of mix and stress level the number of samples and the mean of air voids, fatigue life, initial stiffness of the mix, and initial strain. [51]

[51] The information in Table 6-15 needs to be interpreted with caution. For some stress levels, the unmodified mix appears to perform better than the modified mix. However, the fatigue equations are based on strain

Table 6-15. Number of samples at each stress level in [71] and the corresponding laboratory mean Air Voids, Fatigue Life, Stiffness and Strain.

Type of mixture	Stress Level (kPa)	Number of Samples	Mean Air Voids (%)	Average Number of Cycles Termination @ 20% stiffness	Average Initial Stiffness @ 50th cycle (MPa)	Average Initial strain (mϵ) peak to peak
Unmodified	1000	1	7.16	909,130	3659	273
Unmodified	1200	3	7.04	314,837	4798	251
Unmodified	1350	3	6.63	299,630	5594	242
Unmodified	1500	4	6.57	102,998	5318	287
Unmodified	1700	3	6.27	39,803	4679	372
Unmodified	1850	3	6.54	34,317	5179	363
Number of samples		17				
Modified 1%	1100	1	6.63	849,070	4222	260
Modified 1%	1200	6	7.04	368,733	4359	278
Modified 1%	1350	6	7.43	139,190	4296	324
Modified 1%	1500	7	6.97	61,917	4125	368
Modified 1%	1700	6	7.23	41,952	4363	394
Modified 1%	1850	4	6.91	34,988	4355	433
Number of samples		30				

In general, in Munar-Castaneda's study [71], the values of flexural stiffness for the unmodified mix specimens are about 17% higher on average than the stiffness for the Elvaloy-modified samples. This can be explained by the reduction in stiffness effect that polymer modification has in asphalt mixtures. A more flexible mix under cyclic loading delays the appearance of tension cracking, leading to higher fatigue performance.

6.4.2 Complete MEPDG Fatigue Relationship

As discussed in section 5.4.2.1, fatigue cracking is modeled in the MEPDG with a three-parameter model that predicts the allowable number of load repetitions for a given strain level on a mix with a given flexural stiffness (see equation (5-1) on page 201). Equation (5-1) is nothing but a modification of a similar equation developed from beam fatigue laboratory tests similar to the ones discussed in the previous section. The laboratory model takes the form:

not stress. As discussed below, the modified mixes provide a longer fatigue life for a given strain level. Note also that in Table 6-15 the first stress level for the unmodified mix is higher than for the unmodified mix.

$$N_f = k_1 \varepsilon_t^{-k_2} S^{-k_3} \quad (6\text{-}31)$$

where:

N_f = number of repetitions to failure (fatigue life),

S = flexural stiffness, σ/ε_t, (σ = extreme fiber stress and ε_t = extreme fiber tensile strain),

k_1, k_2 and k_3 = experimentally determined regression parameters.

It is important to clarify the meaning of flexural stiffness since the literature is not always very precise about it and stiffness has a different meaning in strength of materials. As defined above, *S* is nothing more than a normal modulus of elasticity. However, often, a correction is introduced to consider the shear deformation on the extreme one thirds of the beam. The correction depends on the beam specimen and ranges from 1.04 to 1.16 for the specimens sizes that have been traditionally used [34]. For the tests perform at UH, the factor is about 1.07. The second important consideration is that the flexural stiffness measured in a beam fatigue test is substantially smaller than the dynamic modulus obtained in the AMPT for a given frequency and temperature combination. For the tests performed at UH, the ratio of S/|E*| is about 0.7. Several differences between these tests such as specimen geometry, sinusoidal loading vs. pulse loading with rest periods, shape of the load pulse, etc. help to explain this discrepancy. The most significant, however, is the fact that in the dynamic modulus test the sample is subjected to compression whereas in the beam fatigue test it is subjected to tension and compression. Thus, the modulus derived from the beam fatigue test is really a combined modulus for these two conditions. Since both the asphalt binder and the aggregate contribute to the modulus in compression but for the most part only the asphalt binder contributes in tension, it follows that the stiffness in the beam fatigue test appears to be always smaller than |E*|.

The above observations notwithstanding, whether S or |E*| has been used in a particular model is of not much practical consequence since use of one or the other translate only in a different value of k_1 when S = constant × |E*|. Estimation of the parameters k_1, k_2, k_3 with linear regression leaves the parameters k_2 and k_3 unaltered. Furthermore, k_1 is multiplied, among other things, by a calibration factor to account for the differences between laboratory and field conditions. Thus, use of *S* or |E*| would only affect that calibration factor.

The complete expression used by the MEPDG to compute the allowable number of repetitions for a given tensile strain is [22]:

$$N_{f-HMA} = k_{1f}(C)(C_H)\beta_{f_1}(\varepsilon_t)^{k_{f2}\beta_{f2}}(|E*_{HMA}|)^{k_{f3}\beta_{f3}} \quad (6\text{-}32)$$

where:

$N_{f\text{-}HMA}$ = Allowable number of axle-load applications for a flexible pavement and HMA overlays,

ε_t = Tensile strain at critical locations and calculated by the structural response model, in/in,

$|E^*_{HMA}|$ = Dynamic modulus of the HMA measured in compression, psi,

k_{f1}, k_{f2}, k_{f3} = Global field calibration parameters (from NCHRP 1-40D recalibration; k_{f1} = 0.007566, k_{f2} = -3.9492, and k_{f3} = -1.281), and

β_{f1}, β_{f2}, β_{f3} = Local or mixture specific field calibration constants; for the global calibration effort, these constants were set to 1.0.

$$C = 10^M \quad (6\text{-}33)$$

$$M = 4.84\left(\frac{V_{be}}{V_a + V_{be}} - 0.69\right) \quad (6\text{-}34)$$

where:

V_{be} = Effective asphalt content by volume, %,

V_a = Percent air voids in the HMA mixture, and

C_H = Thickness correction term, dependent on type of cracking.

For bottom-up or alligator cracking:

$$C_H = \frac{1}{0.000398 + \frac{0.003602}{1 + e^{(11.02 - 3.49 H_{HMA})}}} \quad (6\text{-}35)$$

For top-down or longitudinal cracking:

$$C_H = \frac{1}{0.01 + \frac{12.00}{1 + e^{(15.676 - 2.8186 H_{HMA})}}} \quad (6\text{-}36)$$

where:

H_{HMA} = Total HMA thickness, in.

6.4.3 UH Fatigue Data Analysis

Figure 6-52 shows the relationship between initial tensile strain and number of repetitions to failure for the unmodified mixes. Figure 6-53 shows the same relationship for the PMA mixes. Both figures are plotted using logarithmic scales for both axes. As expected, both log-log plots show an approximate linear trend between the two variables. Thus, even without consideration of the mix stiffness, the strain level gives a good indication of the fatigue life. The linear relationships in the figures are expressed mathematically as:

Unmodified Mix:

$$Log_{10}(N_f) = 16.445 - 4.610 \cdot Log_{10}(\varepsilon_t) \quad (6\text{-}37)$$

$$N_f = 2.79 \times 10^{16} (\varepsilon_t)^{-4.610} \quad (6\text{-}38)$$

Elvaloy-modified Mix:

$$Log_{10}(N_f) = 17.286 - 4.872 \cdot Log_{10}(\varepsilon_t) \quad (6\text{-}39)$$

$$N_f = 1.93 \times 10^{17} (\varepsilon_t)^{-4.872} \quad (6\text{-}40)$$

The exponent of strain is similar in both cases, though the modified mix is a bit more sensitive to the strain level. Both values agree quite well with reported values in the literature.

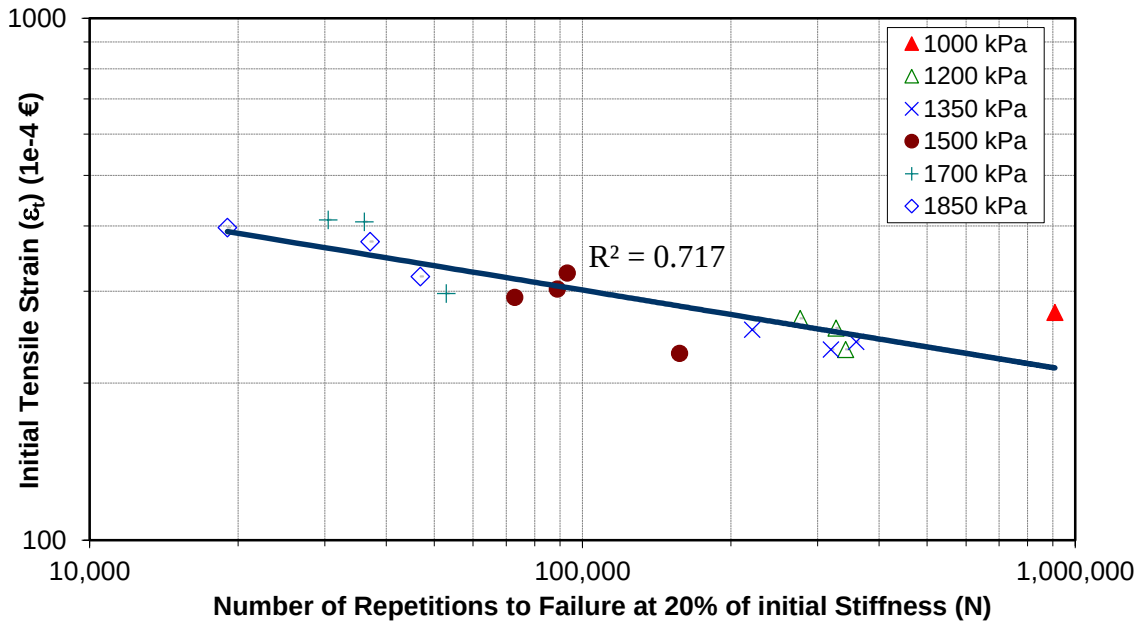

Figure 6-52. Fatigue Test Results (Unmodified Binder) - Relationship between Repetitions and Initial Strain grouped by Test Stress Levels.

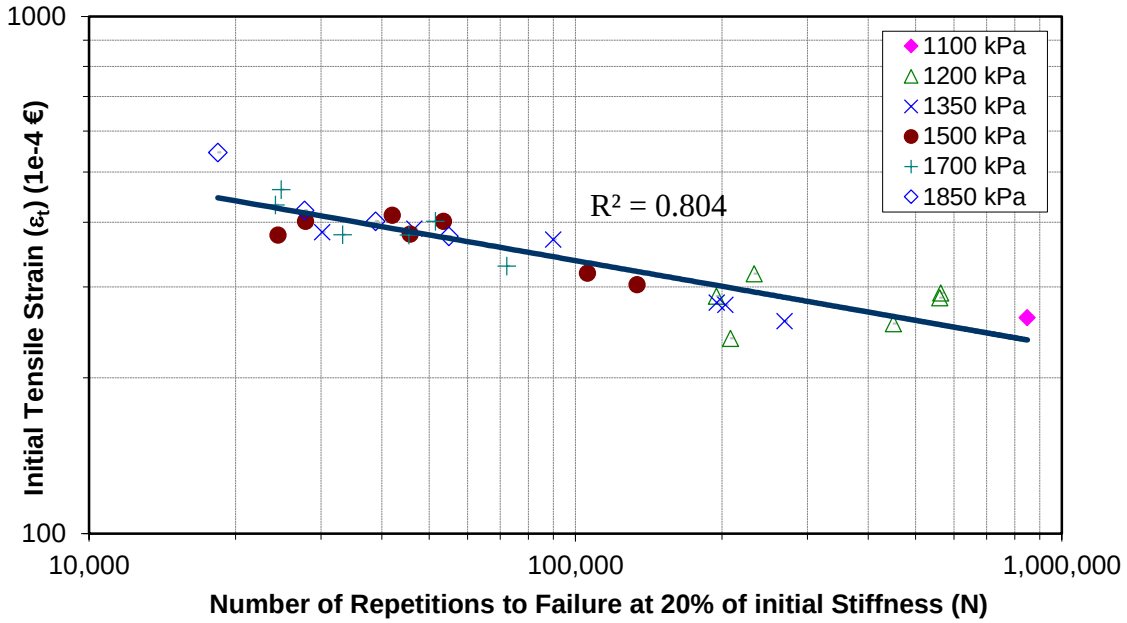

Figure 6-53. Fatigue Test Results (PMA Binder) - Relationship between Repetitions and Initial Strain grouped by Test Stress Levels.

Figure 6-54 compares the fatigue performance of the two types of mixtures. Note that the axes are reversed to show the information in the typical form. There is a clear improvement, on average, with the modified over the unmodified mix.

As shown in Table 6.16, the fatigue performance improvement goes from 29% to 73% depending on the tensile strain level applied to the asphalt layer.

Since all the tests were performed at a single target temperature, the effect of stiffness is more difficult to identify. Nevertheless, as explained next, application of multiple linear regression analysis using equation (6-31) resulted in a statistical significant parameter for stiffness [71].

To apply multiple linear regression, a logarithmic transformation was performed to obtain a linear model in the parameters.

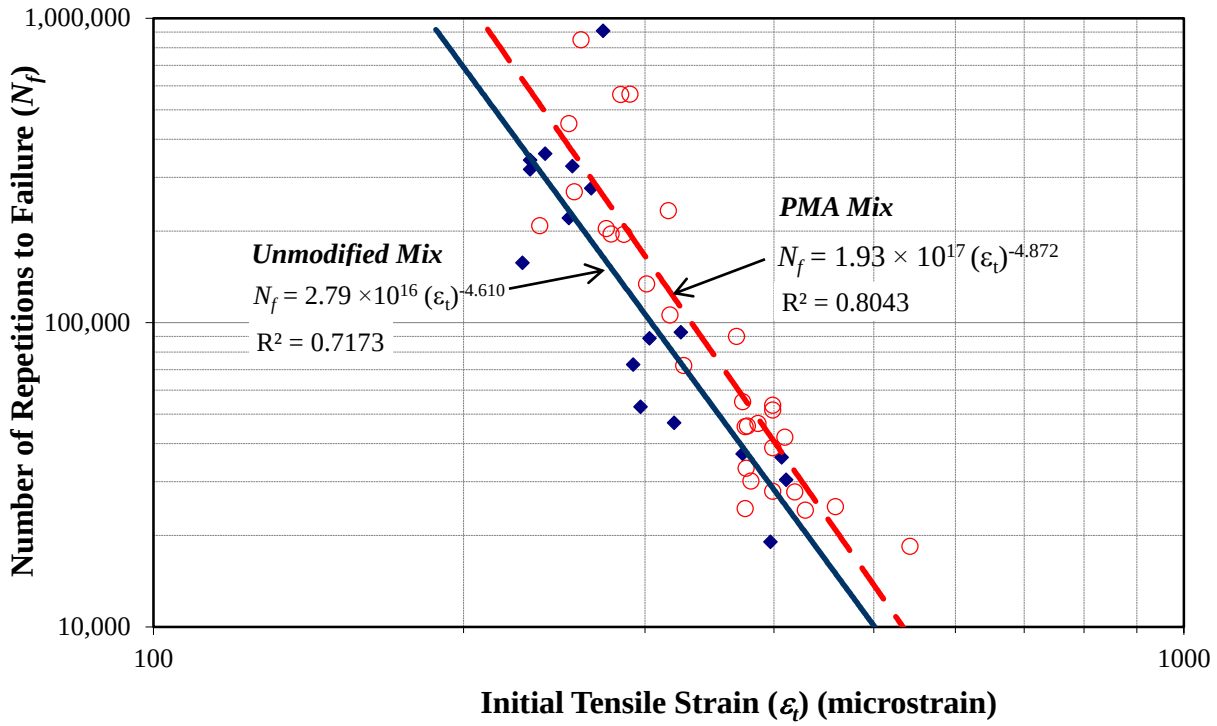

Figure 6-54. Fatigue performance comparison of unmodified and PMA modified mixes.

Table 6.16. Fatigue performance improvement of PMA mixture compared to the unmodified mixture at different tensile strain levels.

Strain Level (1×10^{-6})	Estimated average fatigue life (N_f) unmodified	Estimated average fatigue life (N_f) PMA	Difference	Improvement (%)
200	688,424	1,188,336	499,912	73
250	246,094	400676	154,582	63
300	106,188	164,825	58,637	55
350	52,174	77,778	25,605	49
400	28191	40,581	12,390	44
450	16,379	22,862	6,482	40
500	10,077	13,683	3,605	36
550	6,494	8,600	2,106	32
600	4,348	5,629	1,280	29

$$\log_{10}(N_f) = \log_{10}(k_1) + k_2 \cdot \log_{10}(\varepsilon_t) + k_3 \cdot \log_{10}(S) \quad (6\text{-}41)$$

Applying regression analysis to equation (6-41) with $\log_{10}(N_f)$ as the dependent variable and $\log_{10}(\varepsilon_t)$ and $\log_{10}(S)$ as the independent variables produces estimates of $\log(k_1)$, k_2, and k_3. All the parameter estimates are statistically significant as indicated by the low p-values. The fatigue performance model for the PMA mixes has a R^2 value of 0.842, whereas for the unmodified mixes the coefficient of determination reaches the 0.957 value.

From the results of the regression analysis, linear relationships for the two types of mixes can be created. Transformation of the linear associations using the antilogarithm function can be made in order to define every model in terms of the original variables.

Table 6-17 and Table 6-18 present the results of the regressions performed on the data set for unmodified and the PMA mixes, respectively.

From the results of the regression analysis, linear relationships for the two types of mixes can be created. Transformation of the linear associations using the antilogarithm function can be made in order to define every model in terms of the original variables.

Unmodified Mix:

$$Log_{10}(N_f) = 35.788 - 6.157 \cdot Log_{10}(\varepsilon_t) - 4.197 \cdot Log_{10}(S) \quad (6\text{-}42)$$

$$N_f = 6.14 \times 10^{35} (\varepsilon_t)^{-6.157} (S)^{-4.197} \quad (6\text{-}43)$$

PMA Mix:

$$Log_{10}(N_f) = 27.175 - 5.726 \cdot Log_{10}(\varepsilon_t) - 2.128 \cdot Log_{10}(S) \quad (6\text{-}44)$$

$$N_f = 1.50 \times 10^{21} (\varepsilon_t)^{-5.726} (S)^{-2.128} \quad (6\text{-}45)$$

The testing results from the unmodified mixture revealed that fatigue life occurrence between 10,000 and 1,000,000 load repetitions corresponds to a range of initial tensile strain between 220 to 420 microstrain (1×10^{-6} in./in.), whereas the range for the polymer-modified asphalt mix ranges from 240 to 550 microstrain. Therefore, there is a noticeable difference regarding fatigue behavior between these two mixes.

The empirical relationship between the number of load repetitions (N_f) and initial tensile strain (ε_t) gives acceptable results for both mixtures analyzed. The fitted models have reasonably high coefficients of determination (i.e. R^2) and are statistically significant.

As expected, a reduction in flexural stiffness generates higher fatigue performances for both mixtures.

Equations (6-43) and (6-45) can be visualized in a three-dimensional graph as shown in Figure 6-55 for both asphalt mixtures. The planes illustrated in the graph present different slopes in the strain and stiffness directions.

Table 6-17. Multiple Linear Regression results. N_f vs. ε_t and S model - Unmodified mix.

REGRESSION ANALYSIS	
R Square	0.957
Adjusted R Square	0.951
Standard Error	0.106
Observations	17

ANOVA

	df	***SS***	***MS***	***F***	***Significance F***
Regression	2	3.528	1.764	157.559	2.52E-10
Residual	14	0.157	0.011		
Total	16	3.685			

REGRESSION ANALYSIS

Variable	***Coefficients***	***Standard Error***	***t Stat***	***P-value***
Intercept	35.788	2.298	15.572	3.10E-10
Log **(ε_t)**	-6.157	0.347	-17.752	5.38E-11
Log **(S)**	-4.197	0.472	-8.891	3.92E-07

Table 6-18. Multiple Linear Regression results. N_f vs. ε_t and S model – PMA modified mix.

REGRESSION ANALYSIS	
R Square	0.842
Adjusted R Square	0.830
Standard Error	0.197
Observations	30

ANOVA

	df	***SS***	***MS***	***F***	***Significance F***
Regression	2	5.576	2.788	71.780	1.56E-11
Residual	27	1.049	0.039		
Total	29	6.625			

REGRESSION ANALYSIS

Variable	***Coefficients***	***Standard Error***	***t Stat***	***P-value***
Intercept	27.175	4.056	6.700	3.42E-07
Log **(ε_t)**	-5.726	0.536	-10.679	3.40E-11
Log **(S)**	-2.128	0.843	-2.525	1.77E-02

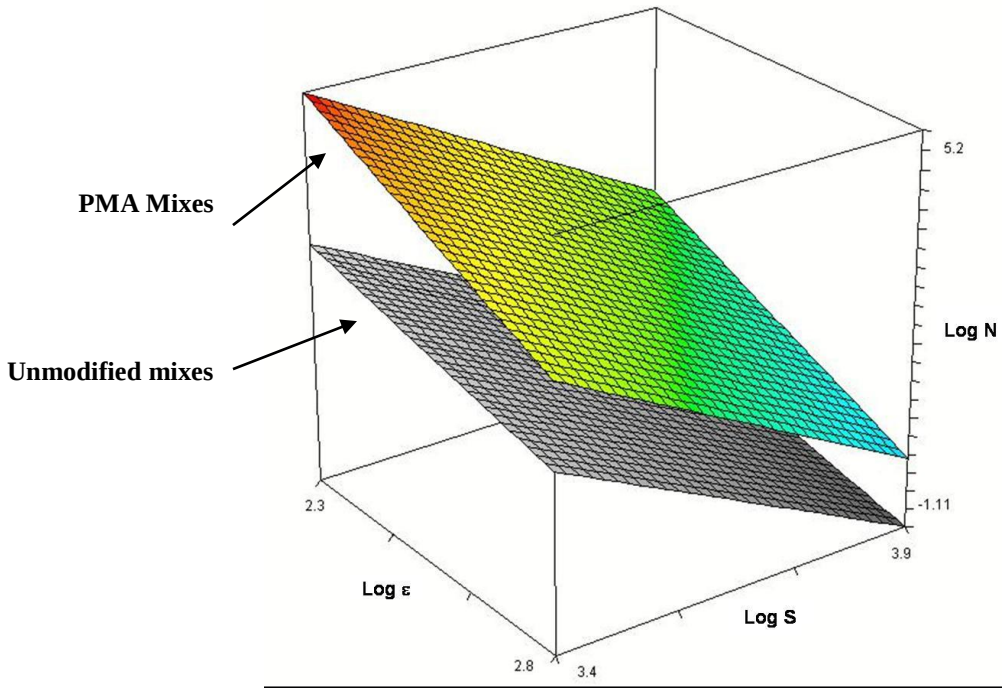

Figure 6-55. Three-dimensional representation of fatigue performance models.

In summary, the modified asphalt mixture presented on average better fatigue performance than the unmodified mix.

6.5 PERMANENT DEFORMATION

As discussed in section 5.4.2.2, in the MEPDG the vertical compressive strains computed by the pavement response model at mid-depth of each sublayer of the pavement structure are used to predict rutting over time. Specifically, for each Hot Mix Asphalt (HMA) sublayer, the field calibrated form of the permanent deformation model, equation (5-7) (shown in page 219), is used to predict the sublayer contribution to rutting for each period. Equation (5-7) was originally derived from the permanent deformation test in the form of equation (5-6) described in section 5.4.2.2.

In addition, the MEPDG estimates the contribution of unbound layers to rutting in a similar fashion, as described also in section 5.4.2.2. However, it has been reported that the MEPDG tends to overestimate rutting originating in these layers. An example for Kansas is provided in [31]. Given the thick HMA layers used in HDOT designs for new sections, rutting originating in unbound layers appears to be minimal. Most of the rutting in new pavement sections on state roads in Hawaii appear to be originating in the HMA. As explained chapter 7 in relation to the calibration of the MEPDG; for this study, rutting originating in unbound layers has been limited to a small value. Therefore, the rest of this section concentrates on the rutting originating in HMA layers.

6.5.1 Characterization of Permanent Deformation

A substantial amount of work has been done to characterize local Superpave 12.5 mm mixes (with gradations also meeting State Mix IV requirements) for permanent deformation. Much of that work has been documented in another research report [46] and journal papers ([50], [52], and [73]). Therefore, the discussion here is limited.

In the MEPDG, the prediction of permanent deformation uses results from both the dynamic modulus test ($|E^*|$) and repeated axial load permanent deformation tests. However, their use is asymmetric in the sense that project specific $|E^*|$ values can be considered (measured or as a function of other mix properties), whereas the permanent deformation parameters enter only through the permanent deformation model, which is calibrated to local conditions at best. It is assumed that the effects of mixture properties such as air void content, effective binder content, and binder grade are already adequately incorporated into the permanent deformation simulation

through |*E**| values. Mixture properties are accounted for only by the elastic response (i.e., ε_r). As a result, it is possible that only a portion (instead of the full extent) of the variability induced from some mixture properties is being taken into account.

Limitations arising from the use of |*E**| alone for rutting characterization have been reported in the literature. A summary of the literature that is critical in this respect is presented in reference [52], on which it is also concluded that predicting rutting performance by means of elastic response alone (universal values for permanent deformation model parameters, regardless of mixture properties) does not fully take into account mixture-specific contributions to rutting. Thus, Archilla and Diaz [52] describe the development of models that make the parameters k_1 and k_3 of equation (5-6) functions of mix characteristics. The data for the same specimens used for the development of the |E*| model presented in section 6.2.4.2 were used for the development of this model. Therefore, the description of the gradations and binders presented in that section are still applicable. The functions for k_1 and k_3 can be useful for the calibration of the permanent deformation model as these are the parameters that more often need modification.

6.5.1.1 Parameter k3

The function for k_3 is:

$$\log(k_3) = \beta_1 + \beta_2 D_{B6416} + \beta_3 D_{A70XX} + \beta_4 D_{B70XX} + \beta_5 D_{A7022} + \beta_6 D_{B7022} + \\ + \beta_7 \log(V_a) + \beta_8 \log(P_{beffVol}) + \beta_9 \log(V_a)\log(P_{beffVol}) \quad \text{(6-46)}$$

where

D_{B6416} = 1 if Gradation B and binder is PG 64-16 and 0 otherwise,

D_{A70XX} = 1 if Gradation A and binder is PG 70-XX and 0 otherwise,

D_{B70XX} = 1 if Gradation B and binder is PG 70-XX and 0 otherwise,

D_{A7022} = 1 if Gradation A and binder is PG 70-22 and 0 otherwise,

D_{B7022} = 1 if Gradation B and binder is PG 70-22 and 0 otherwise,

V_a = air void content (%), and

$P_{beffVol}$ = effective binder content by volume (%).

In addition to considering the effects of air void content, effective binder content, and their interaction, Equation (6-46) allows for different intercepts for the different binders and gradations for log(k_3) (β_1 for Gradation A with PG 64-16, $\beta_1 + \beta_2$ for Gradation B and PG 64-16, $\beta_1 + \beta_3$ for Gradation A and PG 70-XX, $\beta_1 + \beta_4$ for Gradation B and PG 70-XX, $\beta_1 + \beta_5$ for Gradation A and PG 70-22, and $\beta_1 + \beta_6$ for Gradation B and PG 70-22).

Table 6-19. Parameter Estimates for log(k_3).

Parameter Name	Variable ID	Value	Standard Error	t-value	p-value	No of observations associated with the parameter
β_1	Intercept	-2.223	0.692	-3.21	0.002	63
β_2	D_{B6416}	0.018	0.017	1.04	0.302	16
β_3	D_{A70XX}	-0.118	0.019	-6.08	0.000	10
β_4	D_{B70XX}	-0.106	0.018	-5.91	0.000	14
β_5	D_{A7022}	-0.111	0.025	-4.37	0.000	5
β_6	D_{B7022}	-0.033	0.027	-1.22	0.228	4
β_7	$\log_{10}(V_a)$	2.369	0.793	2.99	0.004	63
β_8	$\log_{10}(P_{beffVol})$	2.355	0.670	3.52	0.001	63
β_9	$\log_{10}(V_a)\ \log_{10}(P_{beffVol})$	-1.907	0.773	-2.47	0.017	63

Residual standard error: 0.04625 on 54 degrees of freedom.

Multiple R-Squared: 0.8362

F-statistic: 34.45 on 8 and 54 degrees of freedom, the p-value is zero. Sample size = 63

Except for parameters β_2 and β_6, the parameter estimates are statistically significant at a 95% confidence level. The very low p-values for β_7, β_8, and β_9 statistically confirm the significance of the effects of air voids, effective binder content, and their interaction on k_3.

The fact that the estimate of β_2 is not statistically significantly different from zero simply indicates that there is no discernible difference between mixes with unmodified binder prepared with either gradation.

A somewhat surprising result is that the estimate of parameter β_6 is not statistically significant, which would indicate that there is no difference between a mix prepared with gradation A and the PG64-16 binder (or given that β_2 was not statistically significantly different from zero, a mix with gradation B and PG64-16 binder) and another mix prepared with gradation B and the PG70-22 binder. It is believed that this is just an anomaly in one or more of the only four data points available for the combination of gradation B and the PG70-22 binder. (It is recognized that by following the same logic (i.e. low number of data points), the conclusion drawn for the combination of gradation A and PG70-22 binder could be challenged; however, it is important to note that these results indicate that the performance of the mixture with the modified binder is better than the one observed in the unmodified mixture, which is logical according to extensive literature reports, and consistent with the results obtained with the mixtures prepared with PG70-XX binder, which have more experimental observations).

The estimates for the other three parameters (β_3, β_4, and β_5) are all statistically significantly different from zero, which indicates that all these mixes performed better than the unmodified mixes. The three parameter estimates are similar, thus indicating that these mixes accumulate permanent deformation at comparable rates. The R^2 is 0.836, which indicates an acceptable fit.

The finding that the parameter k_3 is a function of mix characteristics is quite important. Currently, the MEPDG assumes that the elastic response alone (ε_r), which is a function of |E*|, can take completely into account all the effects that individual mixture characteristics have on the permanent deformation response and thus, it assumes that k_3 is a constant. The above results indicate that this may not be the case.

6.5.1.2 Parameter k_1

The procedure to estimate parameter k_1 proposed in [50] is a little more involved. It requires first the estimation of the permanent deformation (ε_{p100}) after 100 load repetitions[52]. The model developed for ε_{p100} for the loading conditions in [50] is:

$$\log(\varepsilon_{p100}) = \lambda_1 + \lambda_2 D_{B6416} + \lambda_3 D_{A70XX} + \lambda_4 D_{B70XX} + \lambda_5 D_{A7022} + \lambda_6 D_{B7022} + \lambda_7 \log(V_a) + \lambda_8 \log(Pb_{effVol}) + \lambda_9 \log(V_a) \log(Pb_{effVol}) \quad (6\text{-}47)$$

where,

D_{B6416} = 1 if gradation B and binder is PG64-16 and zero otherwise,

D_{A70XX} = 1 if gradation A and binder is PG70-XX and zero otherwise,

D_{B70XX} = 1 if gradation B and binder is PG70-XX and zero otherwise,

D_{A7022} = 1 if gradation A and binder is PG70-22 and zero otherwise,

D_{B7022} = 1 if gradation B and binder is PG70-22 and zero otherwise,

V_a = air voids (%), and

$P_{beffVol}$ = effective binder content by volume (%).

The parameters of the model described in Equation (6-47), including the results from the regression analysis, are summarized in Table 6-20.

[52] Loading consisted of an axial deviator stress of 828 kPa (120 psi), a contact stress of 41.4 kPa (5.1 psi), and a confining stress of 138 kPa (20 psi).

Table 6-20. Parameter Estimates for $\log(\varepsilon_{p100})$.

Parameter Name	Variable ID	Value	Standard Error	t-value	p-value	No of observations associated with the parameter
λ_1	Intercept	-5.169	1.690	-3.06	0.004	63
λ_2	D_{B6416}	-0.050	0.041	-1.21	0.232	16
λ_3	D_{A70XX}	-0.364	0.048	-7.66	0.000	10
λ_4	D_{B70XX}	-0.353	0.044	-8.09	0.000	14
λ_5	D_{A7022}	-0.133	0.062	-2.14	0.037	5
λ_6	D_{B7022}	-0.117	0.065	-1.80	0.078	4
λ_7	$Log_{10}(V_a)$	10.001	1.937	5.16	0.000	63
λ_8	$Log_{10}(P_{beffVol})$	28.394	1.635	5.14	0.000	63
λ_9	$\log_{10}(V_a)\ \log_{10}(P_{beffVol})$	-8.604	1.887	-4.56	0.000	63

Residual standard error: 0.1129 on 54 degrees of freedom.

Multiple R-Squared: 0.8872

F-statistic: 53.11 on 8 and 54 degrees of freedom, the p-value is zero. Sample size = 63

Interpretation of the results is analogous to the interpretation of the results for k_3. Again, the parameters for D_{B6416} and D_{B7022}, λ_2 and λ_6, are not statistically significant at a 95% confidence level. The fact that the estimate of λ_2 is not statistically significantly different from zero simply indicates that there is no discernible difference between mixes with unmodified binder prepared with either gradation. As for λ_6, the same potential anomaly described earlier for β_6 may effect this parameter estimate.

The essentially zero p-values for λ_7, λ_8, and λ_9 statistically confirm the significance of the effects of air voids, effective binder content, and their interaction on ε_{p100}.

The estimates for the other three parameters (λ_3, λ_4, and λ_5) are all statistically significantly different from zero and negative, which indicates that all these mixes performed

better than the unmodified mixes (i.e., they show smaller permanent deformations after 100 cycles). λ_3 and λ_4 have similar magnitudes, indicating that the mixes with PG70-XX performed similarly regardless of whether gradation A or gradation B was used. On the other hand, the absolute value of λ_5 is smaller than either λ_3 or λ_4, which indicates that the mixes prepared with PG70-22 binder and gradation A performed slightly worse than those with PG70-XX but still better than those PG64-16. The R^2 of almost 0.89 indicates again an acceptable fit for ε_{p100}.

With ε_{p100}, the value of k_1 can be estimated by

$$k_1 = \log_{10}\left(\frac{\varepsilon_{p100}}{\varepsilon_r}\right) - k_3 \log_{10}(100) - k_2 \log(T) \qquad (6\text{-}48)$$

where

ε_{p100} = cumulative permanent deformation after 100 loading repetitions,

ε_r = resilient strain for the state of stresses, loading frequency and temperature conditions during the test (10Hz and 54°C = 129.2°F),

k_3 = parameter k_3 as estimated by equation (6-47);

k_2 = parameter for temperature (see below),

T = test temperature expressed in °F (129.2°F).

Due to the limitation of having only one temperature level (i.e. 54ºC=129.2°F), the parameter k_2 was assigned a value of 1.734, which is the *laboratory* based value used to calibrate the MEPDG rutting prediction model [1]. This assumption only affects the laboratory estimates of k_1 but it has little effect on the main conclusions. A more detailed description of the rationale for the above equations is presented in [50]. Reference [74] shows that adjusting the permanent deformation model parameters of the polymer modified mixes relative to the unmodified mixes produce more reasonable results. Otherwise, the MEPDG could even predict a lower performance with the modified mixes, which is not logical.

6.5.2 Additional Laboratory Tests

Rayapeddi Kumar [47] performed additional repeated load permanent deformation tests. These tests were performed on the same samples used to measure |E*| described in section 6.2.4.2.4. His most relevant conclusions were:

1. The Flow Number (FN)[53] values of mixes prepared using polymer modified mixes at low and medium air voids are higher compared to the FN values for other types of laboratory prepared mixes at the same approximate air voids. For higher air voids (~7%), the FN for PMA mixes are higher than the FN for the mixes prepared using unmodified binder.
2. The FN values for all specimens prepared using fibers are relatively constant at all air voids.
3. The average slope (k_3) for polymer modified asphalt concrete mixtures is the lowest compared to virgin and fiber reinforced concrete mixtures at low air voids (~3%). At intermediate and higher air voids, the fiber reinforced asphalt concrete mixtures had the lowest k_3 value.
4. The average k_3 values for fiber reinforced asphalt concrete mixes show a relatively lower strain rate compared to mixtures prepared using virgin binder at corresponding target air voids.
5. The plant produced and laboratory produced mixes using unmodified binder do not show a particular trend with respect to the rate of accumulation of permanent strain.

[53] The flow number is the number of load repetitions needed for the permanent deformation curve to reach the inflexion point or flow point (see Figure 5-23, page 216). It is used as an indicator of mix resistance to permanent deformation. The higher the number the more resistant the mix.

6.6 BINDER CHARACTERIZATION

Limited binder characterization of PG64-16 binder was performed in terms of its rotational (Brookfiled) viscosity and dynamic shear modulus (|G*|) [46]. In addition, a few repeated creep and recovery tests were also performed. These tests were performed before Asphalt Hawaii started supplying most of the binder used in the state. Therefore, they may not be entirely representative of current conditions. Nevertheless, as discussed before, relatively minor changes in dynamic moduli and permanent deformation were observed with the Asphalt Hawaii binder. Moreover, simulations with the MEPDG with level 1 or pseudo-level 1 data as generated with the local |E*| models described in section 6.2.4.2 do not produce appreciably different results with variations in binder characteristics when compared with the effects of other variables analyzed. This is not surprising, since when using level 1 dynamic modulus inputs, the binder characteristics are used only in a global aging model to determine the effect of aging of the binder in |E*|. Except for the effect of aging, the master curve is defined mostly by the input |E*| values. With respect to permanent deformation, as discussed in section [50], it is believed that different calibration factors should be developed for significantly different binders (modified vs. unmodified.)

Figure 6-56 shows the viscosity characteristics of Rolling Thin Film Oven (RTFO) aged samples of the PG64-16 and the PG70-XX binders[54]. The viscosities were obtained with a rotational viscometer (Brookfield viscometer) over a wide range of temperatures and also estimated from dynamic shear modulus (|G*|) and phase angle (δ) measurements at 10 rad/s obtained with a Dynamic Shear Rheometer (Bohlin CVO-100) using the following conversion equation from the MEPDG [1]:

[54] The PG70-XX binder is the PG64-16 binder modified with 1% of Elvaloy RET®. As discussed in previous sections, polymer modification appears to have a similar effect on the performance of mixes with the binder supplied by Asphalt Hawaii.

$$\eta = \frac{|G^*|}{10}\left(\frac{1}{\sin\delta}\right)^{4.8628} \qquad (6\text{-}49)$$

where

|G*| = binder shear modulus, Pa

δ = binder phase angle, º

η = viscosity, cP

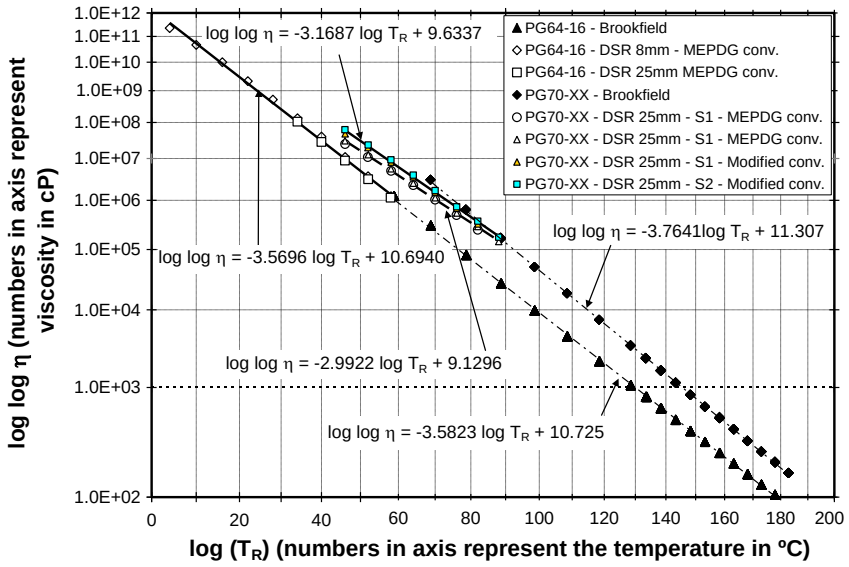

Figure 6-56. Viscosity (η) vs. temperature relationships for local binders (before Asphalt Hawaii started to supply binder).

Two samples of each binder were tested with the DSR. One test was performed with 8 mm plates and the other three with 25 mm plates. For the PG64-16 binder the estimated viscosity trends with both instruments are very similar when both sets of DSR measurements are included as shown in the figure. The estimated A and VTS parameters (the intercept and slope respectively of the log log η vs. log T_R equation, where η is the viscosity in cP and T_R is the temperature in Rankine as used in the MEPDG) differ somewhat when each individual DSR series for the PG64-16 binder is considered separately. Nevertheless the trends with both instruments for the PG64-16 still show relatively good agreement.

On the other hand, the trend of the viscosities estimated for the modified binder with |G*| and δ using equation (6-49) (labeled "MEPDG conv." in the figure) differs significantly from the trend obtained with the rotational viscometer. Despite the differences that result in the A and VTS parameters from both instruments, simulations with the MEPDG with level 1 data for the modified binder did not produce appreciably different results when these variations in A and VTS where considered when compared with the effects of other variables analyzed.

The binder performance was also evaluated with the repeated shear creep and recovery tests. The tests were performed with 100 cycles each composed of a loading period of 1 second with a shear stress of 300 kPa followed by a rest period of 9 seconds at different temperatures. Figure 6-57 shows the results for the 50th cycle at two relevant temperatures. The improvements in rutting resistance and elastic recovery of the modified binder over the unmodified binder are notable. As described in previous sections, these binder improvements translate in performance improvements of the mix.

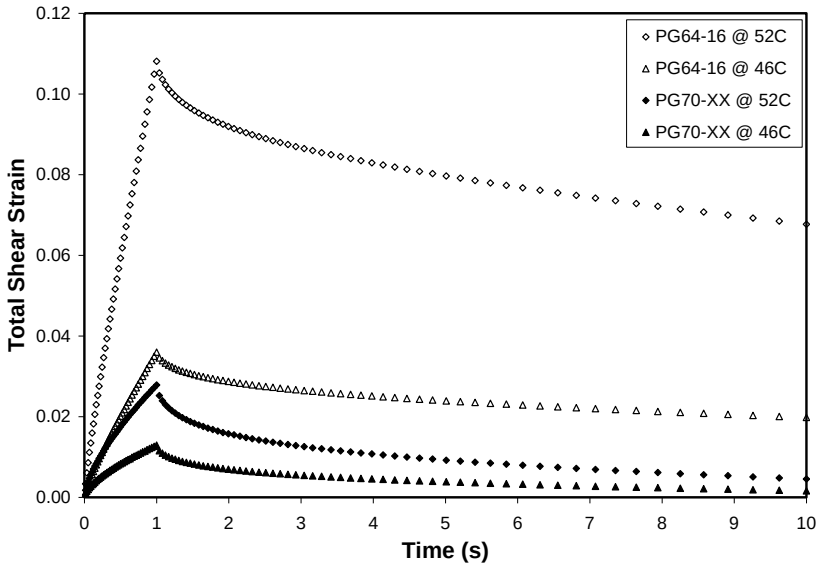

Figure 6-57. Repeated shear creep and recovery test results at 46 and 52°C (50th cycle of local binders (before Asphalt Hawaii started to supply binder).

Although the binder properties are important, for modeling with the MEPDG with pseudo level 1 data (i.e., using the locally developed model as proposed here) they do not play a substantial role. Furthermore, as discussed in chapter 7, other factors such as the resilient

modulus of unbound materials can have a more substantive effect on the predictions. Therefore, for MEPDG use, it is recommended to use input values based on the results of this section. Using default binder characteristics is also considered acceptable.

6.7 DESIGN CONSIDERATIONS FOR COMBATING MOISTURE

One of the tasks for this project included evaluation of the use of the permeable base requirement in HDOT's existing pavement design guideline and to consider alternative solutions. This issue was studied near the beginning of the project and was reported an interim report. This section provides an overview of the findings and recommendations.

Water can enter into the pavement as surface water through cracks, joints, asphalt concrete infiltration, and groundwater from infiltrated aquifers, such as a high water table or a localized spring. The saturation of, or the presence of, water in the pavement structural section decreases the supporting strength, or load-carrying capacity, of succeeding untreated layers underlying the asphalt concrete. This results in increased deflection under traffic loads, thereby leading to structural cracking and pumping action which accelerates the fatigue failure of asphalt concrete.

Both sources of water must be considered and provisions must be made to handle both. The structural section drainage system, which is designed to handle surface water inflow, is generally separate from the subsurface drainage system that is designed to accommodate encroaching groundwater.

The discussions herein are intended only for surface water inflow and not encroaching groundwater. The estimated groundwater inflow should be determined separately by a combination of field investigations, analytical techniques and graphical methods.

Because of the problems associated with high moisture levels within the pavement structure, the pavement designer must try to keep the base, subbase, subgrade, and other susceptible paving materials from becoming saturated or being exposed to high moisture levels over long periods of time. As indicated in [1], four approaches commonly employed to control or reduce moisture problems are:

- Prevent moisture from entering the pavement system.
  - Pavement geometry – surface drainage: Adequate cross-slopes and longitudinal slopes.
  - Joint and crack sealing.
- Use materials that are less sensitive to the effects of moisture.
  - Treated bases.
- Incorporate design features to minimize moisture damage.
  - Dowel bars at transverse joints of sufficient size and spacing.
  - Widened slabs 2 ft to reduce deflections, faulting, and cracking.
  - Tied concrete shoulders to keep the lane/shoulder joint tight and reduce the potential for pumping by reducing the edge deflections.
  - Provision of a granular layer between the subgrade and stabilized base course to reduce erosion beneath the base course and to allow bottom seepage.
  - Provision of adequate side ditches with flow lines beneath the pavement structure.
  - Full-width paving to eliminate the lane/shoulder cold joint.
- Quickly remove moisture that enters the pavement system.

Typically, a combination of approaches are needed to combat the detrimental effects of moisture on the pavement structure. Salient aspects of each of these approaches are discussed in [1]. Here, the design of the drainage system to quickly remove the moisture entering the pavement system is discussed starting with the consideration of whether such a system is warranted in the first place.

Appendix A of this manual presents a literature review about the use of permeable bases in pavement structures, including materials and thicknesses. As shown in that appendix, there is no general consensus about the cost-effectiveness of the use permeable layers. As expressed in [75] "In recent years, many state highway agencies have become less enthused about subsurface pavement drainage because of concerns about construction difficulties, the need to conduct frequent maintenance of edgedrains and their outlets, and scant evidence of performance benefits that justify the costs of drainage system installation and maintenance."

The same authors also conclude "While subsurface drainage systems may still be needed to achieve good performance for some pavements built in some places, it appears to be far less true than it was twenty or more years ago that subsurface drainage systems are needed to achieve good performance for most pavements in most places" [76].

This view also appears to be reflected in the MEPDG manual of practice which indicates "The current state of the art is such that conclusive remarks regarding the effectiveness of pavement subsurface drainage or the need for subsurface drainage are not possible" [22]. Nevertheless, the MEPDG recommends that water not be allowed to accumulate within the pavement structure for reasons similar to those expressed at the beginning of this section.

Given this inconclusive evidence, it would be extremely risky to eliminate the use of subdrainage altogether. Therefore, it is recommended to adopt many of the MEPDG recommendations which are less demanding (in terms of when a permeable base is needed) than the 2002 HDOT Pavement design guidelines [13] but that still require the use of a permeable base in most heavily trafficked roads and in some roads with moderate traffic loadings. The following subsections summarize the MEPDG recommendations tailored for Hawaiian conditions.

6.7.1 Subdrainage Components

Rapid drainage of a pavement structural section can be achieved by placing a highly permeable drainage layer system under the full width of the pavement surface during initial construction. The basic components of the drainage system include [77]:

- a permeable base layer,
- a geotextile separator,
- a collector system (edgedrain structures and outlet pipes) to transport the intercepted water within the pavement structure to an outside drainage ditch, or water sewer system, and
- vents and cleanouts

The essential components of an edgedrain structure include [77]:

- a trench filled with open graded aggregate wrapped with a geotextile filter;
- a longitudinal conduit consisting of a perforated pipe.

The rest of this section concentrates on the permeable base layer component only. It should be understood that if subsurface drainage is provided, the other components have to be present as well to provide an effective drainage system.

6.7.2 Permeable Base

As indicated in [1], the primary function of the permeable base layer is to dissipate water infiltrating the pavement surface by moving it laterally towards the edge of the pavement within an *acceptable* time frame. Acceptability is measured with the time-to-drain parameter, which is the time to drain 50 percent of the drainable (free) water starting with a fully saturated material (i.e., the time it takes to go from $S = 1$ to $S = 0.50$, where S is the saturation of the material as defined in geotechnical engineering, in decimal). Based on this parameter, AASHTO rates the permeable base quality of drainage from "Excellent" to "Poor as shown in Table 6-21.

For Interstate highways and freeways, draining 50 percent of the drainable water in approximately 2 hours is desired [78]. For other roads, "good" drainage (i.e., time-to-drain < 24 hours) is acceptable. Using the computer software DRIP developed by Applied Research Associates for FHWA and available with the research version of the MEPDG software, it was determined that a material with a permeability of about 5,000 ft/day would exhibit excellent drainage for all roads with three lanes or less in one direction (a slightly higher permeability is required for a higher number of lanes in one direction all draining to the same side of the road). Figure 3-2 shows how the time-to-drain typically changes with permeability. The figure also illustrates that a permeability of 1,000 ft/day provides good drainage (< 24 hours) for the conditions cited in the figure.

Table 6-21. Quality of drainage based on the time to drain parameter.

Quality of Drainage	Water Removed Within
Excellent	2 hours
Good	1 day
Fair	1 week
Poor	1 month
Very Poor	Does not drain

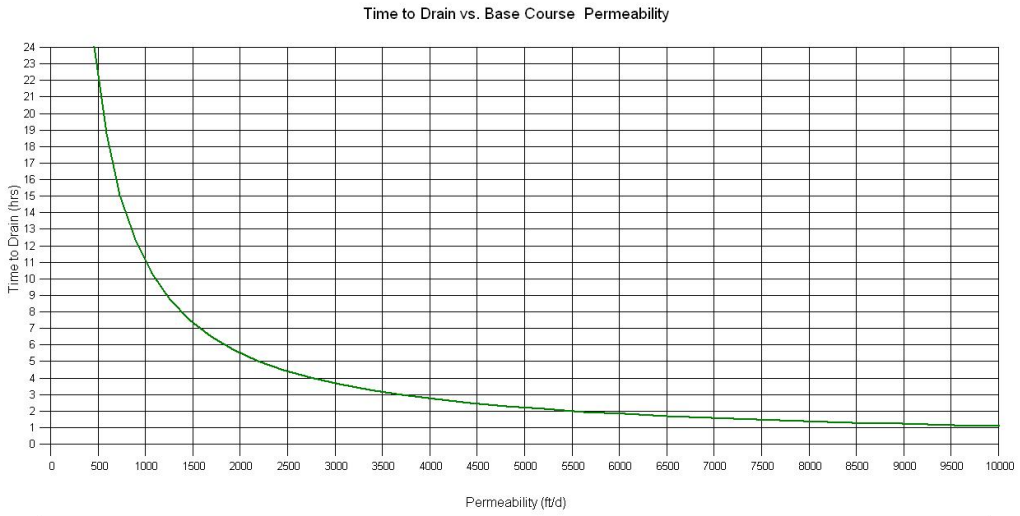

Figure 6-58. Time-to-drain versus permeable base permeability (pavement width = 36 ft, shoulder with = 10 ft, longitudinal slope = 1%, cross slope = 2 %.)

6.7.2.1 Permeable Layer Need

The 2002 HDOT pavement design manual [13] essentially requires a permeable layer for all pavements with the exception of locations with rainfall less than 5 inches or where the basement soil is free draining (a permeability greater than or equal to 100 ft/day). Other exceptions must be justified in the structural section submittal.

On the other hand, the MEPDG provides different recommendations about the need of subdrainage for four different climatic zones of the country. Much of Hawaii falls within the Wet-No freeze climatic conditions defined in the MEPDG (Annual precipitation > 508 mm (20 in) and annual freezing index $\leq$ 83 °C-days (150 °F-days)). For these conditions, the MEPDG provides the recommendations in Table 6-22. These are less restrictive than the current HDOT requirements and leave more room to the designer to determine when a permeable layer is needed.

With respect to the need for a permeable layer, it is recommended to adopt the MEPDG guidelines in reference [1]. Specifically, the use of a permeable base would be required only for higher traffic loadings (greater than 12 million 20-year design lane heavy trucks) and subgrade permeability lower than 100 ft/day (30 m/day). For intermediate traffic loadings (between 2.5 and 12 million 20-year design lane heavy trucks), the MEPDG recommendations would require the use of a permeable layer for subgrades with permeability of 10 ft/day (3 m/day) or less. With

less than 2.5 million 20-year design lane heavy trucks, subsurface drainage would not be required for subgrades with coefficients of permeability of 10 ft/day (3 ft/day) and above. These recommendations relax the requirements of the current pavement design guide but still require a drainage layer for the conditions when it can be most cost-effective. The MEPDG also indicates that additional factors must be considered in the decision for installing permeable bases over subgrades with higher permeability.

Table 6-22. MEPDG subdrainage recommendations for Wet-No freeze zone [1].

	$k_{subgrade}$ **< 10 ft/day (< 3 m/s)**	$k_{subgrade}$ **10 to 100 ft/day (3 to 30m/s)**	$k_{subgrade}$ **> 100 ft/day (> 30m/s)**
Greater than 12 million 20-years design lane heavy vehicles	R	R	F
Between 2.5 and 12 million 20-years design lane heavy vehicles	R	F	F
Less than 2.5 million 20-years design lane heavy vehicles	F	NR	NR

$k_{subgrade}$ = subgrade permeability.

R= some form of subdrainage or other design features are recommended to combat potential moisture problems.

F= Providing subdrainage is feasible. The following additional factors need to be considered in the decision making:

- Past pavement performance and experience in similar conditions if any.
- Cost differential and anticipated increase in service life through the use of various drainage alternatives
- Anticipated durability and/or erodability of paving materials

NR = subsurface drainage is not required in these conditions.

Heavy vehicles include FHWA classes 4 through 13.

When lava rock formations are present, permeable bases shall be used to properly drain pavement structures regardless of the above recommendations. Lava bedrock depends on fractures within the rock formation to drain water through the material. Fine material can fill the cracks to prevent water from penetrating freely through the rock formation. This has been observed in actual construction activities.

6.7.2.2 Permeability of the Permeable Base Material

The 2002 HDOT pavement design manual [13] states that permeability of untreated permeable base materials should be *above* 10,000 ft/day [13]. This is in contrast with the requirements in other design manuals, most notable the new Mechanistic-Empirical pavement design guide [1], which requires a *minimum* of 1,000 ft/day for treated or untreated permeable base layers. Obviously, the MEPDG recommendation is a minimum and a higher permeability is desirable. However, higher permeability is usually associated with low stability, which may also be detrimental for the pavement structure. Therefore, there are tradeoffs that need to be carefully evaluated involving the use of a drainage layer, materials used to construct it if needed, and the thickness of the layer.

The permeability of the various drainage layers should consider the long term alterations the material will undergo. It is conceivable that in the permeable base, fine material will cake around the aggregate which will eventually reduce the permeability. Also, degradation of the layer as it undergoes repeated traffic loading is possible. These and other long term effects should be considered in determining the design permeability. In this respect, it must be noted that based on an analysis in Figure 6-58, the permeability must drop below 500 ft/day for the quality of drainage to fall into the fair category. Thus, proper selection of a geotextile separator should be carried out to minimize these potential problems.

In this report, it is recommended that a permeable base be defined as an open-graded drainage layer with a minimum laboratory permeability value of 5,000 ft/day for interstate highways and primary arterials and 1,000 ft/day for all other roads. Notice that these values differ from the 10,000 ft/day required in the current 2002 HDOT guidelines [13]. However, as mentioned before, these lower permeability values are adequate from a drainage standpoint with the advantage that a more stable layer could be obtained in most situations.

6.7.2.3 Minimum Permeable Base Layer Thickness

Another issue with permeable bases is related to their thickness. The Hawaii Pavement design guide provides a methodology to calculate the thickness of permeable base needed to drain the water infiltrating the pavement from the surface but it currently requires a minimum of 6” of permeable base over a geotextile *permeable* separator on a 6” layer granular material to protect the permeable layer from infiltration of fines from the subgrade. In contrast, the design

guides of several states (e.g., CA, FL, and MO) do not use a variable thickness of the drainage layer but rather a fixed value governed by local experience and constructability issues. Layer thickness has the least effect on the "time-to-drain" parameter in a permeable base, which determines in part its effectiveness, while permeability has the greatest effect, as the time to drain decreases exponentially with an increase in permeability. Based on this, the MEPDG recommends 4 inches as an appropriate permeable base layer thickness (maximum and minimum), allowing compaction without segregation while providing an acceptable hydraulic conduit. This justification makes good engineering sense and it is practical. As indicated in the MEPDG, the main assumptions for the hydraulic design of permeable bases are [1]:

- "Water infiltrates the pavement until the permeable base is saturated.
- Excess runoff will not enter the pavement section after it is saturated.
- After the rainfall event ceases, water is drained to the side ditches or storm drains through edgedrains or by daylighting."

A thickness of 4 inches for the permeable base is adequate to satisfy those assumptions. However, selection of an appropriate minimum thickness should also depend on the material used for constructing the permeable layer. Untreated permeable bases (UPB) with gradations in accordance with Section 306 of the Hawaii Standard Specifications for Roads and Bridge Construction should be constructed with a thickness of 6 inches to accommodate the large aggregate sizes. For other materials with maximum aggregate sizes of 1 inch, a thickness of 4 inches is recommended.

The previous practice of fixing the subbase to a thickness of 6 inches and designing a drainage layer to absorb as much water as it can infiltrate the pavement surface is discourage since the additional permeable material may lead to stability problems and not much benefit is obtained in terms of time-to-drain.

6.7.2.4 Permeable Base Material

The permeable layer could be asphalt-treated, cement-treated, or untreated, depending on structural requirements.

The 2005 Hawaii Standard Specifications for Road and Bridge Construction [79] require a gradation for the coarse fraction of *untreated* permeable bases to have 100% passing the 2-in

sieve and between 75 and 100% passing the 1.5-inch sieve. For untreated permeable bases, the use of a filler material with 100% passing the ½-inch sieve is also required [79]. Based on this and the information in Appendix A, it is seen that Hawaii uses one of the coarser gradations since the filler changes the gradation only in the upper part of the permeable layer, which may explain some of the construction difficulties with permeable layers in Hawaii and may lead to low stability values as well. In fact, Appendix SS in the MEPDG [1] states "To guarantee reasonable stability, a minimum coefficient of uniformity value, C_u, of 3.5 is required for an untreated permeable base. If this cannot be achieved, the base should be treated with either asphalt or Portland cement." It should be noted that although HDOT's gradation requirements for the coarse fraction of the permeable base material could potentially produce a $C_u > 3.5$, it does not guarantee it and it is quite possible to have lower values and consequently associated low stabilities.

As discussed in Appendix A, other states allow other gradations that provide both adequate permeability and stability. It is worth mentioning that aggregates such as 3-Fine commonly used in Hawaii as one of the HMA aggregates may fell within the gradation limits for the Wisconsin OGBC No. 1[55], one of the commonly accepted gradations for permeable bases. Therefore, it was decided to test samples of 3-Fine material from the Makakilo quarry for permeability. This same material was used in 2006 at the Honolulu Airport to pave with Densiphalt. It is permeable enough that allows the penetration of a cement slurry into the aggregate and this may also indicate its possible use in treated permeable bases. Figure 6-59 shows how the material can be laid down with a paver.)

[55] OGBC = Open Graded Base Course

Figure 6-59. Laying of asphalt treated 3-Fine material for Densiphalt at the Honolulu Airport.

A 6" diameter Sand and Gravel Permeameter (Figure 6-60) was used to obtain the permeability of 3-Fine material to assess its potential use in the construction of untreated permeable layers. This device meets the requirements listed in ASTM D 2434-68.

The permeability values observed during laboratory tests of the 3-Fine material ranged between 36,000 and 140,000 ft/day, well above the minimum values recommended by the HDOT current design guide. This indicates that the material tested is extremely permeable. The capacity of the material to allow water to pass through was so high that in most instances laboratory measurements were difficult (as illustrated by the wide range of values measured) since the loss of energy (i.e. head loss) between the two manometers along the permeameter was very small. Thus small errors in the readings translated into large errors in permeability values. It is clear though that the permeability of the material was higher than required.

As discussed in Section 6.3.1.2.3.5, the resilient modulus of the 3-Fine material is not much lower than that of other base materials. The main point of this discussion, however, is not so much about the adequacy of the 3-Fine material for use in permeable base construction but instead in the need to allow the use of alternative materials if the proper engineering tests are performed (permeability, resilient modulus, and crushed faces). That is, if a material provides adequate permeability and its modulus can be evaluated with confidence (the modulus is used directly in M-E design) then there should be no reason from a mechanistic point of view to

restrict its use. Smaller maximum aggregate sizes may allow better compaction of the permeable base and thus reduce problems during construction.

Thus, alternative gradations composed of 100 percent crushed stone should be acceptable if testing results show that they have adequate stability and permeability of at least 5,000 ft/day for interstate and primary arterials or at least 1,000 ft/day for other highways. Table 6-23 shows gradations that provide a careful trade-off of constructability/stability and permeability. The New Jersey gradation provides satisfactory permeability for many roads (greater than 1,000 ft/day) and good stability during construction [80]. The coefficient of permeability of the AASHTO No. 67 gradation is at least 5,000 ft/day. It should be noted that what is locally known as 3-Fine aggregate usually meets the gradations requirement of the AASHTO No. 67 gradation and results in much higher permeability values as described in the previous page. The New Jersey gradation may provide a viable alternative for those cases labeled F in Table 6-22.

The thickness of the untreated permeable base layer constructed with these alternative suggested gradations should be 4 inches. As discussed before, this ensures an adequate hydraulic channel for the free flow of water and places an upper limit on the thickness of this potentially unstable layer [1].

Figure 6-60. Layout of the Sand and Gravel Permeameter with the 3-Fine material inside.

As for the separator layer between the permeable base and the subgrade, the minimum thickness recommended in the MEPDG is also 4” instead of 6” and a geotextile is not always required if the separator layer meets the filter criteria with subgrade material and the permeable base. The research team’s view is that if a permeable base layer is deemed necessary, the

geotextile is an insurance against its potential premature failure that protects the additional investment. Thus, it is recommended to continue using geotextiles to avoid contamination of the permeable base with fines.

Table 6-23. Alternative untreated permeable base gradations.

Sieve Size	Percent Passing By Weight	
	New Jersey Gradation	AASHTO No. 67
1.5”	100	
1”	95 – 100	100
0.75”		90 – 100
0.5”	60 – 80	
0.375”		20 – 55
No. 4	40 – 55	0 – 10
No. 8	5 – 25	0 – 5
No. 16	0 – 8	
No. 50	0 – 5	

6.8 COEFFICIENT OF THERMAL EXPANSION OF LOCAL PCC MIXES

The coefficient of thermal expansion (CTE) of Portland Cement Concrete (PCC) mixes plays a fundamental role in the mechanistic-empirical design of PCC pavements. As indicated before, no data was available for calibration of the MEPDG for PCC pavements. Nevertheless, much of the information analyzed for flexible pavements such as the traffic loading characterization and the subgrade and unbound material properties are useful for their analyses. Thus, it was considered important to determine some additional parameters that will facilitate the implementation of the MEPDG for PCC pavements in the future. Since strength characteristics of PCC (from which stiffness can be estimated) are relatively well understood, efforts were directed at estimating the CTE because of its important effect on PCC faulting, which appears to be the distress that has triggered rehabilitations of PCC pavements in the recent past. Appendix B provides the details of this effort. Only a brief description of the study is presented here.

The primary objective of the study was to determine CTE values of PCC mixes used in Hawaiian pavements. A secondary objective was to study the effect of curing time on the CTE.

To achieve these objectives, 45 concrete specimens were prepared onsite at three Hawaiian concrete companies using local basaltic aggregates. For each site, 15 replicate test specimens (five sets of three) were cured in a 100% humidity room for 3, 7, 14, 28, and 56 days before determining their CTEs following AASHTO T-336. It was found that CTE values vary significantly with curing time. It was also observed that the CTEs at 28 days computed in this study, ranging from 6.1×10^{-6}/°F to 6.6×10^{-6}/°F (11.0×10^{-6}/°C to 11.9×10^{-6}/°C), differ significantly from the value recommended in the MEPDG Manual of Practice for concrete specimens with basaltic rock as a constituent (5.2×10^{-6}/°F or 9.4×10^{-6}/°C), which can lead to designs with overestimated performance. The variation caused by curing time is similar in magnitude to the variation caused by the use of different mixes for a giving curing time. Thus, the study results support the need to establish a standard curing time when determining an appropriate CTE for design. Furthermore, use of a non-representative default value can have a higher effect than that produced by differences between mixes or curing times, which highlights the importance of performing research to establish local CTE values. Based on the results, it is recommended to use the CTE obtained after 28 days of curing for design.

CHAPTER 7. MEPDG CALIBRATION FOR NEW HMA PAVEMENT SECTIONS

7.1 INTRODUCTION

This chapter describes the efforts to calibrate the MEPDG for flexible pavements. It attempts to integrate and use much of the information described and analyzed in previous chapters, i.e.: traffic loading, material characterization, and pavement condition. Calibration of the MEPDG for PCC pavements was not attempted because of the lack of appropriate historical distress information. Furthermore, even for flexible pavements calibration had to be limited to new pavement sections because of the limitations in the available distress information.

The chapter is organized is follows. Section 7.2 briefly describes the pavement sections used for the calibration effort. Section 7.3 describes the factors that limits the calibration in more detail. Even with the significant amount of information available, several issues had to be addressed for calibration of the MEPDG including usability of the distress information and unbound material moduli. Section 7.4 provides what in the view of the writer is a very interesting and challenging issue for use of mechanistic-empirical procedures, which is the selection of adequate unbound material moduli when non-linear effects are significant. Section 7.5 discusses the results of the calibration effort and describes a procedure to reduce the number of simulations required for calibration. Then, section 7.6 analyzes the issue of top down fatigue cracking and presents a hypothesis that may explain the widespread appearance of longitudinal fatigue cracking on Hawaii's roads. The chapter closes with a summary and other observations for use of the MEPDG.

7.2 PAVEMENT SECTIONS USED FOR CALIBRATION

The pavement structure processing tool described in chapter 2 was used with information updated by personnel from the Material Testing and Research Branch to estimate the pavement structural information for a set of routes in the State. These data, which were provided in 2012 in an excel spreadsheet, were used to identify candidate sections for calibration.

A set of sections that could be considered new sections or reconstructions were identified. This, by itself, was challenging since at present most construction work involves pavement rehabilitations. Consequently, only 29 sections were identified on that part of the network for which pavement structural information had been developed. Table 7-1 provides a summary of basic information for the sections in the calibration set. Annual Average Daily Truck Traffic (AADTT) was estimated from the Annual Average Daily Traffic (AADT) and percentage of trucks on HDOT's Road Information System (RIS) for the construction year by extrapolating backwards the historical AADT information available in the RIS. The lane distribution percentages are assumed values based on the number of lanes on the section and the analysis of section 3.7. These values differ slightly from the values recommended in section 3.7 as they are intended to represent average conditions whereas the ones suggested there are intended to be used in designs with the old design procedure.

Table 7-2 provides the vehicle class distribution for each section. These distributions were obtained from data for 2011 provided by the Planning Branch. The implicit assumption with the use of these values is that the distributions have not changed much over the years.

Table 7-3 provides the structural information. In this table, Mix III, IV, and V are standard State mixes type III, IV, and V respectively, GCB is Glassphalt Concrete Base, ACB is Asphalt Concrete Base, ATB is Asphalt Treated Base, AB is Aggregate Base, ASB is Aggregate Subbase and UPB is Untreated Permeable Base. For one of the pavement sections (section 26), the subgrade material varies after a depth of 22 in. Thus, the pavement structure was modeled with a layer of 22 in with the characteristics of that subgrade material (labeled as SB1) on top of another subgrade material. The information for section 18 (Route 50, MP 21.71-21.81) was not used for calibration as it appear to show abnormal deterioration with a pattern that resembles more reflection cracking from an old PCC pavement instead of the patterns typically observed on conventional flexible pavements.

Table 7-1. Basic information for pavement sections in the calibration set.

Section	Route	Begin MP	End MP	Construction Year	No. of Lanes (One-way)	AADTT	Lane distribution	Operational speed	Island
1	H-1	19.37	19.65	2003	3	17,551	50	20	Oahu
2	H-2	0.21	0.39	1997	2	2,004	70	50	Oahu
3	H-3	0.06	0.26	1995	2	665	70	50	Oahu
4	11	0.75	1.00	1997	3	1,299	50	45	Hawaii
5	11	6.45	6.65	1985	2	1,006	70	45	Hawaii
6	19	1.32	1.42	1988	2	1,666	70	35	Hawaii
7	19	9.80	9.90	2004	1	301	100	45	Hawaii
8	19	31.76	31.91	2002	1	585	100	55	Hawaii
9	19	32.07	32.22	2002	1	585	100	55	Hawaii
10	19	96.89	97.17	2000	1	1,240	100	55	Hawaii
11	31	0.00	0.35	2006	2	858	70	45	Maui
12	32	0.40	0.51	2000	1	390	100	25	Maui
13	311	0.00	0.50	2002	2	665	70	35	Maui
14	380	1.50	2.00	2000	2	780	70	35	Maui
15	50	0.00	0.13	1998	2	489	70	35	Kauai
16	50	15.08	15.69	2006	1	188	100	35	Kauai
17	50	18.93	19.10	2000	1	144	100	35	Kauai
18	50	21.71	21.81	2001	1	148	100	35	Kauai
19	50	25.19	25.35	1993	1	216	100	35	Kauai
20	56	8.23	8.49	2007	1	302	100	25	Kauai
21	72	14.90	15.40	1993	3	1,158	50	35	Oahu
22	83	1.86	2.11	1991	1	425	100	30	Oahu
23	83	16.09	14.19	1998	1	470	100	30	Oahu
24	83	16.22	16.30	1998	1	470	100	30	Oahu
25	83	40.24	40.44	1994	2	1,162	70	35	Oahu
26	93	9.00	9.20	1996	2	1,039	70	35	Oahu
27	95	0.60	1.00	1988	2	505	70	35	Oahu
28	95	0.60-	1.00-	1988	2	505	70	35	Oahu
29	99	16.30	16.60	1995	2	1,140	70	35	Oahu

Table 7-2. Vehicle class percentages for pavement sections in the calibration set.

Section	Route	Begin MP	End MP	Growth (%)	Vehicle Class Percentage (by volume of trucks)									
					4	5	6	7	8	9	10	11	12	13
1	H-1	19.37	19.65	0.34	3.99	83.52	4.3	0.41	1.44	5.83	0.41	0.00	0.00	0.10
2	H-2	0.21	0.39	3.89	2.96	65.63	9.81	0.00	0.56	9.85	0.00	6.98	0.00	4.21
3	H-3	0.06	0.26	5.00	4.96	62.28	11.64	1.72	3.88	14.66	0.43	0.00	0.21	0.21
4	11	0.75	1.00	0.62	5.56	75.36	6.28	1.93	2.42	8.21	0.24	0.00	0.00	0.00
5	11	6.45	6.65	2.16	4.88	73.95	9.53	0.47	4.19	6.28	0.47	0.23	0.00	0.00
6	19	1.32	1.42	0.00	4.17	59.55	7.06	0.64	3.69	24.57	0.32	0.00	0.00	0.00
7	19	9.80	9.90	0.19	19.08	26.32	13.82	1.31	5.59	29.28	1.31	0.66	0.33	2.30
8	19	31.76	31.91	2.25	4.17	59.55	7.06	0.64	3.69	24.57	0.32	0.00	0.00	0.00
9	19	32.07	32.22	2.25	4.17	59.55	7.06	0.64	3.69	24.57	0.32	0.00	0.00	0.00
10	19	96.89	97.17	4.28	4.26	79.66	4.82	0.10	2.62	8.13	0.39	0.00	0.01	0.01
11	31	0.00	0.35	3.19	11.41	66.67	9.61	0.60	5.71	4.20	1.20	0.00	0.00	0.60
12	32	0.40	0.51	-1.86	12.37	75.26	6.19	0.00	2.58	2.58	0.51	0.00	0.00	0.51
13	311	0.00	0.50	-0.3	7.17	32.67	26.69	0.80	10.36	15.14	2.39	3.19	0.00	1.59
14	380	1.50	2.00	3.11	5.26	31.93	27.02	10.88	4.03	10.18	6.49	0.00	0.00	4.21
15	50	0.00	0.13	0.51	1.55	18.04	20.1	4.12	30.93	10.31	5.67	6.19	1.03	2.06
16	50	15.08	15.69	1.04	10.07	23.02	24.46	1.44	7.19	28.06	2.88	0.72	0.00	2.16
17	50	18.93	19.10	2.44	10.07	23.02	24.46	1.44	7.19	28.06	2.88	0.72	0.00	2.16
18	50	21.71	21.81	2.44	10.07	23.02	24.46	1.44	7.19	28.06	2.88	0.72	0.00	2.16
19	50	25.19	25.35	1.31	10.45	34.57	19.33	2.28	6.51	22.10	2.19	1.41	0.00	1.16
20	56	8.23	8.49	1.50	21.34	13.39	33.47	3.77	17.15	2.09	2.51	4.50	0.84	0.84
21	72	14.90	15.40	1.24	14.62	50.94	12.74	0.94	11.32	6.14	0.94	0.00	0.00	2.36
22	83	1.86	2.11	2.65	22.89	48.95	8.42	0.26	6.32	12.10	0.80	0.00	0.00	0.26
23	83	16.09	14.19	1.32	24.78	58.26	4.24	0.22	3.57	7.81	0.45	0.00	0.00	0.67
24	83	16.22	16.30	1.32	24.78	58.26	4.24	0.22	3.57	7.81	0.45	0.00	0.00	0.67
25	83	40.24	40.44	2.05	13.58	39.43	32.38	1.57	5.22	5.74	1.04	0.00	0.00	1.04
26	93	9.00	9.20	0.90	15.84	40.17	13.49	0.29	17.60	9.68	1.17	0.00	0.00	1.76
27	95	0.60	1.00	1.25	8.15	28.83	22.73	0.74	4.38	30.88	3.96	0.00	0.00	0.33
28	95	0.60-	1.00-	1.25	8.15	28.83	22.73	0.74	4.38	30.88	3.96	0.00	0.00	0.33
29	99	16.30	16.60	0.49	26.67	31.11	17.46	2.22	9.53	6.98	1.59	0.00	0.00	4.44

Table 7-3. Pavement structural information for sections in the calibration set.

Section	Route	Begin MP	End MP	Layer Type – Thickness (in)			
				1	2	3	4
1	H-1	19.37	19.65	Mix IV – 2.5	GCB – 14.0	AB – 4.0	ASB – 12.0
2	H-2	0.21	0.39	Mix IV – 3.5	ACB – 2.5	ATB – 4.75	ASB – 14.0
3	H-3	0.06	0.26	Mix IV – 2.5	Mix III – 3.0	ATB – 6.5	ASB – 18.5
4	11	0.75	1.00	Mix IV – 1.5	ACB – 6.5	UPB – 6.0	
5	11	6.45	6.65	Mix V – 3.0	ACB – 5.0	ASB – 6.0	
6	19	1.32	1.42	Mix V – 6.0	AB – 8.0		
7	19	9.80	9.90	Mix IV – 4.0	ACB – 8.0	UPB – 6.0	ASB – 6.0
8	19	31.76	31.91	Mix IV – 3.5	ACB – 7.0	UPB – 6.0	ASB – 6.0
9	19	32.07	32.22	Mix IV – 3.5	ACB – 7.0	UPB – 6.0	ASB – 6.0
10	19	96.89	97.17	Mix IV – 3.5	ACB – 7.0	UPB – 6.0	ASB – 6.0
11	31	0.00	0.35	Mix IV – 3.5	ACB – 8.0	UPB – 6.0	ASB – 6.0
12	32	0.40	0.51	Mix IV – 3.0	ACB – 9.0	Broken Stone – 2.0	
13	311	0.00	0.50	Mix IV – 3.5	ACB – 8.0	UPB – 6.0	ASB – 6.0
14	380	1.50	2.00	Mix IV – 3.5	ACB – 8.0	UPB – 6.0	ASB – 6.0
15	50	0.00	0.13	Mix IV – 5.5	ACB – 8.0	UPB – 6.0	ASB – 6.0
16	50	15.08	15.69	Mix IV – 2.0	ACB – 12.0	ASB – 6.0	
17	50	18.93	19.10	Mix IV – 2.0	ACB – 12.0	ASB – 6.0	
18	50	21.71	21.81	Mix IV – 2.25	ACB – 7.75	ASB – 1.25	
19	50	25.19	25.35	Mix V – 1.5	ACB – 4.0	ASB – 6.0	
20	56	8.23	8.49	Mix IV – 1.5	ACB – 6.5	AB – 1.5	
21	72	14.90	15.40	Mix IV – 1.5	Mix III – 2.5	ATB – 6.5	ASB – 18.5
22	83	1.86	2.11	Mix V – 3.5	ACB – 6.0	ASB – 18.5	
23	83	16.09	14.19	Mix IV – 4.0	GCB – 6.0	AB – 6.0	ASB – 20.0
24	83	16.22	16.30	Mix IV – 4.0	GCB – 6.0	AB – 6.0	ASB – 20.0
25	83	40.24	40.44	Mix IV – 4.0	ACB – 9.0	UPB – 10.0	ASB – 6.0
26	93	9.00	9.20	Mix IV – 4.0	ACB – 9.0	SB1 – 22.0	
27	95	0.60	1.00	Mix V – 2.5	ACB – 5.0	ASB – 6.0	
28	95	0.60-	1.00-	Mix V – 2.5	ACB – 5.0	ASB – 6.0	
29	99	16.30	16.60	Mix IV – 3.0	ACB – 12.0		

7.3 CALIBRATION LIMITATIONS

As described in chapter 4, significant effort was directed towards the processing and visualization of the existing distress information for use in PMS and the MEPDG calibration. In addition to the issues discussed in that chapter, there were some concerns about the approximate nature of how the cracking data were obtained. In fact, some inconsistencies were found in the information about cracking during this MEPDG calibration phase. In general, as shown in Figure 7-1 for those sections with information in both 2006 and 2009, the fatigue cracking in 2009 was much higher than the fatigue cracking in 2006. The 2006 data provided almost no useful information for calibration of the MEPDG. Although for a few sections a high increase in cracking in a three year period is feasible, it is simply not realistic to observe this for *all* sections. It was very suspect that not a single point was closer to a 45° line in this graph.

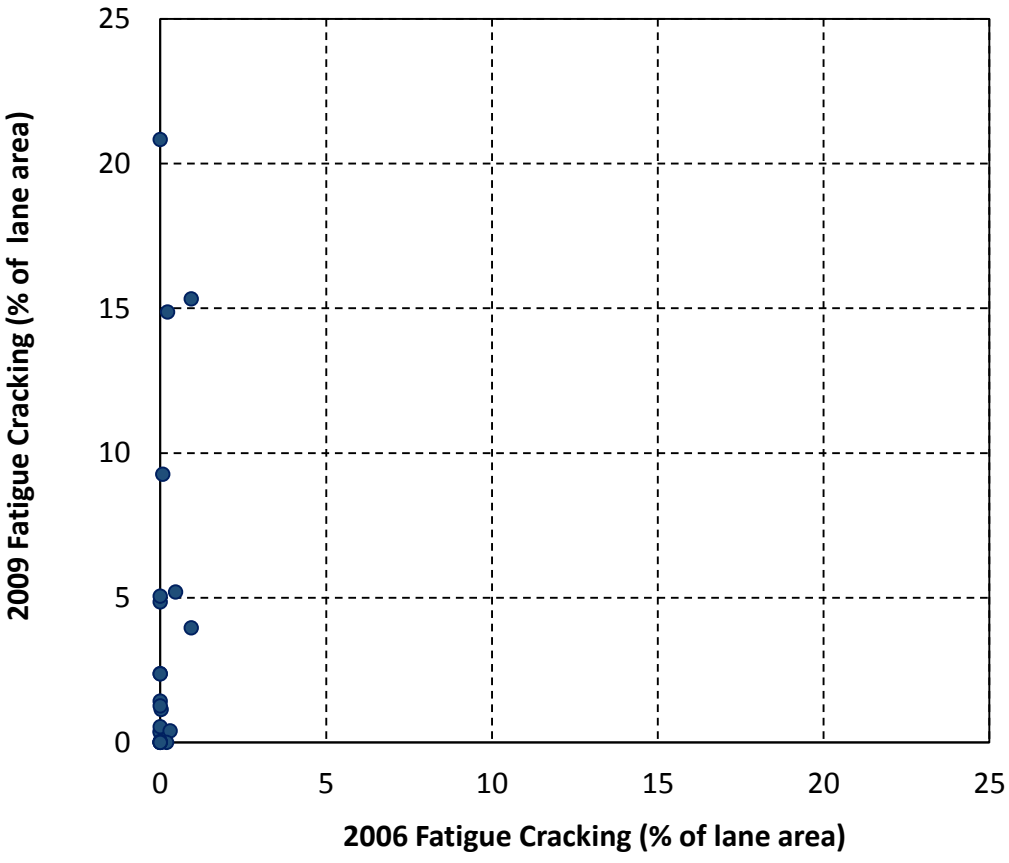

Figure 7-1. Fatigue Cracking for 2009 vs. Fatigue Cracking for 2006.

The above observation prompted a more thorough review of HDOT's RIS photo logs. It soon became evident that the cracking information, particularly for 2006, was not always reliable. This, coupled with the fact that the number of observations available was small, led the research team to perform an additional effort to collect cracking information from the historical video logs. Cracking information was collected for the rightmost lane for each of the sections selected on years ranging from 2003 to 2012. The number of sections with 2, 3, 4, 5, and 6 observations are 2, 6, 9, 3, and 8, respectively. Thus, the data set contains a total of 121 cracking observations. Although this is a significant improvement over the information originally available, it still represents only a starting point for calibration of the MEPDG since many of these observations are zero. In addition, the unbalance of the panel data set (i.e., the different number of observations per section) is generally problematic. However, as discussed below other issues are considered even more limiting at this point.

The data collection process was extremely slow and time consuming as a frame by frame analysis was performed to quantify cracking.[56] Consequently, it was possible to collect the information only for new pavement sections. Collecting cracking information for rehabilitated pavement sections following the same procedure is possible but to make such effort worthwhile for calibration of the MEPDG it is also desirable that is accompanied by FWD testing to limit the uncertainties in the calibration process.

The rightmost lane was selected for the data collection, as this is typically the lane for which pavements are designed. In most States, the rightmost lane typically carries the heaviest traffic loads. In retrospect, this may not have been the best choice in Hawaii. On multi-lane highways, it was often observed that adjacent lanes exhibited larger deterioration levels than the rightmost lane. As was shown in Table 3-25 (page 108) in section 3.7; in Hawaii, it is often the case that lanes other than the rightmost lane carry the heaviest traffic loading. Unfortunately, the analysis of the lane distribution was performed relatively late and thus there was not time to

[56] The photolog is collected with one frame for every 0.002 mi or 500 frames per mile. Thus, for example, reviewing a 0.5 mi section on given year involved the observation of 250 frames. Since the network connection speed was at times very slow, reviewing a single section for a given year sometimes was a process that took hours.

collect distress information for other lanes. Doing this in a future study may result in better calibration results.

Figure 7-2 shows an example on the H-3 freeway that displays cracking on the inside lane not existent on the rightmost lane. Figure 7-3 shows a similar example for route 11 in the Big Island, where the center lane has deterioration not seen in the other lanes. This phenomenon appears to be quite prevalent in multilane highways in Hawaii. This is illustrated in yet another example on the H-1 freeway which is not part of the calibration sample. Of course, looking at only one screenshot, as in these figures, may be misleading. However, although it was not quantified, the observation that often higher deterioration occurs in lanes other than the rightmost lane is based on what was noted over the length of the segments during the data collection.

One of the patterns that were detected during the data collection process was that most of the cracking in State roads appear as longitudinal cracks in the wheel paths. The cracking shown in Figure 7-4 is in a relatively advanced state. Figure 7-5 shows other typical situations. On the left wheel path, there is a very straight longitudinal crack. Although on a few occasions a longitudinal joint was the cause of similar cracking, in many cases this type of cracks could not be attributed to a joint since oftentimes the location of the longitudinal joint was also visible in the photographs. Notice also the position of the pickup truck in the photo with its wheel almost on top of the crack.

Figure 7-2. Example of higher deterioration on the inside lane (Route H-3, MP 0.108).

Figure 7-3. Example of center lane with more deterioration than the rightmost lane (Route 11, MP 6.478).

Figure 7-4. Example of left lane with more deterioration than the rightmost lane (Route H-1, MP- 21.027).

The crack on the right on Figure 7-5 also shows a typical situation. The crack orientation is generally longitudinal but often times it jumps from one side of the wheel path to the other. This may be simply related to heterogeneities in the pavement. In the particular example of Figure 7-5, the cracking pattern may also be affected by the traffic entering from the intersection. Note also how the crack on the right moves towards the center of the lane on the bottom of the photograph. It is not unusual to observe this on Hawaii roads. Normally, cracking between the wheel paths would be associated with environmental effects but in most of these cases it was apparent that most of the observed cracking was load associated.

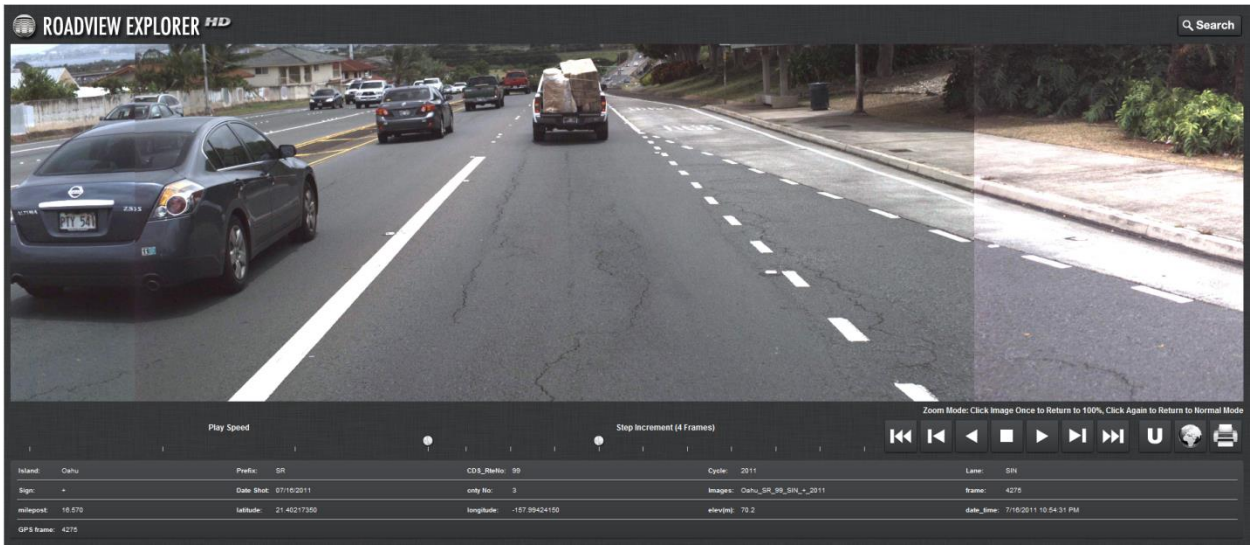

Figure 7-5. Load associated longitudinal cracking (Route 99, MP 16.570).

It was also observed that cracking rarely developed into the typical alligator cracking pattern associated with bottom up fatigue cracking. Figure 7-6 shows an example for a pavement with one of the thinnest HMA layers in the samples (about 6 inches of HMA) and Figure 7-7 shows an example for a thicker HMA layer (~11 inches). In general, on pavements with thinner HMA layers the cracking pattern is more random than on the thicker HMA layers. Still, in both situations, a more typical alligator cracking pattern such as the one shown in Figure 4-24 (page 141) was seldom observed. Instead, on pavements with thick HMA layers, as cracking progresses a second longitudinal crack may be observed on the same wheel path with occasional secondary cracking. On pavements with thinner layers but with relatively good support (as the one in Figure 7-6 apparently has) secondary transverse cracks between the two wheel paths or across lanes were also observed. It is important to note that in the example of Figure 7-6, the longitudinal cracking appeared before the transverse cracking. For someone who has not seen how this cracking developed the pattern may look like block cracking. Although the reason for the secondary transverse cracking is not known, clearly the main cause of the longitudinal cracking is load associated.

Since it is difficult to quantify areas of cracking from forward photographs, the length of longitudinal cracking that was considered to be load associated was quantified instead. Note that

this means that when both wheel paths are completely cracked, the measured length is 10,560 ft/mi. To estimate the percent of the lane area with fatigue cracking the length of cracking was conservatively multiplied by 2 ft. This is twice the value suggested in the MEPDG Manual of Practice to translate longitudinal cracking into fatigue cracking [22]. Note that when cracks start meandering, they can easily affect 2 ft of pavement. This also account for occasional small secondary transverse cracking. Although 2 ft may lead to a slight over estimation of cracking for low deterioration levels, it is a more conservative conversion. That is, with 2ft a given threshold of percent of area cracked will be achieved earlier. The best solution to this problem would be to use a technology capable of measuring the actual areas.

Figure 7-6. Fatigue cracking on Route 50, MP 25.208 in 2012.

Figure 7-7. Fatigue cracking on Route 72, MP 15.994 in 2011.

As indicated earlier, the AADTT was obtained from historical AADT information and percentage of trucks. The historical AADT was extrapolated backwards by fitting the function:

$$AADT_x = AADT_c\left(1+\frac{r}{100}\right)^{(x-c)} \qquad (7\text{-}1)$$

where:

$AADT_x$ = AADT in year x

$AADT_c$ = AADT in the construction year c, and

r = growth rate (%).

The fitting process produced the parameters $AADT_c$ and r. Figure 7-8 shows as an example the line fitted for the section between mile points 0.06 and 0.26 on the H-3 freeway. The construction year for this section is 1995. As observed in the figure, the estimated AADT for that year is 14,315 and since the percentage of trucks on this section was estimated as 4.64%, the AADTT for 1995 was estimated as 665 as reported in Table 7-1. At the same time, the growth rate for this section was estimated as r = 5%. This type of analysis was performed for each section in the sample.

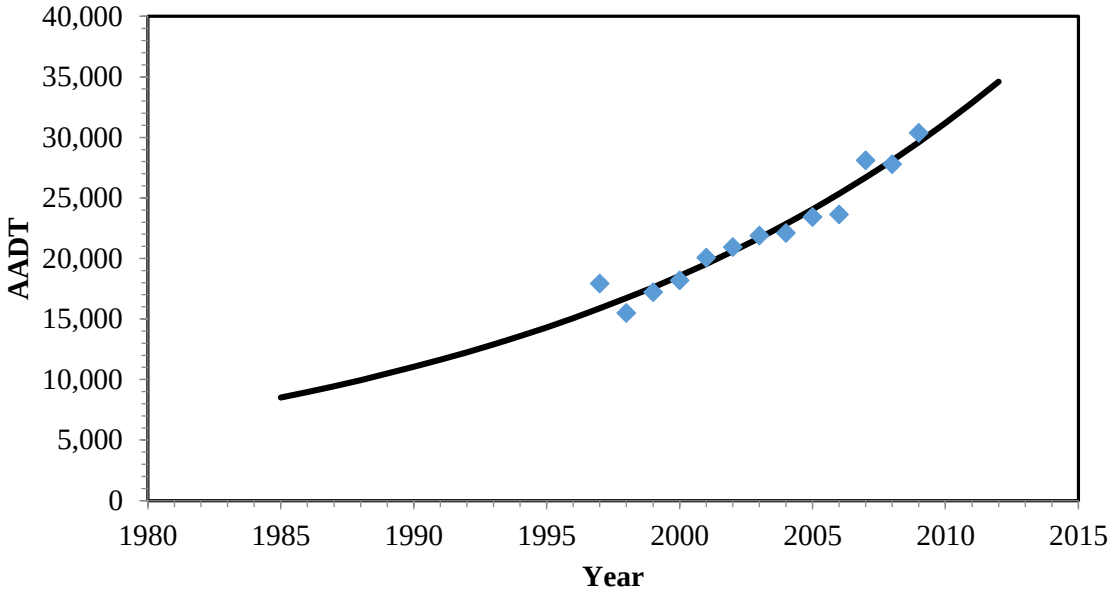

Figure 7-8. Example of the line fitting process used to predict design year AADT and growth rate.

7.4 UNBOUND MATERIAL MODULI

As discussed in Section 6.3, the laboratory resilient modulus, M_r, of unbound materials and soils are almost always stress dependent (see equation (6-23) on page 285). However, in the current version of the Pavement ME Design software the option of entering the nonlinear parameters is not available. Thus, users of the software are forced to select a single modulus value for each layer.

The user is also given the option of allowing the software to modify the M_r input value by temperature/moisture, to enter monthly representative values, or to enter an annual representative value. Entering monthly representative values may be reasonable only if an extensive Falling Weight Deflectometer study is performed, which is not currently the situation in Hawaii. Thus, either the first or the third options must be considered. The following section discusses this issue in more detail.

7.4.1 Temperature/Moisture Effects

One of the big advances of the MEPDG over other design methodologies is the integration of the Enhanced Integrated Climatic Model (EICM), which allows the computation of evolution of temperature and moisture within the pavement structure over time. The EICM makes the computation of these climatic variables and then the MEPDG uses them to predict the changes in moduli of the different layers. In regions with freezing and thawing, modeling the climatic effects on unbound materials is extremely important since it allows accounting for the dramatic changes in modulus occurring from freezing conditions, saturated conditions produced by thawing, and normal conditions. Freezing and thawing, however, have little relevance to Hawaiian conditions. For Hawaii, the changes due to precipitation are the most relevant for unbound materials.

Clearly, if the MEPDG were able to provide accurate estimates of the changes of modulus with moisture, then using the option to allow the program to modify the M_r values with temperature/moisture would be the most logical one.

The MEPDG requires entering the modulus at optimum moisture content and 100% relative compaction. This value is then modified internally to account for whether the unbound material element is in a frozen state, recovering from a frozen state, or unfrozen.

For the unfrozen state, the modulus is changed with the moisture content or more specifically with the saturation level as described in equation (6-24) on page 286. For most Hawaiian conditions, this is really the only relevant factor in the MEPDG affecting the modulus. It is important to note that for fine grained materials, for which the MEPDG uses a = -0.5934, b = 0.4, and k_m = 6.1324; the change of the modular ratio Mr_{max}/Mr_{opt} implied by equation (6-24) is $10^{0.4} \approx 2.5$. Based on the local model for fine grained soils described in section 6.3.1.2.3.1 (page 290), a modular ratio of 2 to 2.5, depending on the state of stresses, can be achieved with a reduction of moisture content of just about 2% (molding moisture contents of the samples used to develop the model were varied by at most ±2%). According to the local model, for drier soils, the increase in modulus could be even higher (as high as 6). However, predictions for moisture contents more than 2% below optimum represent extrapolations beyond the range for which the local model was developed. Thus, they should be used with caution. Furthermore, the local model was developed with different molding moisture contents as opposed to compacting specimens at optimum and letting the moisture content change to something different from optimum. Nevertheless, it provides a check of the reasonableness of the MEPDG assumptions. Without other information, use of the MEPDG assumptions seem a reasonable first approximation.

For coarse grained materials, for which the MEPDG uses a = -0.3123, b = 0.3, and k_m = 6.8157; the change of the modular ratio Mr_{max}/Mr_{opt} implied by equation (6-24) is $10^{0.3} \approx 2.0$. Unfortunately, there is no local *model* to check this assumption for these materials.

According to the MEPDG [1], the parameter b was chosen to "*conservatively*" produce the aforementioned modular ratios for fine and coarse grained materials. It is believed that by *conservatively* it is meant that the modular ratio could actually be higher, which is what the local model for fine grained soils imply. The word conservatively should be used with caution since limiting the modulus of a layer artificially may not always result in reduced distresses. For example, the predicted bottom up fatigue cracking would be increased with a lower modulus but the predicted top down fatigue cracking would tend to decrease. Depending on which distress is most prevalent, this may not be desirable.

In summary, the information available for fine grained soils supports the modeling in the MEPDG, although the MEPDG may underestimate the values for some dry of optimum conditions for fine grained soils.

The following section presents a discussion of the challenges to select reasonable values of resilient modulus at optimum water content. Before turning attention to that important topic, it is convenient to illustrate how the MEPDG internally changes the input values according to its predictions of changes in the moisture content. Such predictions are highly dependent on the prediction of the depth to the water table, which is an input into the MEPDG simulations. Very rough estimates can be obtained of the water table depths from the Soil Conservation Service Web Soil Survey site. Note, however, that these may be not be representative depending on the grade of the road with respect to where the information was obtained. Since many HDOT pavement justification reports include description of soil borings that in many cases indicate the depth of the water table or if water table was not observed to a certain depth, it would be important to perform an additional study to determine if such information is useful for mapping water table depths along state roads and to start including the information from any new study in a database.

For most of the simulations, a water table depths of 3 ft was assumed. For illustration purposes, figures for only three cases are presented below. The reasonableness of the input values will be discussed in the next section. Figure 7-9 shows the predicted granular base moduli over time for Route 83 around mile point 40. This section had a 10 inch base on top of a 6 in subbase. The resilient modulus at optimum moisture content and 100% relative compaction for the base was assumed to be 17,000 psi and the one for the subbase was assumed to be 20,000 psi. The MEPDG subdivides thick layers into sublayers. In this particular example, the 10-inch granular base was subdivided into one 2-inch sublayer (labeled GB3(8) in the figure) and two 4-inch sublayers (GB3(9) and GB3(10)), whereas the granular subbase is represented by a single sublayer (GB4(10)). As can be observed, the modulus of the granular base is about twice the input value while that of the subbase was almost halved. This is because the subbase layer is within the zone of capillary action whereas the base is not. Thus, the MEPDG predicts that the equilibrium state for the base is dry of optimum and thus the modulus is significantly higher than that at optimum (notice that the factor is the same as the modular ratio discussed earlier for coarse grained materials.) The subbase on the other hand is wet of optimum and thus its modulus

is reduced. These significant differences in the predicted moduli illustrate the importance of accurately predicting water table depths.

Figure 7-10 illustrates the predicted moduli for the different subgrade layers of the same section on Route 83. In this case, all the subgrade sublayers are wet of optimum and the modulus is thus reduced from the input value of 12,608 psi to about 7,000 psi. As seen in the last two figures, the MEPDG does not predict any significant fluctuation of the modulus over time based on the environmental conditions on this section of route 83. This is mainly a consequence of having entered a single value of water table depth for the whole year and also depends on the gradations of the materials. Inputting seasonal water table depths would result in more reasonable moduli fluctuations.

Figure 7-11 illustrates a situation where the modulus for some of the granular base sublayers transition over a relatively short period into an equilibrium situation (6 months to 1 year). Again, the predicted moduli fluctuations with climatic changes over time after the initial transition are negligible. For this section, the top sublayer is predicted to be dry of optimum and thus its modulus is again twice the input value (Mr_{opt}). On the other hand, for the other granular base sublayers the modulus is reduced to about half the input value. The reduction in modulus from the optimum for the subgrade material, illustrated in Figure 7-12, is entirely similar to the reduction predicted for the section in route 83 described above.

Figure 7-13 shows another example, this time on route 11 on the Big Island. For this location, a noticeable pattern due to climatic effects can be noted on the predicted resilient modulus of the granular base materials. Note, however, that the most significant differences apparently occur on climatic differences from year to year as opposed to seasonal changes. Still, these differences, which are at most of about 2,000 psi, are still minor compared to the predicted change from the input value of Mr_{opt} = 28,000 psi to the equilibrium value that varies between 39,500 and 41,500 psi. In this example, the modulus of the subgrade shown in Figure 7-14 is again reduced from the input value, although the reduction is not the same for all the sublayers.

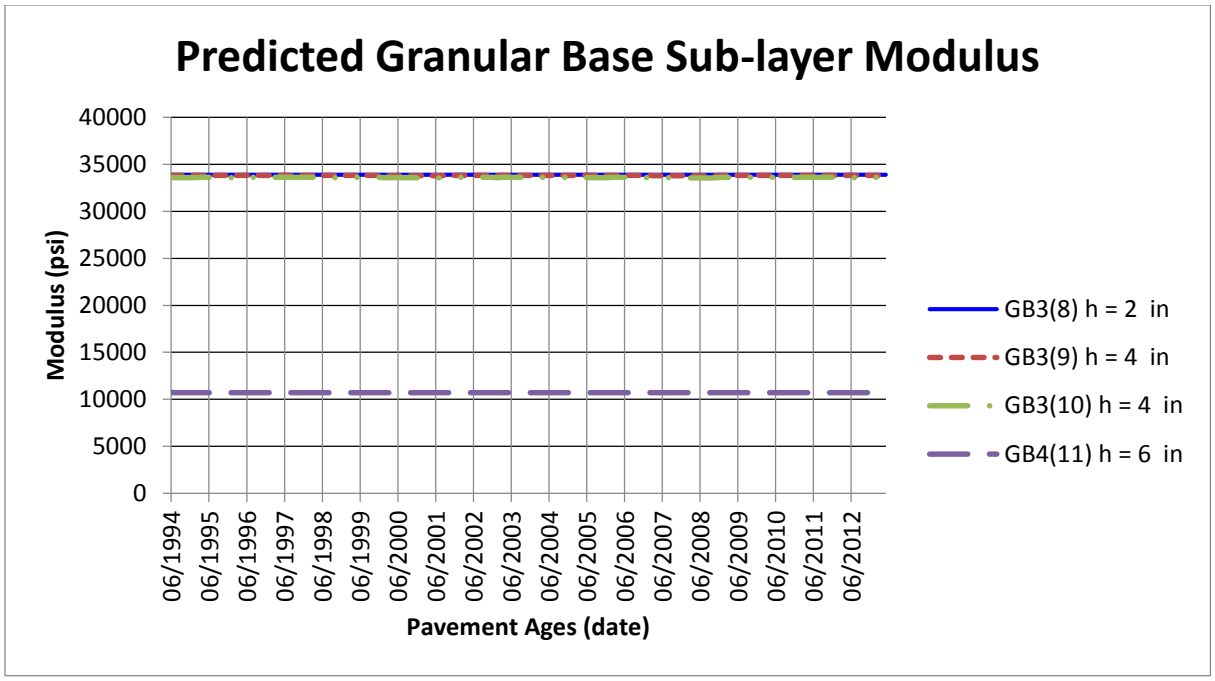

Figure 7-9. Base modulus changes in Route 83 – around MP 40. Input base modulus at optimum water content = 17,000 psi.

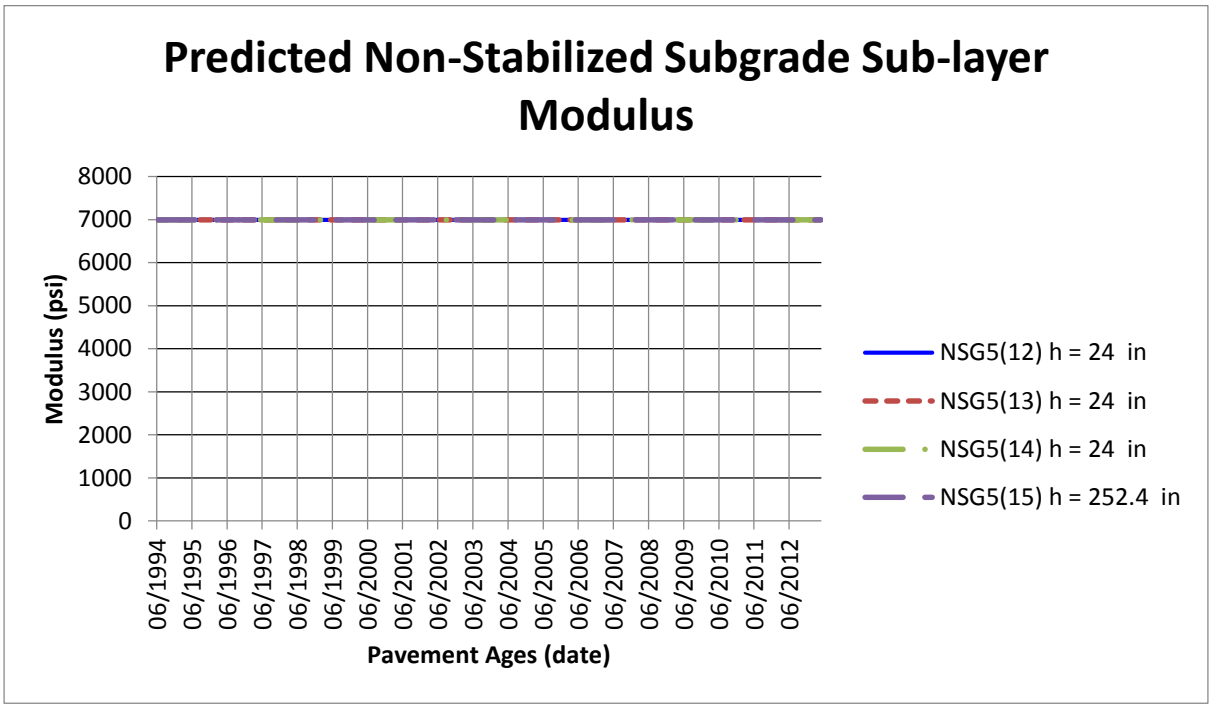

Figure 7-10. Subgrade modulus changes in Route 83 – around MP 40. Input subgrade modulus at optimum water content = 12,608 psi (assumed water table depth = 3 ft).

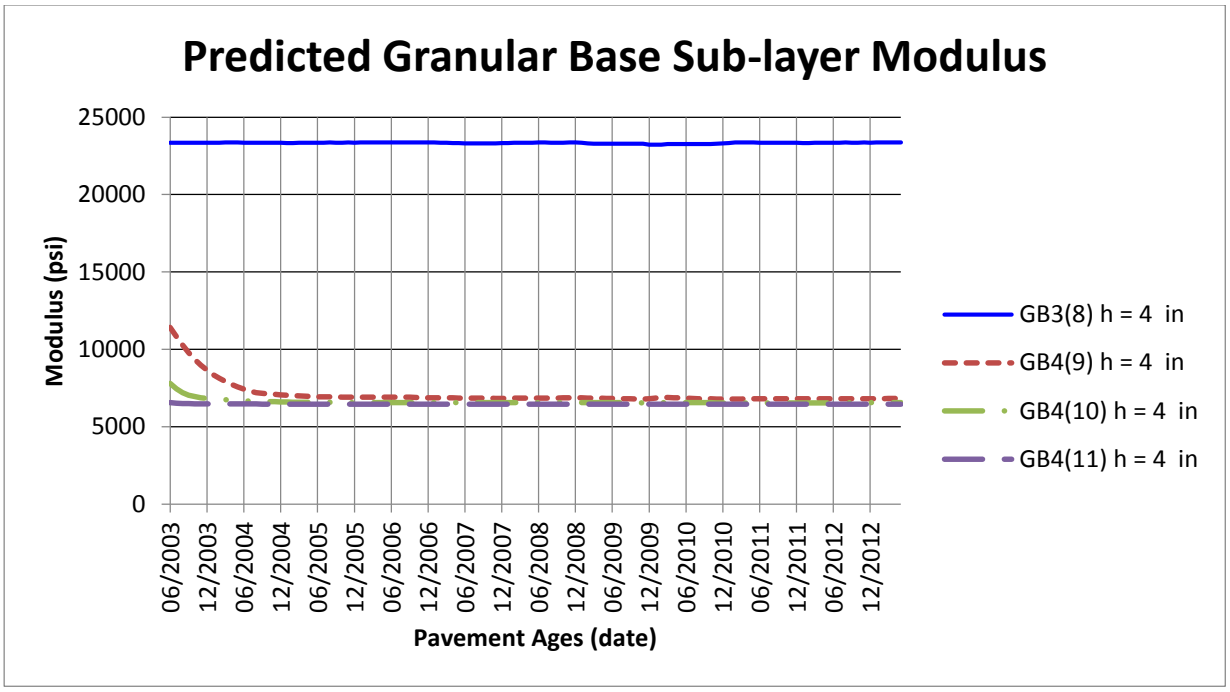

Figure 7-11. Base modulus changes in Route H1 – around MP 19.5. Input base modulus at optimum water content = 12,000 psi (assumed water table depth = 3 ft).

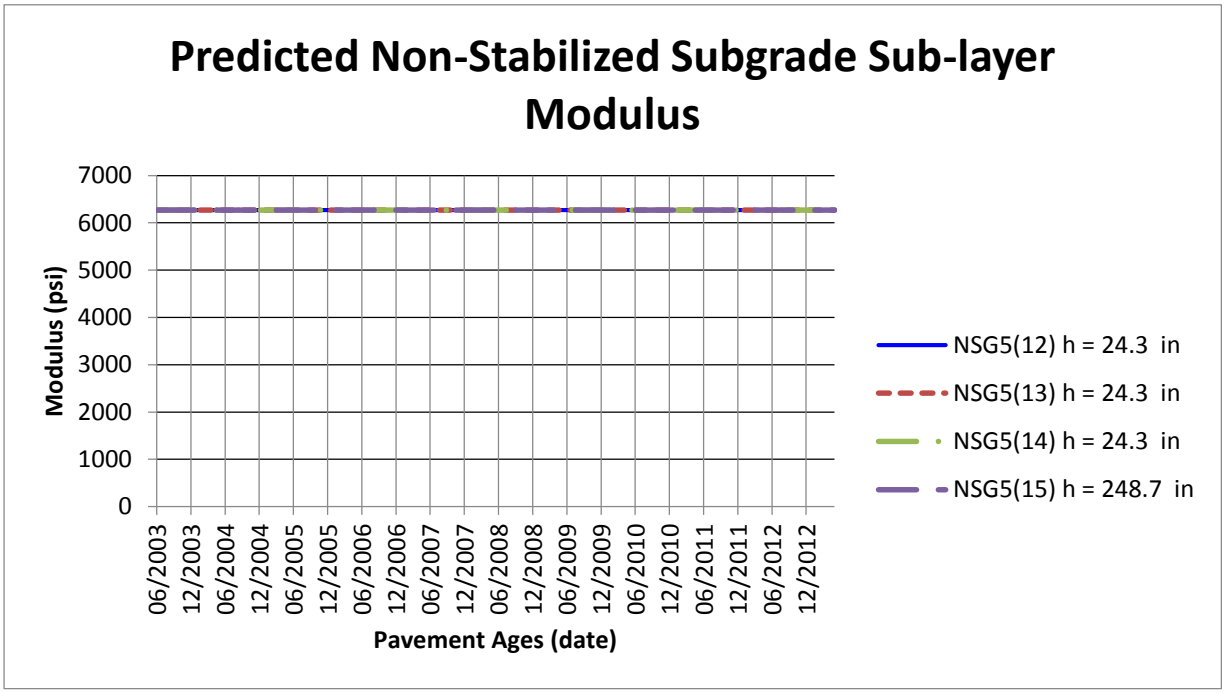

Figure 7-12. Subgrade modulus changes in Route H-1 – around MP 19.5. Input subgrade modulus at optimum water content = 11,400 psi (assumed water table depth = 3 ft).

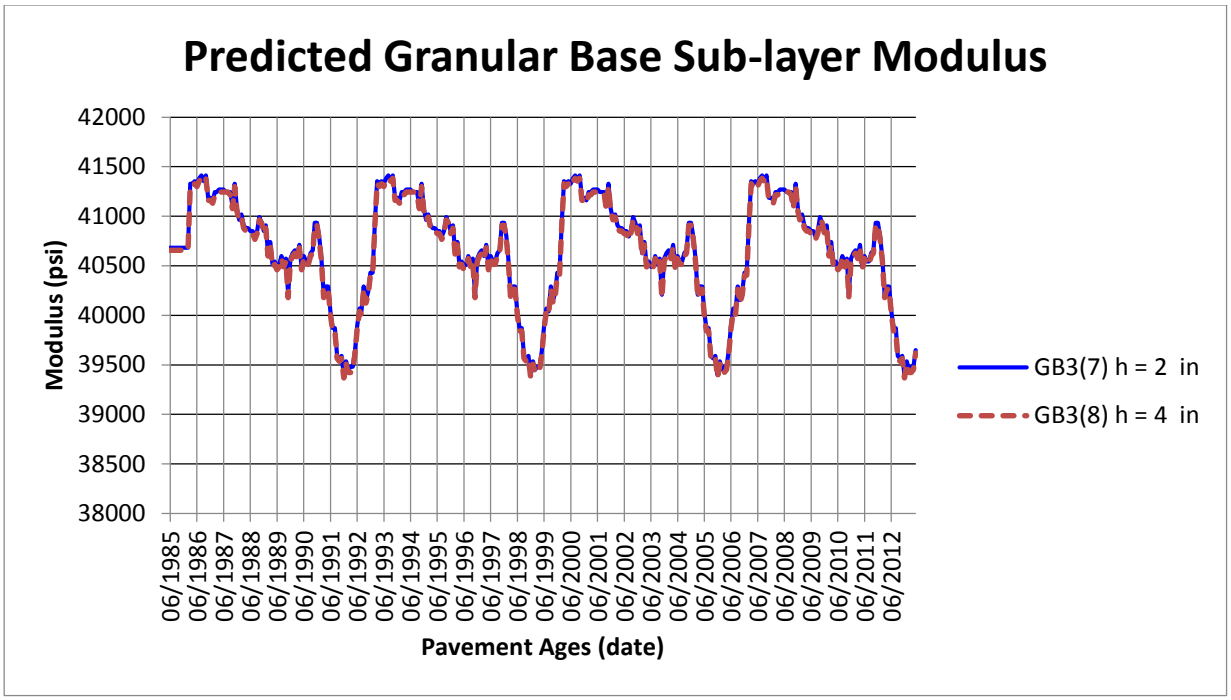

Figure 7-13. Base modulus changes in Route 11 – around MP 6.50. Input base modulus at optimum water content = 28,000 psi (assumed water table depth = 3 ft).

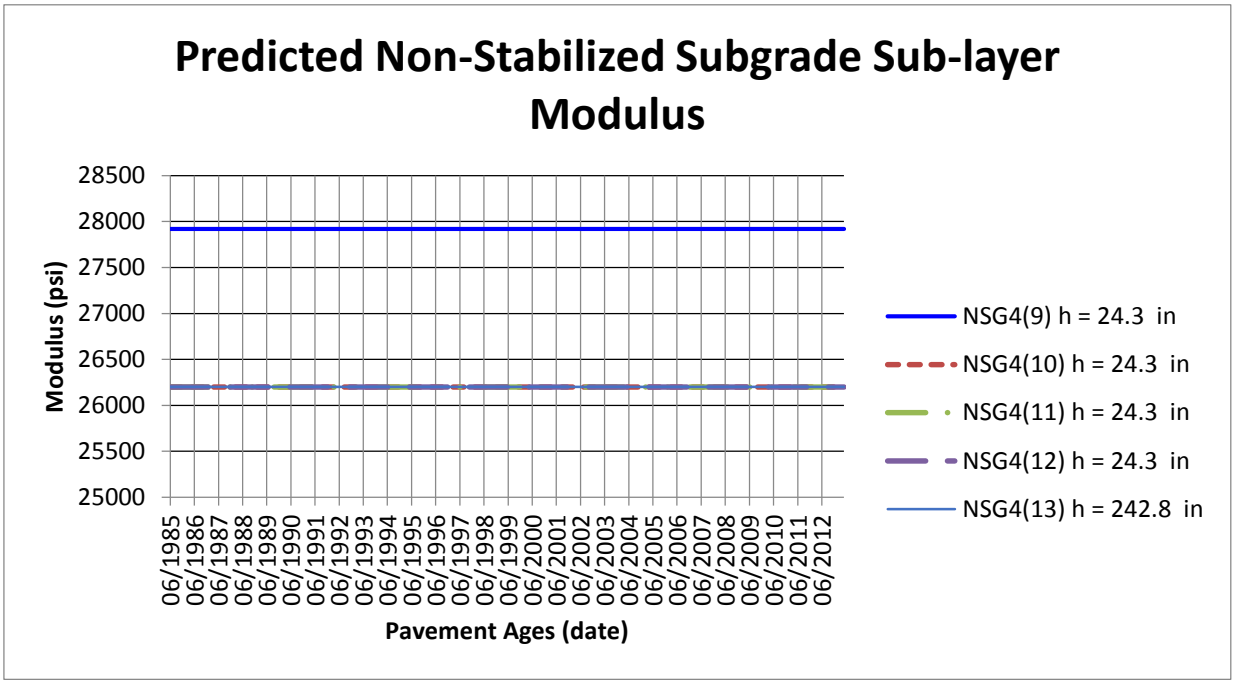

Figure 7-14. Subgrade modulus changes in Route 11 – around MP 6.50. Input subgrade modulus at optimum water content = 40,000 psi (assumed water table depth = 3 ft).

The above analysis shows that there are still some elements of concern about the moduli changes with climate. In all the examples, when the base modulus changes from one sublayer to the next it does so quite dramatically as shown in Figure 7-9 and in Figure 7-11. There are usually no transitions from a wet to a dry condition. There is currently no information to validate this but such predictions appear a bit extreme.

7.4.2 Stress Dependency

As discussed in section 6.3, laboratory determinations of resilient modulus of unbound materials always exhibit stress dependency. However, for the analysis with the MEPDG (or any other software based on linear layer elastic analysis), a single modulus is required for each layer. This presents a difficult dilemma for the designer. As discussed in the previous section, the MEPDG requires the input of the resilient modulus at optimum water content and 100% relative compaction. However, it must be realized that this value depends on the state of stresses selected.

This section analyzes the estimated variation of the resilient moduli within non-linear layers. A large number of finite element simulations with non-linear constitutive models were performed with variations in HMA layer thickness (6 and 12 inches), HMA modulus (100,000 psi, 500,000 psi, and 1,500,000 psi) and base thickness (6 and 12 inches). The above layer thicknesses encompass common situations found in the calibration data set. The three HMA moduli selected are intended to simulate high temperatures, intermediate temperatures, and low temperatures representative of Hawaiian conditions. Most of the predicted HMA moduli using the MEPDG with Hawaii climatic stations result in HMA modulus values within 100,000 psi to 1,500,000 psi. Nevertheless, modulus values as high as 2,500,000 psi are predicted for the lowest temperatures. Most of the simulations were performed with a wheel load of 9,000 lb (representing a standard axle load) applied over a circular area of 5.91 inches (as it could be applied, for example, with a Falling Weight Deflectometer, FWD). In order to illustrate the effect of the load level, a few simulations were also performed for a load of 14,000 lb. The simulations were performed using parameters for different materials evaluated in section 6.3. Poisson ratios were assumed to be 0.35, 0.35 and 0.40 for the HMA, base, and subbase, respectively. For this analysis, the values assumed were deemed appropriate but a more thorough study of Poisson ratio is probably warranted in the future. Only some illustrative examples are presented in what follows.

Figure 7-15 shows the estimated M_r's for a section loaded with a 9,000 lb load and with a 6" HMA layer, a 12" base with the characteristics of the Makakilo base material presented in page 316 (k_1 = 870, k_2 = 0.40, and k_3 = 0.82) and a 182" subgrade with k_1 = 1,821, k_2 = 0.42, and k_3 = -3.86 (these parameters were obtained with the model presented in section 6.3.1.2.3, Local Models of M_r, for a soil with w = 29%, w_{opt} = 27.4%, e = 0.93, e_{opt} = 0.93, P_{Silt} = 45%, S = 0.90, S_{opt} = 0.85, and G_s = 2.90). A total depth of 200 inches was used to minimize the boundary effects. These figures clearly show that according to the laboratory results, resilient modulus of the base material varies widely. It is also quite evident that as the modulus of the HMA increases the modulus of the base decreases. This is logical as with an increase of the HMA modulus the load is spread out over a wider area and thus the stresses on the underlying base layers are lower, which in turn results in lower base moduli. On the other hand, for the subgrade, which has a relatively large and negative k_3 and thus, it is sensitive to shear, the modulus is lower with the softer HMA layer than with the stiffer layer. Clearly, there is no such thing as a single equivalent modulus for each layer that would produce the same effects for all types of distresses that one would want to predict. Thus, any value selected would be a compromise.

Figure 7-16 illustrates a situation with a thicker HMA layer (12 inches) and a stronger subgrade with k_1 = 2,765, k_2 = 0.62, and k_3 = -3.72 corresponding to w = 13.0%, w_{opt} = 12.0%, e = 0.46, e_{opt} = 0.41, P_{Silt} = 52.0%, S = 0.75, S_{opt} = 0.77, and Gs = 2.64. The base material is the same as in the previous example. This example illustrates that the effect of a thicker layer is similar to having a stiffer layer, i.e. spreading the load over a larger area reduces the stresses on the base and result in lower base moduli. The example also shows (for a 9,000 lb load) that the approximations of linear elastic analysis (i.e., constant modulus) are much more reasonable than for thinner HMA layers.

Figure 7-17 shows the same structure used in the previous figure but subjected to a load of 14,000 lb instead of 9,000 lb. Comparison of these results with those shown in Figure 7-16 illustrate the effect of the loading level on the resilient modulus.

Figure 7-18 shows the modulus distribution for the coral base with k_1 = 1,760, k_2 = 0.18, and k_3 = 0.932 and a subgrade with k_1 = 1,821, k_2 = 0.42, and k_3 = -5.51. Once again, the lateral and vertical variations of the modulus are substantial even with a 12 in HMA layer.

Figure 7-19 shows a simulation with the 3-Fine material with k_1 = 1,230, k_2 = 0.495, and k_3 = 0.0 over the subgrade with k_1 = 1,821, k_2 = 0.42, and k_3 = -5.51 and under a 6 inch HMA layer. Compared to the response of the base material in Figure 7-15 (in both cases the HMA thickness is 6 inches), it is seen that the 3-Fine material provides a slightly softer support but the differences do not appear to be substantial. Of course, with the 3-Fine material Mr is likely to change little with changes in moisture but the conventional base material Mr would tend to increase significantly dry of optimum and decrease wet of optimum.

Figure 7-20 shows a simulation with a Foamed Asphalt (FA) base material with k_1 = 2,955, k_2 = 0.39, and k_3 = -0.14 and a subgrade with k_1 = 1,821, k_2 = 0.42, and k_3 = -5.51 for a load of 9,000 lb and HMA thickness of 12 inches. Clearly, under optimum conditions the FA base material has the potential of increasing the resilient modulus. An interesting question is how the modulus of this material would change with changes in post-compaction moisture content. There is currently no local information to address this question.

As illustrated by the previous examples, the number of combinations are endless. Notice that the figures presented show only some specific conditions (for example, a given subgrade condition, one HMA thickness, and one load level.) Many other situations were analyzed but they are not presented here. Note that in some cases, with thin HMA sections and high loads, the bulk stress can become very small in the base or even negative, which causes some instabilities in the predictions. Unfortunately, none of the models are well defined for those conditions and thus either a lower limit has to be used (as has traditionally being done) or a study of base material behavior at low stress levels need to be carried out.

In general, it can be seen that for optimum water content and maximum dry density, the resilient modulus values are substantially lower than those generally suggested for design. For example, the MEPDG manual of practice suggested values for materials classified as A-1-a, A-1-b, A-2-4, A-2-5, A-2-6, A-2-7, and A-3 are 40,000 psi, 38,000 psi, 32,000 psi, 28,000 psi, 26,000 psi, 24,000 psi, and 29,000 psi respectively [22]. These values are probably intended to represent average conditions over the service life. Note that in many of the examples above, even doubling the maximum simulated value to account for drying of the base would result in values lower (sometimes substantially lower) than those typically suggested. Of course, arbitrary picking the maximum value on the base is also questionable.

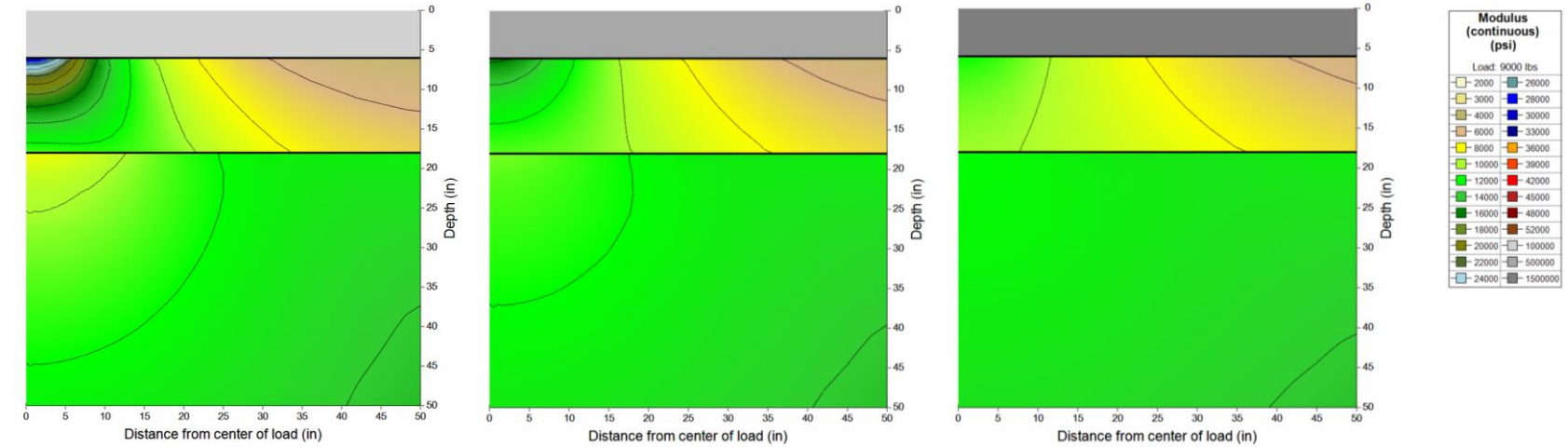

(a) |E*| = 100,000 psi (b) |E*| = 500,000 psi (c) |E*| = 1,500,000 psi

Figure 7-15. Resilient modulus distributions for an aggregate base with Makakilo characteristics (see page 316) and a weak subgrade ($w > w_{opt}$) according to the model of section 6.3.1.2.3.1. Load = 9,000 lb.

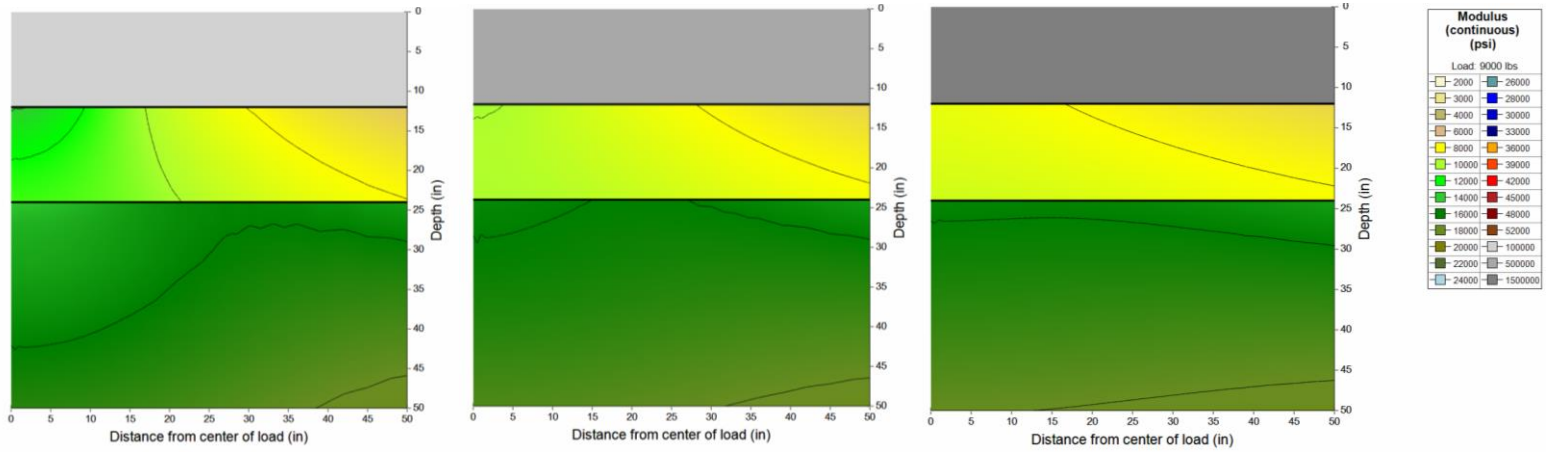

(a) |E*| = 100,000 psi (b) |E*| = 500,000 psi (c) |E*| = 1,500,000 psi

Figure 7-16. Resilient modulus distributions for an aggregate base with Makakilo characteristics (see page 316) and a stronger subgrade according to the model of section 6.3.1.2.3.1. Load = 9,000 lb.

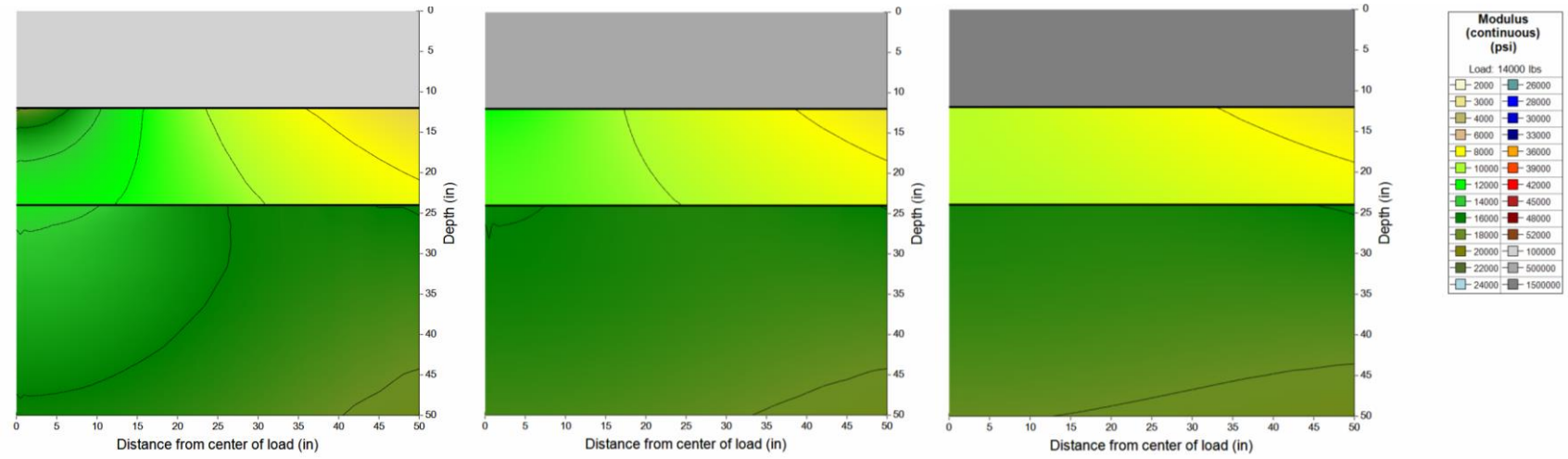

(a) |E*| = 100,000 psi (b) |E*| = 500,000 psi (c) |E*| = 1,500,000 psi

Figure 7-17. Resilient modulus distributions for an aggregate base with Makakilo characteristics (see page 316) and a stronger subgrade according to the model of section 6.3.1.2.3.1. Load = 14,000 lb.

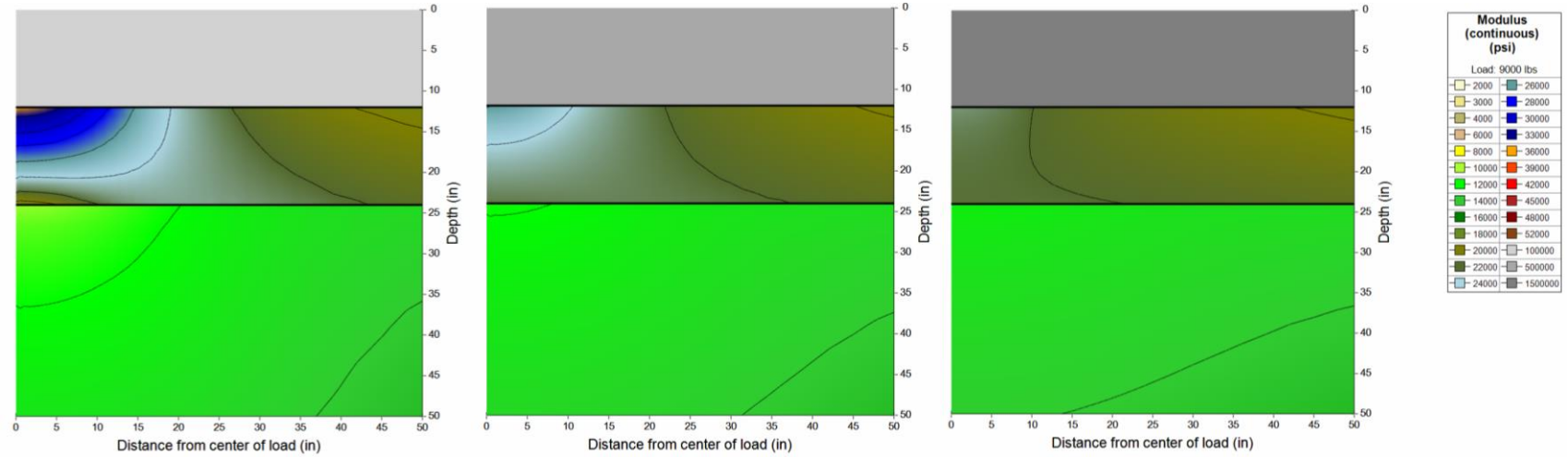

(a) |E*| = 100,000 psi (b) |E*| = 500,000 psi (c) |E*| = 1,500,000 psi

Figure 7-18. Resilient modulus distributions for a Coral Base (page 300) and weak subgrade ($w > w_{opt}$) according to the model of section 6.3.1.2.3.1. Load = 9,000 lb.

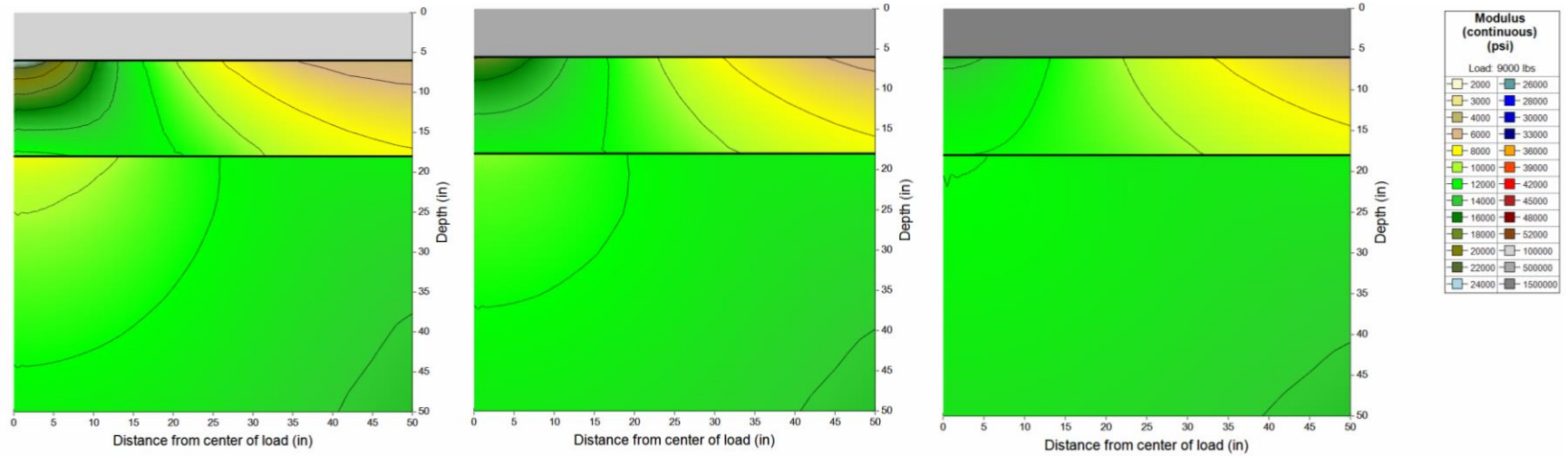

(a) |E*| = 100,000 psi (b) |E*| = 500,000 psi (c) |E*| = 1,500,000 psi

Figure 7-19. Resilient modulus distributions for the 3-Fine aggregate (see Table 6-11 on page 314) and weak subgrade ($w > w_{opt}$) according to the model of section 6.3.1.2.3.1. Load = 9,000 lb.

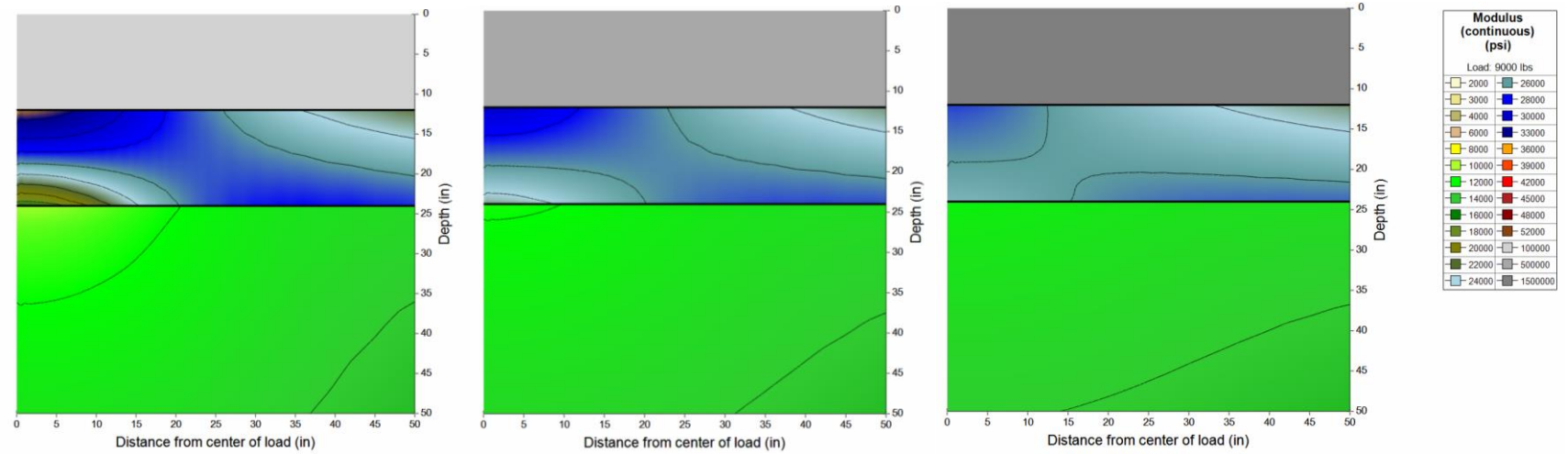

(a) |E*| = 100,000 psi (b) |E*| = 500,000 psi (c) |E*| = 1,500,000 psi

Figure 7-20. Resilient modulus distributions for the Foamed Asphalt base with k_1 = 2,955, k_2 = 0.39, and k_3 = -0.14 and a subgrade with k_1 = 1,821, k_2 = 0.42, and k_3 = -5.51. Load = 9,000 lb.

If the procedure described by Von Quintus and Killingsworth is used ([81] and [82]), the modulus under the center of the load and at a depth of ¼ of the base layer height should be selected, which result in even lower values. In fact, it is not clear to the PI why a value selected at that location would be the most representative one to use. As described in Huang [34], different stress points are appropriate depending on what the designer is interested in predicting (vertical compressive strains, tensile strains at the bottom of the HMA, tensile strains at the top of the HMA, etc.) In any case, the observation about the low M_r values created some concern about the validity of the local observations. Thus, laboratory results reported for other locations were used to analyze the predicted M_r values. Figure 7-21 shows the results of simulations performed using the resilient modulus model parameters for granular base materials used in New Jersey reported by Bennert and Maher [60]. Specifically, the values of k_1 = 992.4, k_2 = 0.594, and k_3 = -0.0285 were used. Only the simulations with a $|E^*|_{HMA}$ = 100,000 psi are presented since these result in the highest predictions of M_r for the base. Figure 7-21 shows the results side by side for a 6-inch HMA layer thickness and a 12-inch HMA layer thickness. As for the local materials, the maximum predicted M_r values are relatively low (less than 20,000 psi for the 6-inch HMA) and less than 12,000 psi for the 12-inch HMA). Of course, at ¼ depth of the base, the values are even lower. Thus, for this material, if the user were to enter a value of 12,000 psi at optimum water content and maximum dry density, the MEPDG would predict for dry of optimum conditions a resilient modulus value of at most 24,000 psi, which is again lower than the value typically suggested even though, based on the laboratory resilient modulus, the 12,000 psi input is probably an overestimate of the effective modulus. These simulations provide some independent validation to the predictions with the local materials.

Finally, it is interesting to note the work of Sagario [83], who tested RCA (Recycled Concrete Aggregate) and RAP (Reclaimed Asphalt Pavement) compacted in two cross-linked polyethylene storage tanks 4-foot high and 3-foot diameter. She used a Portable Falling Weight Deflectometer (PFWD) and a GeoGauge to measure the stiffness of the compacted material to compare the measurements with these two devices. Interestingly, the PFWD stiffnesses measured on the top layer were 16,550 psi and 15,000 psi for the RCA and RAP, respectively. These results are of the same order of magnitude as those presented earlier for granular bases with 6-inch HMA layers. It must be noted that the vertical stress at the top of the base predicted

for a 9,000-lb load on a 6-inch HMA layer with low to intermediate stiffness on top of the granular base is similar to the vertical stress applied by the PFWD (on the order of 21 psi).

Furthermore, Sagario [83] also found that the modulus for RAP almost doubled with time. This was possibly attributable to the fact that the moisture content of RAP decreased over the duration of the experiment due to a downward percolation of the water in the RAP.

7.4.3 Mr values used for calibration

The previous sections have illustrated the challenges for selecting reasonable M_r values for use in calibration of the MPEDG. Since the unbound materials response is non-linear but in the MEPDG it is assumed to be linear for simplicity, it is clear that no single modulus value would result in an equivalent strain for each load level and environmental conditions[57]. Furthermore, the location of a stress point to compute an equivalent M_r also depends on the type of distress of interest. For example, the most appropriate modulus to compute the strains for permanent deformation modeling is not the same as the one for computing bottom up fatigue cracking. Yet, a single value needs to be input into the MEPDG.

Von Quintus and Killingsworth [84] use the M_r values at one quarter of the layer depth for bases and subbases and 18 inches into the subgrade[58]. However, as reported by the same authors, the procedure was based on result from other studies. In their study, they found that in 75% of the sections the back-calculated values significantly exceeded those values measured in the laboratory, such as there is no stress state for which the two moduli are equal[59]. As illustrated in section 7.4.2, the lateral variation of the modulus can be quite substantial as well. This also affects the deflections on sensors further from the load and the overall backcalculation results.

---

[57] Recall that temperature changes result in changes of the HMA modulus. As a result of a change in the HMA modulus, for a given load magnitude the stresses transmitted to the underlying layer by the HMA would also change and thus, the modulus of the underlying unbound non-linear layer would also change.

[58] Although not explicitly specified, it is apparent that the values are computed directly underneath the load.

[59] Put another way, as they computed values of M_r corresponding to the state of stress for points at different depths in a given layer, they found that for 75% of the sections none of those M_r values matched the back-calculated value.

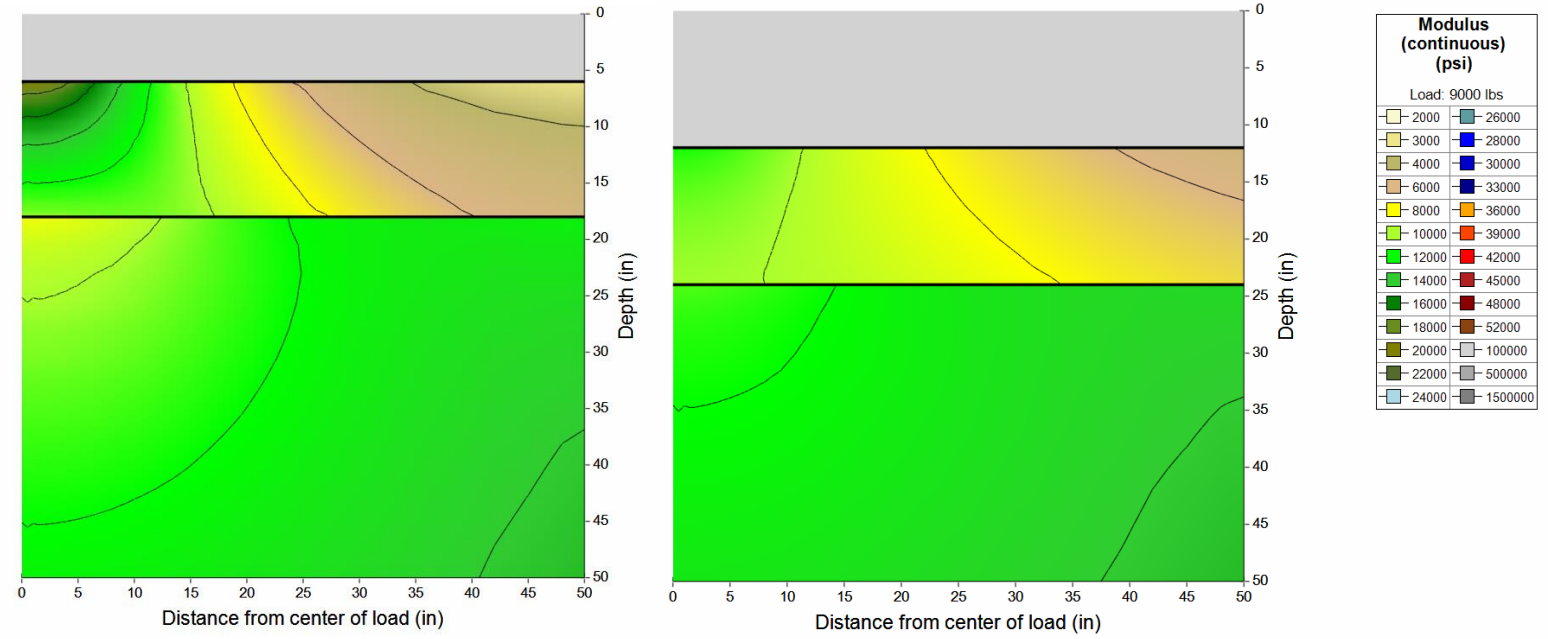

(a) h_{HMA} = 6 inches (b) h_{HMA} = 12 inches

Figure 7-21. Resilient modulus distributions of base material tested by Bennert and Maher [60] for the New Jersey (k_1 = 992.4, k_2 = 0.594, and k_3 = -0.0285 and a subgrade with k_1 = 1,821, k_2 = 0.42, and k_3 = -5.51. Load = 9,000 lb. $|E^*|_{HMA}$ = 100,000 psi.

For this study, the following simplified procedure was adopted to account for the effect of the thickness of layers above the base and for the subgrade characteristics.

For bases/subbases, a value of 12,000 psi was used for an HMA thickness of 16 inches or more, and 2,000 psi were added for each 1-inch reduction in HMA thickness. Thus, for a 10-inch HMA layer, the assumed modulus of the base is 12,000 psi + 2,000 psi/inch × (16 – 10) inch = 24,000 psi. This should produce values that are a reasonable approximation to the values corresponding to 100% compaction and optimum moisture content (in most situations, the values will be within the ranges simulated in section 7.4.2.) When a subbase was present, a 3,000 psi were added to the Mr of the subbase to account for the usually higher confinement of this layer. Notice that subbases are more likely to be affected by moisture since they are closer to the water table. Thus, the slightly higher input modulus does not necessarily result in a higher modulus than that of the base when the simulations are performed with the MEPDG. Other characteristics were obtain from the results of Rayapeddi Kumar [47].

For subgrades, the Arizona State University Soil Unit Map Application (http://nchrp923b.lab.asu.edu/index.htm) developed under NCHRP Study 9-23b [68] was utilized to estimate the resilient modulus and other characteristics. However, as observed in Section 6.3.1.2.3.3, Hawaiian soils are stiffer than the mainland counterparts with similar characteristics. Based on the analysis of that section, and for simplicity *it is recommended that the resilient modulus estimates from the NCHRP 9-23B website be increased by 100% (i.e., to multiply them by 2).*

7.5 CALIBRATION EFFORT FOR NEW PAVEMENTS

With the information described in previous sections, an effort was made to provide a first calibration of the MEPDG for new pavement segments. As discussed in Section 7.3, some of the distress data available from HDOT, particularly for 2006, were questionable. Furthermore, the historical information was not detailed enough for calibration.

Even with the limited scope of the calibration attempt, the effort was challenging as some of the input information, such as resilient moduli of unbound materials, axle load spectra for each section, or even percentage of heavy trucks on the calibration lane are only approximate.

Traffic loading inputs used for calibration for each section were assigned following the recommendations presented in section 3.4. Resilient moduli of unbound materials were assigned according to the rules described in the previous section with the option of modifying input values for temperature/moisture. HMA dynamic moduli for State Mix Type IV and Superpave mixes were entered as if they were input level 1 (i.e., pseudo-level 1), which requires entering a set of values corresponding to a set of frequency and temperature pairs. The values entered as pseudo-level 1 for these type of mixes were derived from the local model presented in Section 6.2.4.2 using the volumetrics corresponding to a mix with 5.2% binder content and 7.5% air voids. This was considered preferable than entering level 3 information. For asphalt concrete bases, inputs were at level 3 using the gradation in the HDOT specifications. The closest climatic weather station was assigned for each pavement section.

Figure 7-22 shows an example of HMA dynamic modulus, Figure 7-23 provides an example of some of the traffic inputs, and Figure 7-24 shows binder inputs required when level 1 data is input for the HMA dynamic modulus.

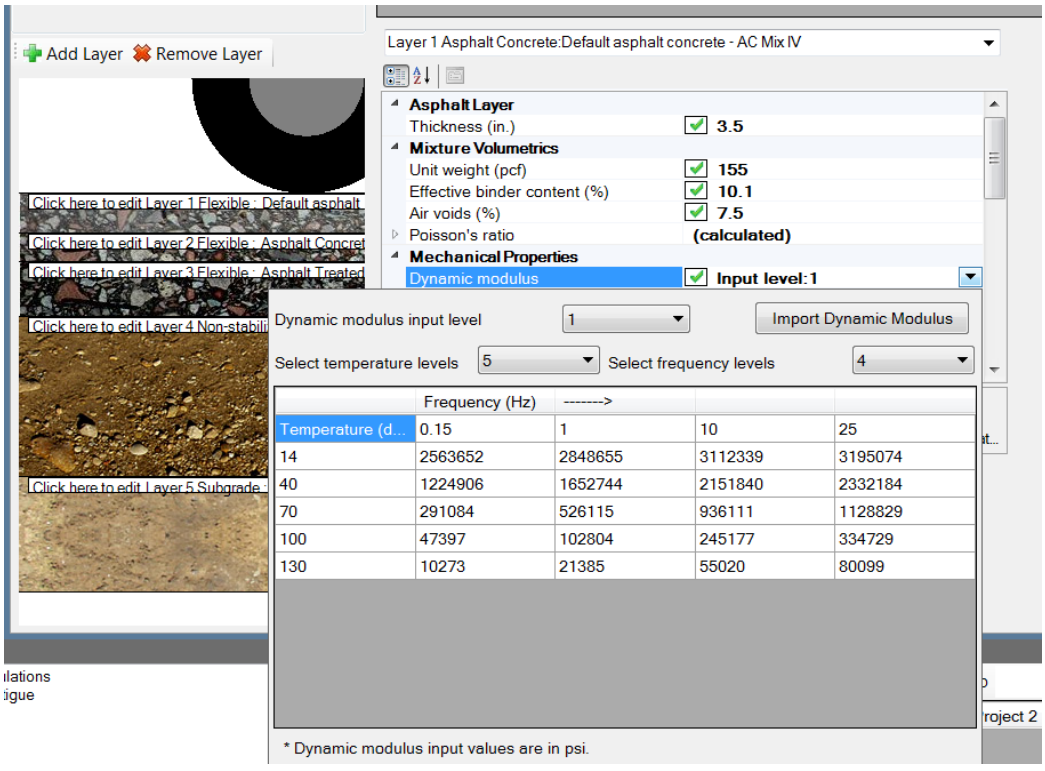

Figure 7-22. Example of HMA Dynamic Modulus input.

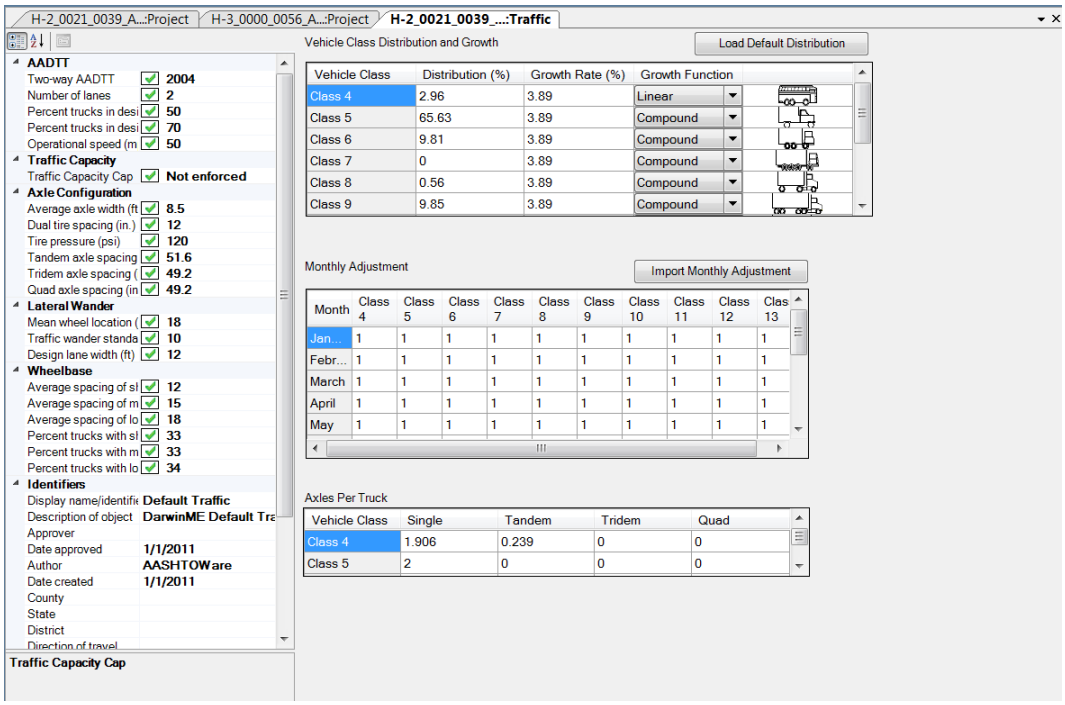

Figure 7-23. Example of Traffic Loading input.

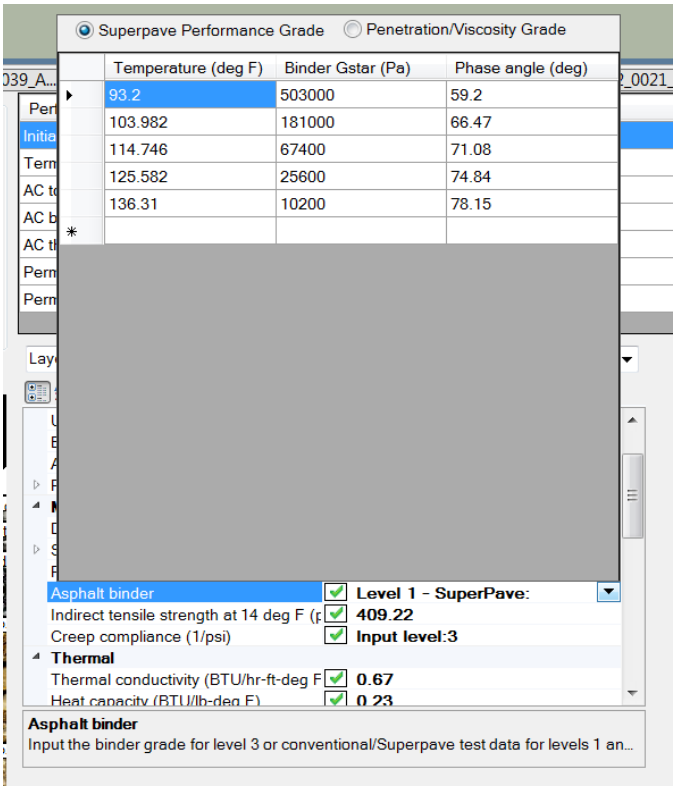

Figure 7-24. Example of Binder Dynamic Shear Modulus and Phase Angle input.

Several runs were needed to calibrate the prediction of rutting, cracking and roughness. Thermal cracking was always predicted to be zero no matter what values of the calibration parameters were used. Given the Hawaiian climate, this is quite logical. The results for the other distresses are discussed in more detail in the following subsections.

The AASHTO Guide for the Local Calibration of the Mechanistic-Empirical Pavement design Guide [31] provides a Step-by-Step procedure for local calibration. The 11 steps include:

1. Selecting a Hierarchical Input Level for Each Input Parameter
2. Developing Local Experimental Plan and Sampling Template
3. Estimating Sample Size for Specific Distress Prediction Models
4. Selecting Roadway Segments
5. Extracting and Evaluating Distress and Project Data
6. Conducting Field and Forensic Investigations
7. Assessing Local Bias: Validation of Global Calibration Values to Local Conditions, Policies, and Materials
8. Eliminating Local Bias of Distress and IRI Prediction Models
9. Assessing the Standard Error of the Estimate
10. Reducing Standard Error of the Estimate
11. Interpreting the results, deciding on Adequacy of Calibration Parameters

Unfortunately, as illustrated by the complexities and data issues discussed in previous chapters, most of the steps in the procedure could not be applied. For example, it is simply not possible to develop an experimental plan with only 29 pavement segments (step 2). Also, estimating an appropriate sample size and selecting the roadway segments are simply academic exercises for the new pavement sections since the sample was so small that all observations needed to be used. These are tasks that could be performed for rehabilitated sections but more reliable distress records are needed in these cases, particularly for cracking. Furthermore, documenting the condition of the pavement before rehabilitation complemented with FWD testing is also needed. Forensic investigations are desirable but they were beyond the scope of this project. Finally, the information was simply too limited to assess standard errors. Therefore, most of the effort was directed towards attempting to eliminate the bias and reduce the errors.

7.5.1 Rutting or Permanent Deformation

Calibration of the rutting model consists of changing one, two, or three of the parameters available in the MEPDG for this purpose until the errors and the bias in the predictions are minimized. Recall that rutting prediction in the MEPDG is based on equation (5-7), which is reproduced here for convenience:

$$\Delta_{p(HMA)} = \varepsilon_{p(HMA)} h_{HMA} = k_z \beta_{r1} 10^{k_1} T^{k_2 \beta_{r2}} n^{k_3 \beta_{r3}} \varepsilon_r h_{HMA} \quad (7\text{-}2)$$

In this equation T is the temperature, n is the number of load repetitions producing a certain strain ε_r, and h_{HMA} is the thickness of the HMA layer. k_z provides an adjustment for the effect of confinement with depth and k_1, k_2, and k_3 are the laboratory developed model parameters that were adjusted during the global calibration process. The parameters β_{r1}, β_{r2}, and β_{r3} are provided specifically for local calibration of the guide to field conditions. They provide a simple way to modify the parameters k_1, k_2, and k_3.

After several runs and together with the experiences with the development of the local permanent deformation model presented in section 6.5.1, the following calibration parameters were used: β_{r1} = 0.11, β_{r2} = 1, and β_{r3} = 1.35. In addition, since it has been reported that the MEPDG overestimates the rutting contributed by the unbound layers and it appears that in most locations with significant rutting most of the rutting originates in the HMA, the calibration parameter for unbound materials were reduced significantly, β_{s1} = 0.01. This had the effect of significantly limiting the contribution of the unbound layers to rutting. As shown in Figure 7-25, simulations with these calibration parameters provide modestly reasonable predictions and a significant improvement over the predictions obtained with the initial runs without calibration shown in Figure 7-26. Note that a slight upward bias still remains as there are more points above the equality line than below. It is important to note that a slightly better fit could have been obtained with other calibration parameter combination. However, in addition to the overall fit, the predictions for each individual section were also considered.

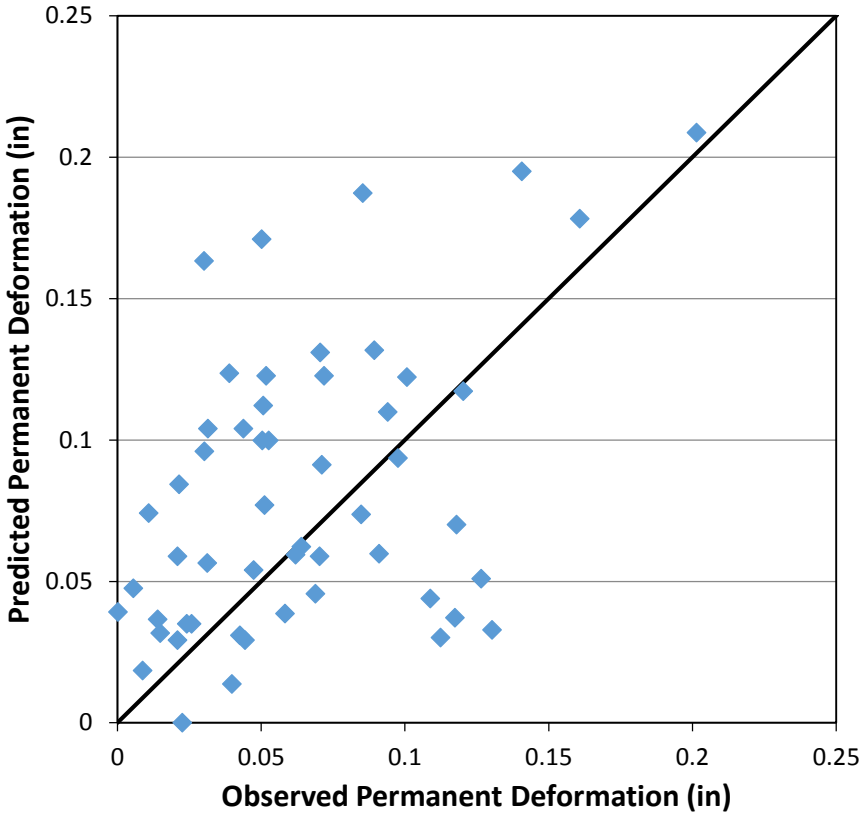

Figure 7-25. Observed vs. Predicted Permanent Deformation after calibration.

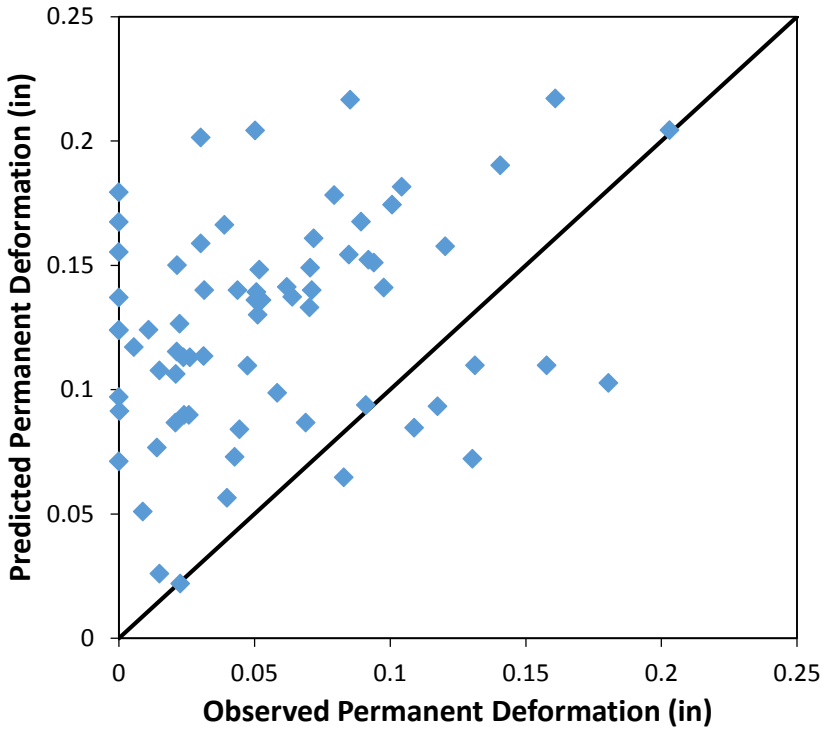

Figure 7-26. Observed vs. Predicted Permanent Deformation without calibration.

As shown in Figure 7-27, the predictions for individual sections are more or less parallel to the 45° line although in general they have a slope of less than 45°. Further reduction of the bias made these slopes worse than the ones shown here. Thus, elimination of the overall bias without consideration of individual section predictions can be dangerous since the model may not simulate well the individual section rutting performance. Considering the level of precision with which the data is currently collected (i.e., with only 3 sensors per wheelpath), the rutting predictions are modestly acceptable.

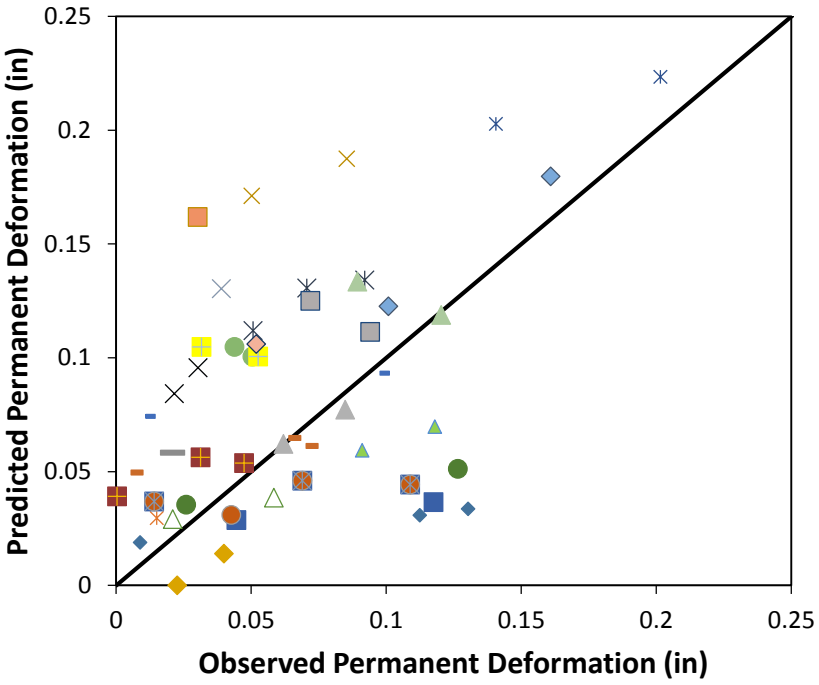

Figure 7-27. Observed vs. Predicted Permanent Deformation after calibration with different symbols for each individual pavement section.

7.5.2 Fatigue Cracking

Calibration for fatigue cracking became a large effort since analysis of the original data led to the conclusion that there were inconsistencies with them. Thus, as explained in Section 7.3, a big part of the effort was directed towards obtaining the data used for calibration from the HDOT's photo logs. Even after this effort, the attempt to reduce the bias was a difficult endeavor. It is important to note, however, that this is not a unique situation for Hawaii. Some of the same issues that will discussed with the Hawaiian data can be pointed out for other studies with more controlled data.

Specifically, consider the results shown on Figure 7-28 reproduced from Figure 3 in the article by Timm et al. [85]. The figure was created with data from the National Center of Asphalt Technology Test track. Despite this being a very well controlled full-scale experiment with known layer thicknesses, materials, traffic and environment, there is a large degree of scatter within the data with reasonably accurate predictions for only two sections. This was noted by the authors of the article who further pointed out

"The remaining sections were grossly over- or under-predicted, which would lead to inefficient designs. Unfortunately, after attempting many combinations of calibration coefficients, a better fit between measured and predicted cracking was not found. …"

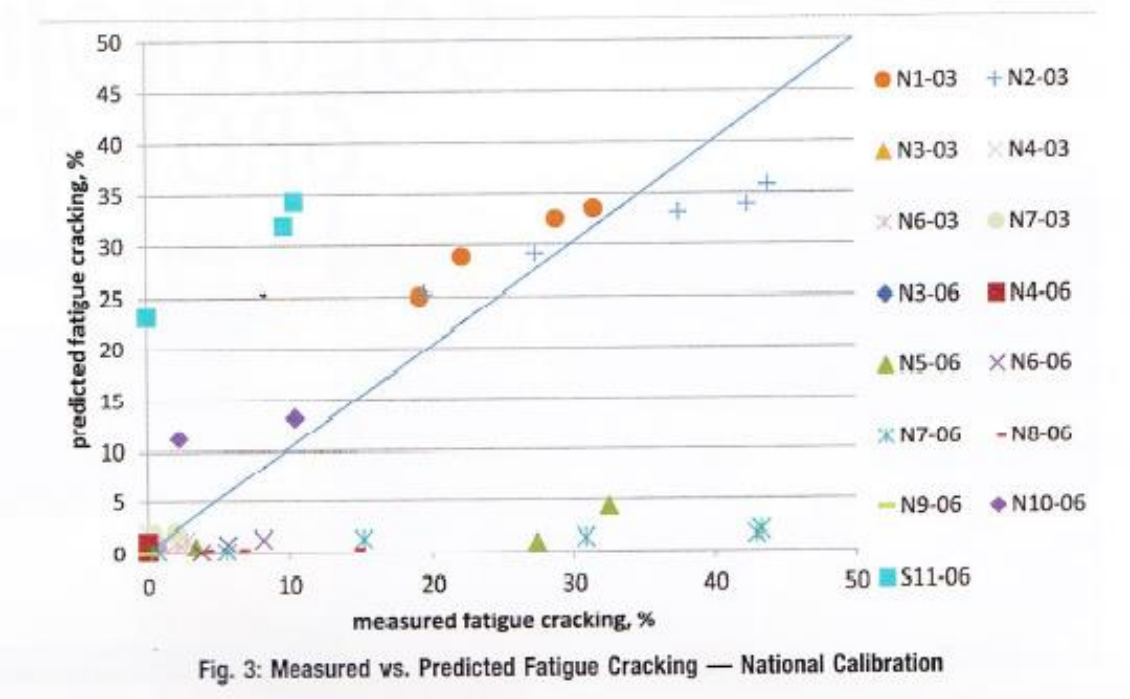

Figure 7-28. Measured vs. Predicted Fatigue Cracking with the National Calibration obtained at NCAT (Source: [85]).

It is also instructive to see results for top-down fatigue cracking from another MEPDG calibration effort. Figure 7-29 shows the results reported in [86] during the NCHRP study 1-40D. The similarity with the results in Figure 7-28 is that in both cases a high proportion of the data lie on the axes. The data lying on the x-axis in Figure 7-29 correspond to zero predictions when top-down cracking is actually observed and those on the y-axis correspond to predictions of cracking when non cracking is observed. In many cases, the differences are substantial. A cursory view of the figure may lead the casual observer to believe that the fit is actually quite good. However, a careful view indicates that this is not the case. This is because the fit is based on 312 observations whereas the trend is governed mostly by about 25 to 30 points that lie close to the 45° line. Most other points lie on the axes or on the origin. Thus, despite the large amount of data points, many of them do not provide very useful information for calibration.

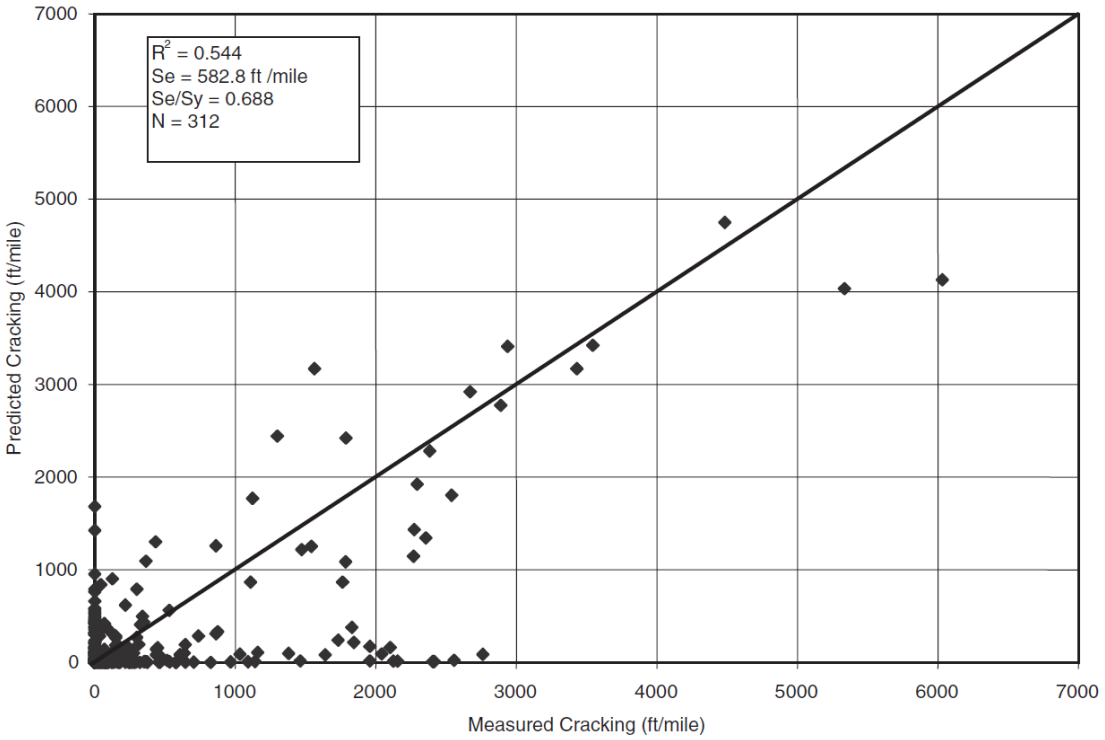

Figure 7-29. Measured vs. Predicted Top-Down Cracking results obtained during the global calibration of efforts of the NCHRP 1-40D study (Source: [86]).

The results described above are quite relevant to the Hawaii calibration effort as similar issues were encountered. The full fatigue cracking expression used in the MEPDG to relate the number of repetitions to failure to strain level was presented as equation (6-32) in Section 6.4.2. The expression is repeated below for convenience.

$$N_{f-HMA} = k_{1f}(C)(C_H)\beta_{f_1}(\varepsilon_t)^{k_{f2}\beta_{f2}}(|E^*_{HMA}|)^{k_{f3}\beta_{f3}} \quad (7\text{-}3)$$

As for the rutting model, this equation contains three parameters β_{1f}, β_{2f}, and β_{3f} provided to facilitate the local calibration. Recall that the number of repetitions to failure for each strain (or equivalently, for each load and environmental conditions on the specific pavement structure) is used with the expected number of repetitions over a time interval to estimate the increment in damage caused by the given load on the interval and then the cumulative damage is used to predict the amount of cracking using the following equation:

$$FC_{Bottom} = \frac{6{,}000}{1+e^{\left(C_1 \times C_1' + C_2 \times C_2' \log 10(D \times 100)\right)}} \times \frac{1}{60} \qquad (7\text{-}4)$$

Notice that with $C_1 = C_2 = 1$ and $C_2' = -2\ C_2'$ this expression is identical to equation (5-3) presented in Section 5.4.2.1. Recall that in this expression D is the cumulative damage and C_2' is a function of thickness (see page 206). The parameters C_1 and C_2 are also provide to facilitate the local calibration of the MEPDG.

The results of running the MEPDG for each section with the default global calibration factors (i.e., $\beta_{1f} = \beta_{2f} = \beta_{3f} = C_1 = C_2 = 1$) are presented in Figure 7-30.

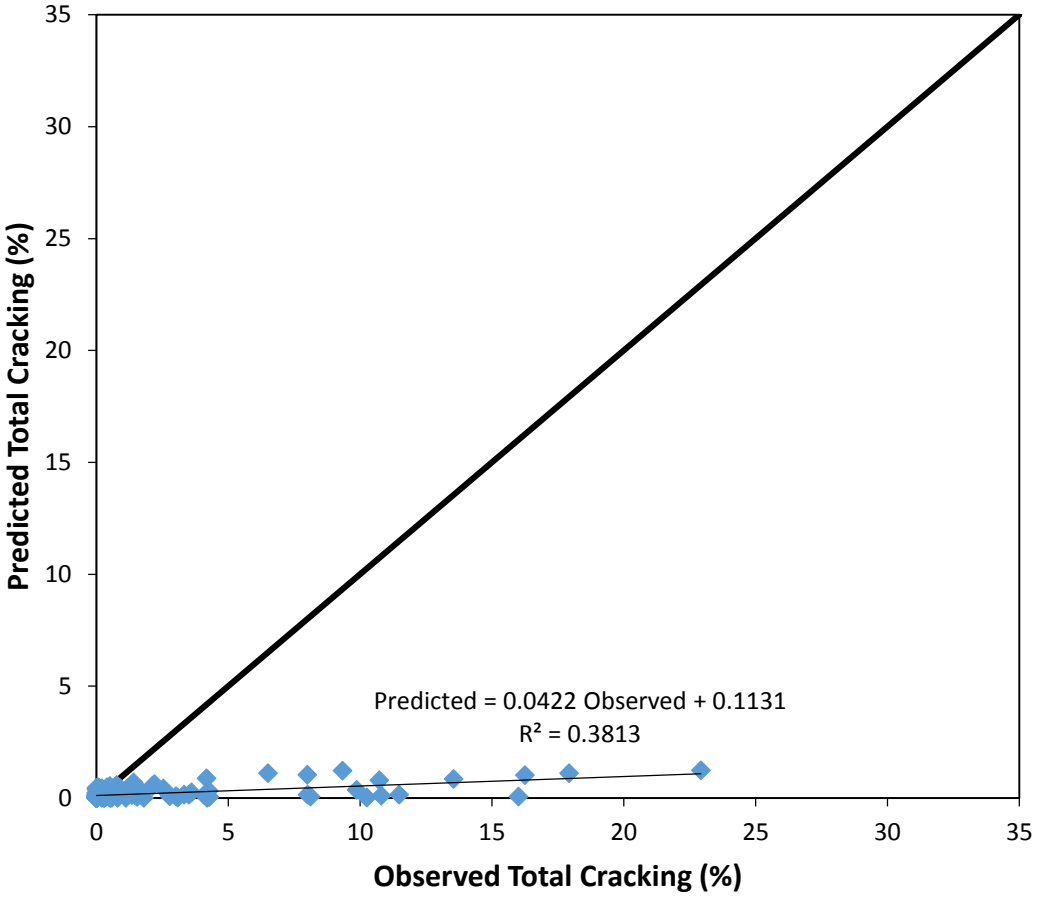

Figure 7-30. Measured vs. Predicted Fatigue Cracking results with the default global calibration factors.

Clearly, the predictions with the global calibration factors are biased downward. Actual fatigue cracking values are much larger than predicted. Thus, modification of the parameters β_{1f},

β_{2f}, β_{3f}, C_1, and C_2 was evaluated. The initial calibration efforts were performed by changing the parameters by trial and error combined with engineering judgment. The process is extremely slow and depending on the analyst intuition it may require an unnecessarily high number of runs. However, as explained below, if only parameters β_{1f}, C_1 and C_2 are considered for calibration then the process can be considerably simplified. Attempting the calibration with parameters β_{2f} and β_{3f} would be worthwhile if reliable local fatigue cracking information were available. As presented in Section 6.4, the beam fatigue data developed locally had some limitations in the compaction procedure and thus there appeared to be too much variation on the exponent of the stiffness. Nevertheless, the results provide guidance about potential calibration factors. For example, comparing the global exponent of the strain with those obtained with the local mixes suggest using values of β_{2f} of 1.56 for unmodified mixes and 1.45 for modified mixes. Given all the uncertainties in the inputs, these values have not been tried yet but should be considered in further calibration attempts.

So far, calibration has been attempted only with the use of parameters β_{1f}, C_1 and C_2. Using these three parameters, the procedure used to calibrate for fatigue cracking is relatively simple since it requires a single run for each section with $\beta_{1f} = 1$. This defines a basic level of damage for each section. Notice that the effect of the parameter β_{1f} is to simply scale the damage. For example, if β_{1f} is 0.5, N_f is halved and consequently the damaged is doubled. Thus, the damage changes inversely proportional to the value of β_{1f}. Notice that this observation is valid for every value of the strain and mix modulus. Therefore, calibration can be achieved by simply scaling the damage for each section by the same factor (which is equivalent to varying β_{1f}) and simultaneously changing the parameters C_1 and C_2 to obtain the best fit possible. This can be easily achieved with a tool such as Solver in Microsoft Excel® with the objective of minimizing the sum of the squared residuals.

Application of the above procedure resulted in $\beta_{1f} = 0.137$, $C_1 = 1.639$, and $C_2 = 2.277$. The corresponding observed vs. predicted chart is shown in Figure 7-31. Clearly, there is a significant improvement over the fit shown in Figure 7-30. Nevertheless, similarly to other studies, a significant number of observations can be observed along one of the axes (the observed axis in this case). Furthermore, the slope of the observed vs. predicted line is 0.55, which is significantly different from 1.

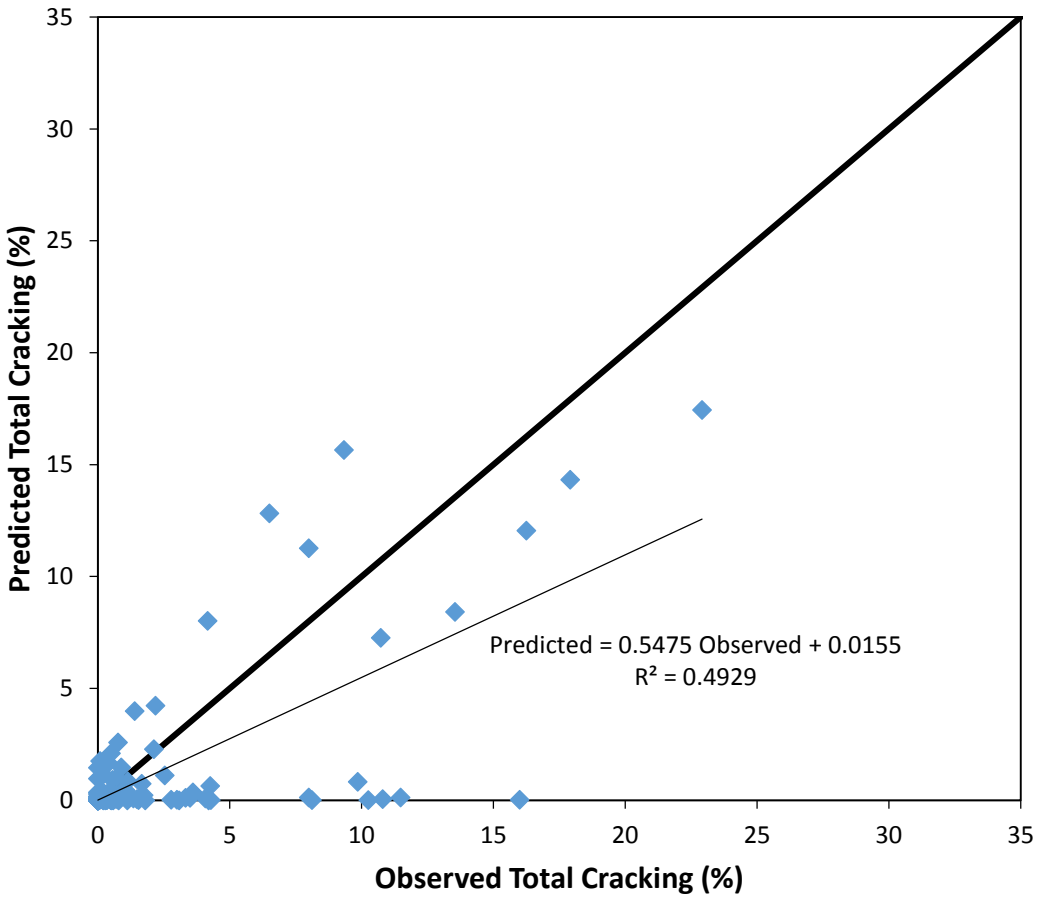

Figure 7-31. Measured vs. Predicted Fatigue Cracking results obtained with β_{1f} = 1.188, C_1 = 1.6394, and C_2 = 2.277.

One of the premises of the local calibration is to eliminate the bias, as described by step 8 on page 390. This can also be done with a modification of the procedure described earlier. All it takes is to write an equation in Excel to find the slope of the regression of the predicted values on the observed values, and then create a restriction in Solver that limits the value of the slope to a value close to 1 (say, Slope > 0.99 and Slope < 1.01; only the first restriction was needed with the Hawaiian data.) Performing this analysis resulted in in β_{1f} = 0.771, C_1 = 0.686, and C_2 = 2.506 and the Observed vs. Predicted Cracking shown in Figure 7-32. The line fitting the data is now almost indistinguishable from the 45° line. Clearly, since this is a more constrained optimization problem than the one without the constraint in the slope, the fit is reduced substantially. Although the fitting line is now at almost 45°, there is a clearly seen larger scatter of the data around this line.

In this case, eliminating the bias is perhaps questionable. Comparing the results in Figure 7-32 with those in Figure 7-31 shows that points on the x-axis or very close to it have moved by imperceptible amounts. Thus, all that is gained is a theoretical unbiasedness at the expense of significantly more scatter. The calibration has not really taken care of the real reason behind the under prediction for the observations on the x-axis. This is yet unknown here and apparently in other studies. Thus, until more data are obtained for a more robust calibration, it is recommended to use the values $\beta_{1f} = 0.13697$, $C_1 = 1.6394$, and $C_2 = 2.277$.

It is interesting to note that the observations below the equality line in Figure 7-32 correspond to thick sections and those above mostly to thinner sections. This may indicate that two different mechanism are acting or that top down cracking is the main mechanism. Top down cracking is suspected to be the mechanism in many of the sections in the sample for several reasons: 1) cracking usually appears longitudinally (which per se may be top-down or bottom-up) but it stays like that for a very long time. It rarely develops into a typical alligator cracking pattern; 2) as shown later in Section 7.6.4 (page 420), there are certain combinations of moduli that may result in minimum principal strain distributions with maximum tensile strains near the top of the surface; and 3) some of the sections are simply very thick (about 13 inches of HMA with traffic loading that is apparently not too high.)

Calibration attempts were also performed using the top-down fatigue equations. Similar issues were confronted. Since at present there is uncertainty about the mechanism of cracking, these results are not presented. However, it is recommended to perform forensic studies on different type of pavements (soon after cracking is first detected) to determine how cracking initiates so as to better guide its modeling. Confirmation of the prevalence of top-down fatigue cracking would indicate the need of further research to more accurately model this distress mechanism.

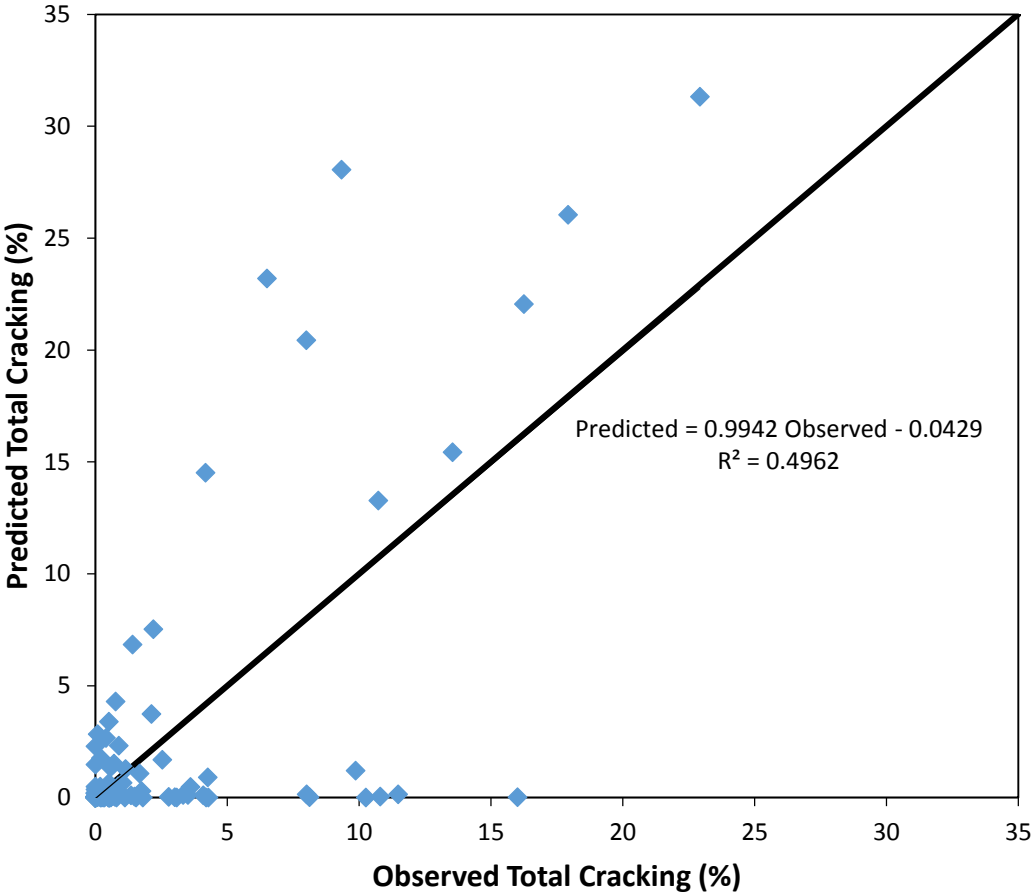

Figure 7-32. Measured vs. Predicted Fatigue Cracking results with the default global calibration factors.

7.5.3 International Roughness Index (IRI)

The MEPDG predicts IRI based on the initial IRI after construction (IRI_0), a site factor (*SF*), area of fatigue cracking as a percent of the total lane area (FC_{Total}), transverse cracking (*TC*), and rut depth (*RD*). The equation relating these variables is:

$$IRI = IRI_0 + C_1 RD + C_2 FC_{Total} + C_3 TC + C_4 SF \quad (7\text{-}5)$$

where

IRI_0 = Initial IRI after construction, in/mi,

RD = average rut depth, in,

FC_{Total} = Area of fatigue cracking (combined alligator, longitudinal, and reflection cracking in the wheel path), percent of total lane area. All load related cracks are combined on an area basis – lengths of cracks is multiplied by 1 ft to convert length into an area basis [22].

TC = Length of transverse cracking (including the reflection of transverse cracks in existing HMA pavements), ft/mi, and

SF = Site factor, computed with equation (7-6) below, and

C_1 to C_4 = model coefficients.

$$SF = Age\left[0.02003\left(PI+1\right)+0.007947\left(\mathrm{Pr}ecip+1\right)+0.000636\left(FI+1\right)\right] \qquad (7\text{-}6)$$

where

Age = Pavement age, yr.,

PI = Percent plasticity index of the soil.

FI = Average annual freezing, °F-days, and

$Precip$ = Average annual precipitation or rainfall, in.

For most Hawaiian locations, FI is zero. The default coefficients of equation (7-5) in the MEPDG are C_1 = 40.0, C_2 = 0.400, C_3 = 0.0080, and C_4 = 0.0150. Calibration of the IRI model in the MEPDG consists of essentially changing these parameters to eliminate the bias and reduce the error. In addition to the above parameters, the predictions are highly dependent on the initial value of IRI, IRI_0. Unfortunately, IRI_0 was known for only a few sections in the calibration sample.

Simulation runs with the default coefficients C_1 = 40.0, C_2 = 0.400, C_3 = 0.0080, and C_4 = 0.0150 performed after calibration of the cracking and rutting models presented earlier and with a default IRI_0 = 63 (default value in the MEPDG) resulted in the predicted vs. observed values presented in Figure 7-33. Clearly, there is a substantial under-prediction of roughness. Since the global calibration of the MEPDG was performed with national data, these results indicate that most of the new pavements/reconstructions in the State are being built with considerable more roughness than in the mainland US.

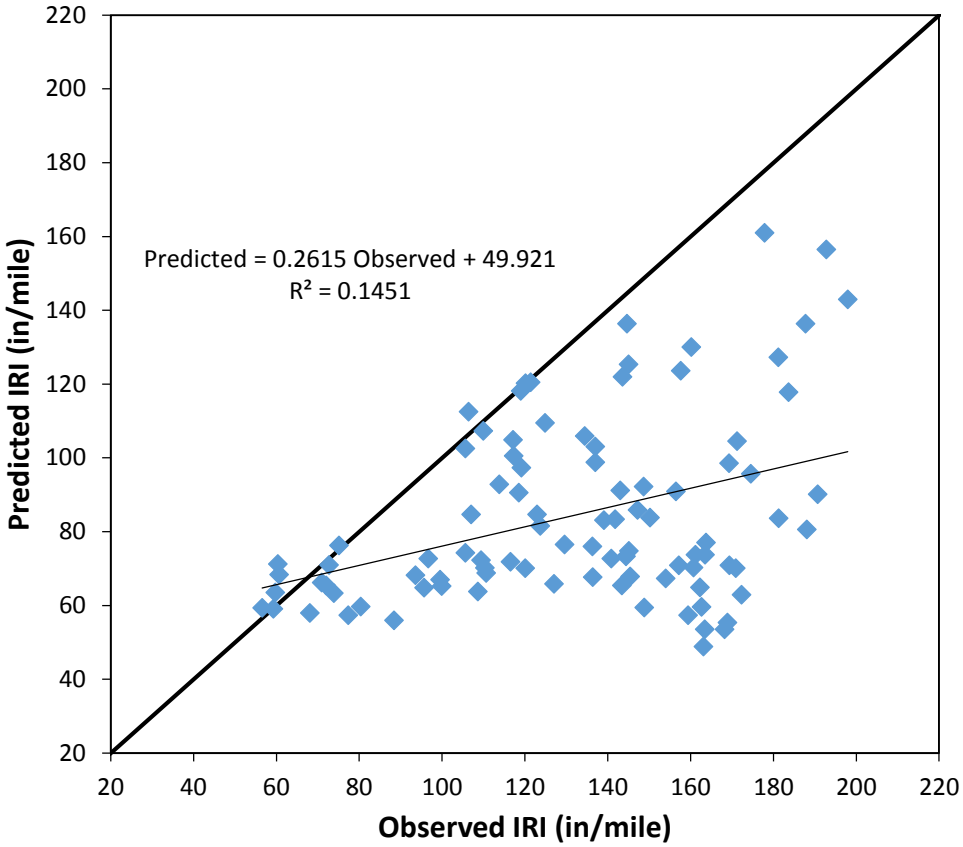

Figure 7-33. Predicted vs. Observed results with the default global calibration factors and $IRI_0 = 63$.

The large cluster of points on the lower right of Figure 7-33 also appears to indicate that there is a group of pavements that have substantially more roughness than expected (roughly 75 in/mile more than other sections). The only common feature that was identified for these sections is that in general, they are fill sections with relatively important embankments. Sections in this group included the sections for H-2 0.21-0.39 (fill section), H-3 (fill section), R83 16.09-16.19 and 16.22-16.30 (fill on bridge approach), R50 0.00-0.13 (fill section), R50 18.93-19.10 (widening), R50 21.71-21.81 (fill section), R32 0.40-0.51 (fill section between retaining walls). This may indicate that the specification, materials, and construction practices of this type of embankments may need to be evaluated further. Hawaii is rated consistently among the States with worst pavements in the nation with ratings that are based mostly on IRI. Thus, in addition to potentially improving the ride conditions for the traveling public, determining the causes of the substantially higher roughness on embankments may help improve the overall State rating.

As indicated earlier, for a few sections (actually, for eight sections), IRI_0 could be estimated from the information available on the construction year. Figure 7-34 shows the results of the simulations with the same inputs used to generate Figure 7-33 but with the actual IRI_0 value for each of the eight pavement sections. Clearly, using this additional information helps with the predictions for the sections in question.

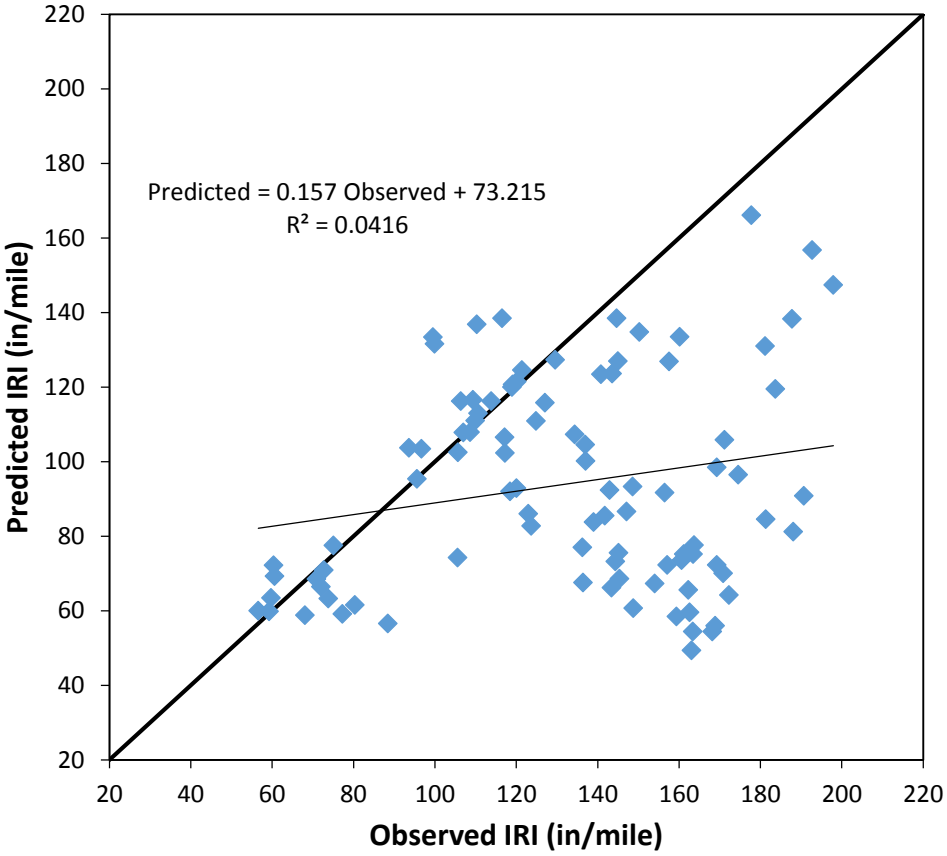

Figure 7-34. Predicted vs. Observed results with the default global calibration factors and actual IRI_0 for sections with known values and IRI_0 = 63 for the rest of the sections.

The goal of the calibration is to obtain appropriate values of C_1, C_2, C_3, and C_4[60]. It is also desirable to obtain a reasonably representative value of IRI_0 to use in the simulations. However, IRI_0 is not available for every section, which poses a challenge for calibration of C_1, C_2, and C_4.

[60] As indicated before, thermal cracking is not relevant for Hawaii, so using the default value is acceptable.

This challenge was overcome by minimizing the sum of squared residuals by varying the parameters C_1, C_2, and C_4 and simultaneously varying the values of IRI_0 for each section. Thus, in addition to the three parameters C_1, C_2, and C_4, an additional value was estimated for each section. It is important to note that the only goal of this exercise was to obtain unbiased estimates of C_1, C_2, and C_4. The estimated values were $C_1 = 23.1$, $C_2 = 0.323$, and $C_4 = 0.015$[61]. Figure 7-35 shows the results. This figure clearly shows that with good estimates of IRI_0 the model has the potential of providing better predictions.

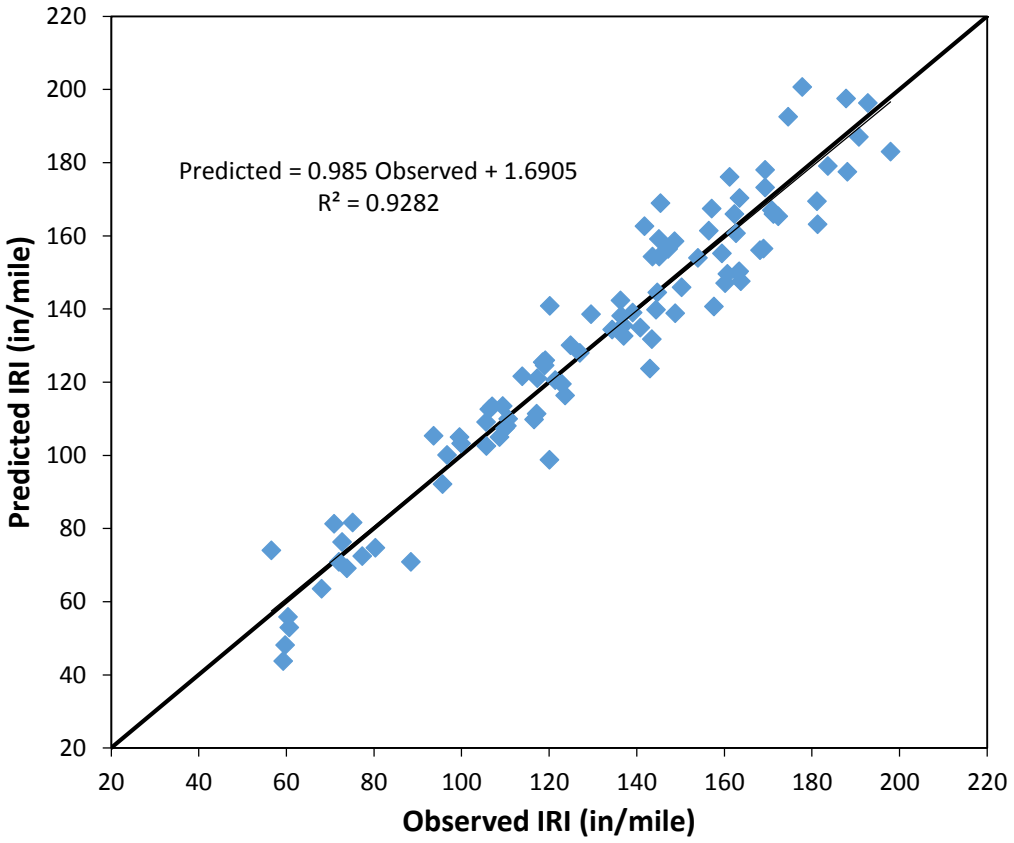

Figure 7-35. Predicted vs. Observed results with the estimated C_1, C_2, and C_4 and IRI_0 values estimated for each section.

[61] The optimizations resulted in a value for C_4 of zero. Since the data used for the site factor are not entirely reliable, it was preferred to fix the value of C_4 to be the same as the global calibration factor, i.e., $C_4 = 0.015$.

With the estimated values of C_1, C_2, and C_4 in hand, attention was turned again to obtain a reliable estimate of IRI_0. An alternative would have been to use the average of the IRI_0 values for all sections estimated when obtaining C_1, C_2, and C_4. However, this was not considered appropriate because as indicated before, two groups with very different IRI_0 values appear to be present in the sample. Therefore, the two groups of pavements were assumed to have different representative IRI_0 values and these were estimated by minimizing the sum of squared residuals with the values of $C_1 = 23.1$, $C_2 = 0.323$, and $C_4 = 0.015$ and varying the IRI_0 value for each group. These resulted in $IRI_0 = 78.0$ in/mile for "normal" sections and $IRI_0 = 150.5$ in/mile for fill sections. Figure 7-36 shows the predicted vs. observed results.

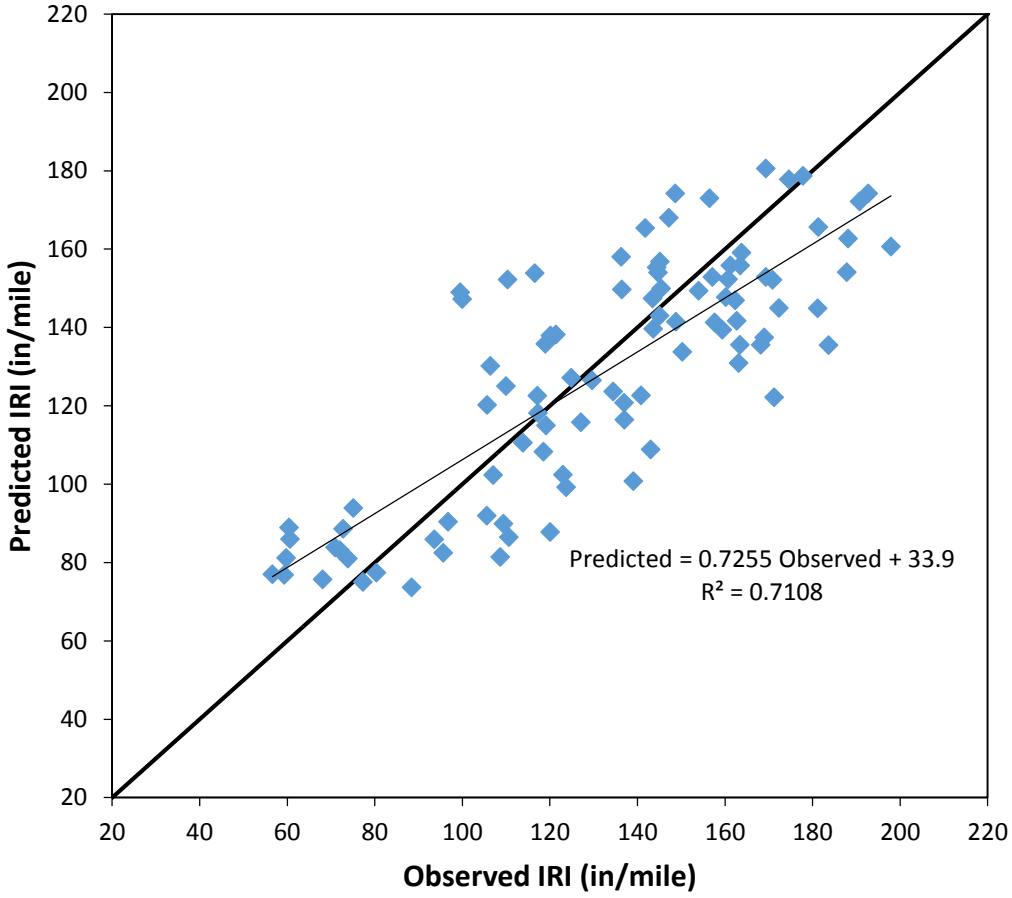

Figure 7-36. Predicted vs. Observed results with the estimated C_1, C_2, and C_4 and $IRI_0 = 78.0$ in/mile for "normal" sections and $IRI_0 = 150.5$ in/mile for fill sections.

Considering the uncertainty in the IRI_0 and other input values, the predictions above are quite reasonable. Of course, additional data are needed to validate these results.

It is important to note that IRI_0 = 78.0 in/mile is 15 in/mile higher than the default recommended value. This again, points out that for some reason the pavements in our State appear to have larger built-in roughness. For sections in fill, the values of IRI_0 = 150.5 in/mile is almost doubled the value for other sections, which is something that needs to be investigated in more detail.

7.6 TOP-DOWN FATIGUE CRACKING

As noted in section 7.5.2, it is suspected that top-down fatigue cracking may be the main mechanism of cracking on state roads with thick HMA layers. This section presents an analysis supporting this hypothesis.

The variation of the HMA modulus with depth has an important bearing on the strain distribution within the HMA layers and in turn on the location with the largest fatigue damage. The MEPDG currently assumes that that location of largest fatigue damage is at the bottom of the HMA for bottom-up fatigue cracking or at the surface or 0.5 in below the surface for top-down fatigue cracking. As was illustrated in Figure 6-9 on page 246, the MEPDG typically predicts that the modulus of the HMA decreases with depth, which implies that the effects of frequency and aging on the HMA modulus always supersede the effect of temperature. In all the simulations performed for this research project with Hawaiian climatic stations, the MEPDG has always predicted a decrease in modulus with depth. Since with Hawaii's weather one should expect to have a large proportion of time with high temperatures at the top accompanied by a relatively large gradient with decreasing temperatures with depth, the consistent decrease of modulus with depth predicted by the MEPDG is a bit puzzling. Therefore, the following subsections analyze this issue in more detail.

7.6.1 Frequency of Loading Calculations

As discussed in section 6.2, the frequency of loading has an important effect on the dynamic modulus, |E*|. Unfortunately, as mentioned on footnote 41 on page 246, there is still some controversies about its calculation. The goal of this section is not to take sides on the controversy but instead to analyze the reasonableness of the |E*| calculations with depth in the

MEPDG. Therefore, the following paragraphs present only the method used in the MEPDG to compute the frequency of loading. If the frequency variation with depth were less severe, as indicated by the results of other researchers [87], the findings on the following subsections would be reinforced even more.

The MEPDG uses the following equation to relate the time of loading to the vehicle speed (velocity) and the effective length of the load pulse.

$$t = \frac{L_{eff}}{17.6\, v_s} \tag{7-7}$$

where

t = time of loading (sec),

L_{eff} = effective length of the load pulse (inches), and

v_s = velocity (mph).

According to the MEPDG documentation (Appendix CC in [1]), the effective length at a given point in the above equation is the duration of the haversine stress pulse and is dependent upon the layer properties and the loading configuration (axle spacing and the radius of contact). Since HMA layers are at or close to the surface of the pavement, the loading configuration has practically no effect on the frequency calculations and thus, only the case with single axles are described here. After computing the time of loading with the equation (7-7), the corresponding loading frequency (f) is estimated according to the following relationship:

$$f = \frac{1}{t} \tag{7-8}$$

Therefore, the key to computing the time of loading or the frequency of loading is in the determination of the effective load pulse length with depth.

7.6.1.1 Effective Length Calculations

The effective length is the length that defines the extent of the stress pulse at a specified depth within the pavement system. The MEPDG represents this schematically as shown in Figure 7-37.

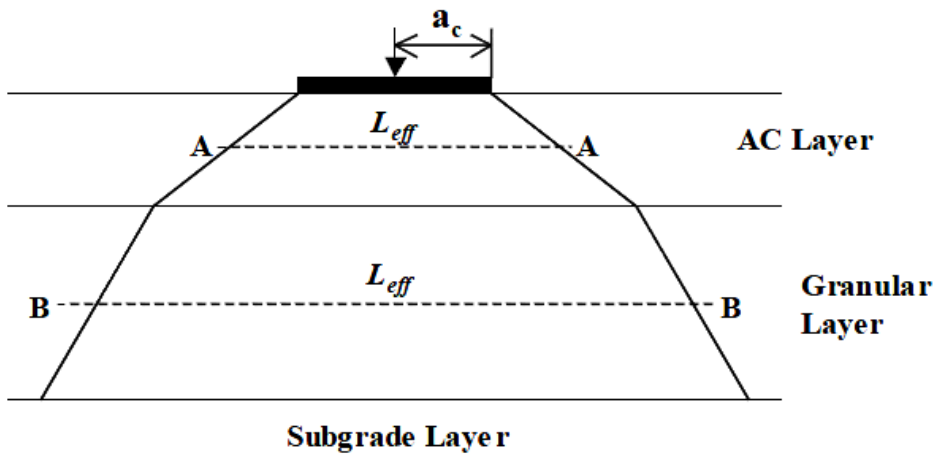

Figure 7-37. Effective Length Concept within the Pavement System (Source: [1]).

In Figure 7-37, the segment AA represents the effective length of the load pulse at a certain depth within the asphalt concrete (AC) (or HMA) layer (typically, the mid depth would be considered). The segment BB represents the effective length at another depth in a granular layer. To interpret these, one needs to imagine a moving load. As the load moves, points outside the segment experience zero load, points within the effective length experience a load that increases to a maximum under the center of the load. Clearly, the longer the effective length the longer is the time of loading.

As indicated in the MEPDG [1], stiffer materials tend to distribute the stresses over a much wider area compared to less stiff materials, which is why the slope of the lines delimiting the effective lengths in Figure 7-37 are considered to vary with material stiffness. In order to account for this, the MEPDG uses a simplified procedure based on an equivalent thickness concept first establish by Odermark. The method is based on the assumption that the stresses and strains below a layer depend on the stiffness of that layer only. If the thickness, modulus and Poisson's ratio of a layer are changed, but the stiffness remains unchanged, the stresses and strains below the layer should also remain (relatively) unchanged [1].

The stiffness of a layer is proportional to:

$$\frac{h^3 E}{(1-\upsilon^2)} \tag{7-9}$$

where

h = thickness

E = elastic modulus

ν = Poisson ratio

With the concept of equivalent thickness based on stiffness, a two-layer system with layer 1 having thickness h_1, modulus E_1, and Poisson ration ν_1 and layer 2 having modulus E_2 and Poisson ration ν_2 can be converted into a single layer system with modulus E_2 and Poisson ratio ν_2 by converting the thickness of layer 1 into an equivalent thickness h_e and simultaneously changing the properties of layer 1 such that the stiffness of layer 1 is unaltered (Figure 7-38). The stresses and strains computed in layer 2 in both systems should be approximately the same. Note that if another layer exists above layer 1 the same transformation can be applied to that layer as well. Thus, the method works for any number of layers

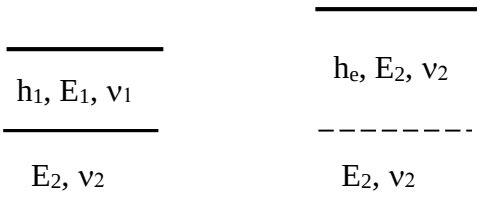

Figure 7-38. Odemark's transformation of a layered system (Source: [1]).

Mathematically, the transformation is given by:

$$\frac{h_1^3 E_1}{(1-\upsilon_1^2)} = \frac{h_e^3 E_2}{(1-\upsilon_2^2)} \quad \therefore \quad h_e = h_1 \sqrt[3]{\frac{E_1}{E_2}\frac{(1-\upsilon_2^2)}{(1-\upsilon_1^2)}} \tag{7-10}$$

If the Poisson ratio is assumed to be the same for all layers, an assumption that is justified in the MEPDG because Poisson ratio is seldom known with any degree of accuracy, the transformation simplifies to:

$$h_e = h_1 \sqrt[3]{\frac{E_1}{E_2}} \tag{7-11}$$

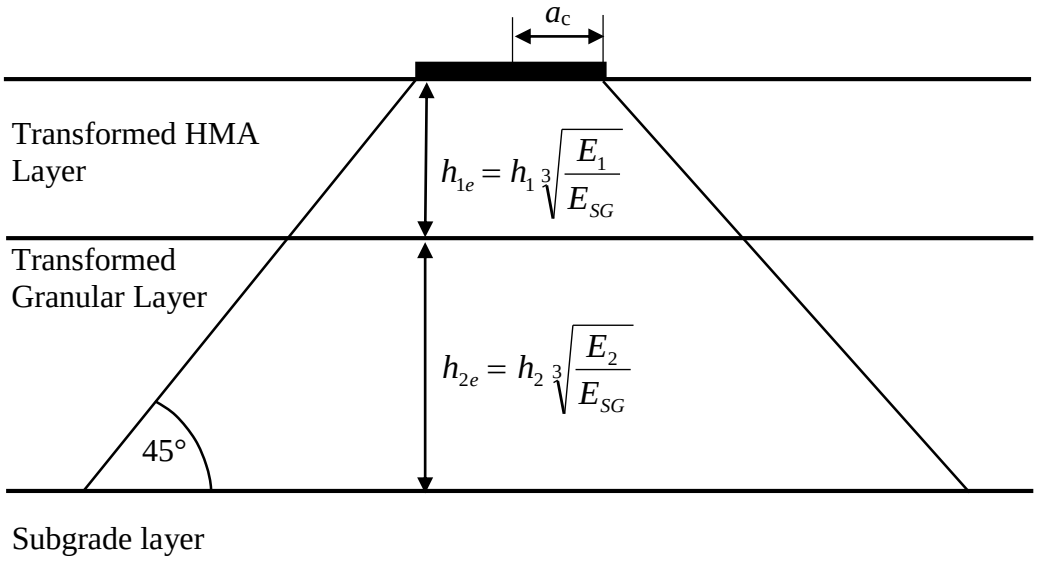

Figure 7-39. Equivalent Layer Thickness (Source: [1]).

For any pavement layer, the effective length of the stress pulse is computed at a specific depth (typically at mid depth) for which the loading frequency is needed for the computation of the modulus. This depth is the transformed depth and is termed as effective depth (Z_{eff}). The effective depth is computed by the following relationship:

$$Z_{eff} = \sum_{i=1}^{n-1} \left(h_i \sqrt[3]{\frac{E_i}{E_{SG}}} \right) + h_n \sqrt[3]{\frac{E_n}{E_{SG}}} \tag{7-12}$$

where E_i is the modulus of layer i, h_i is the thickness of layer i, E_n is the modulus of the layer containing the point at which the frequency is desired, and h_n is the depth from the top of the layer to the point for which the time or frequency of loading is being determined. If the effective

depth is needed at the mid-depth of the layer in the pavement structure, then h_n is half the layer thickness.

To compute the effective length, it is assumed for simplicity that the stress in the transformed structure is distributed at angle of 45° as shown in Figure 7-40. Then, the effective length or the length of the stress pulse at any depth is defined by the following equation:

$$L_{eff} = 2(a_c + Z_{eff}) \tag{7-13}$$

The effective length can then be used with equation (7-7) to estimate the time of loading. This is then used with equation (7-8) to estimate the frequency of loading for the single axle configuration. As indicated before, overlapping of stresses need to be considered for other axle configurations but this is typically not relevant when computing moduli in HMA layers.

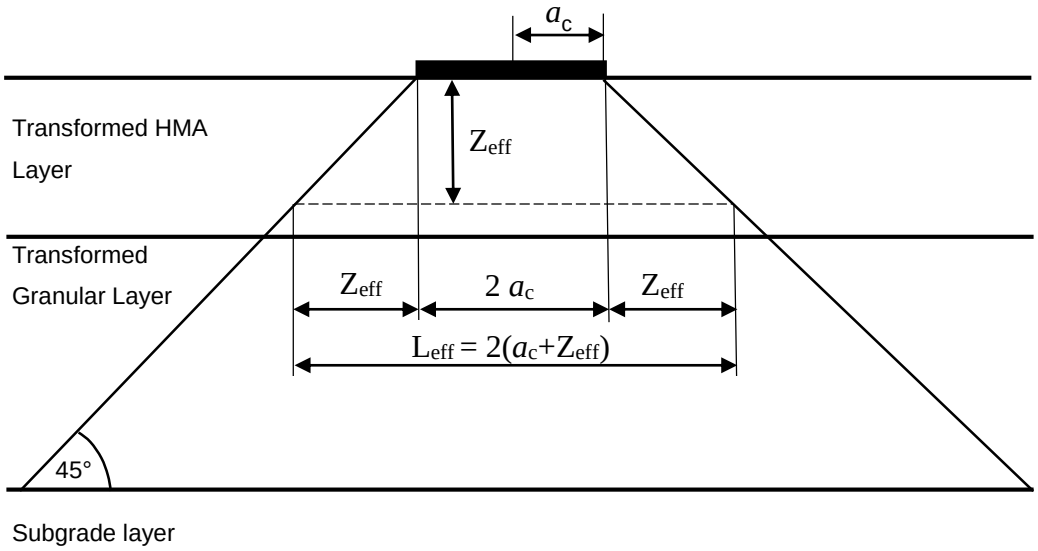

Figure 7-40. Effective Length Calculations using Transformed Thicknesses (Source: [1]).

7.6.2 Temperature Gradients

In order to estimate the variation of modulus with depth, it is also necessary to estimate the temperature variation with depth. For this purpose, a simplified analysis was performed to determine the heat flow within the pavement structure.

The one-dimensional diffusion law that governs the movement of heat within the pavement layers is:

$$\frac{\partial^2 T}{\partial z^2} = \frac{\rho c}{k} \frac{\partial T}{\partial t} \tag{7-14}$$

where

T	=	temperature,
t	=	time,
z	=	depth within the layer,
ρ	=	density,
k	=	thermal conductivity,
c	=	mass-specific heat of the material.

As explained in [36], equation (7-14) can be solved using a numerical technique such as the finite difference procedure. The finite difference equation used to advance the solution from time t to time t+1 is [36]:

$$T_i^{t+1} = \frac{k}{\rho c} \frac{\Delta t}{\Delta z^2} \left(T_{i+1}^t + T_{i-1}^t \right) + \left(1 - 2 \frac{k}{\rho c} \frac{\Delta t}{\Delta z^2} \right) T_i^t \tag{7-15}$$

with superscripts denoting time, subscripts denoting location, and Δz and Δt distance and time steps respectively.

At the boundary between layers (with different k, ρ, and c), the equation needs to be modified to account for the different material properties above and below the boundary:

$$T_i^{t+1} = \frac{\Delta t}{\Delta z^2} \left(\frac{k}{\rho c}\bigg|_1 T_{i+1}^t + \frac{k}{\rho c}\bigg|_2 T_{i-1}^t \right) + \left(1 - \frac{\Delta t}{\Delta z^2} \frac{k}{\rho c}\bigg|_2 - \frac{\Delta t}{\Delta z^2} \frac{k}{\rho c}\bigg|_1 \right) T_i^t \tag{7-16}$$

Examples of the use of these equations are presented in [36]. These can be easily implemented in a spreadsheet if the temperature at the pavement surface is known and it is assumed that there is no significant heat flow below at certain depth.

Using the values for the HMA layer and granular materials used in the simulations with the MEPDG (i.e., thermal conductivity k = 0.67 BTU/hr/ft/°F, heat capacity c = 0.23 BTU/lb/°F,

and ρ = 155 lb/ft^3), heat profiles were computed for different scenarios for 1 inch intervals. The scenarios were based on plausible situations in Hawaii. During the day, at about 2:00 PM in a sunny day, it is quite possible measure temperatures of up 140°F (60°C) at the surface of the pavement. Actually, measurements of that order were obtained by the PI with an infrared thermometer on some occasions. Furthermore, these temperatures are consistent with the PG binder grading system, which for Hawaii's climate requires a high temperature grade of 64°C at 98% reliability. A temperature of 58°C is often appropriate for a 50% reliability, which means that there is a 50% chance that the mean highest pavement temperature over the course of the hottest week will exceed this value.

Scenarios, with maximum temperatures at the surface of 131°F (55°C), 122°F (50°C), and 112°F (45°C) were also considered to evaluate the conditions with smaller gradients. At a depth of 400 inches (~33 ft or 10 m), a constant temperature of 68°F (20°C) was assumed as a reasonable estimate of temperature with depth (and this was also the initial temperature at all depths). As a result of these simulations, the interpolated temperatures profiles shown in Table 7-4 were obtained with depth after 8 hours of constant temperature at the surface. The values presented in the table were interpolated to correspond with the mid depth of each sublayer that would be created by the MEPDG with its automatic sub layering process. Thus, these values are appropriate for HMA layers up to 12 inches thick.

Three additional scenarios were simulated with 78.8°F (26°C) as the constant temperature at a depth of 400 inches The value of 78.8°F (26°C) was also used as the temperature at all depths at t =0. This value was based on measurements obtained under a bridge by the co-PI. In these additional scenarios, instead of maintaining the temperature at the surface constant, a more realistic situation was created in which the temperature increases slowly from 78°F (26°C) to 140°F (60°C) over a period of 5 hours (a quite reasonable assumption from 8:00 AM to 1:00 PM), stays at that temperature for 1 hour, and then it decreases to about 113°F (45°C) over a period of 2 hours. The columns for these scenarios are under the title "Variable Surface Temperature" in Table 7-4. The temperatures used were the ones computed after 4, 6, and 8 hours.

The estimated variations of temperature with depth for the variable surface temperature scenarios are shown in Figure 7-41 after 2, 4, 6, and 8 hours.

In the next subsection, the temperatures presented in Table 7-4 are used together with the estimated frequencies with depth (obtained using the approach of the previous subsection) to estimate dynamic modulus of HMA with depth.

Table 7-4. Temperatures with depth (°F) for different surface temperature scenarios.

Depth (inches)	Temperature at the surface						
	113°F (45°C)	122°F (50°C)	131°F (55°C)	140°F (60°C)	Variable Surface Temperature		
					4 hr	6 hr	8 hr
0.25	111.6	120.4	129.1	137.8	124.2	136.99	112.1
0.75	108.9	117.1	125.3	133.5	116.9	130.96	113.2
1.5	104.9	112.3	119.7	127.1	107.8	122.35	113.0
2.5	99.7	106.1	112.4	118.8	98.4	111.93	110.4
3.5	94.8	100.2	105.6	110.9	91.7	103.16	106.2
6.0	84.3	87.6	90.8	94.1	82.7	88.65	94.4
10.0	73.8	75	76.2	77.3	79.2	80.56	83.3

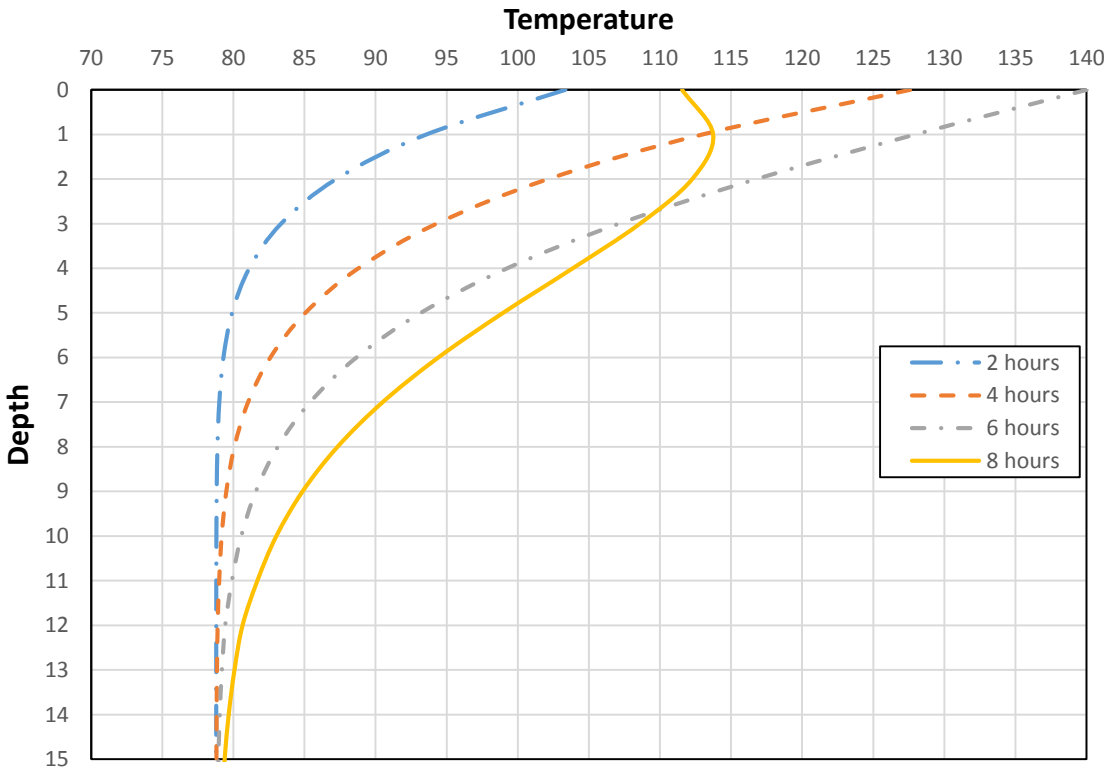

Figure 7-41. Temperature profile with depth after 2, 4, 6, and 8 hours for the scenario with variable pavement surface temperatures.

7.6.3 Combined Effect of Frequency and Temperature on |E*|

The temperatures and frequencies with depth estimated using the procedures in the previous two sections were used to compute the dynamic modulus using equations (6-6) and (6-7) (see page 241) for a mix with parameters $\delta = 2.637$, $\alpha = 3.950$, $\beta = -1.268$, $\gamma = 0.418$, A = 2.15×10^{-4}, B = -0.105, and C = 6.30, which corresponds to the mix type IV utilized for most simulations with the MEPDG.

Since the calculation of the effective load pulse length used to compute frequency of loading depends on the modulus of the layer and the layers above it, an iterative procedure needs to be used to determine the modulus. This was implemented in Excel® in the form shown in Table 7-5. The simulations were performed for a wheel radius of 4 inches and a subgrade modulus of 12,000 psi[62].

With reference to Table 7-5, the calculations were performed as follows. The temperatures for one of the scenarios estimated with the procedure described in section 7.6.2 are listed in column (2) for each of the depths shown in column (1) (these depths correspond to the mid depth of each sublayer). In column (3), an assumed value of |E*| is entered to start the calculations. Initially, these values would be different from those listed in column (11), which are described below. With an estimate of the modulus, the effective depth shown in column (4) is computed using equation (7-12). Then, the effective length of the load pulse in column (5) is computed with equation (7-13). Equation (7-7) is used to compute the time of loading shown in column (6) and equation (7-8) is used to compute the frequency shown in column (7). Equation (6-7) on page 242 is then used to calculate the logarithm of the shift factor in column (8). The corresponding shift factor is shown in column (9). The shift factor is then multiplied by the frequency to obtain the reduced frequency (column 10) and with these, the |E*| values are calculated using equation (6-6) on page 241. Since, the assumed values of |E*| used to compute the frequencies are not necessarily the same as the values obtained in column (11), in column 12 the differences between the assumed and predicted values are computed. Ideally, one would like to make the differences equal to zero so that the frequency calculations correspond to the |E*|

[62] A wheel radius of 4 inches was selected conservatively to obtain a severe effect of frequency at the surface.

values calculated from the master curve. This is accomplished with solver by minimizing the sum of the values in column (12) by varying the assumed modulus values. As shown in Table 7-5, this is easily accomplished with Excel®.

In order to account for aging, the values obtained with the above procedure were multiplied by a factor that varied from 1.56 for the top sublayer to 1.10 for the last sublayer. The multipliers are based on the typical increase of |E*| with time simulated by the MEPDG for the Hawaiian conditions. In this way, an approximation to the simulation of aging in the MEPDG is obtained without having to implement the Global Aging System used by the MEPDG.

Table 7-6 shows the modulus values obtained under the different temperature scenarios described in the previous section and for a speed of 45 mph. The computation of these values already account for temperature, frequency, and aging.

Clearly, the values under the four first scenarios are in distinct disagreement with all the simulations that have been performed in this project with the MEPDG in that the modulus increases with depth instead of decreasing as the MEPDG suggests. This is very puzzling, as the same procedure supposedly used by the MEPDG has been followed closely. Note that even for the variable surface temperatures scenarios, the modulus often increases with depth. Only in the last scenario, it decreases at first with depth but then it increases at higher depths. The results of this analysis actually coincide with a priori expectations for high temperature gradients in which the temperature decreases with depth (which is why the analysis was performed in the first place.)

A potential source for the discrepancy is that the MEPDG does not model every single situation but instead it models only five quintiles as was described in Figure 5-17 on page 212. The scenarios described would be completely missed by the MEPDG if they represented about less than 10% of the potential situations. Yet, as described below, most of the top-down fatigue cracking is likely to be generated during situations such those described by this type of scenarios. The MEPDG modeling may be too coarse to capture these conditions. At least for top-down fatigue, instead of subdividing the pavement temperatures in each analysis period into five equal quintiles, a more detailed analysis of the highest temperatures may be more appropriate. Arguably, this may also be convenient for rutting predictions.

Table 7-5. Illustration of the procedure used to estimate |E*| as a function of frequency and temperature.

Depth (in) (1)	**Estimated temperature** (°F) (2)	**Assumed modulus** (psi) (3)	**Effective Depth** (in) (4)	**Effective Length** (in) (5)	**Time of loading** (sec) (6)	**Frequency** (Hz) (7)	**Log Shift Factor** (8)	**Shift Factor** (9)	**Red Freq** (Hz) (10)	**|E*|** (psi) (11)	**|E*|- |E*$_{assumed}$|** (psi) (12)
0.25	112.1	286,267	0.72	9.44	0.0119	83.9	-2.772	0.00169	0.142	286,267	0
0.75	113.2	249,270	2.13	12.25	0.0155	64.6	-2.834	0.00147	0.095	249,270	0
1.5	113.0	227,610	4.15	16.29	0.0206	48.6	-2.822	0.00150	0.073	227,610	0
2.5	110.4	232,227	6.82	21.65	0.0273	36.6	-2.674	0.00212	0.077	232,227	0
3.5	106.2	261,359	9.56	27.12	0.0342	29.2	-2.429	0.00372	0.109	261,359	0
6	94.4	390,809	17.35	42.69	0.0539	18.6	-1.699	0.01998	0.371	390,809	0
10	83.3	558,452	30.93	69.85	0.0882	11.3	-0.958	0.11012	1.249	558,452	0
14	79.7	594,948	45.47	98.93	0.1249	8.0	-0.706	0.19664	1.574	594,948	0

Table 7-6. HMA modulus (psi) values obtained with depth under different scenarios.

Depth (inches)	Temperature at the surface						
	113°F (45°C)	122°F (50°C)	131°F (55°C)	140°F (60°C)	Variable Surface Temperature		
					4 hr	6 hr	8 hr
0.25	456,353	310,980	213,117	147,572	168,894	97,826	446,577
0.75	458,092	321,520	225,547	159,324	214,299	116,816	388,862
1.5	468,962	341,711	248,374	181,047	290,961	154,794	355,072
2.5	521,596	398,330	304,325	231,239	400,154	224,425	362,274
3.5	593,672	475,337	378,799	302,461	496,830	309,149	407,721
6.0	743,084	655,426	578,857	507,636	636,869	509,049	609,663
10.0	961,206	926,795	893,039	863,591	648,908	626,486	871,185

As shown in Figure 7-41, the maximum temperature at a given depth does not necessarily coincide with the maximum temperature at another depth. Thus, since the guide apparently picks the temperature quintiles for each layer independently, it is likely that situations like those in Figure 7-41 are also being missed.

As shown in the next section, the above observations could have important consequences in the predictions of top-down fatigue cracking.

7.6.4 Minimum Principal Strain Distributions and Their Consequences

The consequences of the moduli variation with depth obtained in the previous section are now explored. For this purpose, simulations were performed for a 9,000 lb load on a pavement structure with subgrade modulus of 12,000 psi and Poisson ratio of 0.4; granular base modulus of 30,000 psi, Poisson ratio of 0.35, and thickness of 12 inches; and an HMA thickness of 12 inches. The HMA layer was subdivided into 7 sublayers of 0.5, 0.5, 1.0, 1.0, 1.0, 4.0, and 4.0 inches, respectively, as these sublayer thicknesses are selected automatically by the MEPDG. The moduli used for each HMA sublayer are those shown for each scenario in Table 7-6. The HMA Poisson ratio was computed by the default MEPDG equation:

$$\mu = 0.15 + \frac{0.35}{1 + e^{a+b|E^*|}} \qquad (7\text{-}17)$$

with a = -1.63, $b = 3.84 \times 10^{-6}$, and with $|E^*|$ expressed in psi.

Figure 7-42 shows the minimum principal strain distributions corresponding to the first four moduli scenarios shown on Table 7-6. Except for the 113°F (45°C) scenario, it is clear that in all other situations the maximum tensile strain occurs near the surface of the pavement instead of at the bottom as it would be predicted with modulus values that decrease with depth. Although during a whole day the higher temperature situations may be less frequent, the magnitude of the strains are also much higher and so may be the potential for fatigue cracking. Notice that the previous sentence is purposely weak as the fatigue cracking potential is affected not only by the strain but also by the stiffness of the mix (see equations (5-1) on page 201 or equation (7-3) on page 397.) Thus, the location of the critical point cannot be determined solely by the strain. Consequently, an analysis was made to obtain the number of repetitions to failure, N_f, for each strain level as estimated from equation (6-32) on page 324 with C = 1 and C_H = 0.1 (the exact value of C_H for a 12 inch HMA layer is 0.083). In order to deal with smaller numbers, the logarithm of the number of repetitions to failure (log N_f) was calculated.

Clearly, the lower the number of repetitions to failure the higher is damage ratio. Thus, the critical points are located were the lowest numbers are found. The results are shown in Figure 7-43. As observed in the figure, apparently, the effect of the change in modulus is not generally high enough to affect the location of the critical point, except when the strains near the top and at the bottom of the layer are of similar magnitude such as the case with 122°F (50°C).

It is important to stress that although the situations depicted in these figures may occur over a relatively short intervals during the day (say, 1, 2, or 3 hours depending on actual conditions), the damage occurring during these periods can be substantial. Notice that the differences in the log N_f between the scenario with 140°F (60°C) maximum temperature and that with 122°F (50°C) maximum temperature imply a six fold change in N_f for the 9,000 lb load. For higher loads the differences would be even higher. This may be a significant factor affecting the predictions of fatigue cracking.

Figure 7-44 shows the minimum principal strain distributions for the last three scenarios in Table 7-6 (all three including the aging effect). For the 8-hours scenario, the simulation was performed with and without aging. Figure 7-45 shows the coresponding log N_f distributions. The observations are similar to the ones presented above. Again, the longer the pavement is heated from the top the more likely the fatigue cracking starts at the top and as the pavement cools down, fatigue from the bottom becomes more likely.

A comparison of parts c) and d) of Figure 7-45 shows that the location of the critical point changes from the top inmediately after construction to the bottom after a few years. Of course, damage accumulates continuously and at which point cracking will initiate depends on many factors.

The above analysis illustrate some of the complexities involved in predicting fatigue cracking. For example, based on the above, if a substantial portion of the loading occurs during the periods with high temperature gradients (hotter on top), then the likelihood of top-down cracking appearing before bottom-up fatigue cracking increases. On the other hand, if not much loading occurs during the hotter periods, then top-down cracking is less likely. The above analysis is very limited as it was performed for a single load magnitude and one layer thickness. Clearly, these factors also play an important role. The main point of the analysis, however, is that the critical conditions for top-down fatigue cracking currently may not be accounted for properly in the MEPDG. Unfortunately, there is nothing that the user can do at this point to address this issue. This analysis also sheds some light on why top-down fatigue cracking appears to be a prevalent distress in Hawaii roads, which is an assumption that needs to be verified. Confirmation of this assumption could also impact the analysis of reinforcements such as glass grids and mix with fiber and polymers.

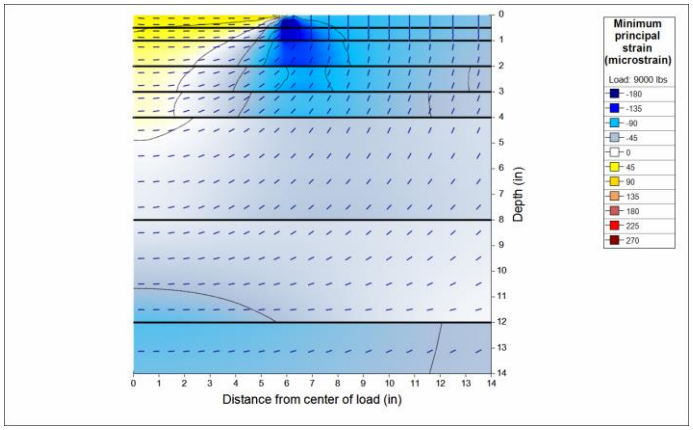

a)

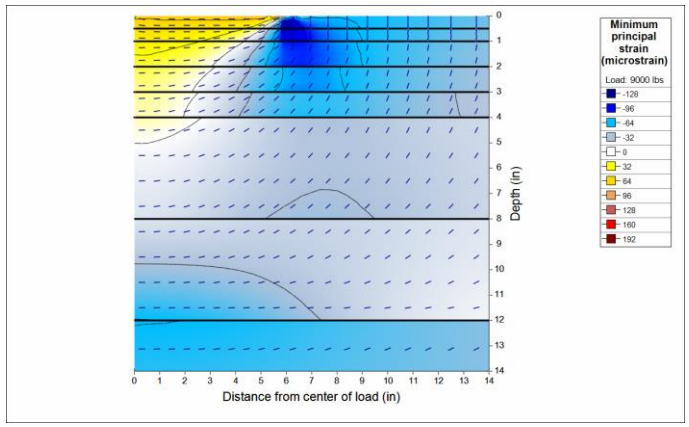

b)

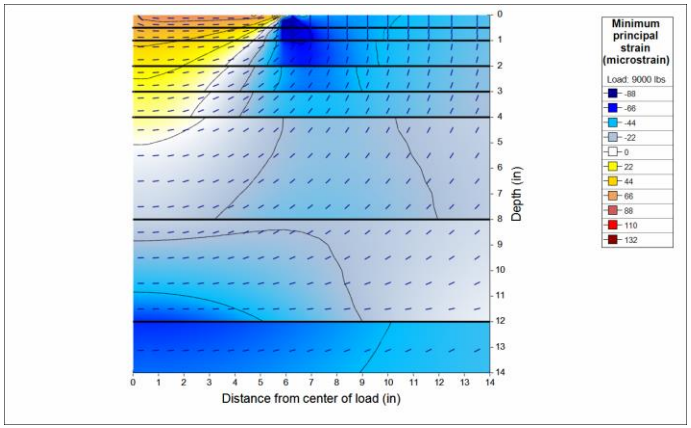

c)

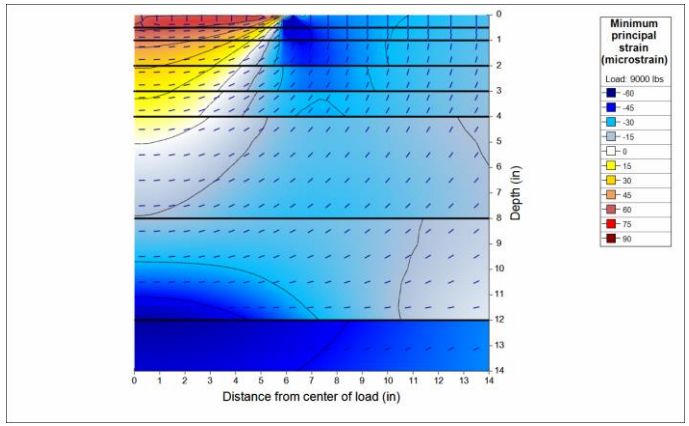

d)

Figure 7-42. Minimum principal strain distributions for a speed of 45 mph and maximum surface temperature for 8 hours of a) 140°F (60°C), b) 131°F (55°C), c) 122°F (50°C), and d) 113°F (45°C).

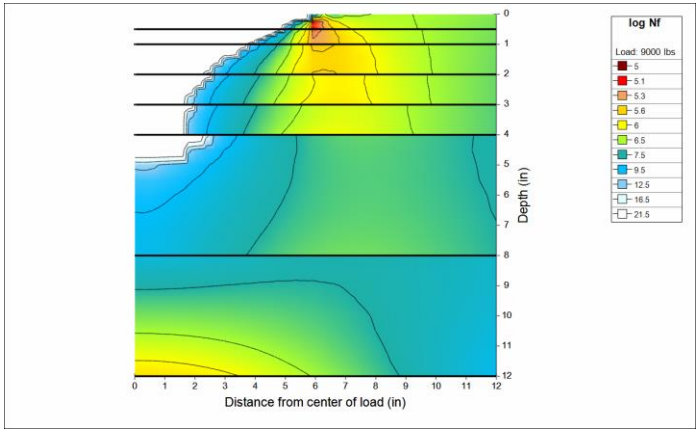

a)

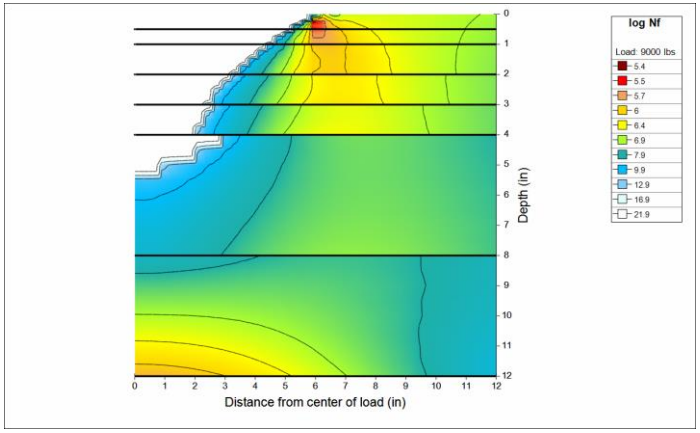

b)

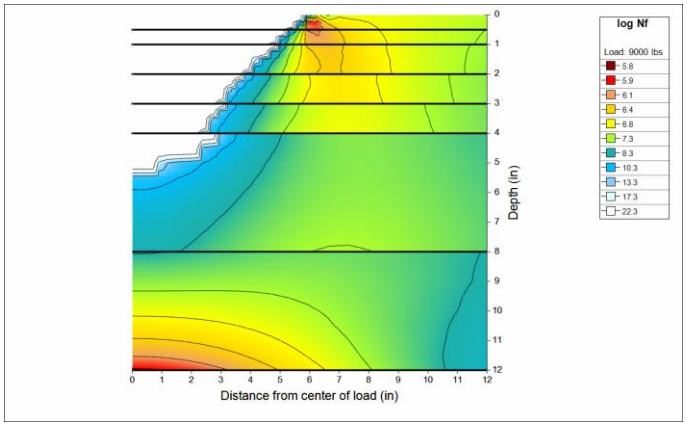

c)

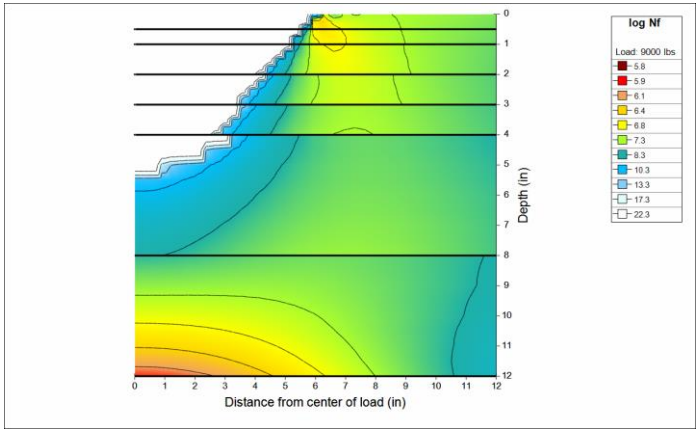

d)

Figure 7-43. Number of repetitions to failure for a speed of 45 mph and maximum surface temperature for 8 hours of a) 140°F (60°C), b) 131°F (55°C), c) 122°F (50°C), and d) 113°F (45°C).

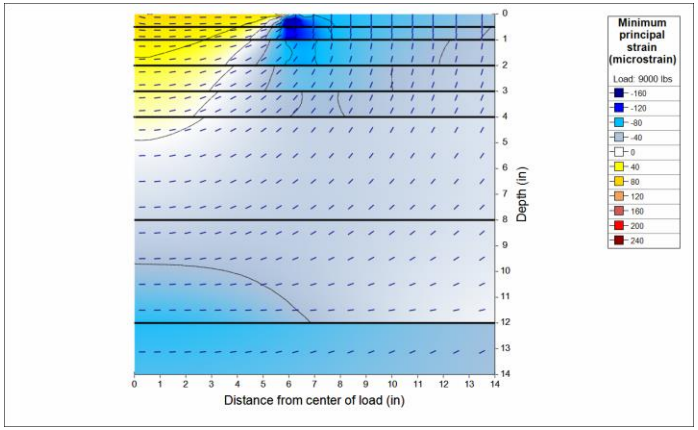

a)

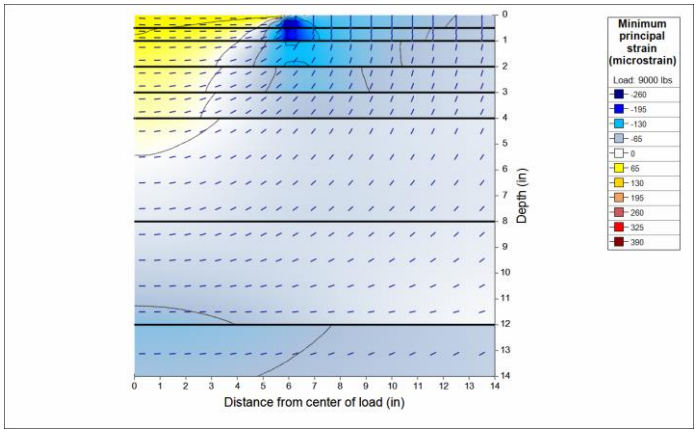

b)

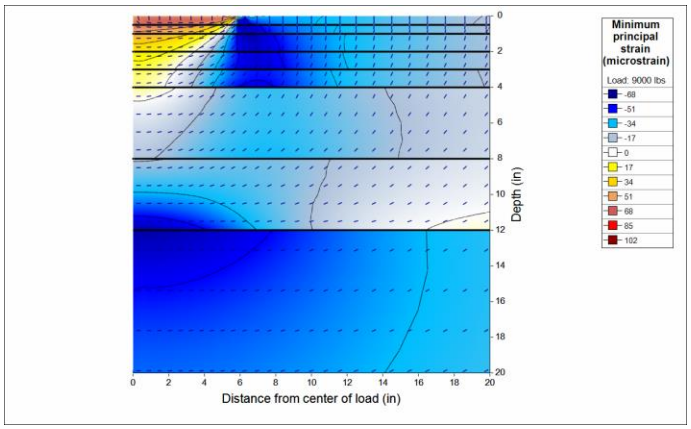

c)

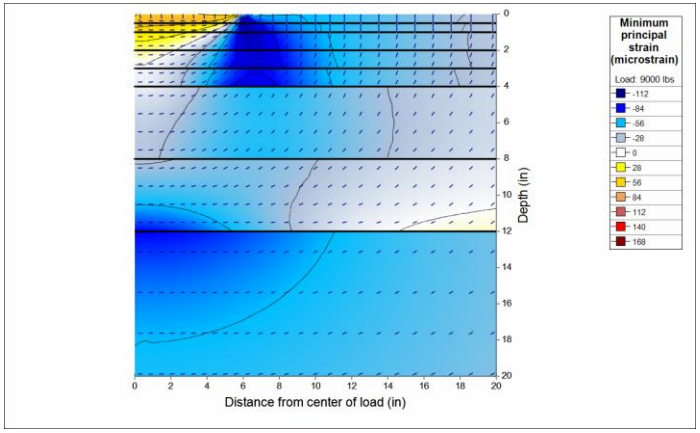

d)

Figure 7-44. Minimum principal strain distributions for a speed of 45 mph and varying surface temperature a) After 4 hours, b) After 6 hours, c) After 8 hours, and d) After 8 hours – no aging.

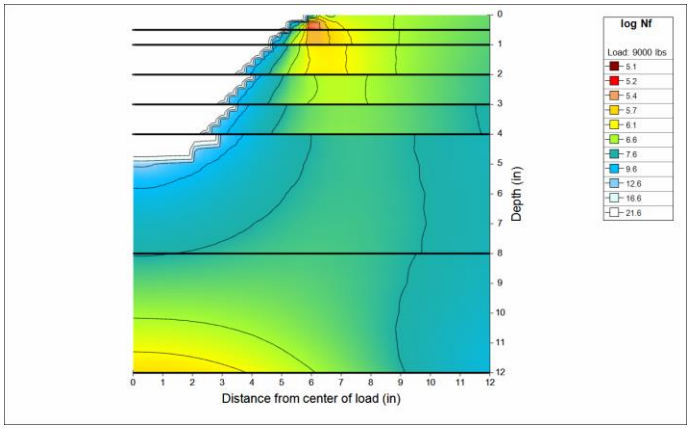

a)

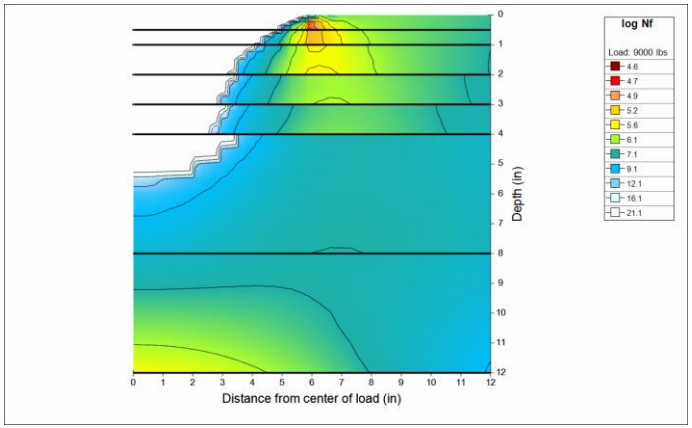

b)

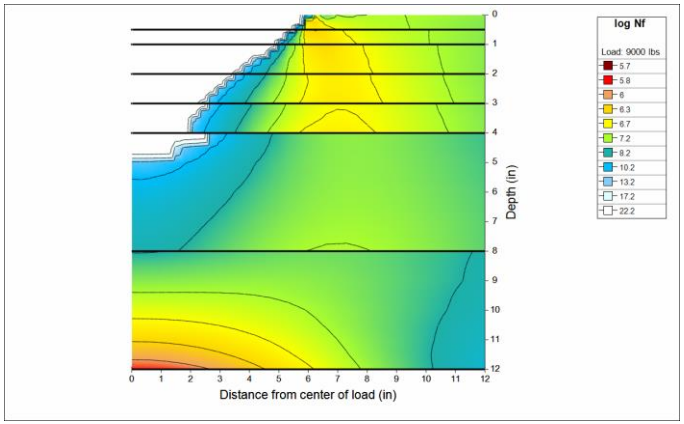

c)

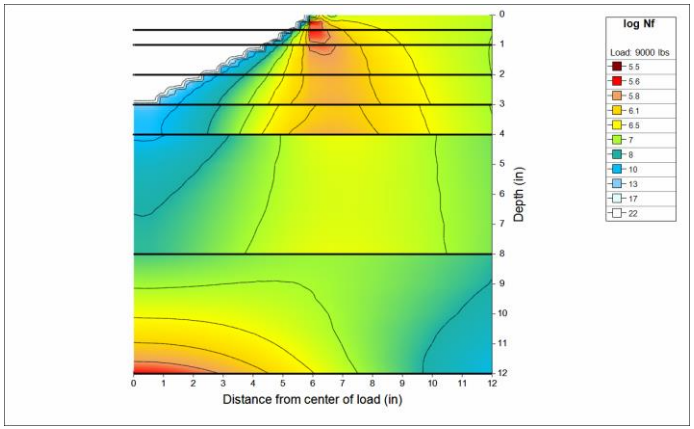

d)

Figure 7-45. Number of repetitions to failure for a speed of 45 mph and variable maximum surface temperature a) After 4 hours, b) After 6 hours, c) After 8 hours, and d) After 8 hours – no aging.

7.7 SUMMARYAND A FEW OTHER OBSERVATIONS

In this chapter, the efforts towards calibration of the MEPDG have been described in detail. Because of data limitations, the calibration attempt has been limited to new HMA pavements. Significant challenges have been faced with the calibration for rutting, fatigue cracking, and roughness. This first calibration attempt presents some very promising results as it shows that predictions can be within reasonable ranges. Nevertheless, considerable work is still needed for regular use of the MEPDG.

In particular, it is imperative to obtain distress and FWD information for calibration of the rehabilitation procedures. Furthermore, usable information for a larger sample of sections is needed to obtain standard error estimates. Although with the local calibration the predictions for mean behavior of new pavement sections may be reasonable, the standard errors (and consequently the reliability analysis) would still be based on the global calibration results.

Calibration needs to be redone considering that in the State, the most trafficked lane is not necessarily the rightmost lane (or simply considering the adequate lane distribution factors based on more specific lane distribution factors for the pavement sections in the calibration data set.) In addition, based on the roughness information and video logs, it is believed that in some situations the construction date may be off by one, two or three years, which may have adversely influenced some of the predictions. In other occasions, there may have been temporary construction traffic. For low volume roads, a big construction project may end up being equivalent to a few years of load applications under normal circumstances, so documenting when such situations occur is desirable to account for them during calibration.

One of the major features of the MEPDG is the predictions of the effects of environmental factors on pavement performance. In this respect, however, to take full advantage of the MEPDG it is desirable to develop information for new weather stations to account, for example, for the differences in weather (rain, cloud cover, wind, etc.) between the different sides of the islands. Furthermore, mapping water table depths could go a long way to improve the predictions of resilient moduli of unbound materials.

As described in section 7.4, non-linearities creates substantial uncertainty in the selection of appropriate resilient moduli for design. This may be complicated even further with the wetting

and drying that occurs with soils in practice. It would be desirable to perform a study of the resilient moduli of unbound materials and soils by varying the post-compaction moisture content (as opposed to compacting the materials at different moisture content). This could help guide in the interpretation of backcalculation results, particularly if non-linearities are considered. Field backcalculation studies with different load levels are also desirable to determine the effect of non-linearities on the resilient modulus of bases. For subgrades, it would be important to start documenting in a database their characteristics encountered in rehabilitation or reconstruction projects. Ideally, resilient modulus determinations would be desirable.

Finally, it would be extremely important to conduct forensic studies on thick pavements with recently formed cracks to determine where they originate and also monitor pavement temperatures so as to validate or invalidate the belief that a significant proportion of the fatigue cracking observed on the State on pavements with thick HMA layers originates near the top of the HMA.

CHAPTER 8. PAVEMENT MANAGEMENT SYSTEM

8.1 Introduction

One of the most important aspects of a PMS is its ability to determine effective maintenance and rehabilitation strategies. Many agencies use assignment procedures or decision trees to connect a type of pavement and condition of the pavement with a treatment at the network level [88]. The selection of strategies range from selecting an M&R category for each condition level and pavement type category to more elaborate trees or decision matrices (based on either pavement condition, roughness, deflections, friction or a combination of these pavement characteristics) sometimes combined with cost-effectiveness calculations or optimization. Hass et al. [3] give examples of different treatment selection strategies whereas Wolters et al. [89] provide a more contemporaneous description of software capabilities.

In general, to determine cost-effective strategies, some sort of "optimization", as used by some PMS programs, is needed to identify trade-offs caused by treatments with different costs and performance lives as well as the timing of treatment application and the consideration of budget constraints. For these programs, the policies consist of parameters that will be used in the "optimization" to determine the most desirable strategy as opposed to fixed rules of what should be done for each pavement section. The word "optimization" is presented in quotes, as in reality most programs use some form of optimization combined with "heuristics"[63] to obtain reasonable strategies.

Pavement management systems (PMS) help in the selection of effective maintenance and rehabilitation strategies. The terminology on maintenance and rehabilitation treatments varies widely in the literature, therefore section 8.2 provides the description of commonly used terms.

[63] Heuristics are simple sets of rules that in general provide a near optimal solution but are not guaranteed to find it.

The implementation of a pavement management system (PMS) requires the selection of appropriate software to store, manage, and process the large amount of information needed to administer the pavement network. A large number of software packages are available with different capabilities. Thus, section 8.3 provides a brief summary of those most commonly used by DOTs and local agencies in North America. Most of the discussion in that section is based on reviews by other researchers or on claims from the vendors' websites. In contrast, section 8.4 concentrates on specific features of three of the programs for which licenses were obtained at different points during this project. The goal of that section is to provide a more detailed description of software capabilities (based on experiences and/or the software documentation) that may aid in the final selection of a PMS program. Although not every single issue that may be encountered during implementation is covered, some important aspects that need to be considered are discussed.

It is important to stress that the use of a modern PMS software is only one of the requirements for a successful PMS implementation. Among others, data quality, workforce assignment and training, personnel buy-in, communication protocols, institutional barriers, and trade-offs with other highway assets are also important. Section 8.5 (page 568) provides some observations on some of these aspects.

8.2 Maintenance and Rehabilitation Categories

There is an abundance of terms used in the pavement literature referring to pavement maintenance and rehabilitation (M&R). The following are relatively common terms. These are not always mutually exclusive. Thus, some treatments may fall under more than one of the categories described below.

Pavement preservation, pavement rehabilitation and pavement reconstruction are the three general treatment categories used for Pavement Management.

8.2.1 General Definitions of Treatment Categories

Pavement Preservation, as defined by the Federal Highway Administration's (FHWA) Pavement Preservation Expert Task Group is: "A program employing a network level, long-term strategy that enhances pavement performance by using an integrated, cost-effective set of

practices that extend pavement life, improve safety, and meet motorist expectations." Since the above definition is not very specific about what it involves, pavement preservation can also be thought of as the sum of all activities undertaken to provide and maintain serviceable roadways, including *preventive maintenance (defined below), corrective maintenance as well as minor rehabilitation projects*. Thus, pavement preservation is a more general term than preventive maintenance (http://www.fhwa.dot.gov/pavement/preservation/091205.cfm.)

Pavement maintenance activities are the key to pavement preservation. An effective pavement preservation program integrates many maintenance strategies and treatments. Pavement maintenance is described as doing inexpensive repairs on good roads to keep them good [90]. According to the Asphalt Institute's Asphalt Handbook [91], there are three categories of pavement maintenance, namely, Preventive Maintenance, Corrective Maintenance, and Emergency Maintenance.

Preventive Maintenance activities are those performed with the primary objective of preserving the existing pavement and extending the life of the pavement by slowing its rate of deterioration. It is a strategy of surface treatments and operations intended to retard progressive failures. It is important to note that preventive maintenance activities are not intended to increase structural capacity. On flexible pavements, it includes crack sealing, surface treatments, thin overlays, drainage maintenance, etc. Surface treatments that are less than two inches in thickness, which are not considered as adding structural capacity, fall under this category.

Corrective Maintenance is performed after a deficiency occurs in the pavement, such as loss of friction, moderate to severe rutting, or extensive cracking. This may also be referred to as "reactive" maintenance. An example is a chip seal used to repair a low friction condition or the filling of ruts with slurry seal mix.

Emergency or Safety Maintenance is a stop-gap measure (also known locally as first-aid) performed shortly after an emergency situation, such as a severe pothole on a high volume roadway that needs repair immediately mostly for safety reasons and to maintain a road operational. This could also include temporary treatments that hold the surface together until a more permanent treatment can be performed.

Pavement Rehabilitation is work undertaken to extend the service life of an existing pavement. This includes the restoration of the structural capacity, placing of a structural overlay to accommodate projected traffic loading, and/or other work required to return an existing roadway to a condition of structural and functional adequacy. Rehabilitation can be subdivided into minor and major. According to the Asphalt Handbook [91], minor rehabilitation treatments include non-structural enhancements such as thin functional overlays. Notice that a thin, non-structural overlay can also be considered a preventive maintenance treatment, which explains why there is usually confusion about the use of some of these terms. Another example may involve placing of a deep patch on a medium size area exhibiting a locally high level of cracking. Major pavement rehabilitation, such as a thick overlay, adds structural enhancements to a pavement section [91].

Pavement Reconstruction consists of construction of the equivalent of a new pavement structure which usually involves complete removal and replacement of the existing pavement structure including new and/or recycled materials.

8.2.2 Treatment Trade-offs

A major determinant of the most appropriate maintenance treatment is the current condition of the pavement. According to reference [92], preventive maintenance is most appropriate for pavements in good condition, corrective maintenance is appropriate for pavements in fair condition, whereas emergency maintenance and rehabilitation are appropriate for pavements in poor condition (Figure 8-1). There are no clear boundaries between when a treatment is preventive versus corrective, or corrective versus emergency.

Often, preventive maintenance methods are designed to repair damage caused by the environment. The renewal of the pavement surface prevents water from penetrating into the pavement structure by sealing the surface and controlling the effects of oxidation, raveling, and surface cracking. Since environmental conditions remain fairly consistent over time, so should the maximum time between preventive maintenance treatments. Thus, preventive maintenance is generally planned and cyclical in nature.

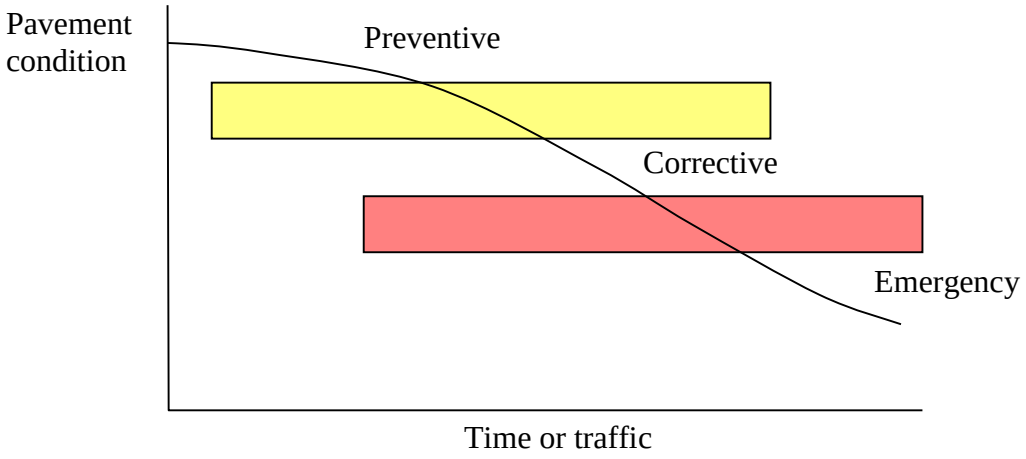

Figure 8-1. Maintenance Categories (source: [92]).

Preventive maintenance activities can include conventional treatments such as crack sealing, chip sealing, fog sealing, rut filling, and thin overlays. They can also include newer technologies such as ultra-thin wearing courses, very thin overlays, and microsurfacing applications. Aside from crack treatments, all of these treatments leave the pavement with a new wearing surface. A fog seal provides a new wearing surface, although it will generally provide lower friction than the original surface.

Figure 8-2 shows the relationship between pavement condition and time (or traffic). Since a PMS must strive to *complete the right repair on the right road at the right time,* it needs to use the pavement deterioration curves along with cost information to analyze the trade-offs between strategies with recurrent preventive maintenance activities and those with longer spaced rehabilitations. Furthermore, it must do this for all sections in a network simultaneously and accounting for budget constraints. Since it is typically reported that strategies including preventive maintenance are more cost-effective than those that do not, use of the PMS should result in a more widespread use of preventive maintenance activities. For example, the Minnesota Asphalt Pavement Maintenance Manual, [92] indicates that preventive maintenance is six to ten times more cost-effective than a “do-nothing” maintenance strategy (i.e. one including only Major M&R).

In the past, several factors precluded a more intensive use of preventive maintenance activities. Quoting Johnson [92]:

- "Many of the available preventive maintenance treatments were considered unsuitable for high-volume roadways.
- Lack of federal aid for maintenance encouraged agencies to allow pavements to deteriorate sufficiently to qualify for rehabilitation that was funded by federal aid.
- Information was lacking about the performance and cost-effectiveness of preventive maintenance practices.
- Highway agencies wished to minimize driver exposure to roadway operations and lane closures. This prevailing philosophy is reactive rather than proactive or preventive."

It is also more difficult to explain to the public the benefits of treating pavements in good condition when there is a large backlog of pavements in poor condition within the system. There is a tendency to concentrate on the urgent problems (e.g., pothole repair) at the expense of preventive maintenance. Although potholes must be repaired for safety reasons, that should not deter an agency from developing a cost-effective preventive maintenance program.

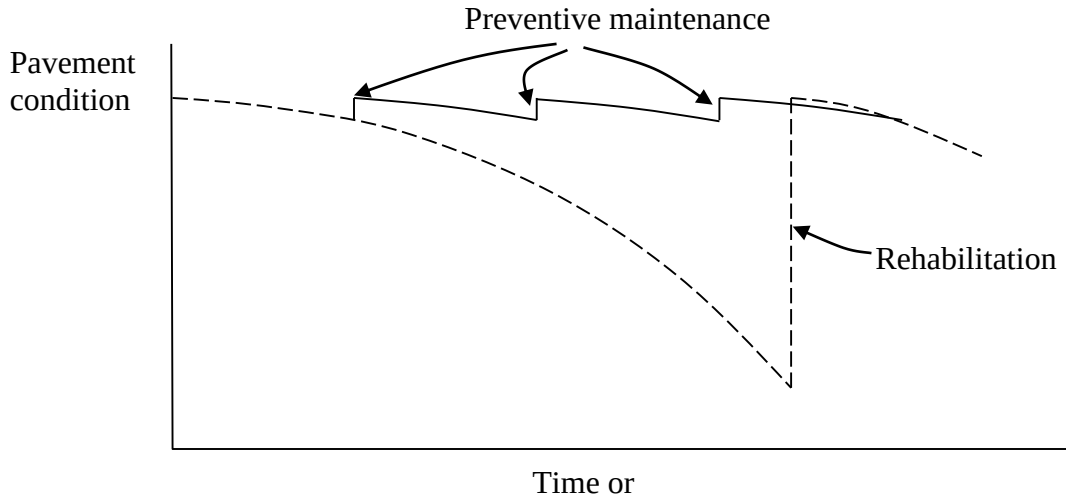

Figure 8-2. Performance of Preventive Maintenance Treatments.

8.2.3 Description of Some Maintenance Treatments

There are many different pavement maintenance techniques, including the do-nothing alternative. Before selecting a technique, one should be familiar with the choices available. Given the renewed interest in preventive maintenance treatments and their current little use in

Hawaii, the list below provides an brief description of several techniques falling in that preventive category (the only exception is pothole patching, which is an emergency repair.). Most of the following descriptions are adopted with minor modifications from Minnesota [92] and Michigan [93] manuals.

Crack sealing. A localized treatment method used to prevent water and debris from entering a crack, which might include routing to clean the entire crack and to create a reservoir to hold the sealant. It is only effective for a few years and must be repeated. However, this treatment is very effective at prolonging the pavement life. It typically includes the following two crack repair methods:

Clean and seal: Used on all types of cracks, it involves using a hot air lance or compressed air to blow out the debris in the crack, then filling with a sealant.

Route and seal: Used on transverse and longitudinal cracks. It involves using a pavement saw or router to create a reservoir centered over existing cracks, and then filling with a sealant.

Crack filling: Differs from crack sealing mainly in the preparation given to the crack prior to treatment and the type of sealant used. Crack filling is most often reserved for more worn pavements with wider, more random cracking.

Full-depth crack repair: A *localized* treatment method to repair cracks that are too deteriorated to benefit from sealing or filling. Secondary cracking requires the reestablishment of the underlying base materials.

Fog seal: An application of diluted emulsion (typically at a rate of 1:1) to enrich the pavement surface and delay raveling and oxidation. This is considered a temporary treatment.

Chip seal/Seal coat: Used to waterproof the surface, seal small cracks, reduce oxidation of the pavement surface, and improve friction.

Double chip seal: An application of two single seal coats/chip seals. The second coat is placed immediately after the first. This treatment waterproofs the surface, seals small cracks, reduces oxidation of the pavement surface, and improves friction.

Slurry seal: A mixture of fine aggregate, asphalt emulsion, water, and mineral filler, used when the primary problem is excessive oxidation and hardening of the existing surface. Slurry seals are used to retard surface raveling, seal minor cracks, and improve surface friction.

Microsurfacing: Microsurfacing is a mix of polymer-modified emulsion, well-graded crushed mineral aggregate, mineral filler (normally Portland cement), water, and chemical additives that control the break time. Microsurfacing differs from slurry seals in that it uses polymer modified asphalt and in that the curing process for microsurfacing is a chemically controlled process, versus the thermal process used by slurry seals and chip seals. Microsurfacing also may be used to fill ruts [92].

Thin hot-mix asphalt (HMA) overlays: These include dense, open, and gap-graded HMA mixes that improve ride quality, reduce oxidation of the pavement surface, provide surface drainage and friction, and correct surface irregularities.

Pothole patching: Includes using cold- and hot-asphalt concrete mixture, spray injection methods, as well as slurry and microsurfacing materials, to repair distress and improve ride quality.

8.3 Commonly used PMS Software

Many public and private domain programs are available. A good summary of the capabilities of most of these programs is provided by Wolters et al. [89]. The public domain programs included in their review are:

1) MicroPAVER® (now named PAVER™) (U.S. Army Corp of Engineers),
2) RoadSoft® (Michigan Tech Transportation Institute at Michigan Technological University),
3) StreetSaver® (Metropolitan Transportation Commission of the San Francisco Bay Area, California), and
4) The Utah LTAP Transportation Asset Management System (TAMS).

The private software programs reviewed by these authors are:

1. PAVEMENTview and PAVEMENTview Plus by Cartegraph,
2. PavePRO Manager by Infrastructure Management Services,
3. PubWorks by Tracker Software Corporation, and
4. RoadCare by Applied Research Associates, Inc.

Table 8-1 reproduces the comparison provided by Wolters et al. [89] of the various features of these eight PMS software programs. Additional details of each program are provided in [89]. Some of the information in Table 8-1 should be looked with caution as it may be outdated. In particular, this is known to be the case for the cost information.

Probably because the report of Wolters at el. [89] was geared towards PMS implementations for local agencies, widely used enterprise asset management systems, such as those of Deighton [94] and Agile Assets [95], were not included in their review. These two companies provide PMS modules with capabilities rivaling those of any of the systems mentioned above and can also be integrated with other asset management modules (signs, markings, culverts, etc.) offered by the same companies. Allegedly, they also allow optimal allocation of resources across different asset classes[64] and can be integrated with work order systems. Furthermore, these companies also provide services to maintain the databases and implement the systems, such as customization, configuration, user interface development, training, etc.

[64] These claims have not been evaluated and it is beyond the scope of this project.

Table 8-1. Comparison of Pavement Management Software Features (Source: [89]).

Criterion Description	PAVEMENT MANAGEMENT SOFTWARE PROGRAMS							
	PUBLIC				PRIVATE			
	MicroPAVER	**RoadSoft GIS**	**Utah LTAP TAMS**	**StreetSaver**	**RoadCare**	**PAVEMENTview Plus**	**PubWorks**	**PavePro Manager**
Vendor	U.S. Army Corps of Engineers	Michigan Technological University – Center for Technology & Training	Utah Local Technical Assistance Program	Metropolitan Transportation Commission	Applied Research Associates	Cartograph	Tracker Software Corporation	Infrastructure management Services
Website	www.apwa.net	www.roadsoft.org	www.utahltap.org	www.mtcpms.org	www.ara.com	www.cartegraph.com	www.pubworks.com	www.ims-rst.com
Laptop Data Collection	Yes	Yes	Yes	Additional Program Needed	*	Yes	Yes	*
Ability to Analyze Other Assets	No	Yes, signs, pavement markings, traffic counts, and traffic crashes	Yes	Yes, sidewalks, lights, signs, curb and gutter, & user defined.	*	Yes, sewer, signal, sign storm, bridge, & lights	Yes, bridges, signs, culverts, guardrails, parks, & buildings.	*
Default Pavement Condition Rating Measure	PCI	PASER	RSL	PCI	PCI, IRI	OCI	PASER	*
Analyzes Different Maintenance Strategies	Yes	Yes	Yes	Yes	Yes	Yes	No	Yes
GASB 34 Reporting	No	Yes	No	Yes	*	Yes	Yes	*
GIS Integration	Yes	Yes	Additional Software Needed	Additional Software Needed	Additional Software Needed	Additional Module-GIS director or own software	Addition module MapViewer needed	Additional Software Needed
Customization Capabilities	Yes	Only certain aspects	Yes	Yes	*	*	Additional modules available	Additional modules available
Costs (2011)	APWA members $995; non-members $1095	Contact vendor for more information	Utah-free/Out of state $500	$1500+, contact vendor for more information	Varies, contact vendor	Varies, contact vendor	Varies, contact vendor	Varies, contact vendor
User's Manual	Yes	Yes	Yes	Yes	*	Yes	Yes	*
Technical Assistance	Training courses or four-part web-based training	Telephone or web-based training	Free Telephone or paid on-site arrangements	4-day training class twice per year and customized on-site training.	*	On-site or web based training, technical support by phone	Formal training at 1 day per module, free updates, software helpdesk	*

Consideration of different assets and training opportunities are also true for some of the other programs in Table 8-1. For example, RoadSoft® also includes modules for other assets and MTU (Michigan Technological University) provides services and training.

The programs listed above are by no means an exhaustive list of options for managing pavement networks. Two important programs not included above are the Highway Development and Management Model (HDM-4) and the Highway Economic Requirements System - State Version (HERS-ST).

HDM-4 [96] is the successor of HDM-3 (the Highway Design and Maintenance Model) developed by the World Bank. This is one of the most commonly used PMS programs in the world because it is required for evaluation of projects financed by the World Bank. It is based on rigorous economic principles where costs and benefits are compared using decision criteria such as Net Present Value and Internal Rate of Return. It includes agency and user costs (vehicle operating costs and delay costs.)

HDM-4 does not appear to have been used much in the US perhaps because their pavement deterioration models, speed prediction models, and vehicle operating costs models were developed from large scale research projects funded by the World Bank in developing countries. An interesting feature of HDM-4 is that models individual distresses separately.

In the US, a tool that is available for all states is the Highway Economic Requirement System – State Version (HERS-ST) [97]. Reference [97] describes it as:

> "HERS-ST is an engineering/economic analysis (EEA) tool that uses engineering standards to identify highway deficiencies, and then applies economic criteria to select the most cost-effective mix of improvements for system-wide implementation. HERS-ST is designed to evaluate the implications of alternative programs and policies on the conditions, performance, and user cost levels associated with highway systems."

HEST-ST does incorporate many of the elements of PMS systems and similarly to HDM-4, it accounts for things such as travel time, safety, and vehicle operating and emissions costs that are not part of some other PMS systems. It uses a rigorous incremental benefit cost analysis to optimize highway investment. It also uses travel forecasts for each highway facility included in the Highway Performance Monitoring System (HPMS) sample database to predict future pavement and capacity deficiencies ([97], [98]).

The HERS-ST program was studied at the beginning of this project but it was determined that it was more appropriate for long term planning. Pavement deterioration predictions in HERS-ST [99] are based on structural number (SN) for flexible pavements or the slab thickness (D) for rigid pavements, on the present serviceability rating (PSR), and on the deterioration models of the AASHTO 1993 Design Guide [12]. Since the program assumes a one-to-one relationship between PSR and roughness (IRI), IRI could be used instead of PSR.

Although the program provides for a large number of highway improvements (e.g., addition of lanes and highway re-alignments), it considers only two pavement treatments: resurfacing and reconstruction. It is not clear how other pavement preservation treatments could be considered. Thus, it appears that the analysis is too coarse at this time for some desirable PMS activities. Nevertheless, if the program were updated to incorporate the new HPMS data fields [9] and improved to account for some of the factors mentioned above, it could be a viable and low cost alternative.

With the varied capabilities of the different programs, it is clearly not possible to say that one program is better than another in all respects. Preference for implementation of one program over another depends on many factors, many of which are non-technical: implementing agency goals; upper level management commitment to implementation; budget allocated for software purchase, maintenance, and service; internal organizational structure; intended users of the system (centralized, at the county level, or combination); database location, security and availability within districts; current data availability and future commitments for data collection; preferences for quantifying pavement condition; etc.

Early in the project, consideration of the expertise of HDOT's Materials Testing and Research Branch personnel assigned to work on the PMS and suggestions by one of the project managers together with the understanding of the resources already available at the Planning Branch led to the selection of three of the above systems for further study: StreetSaver®, RoadSoft®, and PAVER™. Two of these (StreetSaver® and PAVER™) are self-contained PMS programs and the other (RoadSoft®) can deal with several assets, including pavements. All three have a relatively low purchase cost and annual renewal cost. The following section describes these programs in more detail.

Before turning attention to these programs, it is important to note that the recent enactment of the MAP-21 legislation, the Moving Ahead for Progress in the 21st Century Act, signed into law on July 6, 2012, has revived the interest on the PMS and other asset management systems. This project started prior to the enactment of this legislation and its focus was on self-contained PMS software that could be implemented at HDOT's Materials and Research Testing (MT&R) Branch. Nevertheless, prior to MAP-21, the principal investigator consulted with the project manager at the time (around 2007-2008) about pursuing the study of the Deighton system in detail. However, not much interest in pursuing this possibility was shown at that time. Clearly, such systems cannot be evaluated without significant involvement from the agency. Therefore, this possibility was not evaluated further. Nevertheless, MAP-21 may have made the consideration of these enterprise systems more appealing since within 18 months of enactment, a process will be published for States to use in developing a risk-based, performance-based asset management plan for preserving and improving the condition of the National Highway System (NHS). Thus, the need to consider different assets and the risk of losing funding because of not meeting performance standards has made the investment on more comprehensive albeit more expensive asset management system software more attractive. However, considering the current personnel expertise, it is unlikely that if one of such system is selected it could be maintained at the MT&R branch without support from other branches.

8.4 PMS Software Evaluated

For this project, several options were considered. As indicated earlier, at the beginning of the project consideration was given to Asset Management Software such as dTIMS CT (Version 8) by Deighton [94]. At that time, it was implemented in seventeen State DOTs in the US and twenty one Canadian municipalities. They had 250 users worldwide. Several of the features claimed by the vendor include: data integration, centralized data management, client definable framework integrating client business processes, interaction with maintenance management systems, centralized data base, reporting via LAN or Web, cross asset optimization, advanced reporting and charting capabilities, and integration with GIS. The current version of this software is Version 9. However, in addition to the lack of interest on this software by the project manager (at the time this was suggested), it was not clear what data were available to feed the program, it represented a relatively high investment, and it would have required additional commitments

from different branches of HDOT. For all the above reasons the software in the end was not evaluated.

The licenses for three different programs were acquired at different points throughout the project: StreetSaver®, RoadSoft®, and PAVER™. The following subsections provide more details about these. The length of the descriptions are related to how much was accomplished with each program for the reasons described in each case.

8.4.1 StreetSaver®

The first version of StreetSaver® was released in 1987 by the Metropolitan Transportation Commission (MTC) – the transportation planning, financing and coordinating agency for the nine-county San Francisco Bay Area, California [100]. In the more than two decades that StreetSaver® has been in use, there have been 109 users in the San Francisco Bay Area and more than 250 users nationwide and internationally [100].

In the past, StreetSaver® was a standalone program. However, the current version of the program, Version 9, is offered online. That is, the user interface is accessed through a web browser. Furthermore, the SQL Server database used by the program resides on MTC servers. This has the advantage of releasing the users of server maintenance and security.

StreetSaver® utilizes a modified version of ASTM Standard D 6433 to identify seven (7) distresses and three (3) severity levels to calculate the condition of pavements surfaced with asphalt concrete and surface treatments. The distress types are: 1) alligator cracking, 2) block cracking, 3) distortions, 4) longitudinal & transverse cracking, 5) patching & utility cuts, 6) rutting and depressions, and 7) weathering & raveling.

For Portland cement concrete (PCC) pavements, the distresses considered include: 1) corner break, 2) divided slab, 3) faulting, 4) linear cracking (longitudinal, transverse and diagonal cracks), 5) patching and utility cuts, 6) scaling/map cracking/crazing, and 7) spalling.

Based on the above distresses, StreetSaver® computes the pavement condition index (PCI) to measure the condition of a given section of pavement on a scale from 0 to 100, with 100 representing a pavement in excellent condition (see section 4.3.1.1.1, page 133) for a brief description of the PCI calculation.

StreetSaver® provides real-time PCI (i.e., computed based on existing distresses) and projected PCI based on projected deterioration and future treatment strategy on each road segment, as well as overall road network.

The prediction of PCI over time is based on the last observed PCI combined with the deterioration curve of the family to which a pavement section belongs. Pavement sections are assigned to different pavement families based on their surface type (AC, AC/AC, ST, AC/PCC, PCC, and Gravel) (Figure 8-3) and on their functional classification (Arterial, Collector, Residential, and Other). The meaning of the symbols for surface types above (other than Gravel, that has an obvious meaning) are: AC = Asphalt Concrete, AC/AC = Asphalt Concrete Overlay over Asphalt Concrete, ST = Surface Treatment (e.g., chip seal, slurry seal, or microsurfacing), AC/PCC = Asphalt Concrete over Portland Cement Concrete, and PCC = Portland Cement Concrete.

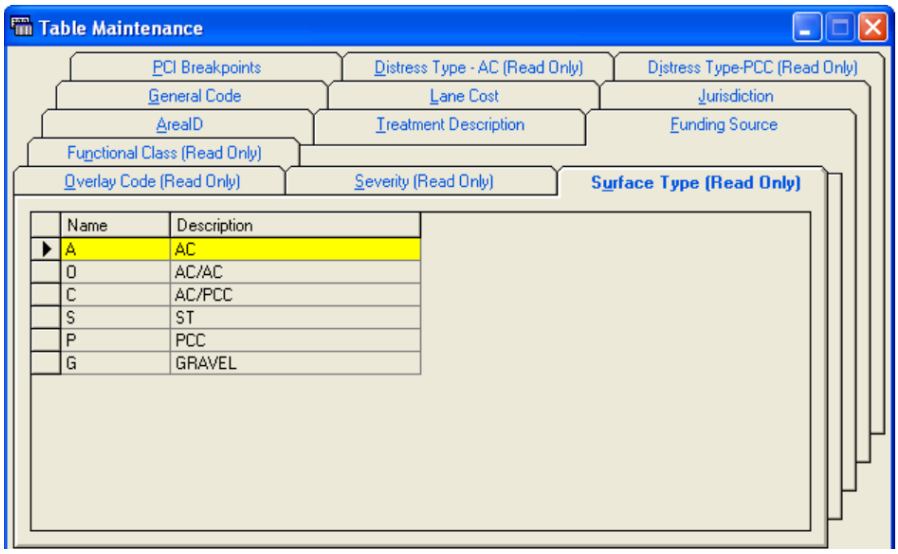

Figure 8-3. Surface types in StreetSaver®.

StreetSaver® uses the computed PCIs and the pavement families' deterioration curves to predict the future condition of each pavement section. The equation used to model deterioration (i.e., PCI vs. Age) is:

$$PCI = 100 - \frac{\rho}{\ln\left(\frac{\alpha}{Age}\right)^{\frac{1}{\beta}}} \quad (8\text{-}1)$$

where ρ, α, *and* β are model parameters.

The parameter α controls the age at which the PCI is projected to reach zero, the parameter β controls how sharp the curve bends, and the ρ parameter controls the location of the curve inflexion point [7].

Budget needs and budget consequences are determined with the help of decision trees. As shown in Figure 8-4, in StreetSaver® different condition categories (I, II, III, IV, and V) are defined for each surface type (AC, AC/AC, AC/PCC. ST, and PCC) within a given highway functional classification (Arterial, Collector, Residential/Local, and Other). For each of the condition categories shown in Figure 8-4, the suggested treatment as well as the cost per unit area (or per unit length for crack sealing) and the number of years between treatments must be defined (this is done is a separate form not shown here.) Then, based on these decision trees, the program can determine budget needs to maintain the network at the optimal level over an analysis period (commonly 5 years, but the program can analyze up to 30 years). The use of the word "optimal" here needs clarification as it depends on whether the decision trees are the most appropriate for the types of pavements analyzed. Note that no "optimization" is really carried out in the budget needs analysis but instead appropriate treatments are identified when each section reaches threshold values in the corresponding decision tree. The premise is that with enough funding, it is cheaper to maintain pavements in good condition. When budgets are constrained, weather a treatment is applied to a given section when it reaches a trigger value depends on the availability of funds and the prioritization described next.

It is important to note that the user has control over what constitute the different condition categories (Figure 8-5).

The budget needs analysis can then be used to analyze several budget scenarios. Typically, funding is insufficient to address the budget needs. Therefore, some form of prioritization needs to be carried out to allocate a given budget. For this purpose, StreetSaver®

computes a Weighted Effectiveness Rating (WER) for each treatment assigned and ranks the sections by WER, from highest to lowest.

The effectiveness rating is based on the ratio of the expected effectiveness[65] for the identified maintenance and rehabilitation treatment per year of influence to their equivalent uniform annual cost per square yard adjusted by a weighting factor. The user is allowed to specify different weighting factors based on functional classification to account for the fact that it is generally less costly to repair residential/local streets, and that in general, they will have longer lives than arterial streets. These weighting factors avoid that all the funding be allocated to streets of lower categories by essentially weighting for roadway usage.

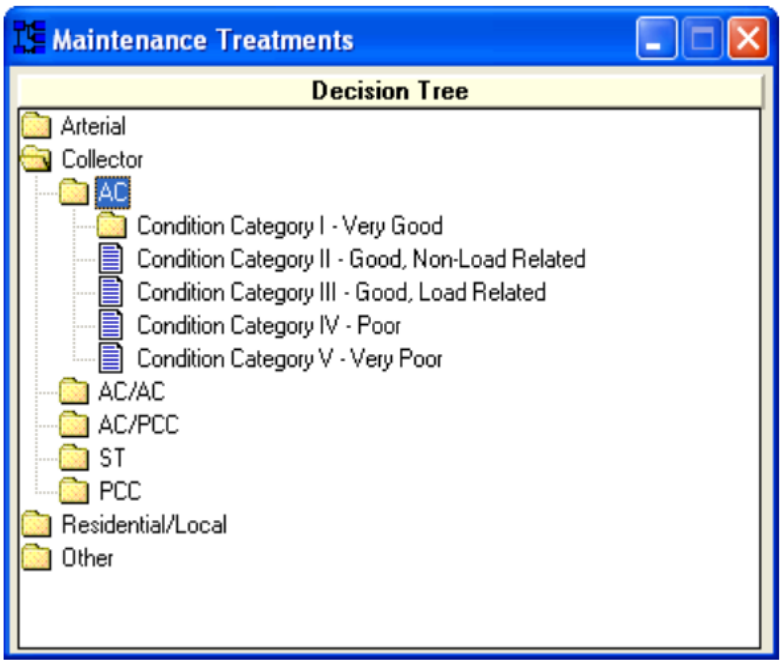

Figure 8-4. Decision tree definition in StreetSaver®.

[65] Effectiveness is typically defined by the area under the deterioration curve.

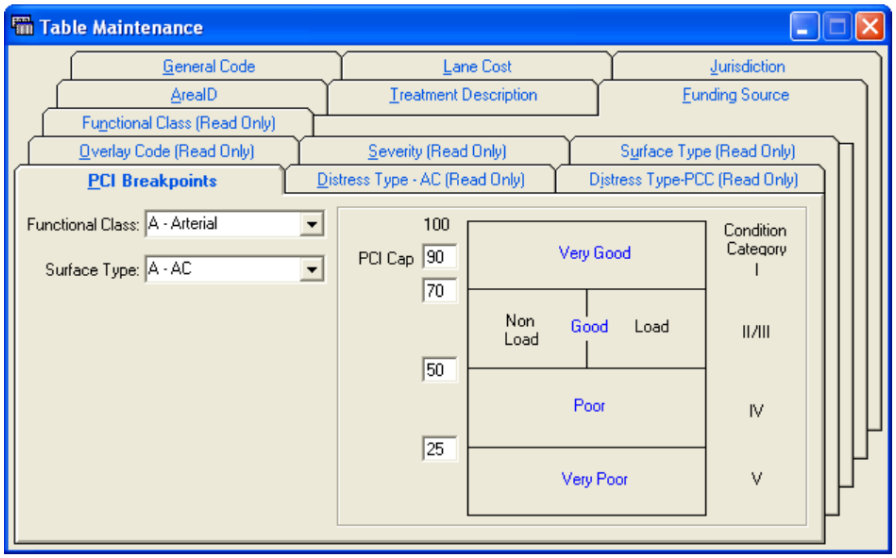

Figure 8-5. Definition categories in StreetSaver®.

StreetSaver® provides the capability to analyze different "Budget Scenarios". For a budget scenario, sections are selected for rehabilitation treatments from the ranked list obtained from the needs analysis until the funds available for rehabilitation projects (equal to the total budget for the year minus the portion reserved for preventive maintenance) have been allocated. The program then totals the amount of deferred maintenance (rehabilitation only), and estimates stop gap costs. The amount of stop gap costs is subtracted from the preventive maintenance budget and then sections are selected for preventive maintenance treatments from the previously developed ranked list. Finally, the program totals the amount of deferred preventive maintenance.[66] These "Budget Scenarios" calculations can be used to determine the impact of various funding strategies.

Other features of StreetSaver® include "Project Selection Analysis" that assists users in translating network pavement repair recommendations into contract packages, XML (extended markup language) importing and exporting of inspections or inventory data from 3rd party software vendors, attachment of supplemental documents (JPG, PDF, Rich Text (.rtf), Word

[66] It is important to note that the user can define what treatments constitute preventive maintence. The above is just a general explanation of the logic used by the program. It is not intended to describe all the options available.

(.doc), Excel (.xls), and MPEG) to provide background information to each individual road segment, and up to 10 customized user-defined fields. The program also provides the capability to generate more than 40 standard reports and graphs, customized reports utilizing a built-in "Custom Report Wizard". Reports can also be exported to various formats (e.g., .xls, .rtf, .txt, PDF, and MDB). In addition, the program has a GASB 34 reporting module to facilitate the reporting of pavement assets to comply with the requirements of the Government Accounting Standard Board's Statement 34 (GASB 34) .

StreetSaver® also provides a GIS Toolbox to allow users to link their street networks to a GIS basemap so that they can display and plot results graphically.

A companion software to StreetSaver®, MobileRater™, is available to assist with the collection of pavement distress data with handheld computers. MTC offers several user services such as virtual on-site and hotline support and training workshops. In addition, it holds a User Week event three times a year (typically in Oakland, California): in March, July and November.

The current cost of the annual license of StreetSaver® outside the San Francisco Bay Area is $1,500 ($2,000 for consultants.) There are additional costs for a Software Support Service Plan, a Technical Support Plan, GIS Mapping Integration, Data Migration, and the MobileRater™ license. The up-to-date costs can be found at http://www.mtcpms.org/products/. Compared to the costs needed to adequately feed any PMS, the above costs are relatively minor.

As part of this research project, the license for this program was paid for a period of two years (2007-2009). Unfortunately, at the time, there was little reliable data to define the sectioning of the network (see the description of the efforts in this respect in the PAVER™ description below) and the corresponding pavement conditions. Consequently, most the program features were not evaluated with actual data.

8.4.2 RoadSoft®

8.4.2.1 General

RoadSoft® is a roadway asset management system for collecting, storing, and analyzing data associated with transportation infrastructure [101]. The Michigan Tech Transportation Institute at the Michigan Technological University (MTU) began its development in 1992 on input and guidance from local road agencies in Michigan. According to [89], clients of

RoadSoft® include the Michigan Department of Transportation, Federal Highway Administration, over 200 cities and villages, and almost 100 county road agencies in Michigan and throughout the U.S.

Roadsoft® is built on a combination of a database engine and GIS mapping tools. Figure 8-6 shows the main interface of the version of RoadSoft evaluated in this project (V7.2.0.7). As shown in that figure, in addition to pavements (as indicated by the layer "Road"), RoadSoft® considers other assets such as culverts, point pavement markings, signs, traffic counts, driveways, sidewalks, and linear pavement markings. Furthermore, according to [101], other assets or data now considered include bridges, crash data, and intersections.

Figure 8-7 shows a screenshot of part of the culvert module and Figure 8-8 shows a screenshot of part of the sign module. Each module contains many more associated windows and details not explained here.

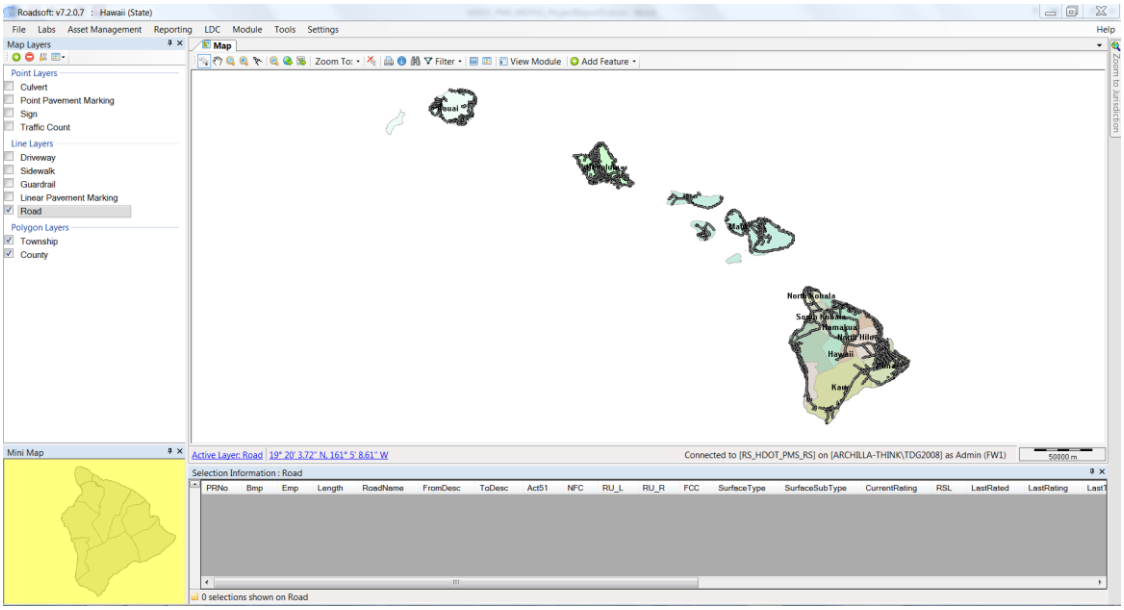

Figure 8-6. RoadSoft® main interface.

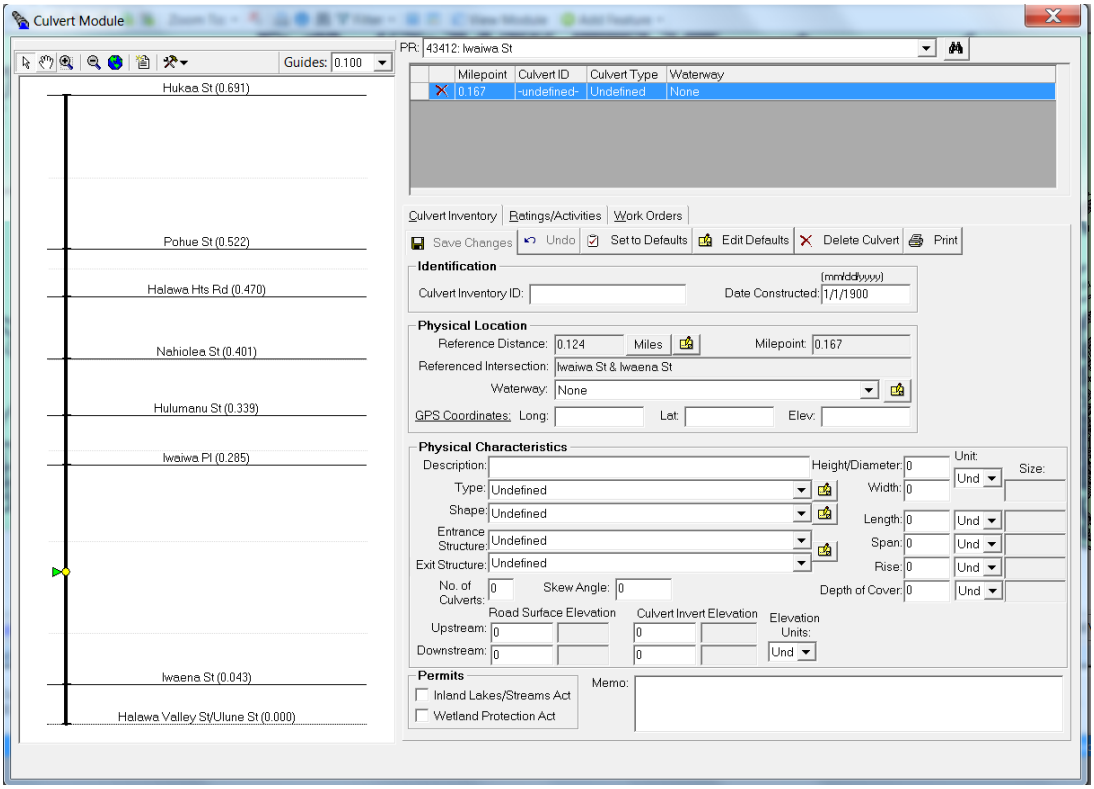

Figure 8-7. RoadSoft® culver module.

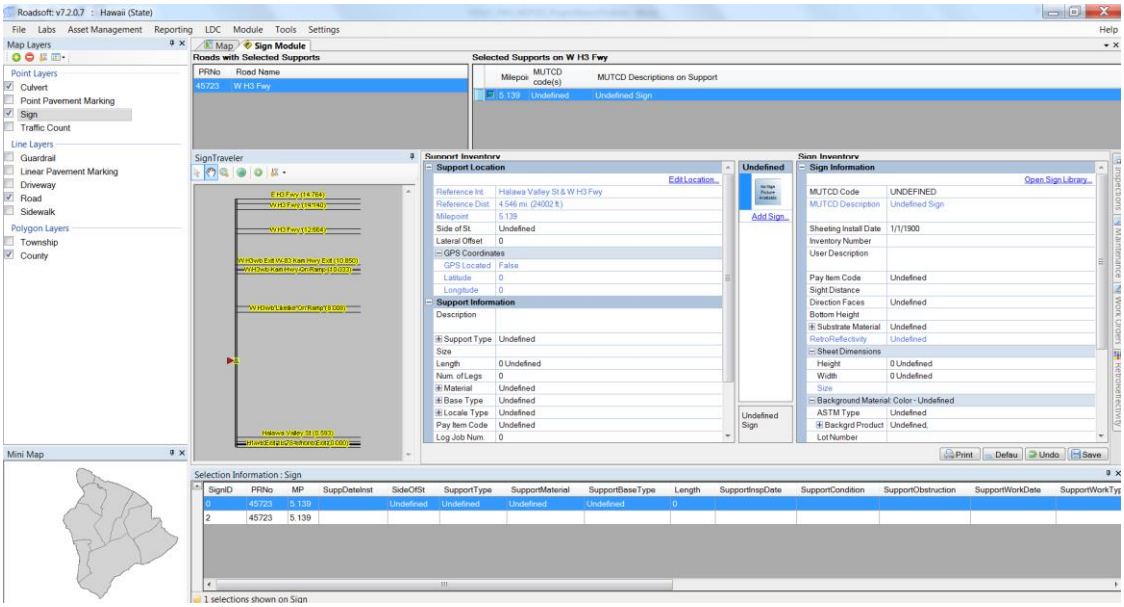

Figure 8-8. RoadSoft® sign module.

8.4.2.2 Inventory and Condition

In RoadSoft®, several pieces of information can be stored. Assets are located in reference to a base map. As illustrated later, in some of its screens, RoadSoft® uses information about cross streets to more easily locate segments. This is a very nice feature of the program but, at least for the version evaluated, it comes at the cost of depending on MTU for its creation and modification. A discussion of this issue is presented later.

Figure 8-9 shows a portion of the base map created by MTU for Hawaii based in part on shapefiles provided by HDOT to the Hawaii Statewide GIS Program in 2011 [102]. Those familiar with Hawaii's State Roads network can recognize that the base map includes much more than just State roads. Once a road segment or set of roads segments are selected by the user, clicking on the View Module button (see the second to last button on the toolbar above the map in Figure 8-9) brings up the Road module screen shown in Figure 8-10, which is where the inventory and condition information is entered.

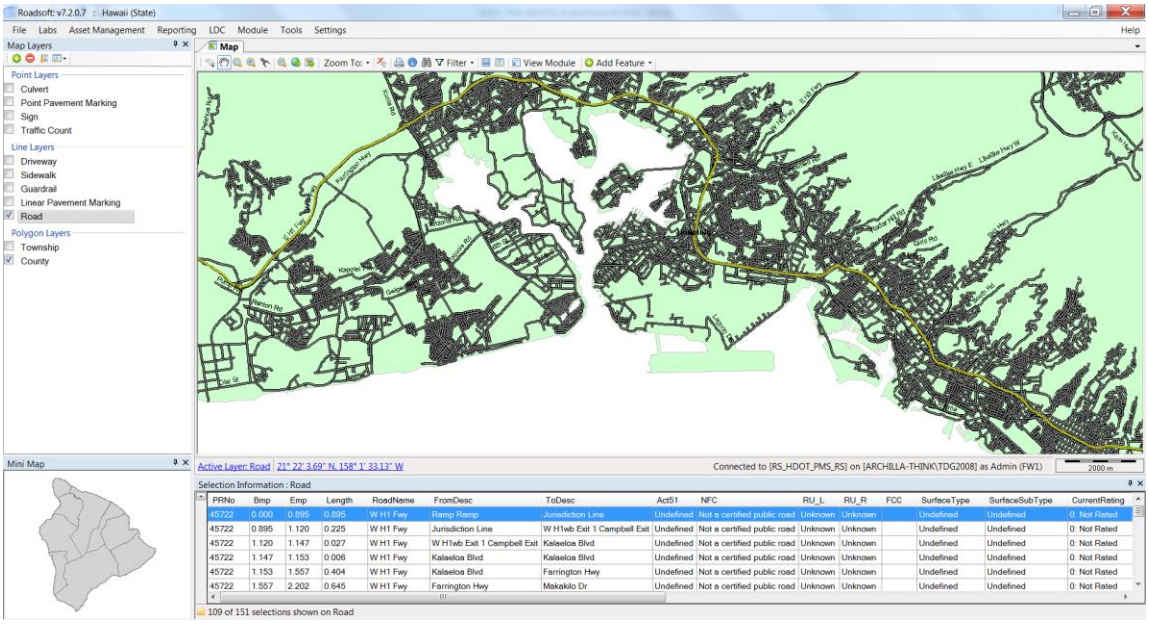

Figure 8-9. Illustration of part of the RoadSoft® base map with a selection set corresponding to the westbound direction of H-1.

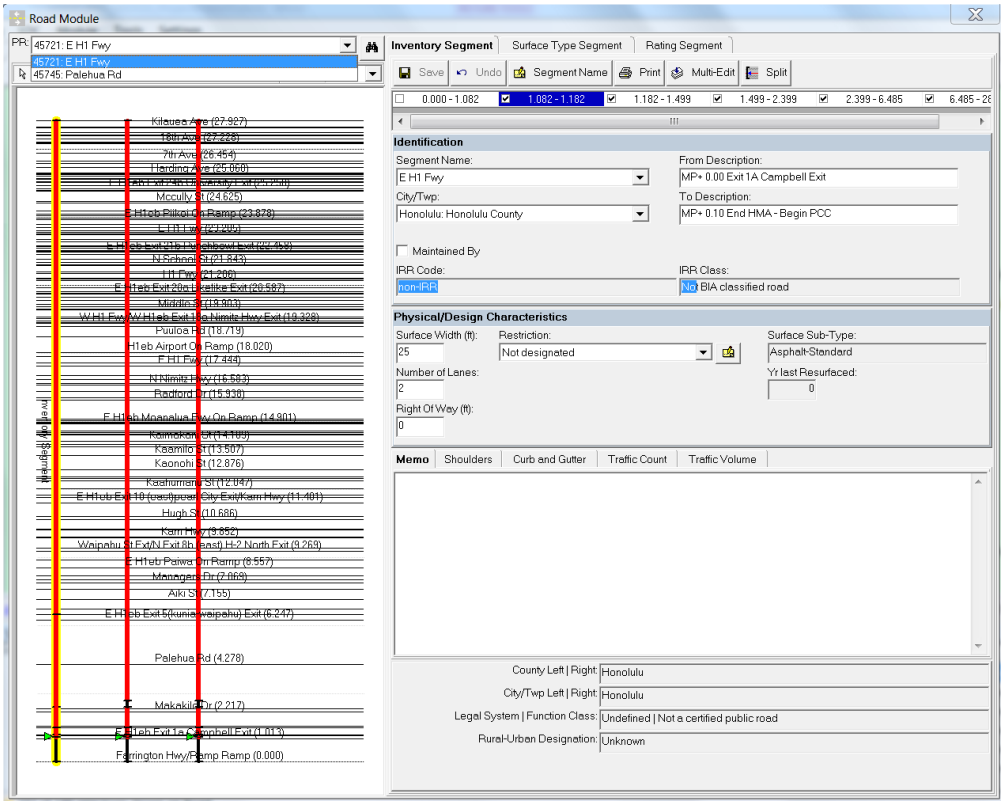

Figure 8-10. RoadSoft® Road module with Inventory Segment tab selected.

At the top-left corner of Figure 8-10, there is a list box (displaying two items in this example.) The items in the list box are the roads for which the user selected at least one segment in the base map in Figure 8-9. For the particular example of Figure 8-10 only two roads were selected. The list box is labeled with the text "PR", which represents a unique number assigned to each **P**hysical **R**oad. Below this list box, there is a chart with three vertical lines, each representing the linear referencing for inventory segments, surface segments, and rating segments, respectively. In this chart, the horizontal lines represent the location of cross-roads and provide a visual cue for users to easily locate segments of interest. As shown in Figure 8-10, for long roads, the information about the cross streets can become cluttered. Fortunately, the program also provides zooming and panning capabilities to overcome this issue. As shown in Figure 8-11, the user can zoom to a level where there is no more clutter on the cross street information.

The three vertical lines correspond to the three tabs located to the right of the "PR" list box, which are used for entering information about inventory, surface type, and rating segments.

The information for each segment on each tab is discussed shortly. The location of these segments (or more appropriately, their endpoints) are created independently for each tab. Thus, for example, the segmentation for inventory may be different from that for surface type and rating segment. This is a very convenient feature, for example, to deal with pavement condition information collected every 0.1 mi (as currently contracted by HDOT). Such information can be entered in RoadSoft® regardless of how the inventory and surface type segments are defined.

As can be observed from Figure 8-10, the inventory information for each segment consists of identification information (e.g., labels for the end points) and physical design characteristics such as surface width, number of lanes, and year of last resurface. In addition, at the bottom of the form, there are different tabs that permit the user to enter information in a memo form as well as shoulder information (surface types and width), curb and gutter information (type, curb reveal, configuration, year built, rating, and rating year), traffic counts, and traffic volumes. The surface width together with the actual length of the segments (taken from the actual end points) are fundamental to compute costs when analyzing funding strategies.

Figure 8-11 displays some of the information shown in the Surface Type tab. Again, the user can enter a description for the endpoints of the segments ("From" and "To" descriptions) and select the surface type (asphalt, brick, composite, concrete, graded earth, gravel-standard, seal coat-standard, undefined, or unimproved earth). The form displays actual material types and thicknesses for each layer (Surface, Base, Subbase, and Subgrade) as well as information about geotextiles, traffic loading in term of ESALs, and structural number. Input of the aforementioned information is actually performed in another form, Figure 8-12, that is accessed by selecting the "Edit Design Characteristics" button shown on Figure 8-11. The types of materials in the Pavement Design form can be easily configured based on agency practices. As shown in Figure 8-12, it is easy to configure the program to accept the labels of local mixes such as State Mixes II, III, IV, and V.

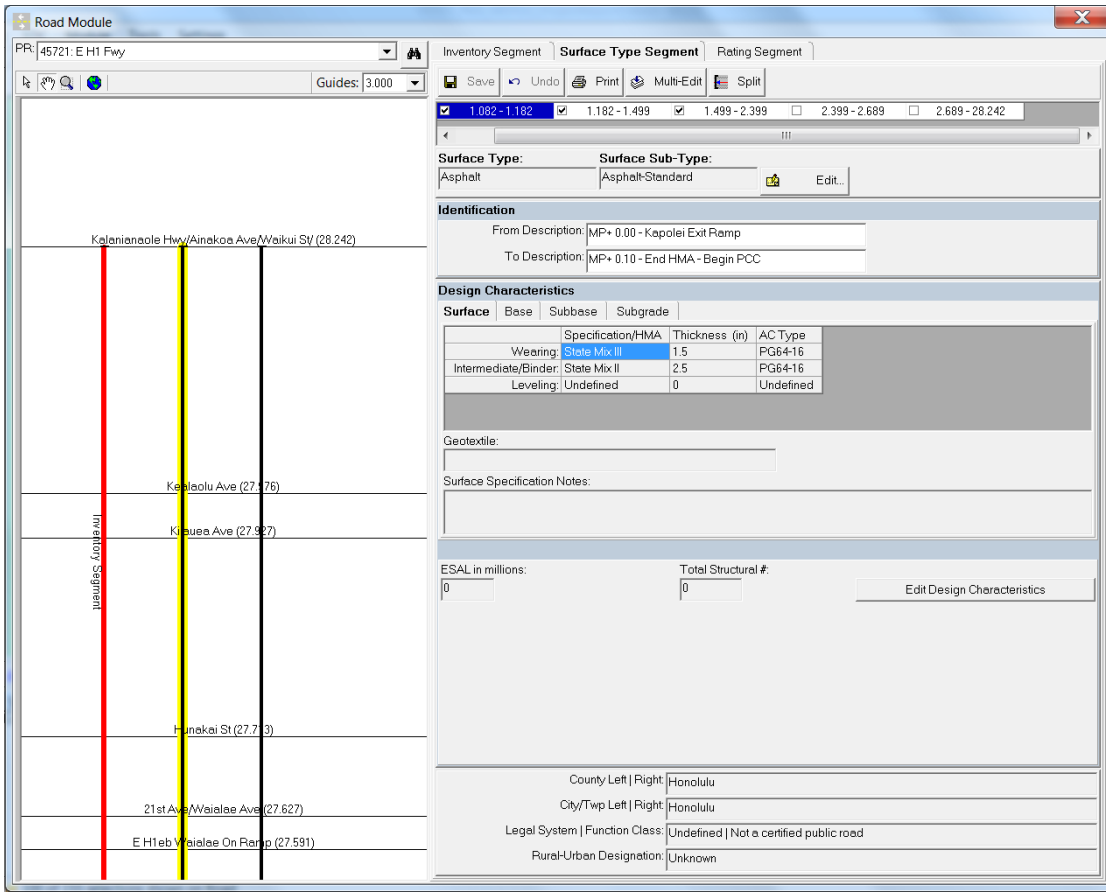

Figure 8-11. RoadSoft® Road module after zooming on an area of interest with Surface Type Segment tab selected.

Figure 8-13 shows the rating form. The form contains two parts. The first part allows inputting section identification information. In the second part, there are three tabs to enter Rating/Construction History Information, displaying Archive Information, and entering Schedule Maintenance Information. Figure 8-14 shows the form to add/edit ratings. The form contains four list boxes for rating the surface, the base, drainage, and ride. For rating of the surface, RoadSoft uses the PASER rating system. In this system, the rating is a subjective value between 1 and 10 with 10 being excellent and 1 being failed. Guidance for rating pavement surfaces using this system is given in reference [10]. The user can actually enter a value of 0 as well, which indicates that a segment has not being rated. For rating the base, drains, and ride, values of 0-failed, 2-Very poor, 4-Poor, 6-Fair, 8-Good or 10-Excellent can be entered.

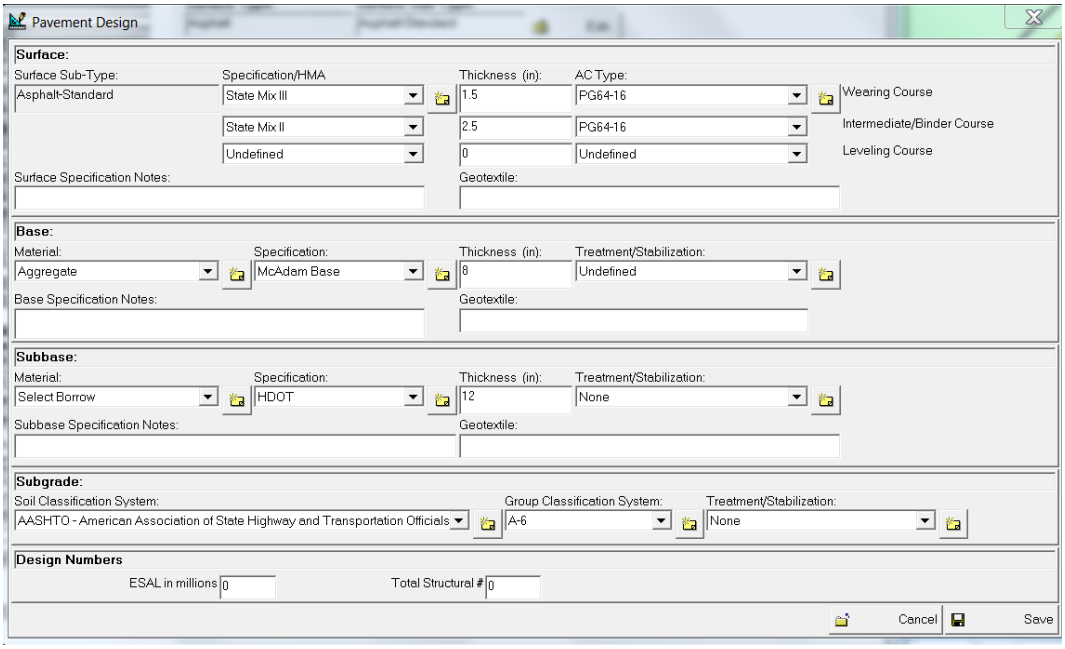

Figure 8-12. Pavement Design information form.

In the Rating Segment tab, the user may also record the activities performed to a given segment as shown in Figure 8-15. As indicated earlier, RoadSoft® is very flexible, allowing ratings at every 0.1-mi segment, as currently collected by the HDOT's Planning Branch. However, most often, activities would be performed over segments much longer than 0.1-mi long. RoadSoft® helps in this respect by providing a Rating Segment Multi-Edit option. Thus, the user does not need to enter the activity information on every 0.1-mi segment.

Within the rating segments tab, RoadSoft® provides the option of entering and editing schedule maintenance activities. This is shown in Figure 8-16.

So far, all the discussion has been about entering information for inventory, surface type, and rating segments but no explanation has been provided about how those segments are defined. Initially, each route (a single PRNo in RoadSoft®) constitutes a single segment. The user can then use the "Split" button (shown in Figure 8-10, Figure 8-11, and Figure 8-13) to split a segment into two. Actually, selecting split provides three options: splitting of a segment, adjusting an existing split, or merging segments. Only the splitting option is discussed here.

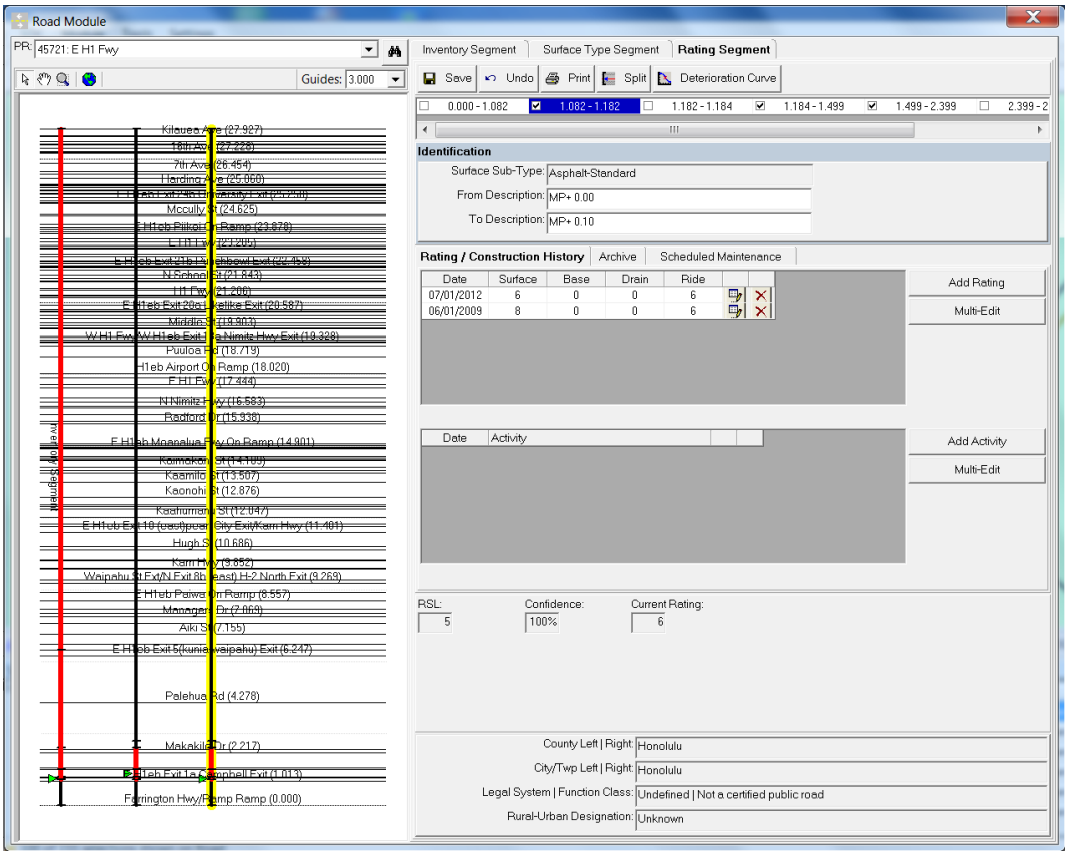

Figure 8-13. RoadSoft® Road module with Rating Segment tab selected.

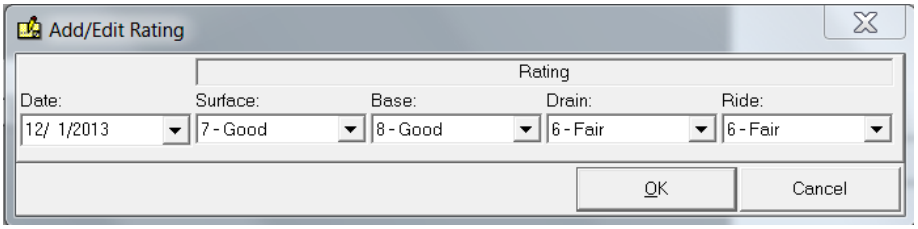

Figure 8-14. Add/Edit Rating form.

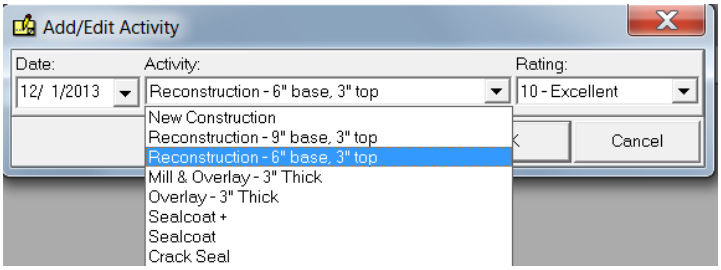

Figure 8-15. Add/Edit Activity form.

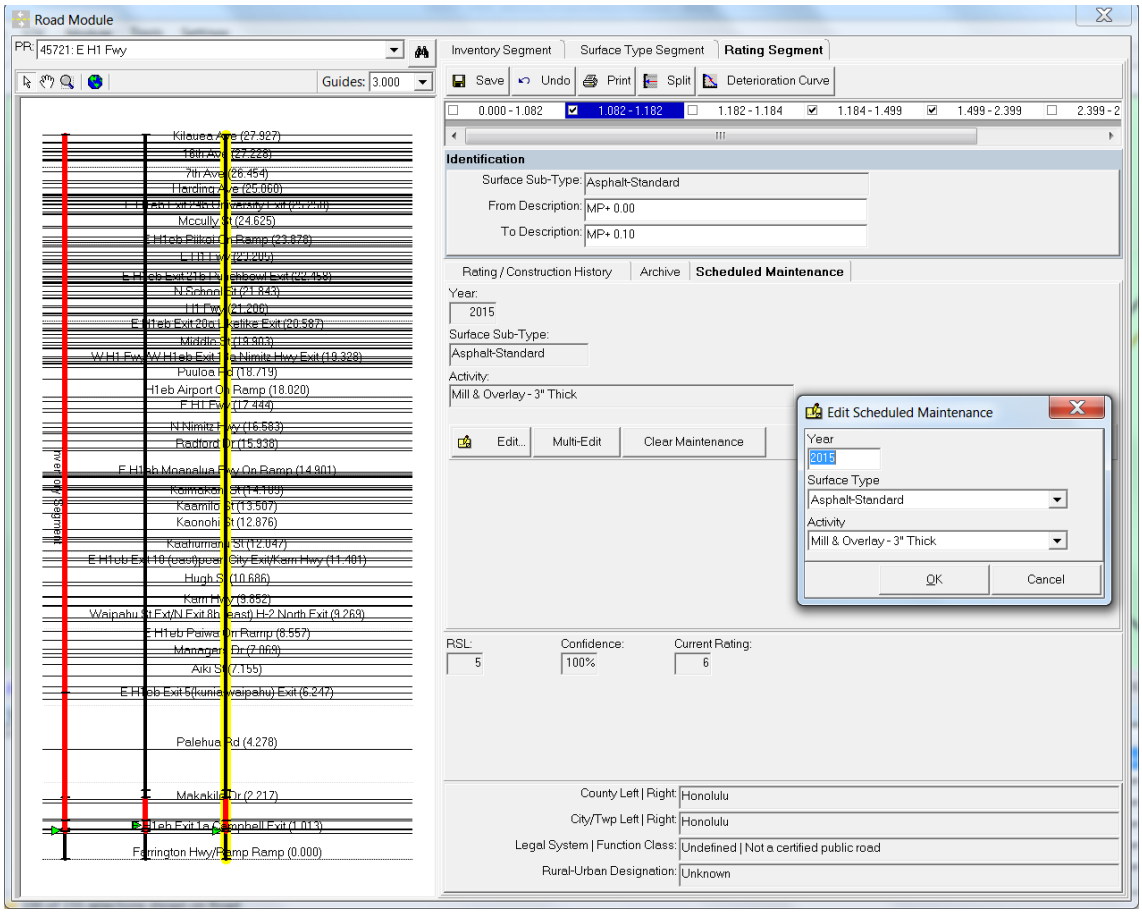

Figure 8-16. Editing Scheduled Maintenance.

The Split Inventory Segment form (shown in Figure 8-17), provides a visually attractive and intuitive way to create segments. The user can drag the splitting point either in the map or in the straight line diagram next to it. In either case, the point is updated simultaneously in the other graph and in the text box at the bottom. Alternatively, the user can also enter a value in the text box to define more precisely the splitting point.

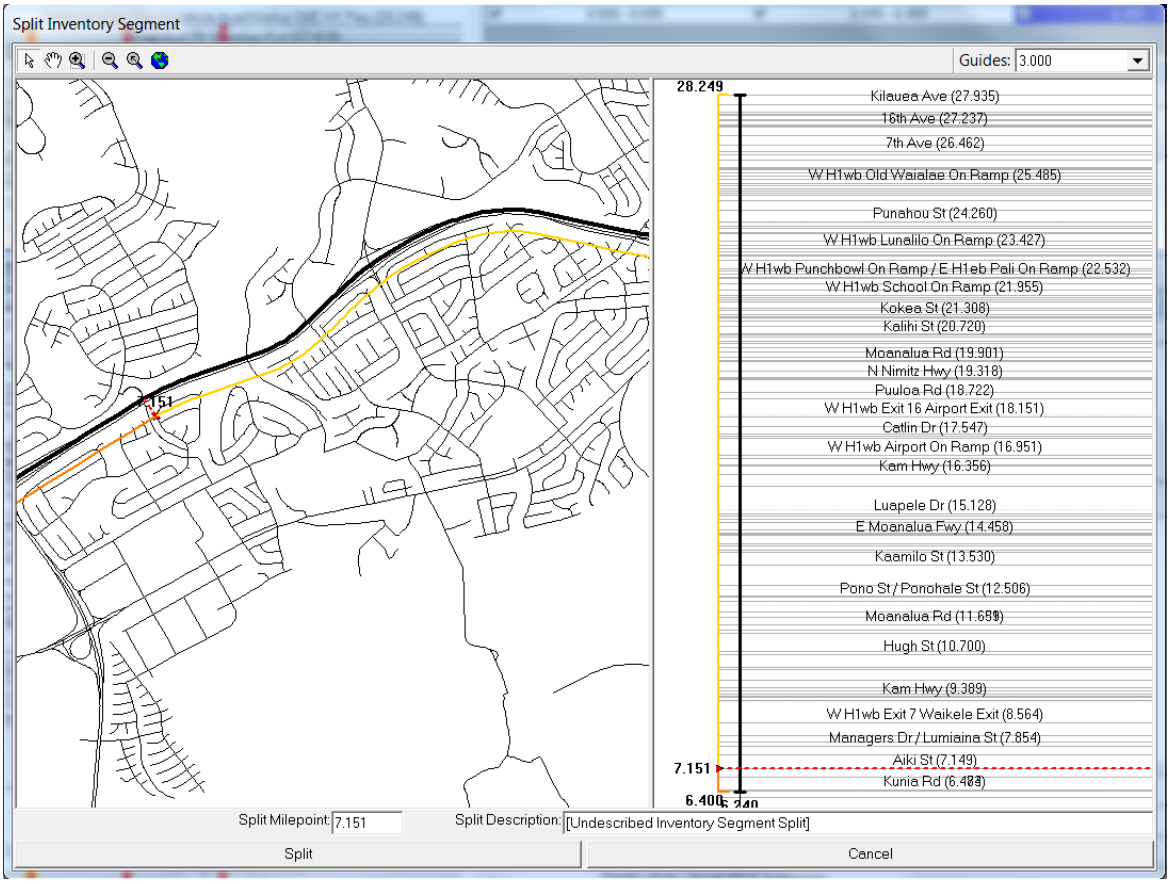

Figure 8-17. Split Inventory Segment form.

8.4.2.3 Strategy Evaluation/Optimization

RoadSoft® has a strategy evaluation/optimization module that allows the evaluation of user defined strategies or the automatic search of near optimal strategies. In either case, the program needs some basic information about the types of treatments available for each surface type. Figure 8-18 shows the Surface Type Definition form in RoadSoft®[67]. As shown in that figure, RoadSoft® recognizes six surface types: Asphalt, Brick, Concrete, Earth, Gravel, and Seal Coat. Within each surface type, the user can create different surface sub-types. For example, in Figure 8-18 two sub-types for the Asphalt surface type have been created: Asphalt-Standard and Composite. Furthermore, as shown in the middle part of Figure 8-18, for each surface sub-

[67] These figure have been created with very little actual data and thus they are not intended to present realistc optimized scenarios. Nevertheless, they provide a picture of the program capabilities.

type, the user can define the type of treatments that can be performed as well as the information needed for evaluating/optimizing strategies (trigger values and costs).

Figure 8-19 shows the screen where the user specifies which treatments to use for optimizing a strategy as well as the inflation rate, the number of years to program, and the budget. Running the optimization results in output such as that shown in Figure 8-20[68], which includes the cost by year, percent of good, fair, and poor by year, lane miles of activity performed by year, and average remaining service life by year.

Clearly, for the selection and evaluation of strategies, the program needs to predict the pavement condition over time. As with other PMS software, RoadSoft® uses the concept of pavement families. As seen at the bottom of Figure 8-18, for each surface sub-type the user must associate a "curve" (meaning a deterioration curve). Deterioration curves are defined as shown in Figure 8-21, in which the number of years that pavements in the family stay in each condition rating must be specified. The user can select among different types of models to fit to the data (Gompertz forced through zero, Gompertz unforced through zero, Logistic Growth forced through zero, Logistic Growth unforced through zero, and Sigmoid S curve).

In one of the approaches used by RoadSoft®, the family curve is adapted for each section to the deterioration observed over time on the particular section. This is illustrated in Figure 8-22.

8.4.2.4 Reporting

Since RoadSoft® is built on GIS mapping tools, it is relatively easy to create map reports identifying features of interest such as pavement conditions, surface types, remaining service life, etc. In addition, the program also provides the capability of creating tabular road reports that are configurable by the user. In order to create and/or edit reports, users need some basic understanding of database queries (as is the case for most PMS software) (Figure 8-23).

[68] Note again that the screenshot was created without almost no data in the program, which explains the very small mileages shown in the figure and the single bar in the cost by year chart.

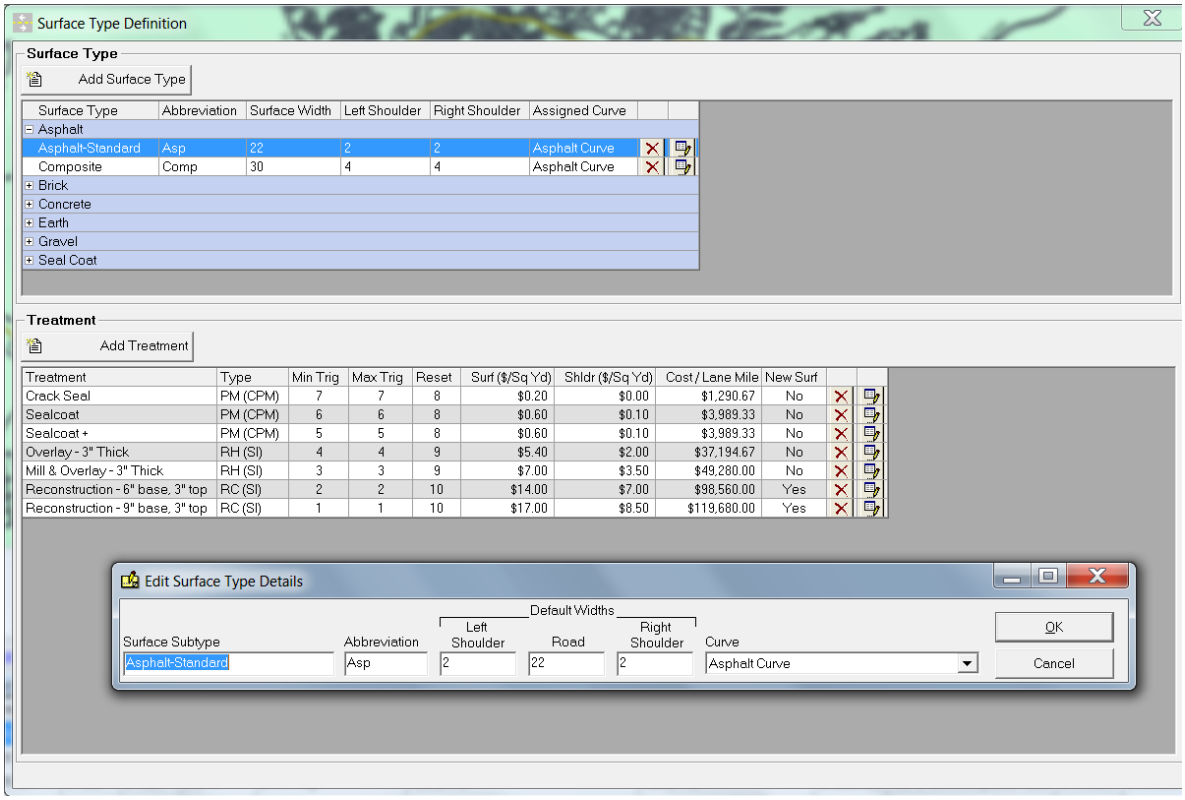

Figure 8-18. Surface types and treatment data in RoadSoft®.

8.4.2.5 Issues to Overcome for Implementation

In general, RoadSoft® presents a very attractive alternative. However, for implementation, a few issues need to be considered and studied in more detail.

The main issue found during the evaluation of the program is a common PMS problem, which is appropriately locating pavement sections. As indicated earlier, as currently implemented, the base map and associated database for RoadSoft® is created by MTU based on information provided by the user. For the evaluation in this study, the shapefiles provided by HDOT to the Hawaii Statewide GIS Program in 2011 [102] were provided to MTU.

After the first delivery, it was noted that the base map in RoadSoft® did not agree in some respects with the shapefiles given to MTU. Specifically, according to the base map in RoadSoft®, H-1 was approximately 8 miles long, whereas in the shapefile and HDOT's RIS H-1 is 27.16 mi long.

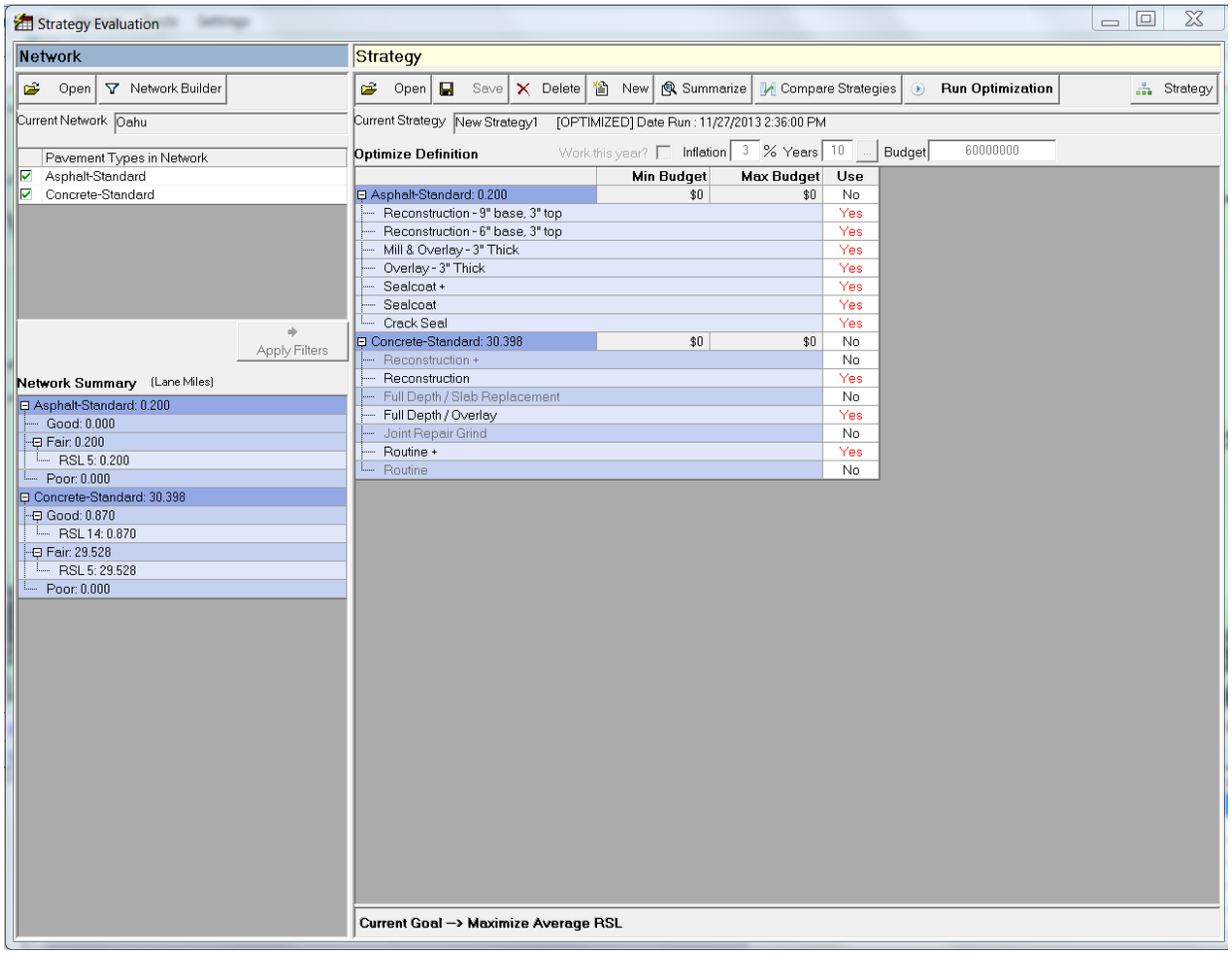

Figure 8-19. Strategy Evaluation/Optimization screen in RoadSoft®.

After discussions with the vendor, it was acknowledged that there had been a problem in the data translation algorithm. Thus, a new database with a new base map was provided to UH. Unfortunately, some issues were also discovered with the new delivery. Specifically, as illustrated in Figure 8-11 (page 453), H-1 is shown as being 28.24 miles long, which is still more than one mile longer than it actually is. A careful analysis of the new base map revealed that the problem with the second database was not with the geometry but with the definition of when a road starts or ends. For the H-1 example, a 1.082-mi long portion of State Route 93 had been assigned as being part of H-1 (conversely, State Route 93 was shorter that it should have been by the same amount.)

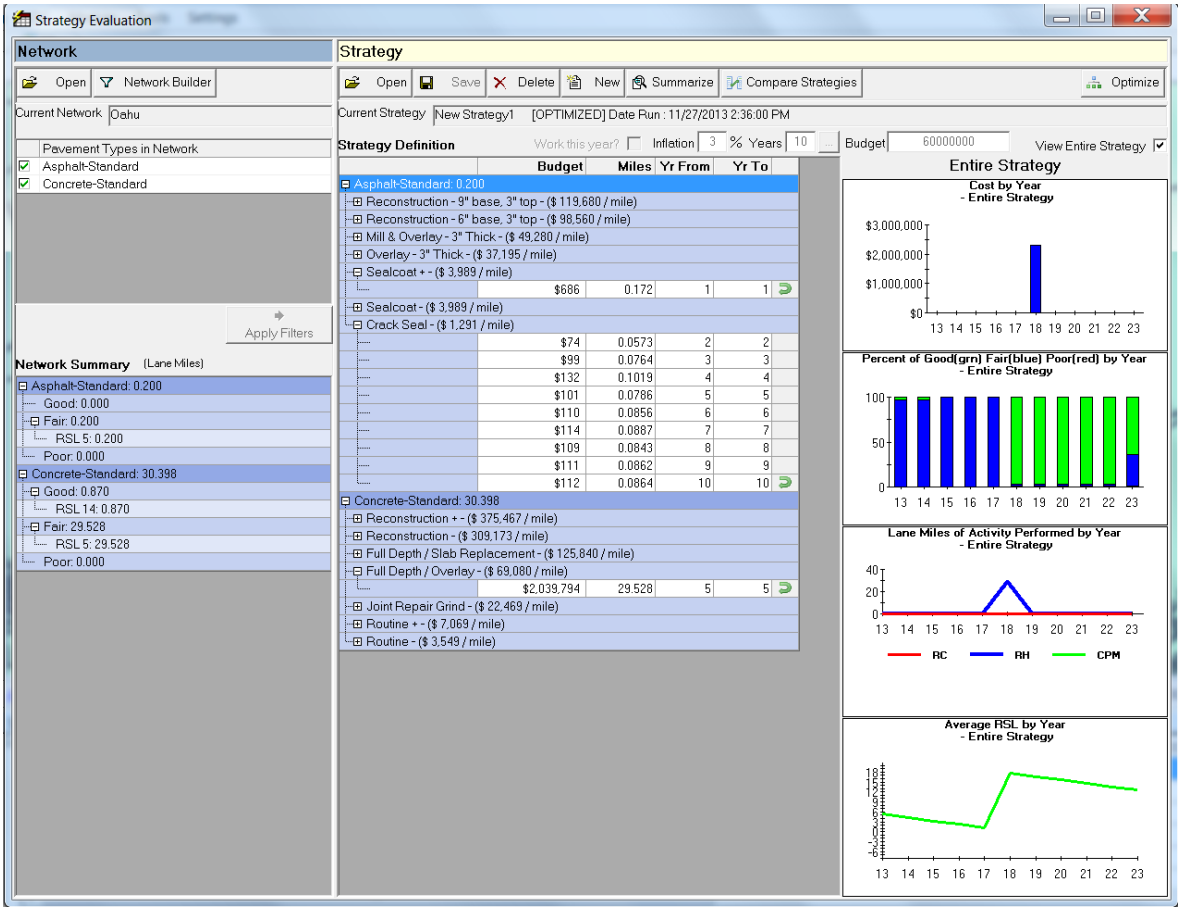

Figure 8-20. RoadSoft® strategy evaluation results.

The issue described above is a perfectly solvable problem but it needs coordination between the vendor and HDOT (with the associated additional service costs that this would entail) if the program is considered further for implementation.

Note that the distress would be located appropriately if the Laptop Data Collector created by MTU together with a GPS unit is used. Also, one could easily enter an offset to define the segment into their appropriate locations. For example, for the selected segment on Figure 8-16 (page 456), which goes from mile points 1.082 to 1.182, the “From” and “To” descriptions were entered as MP+ 0.00 and MP+ 0.10, respectively, which is the results of using an implicit offset of 1.082 miles. However, these “fixes” would most likely results in errors (it is easy to get confused whether an offset has to be added or subtracted, forgetting that an offset needs to be applied, etc.) and require unnecessary additional bookkeeping.

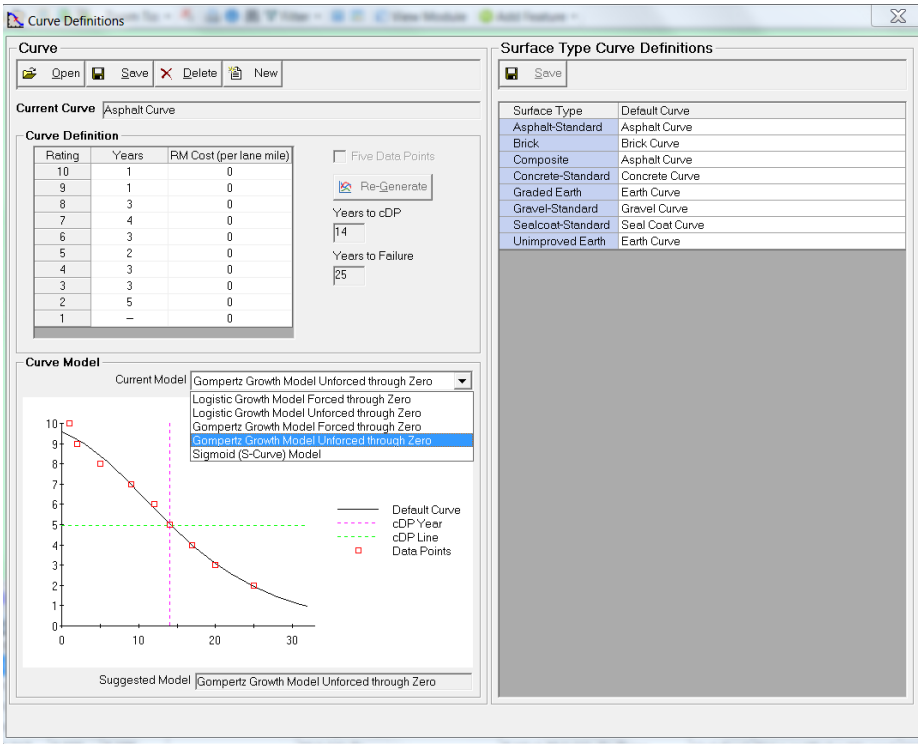

Figure 8-21. RoadSoft® family deterioration curve definition.

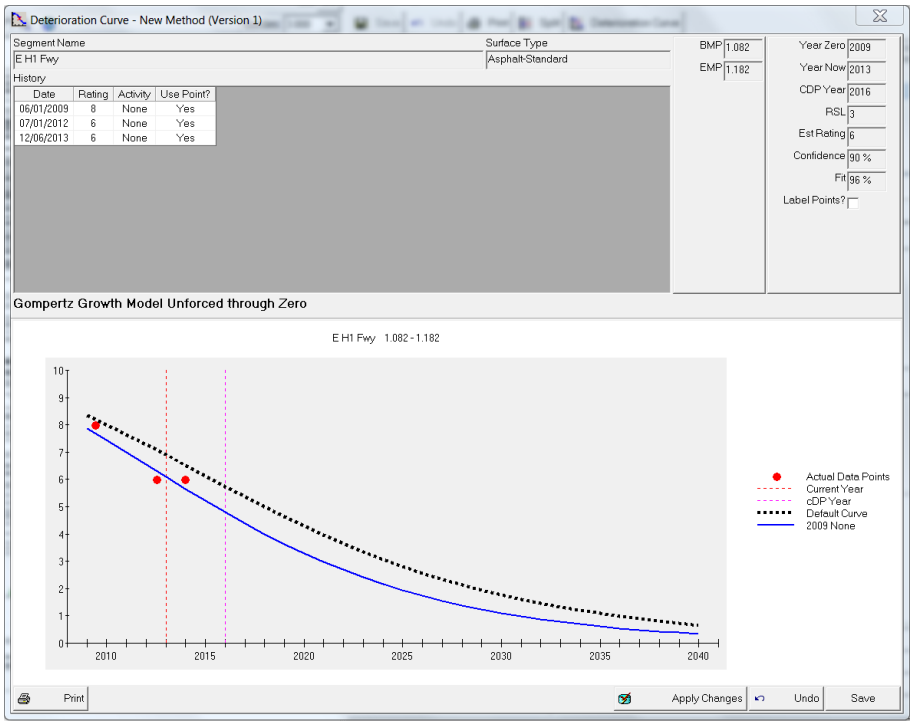

Figure 8-22. RoadSoft® deterioration curve for a given section.

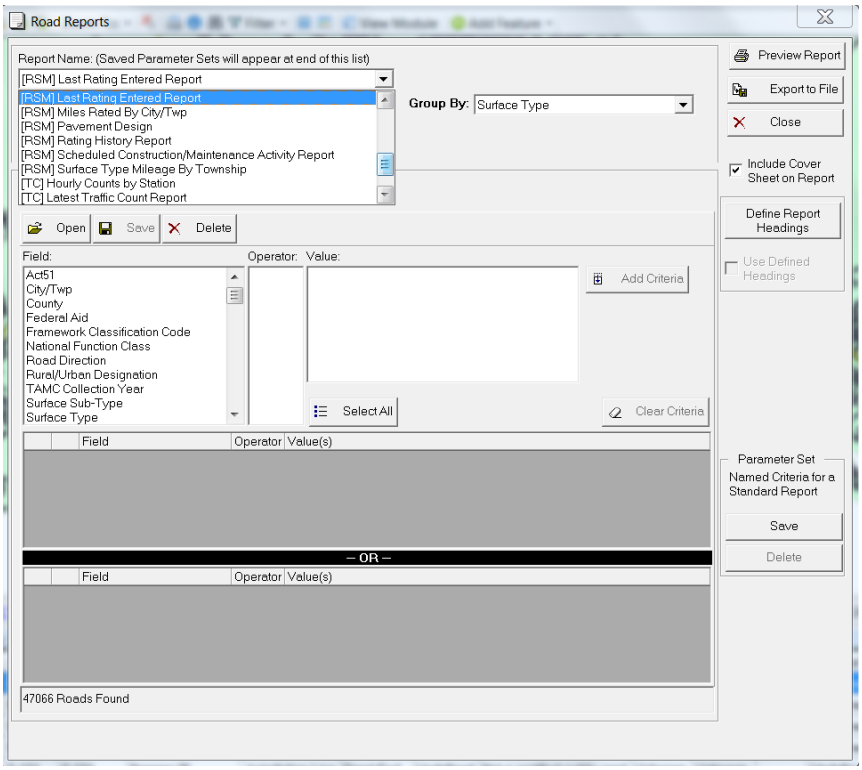

Figure 8-23. RoadSoft® Roads Report form.

These problems are avoided with a correct referencing system in the first place. This issue was the main reason that the database was not populated in RoadSoft® other than to test some of its features. A related issue is that some important divided roads (with two or three lanes in each direction) are represented as a single polyline. For whatever reason, some of these roads have experienced different deterioration and maintenance histories on each direction and it may be convenient to consider different sections on each direction. If it is desired to manage the two directions separately, then two different links should be created in the base map for those roads. This is another issue that should be evaluated carefully with RoadSoft® and other programs that use a similar approach. Similarly, cases of roads where adjacent lanes are of different materials (e.g., HMA vs. PCC) would also require separate links if it is desired to manage them separately.

A second issue that needs to be considered is the index used for characterizing pavement condition. RoadSoft® uses the PASER (Pavement Surface Evaluation and Rating) system [10]. PASER uses visual inspection to evaluate pavement surface conditions. The rating scale ranges from 10-excellent to 1-failed. The ratings are related to maintenance or repair needs: 10 & 9 – no

maintenance required, 8 – little or no maintenance, 7 – routine maintenance, crack sealing and minor patching, 6 & 5 – preservation treatments (sealcoating), 4 & 3 – structural improvements and leveling (overlay or recycling), and 2 & 1 – reconstruction. In contrast, HDOT has been collecting individual distresses and during the last few years computing the Pavement Condition Index (PCI). Thus, use of RoadSoft® would require either a change of rating system or the conversion of PCI into an index from 1 to 10.

Note that the ratings in RoadSoft® are discrete (that is, an integer from 1 to 10.) This is consistent with how PASSER defines the ratings. However, the restriction to integer ratings from 1 to 10 is an important consideration if one wanted to use this program with a different rating system such as PCI. In addition to dividing the index by 10, the values would have to be rounded to integer values. More importantly, it must realized that the two indices may not be directly comparable. For example, for PCI values below 60 or 55, typically no preservation treatments would be recommended. On the other hand, a section with a PASER rating of 5 is still a candidate for treatments such as seal coats. Therefore, if such procedure were use, most likely different trigger values would need to be used. Finally, this may also have some consequences for the contracts for pavement distress data collection. Nevertheless, since HDOT has partnered twice with the county of Hawaii to collect data using using the PASER system, collecting data with this system should not be a problem for the vendor.

8.4.3 PAVER™ (MicroPAVER®)

8.4.3.1 General

The research and development of PAVER™ has been in progress since the early 1970s and continues active to this date. The latest version of PAVER™ used in this project is version 6.5.7. The logic within PAVER™ has not changed throughout the length of this project. However, some significant improvements have been implemented. The improvements have occurred mostly in terms of GIS capabilities and importing/exporting information. The upcoming release of version 7.0 [103] promises also some significant improvements, among others, in GIS/GPS capabilities, splitting of pavement sections, and the choice of single install, network install, or web access installs.

As with other PMS systems, key components include pavement inventory, current and historical conditions of the PMS sections, prediction of future conditions, logic for programming maintenance and rehabilitation activities, and reporting capabilities. The following sections describe these components in some detail.

8.4.3.2 Pavement Inventory

PAVER™ organizes the inventory information into Networks, Branches, and Sections. For HDOT, for example, a network could be all roads in one of the islands. What constitute a network depends on user preferences, as networks could be created for freeways, primary roads, and other roads. Branches are typically the different routes (H-1, 72, 63, etc.) Sections that represent relatively homogeneous areas of pavement are defined by the user. In addition to the organization provided by the network, branch, and section structure, PAVER™ provides three user defined fields used for sorting at the network, branch, and section levels. That is, three fields are available for each level. These fields provide additional flexibility to organize the information.

Structural, traffic loading, and pavement condition information (as discussed in chapters 2, 3, and 4, respectively) are useful for the splitting of roads (branches in PAVER™) into sections. This task is common to all the PMS programs discussed in this report in some detail. However, unlike in RoadSoft® which provides a facility for splitting segments very easily, on PAVER™ more thought is needed[69]. Although the definition of the pavement management sections would typically need to be modified over time, a small number of changes would be required on a given year. Thus, the sectioning described below is mostly a one-time effort that it is needed regardless of the PMS program considered. Of course, every year some modifications may be needed and for those, the use of a program that facilitates joining or splitting sections is advantageous.

[69] As indicated earlier, version 7.0 of PAVER™ is expected to facilitate the splitting of sections within the program, which would be an extremely useful feature addition.

8.4.3.2.1 Sectioning of the Oahu Network

In order to perform a hands on evaluation of PAVER™, creation of a network and importing it into PAVER™ was needed[70]. For this purpose, a network was created for all State roads on the island of Oahu. For the reasons discussed below, this was a major endeavor. To understand this, it is important to note that only recently (with PAVER™ version 6.0), facilities were added to import inventory information from ESRI shapefiles. Furthermore, on that version, only polygons could be imported, which meant that polyline information available at HDOT could not be used. Thus, a big part of the effort described below was related to the need to digitize the polygons representing the road segments, and of course, finding out a reasonable sectioning of each route.

After the release of PAVER™ version 6.5, ESRI Shapefiles with polylines can also be imported. Thus, some of the work described below, performed with polygons for the island of Oahu, could be simplified significantly for the other islands[71]. Nevertheless, digitizing of the sections is only part of the effort, albeit a very time consuming one. Another big part of the effort is studying all the information available to determine reasonably homogeneous segments, work which is needed regardless of the type of geometry used to represent the roads. Furthermore, although the use of polygons is a bit more cumbersome, it is somewhat easier to consider cases where tapers are occurring (a very common occurrence on freeways off- and on- ramps), complex intersections, turning lanes, adjacent lanes with PCC and HMA (e.g. Pali Hwy and Ala Moana), bus pads, etc.

---

[70] It is important to stress that sectioning is also needed with other programs. Although a program such as RoadSoft® allows the splitting/joining of sections within the program, changes of pavement management section definitions should not be overused as this makes the use and interpretation of pavement condition information more difficult (particularly for sections used to develop pavement deterioration models) and depending on the agency's pavement condition data collection method, it may also cause some issues when assigning pavement conditions to pavement sections.

[71] Of course, it is desirable to be consistent and use the same type of geometry to represent road segments for all Islands. Therefore, if polylines are used for the other islands, then they should also be used for Oahu, which would demand some additional effort.

Several sources of information can be used to help the sectioning. In particular, for HDOT personnel, use of the photo log in the RIS together with other information in the RIS and the Straight Line Diagrams (SLD) can be extremely useful. The photo log allows a direct visualization of the number of lanes, surface type, shoulder type, curb and gutters, etc., along with the mile-point and GPS location information. Some of the same information is also given in numeric form in the RIS GIS and the SLD. These sources complement each other and should all be consulted when performing the sectioning to spot gross inconsistencies or outdated information[72]. A field survey with a GPS and a laptop data collector program related to the PMS software used may also be considered.

Unfortunately, for technical and security reasons, access to the RIS and the photo log for the research team was intermittent during the duration of this project. In particular, at the time the Oahu network was digitized, access was not available. Furthermore, even if it had been available, use of the photo log would have been useful mostly for spot checking considering the slow data transmission speeds when accessing it from UH. Consequently, a different approach (described below in Section 8.4.3.2.1.2) was used in the creation of the network for Oahu. It is important to note that the issue of data transmission speeds should be relatively easy to overcome for HDOT, as the option of working near the source of data should be available.

8.4.3.2.1.1 PAVER™ Tool for Creating Inventory from Shape Data

The PAVER™ Engineering Management System contains a separate program (currently, at no additional cost beyond the PAVER™ license) with several tools for manipulating inventory data (Figure 8-24). The last radio button on the set of Inventory Tools shown in this figure allows importing of a network inventory from a shapefile. As indicated earlier, until recently, only shapefiles with polygon data could be imported but now the program also accepts shapefiles with polylines. Selecting this option and selecting a shapefile (as shown in Figure 8-25) brings up the form shown in Figure 8-26.

As can be seen in Figure 8-26, PAVER™ requires three set of fields for networks, branches, and sections, respectively. The fields with an asterisk in Figure 8-26 are mandatory

[72] For this type of information, the quality of the data that was checked during this project was high.

fields. Thus, to import this information into PAVER™, in addition to the geometric information, the shapefile must also contain a table with different fields representing different attributes of the section. In the input form shown in Figure 8-26, the user must select the appropriate field from the shapefile on each of the drop down boxes[73]. Non-mandatory fields can be left blank.

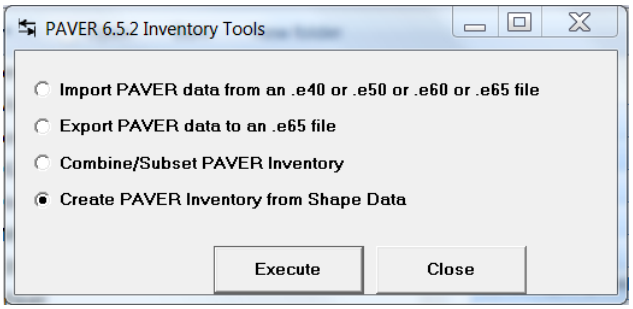

Figure 8-24. PAVER™ Inventory Tools.

8.4.3.2.1.2 Tools used in this study for sectioning

As indicated earlier, the research team did not have access to the photo log and the RIS GIS at the time the Oahu network was created. Although some information from the RIS GIS had been downloaded a few years earlier, the information was limited since it had not been downloaded for creation of the whole network. Consequently, it was decided to use publicly available information from sources such as Google Earth (Figure 8-27) to obtain the geometric information and validate some other data such as number of lanes, surface type, etc. (use of StreetView in GoogleEarth is extremely useful for this purpose and in some cases, to determine whether a section was on fill, cut or a combination of both. Nevertheless, a field survey would be more useful for this last purpose.) In addition, the Pavement Structure Processing Tool (PSPT) described in section 2.4 (page 18) together with the available data from the pavement structure data mining effort were used.

[73] Clicking one of the downward arrows brings up a drop down list with the fields available in the shapefile attribute table. This is not shown in Figure 8-26.

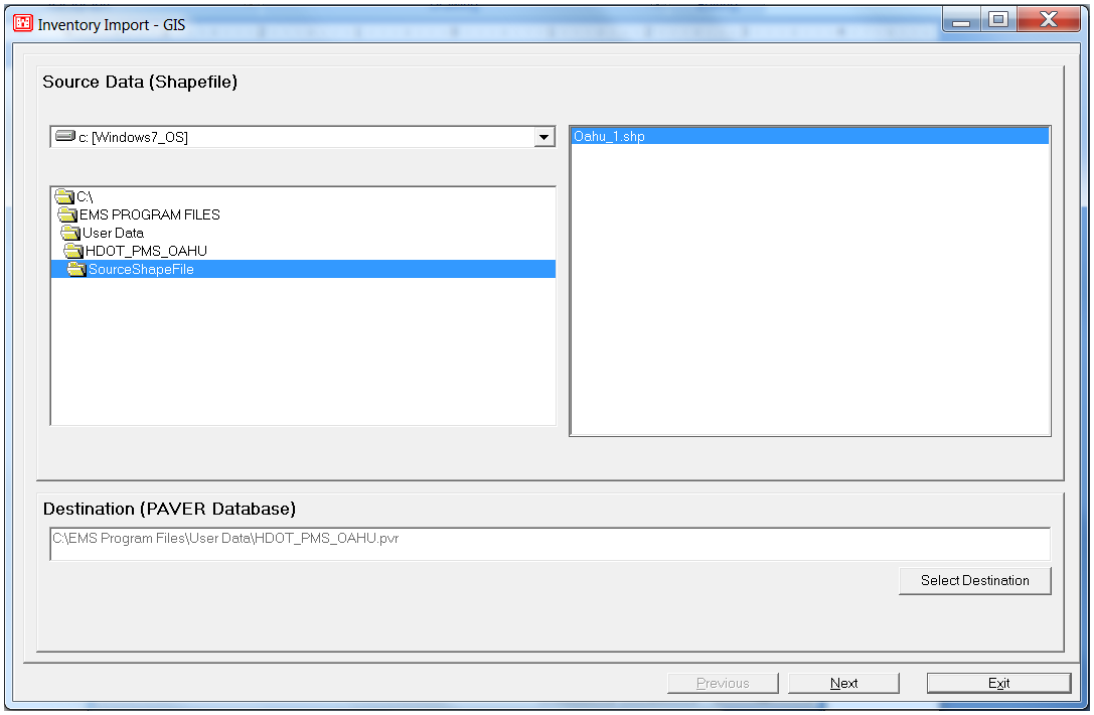

Figure 8-25. PAVER™ Inventory Import – Selecting a Shapefile.

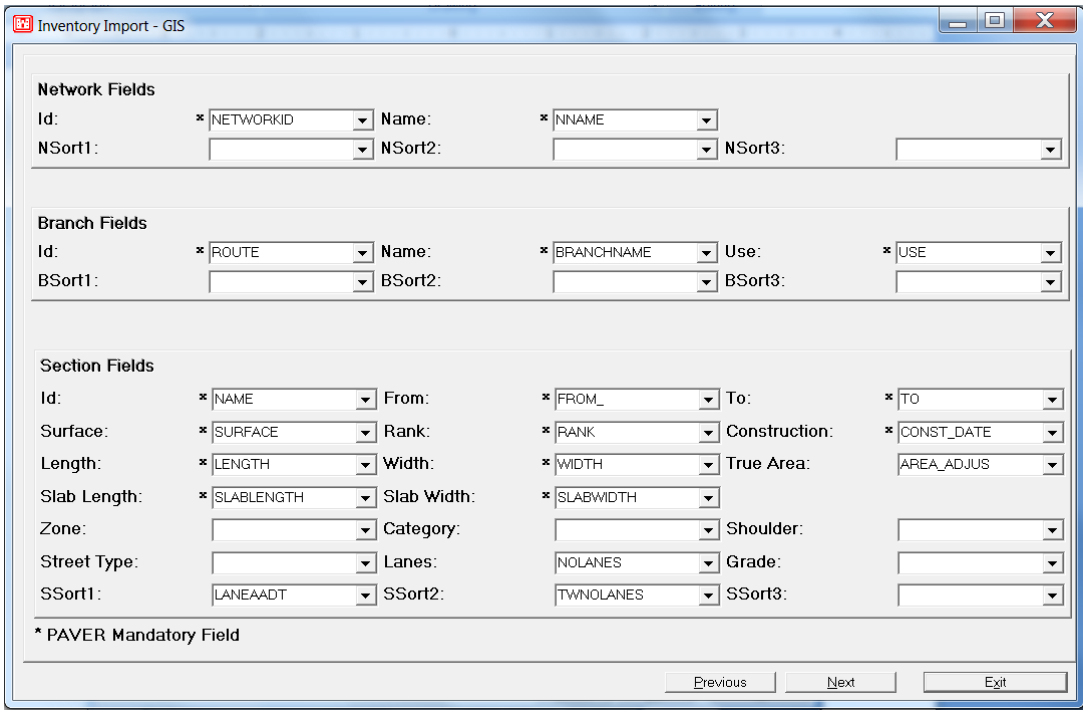

Figure 8-26. PAVER™ Inventory Import – Connecting fields with shape file attributes.

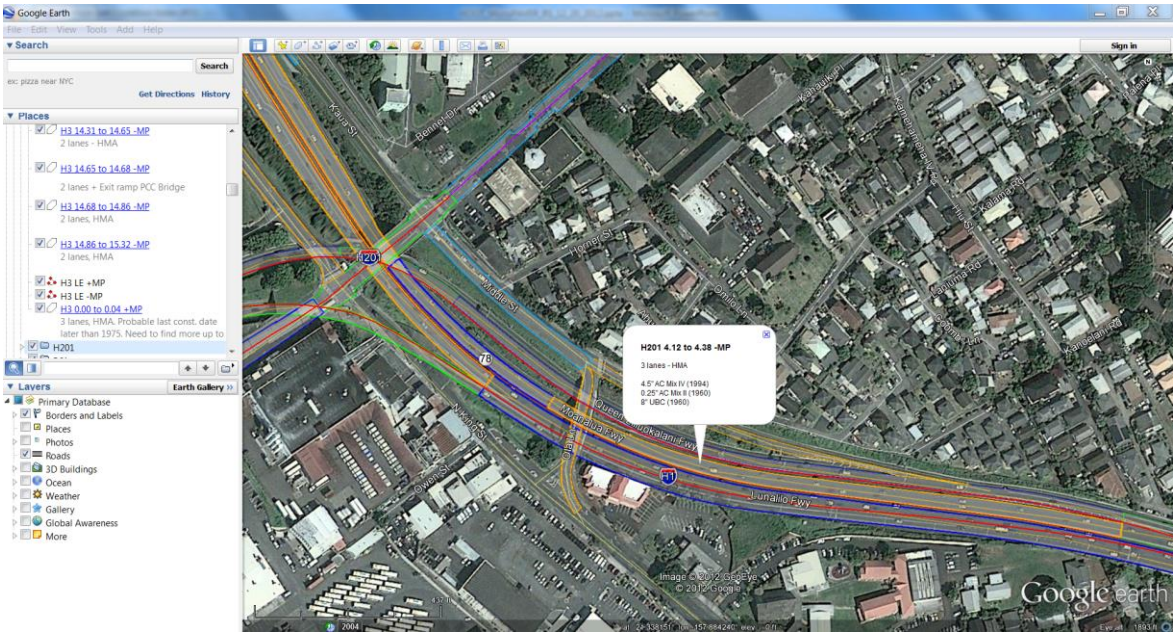

Figure 8-27. Collection of geometric information for each section.

A challenge of this effort was that although the latitude and longitude information for a point of interest can be easily obtained in Google Earth (or for that matter for all points defining the geometry of a section), most of the available data are referenced to milepoints. Thus, in addition to the geometry, it is important to obtain the begin and end milepoints for each section. Having these data for each section is essential for the correct assignment of pavement condition information, which as explained in chapter 4, is currently collected and reported every 0.1 mi. Consequently, in order to obtain the milepoint of any point of interest, a small program was created to translate the latitude and longitude data into Universal Transverse Mercator (UTM) coordinates (UTM zones 4 or 5, depending on the Island). UTM coordinates are plane coordinates, from which it is easy to compute horizontal distances between points. Thus, if the latitude and longitude of the points in a representative line of the alignment of a route (for example, the left edge of the pavement) are known and the exact location of the first point on the route (obtained from the information provided in the SLD) is also known, then the milepoints of any other point of the alignment can be easily obtained.[74]

[74] The decision to compute distances based on plane coordinates is consistent with the stationing used in highway design, where distances along an alignment are measured on the projections on a horizontal plane. This can

Figure 8-28 shows the simple interface of the program that translate latitude and longitude into UTM coordinates (Northing and Easting in meters). As seen in the figure, the program has a button for importing data. When the this button is clicked, the program displays a standard File Open dialog box (not shown) so that the user can select a previously created comma delimited file (csv). The input comma delimited file simply contains a list of latitude and longitude (separated by a comma) of consecutive points in the alignment (with each point on a separate line). After the information is successfully imported, a single click of the "Calculate Coordinates" button populates the rest of the table as shown in Figure 8-29. The column labels in the form are self-explanatory. The column labeled "Cumulative Distance (mi)" provides the correct milepoint if the first point in the list corresponds to the beginning of the route.

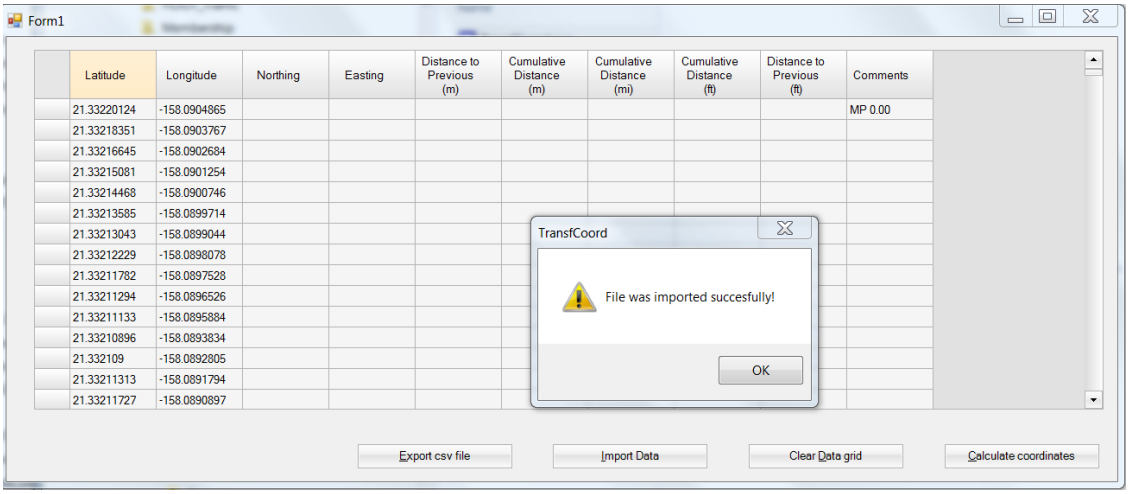

Figure 8-28. Importing latitude/longitude data into the coordinate transformation program.

---

cause small differences with measurements obtained with distance measurement instruments which are affected by the ups and downs of the road. Nevertheless, for most roads, the differences are relatively small. For example, for a road with a sustained grade of 5% the difference is of only 0.124%. Thus, for a 30 miles long road, the difference between the total lengths is of about 0.04 mi. Few roads have sustained grades like this on all its length, so in general smaller differences are expected. Notice that this issue is also relevant because it appears that the Planning Branch is using the elevation information together with the latitude and longitude to obtain distances. This is similar to what one would obtain from a distance measuring instrument. However, since the accuracy with which elevations can be obtained is about half of those for latitude and longitude, the computed distances are expected to have a small upward bias. A consensus on this issue between different branches of HDOT is desirable.

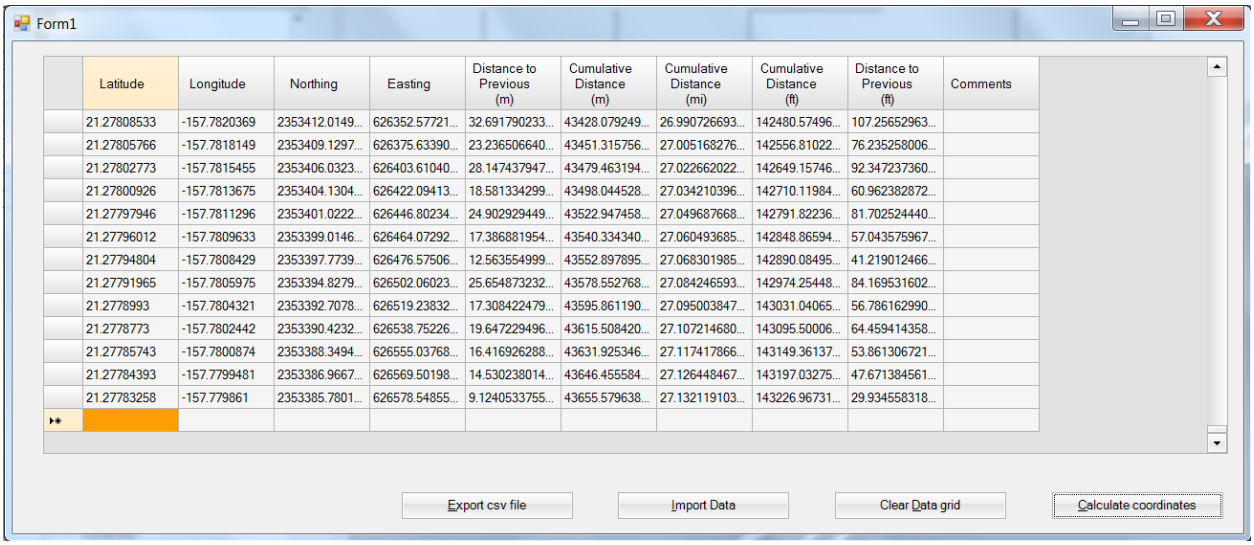

Figure 8-29. Translation of latitude/longitude into UTM coordinates and computation of cumulative distances.

Although the same information can be obtained with a properly linear referenced shapefile, this type of table provided for a simple look-up approach to obtain the end points of prospective pavement sections.

8.4.3.2.1.3 Creation of the shapefile with pavement section attributes

The first step in the creation of the shapefile to import the inventory into PAVER™ consisted on digitizing the left edge of each direction of divided roadways or the centerline of two-lane, two-way highways[75]. The information obtained with Google Earth for each section was exported into KML files (these are text files following XML rules, which among other things contain the latitude and longitude information.) Then, the latitude and longitude data were extracted and modified into the appropriate format using Excel® and imported into the coordinate transformation program. At this point, a simple look-up of the table in the program allowed the determination of the milepoints of points with known latitude and longitude (as seen

[75] This step is not really needed anymore for the other islands since HDOT has the KML files available with the paths followed for each route and ramp during the photolog. Unfortunately, this information was obtained after this task had been completed for Oahu. Furthermore, the same type of information could also be obtained from existing Shapefiles although for this, information on the associated projection is needed.

in Google Earth) or the appropriate location in terms of latitude and longitude of points identified by their milepoint (as given in the other data sources.)

Then, all the sources described earlier were used to identify changes in pavement characteristics such number of lanes, pavement type, begin and end of bridges as seen in Google Earth or as reported in RIS files, significant changes in AADT (typically coincident with on-ramps, off-ramps, and intersections), and points with significant structural changes as indicated by the mined structural information. An attempt was also made to discriminate large fills but time constraints and imaging quality limited this effort.

Once the end points of a section were identified from the above information, the section was digitized. Figure 8-27 (page 470) shows a few of the digitized sections with one of them selected (the section corresponding to H201 between milepoints 4.12 and 4.38 in the westbound direction or negative direction.) Notice that the known information for the section (number of lanes, surface type, and pavement structure) was included whenever possible. Large segments with no apparent changes were subdivided to maintain lengths typically smaller than 0.5 mi long since it is more likely for shorter sections to be more or less homogeneous (However, since this was not done from the beginning of the process, there are many segments that are larger than 0.5 miles.) In addition, smaller sections also provide greater flexibility for grouping sections into projects.

The digitized sections were then exported into KML files and then put together in a single file that was imported into ArcGIS. The sections' geometry was then corrected in ArcGIS so that the edges of adjacent sections matched perfectly. Finally, an attribute table, containing all the fields required by PAVER™ and some of the non-required fields, was populated in ArcGIS. The ArcGIS shapefile and part of the attribute table are shown in Figure 8-30[76]. A total of 1,942 sections were created for the Oahu network.

An essential step in the development of the attribute table is the creation of a field named PID, which is unique for each section to be imported. The PID field must contain the

[76] Actually, in Figure 8-30, the geometry created as described above is hidden by a pavement condition layer generated by PAVER™ with identical geometry.

NetworkID, BranchID, and SectionID of the section as shown in the respective fields of the attribute table separated by double colons (i.e., separated by "::").

8.4.3.2.2 Naming Convention

In order to uniquely identify a pavement section, PAVER™ uses the three key fields: NetworkID, BranchID, and SectionID. For network and branches (routes), PAVER™ has two additional fields (NetworkName and BranchName) that allow the input of longer alphanumerics (including spaces). These two fields are useful for providing more descriptive information of the network and the branches. However, the keys for identifying networks, branches or sections are the ID fields. The NetworkID, BranchID, and SectionID fields accept alphanumeric data with up to 10 characters each (letters or numbers). Thus, given the limited number of characters that can be used, some thought is needed to develop a naming convention that helps the identification of sections without much effort.

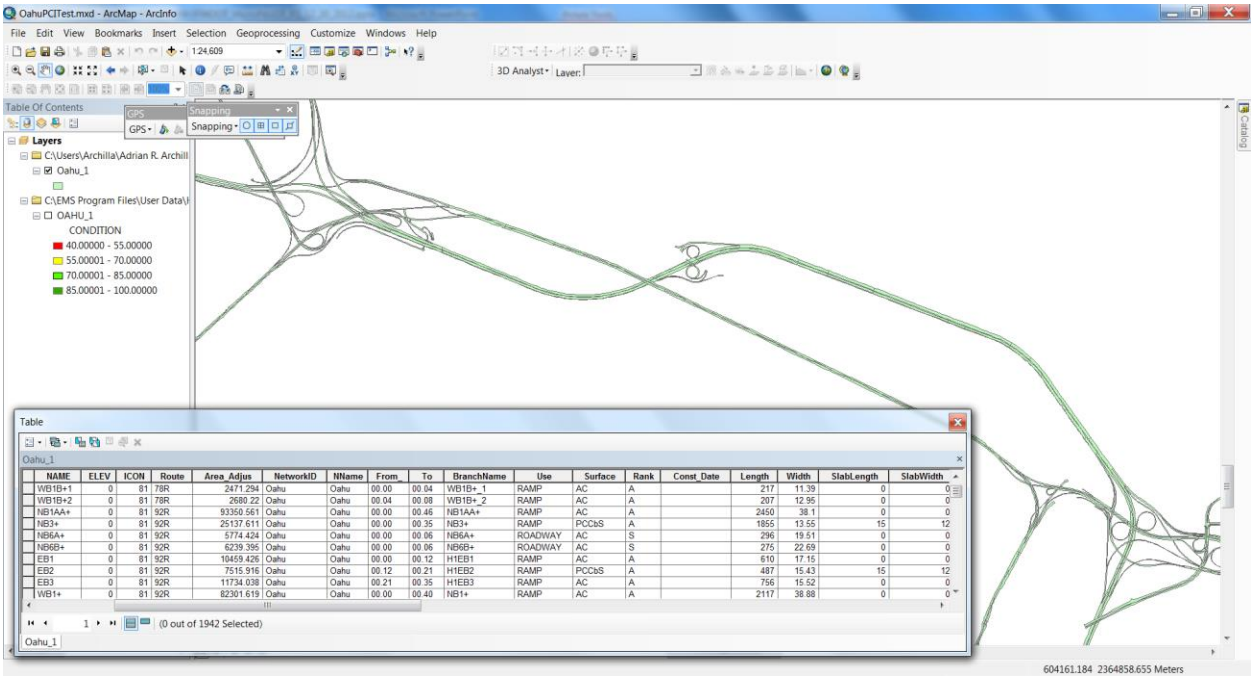

Figure 8-30. Shapefile's attribute table needed for PAVER™ inventory import.

For the Oahu network, the following naming convention was used. For NetworkID, the obvious choice was the text "Oahu". As the network for the other counties are created, the name

of each county can be used. For the county of Maui, one of the network sorting fields could be used to identify roads from the different islands in the county.

For BranchID, different identifiers were used for two different type of branches: routes and connector ramps. For ramps, the main associated route number followed by the letter R was used. Thus, for example, all ramps associated with the H-1 freeway are identified with the BranchID H1R and all ramps for route 63 are identified with the BranchID 63R. Clearly, the convention for ramps differs from the traditional definition of a route in that the sections (the different ramps or portions of them) are not necessarily continuous. Nevertheless, this convention makes finding the ramps for a given route relatively easy. Clearly, in the case of a ramp connecting two roads of equal category, it is not obvious what is meant by the main associated road. However, since the names selected were based on names used in the past by HDOT, it is believed that this convention will not be problematic.

Since roads and freeways are typically identified by the route number (with the prefix H for the interstate freeways), the route number (with the appropriate prefix) was used as the ID to identify these branches.[77]

Some exceptions to the above convention were made for a few roads (mostly in the area of the Honolulu Airport). Many of the connectors in that area appear to share a single route number (e.g., 21103) even though they were not always continuous. Thus, in those situations, the roads were differentiated with arbitrarily letters A, B, etc. Furthermore, some of these were also oriented in different directions. Thus, in those situations, a + or – was also used to differentiate the segments.

The convention for the SectionID field was also different for routes and ramps. For sections on routes, the name was formed by parsing together the begin and end milepoints of the section to the nearest 0.01 mi but without the decimal points. In addition, if a section represents

---

[77] Since for many divided multi-lane highways it may be desirable to manage the two directions separately, consideration was given to include a directional feature in the name of the route. However, this would be problematic for routes that that have segments with only two lanes in both directions and divided multi-lane segments. These routes would have required more than one identifier. Thus, this idea was abandoned in favor of including a directional feature in the name of the section when needed.

one direction of a divided roadway, either the sign + or – is added to the name to indicate that the section is in the direction of increasing milepoints or decreasing milepoints, respectively. For example, the ID of a section on the positive direction of a route between milepoints 0.82 and 1.31 is 00820131+. In addition, in a few occasions, two sections were needed side by side in the same direction. For example, the right lane of a section of the Pali Hwy (route 61) is made of PCC but the two other lanes correspond to an HMA overlay. This is easily accommodated by adding the letter B to one of the sections to differentiate it from the adjacent section (this is the only situation where all the 10 characters of the SectionID field are used.)[78]

Figure 8-31 shows a section of the Pali Hwy with an HMA overlay (identified in PAVER™ with the symbol AAC for the surface type). Note the list selector overlaid to the inventory form at the bottom of the figure. The list selector is one of the tools used to choose a section to work on. As seen in this figure, the Section field in the list selector corresponds to the Section ID in the inventory form. Figure 8-32 shows the information for the adjacent PCC lane. As can be seen by comparing both figures, different information can be entered for the two adjacent sections.

For ramps, the names assigned in the photo log survey were used whenever available. These names are of the form NB7, EB10, WB13A, SB1B, etc., where the first two letters indicate the general destination direction (Northbound, Eastbound, Westbound, or Southbound) and the number(s) following the first two letters is (are) the closest milepoint of the main associated road. It is not entirely clear the meaning of the letters that follow, though they appear to distinguish different branches where a ramp divides into two or where two ramps merge. Even though most ramps are relatively short, it was often necessary to divide ramps into different sections to account for changes in the pavement type. Because of the nature of the ramps, they often include overpasses between two sections in fill or changes in pavement type. Thus,

[78] In restrospect, it is believed that a better convention would be to identify the sections by their lowest milepoint only. This would free characters to accommodate the sections on route 11 on the Big Island, which is longer than 100 miles. In addition, it makes possible to include the decimal point, which makes reading of the milepoint clearer, and perhaps add one more decimal, which is useful for the definition of very short segments such as short span bridges or some ramp sections.

similarly to other roads, it would have been desirable for the name to give some indication of which part of the ramp is covered by the section. However, there is not yet an equivalent of the straight line diagram for ramps indicating the exact start point and their length. Thus, for the time being, a + sign was always added as a simple separator to the end of the name sometimes followed by letters A, B, etc. distinguishing consecutive sections.

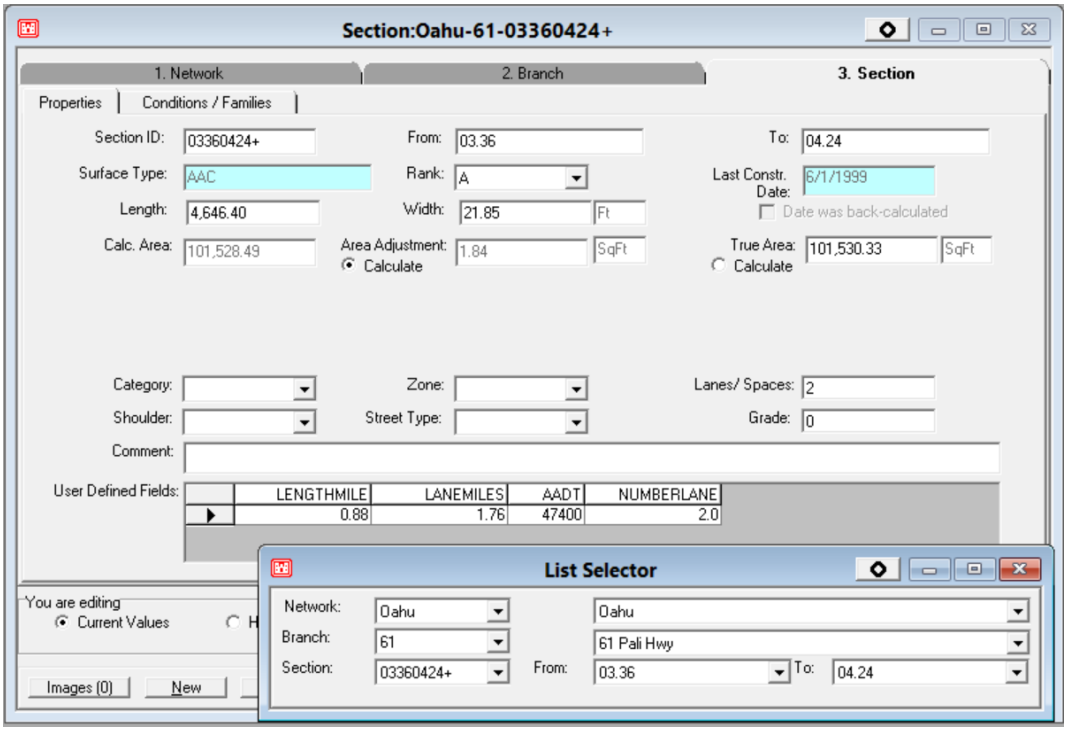

Figure 8-31. Inventory information for an HMA section of the Pali Hwy (Route 61).

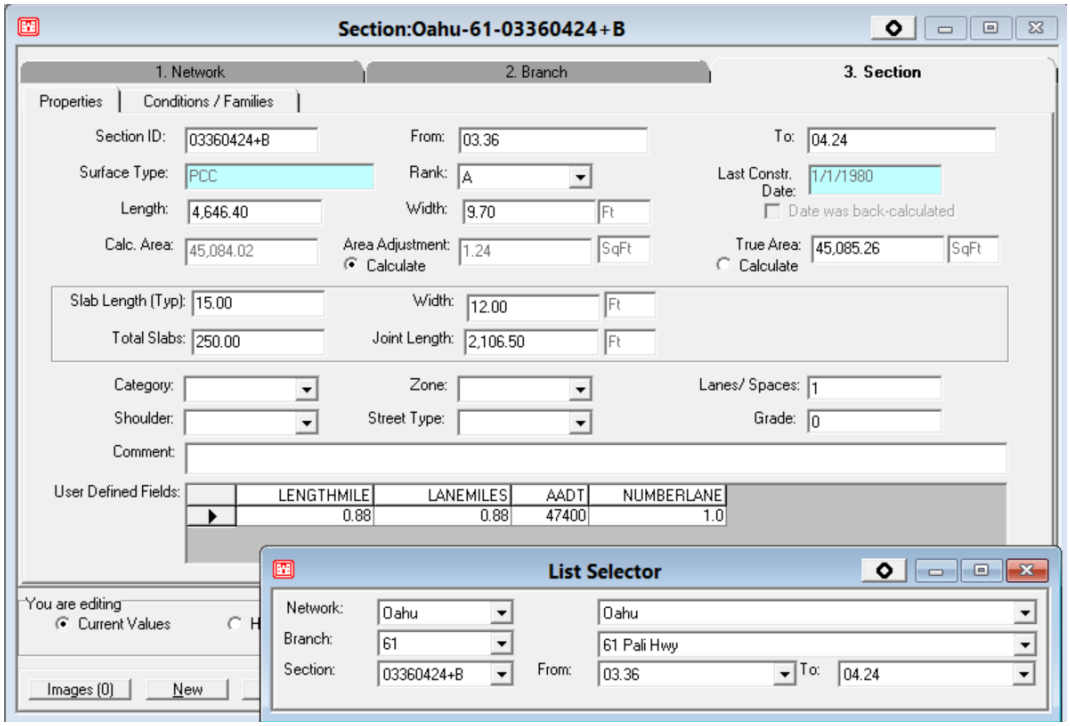

Figure 8-32. Inventory information for a PCC section of the Pali Hwy (Route 61).

Figure 8-33 shows an example of a ramp section using the above convention. Note that the "From" and "To" fields of ramp sections were populated with the approximate distances from the start of the ramp. However, the start of the ramps as defined in the network created in this study for Oahu may not be the same as those currently used to survey the distresses and consequently the automated assignment of distresses to sections may not always be accurate. The reason that the word "approximate" was used above is that many of the off-ramps in the network include a taper, which in many situations is relatively long (see for example, the off-ramp towards the Middle St. shown in Figure 8-27, page 470.) In those situations, the ramps were considered to start at a place such that the multiplication of its length and its width resulted in an area approximately equivalent to the actual pavement surface of the ramp section. In many other situations, it was possible to detect a change in pavement surface perpendicular to the alignment of the ramp after the taper. In those situations, the ramp section was started (or ended) at the pavement change and the taper was considered to be part of the section of the main road connected by the ramp.

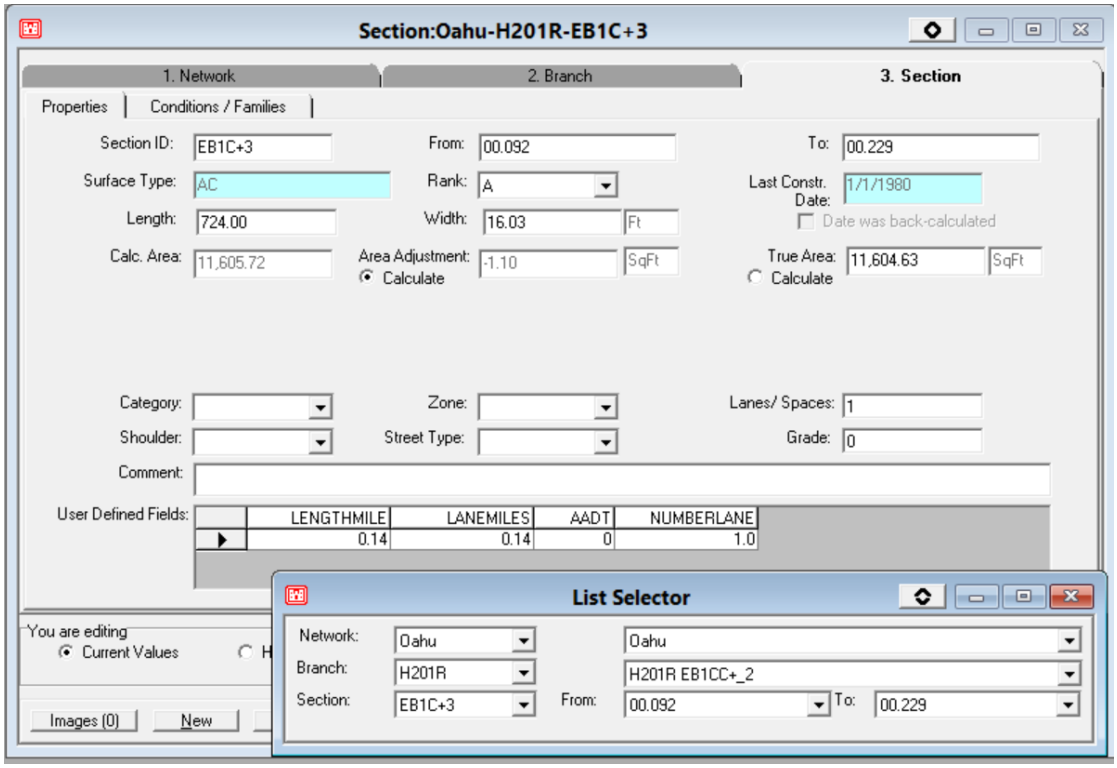

Figure 8-33. Example of inventory information for a ramp section (Route H-201).

As can be seen, the issue of the accurate definition of the locations of the start and end of ramps deserves further study (or consensus) so that the distress surveys are performed consistently with the ramp section definitions. Given the relatively short length of ramps, starting the distress measurements in the wrong location could result in erroneous assignments.

Advances in technology, such as the PAVER™ Image Inspector mentioned later, similar programs associated with other PMS systems, or vendor algorithms can solve the problem relatively easily if a clearly defined network is provided.

8.4.3.2.3 Inventory Import

Once a shapefile with the needed inventory information has been created, the import process into PAVER™ can be started as described in section 8.4.3.2.1.1. As was shown in Figure 8-26 (page 469), after selecting the input shapefile, the user needs to connect the inputs required by PAVER™ with the corresponding attribute fields in the shapefile. This is actually the first of a multi-step process. In the next step, the user can select user defined fields (Figure 8-34.)

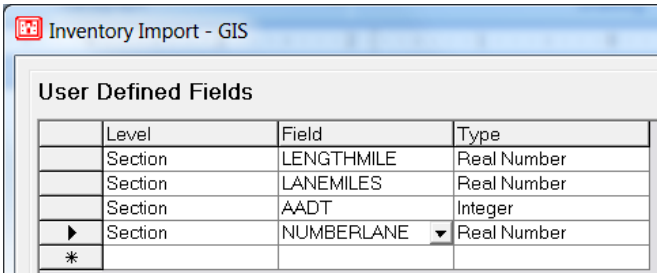

Figure 8-34. Defining user defined fields to import.

In the following step, PAVER™ displays the number of valid and invalid records in the shapefile and shows the information for the valid records in a table. Each record can be reviewed and selected or deselected for import (Figure 8-35). Figure 8-35 also illustrates the PID field described in the previous subsection.

Finally, in the last step, the program just lists the sections as they are added to the PAVER™ database (Figure 8-36). After closing the Import Tool, re-starting PAVER™ and opening the new database, the user can select sections for further manipulation. PAVER™ provides various selection methods. Figure 8-37 illustrates three of them. The user can select sections in the GIS view, the tree view on the left of the GIS view (which in this figure does not really look like a tree because the network root and the branch leaves are out of sight), or with the list selector described earlier and shown near the bottom of the figure. Being able to visualize a selected section within PAVER™ is a very useful feature.

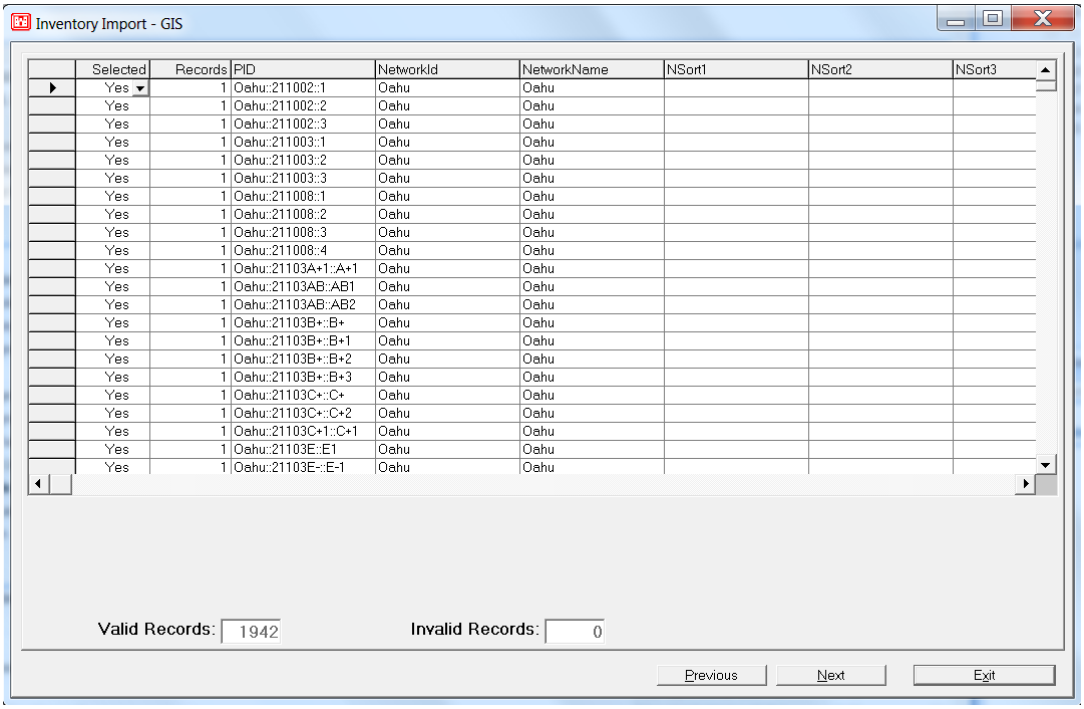

Figure 8-35. Reviewing import data.

Comparison of the generated geometry with GPS data obtained by the vendor during the photo log data collection shows in general very good agreement. In addition, the computed lengths for each route are also close to those reported in the RIS GIS. The locations where the geometry is more suspect are those where the sections are not visible from above, such as Nimitz Highway and Waialae Ave. under the H-1 viaducts, other roads under viaducts in the Honolulu airport area, and the tunnels at the Pali Hwy, the Likelike Hwy, and the H-3 freeway. Since the date of the imagery used preceded the date of the end of the construction of the North-South road, this road was not included in the network (also, the geometry of H-1 at the new interchange may have been altered slightly.)

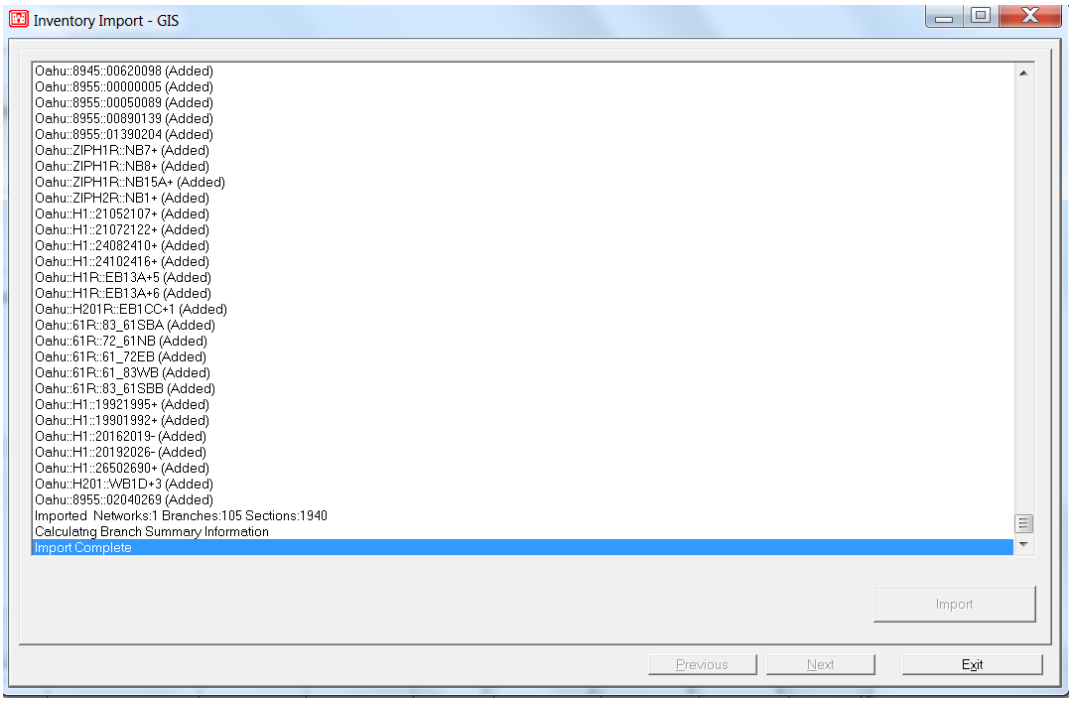

Figure 8-36. Listing of sections as they are imported.

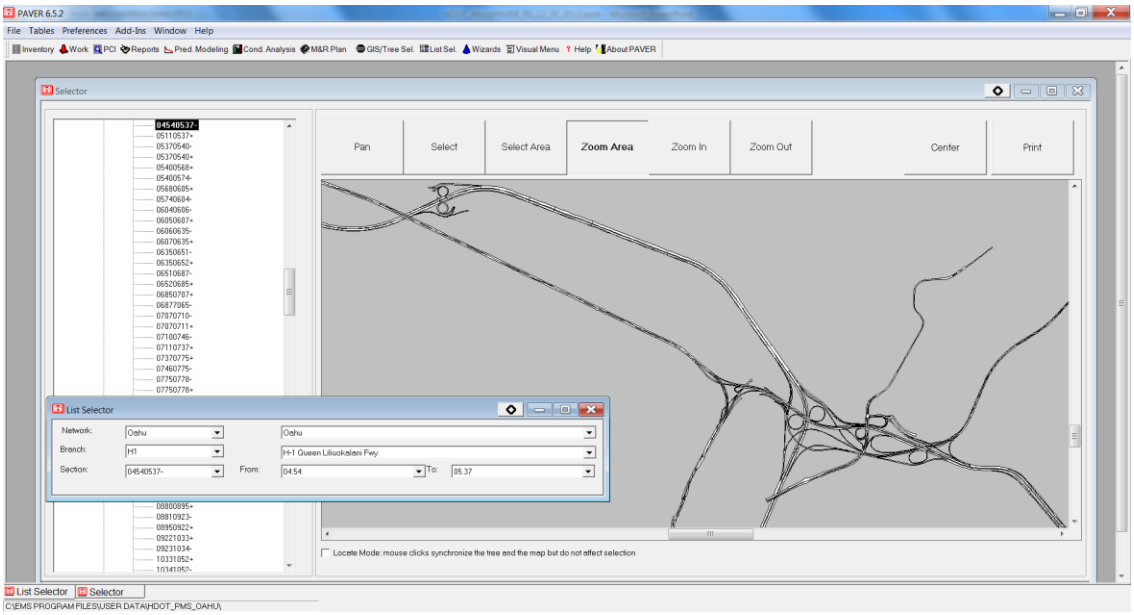

Figure 8-37. Selection of sections after importing them into PAVER™.

Two very important pieces of information required when creating the inventory are the surface type and the last construction date of each section. These are specified when a section is created inside PAVER™ or when imported into PAVER™. After this, the surface type and the

last construction date are only changed for sections receiving a Major Maintenance and Rehabilitation (Major M&R) (as defined later in section 8.4.3.6.6, page 552) or some Global Maintenance and Rehabilitation (Global M&R) (as defined later in section 8.4.3.6.5, page 537). The rules for changing the surface type are given under the headings **Consequent Surface** on the aforementioned subsections.

The following are some of the reporting capabilities of PAVER™ with respect to the inventory information. Figure 8-38 shows the GIS visualization of surface types. The PAVER™ standard surface types shown in this figure include AAC: asphalt concrete overlay over asphalt concrete, AC: asphalt concrete, PCC: Portland cement concrete, and APC: asphalt concrete overlay over PCC. Figure 8-38 also shows user defined surface types, including: ACbS: asphalt concrete over a structure (bridge or viaduct), PCCbS: PCC over structure, and UTW: ultra-thin whitetopping. These were created with the intent to define separate deterioration curves for these types of pavements. However, a few problems have been encountered when these surface types have been created (some systems tables appear to get corrupted) and therefore its usage is not recommended at this point, particularly since assigning different deterioration curves to these sections can still be accomplished within PAVER™ without the need to create new surface types.

Figure 8-39 is one of the standard charts in PAVER™ showing the percent area with each pavement type. Figure 8-40 shows the distribution of ages of the pavement sections in the network. The user has the option to select a subset of the network (e.g., all AC, AAC, and APC pavements, etc.)

It is interesting to note in Figure 8-39 the large percentage of the Oahu network with PCC surfaces (PCC, PCCbS, and UTW). These three surface types represent about 21% of the network area, which is higher than usual. This is in part a reflection of the large percentage of PCC surfaces and viaducts on the interstate portion of the network.

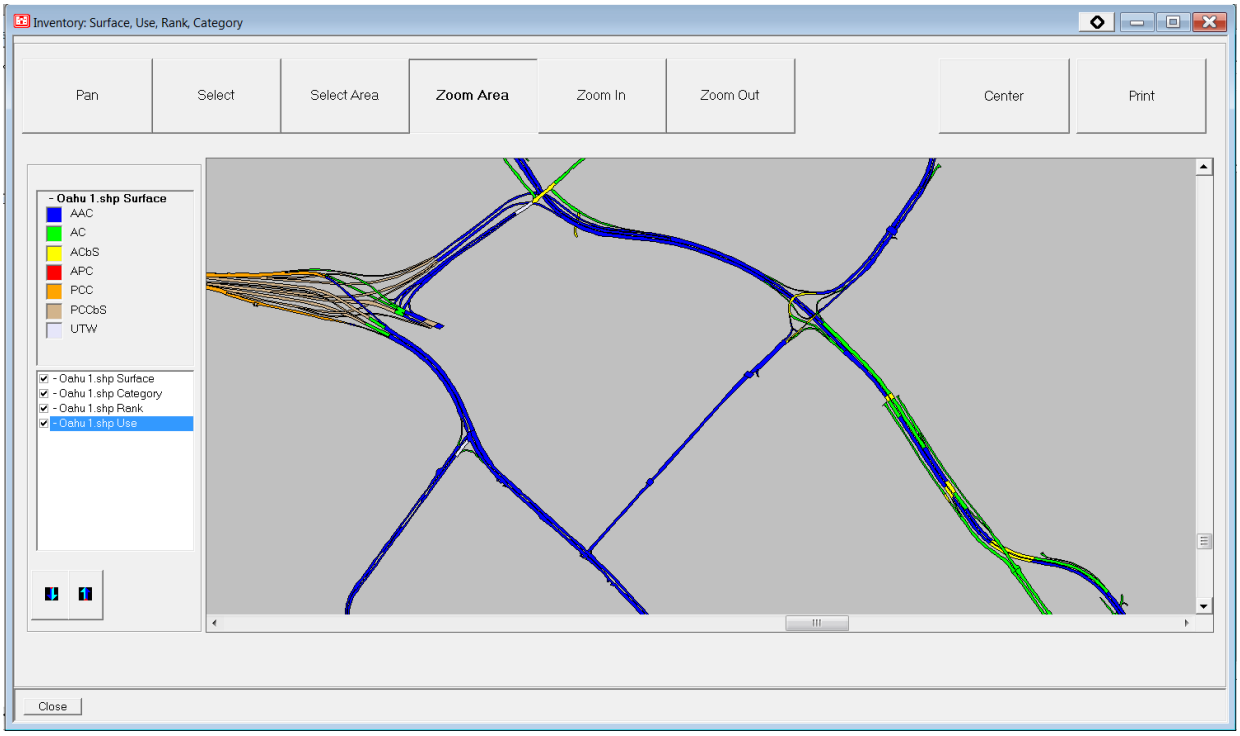

Figure 8-38. GIS Visualization of Pavement Surface Types in PAVER™.

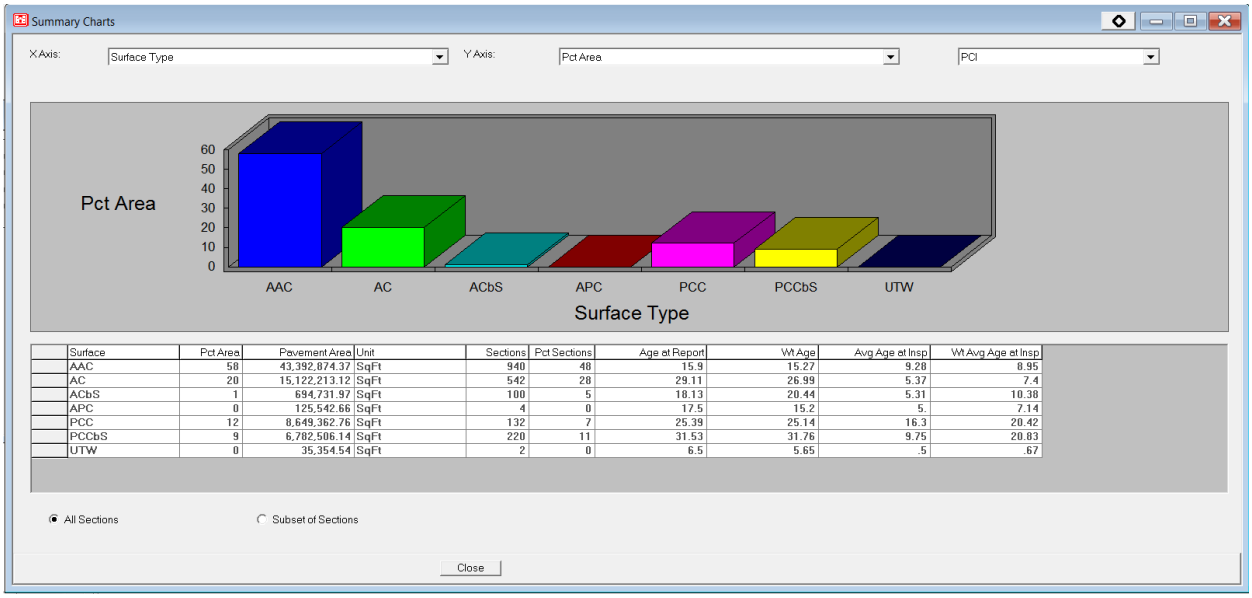

Figure 8-39. Chart of the Percent of Each Surface Type in PAVER™.

On Figure 8-40, it can be observed what appears to be an unusually large percentage (48%) of pavement sections with ages (time since the last reconstruction) above 21 years. This large percentage is explained in part by the large percentage of PCC pavements in the network. Nevertheless, even though some sections are known to have lasted a long time, the percentage remaining after accounting for the PCC pavements appear unusually high. This indicates that there are still holes in the data. Particularly, it is believed that some important maintenance activities, including overlays, are still missing.

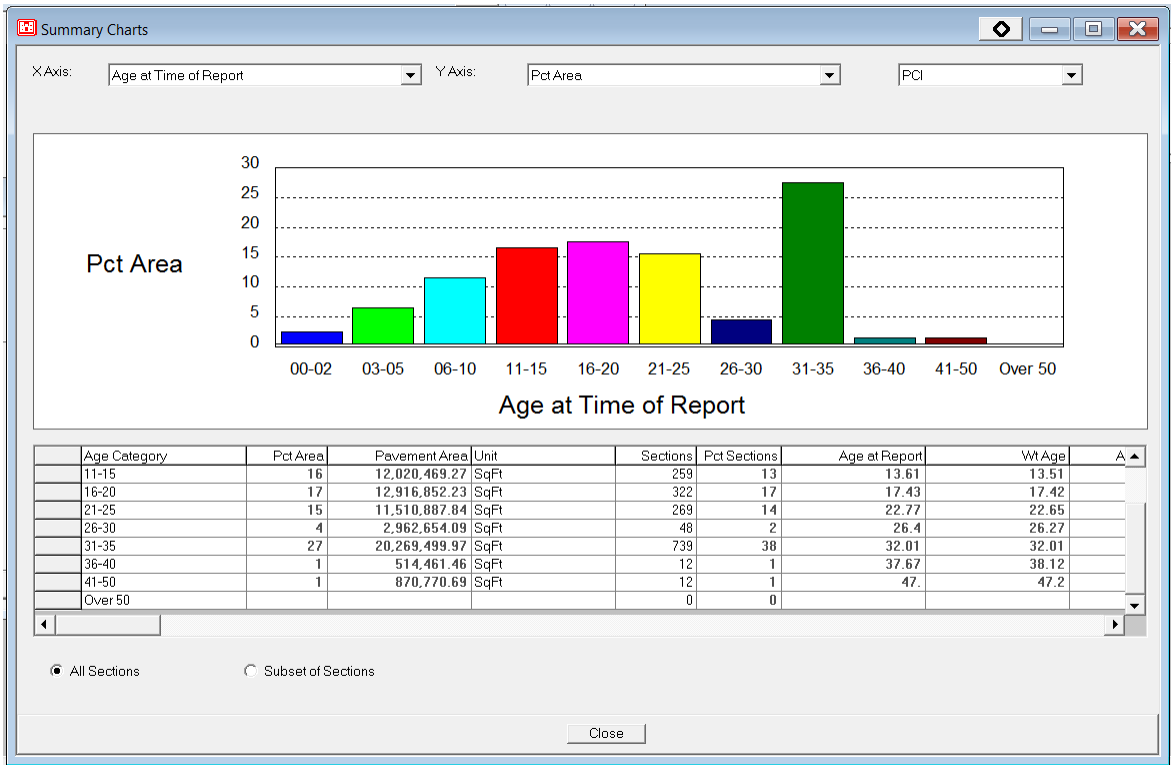

Age Category	Pct Area	Pavement Area	Unit	Sections	Pct Sections	Age at Report	Wt Age
11-15	16	12,020,469.27	SqFt	259	13	13.61	13.51
16-20	17	12,916,852.23	SqFt	322	17	17.43	17.42
21-25	15	11,510,887.84	SqFt	269	14	22.77	22.65
26-30	4	2,962,654.09	SqFt	48	2	26.4	26.27
31-35	27	20,269,499.97	SqFt	739	38	32.01	32.01
36-40	1	514,461.46	SqFt	12	1	37.67	38.12
41-50	1	870,770.69	SqFt	12	1	47.	47.2
Over 50				0	0		

Figure 8-40. Chart in PAVER™ of the Percent Area vs. Age at Time of Report.

8.4.3.3 Pavement Condition

As discussed in the previous section, importing the inventory data requires substantial processing. Nevertheless, this is mostly a one-time effort for the whole network. After this large effort, only a small number of annual record updates may be needed. On the other hand, pavement condition information needs to be input for most of the network recurrently.

8.4.3.3.1 Sampling vs. Continuous Measurements and Survey Frequency

In order to determine the PCI for a pavement section, the section is typically divided into sampling units. ASTM D6433 and the PAVER™ documentation recommend sampling unit sizes of 2,500 ± 1,000 sq. ft. Shahin [7] indicates that at the network level the survey should be performed on sample units representative (not random) of the overall condition of the section since the main objective for budget estimating and network condition assessment is to obtain a meaningful rating with the least cost.

Shahin [7] also points out that a network-level survey can be conducted by surveying only a few sample units per section and provides some guidance on sampling rates. As reported by Shahin [7], some agencies go as low as 10% sampling with more than 40 sampling units (i.e., for large sections). However, it is important to realize that these guidelines were developed mostly for manual data collection efforts.

With respect to sampling rates when automated data collection means are used, some of the relevant findings of NCHRP Synthesis 334 [104] include:

- "Most agencies using automated means of data collection sample continuously, or very nearly so, on the outer traffic lane.
- In a few instances, a worst lane is selected for evaluation and in no case is an agency evaluating all lanes.
- The essentially universal practice is to evaluate the outermost traffic lane (no parking spaces) in one direction for pavements having fewer than four lanes and in both directions for roadways having four or more lanes.
- Three agencies collect cracking data on a segment-by-segment basis (usually defined as a pavement management segment of varying length), whereas five sample 10% to 30% of the roadway, usually on a random sampling basis."

Based on the above, it appears that the practice at HDOT of collecting distress information continuously from images is in line with the practices at many other state DOTs. However, although HDOT practice includes collecting data continuously for one lane, the lane for which the data is collected (on multi-lane highways) is typically not the outermost lane. Instead, it is the innermost lane (or "CTR" lane in the HDOT Planning Branch naming convention.) Although the practice appears to be related to the need to collect other information simultaneously with the distress survey, it also appears to be supported in part by the limited analysis presented in Section 3.7, which showed the leftmost lane to be often the lane with higher

lane distribution factors for heavy vehicles. A more in-depth study is needed of the data from automated vehicle classification stations on multilane highways located throughout the islands to ascertain whether this strategy is appropriate.

As reported in [104], almost all agencies monitor pavement surface distress (cracking, etc.) at 1-, 2-, or 3-year frequencies. That report also indicates that a few agencies do one-half of the system each year, with others doing one-third each year and that a few states monitor interstate pavements at 1-year intervals and other pavements at 2-year intervals. The most common occurrence is capturing of pavement cracking at 2-year intervals.

Wolters et al. [89] provide more recent information on data collection frequency by *local agencies*. According to these authors, most local agencies collect distress information every year (45%), about 9% collect data every two years, 18% every three years, 8% every four years, and 8% every 5 years. Note that it is also common to collect data every year but on only one half or one third of the network. In addition to reducing the costs by a factor of 2 or 3, this also has the advantage of leveling the data collection funding needs.

Therefore, collecting distress data every two years (or alternatively every year on half of the network) is consistent with the need to report HMPS data and a common practice elsewhere. This is probably a good strategy for HDOT as well.

8.4.3.3.2 Importing Pavement Distress Data Into PAVER™

Although PAVER™ provides a form (Figure 8-41) intended for rapid entry of distress information (from which the PCI is computed), the process is slow, tedious, and prone to the introduction of errors. Note that the information entered into the form of Figure 8-41 is at the sample level (in that particular figure, the sample unit is 001). Thus, when dealing with thousands of sections and several sampling units per section, the data input process is slow. Therefore, an automated process for importing distress information or condition information is also desirable. PAVER™ provides a few options for this and this subsection briefly describes the option that was found to be the more useful in this study.

Importing distress information for each section essentially involves the creation of an XML file containing the network, branch, section, sample number and size, and the list of distresses for each sample (including type, severity, and extent.)

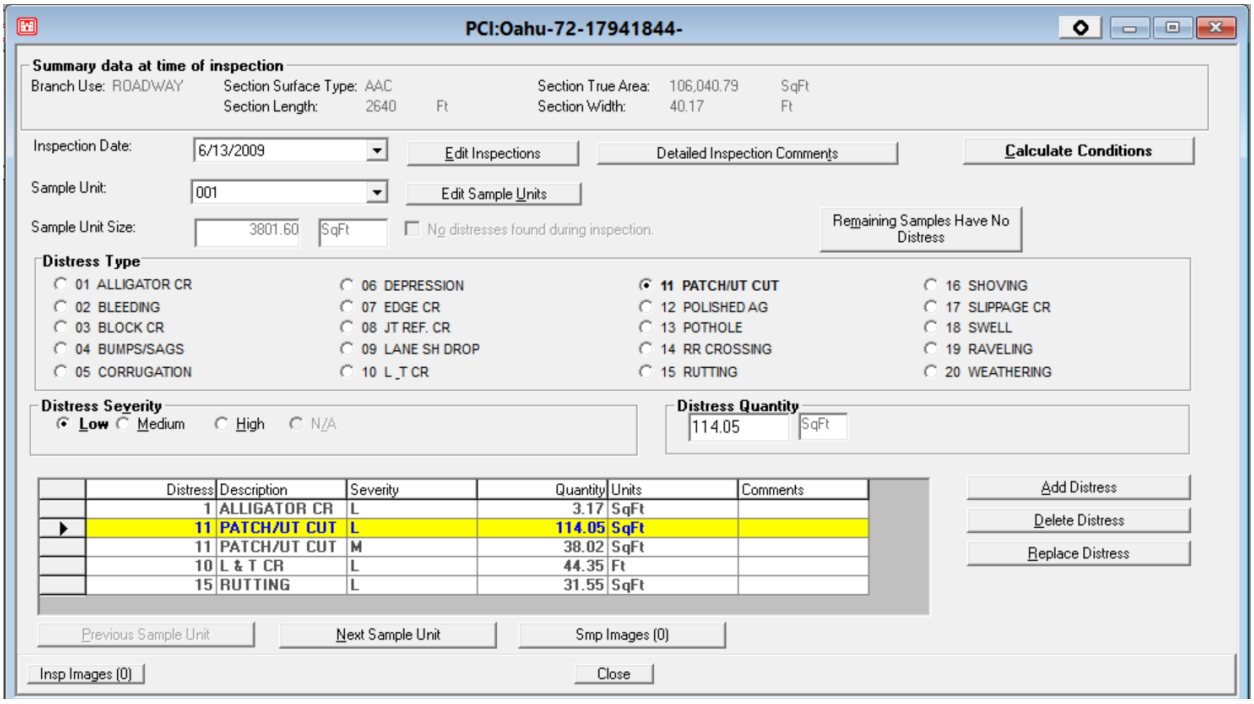

Figure 8-41. PAVER™ form for entering/editing distress information.

As illustrated in Figure 8-42, the data are used to create the attributes of different elements of the file usually identified by two corresponding tags. For example, the information for a sample unit is found between the tags <inspectedElement> and </inspectedElement>. The inspected element is identified by its attributes PID (which identifies the section) and the inspectedElementID (which identifies the sample). The third attribute required for each sample is the size in square feet (which is used to compute distress densities.) For each sampling unit on which distresses are observed, the distresses are listed between the tags <PCIDistresses> and </PCIDistresses>. Each distress record is identified with a single tag that includes attributes <levelDistress severity=”X” quantity=”YYY.YY” distressCode=”YY”>, where X is L, M, or H depending on whether the distress is low, medium, or high severity, respectively, and the Y’s are numbers defining the extent (quantity) of distress and the type of distress (for HMA pavements, the distress codes coincide with those shown in Figure 8-41.) Although this type of file can be created with a text editor (e.g., Notepad), this would not be practical for the whole HDOT network for the same reasons cited for the PAVER™ form shown in Figure 8-41.

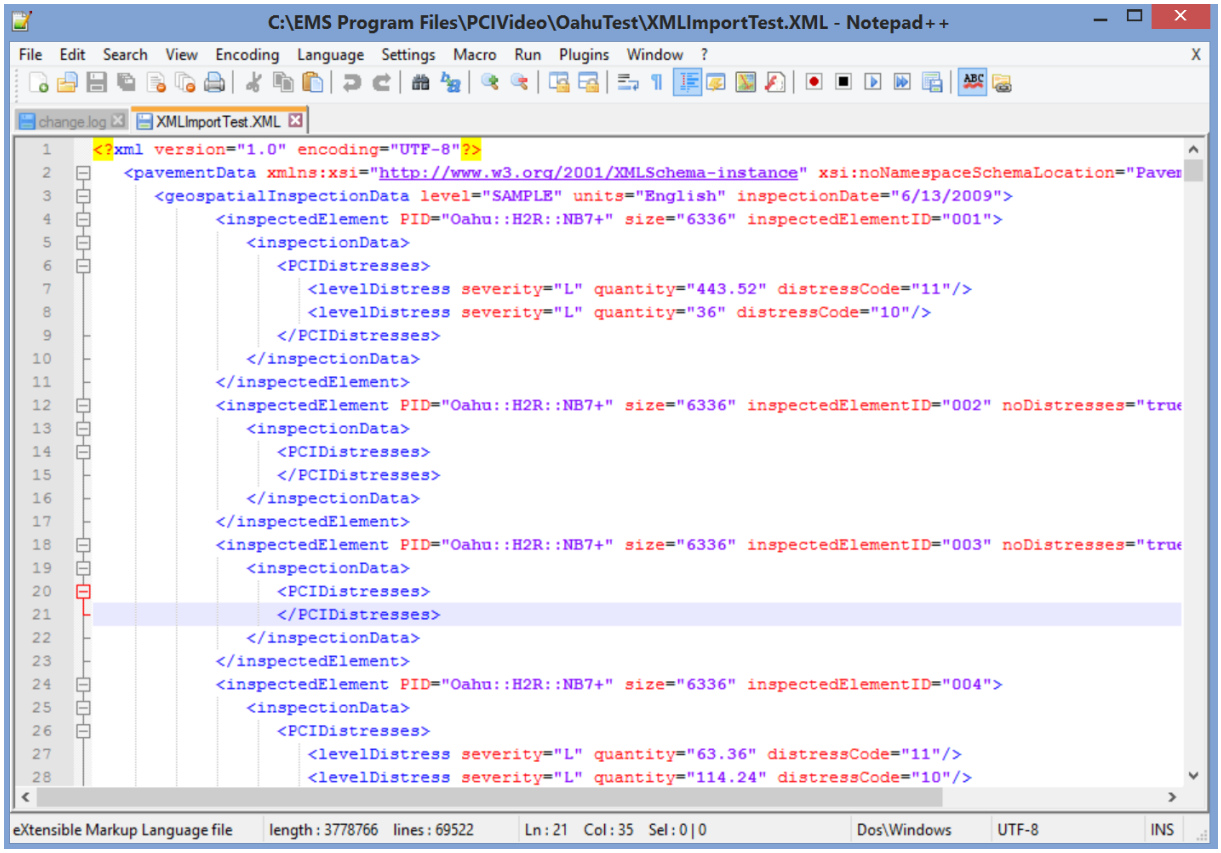

Figure 8-42. Example of XML file with pavement distress information for import into PAVER™.

A fundamental aspect of the file is the PID attribute of the inspected element (a sample unit in this case), which uniquely identifies the existing section within PAVER™ to which the sample belongs. The PID field and the sample number (identified by the inspectedElementID attribute in Figure 8-42) uniquely identify the sampling unit. The PID is the same PID that was described in the discussion of the pavement inventory (section 8.4.3.2.1.3, page 472). Recall that the PID is formed as NetworkID::BranchID::SectionID (i.e., with the IDs for the network, branch, and section, respectively, separated by "::")

Creating this XML file automatically with the information available presented several challenges. These challenges and the steps followed to overcome them are briefly described in the following paragraphs. The description is not abundant in details since, as it will be explained shortly, these issues should be easier to overcome in the near future.

As just noted, the PID field is formed with the information of the network as imported in PAVER^{TM}. Note that this information (NetworkID + BranchID + SectionID) uniquely identifies a section but it does not directly provide information about the location of the section. In addition to the SectionID, PAVER^{TM} also has two fields labeled "From" and "To" that make the identification of sections easier. These fields accept an alphanumeric and could contain descriptive information such as the name of cross streets or the description of some important feature identifying the begin or the end of the section. As described earlier, for Oahu network the milepoints (with an accuracy of 0.01 mi for roads and 0.001 mi for ramps) of the start and the end of the section were used instead for the "From" and "To" fields, respectively.

Then, to assign the distress data to the appropriate sections, a text file was created with the PID and the From and To fields for each pavement section. In addition, the distress data were exported from the vendor provided Microsoft Access® database files into ASCII (text) files.

As indicated in section 4.3.2 (page 142), a custom made program originally develop to compute PCI outside PAVER^{TM} was adapted to compute distress quantities as required by PAVER^{TM}. Recall that the distress data were collected according to the SHRP specifications instead of the ASTM specification used by PAVER^{TM}. Also, recall that the distress data were delivered mostly in 0.1 mi long segments even though the actual data were collected for each video image frame, every 0.002 mi (10.56 ft). Therefore, for simplicity, whenever possible each 0.1 lane-mile segment in the distress survey was considered a sampling unit even though this is about twice the recommended sampling unit length. The computation of distress quantities was based on the transformations for computing distress densities multiplied by estimated sample unit sizes described in section 4.3.2.

An can be seen in many of the examples presented in the development of the Oahu network, it is quite often the case that a pavement management section will not start or end at an exact 0.1-mi multiple. Therefore, the custom program was made to read the information from both text files (one file containing the structural information and the other the distress information). Then, those 0.1-mi segments straddling the boundary of two consecutive pavement management sections were subdivided into two different sampling units (one for each section) and the correponding distress quantities were pro-rated according to the sampling unit sizes. For

those 0.1-mi survey segments completely contained on a pavement mananegement section, a sample unit was simply created and assigned to the PMS section.

Although the above process may not sound too complicated (in terms of the computations needed), there are several special cases that needed to be taken into account. One example is that if a short bridge section is present, say for example 0.02 mi long, a 0.1-mi segment may cover parts of three consecutive sections. Another more common and serious example is if one of the end points of a survey reporting segment is erroneously reported, then the data may be erroneously assigned to many adjacent pavement mangement sections. There were indeed cases of some reporting segments being several miles long. To avoid the problems caused by these segments, the lengths above a certain threshodls were ignored.

With the distress quantities converted and assigned to samplig units, then creating programmatically an XML file (Figure 8-42, page 489) was relatively simple.

Once the XML has been created, importing it into PAVER™ is a relatively simple process as explained next (of course, it is simple provided the file does not contain errors or inconsistencies.) Selecting the "Wizards" button in the main PAVER™ toolbar displays the Wizards form shown in Figure 8-43. Then, selecting the last option in the form and pressing the "Continue" button brings up the form shown in Figure 8-44. In this form, the name of the file to be imported and the directory where it is located must be selected. Pressing the next button on this form shows the form for the next step (Figure 8-45) in which the option "Convert XML into inspection files using PID" needs to be selected and the button "Convert" needs to be pressed. As the program starts converting the distress information, it highlights the section to which a sample is being imported. After this, a confirmation to import the data and the possibility to create a report are presented (these are not shown here.)

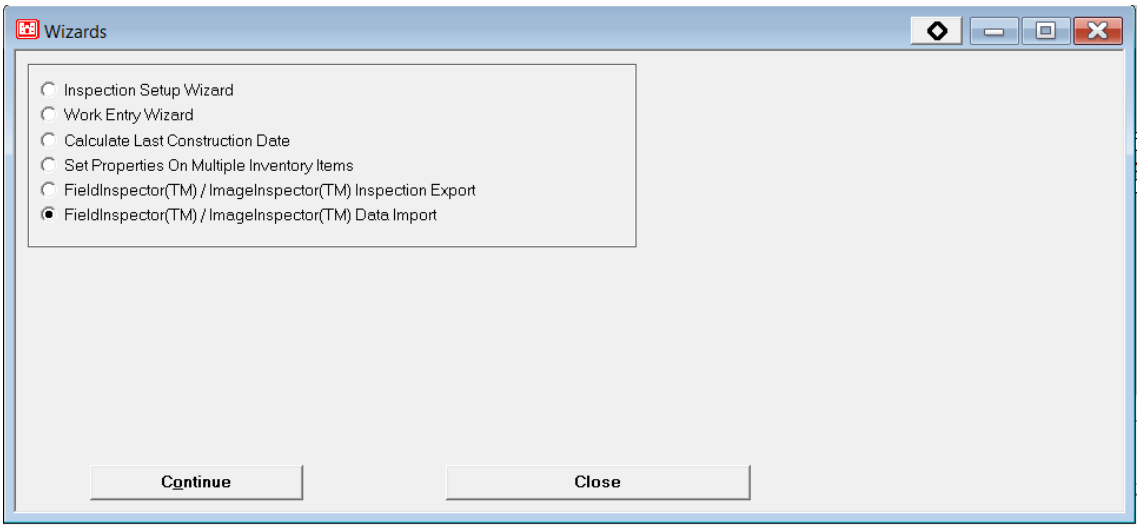

Figure 8-43. PAVER™ Wizards form.

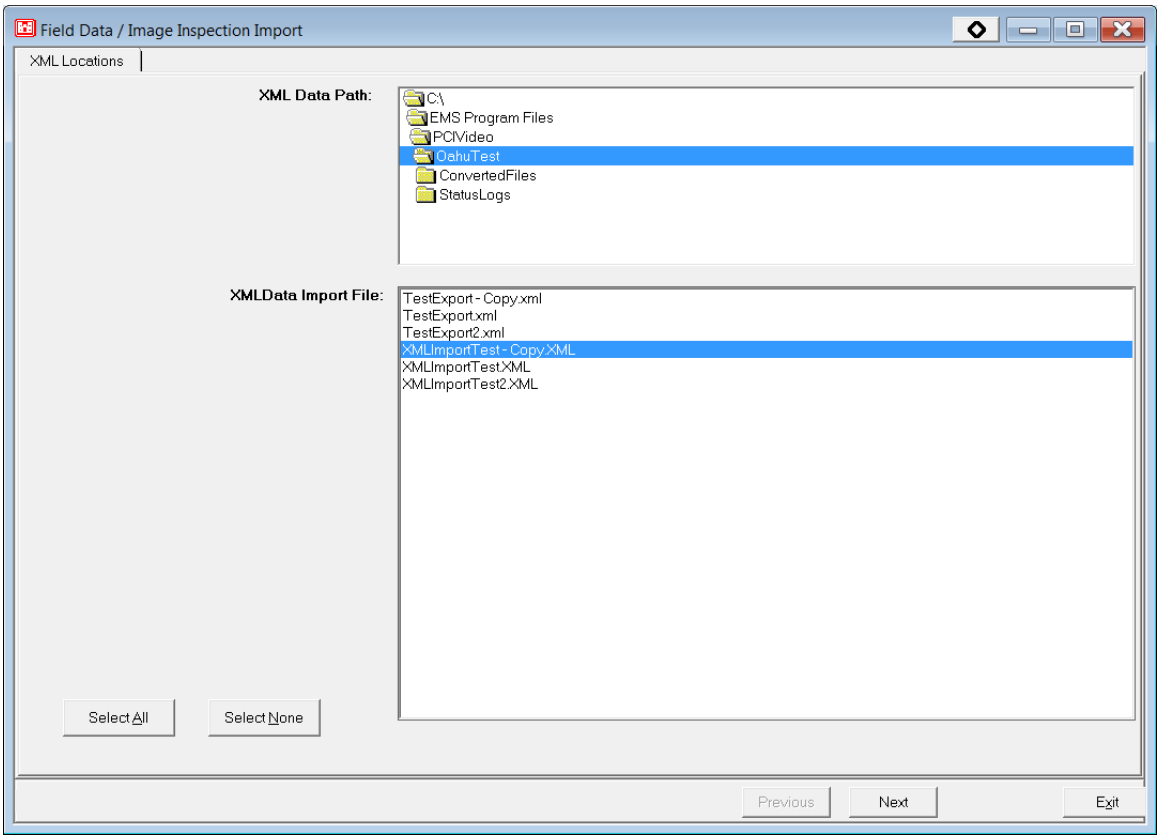

Figure 8-44. PAVER™ form to select the XML containing the distress information.

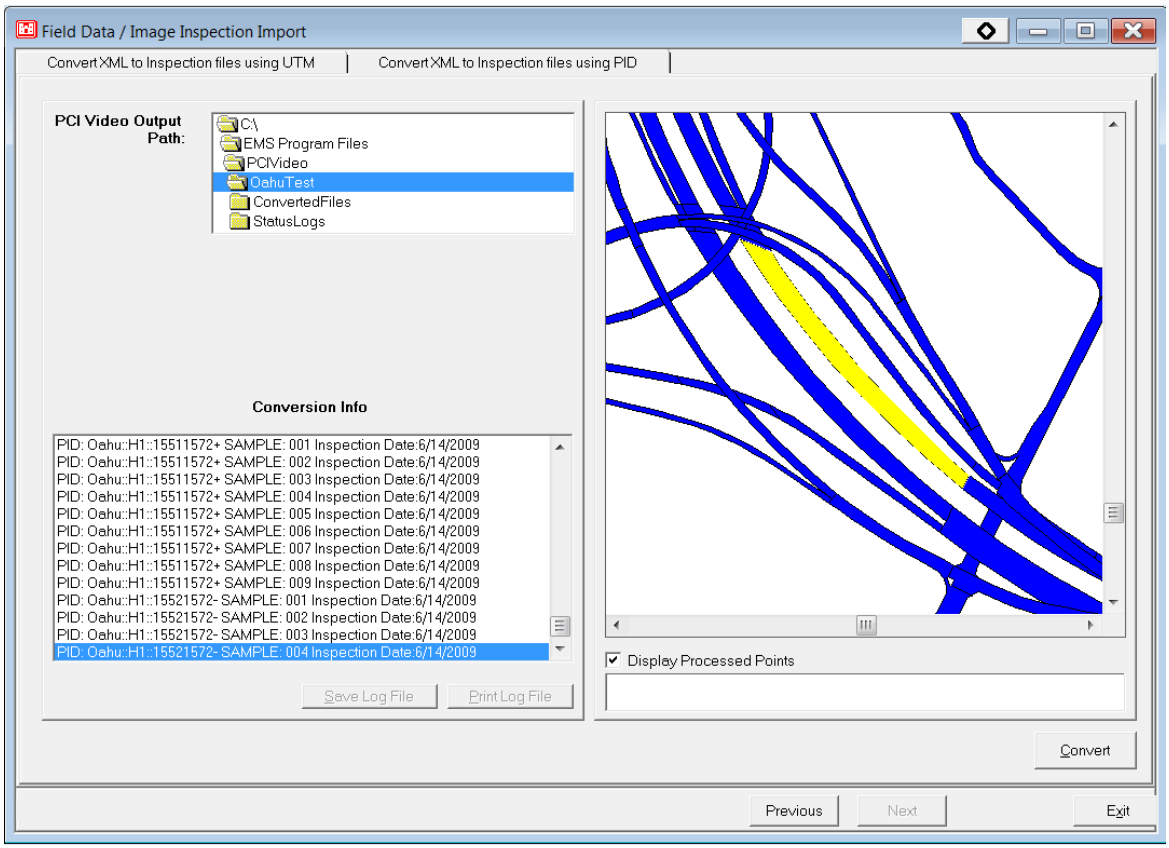

Figure 8-45. Sections containing the sample unit being imported are highlighted by PAVER™.

8.4.3.3.3 Future Distress Surveys

Clearly, a more streamlined and sustainable process without so many manipulations would be required for future surveys if PAVER™ is selected (actually, this would be true for most PMS software.) A few options are available for this. First, notice that in Figure 8-45 another option to import the data includes the use of UTM coordinates. This is an alternative that should be evaluated since the vendor does collect GPS coordinates together with the distresses. In order to create sampling units with the PMS segments and avoid the splitting of sections, the data at the frame level (every 0.02 mi) before aggregation should be used. A clear advantage of this procedure would be that no connection of the inventory and distress data is needed outside PAVER™ (of course, the UTM distress data needs to be consistent with the inventory network.)

A second option, would be the use of the distress data collected every frame (i.e., before aggregating it) using the PID process described above. This process does not add much in terms

of data manipulation savings but it presents fewer problems for correctly assigning the distresses to the PMS sections.

Finally, consideration may also be given to a recently developed tool, PAVER ImageInspector™, which according to the site http://www.paver.colostate.edu/upcoming.php (last accessed 12/28/2013) uses state-of-the-art pavement image data collection methods, automatically assigning collected images to the appropriate pavement section using GIS and Global Positioning System (GPS) technology. It also provides an interface for automatically calculating quantities of identified distresses, and offers real-time PCI™ calculation and data transfer to PAVER™. The PAVER ImageInspector™ is to be licensed separately from PAVER™ and the cost of the license is currently $650. This is listed as the last option since the use of this software may not be compatible with the vendor's workflow.

In any case, probably the best option for HDOT would be to include a requirement to have the data delivered in a format that is easy to import into PAVER™ or any other PMS software selected by HDOT or better yet, already in a databse of the PMS program selected. It is important to note that although all this discussion was centered on PAVER™, many of the issues are not software specific.

8.4.3.4 Pavement Deterioration Modeling

A challenge commonly found in the implementation of a new PMS is the lack of information on the existing pavement structures and the loading imposed on them. In this respect, although the database still needs improvements, significant advances have been made. Fortunately, a common approach used by some PMS programs to model the progression of deterioration, including PAVER™, StreetSaver®, and RoadSoft® is to use the concept of "pavement families", which requires a rough knowledge of the pavement structure. A pavement family consists of a group of pavements that exhibit similar performance because they have similar structures, construction histories, and traffic loading. The advantage of this approach is that existing institutional knowledge can be used to create a rough clustering of existing pavement sections into pavement families to get the PMS going and then that clustering can be improved over time.

The assignment of pavement sections into families is only one part of the equation. The other is the creation of reliable deterioration curves for each family. For this purpose, in

PAVER™, it is important to know the last construction date of each pavement section as well as their pavement conditions over time (as measured by the Pavement Condition Index or PCI).

The Last Construction Date (LCD) corresponds to the date of the most recent major M&R, as defined in PAVER™. In general, this would be the date of any overlay larger than or equal to 2 inches, mill & overlay larger than or equal to 2 inches, or the date of original construction. Notice that the dates of thin overlays used for preventive maintenance (≤ 1.5 inches) or of other preventive maintenance activities such as slurry seals, chips seals, etc., should not be used as LCD.

As indicated earlier on this report, the age of many sections are suspect. It appears that some significant maintenance activities/rehabilitations are missing from the database. Similarly, as discussed in previous sections, there appears to be situations where some distresses (e.g., cracking, raveling, etc.) are being under-reported, which would translate in overestimation of the PCI. The two problems combined may have a significant effect on the deterioration curves.

Figure 8-46 shows the "Prediction Modeling" form used in PAVER™ to develop deterioration curves for families of pavements. The form has six tabs that allow, respectively, the collection of subsets of data from the database for pavement condition modeling, the review of the model data, the application of boundary/outlier filters, the definition of pavement deterioration curve options such as the critical PCI and the number of parameters in the polynomial fit used for the deterioration model, the inspection of the resulting deterioration model equation and statistics, and the assignment of family models to sections in the network. The details for each of these tabs are not discussed here. They are described in the PAVER™ user manual.

The data points shown in Figure 8-46 (both, the green crosses and the red triangles) correspond to PCIs observed on AAC surfaces (HMA overlays of asphalt concrete pavements) with low AADT/lane. This was an attempt to cluster pavements expected to deteriorate similarly. As can be observed, the cloud of points does not exhibit a typical deterioration pattern. Clearly, there is a large number of points that indicate little or no deterioration over time. The two problems mentioned before may be at play here. First, if some distresses are not being captured adequately in the survey, then some of the points should be lower.

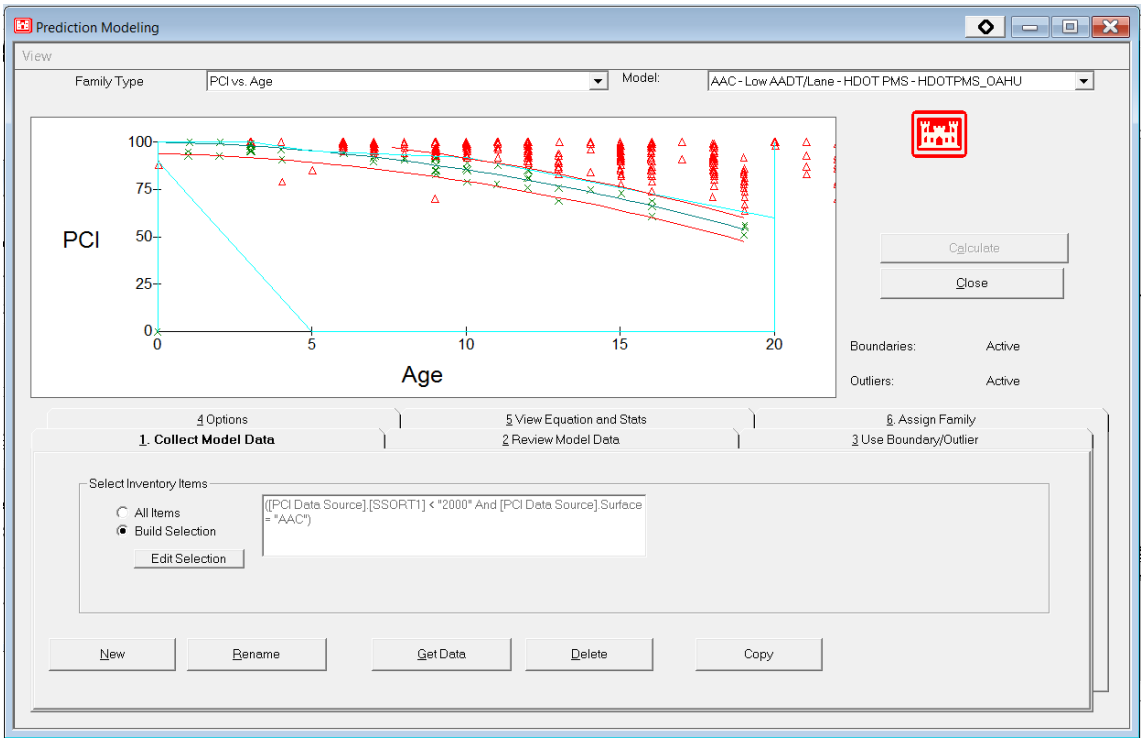

Figure 8-46. PCI prediction modeling in PAVER^{TM}. AAC surfaces with low traffic loading.

Also, on sections on which the last rehabilitation has not been identified correctly, the age would be greatly exaggerated and therefore the corresponding points should be moved substantially to the left. Unfortunately, as shown in Figure 8-47 for AAC surfaces with high traffic loadings, other clustering attempts did not result in any better results.

It also interesting to analyze the time it would take for a section to reach a critical PCI of 60 (a typical threshold below which preventive maintenance is not recommended.) Sections crossing this threshold are good candidates for major rehabilitation. A line fitting all the points in Figure 8-46 (not shown in the figure) would indicate that after 20 years, on average, the threshold would not even be reached. In fact, only a few points are below that threshold. This does not appear realistic or consistent with the needs for pavement rehabilitation.

The original intent with the creation of the Pavement Structure Processing Tool (PSTS) discussed in chapter 2 was the development of distributions of times between rehabilitations/ reconstructions. Unfortunately, the distribution generated with the PSTS for Oahu is suspected to have too many missing projects. Thus, a distribution obtained for the Big Island with the PSTS is instead presented in Figure 8-48. Before comparing the implications from this figure with those

of Figure 8-46, it is important to mention that the two tails of the distribution are also believed to be unrealistic. The left tail is believed to be a simple artifact of artificially created small overlapping sections (a result of small overlaps in milepoints from the data mining) and the right tail is believe to be affected by missing rehabilitation projects.

With these provisos in mind, the rest of the distribution shows that the mode for the time between rehabilitations/reconstructions is between 8 to 12 years (redistribution of some of the tails may affect this result but not dramatically). Assuming that the Big Island is applying a proactive policy, then it could be assumed that the PCI of about 60 is probably reached in about 10 years. This is clearly quite different from the conclusion that one would obtain when using all the points in Figure 8-46. Consequently, filters were setup in PAVER^{TM} to obtain a fitting line close to a lower envelope of the cloud of points. Thus, instead of using all the points, only the points represented by green crosses in Figure 8-46 were used for the deterioration model estimation. Given all the uncertainties on the current data, this appears to produce more realistic results.

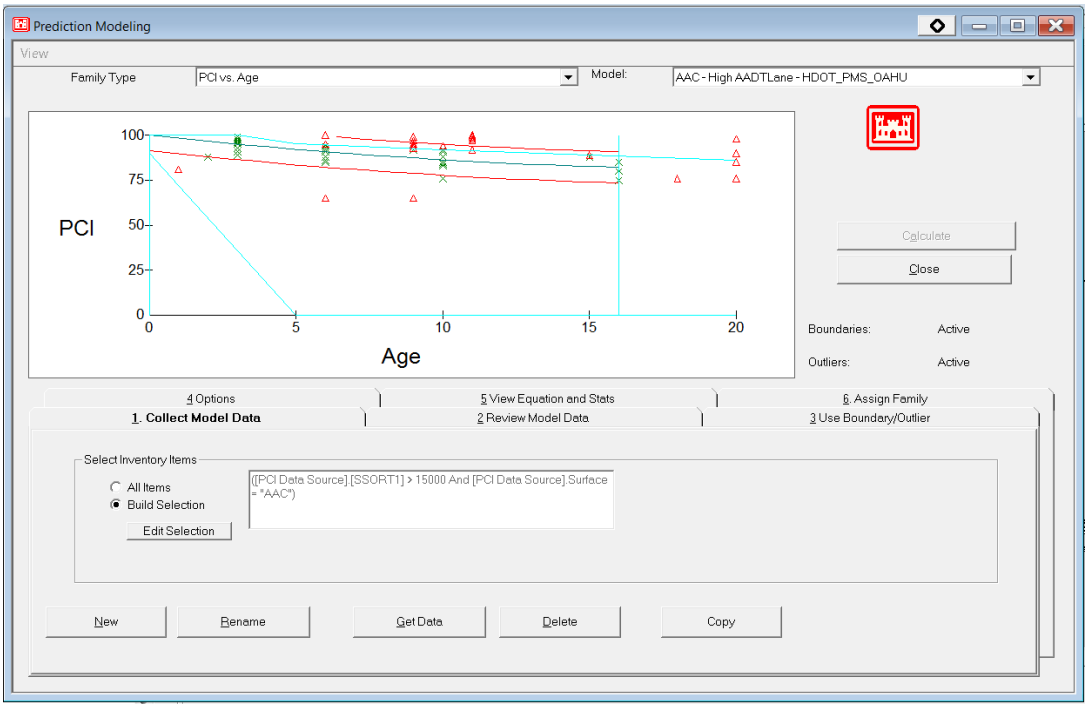

Figure 8-47. PCI prediction modeling in PAVER^{TM} – AAC surfaces with high traffic loading.

The main conclusion from the above discussion is that the current data set does not lend itself to derive reliable deterioration models. Since the family deterioration curves are at the core of the PMS predictions of future conditions (and hence at the selection of efficient strategies), initial use of the PMS will have to rely to some degree on curves borrowed from other agencies. Until data are collected that can provide more reliable estimates, one of the models typically used in the literature or a polynomial model as used by PAVER^{TM} providing a PCI of 60 after, say, 12 years is probably a good option for programming purposes. A selected sample of sections for different pavement categories and for which good information exists about the last construction date should be selected and followed over time to derive more reliable models.

It would also be important at this point to identify those sections that were rehabilitated in the last five years (ideally, it is desirable to identify the timing and type of work, including pavement materials, thicknesses and locations). However, at the very least, the last construction date should be added to the database. Several pavement sections with different ages should be identified for each pavement family so that the trends in the first five years can be identified. Five years is suggested as a compromise since it is most likely that the information will be readily available for recent projects.

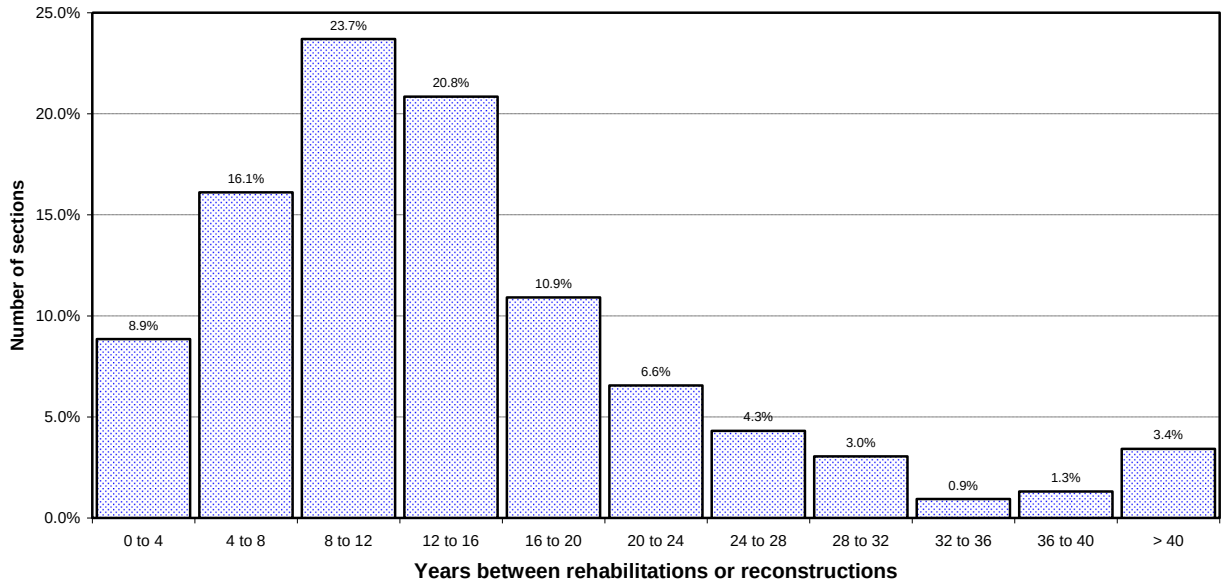

Figure 8-48. Historical times between rehabilitations/reconstructions on the Big Island.

In addition, any new rehabilitation or reconstruction work in between condition surveys must also be recorded to maintain the database. In this way, the system will eventually have the most relevant historic information for all pavement sections in the network.

8.4.3.5 PAVER™ M&R Categories

PAVER™ groups M&R activities into four categories:

- Localized safety
- Localized preventive
- Global preventive
- Major M&R

The definitions of these categories provided by Shahin [7] are:

"Localized safety: Localized safety M&R is defined as the localized distress repair needed to keep the pavement operation in a safe condition.

Localized preventive: Localized preventive M&R is defined as distress maintenance activities performed with the primary objective of slowing the rate of deterioration. These activities include crack sealing and patching.

Global preventive M&R is defined as activities applied to entire pavement sections with the primary objective of slowing the rate of deterioration. These activities are primarily for asphalt surfaced pavements, e.g., surface treatments.

Major M&R: Major M&R is defined as activities applied to the entire pavement section to correct or improve existing structural or functional requirements. Major M&R includes reconstruction and structural overlays. The PCI value after major M&R is assumed to be 100."

Note that in PAVER™ Major M&R includes reconstruction and rehabilitation, while preventive maintenance is separated into two categories (local and global). A relationship between these terms and those described in section 8.2 is presented in [105].

8.4.3.6 Selection of M&R Strategies with PAVER™

This section discusses input parameters and policy factors for treatment selection. Since most of the figures were developed working with part of the City and County of Honolulu

(C&CH) network, reference is often made to the C&CH. However, the discussion is also applicable HDOT.

Before describing the input parameters, a brief introduction to the procedures used by PAVER™ to select M&R strategies is provided. Shahin [7] and the Paver™ 6.5 User's Manual [106] provide more detailed descriptions of the program logic.

8.4.3.6.1 Network-Level M&R Planning in PAVER™

PAVER™ contains a Work Plan tool that is used for planning, scheduling, budgeting, and analysis of alternative pavement maintenance and rehabilitation (M&R) activities. This tool utilizes basic inventory data combined with inspection information, maintenance policies, maintenance costs, and predictions about future pavement condition [106].

The Work Plan tool provides three types of analysis to create M&R plans, identified as:

- Consequence of Localized Distress Maintenance
- Major M&R based on Minimum Condition
- Critical PCI

The first two types of analysis do not generally result in efficient allocation of resources; nevertheless, they are still quite useful. The Critical PCI approach is recommended for developing near optimum multi-year M&R plans.

With "Consequence of Localized Distress Maintenance" localized repairs (either safety or preventive) are assigned for one-year based on existing distress types and severities. This one-year assignment without prioritization is the simplest type of M&R Plan analysis performed by the program. Shahin [7] recommends that an agency develop at least two policies – one for pavements in good condition and one for pavements in bad condition. The type of M&R categories resulting from these two policies were described in section 8.4.3.5 as ***localized safety*** (mostly pothole repairs) and ***localized preventive*** (mostly crack filling and sealing), respectively.

This type of analysis is useful for determining the critical PCI. As defined by Shahin et al. [106], the critical PCI is the PCI value at which the rate of PCI loss increases with time, or the cost of applying localized preventive maintenance increases significantly. The critical PCI is typically a value between 55 and 70 that needs to be determined for the particular deterioration

conditions and costs of each network. The Critical PCI is obtained by estimating two different critical values, one from the deterioration curve and another one using the "Consequence of Localized Distress Maintenance" tool to apply a selected localized maintenance policy to a set of pavement sections belonging to a pavement family and plotting the cost of localized maintenance per unit area versus PCI. By inspecting the cost vs. PCI curve, a "critical PCI" at which the cost increases rapidly with decreasing PCI may be observed and compared with a "critical PCI" determined from a family deterioration curve. The critical PCI value determined from the deterioration curve is that at which a sudden drop on the pavement condition is observed. Shahin [7] recommends determining the critical PCI based on the two critical PCI values described above supplemented with engineering judgment.

Unfortunately, as of the writing of this report, as discussed earlier reliable family deterioration curves have not yet been obtained. However, the critical PCI based on costs can still be analyzed. Figure 8-49 shows the cost of localized preventive maintenance versus PCI generated with PAVER^{TM} for 3,425 pavement sections that were surveyed by a City and County of Honolulu (C&CH) contractor.[79] With so many data points, it may be misleading to simply look at this graph to try to estimate the critical PCI, as for a given PCI, a few points with costs above normal produce the visual impression that the costs start increasing with PCI even for relatively very high PCIs. What this graph cannot show is that for a given PCI, there are multiple sections with zero or very low costs (i.e., a single point in the figure may represent several sections.)

[79] It was preferred to use C&CH distress information since it appears to more realistic capture pavements in bad condition. Very tentative estimates of localized preventive maintenance costs were used to develop this figure. Thus, the figure may not be representative of the actual costs for the C&CH. Similarly to the C&CH, the HDOT needs to obtain cost estimates of the different treatments discussed in the rest of the report.

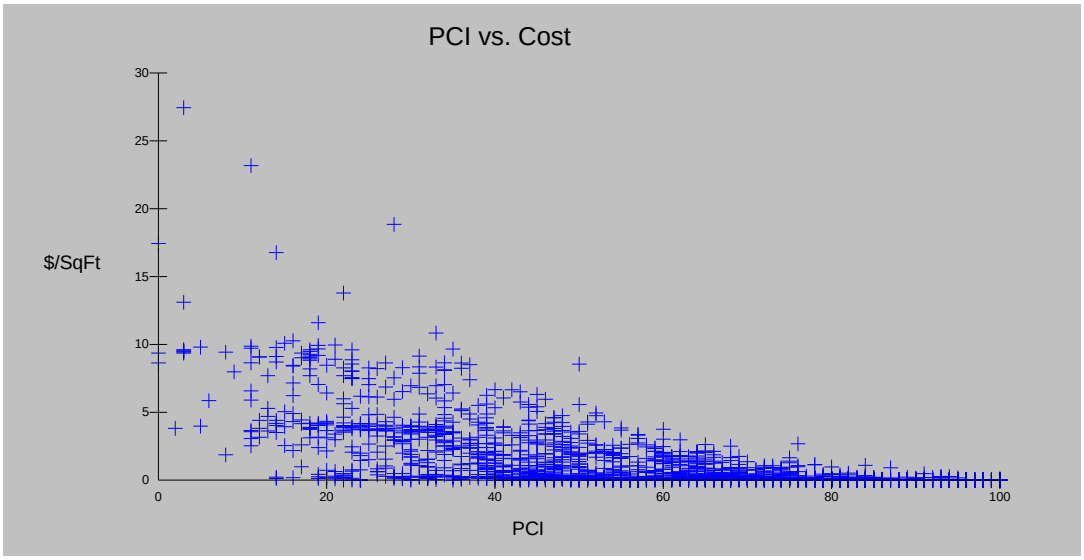

Figure 8-49. Localized preventive maintenance cost ($/sq.yd.) vs. PCI for individual C&CH roads surveyed with Earthmine.

The picture is significantly clearer when the average localized preventive maintenance cost per unit area vs. PCI is plotted as shown in Figure 8-50. Although there is some irregularity in the trend between PCI values of 57 and 67, it is clear that the critical PCI based on costs is apparently between these two values. One of the possible reasons for the irregularity is that at present all the pavements have been lumped together irrespective of traffic level, structural design, etc. Another possible explanation for the drop that starts at a PCI of 60 is that around this PCI the deterioration of many cracks may be accelerated with spalling, raveling or even some potholes that require safety treatments. Thus, around this level the amount of cracking may be reduced simply because those cracks have been transformed into a different distress or into patching areas. In any case, at present, this is the best information available to estimate the Critical PCI.

Based on Figure 8-50, it appears that a good estimate of the critical PCI for the sections analyzed is around **65**. Of course, this value will need to be revised once families with similar deterioration curves can be established. It is nevertheless comforting to see that the estimate is within the typical range of 55 to 70 ([7]).

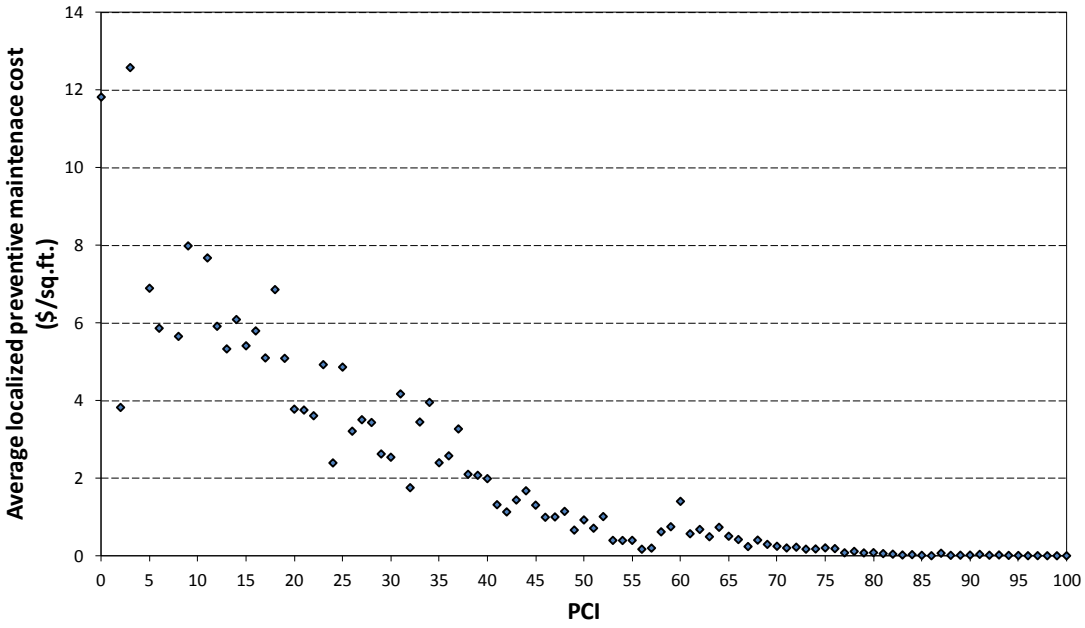

Figure 8-50. Example of average localized preventive maintenance cost ($/sq.ft.) vs. PCI for C&CH roads[80].

The "Major M&R based on Minimum Condition" analysis in PAVER™ is basically a worst first approach without any budget optimization. As it is well known, this is not a cost-effective approach. Under this option PAVER™ provides budget requirements needed to maintain the pavement above a specified condition [7]. The minimum pavement condition can be varied by the user by pavement use and rank. Furthermore, the minimum condition can also be varied by year. By slowly increasing the minimum PCI, the likelihood of developing a plan with a high, unaffordable budget in the first year can be reduced.

Under the "Major M&R based on Minimum Condition" analysis, as stated by Shahin [7] "the cost of applying the major M&R is estimated for each section by projecting the year in which the section will deteriorate to a specified minimum condition and multiplying the section area by the unit M&R cost." For any pavement section needing major M&R in the first year the costs could simply be calculated from the cost of each treatment. However, since the program estimates the condition of the pavement sections in future years, the cost of M&R in the future or

[80] The average costs in the figure are for illustrative purposes only. The C&CH and HDOT need to develop cost estimates more representative of local conditions.

for sections in which the current condition is estimated can only be predicted from a table of major M&R costs versus PCI developed by the user for the specific network.

As explained also in Shahin [7], the **critical PCI approach** was developed by studying results from dynamic programming network optimization analysis and performing many life-cycle cost analyses on many projects. Thus, since the procedure was designed to approximate the results of the optimization it should provide near optimum alternatives. The critical PCI is based on the concept that is more economical to maintain pavements above a certain PCI threshold (the critical PCI defined earlier) than below it [107]. The next section is dedicated to this approach in more detail.

8.4.3.6.2 Critical PCI method for Multi-Year M&R Section Assignment

In the critical PCI method (Figure 8-51), the M&R category assigned to a given section depends on whether the section is above or below the critical PCI. If a section is above the critical PCI, localized preventive and/or global preventive maintenance are applied if the section is structurally adequate or Major M&R is applied if the section is structurally deficient (the actual selection of the specific M&R treatment is explained later.) If a section is below the critical PCI, localized safety or major M&R is applied (again, which treatment is selected is explained later). The actual assignments are performed by trying to optimize the allocation of resources to the different pavement sections and accounting for budget constraints. Thus, the program will attempt to assign a preferred treatment to each pavement section, but depending on the availability of funds on a given section, actions may be deferred. The following paragraphs explain in more detail the assignment of M&R treatments.

8.4.3.6.2.1 M&R Assignment for Sections Above or Equal to The Critical PCI

For sections with a PCI above critical but structurally deficient, the recommended treatment is major M&R. PAVER^{TM} determines whether a section is structurally deficient by comparing the densities (as defined for PCI calculations) of some distresses with the threshold values provided in Table 8-2.

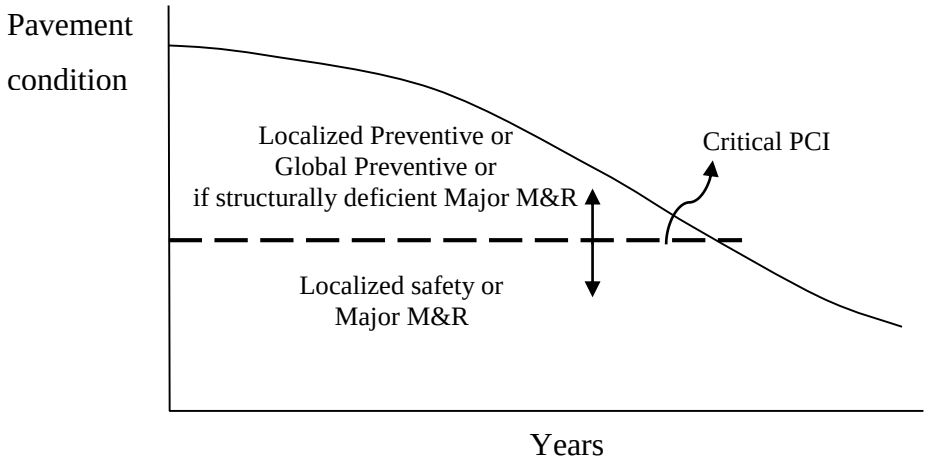

Figure 8-51. Assignment of M&R Category Using the Critical PCI Method (Source: [7])

Table 8-2. List of structural distresses used in Critical PCI method (source: [7]).

Pavement Type	Distress	Severities	Density (%)
Asphalt Pavement			
	Alligator cracking	L+M+H	> 0.5%
	Patching	M+H	> 10%
	Potholes	L+M+H	> 0.1%
	Rutting	M+H	> 1.0%
Concrete Pavement			
	Large Patching	M+H	> 10%
	Corner break +	L+M+H	
	Divided Slab (Shattered	L+M+H	> 5%
	Slab) + Punchout	M+H	

The cost of major M&R is determined based on the PCI vs. unit cost relationship by multiplying the section area by the unit cost. As explained by Shahin [7], the unit cost vs. PCI relationship for Major M&R can be approximated by a straight line interpolation between the

cost at the largest PCI below which reconstruction is needed (PCI ~ 30) to the cost at the lowest PCI at which an overlay is adequate (PCI ~ 75), as illustrated in Figure 8-52.[81]

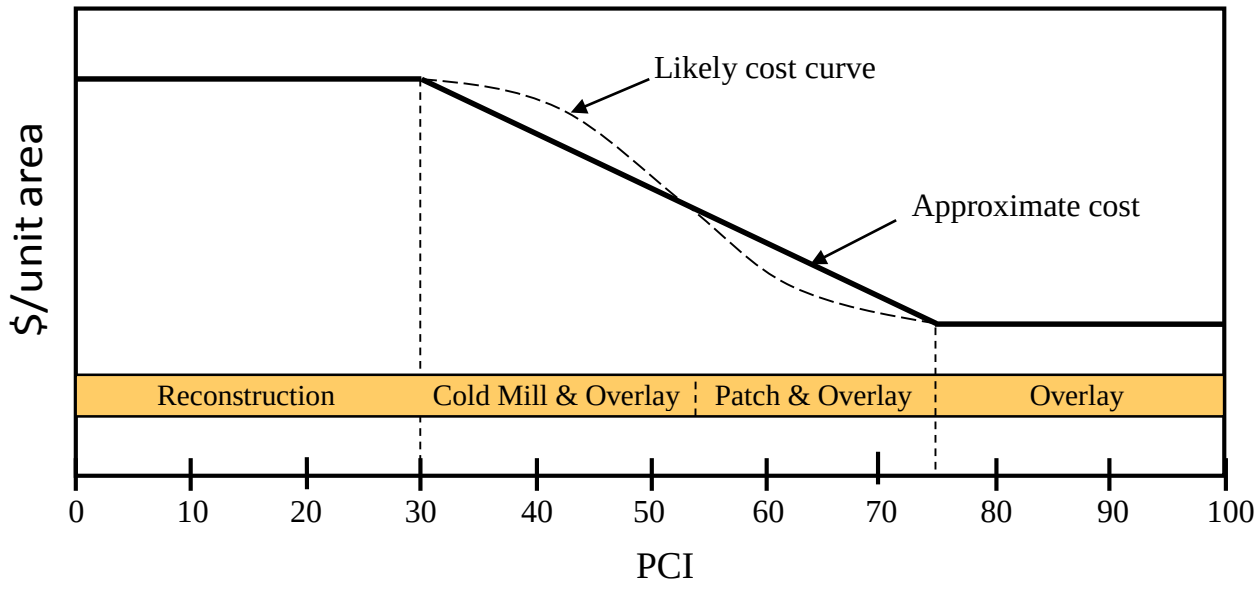

Figure 8-52. Guideline for Development of PCI vs. Unit Cost for Major M&R (source: [7]).

If the section is structurally deficient, the program checks on funds availability and major M&R priorities (as discussed later in the document). If funds are available, major M&R is applied and the PCI value of the section is set to 100. If funds are not available, localized preventive and/or global preventive are applied as explained below for the current year and funds availability for Major M&R is checked in the following years [7].

Pavement sections for which funds for major M&R are not available or that are not structurally deficient receive localized preventive M&R. The cost of application is determined in the first year either based on the results of the most recent distress inspection (if performed within the last year) or through the PCI vs. unit cost relationship. For the second year and beyond, only the PCI vs. cost approach can be used since the program needs to estimate the

[81] An adaptation of this guideline for HDOT is described with the Major M&R policy later in this document.

PCI in future years. The details of the assignment of localized preventive maintenance treatments is explain later in section 8.4.3.6.4.

Global preventive M&R is applied based on the specified interval between applications. Figure 8-53 shows graphically the assignment of M&R treatments for sections above the critical PCI.

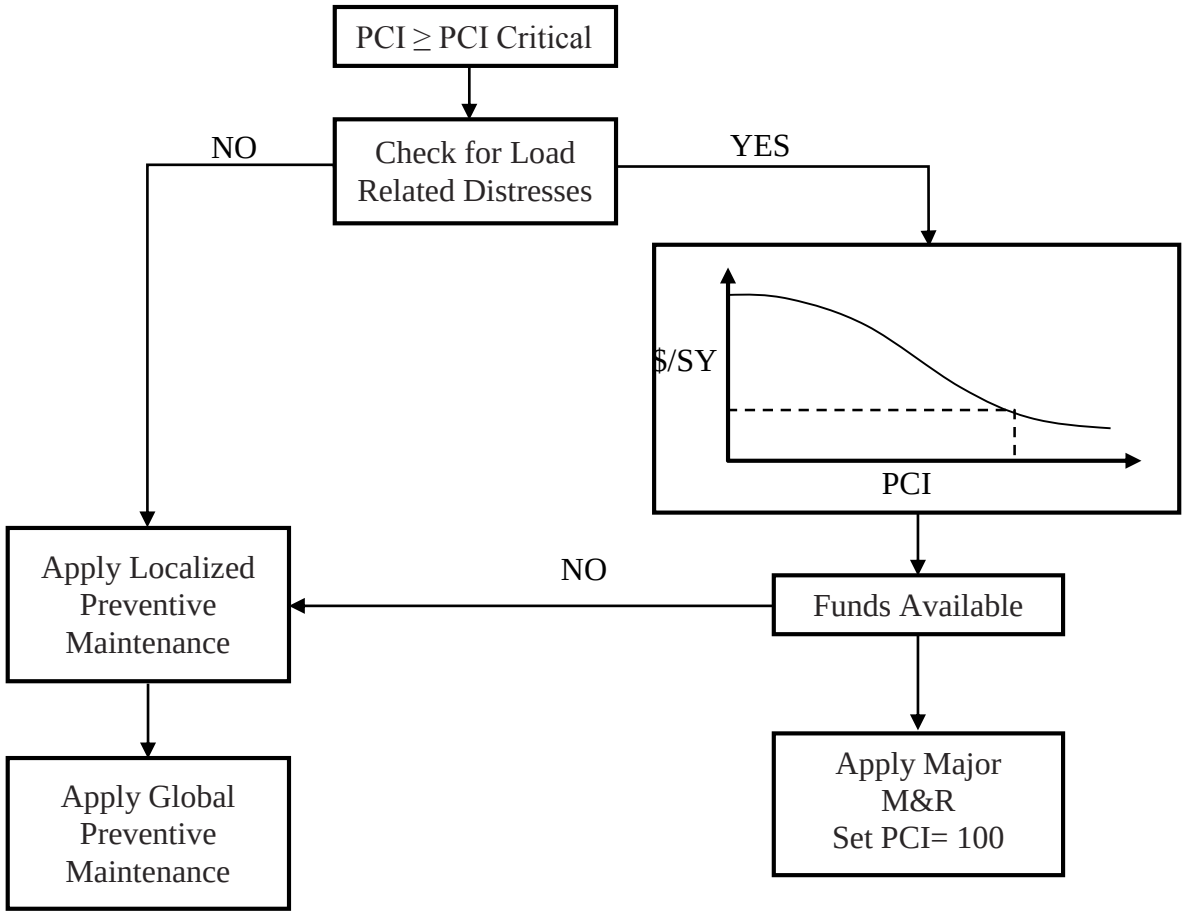

Figure 8-53. M&R Assignment of Sections above or equal to the Critical PCI (Source: [7]).

8.4.3.6.2.2 M&R Assignment for Sections Below to The Critical PCI

Sections below the Critical PCI have typically deteriorated to a point where preventive maintenance activities are not cost effective. Thus, these sections need to be rehabilitated if sufficient funds are available or subjected to safety treatments if funds for major M&R are not available. If Major M&R is applied, then the PCI is set to 100. Figure 4.6 illustrates the process.

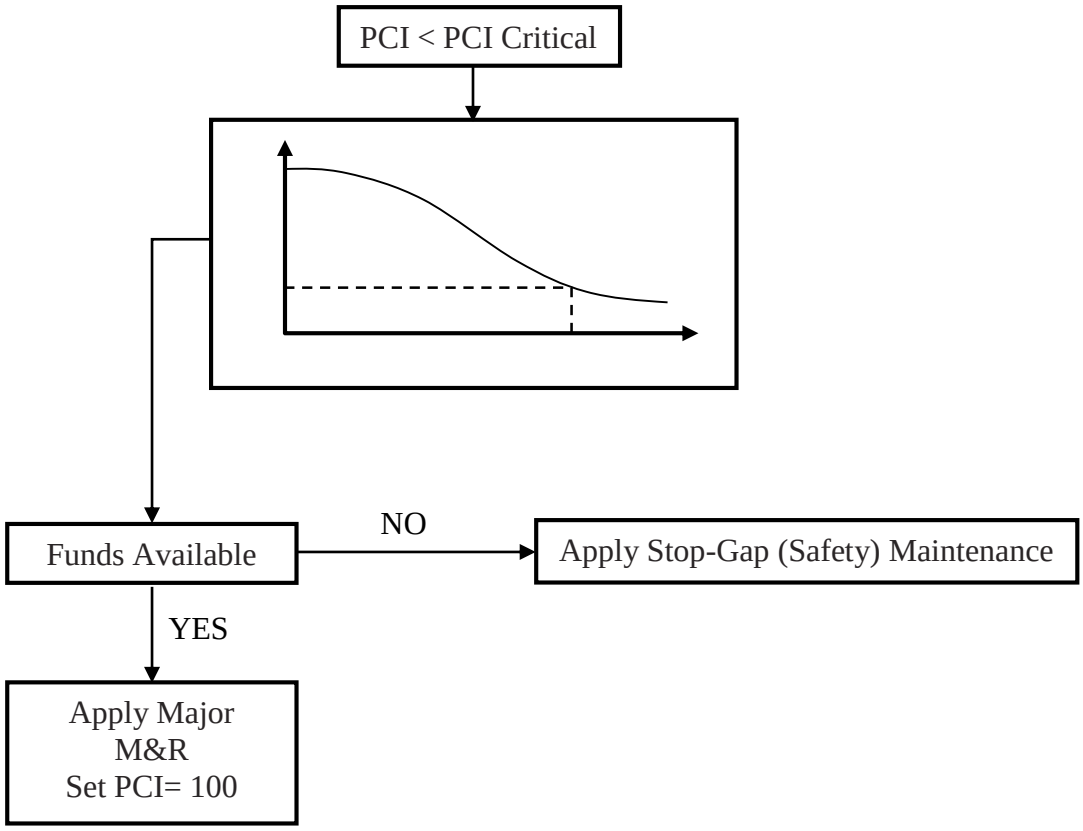

Figure 8-54. M&R Assignment of Sections above or equal to the Critical PCI (Source: [7])

The check for availability of funds for each section is based on budget and the Major M&R priorities explained later.

As for the case of sections with PCI above the Critical PCI, the cost of applying localized safety M&R is determined in the first year either though using the PCI vs. cost relationship or based on the results of the most recent distress inspection. For the second year and beyond, only the PCI vs. cost method can be used.

8.4.3.6.2.3 M&R Budget Prioritization/Optimization

The Critical PCI method places emphasis on preventive maintenance (localized preventive and global preventive) by trying to keep pavements above the Critical PCI, which results in lower M&R spending. Ideally, a pavement section should receive Major M&R immediately after reaching the Critical PCI, bringing its PCI back to 100. This would result in a near optimal allocation of resources for that particular pavement section. However, since several sections may reach the critical PCI at about the same time and budgets may be limited, it is often

necessary to prioritize which sections will receive Major M&R first and for which sections Major M&R will have to be deferred and for how long. For a given prioritization scheme between sections, the optimal allocation of resources is achieved with an optimization algorithm.

Notice that with unlimited funding, there is no need for prioritization between pavement sections. In this case, M&R treatments are assigned following the procedures presented in sections 8.4.3.6.2.1 or 8.4.3.6.2.2 depending on whether the PCI is above or below the Critical PCI, respectively. This should produce a cost-effective treatment assignment. Note also that since it is generally more economical to maintain pavements in good condition, in the long term, the strategy should result mostly in the recurrent application of preventive maintenance treatments without much needs for rehabilitation.

When the available M&R budget is lower than that required by needs alone, prioritization and optimization are needed to obtain the maximum return on investment. The prioritization scheme used in PAVER™ emphasizes budget optimization but it recognizes that certain projects need to be performed to account for factors not considered in the optimization. As pointed out by Shahin [7], some of these factors may include functional requirements (user costs), mission objectives (e.g., increase in traffic loading), and in some cases, political/social realities (e.g., title 6 – environmental justice areas.) The program allows the consideration of projects that must be included for the type of reasons just described. Once those projects are identified, PAVER™ estimates their cost and then it subtract it from the budget to obtain the budget available for the rest of the pavement sections. Finally, PAVER™ selects an approximate cost-effective M&R strategy by allocating the available budget among the candidate pavement sections by following the prioritization scheme described later in the text. Before explaining how the budget is allocated to each pavement section it is convenient to discuss the types of analyses available.

1. Type of Analyses

PAVER™ provides various types of multi-year analyses using the Critical PCI approach. These include determining the consequence of a budget plan or determining budget requirements for:

- eliminating the backlog of Major M&R in a specified period of time,
- maintaining current area-weighted PCI over a specified period of time, or

- reaching the desired area-weighted PCI in a specified period of time.

2. M&R Budget Prioritization/Optimization - Budget Determination

PAVER™ attempts to find the lowest budget that will achieve the specified objective. The objectives for each of these budget requirement plans are considered to be achieved when the following are within certain tolerances [7]:

- Backlog Elimination: No unfunded Major M&R in the last year of the analysis.
- Maintain condition: Compare the area-weighted PCI at the beginning of the analysis period (before M&R) with the value at the end of the analysis period plus one year where no work is performed in the last year.
- Reach a specified condition value: Compare the specified PCI with the value at the end of the analysis period plus one year where no work is performed in the last year.

For any of three objectives, the budget requirements are computed by PAVER™ with the following built in iterative procedure [7]:

Step 1: Determine a plan with unlimited budget and set the maximum budget equal to the highest annual budget during the analysis period (which is usually the first year budget) and set the minimum budget equal to zero.

Step 2: If an unlimited budget cannot achieve the objective, then the desired PCI may be unrealistically high. Thus, the analysis is stopped. If the goal can be achieved go to step 3.

Step 3: Set the current budget equal to the average of the minimum and maximum budgets. If the goal is achieved with the current budget set the maximum budget equal to the current budget and if the goal is not achieved set the minimum budget equal to the current budget.

Step 4: Repeat step 3 until the end condition tolerance is achieved.

Notice that up to this point the method used to select the specific treatment for each section have not been discussed in detail. Now, attention is turned to this important issue.

3. M&R Budget Prioritization/Optimization – Treatment selection

From Figure 8-53 and Figure 8-54, it is clear that with *unlimited funds*, a section will receive either Major M&R or preventive treatment (localized or global) but it will never receive a localized safety treatment. This is reasonable since localized safety treatments are the least cost-effective of all the treatments (as observed every year when potholes are filled with patching mixes only to see many of the same potholes in the same or worst condition the following year.) Proper repair of potholes (e.g., with a deep asphalt concrete patch of an area larger than the pothole and adequately compacted) may ameliorate the problem but it is still not the most cost-effective treatment. Furthermore, the pothole problems typically occur in a short period of time and because of labor force limitations it is typically unfeasible to perform quality pothole repairs. Clearly, the main reason for applying localized safety treatments is for budget constraints. Unfortunately, this is a common situation that takes significant time to reverse if funding levels in previous years have not been adequate.

As indicated by Shahin [7], the first factor in the prioritization is the M&R category, which is given the following priorities:

1. Localized safety
2. Localized preventive
3. Global preventive[82]
    a. Type 1
    b. Type 2
    c. Type 3
4. Major above critical PCI
5. Major below critical PCI

Unfortunately, this description is not clear about how the program proceeds in the allocation of treatments. The following is a possible scenario that is also consistent with the logic of Figure 8-53 and Figure 8-54. Although the actual PAVER™ implementation could vary slightly, it is believed that this is the approximate logic used by the program.

[82] The types of global preventive maintenance are described later in the sequel (see section 8.4.3.6.5.1).

First, for all pavement sections with PCI below critical, the cost of application of ***localized safety*** (e.g., pothole repair) is calculated. Clearly if the sum of localized safety costs were larger than the current budget then not even all the needs for safety treatments could be satisfied. In that case, the sections are selected based on section use and rank priorities. Within each M&R category, PAVER™ assigns a priority factor based on the combination of pavement use (e.g., roadway, parking lot, etc.) and rank (e.g., primary, secondary, etc.). Table 8-3 shows an example priority table.[83]

Table 8-3. Priority based on use/rank (source: [7]).

RANK ► / USE ▼	High	Medium	Low
High	**1**	**3**	**6**
Medium	**2**	**5**	**8**
Low	**4**	**7**	**9**

Typically, budgets are big enough to cover at least the safety treatments.

In the next step, the rest of the budget is allocated to satisfy ***localized preventive*** maintenance needs (e.g., crack sealing). Recall that localized preventive maintenance is applied only to pavement sections with a PCI above the Critical PCI. Again, if the budget is not enough for all sections requiring localized preventive maintenance, then the sections are selected for localized preventive maintenance from the set of sections with PCI above critical based on use/rank priorities (first all the sections with highest priorities are selected, that is with priority 1, then all the sections with second highest priorities, etc.).

Then, the same process is repeated for ***global preventive*** maintenance treatments (e.g., fog seals, slurry seals, etc.)

[83] The user defines what constitutes high/medium/low levels for use and rank in two separate tables. These are described in Section 4.8.

The next priority is given to ***Major M&R for sections above the Critical PCI***. As explained by Shahin [7], the reason that major M&R above Critical PCI has higher priority than Major M&R below Critical PCI is that this strategy minimizes costs. Remember that sections above Critical PCI require major M&R when they show structural distresses. At this point, a 2" overlay (or a 2" mill and overlay if grade needs to be maintained) can be a very effective treatment. Once again, sections are analyzed in the order of their use/rank priorities and treatments are assigned until all sections above Critical PCI with structural distress are treated or until the budget is exhausted. Notice that each time a section above critical PCI is assigned a Major M&R treatment, the previously assigned monies for localized and global preventive for the given section must be released. As shown in Figure 8-53 (page, 507), a section receives a Major M&R if funding is available or Localized Preventive and/or Global Preventive if funding for Major M&R is not available. However, it does not receive both[84].

Finally, sections below critical PCI are considered for Major M&R. Again, sections are analyzed in the order of their use/rank priorities and each time a Major M&R treatment is assigned the cost of the previously assigned localized safety or stop gap must be subtracted. Again, the budget is allocated until all sections are assigned the desired treatment or until the budget is exhausted.

Notice that within a given use/rank priority category there may be hundredths of sections. Thus, within each category some priorities also need to be defined. In this case, PAVER™ breaks ties based on the PCI of each section. In general, within a given user/rank category the program gives higher priorities to sections with PCI closer to the critical PCI. Thus, for sections above the critical PCI, lower PCIs result in higher priorities and for sections below the critical PCI higher PCIs result in higher priorities. The exception to this rule is for localized safety (stop gap) treatments where sections with lower PCIs receive higher priority. The reason is that stop gap treatments are required for safety reasons whereas the other treatments are selected for their cost-effectiveness.

---

[84] Of course, the cost estimates for Major M&R treatments should include the costs of local repairs needed prior to application of the M&R.

8.4.3.6.3 Stop Gap M&R Treatments, Policies, Consequences, and Costs

In order to carry out the Critical PCI analysis described in the previous section, PAVER™ requires the definition of M&R policies as well as their effects and estimates of the different treatment costs. All these parameters need to be defined and entered into different program tables before the program can carry out the analysis.

Figure 8-55 shows one such program table available for Localized Stop Gap (or Localized Safety) M&R (this particular table is also used by the program for Localized Preventive M&R.) This table provides the **Work Types** that can be performed under localized M&R strategies (either stopgap or preventive). The values with yellow background are defaults provided by the program but the user can add other types of work to customize the program to local practice (this is a common feature in PAVER™). It is important to note from this figure that for each M&R policy (localized safety, localized preventive, global preventive and major M&R) there are different tabs with information requirements that need to be completed to perform the analysis. The following subsections explain the M&R policies for each of the M&R categories.

8.4.3.6.3.1 Localized Repairs M&R Policy

Localized repairs (including localized safety and localized preventive maintenance) are assigned based on existing distress types and severities. Two different policies are typically specified for **localized safety/stopgap treatments** (e.g., pothole repair) and for **localized preventive maintenance** (e.g., crack sealing).

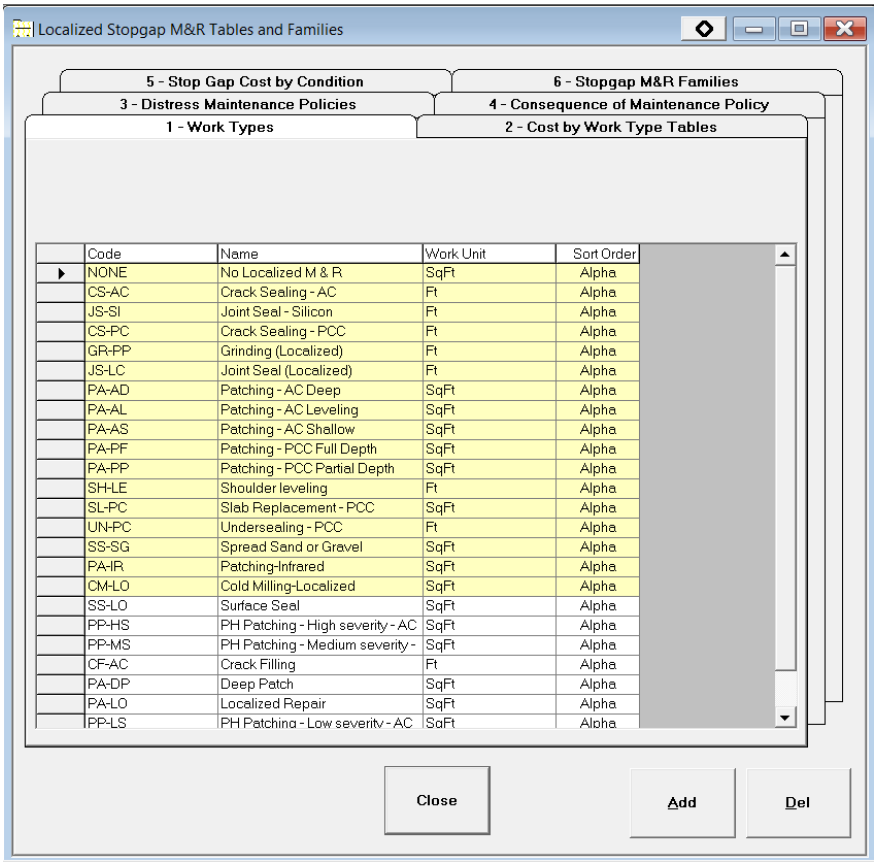

Figure 8-55. Example of M&R Input Table.

8.4.3.6.3.2 Stopgap (safety) M&R Policy

Table 8-4 provides a suggested ***Localized Safety M&R*** policy. The work types in the table are described shortly. It must be emphasized that at this point only the part of the policy related to asphalt concrete distresses has been considered in detail. Note that the part of the policy related to Portland Cement Concrete (PCC) pavements has been reproduced from one of the tables suggested in Shahin [7]. A detailed analysis with input from HDOT should be performed with more information on costs and currently used local HMA and PCC repair practices. The following sections provide more information on the most common work types for flexible pavements in this table.

Table 8-4. Suggested Localized Safety (Stopgap) M&R Policy

Distress	Distress Severity	Description	Work Type	Work Unit
1	High	ALLIGATOR CR	Patching – AC Shallow	SqFt
4	High	BUMPS/SAGS	Patching - AC Shallow	SqFt
5	High	CORRUGATION	Patching - AC Shallow	SqFt
9	High	LANE SH DROP	Shoulder Leveling	Ft
11	High	PATCH/UT CUT	Patching - AC Deep	SqFt
13	High	POTHOLE	PH Patching – High Severity – AC	SqFt
13	Low	POTHOLE	PH Patching – Low Severity – AC	SqFt
13	Medium	POTHOLE	PH Patching – Medium Severity - AC	SqFt
15	High	RUTTING	Patching - AC Shallow	SqFt
16	High	SHOVING	Patching - AC Shallow	SqFt
17	High	SLIPPAGE CR	Patching - AC Shallow	SqFt
21	High	BLOW UP	Slab replacement - PCC	SqFt
21	Medium	BLOW UP	Patching - AC Shallow	SqFt
25	High	FAULTING	Slab Replacement - PCC	SqFt
27	High	LANE SH DROP	Patching - AC Leveling	SqFt
38	High	CORNER SPALL	Patching - AC Leveling	SqFt
39	High	JOINT SPALL	Patching - AC Leveling	SqFt

8.4.3.6.3.3 Stopgap M&R Work types

The work types in Table 8-4 deserve some explanation. Most of the following discussion is related to the pothole repair work types.

A pothole is a localized distress in an asphalt concrete pavement resulting from the breakup of the asphalt concrete surface and possible erosion/breakup of the base course. The pothole is formed when pieces of the asphalt concrete in a distressed area of the pavement are removed under the action of traffic. The effect of traffic in the formation of potholes is typically accelerated under the presence of water.

The primary methods used to perform pothole patching are [108]:

- Temporary (Throw-and-roll)
- Semi-permanent
- Injection patching

Injection patching is an alternative to the "throw-and-roll" method [108]. It requires specialized equipment and it is considered by some as a rapid and effective method for temporary patches. Although it is reported that injection patches typically have longer lives than throw-and-roll patches [108], past experience with this method in Oahu *has been negative* (see for example http://the.honoluluadvertiser.com/article/2003/Feb/26/ln/ln04a.html (last accessed March 2013) and http://the.honoluluadvertiser.com/article/2004/Jan/06/ln/ln10a.html (last accessed March 2013). Whatever the reasons for the past negative experience, the technique is unlikely to be a viable alternative in the short term in Oahu, therefore injection patching is not discussed further in this report.

In the **throw-and-roll technique** [109], the patching material is placed into the pothole with or without cleaning and/or drying of the pothole. Then the material is compacted using the maintenance truck tires (usually 4 to 8 passes). It is recommended for the finished patch to have a ⅛ to ¼ in (3 to 6 mm) of crown to help avoid water ponding. The **throw-and-roll** method is used when weather conditions are too poor for a semi-permanent patch or when the immediate pothole repair demands are so high that performing semi-permanent patches is impractical. The main advantage of this method is productivity in terms of potholes patched per day, although patching appearance is not visually appealing.

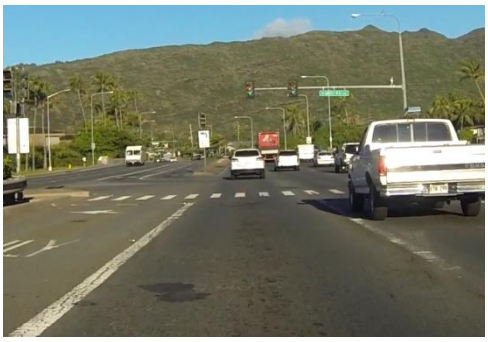

Figure 8-56. Throw-and-roll pothole patch.

Wilson and Romine [110] indicate that **Semi-Permanent** patching (Figure 8-57) is considered one of the best repairing potholes methods, short of full-depth removal and replacement.

Figure 8-57. Example of a semi-permanent patch.

The semi-permanent procedure for repairing potholes includes the following steps (adapted from [110]):

1. Remove all water (the pothole should be reasonably dry) and debris from the pothole.
2. Mark and square off an area at least 6” to 12” beyond the pothole area (using a diamond saw, pneumatic hammer, or a milling machine). The area is cut such that vertical sides exist in reasonably sound pavement.
3. Place the patching material.
4. Compact with a device smaller than the patch area. (Single-drum vibratory rollers and vibratory plate compactors work best.)
5. Open the repaired section to traffic as soon as maintenance workers are cleared from the area.

Before placing the mix, the vertical faces of the pothole may be tacked with a light application of asphalt material to promote bonding between the pothole material and the existing asphalt concrete. An excess of asphalt tack material should be avoided.

As with new pavement construction, achieving adequate density is extremely important. In this respect, the Maintenance Technical Advisory Guide (MTAG) of the California Division of Maintenance [108] recommends that the patch be compacted thoroughly. It is also recommended that the finished patch have a 0.1 in to 0.2 in (3 to 6 mm) crown to account for additional compaction by traffic and to help prevent standing water accumulate in the patching area. Several MTAG recommendations [108] are given in Figures 5-7 to 5-11 of that report, which are reproduced here in Figure 8-58.

Different recommendations are found in the literature about the compaction of the patch material (though they are not always referring explicitly to the semi-permanent pothole patching technique.) For example, for "Deep Patch Repair" of asphalt concrete pavements, Shahin [7] indicates that Hot Mix Asphalt (HMA) should be placed in layers not to exceed 3 in. On the other hand, *for pothole patching* Wolters [111] recommends placing HMA mix in one lift with the loose mixture higher than the patch area. He recommends using only one lift to promote mixture heat retention and obtain maximum in-place density (this is apparently achieved with one lift because most potholes dimensions are small in area.)

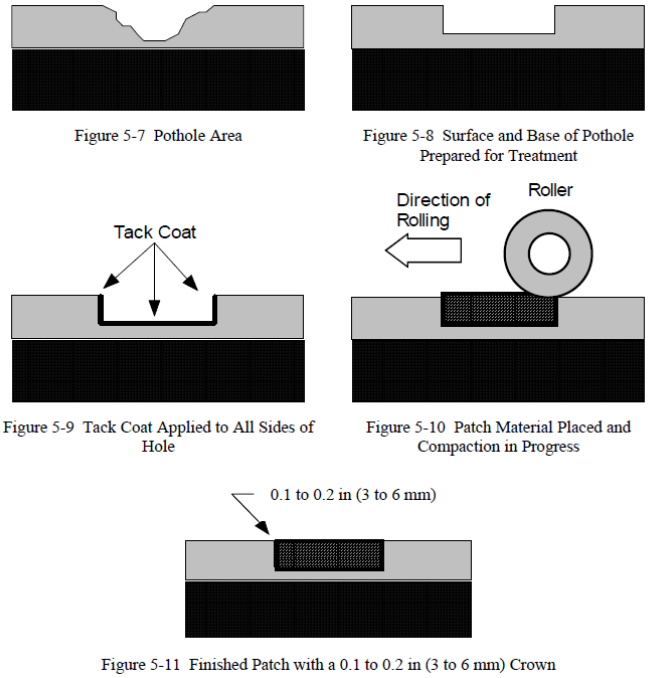

Figure 5-7 Pothole Area

Figure 5-8 Surface and Base of Pothole Prepared for Treatment

Figure 5-9 Tack Coat Applied to All Sides of Hole

Figure 5-10 Patch Material Placed and Compaction in Progress

Figure 5-11 Finished Patch with a 0.1 to 0.2 in (3 to 6 mm) Crown

Figure 8-58. Recommendations for Semi-permanent patches [108].

MTAG [108] also recommends to seal with crack sealant the edges of the patch area. For areas with significant amount of rainfall, they recommend to fog seal the entire patch area. As illustrated by the relatively wide gap between the patch and the rest of the pavement in Figure 8-59, the edges of the patch are a potential route for water to ingress into the pavement structure.

The references cited in the previous paragraphs provide several other valuable recommendations that are worth consulting by maintenance personnel. Another reference providing interesting information of pothole repairs is [112].

For larger patching areas, it is recommended to follow the guidelines for Full-Depth Patching provided in "The Asphalt Handbook" [91]. Note that the Asphalt Institute also recommends backfilling a patch with dense graded HMA but if HMA is not available, they recommend using an appropriate cold mix, specialty mix, or proprietary mix. If the patch is more than 6 in (150 mm) deep, the Asphalt Institute recommends placing the material in layers, each compacted thoroughly with a vibratory plate for smaller patches and a roller in bigger patches. Contrary to the California Division of Maintenance [108] recommendations, the Asphalt Institute [91] indicates that the patch should not be overfilled in anticipation of traffic compaction. This recommendation is consistent with achieving adequate compaction of the patched area (similar to that achieved on new pavements.)

Figure 8-59. Untreated edges in a semi-permanent patch.

8.4.3.6.3.4 Proposed pothole repair policy

As discussed in the previous section, several options are available for pothole patching. In this section, the rationale for the policy on pothole patching proposed in Table 8-4 (page 516) is discussed. The proposed policy is intended to define some general direction on how to proceed with pothole patching. However, more input and discussion is needed from stakeholders to define some important details and obtain a practical policy.

For semi-permanent pothole patches, the vertical faces of the squared off area are intended to provide lateral restraint against movement of the patch, which can be achieved for pavements in relatively good condition (i.e., without not much deterioration other than the pothole in question.) Thus, semi-permanent "pothole" patching is not recommended for a "single" pothole in an otherwise severely deteriorated area since the lateral support will be

difficult to obtain. Furthermore, in a deteriorated area, the cutting operation may dislodge additional pieces. However, semi-permanent patching may still be a good alternative for patching the pothole together with the adjacent severely cracked areas.

In terms of effectiveness, the FHWA's Long Term Pavement Performance (LTPP) Study found that the "throw-and-roll technique proved just as effective as the semi-permanent procedure for those materials for which the two procedures were compared directly" [109]. Considering that the semi-permanent method is more labor and material intensive, the throw-and-roll technique is generally more cost effective if *quality materials* are used.

As indicated by Wilson and Romine [110], MTAG [108] and the Asphalt Institute [91], Hot Mix Asphalt (HMA) concrete is recognized as a preferred alternative for patching operations. However, since pothole repairs often need to be performed quickly after rain events, Cold-Mix Asphalt (CMA) is often used. Patches completed with CMA, however, are most often believed to be for temporary fixes. Nevertheless, most of the consulted pothole repair patching literature provide details of patching with CMA and not much is said about the logistics of handling HMA for pothole repairs.

The observations in the previous paragraphs guided the pothole repair policy in Table 8-4, which is now described in more detail.

Specifically, for low severity potholes it is proposed to continue using the throw-and-roll method with quality CMA. It is important to emphasize that adequate compaction should be provided in all cases. Productivity is of no value if the treatment does not last a reasonable period of time. In Table 8-4 , the *throw-and-roll method for low severity potholes has been termed* ***PH Patching – Low severity - AC*** to account for the fact that the same technique applied to other severity levels has a different average cost. Low severity potholes are probably the most common type of potholes encountered. Therefore, use of the throw-and-roll method would result in an effective operation.

For medium severity potholes (diameter of 18-30" and depth of ½" to 1"[85] or diameter of 8-18" and depth >1" or diameter of 4-8" and depth > 2" according to ASTM D6433), it is also proposed to use the throw-and-roll method with quality CMA. The potholes in this category can still be compacted with the truck tire. Patching for medium severity potholes has been termed ***PH Patching – Medium severity – AC*** in Table 8-4.

Depending on the mix tenderness, it may be more difficult to obtain a smooth surface in larger potholes (Figure 8-60).

Figure 8-60. Questionable smoothness of throw-and-roll patches in larger potholes.

Consequently, for high severity potholes (diameter > 18" and any depth > 1"), semi-permanent patches are proposed. First, as seen in Figure 8-60, even if an effective patch could be performed with the throw-and-roll method, the patching area becomes unattractive and gives the appearance of poor workmanship, which will affect public perception regardless of the patch effectiveness. If the pavement around the potholes is in relatively good condition, the squared-off area will provide good confinement to the patch as required for this method. If the area around the pothole exhibits high severity fatigue cracking, then consideration of a larger patch including the cracked area is warranted.

[85] Some of these "potholes" are probably the result of de-lamination instead of being a real pothole. Thus, if it is evaluated that the mix will not adhere to the existing surface, a different repair technique is required.

Overuse of the throw-and-roll technique can cause situations such as that depicted in Figure 8-61, which should be avoided. Additional throw-and-roll patching in such situations is ineffective, the ride for users becomes unacceptable, the patching is unsightly, and the public perception extremely negative. These, together with the higher likelihood of high severity potholes being in areas severely cracked that may be recommended for patching by the preventive maintenance policy, are the main reasons why the throw-and-roll method is not proposed for high severity potholes. The pothole repair for large severity potholes has been termed ***PH Patching – High Severity – AC*** in Table 8-4.

Figure 8-61. Ineffective throw and roll patching.

For planning purposes, it is assumed that HMA will be used for semi-permanent repair of high severity potholes. For the use of HMA to be effective, the potholes would have to form part of a bigger area to be patched (e.g., because of alligator cracking around the pothole) or several patching operations will need to be coordinated in the vicinity of the pothole.

It is recognized that the proposed policy may require additional efforts and costs compared with the current practice. Nevertheless, increasing the quality of pothole patching combined with other M&R treatments discussed later not only should result in lower M&R costs in the long run but also a lower number of reimbursement claims, thus offsetting even more the additional costs.

8.4.3.6.3.5 Stopgap M&R Costs

For illustrative purposes, this section provides estimates of patching costs for use in M&R analyses scenarios with PAVER™. As discussed in previous sections, two different types of cost information are required by PAVER™ for Stopgap M&R treatments: "Cost by Work Types" and "Stopgap Cost by Condition". Unfortunately, at this point neither of these can be estimated accurately.

Figure 8-62 shows an example of the Cost by Work Types table.

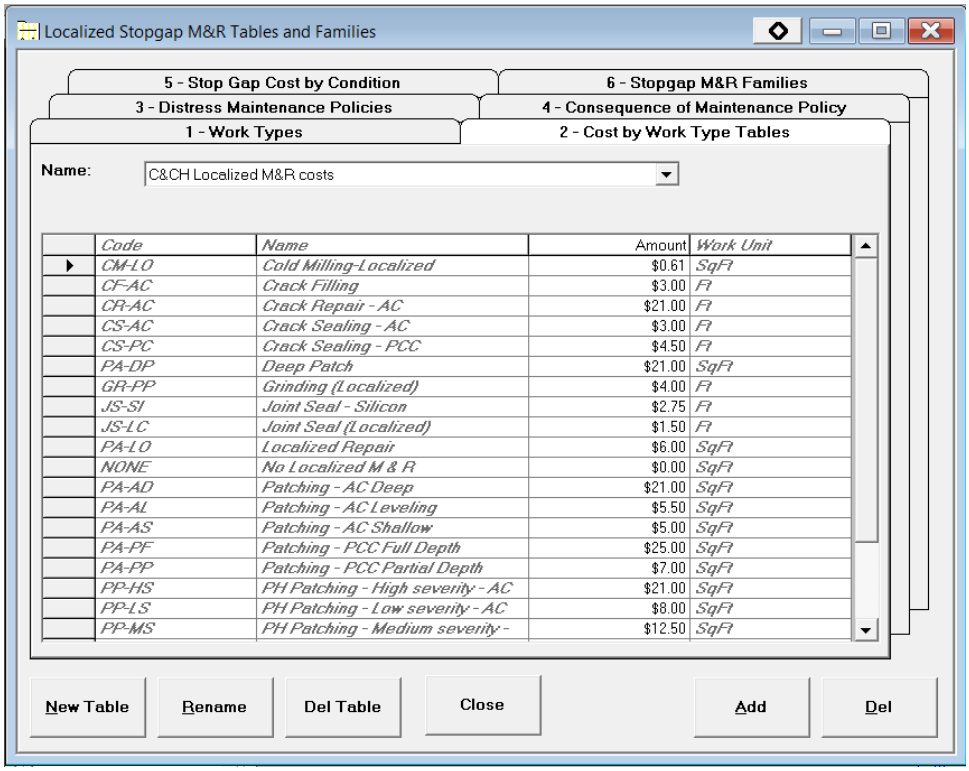

Figure 8-62. Cost by Work Type Table[86]

Wilson and Romine [110] provide detailed procedures for estimating pothole patching costs. Unfortunately, these procedures require very detailed information that has not been collected and analyzed. The information required for the calculations include among other things

[86] The costs in this figure are provided for illustrative purposes only. They may not be representative of local conditions, particularly those for PCC pavements, which are PAVER™.

material purchase costs, number in patching crew, average daily wage per person, equipment costs, daily productivity, and expected patch survival.

The costs in Figure 8-62 are very rough estimates based on extremely simplified assumptions. HDOT needs to develop estimates that are representative of local conditions and patching/sealing practices. The figure illustrates some of the information needed to run PAVER™ (this is also applicable to other software.) In particular, development of the cost estimates requires identifying all the costs involved (materials, labor, equipment, traffic control, police, etc.)

The other costs required by PAVER™ for Stopgap M&R treatments are contained in the "Stopgap Cost by Condition" table illustrated in Figure 8-63. This is important for making future budget needs projections. Typically, the information in this type of table would be obtained by running a "Consequence of Localized Distress Maintenance Plan" with a stopgap policy for which PAVER™ will compute the cost/sq.ft. vs. PCI for the current distresses resulting in a plot similar to that shown in Figure 8-50 (page 503) for preventive maintenance.

Since the values of the costs by work types are not reliable, so are the cost by condition derived from them. Thus, in order to obtain a reasonable table of the cost by condition, the values in the default "Stop Gap Cost by Condition" table in PAVER™ were multiplied by 3 to account for the typically higher labor and material costs in Hawaii compared to the US mainland. Figure 8-63 shows the assumed "Stop Gap Cost by Condition" table. It is important to stress that this table is very tentative. A table more representative of actual local costs needs to be developed by HDOT.

8.4.3.6.3.6 Stop Gap Budget Consequence

In PAVER™, for each treatment, a table needs to be specified with the consequences of the treatment application. Figure 8-64 illustrates the consequences when **Patching – AC Shallow** is applied to different distresses. As can be seen, application of this treatment converts the existing distresses into Patching/Utility Cut Patching of low severity.

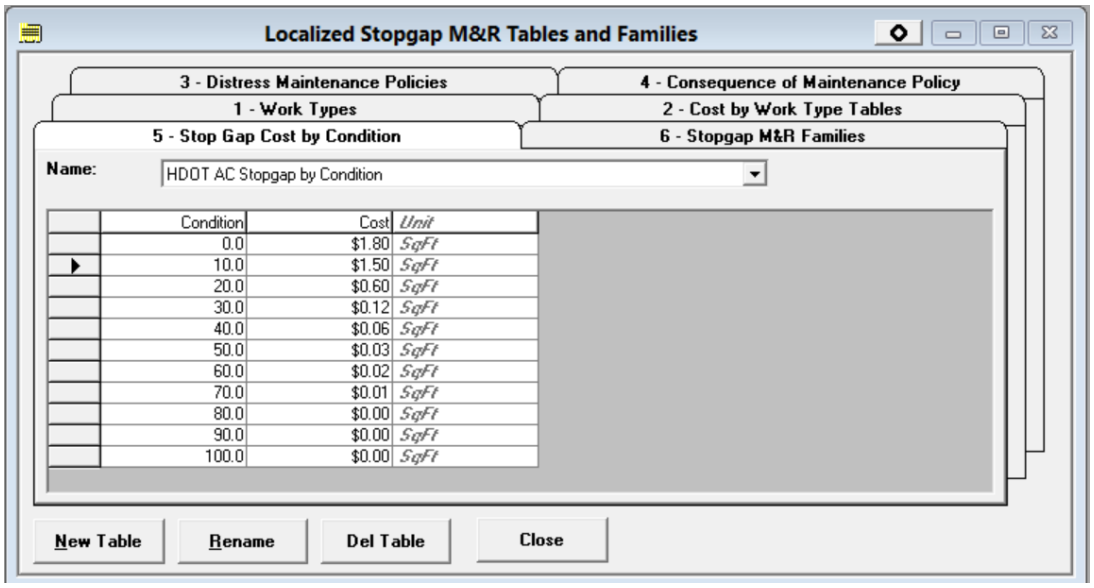

Figure 8-63. Stop Gap Cost by Condition Table.

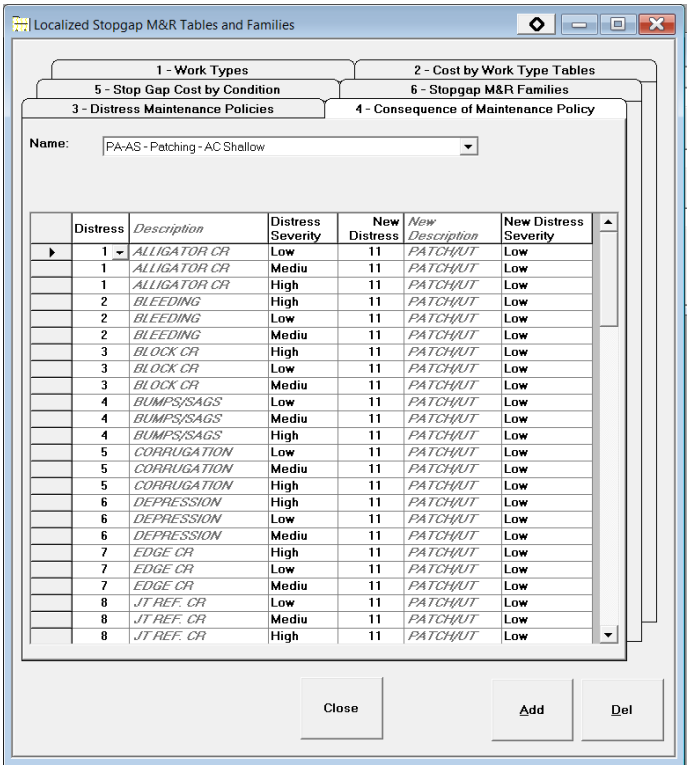

Figure 8-64. Example of Consequence of Maintenance Policy.

The above is considered a logical conversion. No matter how well a patch is constructed, it is never as good as the original pavement. Now, how is this information used by PAVER™?

The program uses this information by first converting distress quantities into work quantities using built-in conversion factors (this, for example, would account for the need to square-off a larger area when patching a high severity pothole) and then each distress is adjusted based on the applied repair method to compute the resulting PCI after the repairs are applied.

As shown in Figure 8-64, low severity potholes are converted to medium severity patches when the work type is **PH Patching – Low severity – AC**. A similar table for **PH Patching – Medium Severity – AC** converts medium severity potholes into medium severity patches. This will result in lower improvements in the PCI and higher future repair costs. In light of the conditions observed in Figure 8-61, this seems a bening assumption. On the other hand, it is assumed that semi-permanent pothole patches (applied to high severity potholes) will result in low severity patches (the corresponding table is not shown here.)

8.4.3.6.3.7 Putting everything together - Stopgap M&R Families

PAVER™ requires additional instructions to put together all of the pieces of information described in the previous sections. This is done on the Stopgap M&R Families tab illustrated in Figure 8-66. In the example of Figure 8-66, the table indicates that a M&R family named **Roadway Stopgap** uses the distress maintenace policy named **C&CH StopGap AC** (the information in Table 8-4 "constitutes this policy) with cost by work types given in a table titled **C&CH Localized** (which contains for example the cost/sq.ft. of the different pothole repair options as well as other treatament costs) and with costs by condition given in a **CCH Safety AC** table (this would be a table similar to the **HDOT AC Stopgap by Condition** shown in Figure 8-63 (page 526)).

Finally, the user needs to define to which Stopgap M&R family each section belongs to. This is done by assigning sections to M&R families as shown in Figure 8-67. As can be seen in that Figure, the stop-gap M&R family selected (that to which sections will be assigned) is **Roadway Stopgap**. When this window is first opened, it will typically show a list of sections on the left pane that have not been assigned to the current family (or to any other family depending on the radio button selection on top of the pane). The user can select a subset of those sections by accessing the PAVER query wizard, which is invoked by selecting the show subset radio button underneath the pane diplaying the sections. Once a set of sections has been selected (filtered) they can be assigned with the button “>>”. Of course, sections can also be assigned/unassigned

one by one as well. In the example of Figure 8-67, all sections were assigned to the Roadway Stopgap family. The user can open the "**Assign Localized Stopgap M&R Families**" dialog box by selecting the **Visual Menu** button in the PAVER^{TM} main toolbar, after which the dialog box shown in Figure 8-68 will be displayed. Then, the user must select the **M&R Familiy Assignment** radio button on the left side of the **Visual Menu** dialog box and the **Assign Localized Stopgap M&R Families** on the right side and finally press the **Continue** button.

Assignment of sections to different rehabilitation families provides great flexibility to accommodate different type of treatments for different road types and different counties.

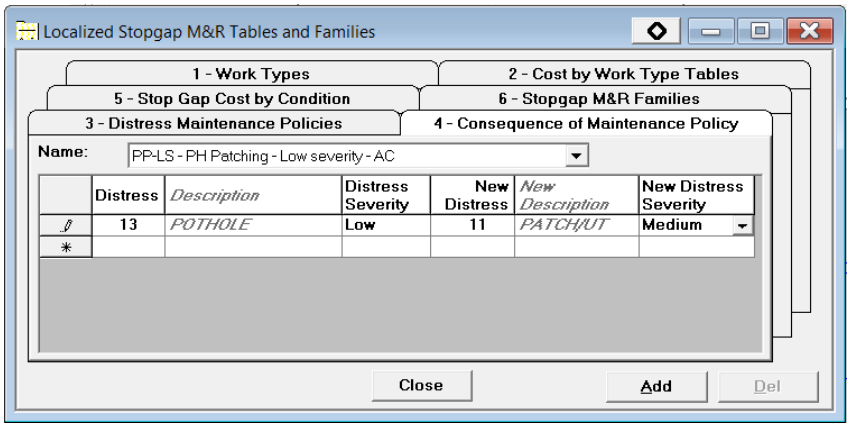

Figure 8-65. Assumed consequence of filling potholes of low severity.

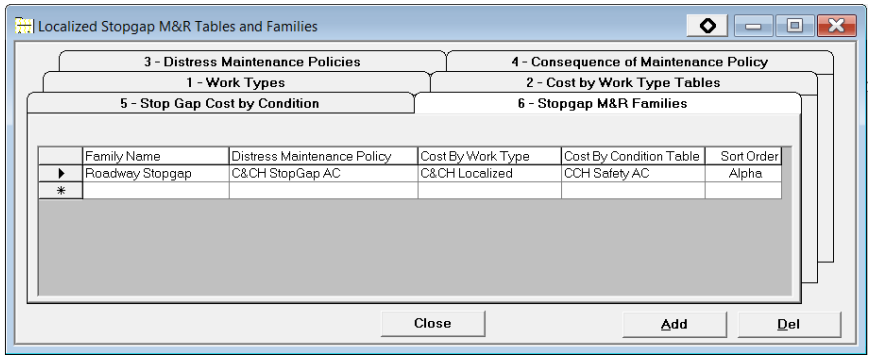

Figure 8-66. Stopgap (Safety) M&R Families.

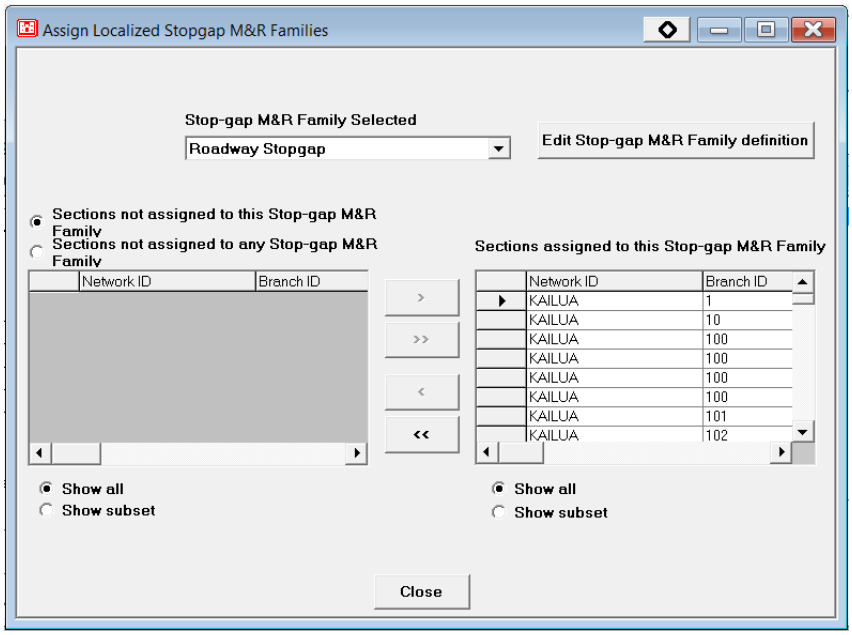

Figure 8-67. Assignment of sections to Stop-gap M&R families.

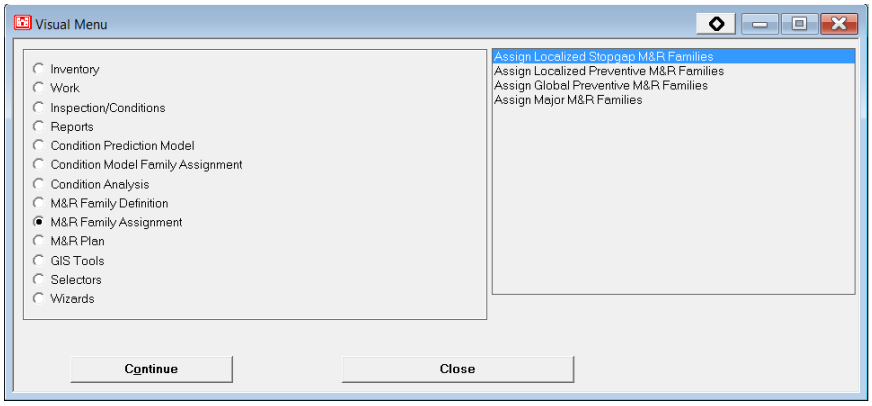

Figure 8-68. Accessing the "Assign Localized Stopgap M&R Families" dialog box.

8.4.3.6.4 Localized Preventive M&R Treatments, Policies, Consequences, and Costs

This section describes the input parameters required to define the Preventive M&R Policies. The structure of the input tables is the same as that explained for Stopgap M&R, thus, only the most significant differences are explained.

The **Work Types** table is the same that is used for Stopgap M&R. This table was presented in Figure 8-55.

8.4.3.6.4.1 Localized Preventive Work types

A main concern with localized preventive maintenance is avoiding the ingress of water through the pavement surface into the pavement structure. Therefore, emphasis should be put into treating cracks. The crack treatments available include:

- Crack filling
- Crack sealing
- Full- and partial-depth crack repair

Crack filling and sealing operations (or crack treatments) can be effective if cracks are moderate in density and show moderate to no deterioration at the edges [113]. Since crack sealing is a preventive maintenance activity that adds no structural capacity, ideal sections for this technique should exhibit minor pavement distresses and have sufficient structural capacity to meet future needs [114]. This is typically the situation of pavements above the Critical PCI for which the localized preventive maintenance policy is applied. Pavements with transverse and non-load associated longitudinal cracks are good candidates for crack sealing.

When cracks are low to moderate in density and have typically progressed to a point of high edge deterioration, ***crack repair strategies***, such as partial-depth patching or spot patching may be warranted. If both the crack density and the edge deterioration level are high, then rehabilitation may be warranted. However, this last situation is unlikely for pavements above the Critical PCI.

The following paragraphs describe the different alternative treatments and the situations in which their use is recommended in more detail.

Crack sealing: Crack sealing is generally described as a *localized* maintenance procedure that involves placement of specialized materials into *working cracks* used to prevent water and incompressibles from entering a crack. Crack sealing involves blowing out the debris in the crack or using a saw or router to create a reservoir which is filled with a sealant. Cracks that are sealed are typically less than 3/4-inch (19 mm) wide. Working cracks are those that have more than 0.1 in (0.25 mm) of annual vertical or horizontal movement. Normally, cracks that are spaced uniformly along the pavement, have limited edge deterioration, and are less than 3/4-inch wide should be sealed.

To effectively seal the cracks, the router or saw must touch both sides of the crack. Cracks that are greater than 3/4-inch wide and are very numerous are not practical to seal, both because the router or saw will not touch both sides of the crack and because of the number of cracks present [92].

Crack Filling: Crack filling is the placement of materials into cracks to reduce the amount of water infiltration into a pavement while also reinforcing the adjacent pavement. It is used in sections that are unsuitable for crack sealing due to excessive crack width, secondary cracking and/or crack edge deterioration/spalling and in *non-working* cracks.

Crack filling should be distinguished from crack sealing. It differs from crack sealing mainly in the preparation given to the crack prior to treatment and the type of sealant used.

The identification of working cracks requires some annual monitoring of crack widths, an activity that is currently not practical for HDOT. Smith and Romine [113] indicate that working cracks are usually transverse in orientation but that some longitudinal and diagonal cracks may meet the 0.1-in movement criterion. For proper sealing, materials placed on working cracks must adhere to the crack sidewalls and flex as the crack opens and closes. This is the reason why rubber-modified materials designed for low-stress elongation, especially at low temperatures, are preferred for treating working cracks.

The *SHRP Materials and Procedures for Sealing and Filling Cracks in Asphalt Surfaced Pavements – Manual of Practice* [113] provides basic definitions of the density of cracking and level of edge deterioration (although density thresholds are not provided). As pointed out in the Michigan DOT Manual "*Sealing and Filling of Cracks for Bituminous Concrete Pavements – Selection and Installation Procedures*" [93], the first step in the process to select crack treatments is to characterize the density of cracking and the level of edge deterioration. The Michigan DOT manual [93] also provides guidance on density thresholds. These are shown in Table 8-5. The threshold between moderate and high densities is based on the approximate point where transverse and longitudinal cracking would be classified as block cracking. The threshold between low and moderate cracking is based on the observation that 2 to 3 transverse cracks in a 100 m (328 ft) section would justify a sealing operation.

Table 8-5. Thresholds to determine crack density levels

Linear Crack Length per 100 m (328 ft) Pavement Section	**Density**
< 10 m (32.8 ft)	Low
10 m (32.8 ft) to 135 m (443 ft)	Moderate
> 135 m (443 ft)	High

Notice that the emphasis put in determining the density of cracking is related to its potential origin. That is, if cracking is related to environmental/construction factors (e.g., block cracking and longitudinal and transverse cracking), application of a crack treatment is appropriate. HDOT collects the distress information in a format that indicates what caused it. Thus, the policy for crack sealing/filling can be defined to a certain extent by the type of cracks.

The other criterion used in those manuals to define the crack treatment is the degree of edge deterioration. Typically, cracks with edges deteriorated in more than 50% of their length should be repaired instead of treated. Since edge deterioration is not a variable on the pavement condition survey performed for pavement management, this criterion cannot be used for budget plan determination. Nevertheless, this can still be used by maintenance crews or the engineer to decide the type of crack treatment/repair to apply during maintenance operations.

As discussed before, the Michigan DOT [93] provides different alternatives for working and non-working cracks. This differentiation between types of cracks is not considered practical for the HDOT at this time. Therefore, the following guideline is recommended for determining budget requirements: for Block, Edge, Joint Reflection, and Longitudinal and Transverse cracks of low and moderate severity *sealing or filling* is recommended and *crack repair* is recommended for the high severity level of these types of cracks.

It is recommended to *seal* cracks less than ¾ in and *fill* the cracks wider than ¾ in. Weather sealing or filling will be needed cannot be determined in the budget plan analysis. This would have to be an operational decision. Notice that based on the width of the cracks for which the two treatments are recommended more sealant will typically be needed for filling cracks than for sealing them. On the other hand, sealing cracks demands more preparation of the crack. In

the following recommendations, the cost estimate for crack sealing is also used for crack filling. However, these should be revised if later it is determined that crack filling costs differs substantially from those of crack sealing.

In general, sealing/filling treatments should be applied when pavement cracks first develop, as this timely treatment will help prevent further pavement deterioration. Therefore, consistent pavement management practice should result in a relatively minor need for *filling* wide cracks. *Crack filling* is not as efficient as *crack sealing*; nevertheless it still reduces water infiltration into the pavement structure and the intrusion of incompressibles into the crack. Thus, its use may still be warranted when crack sealing is not effective as it happens for wide cracks with moderate edge deterioration.

Full- and partial-depth crack repair: This is a localized treatment method to repair cracks that are too deteriorated to benefit from sealing or filling. It involves cutting a trench centered over an existing crack, placing hot-mix asphalt (HMA) into the reservoir in one or more lifts, and compacting it to achieve appropriate density. This treatment is recommended for high severity cracks. The need for this type of treatment should be rare for pavement with PCI above critical (for which the localized preventive treatments discussed in this section are recommended).

Other repairs: For distresses other than cracks or for small areas of fatigue cracking either shallow or deep patching are recommended. Pavements with large areas of fatigue cracking will either not have a PCI above the Critical PCI or if they do, they will typically be recommended for Major M&R if funds are available.

8.4.3.6.4.2 Localized Preventive M&R Policy

Figure 8-69 provides a suggested ***Localized Preventive M&R*** policy. At this point, only the policy for asphalt concrete pavements has been considered in detail.

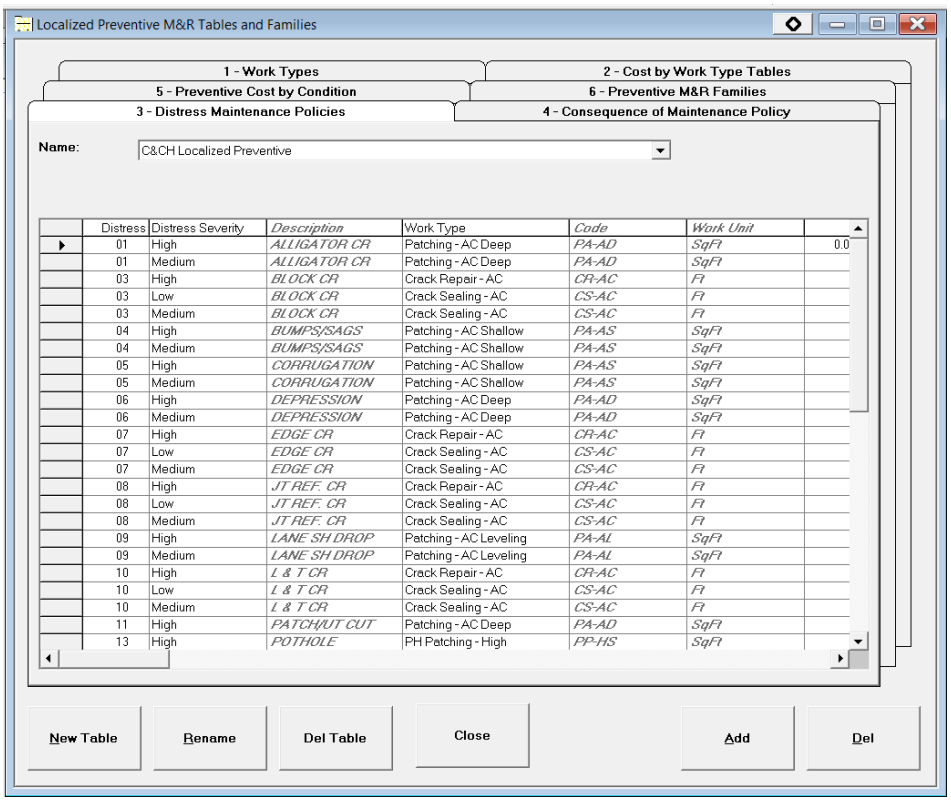

Figure 8-69. Suggested Localized Preventive Distress Maintenance Policy.

The policy calls for sealing of any low or medium severity linear cracking distresses (block, edge, joint reflection, or longitudinal and transverse cracking) and for repairing those with high severity. For crack repair, a patch with a depth of 6 in and 1 ft width is assumed.

For the other distresses in the policy, either deep or shallow patching is recommended. Specifically, **Patching – AC Shallow** (2 in mill and fill) is recommended for bumps/sags, corrugation, shoving, and slippage cracking. **Patching – AC Deep** (6 in mill and fill) is recommended for alligator cracking of medium and high severity, high severity patches, and rutting (rutting is not shown in the figure). In addition, pothole patching is treated in the same way as in the Stopgap policy (not many potholes are expected to be observed in sections with PCI above critical.)

8.4.3.6.4.3 Localized Preventive Maintenance Costs

As for safety maintenance, for illustrative purposes, this section provides rough estimates of patching costs for use in M&R analyses scenarios with PAVER™. As discussed in previous

sections, two different types of cost information are required by PAVER™ for Localized Preventive M&R treatments: "Cost by Work Types" and "Stopgap Cost by Condition". The cost by work types table is the same one that was presented for Stopgap treatments in Figure 8-62.

The other cost information required by PAVER™ for Localized Preventive M&R treatments is contained in the "Preventive Cost by Condition" tab illustrated in Figure 8-70. The information in the table named **C&CH Localized Preventive AC** was obtained by running a "Consequence of Localized Distress Maintenance Plan" for which PAVER™ computes the cost/sq.ft. vs. PCI for the current distresses. The raw results of the analysis were presented in Figure 8-49 (page 502) and the averages cost vs. PCI was presented in Figure 8-50 (page 503). The values in Figure 8-70 provide an approximation to the points in Figure 8-50.

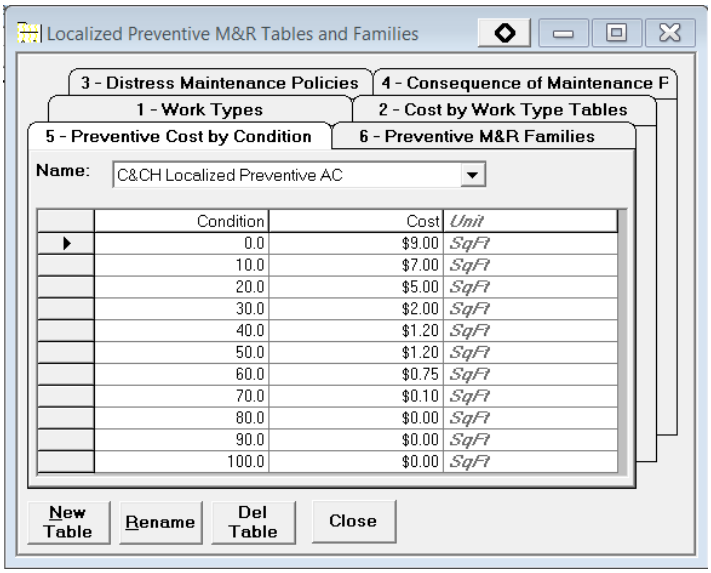

Figure 8-70. Localized Preventive Cost by Condition Table.

8.4.3.6.4.4 Localized Preventive Budget Consequence

As in the case of stopgap treatments, for each localized preventive treatment, a table needs to be specified with the consequences of the treatment application (the list of treatments for localized repair, either stopgap or localized preventive is unique, so these tables need to be specified only once.) Figure 8-71 illustrates the consequences when **Crack Sealing – AC** is applied to different types of cracks. As can be seen, application of this treatment converts the existing cracks to cracks of the same type but of lower severity. Recall that the only purpose of

specifying these consequences is to be able to compute an estimate of the pavement condition immediately after the treatment application.

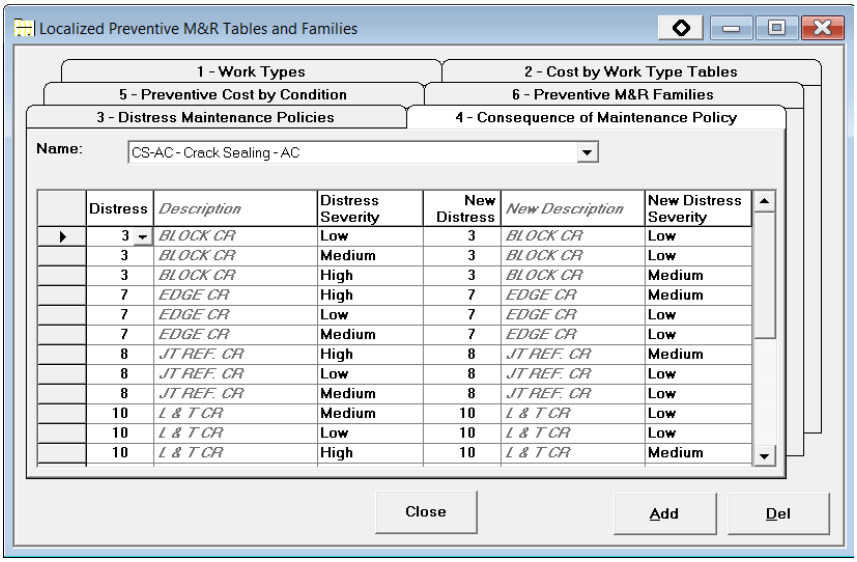

Figure 8-71. Another example of Consequence of Maintenance Policy

The program uses this information by first converting distress quantities into work quantities using built-in conversion factors and then each distress is adjusted based on the corresponding consequence table to compute the resulting PCI.

8.4.3.6.4.5 Putting everything together – Localized Preventive M&R Families

Again, PAVER™ requires additional instructions to put together all of the pieces of information described in the previous sections for localized preventive M&R. This is done on the **Preventive M&R Families** tab illustrated in Figure 8-72. As can be seen, the table indicates that a M&R family named **Roadway Prev.** uses the distress maintenace policy named **C&CH Localized Preventive** (the information in Figure 8-69, page 534, constitutes this policy) with cost by work types given in a table titled **C&CH Localized M&R Costs** and with costs by condition given in the **C&CH Localized** table shown in Figure 8-70.

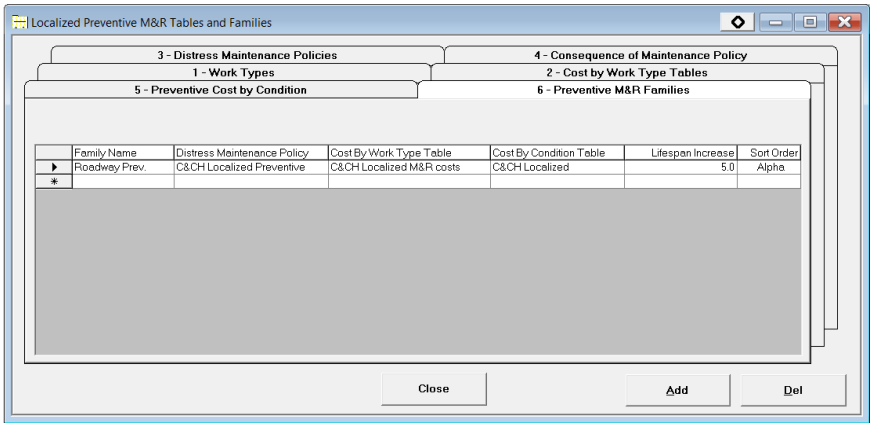

Figure 8-72. Localized Preventive M&R Families.

Finally, the user needs to define to which Localized Preventive M&R family each section belongs to. The procedure is entirely analagous as what was explained for the Stopgap M&R policy. The assignment of sections to the **Roadway Prev.** family is shown in Figure 8-73.

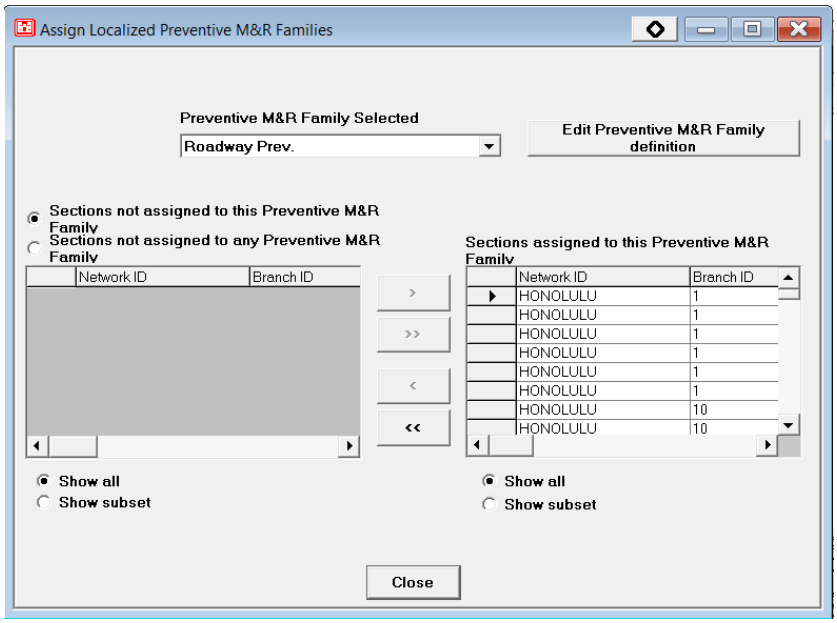

Figure 8-73. Assignment of sections to Preventive M&R families.

8.4.3.6.5 Global Preventive M&R Treatments, Policies, Consequences, and Costs

This section describes the input parameters required to define the Global Preventive M&R Policies. The structure of the input tables in this case is slightly different than the structure

in the previous two cases. The information required is spread in four tabs instead of the six needed for the other M&R treatment families. Figure 8-74 shows the four different tabs: 1 – Work Types, 2 – Consequent Surface, 3 – Costs by Work Types Table, and 4 – Global M&R Families. The Figure also displays the **Work Types** table.

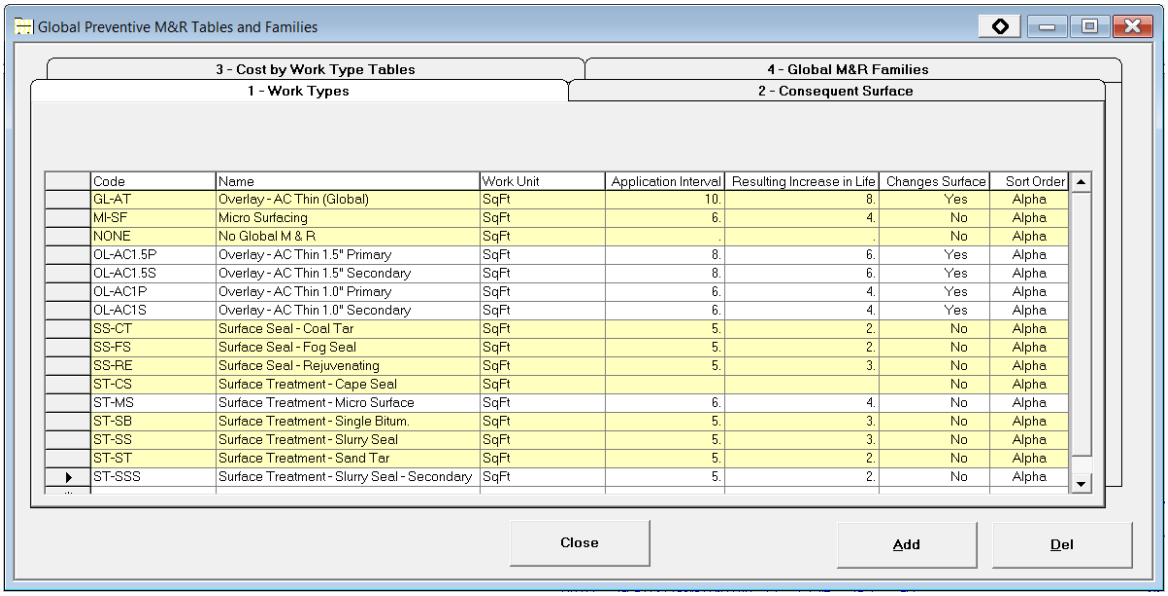

Code	Name	Work Unit	Application Interval	Resulting Increase in Life	Changes Surface	Sort Order
GL-AT	Overlay - AC Thin (Global)	SqFt	10.	8.	Yes	Alpha
MI-SF	Micro Surfacing	SqFt	6.	4.	No	Alpha
NONE	No Global M & R	SqFt	.	.	No	Alpha
OL-AC1.5P	Overlay - AC Thin 1.5" Primary	SqFt	8.	6.	Yes	Alpha
OL-AC1.5S	Overlay - AC Thin 1.5" Secondary	SqFt	8.	6.	Yes	Alpha
OL-AC1P	Overlay - AC Thin 1.0" Primary	SqFt	6.	4.	Yes	Alpha
OL-AC1S	Overlay - AC Thin 1.0" Secondary	SqFt	6.	4.	Yes	Alpha
SS-CT	Surface Seal - Coal Tar	SqFt	5.	2.	No	Alpha
SS-FS	Surface Seal - Fog Seal	SqFt	5.	2.	No	Alpha
SS-RE	Surface Seal - Rejuvenating	SqFt	5.	3.	No	Alpha
ST-CS	Surface Treatment - Cape Seal	SqFt			No	Alpha
ST-MS	Surface Treatment - Micro Surface	SqFt	6.	4.	No	Alpha
ST-SB	Surface Treatment - Single Bitum.	SqFt	5.	3.	No	Alpha
ST-SS	Surface Treatment - Slurry Seal	SqFt	5.	3.	No	Alpha
ST-ST	Surface Treatment - Sand Tar	SqFt	5.	2.	No	Alpha
ST-SSS	Surface Treatment - Slurry Seal - Secondary	SqFt	5.	2.	No	Alpha

Figure 8-74. Global Preventive M&R Tables and Families – Work Types table.

The **Work Types** table differs from that for localized repairs in that in addition to the code, the name, and the work unit of the work type the application interval and resulting increased in life of the treatments need to be specified. The **Application Interval** is the interval at which a work type would be reapplied. The **Resulting Increase in Life**, or change in age, of the pavement is defined as the time (in years) it would take for the condition of the pavement to return to where it was prior to application of the global treatment. If a treatment changes the type of surface then the **Changes Surface** field must be set to Yes, as can be seen for the overlays in the figure. This is simply because an *asphalt concrete* pavement becomes an *overlay over asphalt concrete* pavement after the treatment, which is considered a different surface type (the deterioration curves are usually different.)

8.4.3.6.5.1 Global Preventive Work types

There are a large number of alternatives that fall under the category of surface treatments or seals. These are generally less than one inch or one inch and a half thick. The objective of these seals is to waterproof the pavement, restore skid resistance, and restore oxidized surfaces. In some situations, some of these seals can be used to fill minor ruts. Surface treatments do not add any structural strength [115].

The treatments briefly described in this section include fog seal, seal coat, double chip seal, slurry seal, microsurfacing, and thin hot-mix asphalt overlays. Not all these treatments are currently used on state roads. However, they are included because of their potential use in the future. Sand sealing is not included because quantities are difficult to control, resulting in bleeding or excess sand on the pavement surface [92]. Only some of the more important characteristics of the treatments and a few other details are presented here. For more details on construction and materials specifications, the reader is referred to Johnson [92] (from which most of the descriptions below were extracted) or other DOT/industry manuals on the subject. The HAPI (Hawaii Asphalt Pavement Industry) Asphalt Pavement Guide [116] provides an illustrated introduction to some of the treatments available.

1. Fog Seal

A fog seal is a light application of diluted slow-setting asphalt emulsion without a cover aggregate used to seal and enrich the surface of aged (oxidized) asphalt pavement, seal minor cracks, prevent raveling, and provide shoulder delineation. Typically, an asphalt emulsion diluted mix with 50 percent water (such as CSS-1, CSS-1H) or proprietary rejuvenators are used. A sand cover may be used to improve the surface friction.

For Hawaiian conditions, fog seals are more suitable for low-volume roads (residential streets) or parking lots, which can be closed to traffic for the time it takes for the slow-setting asphalt emulsion to break and set and where the potential for reduced pavement friction is not a concern. Under favorable conditions, two to three hours may be sufficient but normally it takes 4 to 6 hours for the slow-setting asphalt emulsion to break and set. Traffic should be kept off the emulsion until it has cured significantly. Sand should be used to blot up areas of excess application.

Fog seals are effective when light to moderate raveling and/or oxidation and weathering develop. They should be used only where the existing pavement is sufficiently porous to absorb a substantial amount of the emulsion and they should be avoided in areas with a significant number of cracks larger than hairline. All necessary repairs or reconditioning work should be completed before application of the treatment. Furthermore, the fog seal should only be applied when the pavement is dry and clean. Fog seals may be able to temporarily postpone the need for a chip seal or non-structural overlay.

The performance life of this type of treatment is fairly short, ranging from one to three years.

2. Seal Coat/Chip Seal

A seal coat, also known as chip seal or bituminous surface treatment (BST), is a thin protective wearing surface formed by an application of an asphalt (typically a rapid-setting asphalt emulsion) followed immediately with an aggregate cover.

The primary reason to seal coat an asphalt pavement is to protect the pavement from the deteriorating effects of sun and water. Exposure to sun, wind, and water, results in oxidation and hardening of the asphalt. This causes the pavement to become brittle and more prone to cracking. A seal coat provides a waterproof membrane that not only slows down the oxidation process but also helps to prevent water from entering the base material (it seals low-severity cracks and fills raveled surfaces.) A secondary benefit is an increase in the surface friction, which happens because the aggregate adds additional texture to the pavement. In addition, seal coats reduced glare in wet weather and increase the pavement night reflectivity. Pavements that are dry and raveled but in otherwise good condition are good candidates for seal coating.

Traffic should not be allowed on the seal coated surface until after all rolling has been completed and the emulsion has set so that there is no pick up on vehicle tires. Although seal coats provide effective sealing and friction, the possibility of loose chips and broken windshields along with excessive noise has prompted some states to restrict use of chip seals to low-volume roads. Nevertheless, new technique (e.g., use of pre-coated aggregates) have reduced these effects.

Expected life of a seal coat is approximately three to six years.

3. Double Chip Seal

This treatment involves the application of two single seal coats. The second coat is placed immediately after and directly over the first. Sixty percent of the total asphalt binder required is placed in the first pass, with larger aggregate. The remaining forty percent is placed in the second pass, with aggregates half as large as those placed first.

It is strongly recommended that a polymer-modified emulsion be used on double chip seals to increase early retention of aggregate.

Similarly to seal coats, the purposes of double chips seals are to waterproof the surface, seal small- to medium-sized cracks, and improve surface friction. This treatment reinforces the benefits of a single chip seal. As the top layer of aggregate wears off, the bottom layer remains. It offers better aggregate retention overall, as the bottom layer is more deeply embedded. A double chip seal results in a quieter, smoother surface than a single chip seal, and is a good alternative for pavements in fair condition without structural distresses.

Similarly to the other surface treatments described in this document, this treatment is appropriate for stable pavements on a sound base with a good cross section. Visible surface distresses may include moderate raveling, surface wear, longitudinal cracks, and transverse thermal cracks with some secondary cracking and some deterioration along crack faces. A minor amount of patching in good condition is acceptable. The surface may show signs of slight to moderate block cracking, moderate to severe oxidation, and/or slight to moderate flushing or polishing.

Heavy commercial traffic and frequent stopping and turning movements reduce the life of this application and cause local deterioration. Thus, they are also mostly applicable to low volume roads.

4. Slurry Seal

A slurry seal is a mixture of well-graded fine aggregate, asphalt emulsion, water, and mineral filler with a creamy fluid-like appearance during application. The mineral filler most often used is Portland cement. Aggregate, water, filler, and emulsion are proportioned and mixed together in a truck-mounted mixer and applied immediately to the pavement surface with a spreader box.

They are used to seal the existing asphalt pavement surface, retard surface raveling, seal small cracks, and improve surface friction. Slurry seals are similar to chip seals in that they use a thermal break process, requiring heat from the sun and pavement. *This process takes anywhere from two to eight hours depending on the heat and humidity.*

In addition to the required curing time, another challenge for their use in high-volume roads is that friction initially may be reduced until traffic wears some of the asphalt from the surface.

The slurry seal mixes are used as either a preparatory treatment (e.g., pavement leveling and pothole patching) for other maintenance treatments or as a wearing courses. As wearing courses, they are appropriate to maintain pavements when they first develop a moderate density of surface cracking with low to moderate edge deterioration and secondary cracking, or to treat light to moderate raveling and/or oxidation.

Slurry seals are effective where the primary problem is excessive oxidation and hardening of the existing surface. As other surface treatments, slurry seals will not perform well if the underlying pavement contains extensive cracks.

Aggregates for slurry mixes may consist of most hard crushed aggregates such as basalt. They conform to one of three gradations: Type 1, Type 2, and Type 3. The maximum size for slurry aggregates is 2.36 mm (#8 sieve) for Type 1, and 9.5 mm (3/8-inch sieve) for Types 2 and 3. Type 3 has a coarser gradation than Type 2. All slurry gradations have between 5 and 15 percent passing the 75-micron sieve (#200). The slurry is applied basically one aggregate layer thick. A tack coat is not necessary unless the pavement to be sealed is extremely dry and raveled or the slurry is being placed on a concrete surface.

The slurry seals in Hawaii typically contain a latex modified cationic quick set (LMCQS-1h) or cationic quick set (CQS-1h) emulsion [116].

Expected life of a slurry seal is three to five years.

5. Microsurfacing

Microsurfacing is a mix of polymer-modified emulsion, well-graded crushed mineral aggregate, mineral filler (normally Portland cement), water, and chemical additives that control

the break time. Except for the polymer additives, it uses the same basic ingredients as slurry seals and consequently it is sometimes incorrectly referred to as a polymer-modified slurry seal. The major difference however is that *the curing process for microsurfacing is chemically controlled*, whereas slurry seals and chip seals use the thermal process. The aggregate, mineral filler, emulsion, and water are mixed in a truck-mounted traveling plant, which is deposited into a spreader box. No compaction is needed.

Many states have used this treatment for both surfacing and rut filling on roads *with moderate- to heavy-volume traffic*. As a preventive maintenance or surface treatment for an existing AC pavement, microsurfacing provides a skid-resistant surface and reduces the amount of water that enters the pavement layers through the pavement surface. Microsurfacing restores the transverse cross-section profile and may also be used to fill ruts.

As with slurry seals, microsurfacing is effective where the primary problem is excessive oxidation and hardening of the existing surface. It will not perform well if the underlying pavement contains high density of cracks or a moderate density of cracking with high edge deterioration and secondary cracking. Prior to the application of microsurfacing, all necessary repairs or reconditioning work must have been previously performed and the surface must be clean and dry.

Microsurfacing cures and develops strength faster than conventional slurry seals and *can be opened to rolling traffic in about an hour*. *Service life is about seven or more years for high traffic* and considerably longer for low to moderate traffic. Comparative costs reported in the literature indicate that the cost ranges from about the same order as slurry seals [117] to about 17% higher than slurry seals [92] but the differences are sometimes as high as 39% [90].

6. Thin Hot-Mix Overlays

Thin hot-mix asphalt (HMA) overlays are constructed with a thin layer of HMA typically ranging from 3/4 to 1-1/2 inch. Three types of HMAs (dense-graded, open-graded friction courses, and gap-graded) have been used in the United States to improve the functional (non-structural) condition of the pavement. The mixes are often modified with polymers to meet high performance expectations, though to date in Hawaii, the supply modified mixes has been limited.

Thin hot-mix asphalt overlays are used on all types of roadways for functional improvements. Functional improvements are those improvements that enhance the smoothness, friction, and/or profile of the roadway while adding little or no additional load-carrying capacity. They are particularly suitable for high-volume roads in urban areas where longer life and relatively low-noise surfaces are desired. Other benefits include enhanced appearance and reduction of road-tire noise.

As with other preventive maintenance treatments, thin HMA overlays add little structure to the existing pavement and therefore they should not be used on pavements showing structural distress or deterioration, unless the distresses are corrected first. Visible surface distresses to be corrected by thin HMA overlays may include moderate to extreme raveling and longitudinal and transverse cracks with some secondary cracking. A moderate amount of patching in good condition is acceptable. Milling prior to overlay is recommended when severe surface distresses are present. Note, however, that the milled surface should be in generally good condition.

The requirement of having a pavement in relatively good condition cannot be overemphasized. Application of thin hot-mix overlays to pavements in conditions such as the one shown in Figure 8-75 would perform poorly. The cracks and localized pavement failures will quickly reflect through the new surface.

Milling or a leveling course should precede thin HMA overlays where pavements need cross-section improvements. Any minor cracks should be sealed several months in advance prior to application to allow for curing of the sealing material. Excessive amounts of uncured crack sealant should be avoided as they can create bumps and checking on the new asphalt mat due to sealant expansion (see Figure 8-76). A tack coat must be applied when using thin HMA overlays to promote bonding with the existing pavement.

Figure 8-75. Unsuitable conditions for thin hot-mix overlays.

Figure 8-76. Potential problems with sealed cracks

Due to their low mass, thin HMA overlays lose heat to the atmosphere very quickly. Thus, achieving density is only possible if they are compacted very quickly while they are still hot.

The principal problems with thin HMA overlays are similar to those of other thin overlay techniques including: delamination, reflective cracking, poor friction, low durability, excessive permeability, and maintenance problems.

The Hawaii Pavement Guide (HAPI 2013), citing NAPA 1995, lists several construction concerns:

- "Thin lifts require less HMA per foot of road length than thick lifts. This can result in high paver speeds (in excess of 70 ft/min) making it difficult for rollers to keep up.

- Thin lifts will cool quickly. This can result in little time available for compaction before the thin overlay reaches cessation temperature (sometimes as little as 3 to 5 minutes).
- Thin lift construction produces greater screed wear. If the lift depth is less than about twice the maximum aggregate size, the HMA may tear under the paver screed. Very thin lifts (less than 1 inch) can be damaged by the screed dragging large particles.
- Thin lifts are more sensitive to vibratory rolling. Incorrectly chosen amplitude, frequency or roller speed can result in aggregate breakage and damage of the bond between the overlay and the existing pavement.
- Density control is difficult. Thin lifts provide fewer options for aggregate particles to rearrange under compaction. Thus, mat densities will tend to be less uniform than those associated with a thicker lift. This should be recognized if pay is in any way tied to mat density."

The service life of thin HMA overlays is expected to average five to eight years depending on existing pavement condition, overlay thickness, and type of binder. Some states report as low as two to four years; others report as many as ten years.

The cost of thin HMA overlays depends largely on the layer thickness and miscellaneous expenses such as traffic control and pavement markings.[87]

8.4.3.6.5.2 Consequent Surface

As explained at the beginning of section 8.4.3.6.5, each global preventive treatment may change the surface of the pavement. For those treatments who do, the program needs to know how the surface is transformed. Figure 8-77 shows how this is specified in the **Consequent Surface** tab, which shows a table with a different row for each of the global preventive M&R treatments (work types) for which the **Changes Surface** field in the **Work Types** table is Yes (see Figure 8-75, page 545). The table also contains a column for each surface type in the PAVER^{TM} database. For those surface types that get changed by the application of a work type, the user needs to specify the new surface type. Figure 8-77 shows that each of the asphalt concrete overlays transform a conventional asphalt concrete pavement surface, identified with

[87] Note that the costs for milling, traffic control, pavement markings, etc. do not change with the thickness, thus a 15% increase in the cost of the material can translate into about a 10% increase in the overall cost. In other words, in general, the cost/unit area of a 1.5" overlay will typically be less than 1.5 times the cost of a 1" overlay.

the symbol AC, into an overlay over asphalt surface, identified with the symbol AAC. Notice that the program changes the cell background to yellow whenever a work type would produce a change of the pavement surface.

As another example, the overlays in Figure 8-77 would change the surface type of a Portland Cement Concrete (PCC) pavement into an asphalt overlay over PCC. Thus, under a column labeled PCC, the user would need to select APC, which is the symbol for asphalt over PCC to indicate the change of surface.

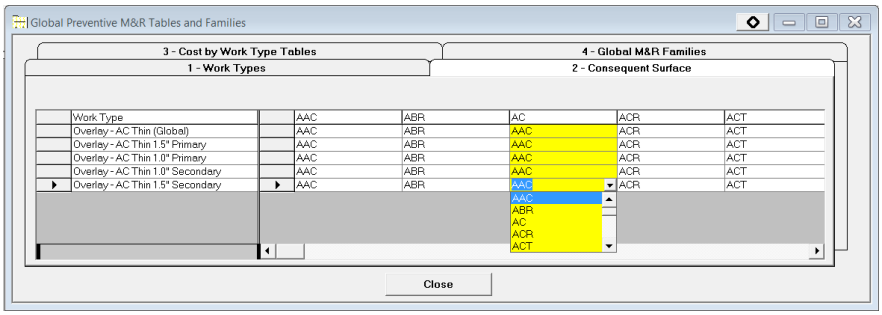

Figure 8-77. Specifying Consequent Surface types.

8.4.3.6.5.3 Global Preventive Costs by Work Types

In the **Costs by Work Type Tables** the user can create a customized table with the cost for each treatment. This is illustrated in **Figure 8-78** in which a table named **C&CH Default Global Preventive** was created. Once again, the cost are provided for illustrative purposes and may not be representative of local conditions.

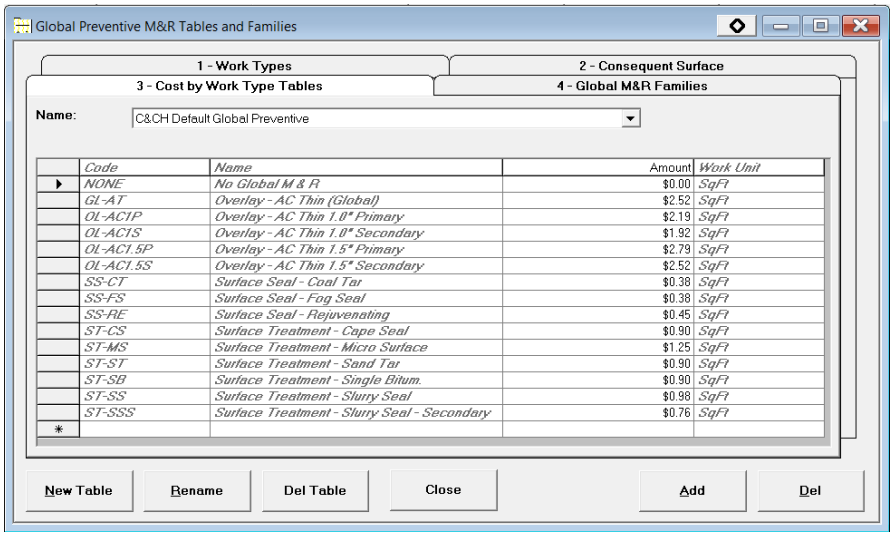

Figure 8-78. Costs by Work Type.

8.4.3.6.5.4 Assignment of Global Preventive Surface Treatments

As mentioned in section 8.4.3.6.2.3 (page 508), PAVER™ considers the application of different types of Global Preventive M&R treatments. The assignment of treatments is based on existing distress types. PAVER™ allows the consideration of up three different types of surface treatments. The methodology is illustrated with the help of Figure 8-79 for an example policy assignment. As shown in the figure, a Type 3 treatment (e.g., a 1" thin overlay on secondary roads) is assigned to pavements with skid-causing distresses such as polished aggregate. Type 2 (a 1.5" thin overlay on secondary roads) is assigned to pavements with climate-related distresses such as weathering and raveling. Finally, Type 1 (fog seal) is assigned to pavements with little or no distress. Notice that a chip seal could be as easily assigned as a Type 1 treatment. The selection of which treatments to apply is a matter of agency policy.

Different policies can be applied to different sets of pavements. For example, Figure 8-80 shows that in addition to the Default Global Policy, four additional policies were created for four different sets of pavements defined by whether the PCI is above or below 70 (termed high PCI and low PCI, respectively in the family names) and by whether the road is a primary or secondary road. The policy shown in Figure 8-79 corresponds to the last row of the table in Figure 8-80 for the family named **HNL Global Low PCI - Secondary**. Notice that the two policies for secondary roads specify a fog seal for Work Type for Minimal Distress (Type 1)

whereas the two policies for primary roads specify **No Global M&R** for Work Type for Minimal Distress (Type 1). As mentioned in the section describing fog seals, these tend to reduce the friction and thus may be a concern on primary roads. A probably better option for a type 1 treatment on secondary roads is a chip seal, which improves friction and seals the surface.

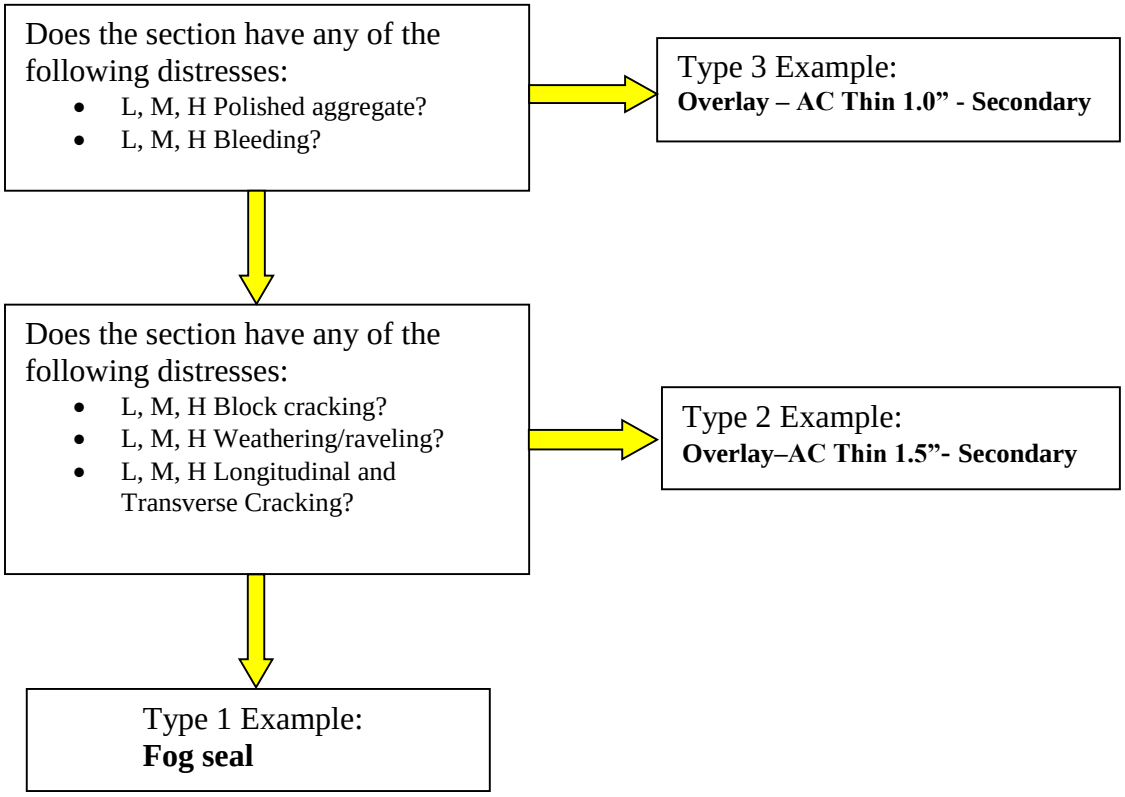

Figure 8-79. Assignment methodology for up to three different treatments.

This type of assignment provides a mechanism to differentiate policies in several ways. For example, the two policies for secondary roads differ in the type of treatment assigned for Work Type for Climate-related Distress (Type 2). For pavements with PCI above 70 (high PCI) a slurry seal would be assigned whereas for pavements with PCI below 70 (low PCI), a 1.5" overlay is assigned. The rationale for this type of assignment is that pavements with PCI between

the critical PCI[88] and 70, though still in satisfactory condition, are more likely to start suffering from some structural deterioration. Thus, a 1.5" overlay would be more effective at delaying the progression of those distresses than a slurry seal. On the other hand, a slurry seal is a perfect candidate to restore the surface for pavements with a PCI above 70.

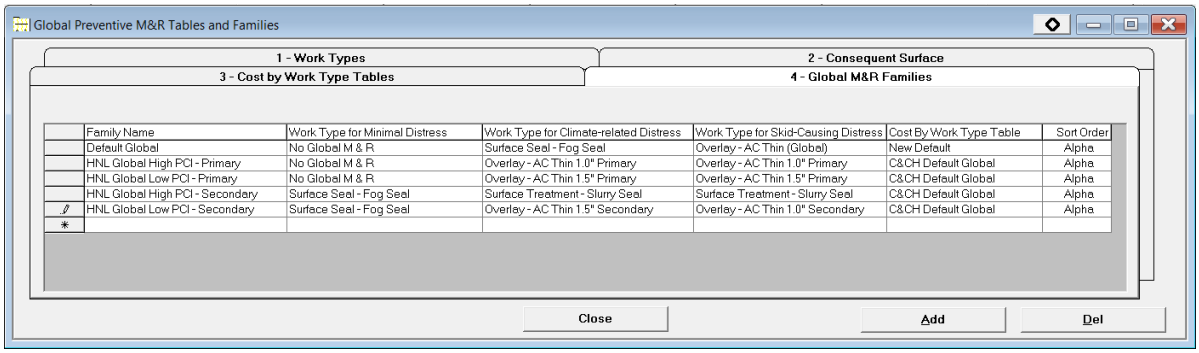

Figure 8-80. Global M&R Families.

Finally, the user needs to define to which Global Preventive M&R family each section belongs to. This is done by assigning sections to M&R families as shown in Figure 8-81. As can be seen in that figure, in this example, the Global Preventive M&R family selected (that to which sections will be assigned) is **HNL Global Low PCI - Secondary**. When this window is first opened, it will typically show a list of sections on the left pane that have not been assigned to the current family (or to any other family depending on the radio button selection on top of the pane). This is exactly the situation shown in the figure. The user can select a subset of those sections by accessing the PAVER query wizard, which is invoked by selecting the show subset radio button underneath the pane diplaying the sections.

[88] Recall that Global Preventive M&R treatments may be assigned only to sections with PCI above the critical PCI.

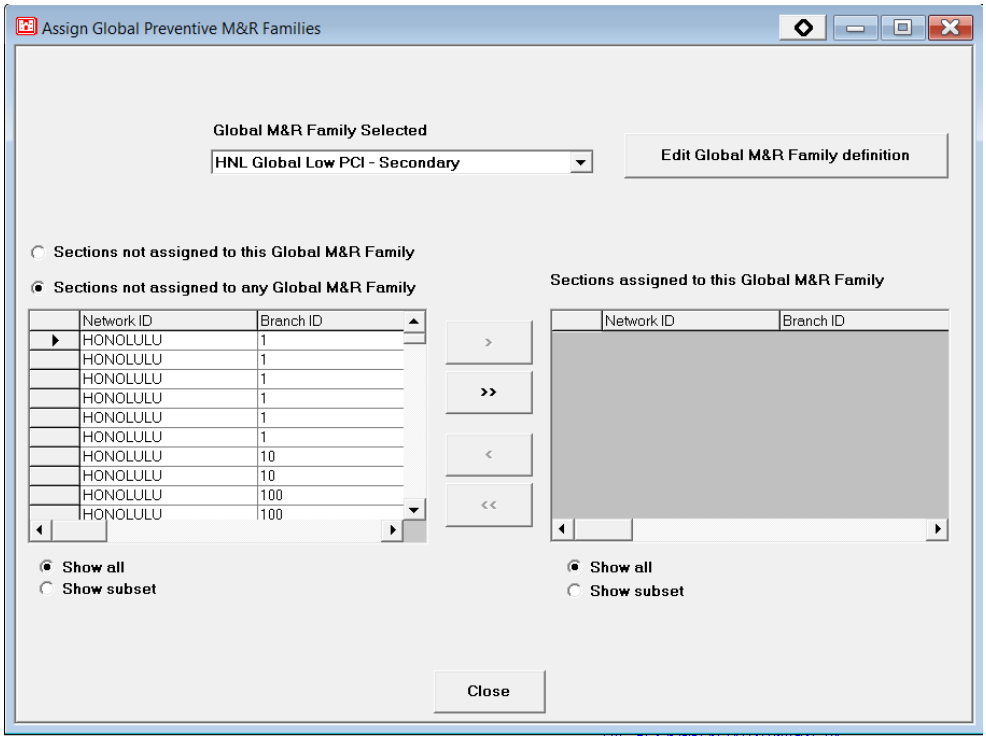

Figure 8-81. Assignment of Global Preventive M&R Families.

Figure 8-82 shows the query wizard with part of the query that will be created to select the secondary pavements with PCI below 70. As shown in this figure, the user has clicked on the **Section** leaf of the tree on the right side pane and then under the **Select Rows** tab has chosen the field **Secion Rank** and set it equal to **S** for secondary roads (the options are only S and P in the current C&CH database). Then, by clicking on the **Latest Conditions** leaf of the tree on the left pane, the user can select first the PCI under field, then set the comparison to "<" and finaly the value to compare to equal to 70 (these actions are not illustrated in the figure). This completes the query that will select secondary pavements with PCI below 70. Pressing the Ok button replaces the selected sections on the left pane of Figure 8-82. Then, the user can proceed to assign them to the Global Preventive M&R familiy selected by pressing the ">>" button. A similar process has to be performed to assign sections to the other families.

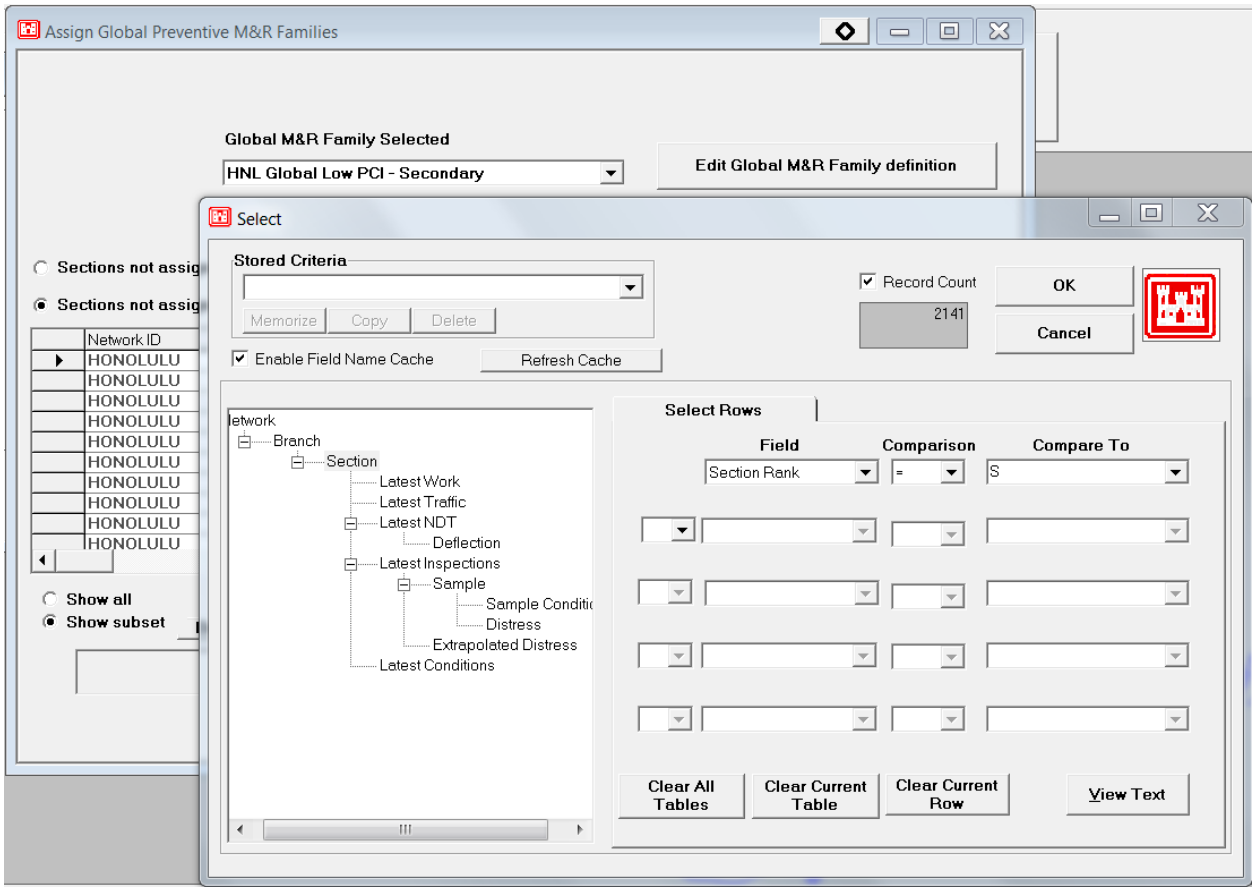

Figure 8-82. Selecting a subset of sections with the query wizard.

8.4.3.6.6 Major M&R Treatments, Policies, Consequences, and Costs

This section describes the input parameters required to define the Major M&R Policies. The structure of the input tables is similar though not identical to those explained for Stopgap and Local Preventive M&R. Therefore, only the most significant differences are explained.

8.4.3.6.6.1 Major M&R Work Types

PAVER™ comes with several default work types and the user can add more. Figure 8-83 shows the Work Types table in PAVER™. As usual, default values are highlighted in yellow. Most of the work types for Major M&R are pretty common and do not require much explanation.

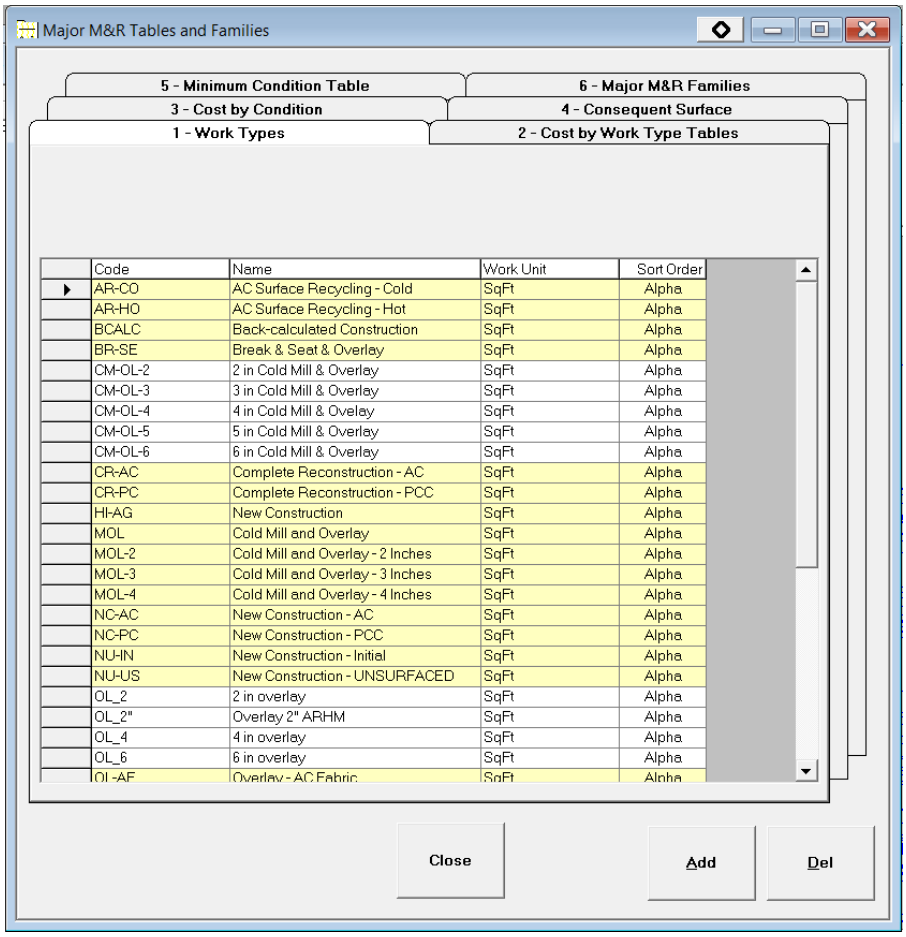

Figure 8-83. Major M&R Work Types.

8.4.3.6.6.2 Major M&R Costs by Work Types

The Cost by Work Types table, shown in Figure 8-84 is self-explanatory[89]. For HDOT, it is expected that the most common Major M&R will consists of mill and fill operations. Although on occasion a single overlay may be adequate, the need to maintain grade makes the overlay option less viable, particularly on primary roads. On secondary or local roads, an overlay may be a more viable option. Thus, several mill and fill of different depth (2 in to 6 in) were created to consider the most common situations as well as one 2" overlay.

[89] Once again, the costs in this table are for illustrative purposes. Cost estimates representative of local conditions need to be developed by the HDOT.

This table appears to be used mostly for documentation purposes as it is not really used in the selection of M&R strategies.

8.4.3.6.6.3 Major M&R Costs by PCI

The recommendations in Figure 8-52 (page 506) were used to develop approximate Major M&R Costs by PCI. Since the Major M&R costs are expected to be different for primary and secondary roads two different tables were created (Figure 8-85).

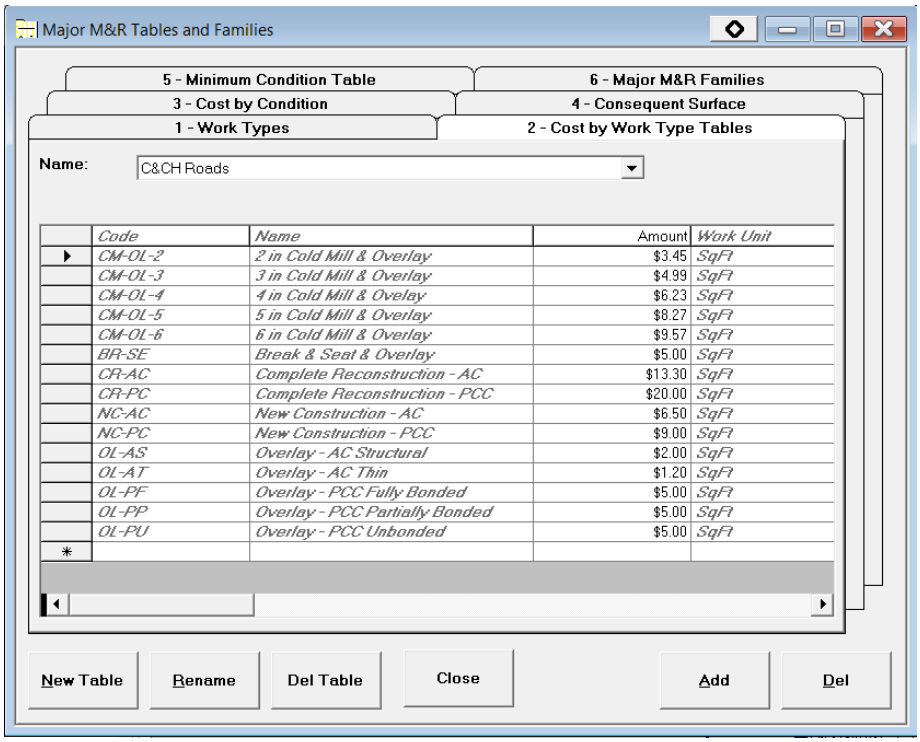

Figure 8-84. Costs by Work Type table.

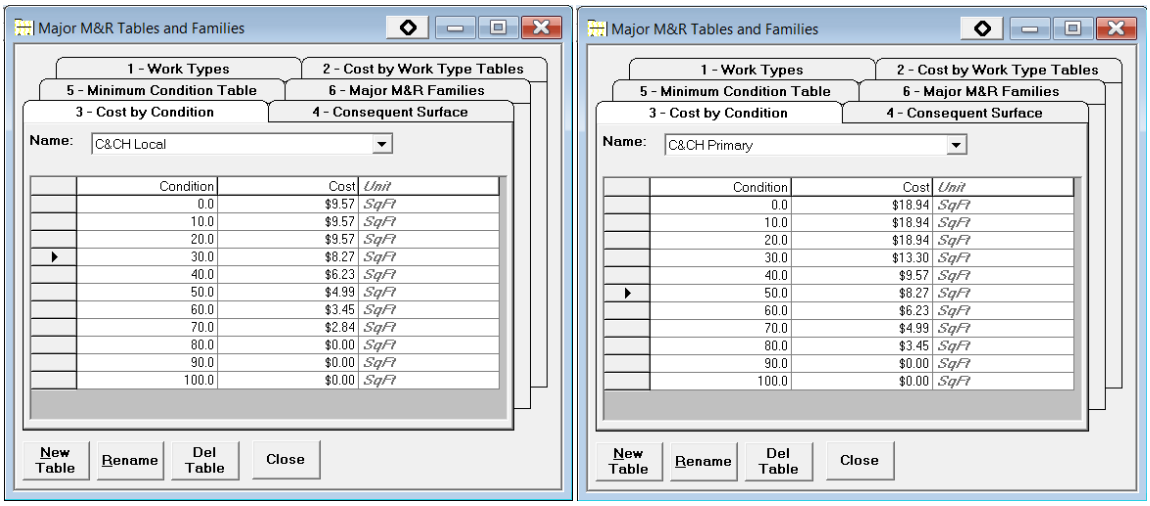

(a) (b)

Figure 8-85. Major M&R Costs by PCI for (a) Local (secondary) and (b) Primary roads.

For secondary roads, it was assumed that the minimum Major M&R would consists of a 2 in overlay and the maximum work would be a 6 in mill and fill.

For primary roads, the minimum Major M&R was assumed to be a 2" mill and fill and the maximum full reconstruction. A $1,000,000 per lane-mile was used to obtain the value corresponding to full reconstruction.

8.4.3.6.6.4 Consequent Surface from Major M&R

As was the case for Global Preventive M&R, each Major M&R may change the surface of the pavement. For those Major M&R that change the surface, PAVER™ needs to know how the surface is transformed. Figure 8-86 shows how this is specified in the **Consequent Surface** tab, which shows a table with a different row for each of the Major M&R work types. The table also contains a column for each surface type in the PAVER™ database. For those surface types that get changed the user needs to specify the new surface type. The procedure is identical to that described in section 8.4.3.6.5.2 for global preventive M&R.

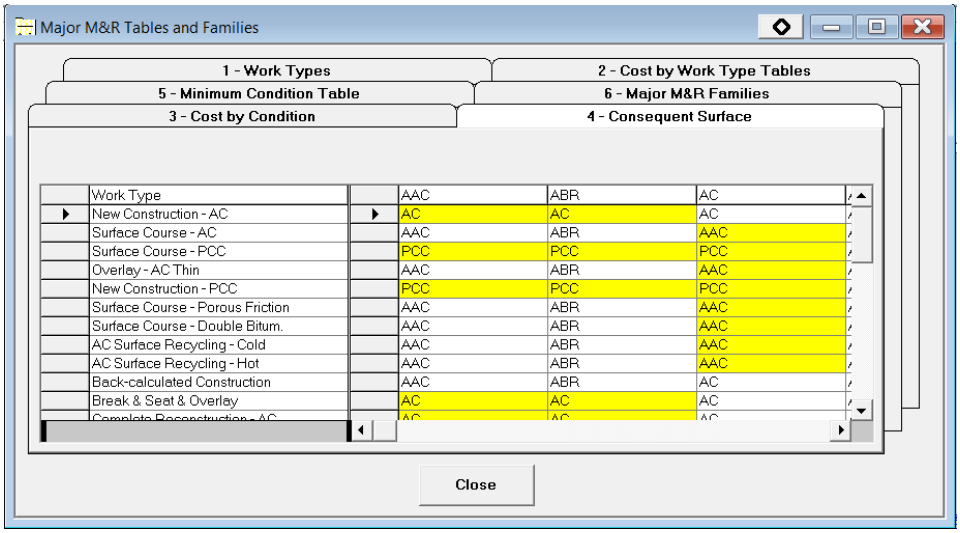

Figure 8-86. Specifying Consequent Surface types for Major M&R.

8.4.3.6.6.5 Major M&R Minimum Condition Table

This table is not used in the Critical PCI analysis. It is described however for completeness. As mentioned in section 8.4.3.6.1 (page 500), one of the M&R Plan options in PAVER™ is Major M&R based on Minimum Condition. When performing this type of analysis, PAVER™ assigns Major M&R whenever a section reaches the minimum condition. The minimum condition in turn can be changed over time to slowly improve the network condition and avoid large budgets in the initial years. As shown in Figure 8-87, the **Minimum Condition Table** simply defines the minimum PCI for each year.

8.4.3.6.6.6 Major M&R Families

As with the other M&R categories, PAVER™ can group pavements sharing costs into families. For Major M&R, these families are defined by the costs and the minimum condition (remember that minimum condition is not used in the Critical PCI analysis). For Major M&R there is no such thing as a maintenance policy. The program does not specify a specific M&R action but instead determines a budget for Major M&R based on the Costs by PCI tables. Whether Major M&R is required for a given section is determined with the logic presented in Figure 8-53 (page 507) and Figure 8-54 (page 508) and the logic presented in section 8.4.3.6.2 (page 504.)

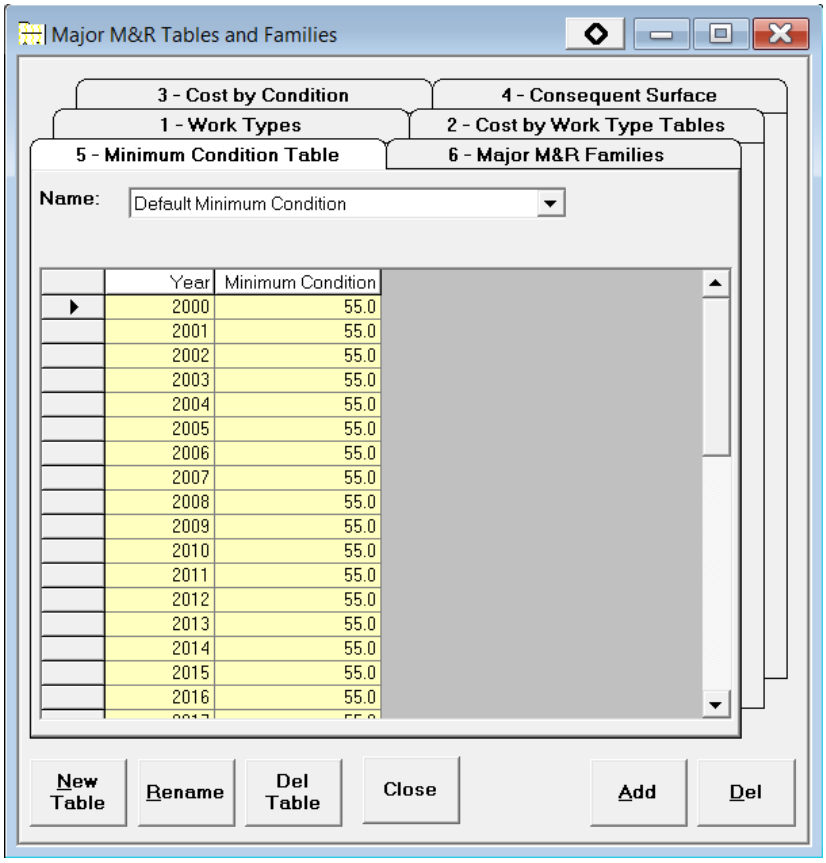

Figure 8-87. Minimum Condition Table used in Minimum PCI analysis.

In section 8.4.3.6.6.3, page 554, two different Costs by PCI tables were created. One for Primary roads and the other for Secondary roads. PAVER™ then needs to know which of these two tables will be used for a specific section. This is accomplished by creating two families, one for primary roads and the other for secondary road. Obviously, the Costs by PCI table corresponding to primary roads will be assigned to the family for primary roads and likewise for secondary roads. This is illustrated in Figure 8-88, where the family for primary roads has been given the same name as the Cost by PCI table, namely **C&CH Primary**. For secondary roads, the family was named **C&CH Locals** with the Costs by PCI table named **C&CH Local**.

Once these families have been defined, the user needs to assign the pavement sections to each family. The process is identical to those described in section 8.4.3.6.5.4, so it is not repeated here.

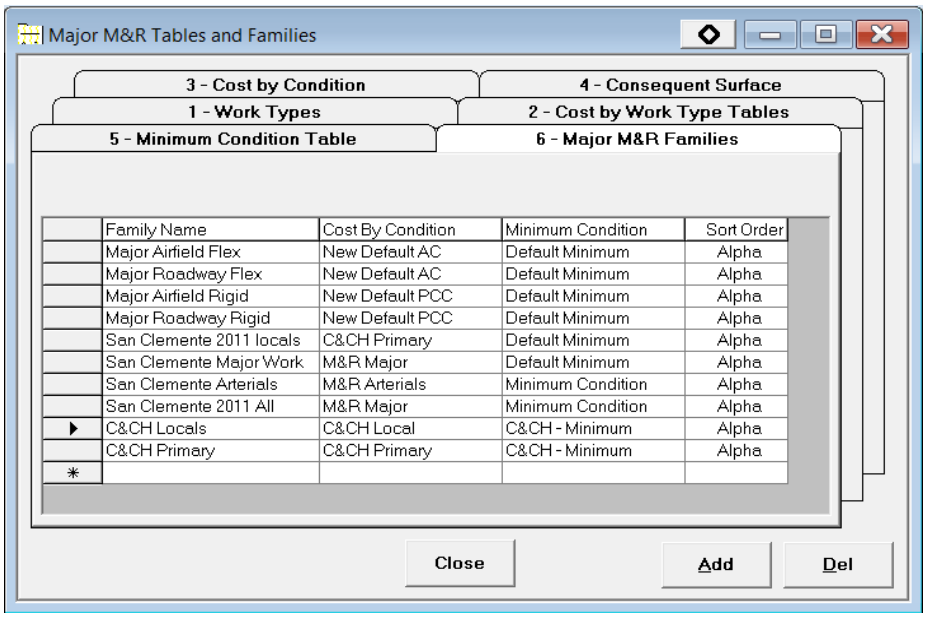

Figure 8-88. Major M&R Families.

4.7 M&R Priority Table

In some situations, PAVER™ utilizes a priority table to prioritize assignment of funds to sections within a given M&R category. The priority indexes based on section use and rank were presented in Table 8-3. For convenience, the same information but as display in PAVER™ is presented in Figure 8-89.

In order to assign a priority index to each section, PAVER™ needs to know whether the rank of the section is Low, Medium or High priority. The user controls this by linking the section rank (an input that is defined for each pavement section) to the priority with the help of the table displayed in Figure 8-90. In the C&CH example, the roads have been categorized as either Primary (P) or Secondary(S). As seen in the figure, primary roads have been assigned a high section rank priority and secondary roads a medium rank priority.

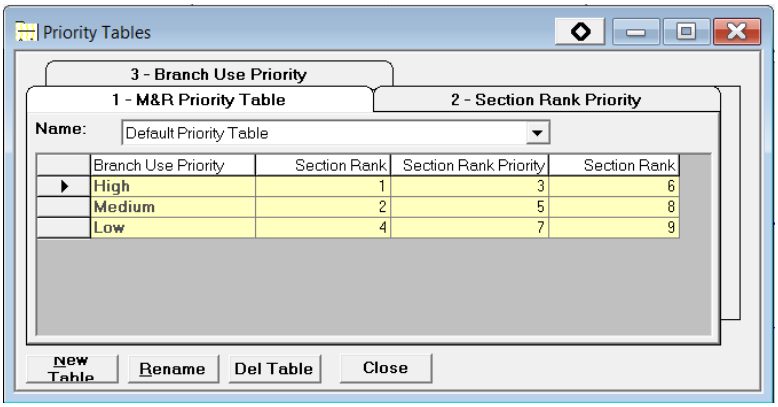

Figure 8-89. Priorities based on section use and rank.

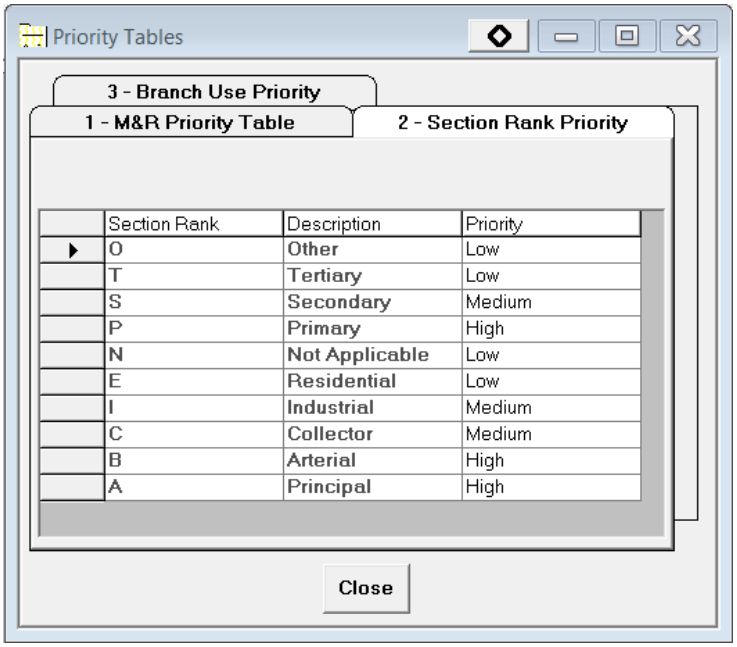

Figure 8-90. Section Rank Priority.

Similarly, PAVER™ needs to know whether the use of the section is Low, Medium or High priority. The user controls this by linking the branch use (also an input that is defined for each pavement section) to the priority with the help of the table displayed in Figure 8-91. In the C&CH example all the roads have been categorized as roadway and given a high priority. Note that except for Parking and Shoulder all the other default branch uses are not relevant for highway pavements. Nevertheless, other branch uses can be easily created by HDOT in the form

shown in Figure 8-91, for example, to give different priority to service roads. Thus, the use of these tables can be customized in the future if other prioritization schemes are required.

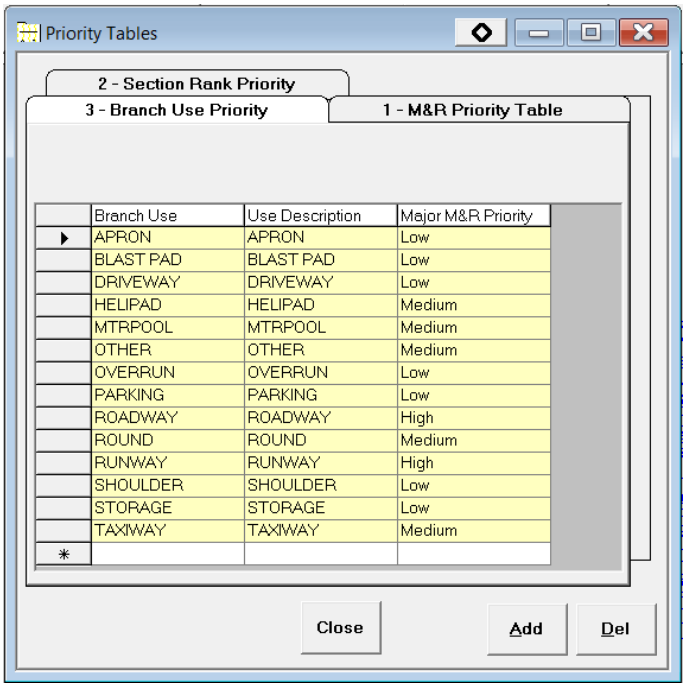

Figure 8-91. Branch Use Priority.

8.4.3.6.7 Summary

This section has presented the logic of how PAVER™ determines M&R plan requirements and the parameters that the program needs for determining such a plan. Since the program performs a (pseudo) optimization, it is not possible to present a simple recipe such as "if the condition is X then do Y". Instead, as described in previous sections, several tables need to be specified with distress maintenance policies and costs for each the four M&R categories. Although many of the tables appear to be of the type "if the condition is X do Y", it has to be remembered that none of these are absolute. The actions depend on conditions, availability of funds and competing resource requirements between sections.

The policy is actually contained on the values provided in each of the tables and the logic described in the previous sections.

8.4.3.7 Program uses

Different uses of the program can be made at different levels.

At a higher level, PAVER™ can produce tables such as the one shown in Figure 8-92, which contains estimates of how much money should be allocated to each M&R category for a given annual budget (the costs have been blown up for easier reading). The program can provide these estimates for multiple years (in the example of the figure only two years were used.) Also, depending on several plan parameters beyond the scope of this report, the user can ask the program to obtain appropriate funding levels to achieve a given overall network condition or to eliminate the backlog in a specified number of years. In any of these cases, the program will produce estimates of the funding that should be allocated to each M&R category. The program also produces estimates of the pavement conditions that will be obtained with those budget allocations.

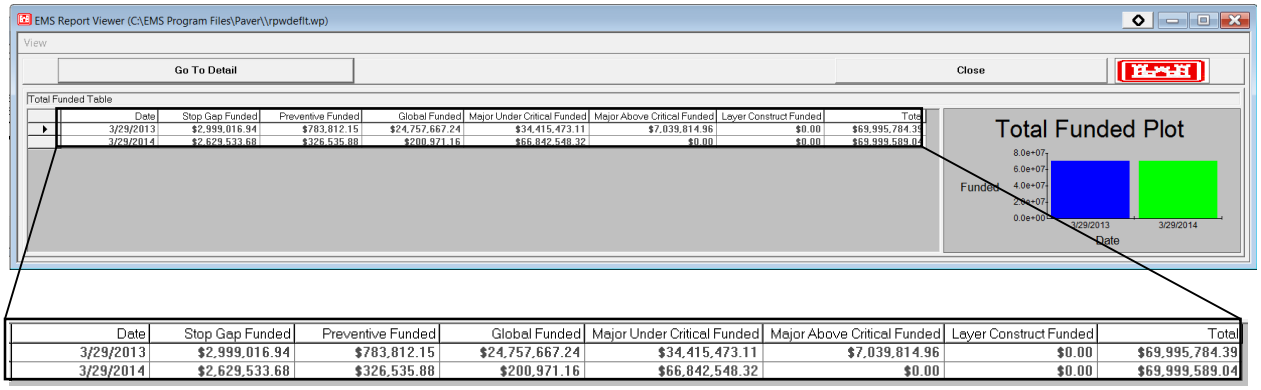

Date	Stop Gap Funded	Preventive Funded	Global Funded	Major Under Critical Funded	Major Above Critical Funded	Layer Construct Funded	Total
3/29/2013	$2,999,016.94	$783,812.15	$24,757,667.24	$34,415,473.11	$7,039,814.96	$0.00	$69,995,784.39
3/29/2014	$2,629,533.68	$326,535.88	$200,971.16	$66,842,548.32	$0.00	$0.00	$69,999,589.04

Figure 8-92. Total funding allocations.

At a lower level, one may be interested in what type of treatments should be applied to each section in the network. PAVER™ also provides some useful outputs for these types of activities.

As shown in Figure 8-93, among other things, the program produces funding allocation tables for each section. Clearly, after studying the assumptions and issues in the previous sections, it should be understood that these are approximate but neverthless useful for programming funding M&R activities.

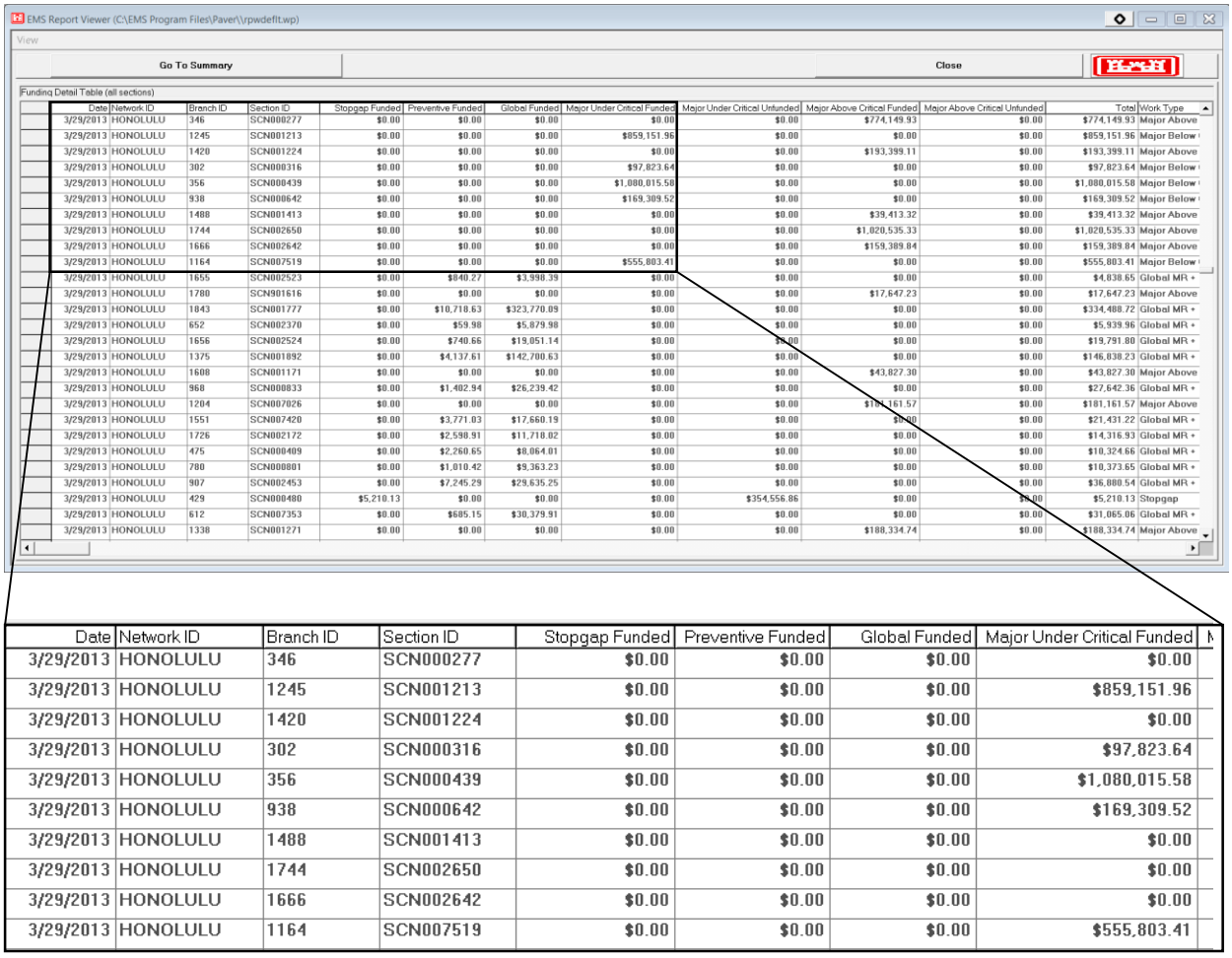

Date	Network ID	Branch ID	Section ID	Stopgap Funded	Preventive Funded	Global Funded	Major Under Critical Funded	Major Under Critical Unfunded	Major Above Critical Funded	Major Above Critical Unfunded	Total	Work Type
3/29/2013	HONOLULU	346	SCN000277	$0.00	$0.00	$0.00	$0.00	$0.00	$774,149.93	$0.00	$774,149.93	Major Above
3/29/2013	HONOLULU	1245	SCN001213	$0.00	$0.00	$0.00	$859,151.96	$0.00	$0.00	$0.00	$859,151.96	Major Below
3/29/2013	HONOLULU	1420	SCN001224	$0.00	$0.00	$0.00	$0.00	$0.00	$193,399.11	$0.00	$193,399.11	Major Above
3/29/2013	HONOLULU	302	SCN000316	$0.00	$0.00	$0.00	$97,823.64	$0.00	$0.00	$0.00	$97,823.64	Major Below
3/29/2013	HONOLULU	356	SCN000439	$0.00	$0.00	$0.00	$1,080,015.58	$0.00	$0.00	$0.00	$1,080,015.58	Major Below
3/29/2013	HONOLULU	938	SCN000642	$0.00	$0.00	$0.00	$169,309.52	$0.00	$0.00	$0.00	$169,309.52	Major Below
3/29/2013	HONOLULU	1488	SCN001413	$0.00	$0.00	$0.00	$0.00	$0.00	$39,413.32	$0.00	$39,413.32	Major Above
3/29/2013	HONOLULU	1744	SCN002650	$0.00	$0.00	$0.00	$0.00	$0.00	$1,020,535.33	$0.00	$1,020,535.33	Major Above
3/29/2013	HONOLULU	1666	SCN002642	$0.00	$0.00	$0.00	$0.00	$0.00	$159,389.84	$0.00	$159,389.84	Major Above
3/29/2013	HONOLULU	1164	SCN007519	$0.00	$0.00	$0.00	$555,803.41	$0.00	$0.00	$0.00	$555,803.41	Major Below
3/29/2013	HONOLULU	1655	SCN002523	$0.00	$840.27	$3,990.39	$0.00	$0.00	$0.00	$0.00	$4,830.65	Global MR +
3/29/2013	HONOLULU	1780	SCN901616	$0.00	$0.00	$0.00	$0.00	$0.00	$17,647.23	$0.00	$17,647.23	Major Above
3/29/2013	HONOLULU	1843	SCN001777	$0.00	$10,718.63	$323,770.09	$0.00	$0.00	$0.00	$0.00	$334,488.72	Global MR +
3/29/2013	HONOLULU	652	SCN002370	$0.00	$59.98	$5,879.98	$0.00	$0.00	$0.00	$0.00	$5,939.96	Global MR +
3/29/2013	HONOLULU	1656	SCN002524	$0.00	$740.66	$19,051.14	$0.00	$0.00	$0.00	$0.00	$19,791.80	Global MR +
3/29/2013	HONOLULU	1375	SCN001892	$0.00	$4,137.61	$142,700.63	$0.00	$0.00	$0.00	$0.00	$146,838.23	Global MR +
3/29/2013	HONOLULU	1608	SCN001171	$0.00	$0.00	$0.00	$0.00	$0.00	$43,827.30	$0.00	$43,827.30	Major Above
3/29/2013	HONOLULU	968	SCN000833	$0.00	$1,402.94	$26,239.42	$0.00	$0.00	$0.00	$0.00	$27,642.36	Global MR +
3/29/2013	HONOLULU	1204	SCN007026	$0.00	$0.00	$0.00	$0.00	$0.00	$181,161.57	$0.00	$181,161.57	Major Above
3/29/2013	HONOLULU	1551	SCN007420	$0.00	$3,771.03	$17,660.19	$0.00	$0.00	$0.00	$0.00	$21,431.22	Global MR +
3/29/2013	HONOLULU	1726	SCN002172	$0.00	$2,598.91	$11,718.02	$0.00	$0.00	$0.00	$0.00	$14,316.93	Global MR +
3/29/2013	HONOLULU	475	SCN000409	$0.00	$2,260.65	$8,064.01	$0.00	$0.00	$0.00	$0.00	$10,324.66	Global MR +
3/29/2013	HONOLULU	780	SCN000801	$0.00	$1,010.42	$9,363.23	$0.00	$0.00	$0.00	$0.00	$10,373.65	Global MR +
3/29/2013	HONOLULU	907	SCN002453	$0.00	$7,245.29	$29,635.25	$0.00	$0.00	$0.00	$0.00	$36,880.54	Global MR +
3/29/2013	HONOLULU	429	SCN000480	$5,210.13	$0.00	$0.00	$0.00	$354,556.86	$0.00	$0.00	$5,210.13	Stopgap
3/29/2013	HONOLULU	612	SCN007353	$0.00	$685.15	$30,379.91	$0.00	$0.00	$0.00	$0.00	$31,065.06	Global MR +
3/29/2013	HONOLULU	1338	SCN001271	$0.00	$0.00	$0.00	$0.00	$0.00	$188,334.74	$0.00	$188,334.74	Major Above

Date	Network ID	Branch ID	Section ID	Stopgap Funded	Preventive Funded	Global Funded	Major Under Critical Funded
3/29/2013	HONOLULU	346	SCN000277	$0.00	$0.00	$0.00	$0.00
3/29/2013	HONOLULU	1245	SCN001213	$0.00	$0.00	$0.00	$859,151.96
3/29/2013	HONOLULU	1420	SCN001224	$0.00	$0.00	$0.00	$0.00
3/29/2013	HONOLULU	302	SCN000316	$0.00	$0.00	$0.00	$97,823.64
3/29/2013	HONOLULU	356	SCN000439	$0.00	$0.00	$0.00	$1,080,015.58
3/29/2013	HONOLULU	938	SCN000642	$0.00	$0.00	$0.00	$169,309.52
3/29/2013	HONOLULU	1488	SCN001413	$0.00	$0.00	$0.00	$0.00
3/29/2013	HONOLULU	1744	SCN002650	$0.00	$0.00	$0.00	$0.00
3/29/2013	HONOLULU	1666	SCN002642	$0.00	$0.00	$0.00	$0.00
3/29/2013	HONOLULU	1164	SCN007519	$0.00	$0.00	$0.00	$555,803.41

Figure 8-93. Sections' funding allocations.

For Global Preventive M&R, the program is very specific since it indicates the type of global preventive M&R treatment that must be applied to each section on every year in the analysis period (only sections on which a treatment is planned in a given year are listed.) This is illustrated in Figure 8-94.

For the other types of M&R categories, the program provides estimated appropriate funding levels and predicts their consequences. Although defining the actual treatments demand some additional work, the output in Figure 8-93 still provides useful information. Furthermore, for the stopgap and local preventive maintenace categories some flexibility is needed since it is very difficult to predict exactly how many potholes will need to be repaired and how many cracks will need to be filled for a particular section. Also, it is difficult to estimate whether cracks should be filled or sealed from the network distress survey alone. These

are more operational issues that can be dealt with with appropriate levels of funding, which is what the program attempts to provide.

Finally, for Major M&R, a more thorough study is needed anyway at the pavement section level (i.e., for a specific section, a formal pavement design needs to be completed to address all the potential problems and obtain more reliable costs estimates.)

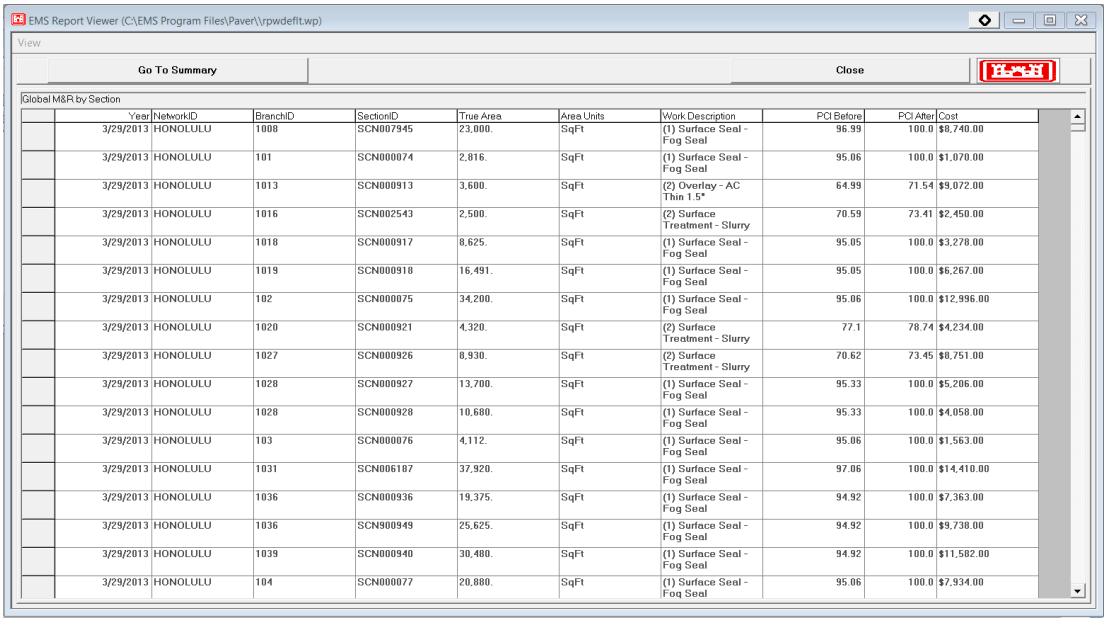

Year	NetworkID	BranchID	SectionID	True Area	Area Units	Work Description	PCI Before	PCI After	Cost
3/29/2013	HONOLULU	1008	SCN007945	23,000.	SqFt	(1) Surface Seal - Fog Seal	96.99	100.0	$8,740.00
3/29/2013	HONOLULU	101	SCN000074	2,816.	SqFt	(1) Surface Seal - Fog Seal	95.06	100.0	$1,070.00
3/29/2013	HONOLULU	1013	SCN000913	3,600.	SqFt	(2) Overlay - AC Thin 1.5"	64.99	71.54	$9,072.00
3/29/2013	HONOLULU	1016	SCN002543	2,500.	SqFt	(2) Surface Treatment - Slurry	70.59	73.41	$2,450.00
3/29/2013	HONOLULU	1018	SCN000917	8,625.	SqFt	(1) Surface Seal - Fog Seal	95.05	100.0	$3,278.00
3/29/2013	HONOLULU	1019	SCN000918	16,491.	SqFt	(1) Surface Seal - Fog Seal	95.05	100.0	$6,267.00
3/29/2013	HONOLULU	102	SCN000075	34,200.	SqFt	(1) Surface Seal - Fog Seal	95.06	100.0	$12,996.00
3/29/2013	HONOLULU	1020	SCN000921	4,320.	SqFt	(2) Surface Treatment - Slurry	77.1	78.74	$4,234.00
3/29/2013	HONOLULU	1027	SCN000926	8,930.	SqFt	(2) Surface Treatment - Slurry	70.62	73.45	$8,751.00
3/29/2013	HONOLULU	1028	SCN000927	13,700.	SqFt	(1) Surface Seal - Fog Seal	95.33	100.0	$5,206.00
3/29/2013	HONOLULU	1028	SCN000928	10,680.	SqFt	(1) Surface Seal - Fog Seal	95.33	100.0	$4,058.00
3/29/2013	HONOLULU	103	SCN000076	4,112.	SqFt	(1) Surface Seal - Fog Seal	95.06	100.0	$1,563.00
3/29/2013	HONOLULU	1031	SCN006187	37,920.	SqFt	(1) Surface Seal - Fog Seal	97.06	100.0	$14,410.00
3/29/2013	HONOLULU	1036	SCN000936	19,375.	SqFt	(1) Surface Seal - Fog Seal	94.92	100.0	$7,363.00
3/29/2013	HONOLULU	1036	SCN900949	25,625.	SqFt	(1) Surface Seal - Fog Seal	94.92	100.0	$9,738.00
3/29/2013	HONOLULU	1039	SCN000940	30,480.	SqFt	(1) Surface Seal - Fog Seal	94.92	100.0	$11,582.00
3/29/2013	HONOLULU	104	SCN000077	20,880.	SqFt	(1) Surface Seal - Fog Seal	95.06	100.0	$7,934.00

Figure 8-94. Global Preventive treatment allocation by section.

In addition to the tabular output, PAVER™ also provides several GIS outputs for a particular plan. The following figures illustrate some of these outputs. For example, Figure 8-95 shows the locations, by year, on which Major M&R should be performed based on a 10-year plan obtained using the Critical PCI analysis for part of the C&CH network. Figure 8-96 shows the Major M&R needed in 2015 (corresponding to year 3 in Figure 8-95) for the same plan. In Figure 8-96, the major M&R is shown separately for roads with PCI below and above critical. Note that with a worst-first approach, the sections with some structural problems above the critical PCI would probably not have been considered for this type of treatment.

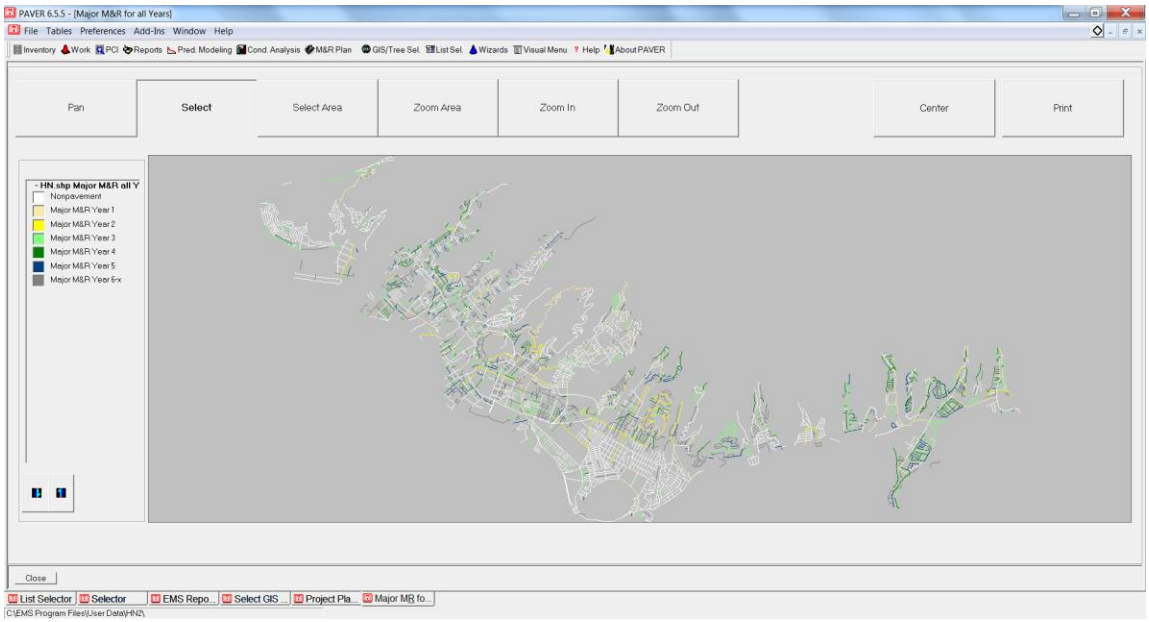

Figure 8-95. GIS output example – Major M&R all years.

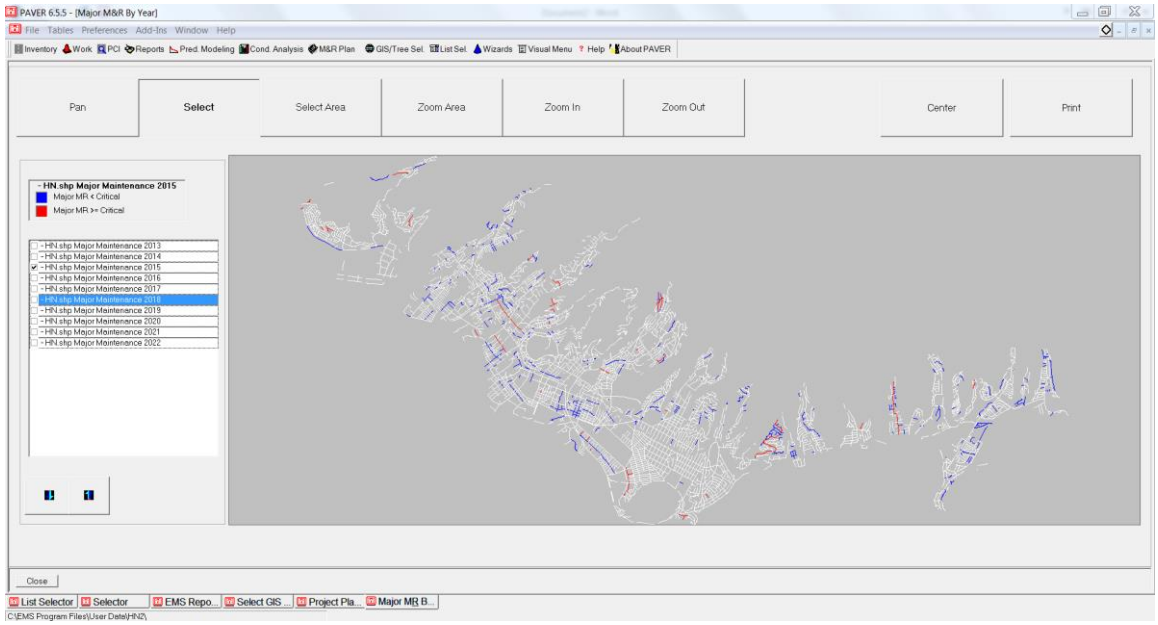

Figure 8-96. GIS output example – Major M&R by Year.

Figure 8-97, Figure 8-98, and Figure 8-99 show the predicted conditions for the same plan at three points in time, 2013, 2017, and 2021, respectively. These types of plots are useful for visualizing the evolution of the network condition over time. One can clearly see the reduction of pavements falling in the lower PCI categories from 2013 to 2017. It can also be

observed an increment in pavements in fair condition from 2017 to 2021, which illustrates the cyclical nature of the rehabilitation problem. In the long term, use of PMS software can help stabilize the budget needs and achieve steadier budget requirements.

PAVER^{TM} also allows grouping of recommended treatments into projects. The user has significant flexibility on how to group pavement sections using queries (e.g., by M&R category, geographically, or based on combinations of factors.) Figure 8-100 shows a hypothetical grouping of some treatments into two projects. One of the projects is for a particular road, while the other is for a set of roads dispersed over the network. Once a programmed project is completed, the information can be set as work completed with the press of a button (in this case, the conditions are updated as needed.)

The shapefiles created by PAVER^{TM} can be easily imported into GIS software to enhance legends, plotting, etc.

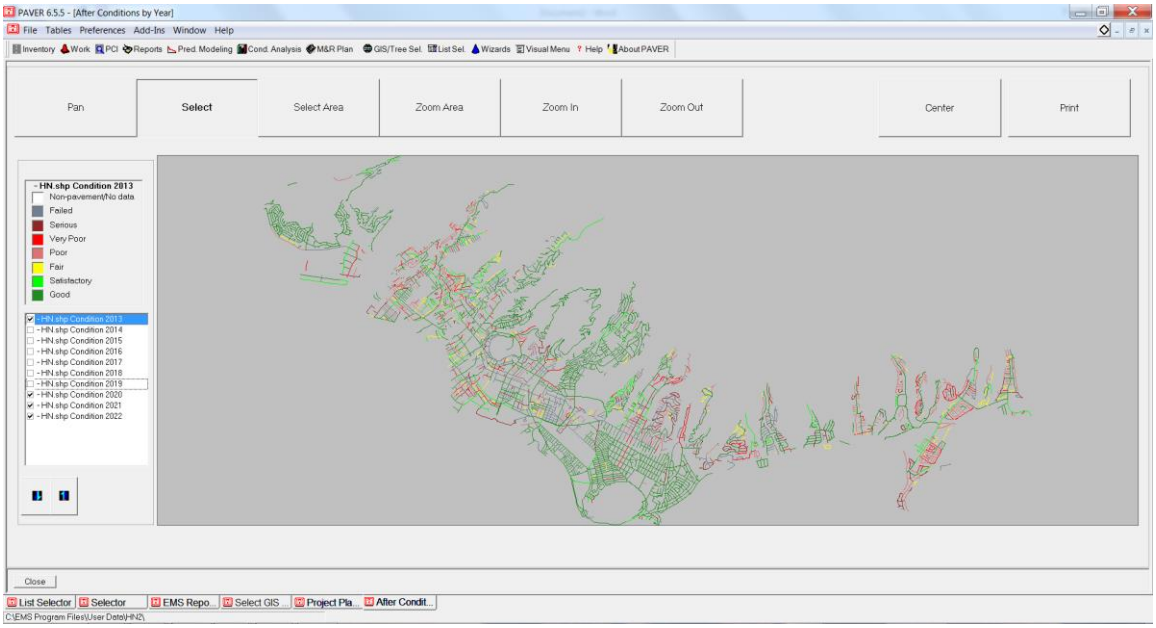

Figure 8-97. GIS output example – Predicted PCIs in 2013.

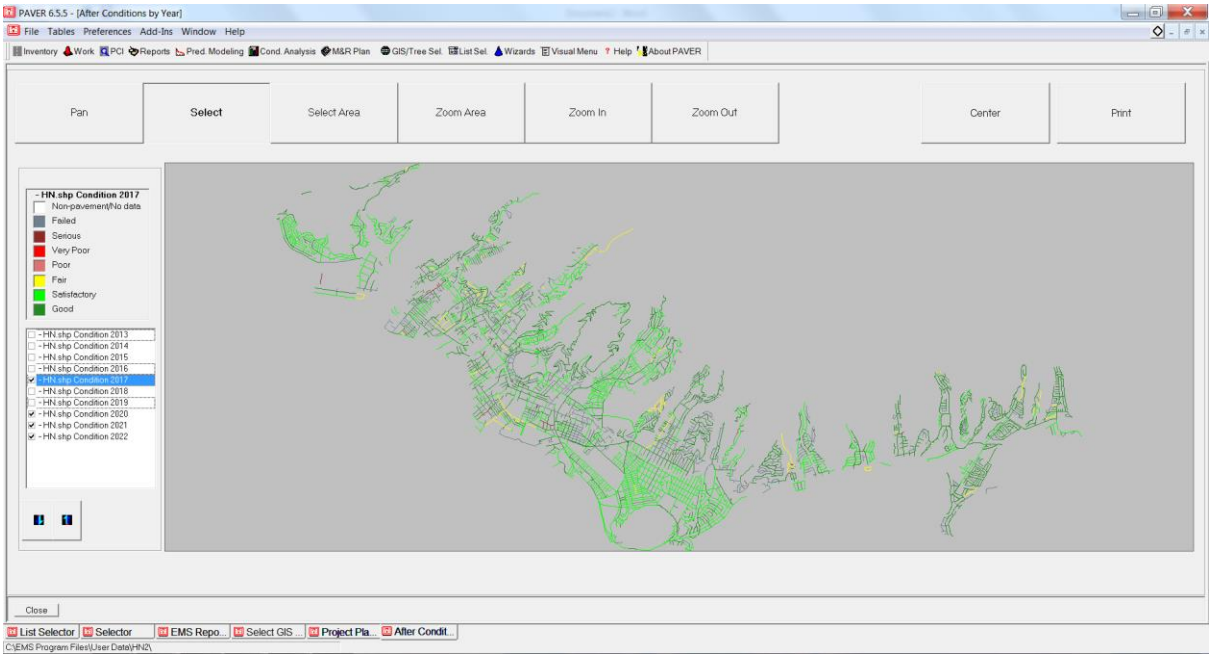

Figure 8-98. GIS output example – Predicted PCIs in 2017.

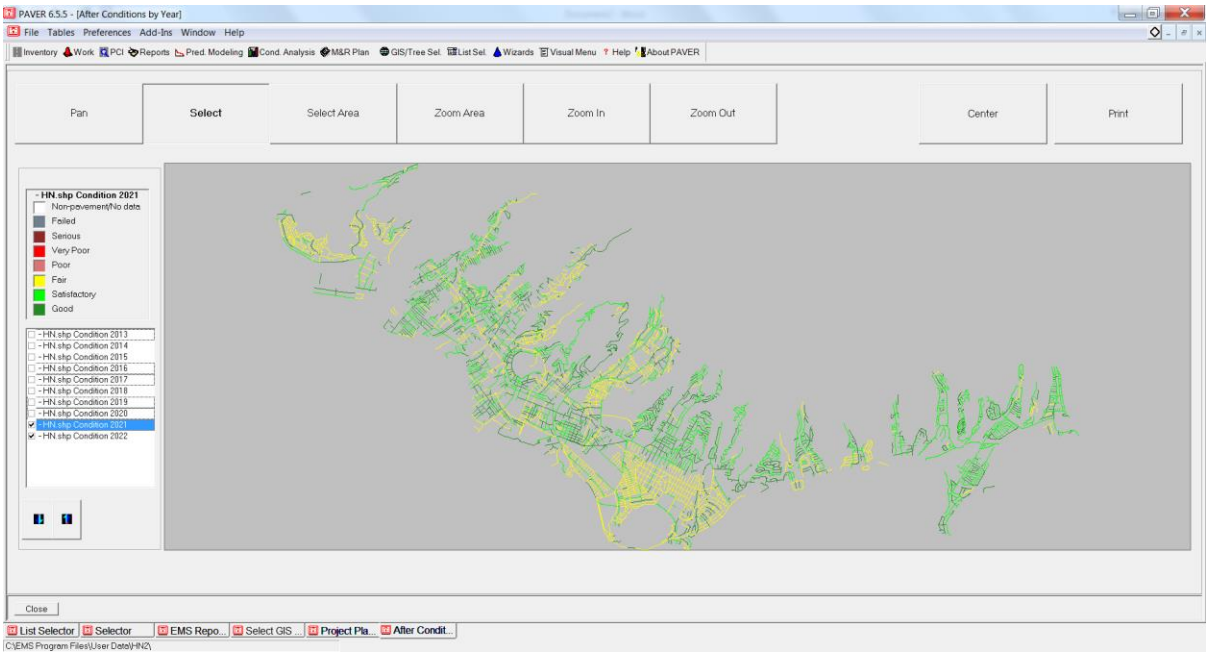

Figure 8-99. GIS output example – Predicted PCIs in 2021.

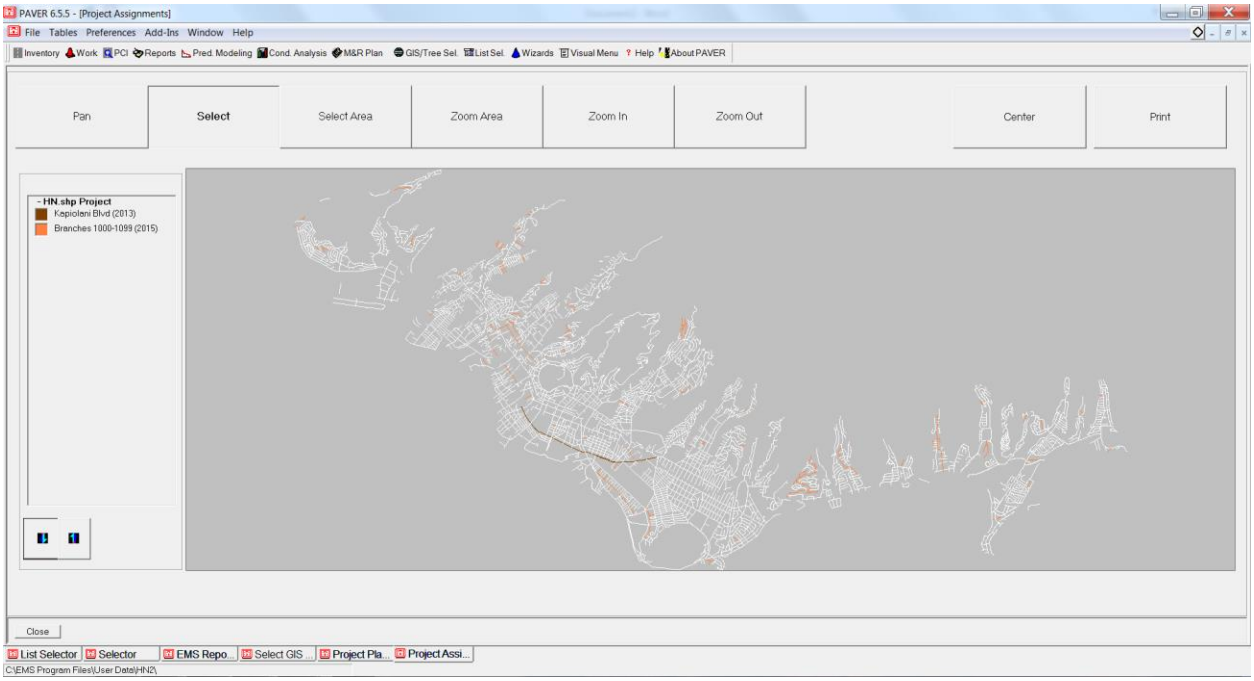

Figure 8-100. GIS output example – Grouping of sections into projects.

8.5 Other PMS implementation challenges

While the use of a modern PMS software is required for a successful PMS implementation, other challenges must be overcome including data quality, workforce assignment and training, personnel buy-in, communication protocols, institutional barriers, and trade-offs with other highway assets. This project has concentrated for the most part on technical issues. However, it is recognized that proper consideration of non-technical issues may be as critical. This section identifies some issues as perceived by the research team.

One of the challenges is for HDOT personnel to really buy-in about the benefits of using a PMS system. Although there is a real sense of urgency of its need, much of it appears to be driven by legislation requirements. Federal requirements help to keep a PMS going but in the long run real buy-in is needed. Thus, having a champion within HDOT that firmly believes in the benefits of a PMS, that can communicate with other stakeholders and foster cooperation within the agency can go a long way. Encouragement and support from upper management can be very useful in this respect.

The success of the PMS relies on adequate staffing levels and resources. Two types of profiles are desirable: a person with good knowledge of pavement engineering and pavement management systems and another with good knowledge on systems, database principles, and GIS. Finding a single person with both sets of skills is usually very difficult and given the amount of information that needs to be managed, it can be overwhelming as well. Thus, appropriate staffing and training should be provided so that the workload is adequate to avoid a rapid turnaround. If hiring staff with appropriate skill sets becomes difficult, it is imperative to invest in properly training existing personnel.

A substantial part of this report has been devoted to data analysis and a lot of good information has been analyzed. However, as shown in previous sections, there are several data issues that may be improved. What appears to be missing is the feedback from the districts since apparently much of the information collected over time is collected mostly for federal reporting purposes instead of (or in addition to) local analysis. Developing an internal feedback mechanism can improve the efficiency and usefulness of the data.

CHAPTER 9. FINDINGS AND RECOMMENDATIONS

This chapter summarizes the findings and provides several recommendations. However, it is recognized that some recommendations are more urgent than others. Also, some are implementable without much effort and others require substantial effort. Thus, recommendations are accompanied with a letter in parenthesis to indicate whether the recommendation is critical (*C*), intermediate (*I*), or desirable (*D*).

9.1 PMS Implementation

As discussed throughout this report, several technical aspects must be considered for implementing a PMS at HDOT, along with institutional aspects that are as important as the technical ones for its successful implementation. All these are discussed in this section.

9.1.1 PMS Software

Clearly, for the size of the network managed by HDOT, the PMS data should be incorporated and processed in a modern commercial PMS program instead of Excel® worksheets. This was also one of the recommendations of the 2009 Pavement Preservation Technical Appraisal [8] and one of the main reasons for performing this research project. Although substantial information is available online through HDOT's RIS, PMS recommendations are still based mostly on analyses carried out on spreadsheets.

As discussed in section 8.3, there is a large number of candidate PMS programs with different capabilities. Most of them would meet HDOT needs from a purely technical point of view. However, consideration of the network size and personnel at HDOT's MT&R branch (HWY-L) lead to the consideration of only three of these for a more detailed evaluation, namely, StreetSaver®, RoadSoft®, and PAVER™ (section 8.4). Again, the technical capabilities of the three programs are believed to be adequate to address HDOT needs. Because of different data and timing issues, the program that was evaluated more thoroughly was PAVER™. The following subsections present a comparison of some of their features and other issues that need to be addressed for a successful PMS implementation.

9.1.1.1 Comparison of some of the features of StreetSaver®, RoadSoft®, and PAVER™

Characterization of Pavement Condition: The three programs use an aggregate index for pavement condition. StreetSaver® and PAVER™ use PCI whereas RoadSoft® uses the PASER system. Thus, implementation of RoadSoft® would require a different paradigm for distress/condition data collection. Although the PASER system has been developed to simplify the determination of pavement condition and the current HDOT distress data collection process is subject to improvements, changing the system may present additional training needs for HDOT personnel.

Modeling of Pavement Deterioration: The three programs also have in common that they all use the concept of pavement families to model pavement deterioration but they differ on the models used.

PAVER™ uses constrained or unconstrained polynomials fitted to PCI values that are computed from distress data. The process is very transparent since the program provides facilities to collect the relevant data from the condition information available for a given network database, filter the data for outliers, select constraints, perform the fitting, and assign the models to pavement sections. Default models are also available.

In RoadSoft®, the creation of models is also relatively simple since the user essentially needs to define for each model (usually for different pavement types) a table containing the consecutive ratings in decreasing order along with the number of years it takes to move from one rating to the next (Figure 8-21, page 462). The most difficult task is really obtaining representative values to fill in the table, something that needs to be done separately.

In StreetSaver® deterioration curves vary based upon surface type and functional classification but apparently these curves are pre-specified, i.e., they cannot be updated based on local data. This presupposes that the default curves are representative of local conditions.

Section Split/Combine Capabilities: RoadSoft® and StreetSaver® currently provide facilities for splitting/combining segments, a feature that is extremely useful for updating the changes that occur in the network. On the other hand, for PAVER™, only recently it has been announced that its next version will also have this feature [103].

Data Import Capabilities: Both PAVER™ and StreetSaver® provide tools to import inventory and distress information (see section 8.4.3.2.3 on page 479 and section 8.4.3.3.2 on page 487 for the descriptions for PAVER™). Since the process of sectioning the Oahu network presented in section 8.4.3.2.1 (page 466) was done after the license for StreetSaver® Online had expired, the import operations were not evaluated with StreetSaver®. Apparently, no such tool is available in RoadSoft®. Thus, the options for a vendor would be to use their laptop data collector (which would transfer the information directly in RoadSoft®) or key in the data. Although the amount of data may be less voluminous, this is still not considered an efficient process.

Strategy Development: One aspect on which the three programs differ is in the development of M&R strategies. For this purpose, StreetSaver® uses decision trees together with a *prioritization* scheme based on a measure of effectiveness. RoadSoft® uses decision trees together with an *optimization* algorithm (though the documentation is not specific as to exactly what function is being optimized and the criteria used formulate the objective function.) PAVER™ uses what is known as the Critical PCI analysis described section 8.4.3.6.2 (page 504). The critical PCI analysis also involves the use of decision trees together with a heuristic to optimize the allocation of funds.

GIS Capabilities: All three program provide some GIS capabilities. RoadSoft® is essentially a GIS based program with several modules for managing different roadway assets (culverts, point pavement markings, linear pavement markings, signs, traffic counts, driveways, sidewalks, bridges, crash data, and intersections) The capability of dealing with different assets is an important advantage of RoadSoft® over the two other programs. Furthermore, since the program is based on a GIS, creation of GIS reports is also relatively simple.

On the other hand, the information on StreetSaver® and PAVER™ is linked to shapefiles. Although this approach may be somewhat less flexible for obtaining the desired GIS reporting results, the GIS reports created are for most purposes adequate. Furthermore, they can be easily enhanced with GIS software.

The disadvantage of using segments in the GIS "framework" to define the set of routes or roadways (as done in RoadSoft®) over having inventory segments linked to GIS segments or polygons (as done in PAVER™) is that in the RoadSoft® approach any misclassification of a

route cannot be corrected unless the base map is re-created, a task that at present can only be performed by the vendor (section 8.4.2.5, page 459.) Similar issues may be encountered when a road alignment is changed substantially, a unidirectional framework segment represents a divided road, or two different pavement types are used for adjacent lanes of a road section.

PAVER ImageInspector™: This is a relatively new tool developed to work with downward images to collect pavement distress information and transfer it directly to PAVER™. It has the potential of simplifying many of the distress issues discussed in the report. However, to benefit from it, downward imaging needs to be captured, which is not currently being collected by HDOT.

Reports: The three programs provide a wide variety of reports. StreetSaver® probably has the widest variety of standard reports. Wizzards to configure reports according to user needs are also available on the three programs.

In summary, the three programs compared in this section, PAVER™, StreetSaver®, and RoadSoft® have the capabilities to satisfy HDOT needs. No single program appears to be superior to the others in all respects. However, for reasons related to the lack of availability of some data when evaluating StreetSaver® or issues with the network definition with RoadSoft®, most of the advances were made with PAVER™. Thus, the possibilities to assist HDOT locally are also greater with PAVER™.

Recommendation 1: *(I) Based on program capabilities, cost, documentation, possibilities of training, and present MT&R branch personnel expertise, it is recommended to consider the evaluated PMS programs in the following order of preference 1) PAVER™, 2) StreetSaver®, and 3) RoadSoft®.*

If PAVER™ is selected for implementation, the upcoming release (version 7.0) should be given preference as, in addition to the improvements noted before, it will improve the approach to account for benefits of preservation treatments (Global Preventive Treatments in PAVER™). The authors recently found that the version evaluated does not automatically update the condition of pavements subjected to preservation treatmenents. Although this can be overcome, it requires unnecessary additional effort by the user.

Note that if HDOT were willing to change its rating system to the PASER system and were to work with the vendor to solve the route linear reference issues, then RoadSoft® could be the top option considering that other assets can be managed with the same software.

The new MAP-21 requirements may have made consideration of more expensive enterprise programs such as those of Deighton [94] and Agile Assets [95] more appealing. Note that by more expensive it is meant only that the cost of purchasing and maintaining the software is higher. Detailed evaluation of these systems is beyond the scope of the project (they require a more direct involvement of HDOT in non-technical aspects) but HDOT may want to consider them as viable alternatives.

9.1.1.2 Inventory and Distress Data

Reliable inventory and distress data are essential to take advantage of the capabilities of any PMS software.

9.1.1.2.1 Inventory

There is substantial valuable inventory information in HDOT's RIS (number of lanes, lane widths, etc.) Furthermore, the data mining effort together with the PSPT tool described in section 2.4 (page 18), have produced a significant amount of structural information. To date, no subgrade and water table depth information has been included, which may significantly affect pavement performance. As discussed in section 7.5.3 (page 402), whether a section is a fill or a cut may be another factor influencing the pavement performance worthy of further investigation.

In addition, there are some known issues with the proper location of treatments within the mined data that need to be corrected. Fortunately, this activity is currently underway at the MT&R branch. However, the data mining effort is still missing important maintenance information from open ended pavement repair/maintenance contracts. Those activities influence significantly the condition of the pavement, and depending on the type of activity, they may also affect the Last Construction Date (LCD) (or equivalently, the pavement age.) Proper determination of the LCD and reporting of all maintenance activities would allow the determination of pavement deterioration models based on local values rather than default models.

As recently suggested by HDOT personnel, one possible source for these data is the AS400 accounting system used by all the districts. The compatibility of the maintenance control sections (MCS) with the PMS segments should be studied. For compatibility, at a minimum, the MCS should provide an indication of the percent of the area of the PMS segments affected by the treatment, the material used, the thickness, and the cost of the treatment. If possible, this could be extended to localized treatments such as crack sealing (measured in linear feet) to quantify the benefits of these types of treatment.

If the above is not possible, HDOT must develop a communication protocol (timing or frequency, type of information to be included, generating and receiving party, etc.) between HDOT sections and branches to ensure that maintenance treatments are included in the PMS database. Although it is recognized that this may involve additional effort, the potential benefits are substantial. Again, it is important to note that the amount of information required for the PMS is relatively minor. For example, the following items are adequate for most practical purposes: date, from milepoint, to milepoint, lane(s) affected, material, area affected (alternatively, average width) and thickness. This task would require that different HDOT branches and districts use the same referencing system. Note that with advances and cost reductions in GPS technology, field crews could be equipped with GPS units to provide the latitude and longitude of the "from" and "to" points instead of their milepoints. A program that automatically translates latitudes and longitudes into route milepoints could then be created to locate these points in the PMS (in software such as RoadSoft®, the location can be done directly with the GPS data.)

Based on the above observations, the following recommendations are provided:

Recommendation 2: *(I) Create PMS segments for the whole state network (similarly to what was made for Oahu in this study). The segments should be delimited by substantial changes in traffic loading (e.g., AADTT/lane), pavement structure, subgrade support, fill/cut sections, number of lanes, and other factors such as bridge ends. The Oahu network created in this study should be revised for consistency with criteria used for the other islands and improvement of the areas with poor imagery (under viaducts, tunnels, etc.).*

Recommendation 3: *(C) The PMS segments (or at least a manageable subset for which good information is available) should be categorized into a relatively small number of families with similar deterioration patterns. Some of the same factors above should be used for this purpose (e.g., heavy and low traffic loading with strong or weak support)*

Recommendation 4: *(C) A relatively small number of PMS segments on each family (20-30) should be monitored over time to obtain reliable deterioration models and to redefine the families if needed.*

Recommendation 5: *(C) A study should be conducted to evaluate the feasibility of using the AS400 accounting system database to obtain maintenance information from open ended contracts for the PMS. Alternatively, a protocol should be developed to feed the maintenance information from open ended maintenance contracts back into the PMS.*

9.1.1.2.2 Distress

In the last few data collection cycles collected by HDOT, the distress surveys have been improved in aspects such as the sampling interval and the specific consideration of PCC distresses. Nevertheless, the widely varying PCI values shown in section 8.4.3.4 (page 494) indicate that improvements are still needed. Some of that variation is explained in part by the artificially long lives created by missing rehabilitation data explained in the previous section and random variation. Also, some distresses (e.g., cracking, raveling, etc.) appear to be under-reported, which would translate in overestimation of the PCI. These problems combined have a significant effect on the deterioration curves.

Cracking characterization could be improved if cracking data are obtained automatically from downward pictures and 3D laser scanning, which as far as the PI knows, is planned for the

next pavement deterioration data collection cycle. It is expected that the lengths and areas of cracking (depending on the type being measured) will be more repeatable with an automated process.

> **Recommendation 6:** *(I) It is recommended that HDOT evaluates the collection of cracking using automated image analysis algorithms from downward images and 3D laser scanning.*

Raveling is a difficult distress to quantify from photographs and appears to be currently under-reported. However, significant technological advances have been made in recent years that may help measuring indicators of raveling at the network level. As discussed in section 8.4.3.4 (page 494) 3D Laser technology has been develop to quantify reveling [33].

> **Recommendation 7:** *(I) It is recommended that HDOT consider evaluating the use of 3D Laser technology to quantify raveling.*

As pointed out in section 8.4.3.4, the same technology can also provide measurements of a Road Porosity Index, with relevance to safety (tire/road friction level, water runoff and aquaplanning conditions) and noise.

Although the interval of 0.1 mi is appropriate for most practical purposes, the allocation of sampling segments to PMS sections oftentimes requires prorating of the 0.1 distress data, which results in additional uncertainty. Since the data are collected on shorter intervals anyway, automatic aggregation should be relatively simple.

> **Recommendation 8:** *(C) Distress information should be aggregated on sampling units entirely within PMS segments. Sampling units straddling the boundary between two PMS sections should be avoided.*

Currently, the distress data are subjected to minimal quality assurance procedures that appear to be limited to consistency checks. However, these data should also be subjected to quality assurance from the pavement engineering point of view.

Recommendation 9: *(I) HDOT personnel should be trained in distress data collection and on the use of the same software as the vendor so that quality assurance can be performed.*

9.1.1.3 Cost information

The strategies recommended by a PMS are heavily dependent on the relative costs of the different treatments (and on user costs for those PMS programs that account for them). For accurate budgeting, the actual costs are needed.

Given that most of the efforts in this project were directed towards determining the pavement lives and conditions and that, as described in the previous sections, these exhibited large uncertainties, a detailed analysis of cost information was deferred for a future study.

In a previous study [46], it was observed that the cost information of HMA layers showed significant variability on some of the items affecting the overall treatment costs (markings, reflectors, police control, traffic control, etc.) Since for preservation treatments the material costs are typically lower, these items may have a larger influence on the overall treatment cost. However, considering the yet scarce application of preservation treatments in Hawaii, there is still a need to develop cost estimates of preservation treatments. In section 8.4.3.6 (page 499) rough cost estimates for the City and County of Honolulu were used instead of the costs for HDOT because some very crude cost estimates for preservation treatments were available from the C&CH. It is important to point out that these were presented for illustration purposes only. Since they are based on some very crude assumptions, they may not represent HDOT's or C&CH's actual costs.

Recommendation 10: *(C) HDOT should perform a parametric study of treatment costs such that only periodic updating of the costs of the items effecting the treatments are needed to maintain them.*

9.1.2 Other issues

This project has concentrated for the most part on technical issues. However, it is recognized that proper consideration of non-technical issues may be as critical.

Recommendation 11: *(I) Staff dedicated to the PMS should be adequate for the tasks required. If possible, two engineers should be assigned to the PMS unit along with a proper level of technical assistance. It is recommended that those engineers work on the same office to minimize communication problems. Adequate training should be provided to the staff.*

Recommendation 12: *(I) The main activities of the PMS unit members should be related to the PMS needs. While the unit members may need to contribute to other activities such as pavement design, the main occupation should be on PMS activities such as quality assurance of condition data; updating of inventory, condition, and cost information; communication with stakeholders; development of plans; creation of reports, and overseeing research on PMS issues.*

Recommendation 13: *(I) Coordination and communication between stakeholders needs to be improved. As mentioned before, an area that appears to need improvement is in the coordination of the location referencing system used by different branches/districts.*

9.2 Pavement ME Design

Because of its nature, implementation of the Pavement ME Design guide (MEPDG) requires a significant amount of effort in terms of training and in terms of calibration for which the appropriate data need to be gathered and assembled. In this study, considerable progress has been made towards the calibration of the guide. As with the PMS efforts, the availability of data has limited what could be accomplished and therefore the calibration so far has been constrained to new HMA pavement sections. The following paragraphs summarize the major areas where advances have been made and provide recommendations for those areas where substantial work is still needed.

9.2.1 Traffic Loading

A large amount of data collected by the Planning Branch over the years for a limited number of WIM stations was analyzed and substantial progress was made on several aspects of this important input for ME design. Nevertheless, although the WIM data available in the state is voluminous, the criteria recommendations in the Traffic Monitoring Guide [15] to test the quality of selected truck weight ***groups*** cannot be applied because of the small number of WIM stations.

The axle load spectra (ALS) (or axle load weight distributions) for the different axle configurations (single, tandem, tridem, and quads) were obtained for vehicle classes 4 to 13 for individual stations. In addition, the data from seven stations with reliable information were used to obtain interpolated ALSs. Significant effort was put to clean the data by eliminating the information with potential calibration problems. The derived ALS (those that were identified as reliable) are believed to be adequate for the design of most state roadways.

Recommendation 14: *(I) For pavement designs performed with the Pavement ME Design software, use of the ALS derived in this study is recommended (see Table 3-21, page 98 for the recommended assignment of ALS to individual roadways).*

Clearly, most of the current WIM locations have been appropriately selected to capture heavy traffic loading in the islands. However, it would also be desirable to obtain weight information on locations that provide a greater geographic coverage. Currently, most stations with reliable data are located either on freeways or on roadways with some particular characteristics, such as access roads to ports (e.g., Station C202B on San Island Access Road), on roads with industrial traffic (e.g., Station 10W on Kalaeloa Blvd.), or roads with heavy bus traffic and weight loading (e.g., Station 438 on Ala Moana Blvd.) Unfortunately, no reliable information is currently available for the stations that could provide ALS on roadways with suspected lower traffic loadings such as Station 023 on the Likelike Hwy in Oahu or Station C12E on the Honoapiilani Hwy in Maui. With any new WIM deployments, it would be desirable to locate some stations that could provide axle loading information on the Windward and East side of Oahu, the Hilo side of Hawaii, as well as on the other islands.

Recommendation 15: *(D) With any new WIM station's deployment, consider locating some WIM stations at locations providing a larger geographic coverage so that more economical designs at locations with lower traffic loadings can be accomplished if appropriate.*

Although the ALS can always be improved, it is also necessary to look at other factors affecting the estimation of the number of load applications. The lane distribition factor (LDF) has not received much attention in the recent past for pavement design in Hawaii probably because its value is specified in the design procedure. However, use of unrealistic lane distribution factors can have almost as much of an adverse effect (over or under design of a pavement) as any other traffic loading input.

Currently, in some situations, the percentage of trucks in the design lane may be overestimated. The 2002 HDOT Pavement Design Manual [13] assumes 100% for 2 lanes in one direction, 80% for 3 lanes in one direction and 75% for 4 lanes in one direction. These values (particularly those for 3 and 4 lanes) appear to be extremely conservative. Values of percentage of trucks in the design lane based on the most recent WIM and AVC measurements (albeit limited) indicate that in general these values are too high. It must be recognized that many older design procedures used conservative values of many factors (including LDF) to provide a factor of safety. However, even in this case the values appear too conservative. Furthermore, in the MEPDG, the factor of safety is controlled by the reliability chosen for the design and thus average values should be used as input values.

Recommendation 16: *(I) Conduct a study of the data from automated vehicle classification stations on multi-lane highways and streets throughout the islands to improve the estimates of prevailing lane distribution factors for each vehicle class for use in pavement design.*

In the MEPDG, the lane distribution factor is defined by the primary truck class for the roadway, where the primary truck class is defined as "the truck class with the majority of applications using the roadway." Since this statement is vague, use of a more specific definition of predominant truck class is recommended.

Recommendation 17: *(I) For Hawaii, it is recommended to estimate what truck class has the most damaging power and use it as the predominant truck class. A simple way proposed here to estimate which vehicle class has the most damaging power is simply to multiply the percentage of vehicles in each class by the corresponding ESALC appropriate for the section and selecting the class with the largest product. In cases where the numbers for the two top classes are close (say, withing 20% of each other), an average of the lane distribution factors for those two classes could be used instead of simply selecting the one for the largest.*

A particularly useful quality assurance procedure to discriminate between potential calibration problems and actual seasonal changes in ALS was the observation of whether any temporal shifts in the distributions within a given year for a given axle/vehicle class combination or GVW were repeated for different vehicle classes and axle types on the same year. In particular, the comparison between the shifts in the distributions of class 9 vehicles (semi-trailers) and class 4 vehicles (buses) was extremely useful, with similar shifts indicating a potential calibration problem.

Recommendation 18: *(I) Use the comparison of the types of shifts in the ALS of the axles of buses and semitrailers (and other vehicle classes as appropriate) as a quality assurance procedure to identify data with WIM calibration issues.*

Although the literature presents extremely valuable suggestions for verifying the quality of WIM data, the application of some of the rules are sometimes subjective.

Recommendation 19: *(I) All WIM data quality controls need to be applied carefully as in Hawaii there appear to be many loading situations that do not conform to what is considered "normal". It is recommended that the procedures used in this report (which were based on judgment of the analyst helped with knowledge of local conditions and proper data visualization tools) are considered for further use. Completely automated procedures may discard substantial valid information and should be used with care.*

At some WIM stations, it was observed that the ALS had long tails to the right, which may indicate that there is a relatively high proportion of overloaded trucks crossing these stations.

Recommendation 20: *(I) Consider increasing weight limitation enforcement and limiting special weight permits since these measures can pay off substantially in terms of the reduction of maintenance costs.*

For some WIM stations, averaging the directional distributions would have only a modest effect on designs. For those stations, it is recommended to use the average of the directional ALS. However, for other stations the differences are so significant that separate consideration of the heavier loaded direction is warranted.

9.2.2 Material's Characterization

9.2.2.1 Dynamic Modulus

The two models currently used in the MEPDG for levels 2 and 3 (NCHRP 1-37A and NCHRP 1-40D) provide in general reasonable estimates of |E*| for those levels of analysis, although for the mixes analyzed in this study, the results appear to be biased.

A local model for predicting dynamic modulus (equations (6-12) to (6-16), page 261) estimated with data from State Mix IV is available to generate |E*| values for selected temperatures and frequencies as pseudo-level 1 input into the MEPDG. Relatively accurate results can be achieved with this model, which is based on local material characteristics. It also provides a better alternative to the use of level 2 or 3 inputs, which are based solely on gradation and binder characteristics.

Recommendation 21: *(C) For State IV mixes, use the locally developed model to generate pseudo-level 1 |E*| input values for designs with the Pavement ME. Since no local model has yet been estimated for other type of mixes, level 3 inputs (gradation and binder grade) need to be used for these.*

The above model was validated in this study with additional HMA specimens compacted and tested for dynamic modulus and permanent deformation. Since the aggregates were from a different quarry (Kapa'a instead of Makakilo) and the binder also changed from the old Tesoro PG 64-16 to the somewhat softer PG 64-22 supplied by Asphalt Hawaii (crude source: Saudi Arabia), small adjustments to two of the model parameters were needed. However, the model still replicates the mix behavior extremely well.

Recommendation 22: *(C) For new designs with State Mix IV, use the adjustments for the parameters δ and α of the local |E*| model developed in section 6.2.4.2.4.2 (page 275).*

The |E*| model is applicable to mixes prepared with unmodified and modified (with SBS or Elvaloy®) binders. It is also applicable to mixes prepared with Forta FI® HMA blend fibers. Since the source of the binder has changed once again (it is currently imported from Venezuela), it is likely that some additional small adjustments to some of the model parameters will be needed. Nevertheless, no dramatic changes are expected.

Recommendation 23: *(D) Perform further testing with the new source of binder to obtain corrections to the |E*| model parameters for State IV mixes. Perform testing with other commonly used mixes to obtain their master curve model parameters.*

More research is needed to develop models that determine |E*| as a function of confinement level since without confinement, the |E*| values at high temperatures and low frequencies of loading appear to be conspicuously low for some mixes. Another related issue is that all the |E*| testing is performed in compression, where the aggregate and the binder contribute to the modulus. However, in tension, the modulus is expected to be more dependent on the binder.

Recommendation 24: *(D) It is desirable that constitutive models for |E*| that account for the state of stresses (level of confinement) and the different moduli in compression and tension be developed.*

9.2.2.2 Resilient Modulus of Unbound Materials

For fine grained materials, the available resilient modulus information indicates that, all else equal, the resilient modulus of a Hawaiian fine grained soil is between 50% to 210% higher than that of a soil from the continental US with similar parameters (gradation, plasticity, voids ratio, etc.) In addition to the soil characteristics, the resilient modulus is significantly affected by moisture conditions and the state of stresses (which are in turn affected by the load level and the depth of layers above the subgrade). However, for input levels 2 and 3 (the only levels currently active for resilient modulus input in the Pavement ME Design software) the non-linearities due to the state of stresses are not considered. Furthermore, water table depth information in the State (which may have a significant effect on the computed adjustment for moisture conditions) is not currently available for calibration. Thus, important simplifications are needed to input resilient modulus in the MEPDG. Consequently, any input value is a compromise that provides a reasonable value of M_r at optimum conditions for different loading levels, HMA thickness and stiffness, etc. Thus, the following is recommended to select a reasonable input value for subgrade soils:

Recommendation 25: *(I) At this time, for those projects on which no other information can be obtained (either through sampling and FWD testing) it is recommended as a practical alternative for subgrade soils to use the NCHRP 9-23B website to obtain a first estimate of the resilient modulus and increase it by 100% (i.e., multiply by 2). The 100% increase with respect to continental US soils was found to be a reasonably good compromise value (see Section 6.3.1.2, page 287).*

Since base/subbase materials are typically subjected to higher state of stresses than subgrade soils, their resilient moduli are much more affected by the state of stresses than those of subgrades. However, for input level 3, the Pavement ME Design software (MEPDG) [2] still

requires the input of a single value of M_r. The user has the option of allowing the program to modify the value according to the temperature and moisture predictions or to use the value entered as an annual representative value. For input level 2, the software adds an option of entering monthly representative values instead of a single value. Unfortunately, not much information is currently available on monthly M_r changes. Clearly, there is no such thing as a single equivalent modulus for each layer that would produce the same effects for all types of distresses that one would want to predict. Thus, any value selected would be a compromise.

Based on the results of a large number of finite element simulations using resilient modulus parameters obtained from tests of local base/subbase materials, the following simplified procedure was used to determine a compromise input M_r value at optimum conditions for base/subbase materials. This simplified procedure accounts to some extent for the effect of the thickness of layers above the base and for the subgrade characteristics.

Recommendation 26: *(I) For bases/subbases, use a value of 12,000 psi for an HMA thickness of 16 inches or more, and add 2,000 psi for each 1-inch reduction in HMA thickness. Thus, for example, for a 10-inch HMA layer, the assumed modulus of the base at optimum is 12,000 psi + 2,000 psi/inch × (16 – 10) inch = 24,000 psi. This should produce values that are a reasonable approximation to the values corresponding to 100% compaction and optimum moisture content (in most situations, the values will be within the ranges observed in the finite element simulations in section 7.4.2.) When a subbase is present, add 3,000 psi to the Mr of the subbase to account for the usually higher confinement of this layer. Notice that subbases are more likely to be affected by moisture since they are closer to the water table. Thus, the slightly higher input modulus does not necessarily result in a higher modulus than that of the base when the simulations are performed with the MEPDG.*

The above simplified procedure provides values that are in general within the ranges simulated under the load with the finite element analysis at optimum. Note that for very thick HMA layers (say 12 to 16 inches) the input values range from 20,000 psi to 12,000 psi. These values are much lower than those recommended in the MEPDG Manual of Practice [22] (Table

6-13, page 319). However, they are more compatible with the larger scale results of Sagario [83], who tested RCA and RAP compacted in cross-linked polyethylene storage tanks 4-foot high and 3-foot diameter with a Portable Falling Weight Deflectometer. They also agree better with a few backcalculations results performed locally. Nevertheless, regardless of the ***input*** resilient modulus values, the MEPDG very quickly converges to a modulus corresponding to an "equilibrium". The reason is that it uses the EICM (Enhanced Integrated Climatic Model) to compute moisture and temperature changes throughout the design life. In most situations, the MEPDG will double the M_r values when the moisture transitions to dry of optimum. Note that even when doubled, the values for very thick layers are lower than those usually assumed. The values for thinner HMA layers are more in line with traditional recommendations (which were probably developed using data from older pavements that were in general thinner.) For example, for a 6-inch layer, the recommended value is 32,000 psi. Using the MEPDG Manual of Practice values and allowing the program to make corrections for moisture conditions results in values that are generally too high. If the MEPDG Manual of Practice recommended values are used, then the adjustment for environmental effects should be disabled.

Recommendation 27: *(C) If the MEPDG Manual of Practice recommended M_r values are used, then the option to adjust the modulus for environmental effects should be disabled.*

It must be noted that the procedure recommended here is only for HDOT unbound bases and it is very approximate since the state of stresses on a given unbound material element can vary widely depending on other factors such as the thickness of the HMA layer, stiffness of the HMA layer, stiffness parameters of other layers in the pavement, and thicknesses of other layers in the pavement. The suggested procedure gives some consideration to the thickness of HMA.

9.2.3 Calibration Effort For New Pavements

An effort was made to provide a first calibration of the MEPDG for new pavement segments. Even with the limited scope of the calibration attempt, the effort was challenging as some of the input information, such as resilient moduli of unbound materials, axle load spectra for each section, or even percentage of heavy trucks on the calibration lane are only approximate.

The AASHTO Guide for the Local Calibration of the Mechanistic-Empirical Pavement Design Guide [31] provides an 11-step procedure for local calibration, most of which could not be applied locally with the existing data. Thus, most of the effort was directed towards attempting to eliminate the bias and reduce the errors. The information was simply too limited to assess standard errors as indicated in one of the steps.

9.2.3.1 Rutting or Permanent Deformation

After several runs and together with the experiences with the development of the local permanent deformation model, the following calibration parameters were used: β_{r1} = 0.11, β_{r2} = 1, and β_{r3} = 1.35. In addition, the calibration parameter for unbound materials was set at β_{s1} = 0.01, which had the effect of significantly limiting the contribution of the unbound layers to rutting. Simulations with these calibration parameters provided reasonable predictions and a significant improvement over the predictions obtained with the initial runs without calibration.

Recommendation 28: *(C) For rutting use the calibration factors* β_{r1} *= 0.11,* β_{r2} *= 1, and* β_{r3} *= 1.35 for HMA layers and* β_{s1} *= 0.01 for unbound materials.*

A slight upward bias (overprediction) still remains as there are more points above the equality line than below. Although this bias could have been slightly reduced, this would have been at the expense of worsening the trends for each individual section. Nevertheless, the fit is considered acceptable given that the rut depth data is based on three sensors only and that the contribution to rutting from unbound layers has been limited substantially.

9.2.3.2 Fatigue Cracking

The Hawaii predictions using the global calibration factors were found to be biased downwards. Actual fatigue cracking values are much larger than predicted. Thus, modification of the parameters β_{1f}, β_{2f}, β_{3f}, C_1, and C_2 was evaluated.

Since changing the parameters by trial and error is extremely slow, a process was devised to perform the calibration using only the parameters β_{1f}, C_1 and C_2 with a single set of simulations. If modifications in parameters β_{2f} and β_{3f} are also needed, a combination of the proposed procedure with the trial and error process for these two parameters can be used. That is,

a single set of runs is needed for each combination of parameters β_{2f} and β_{3f}. Trial and error is needed to find the combination of β_{2f} and β_{3f} that results in the best fit when the other three parameters are obtained with optimization. Although the process in this case is a bit more involved, it can still decrease the number of trial and errors substantially.

Recommendation 29: *(I) The procedure developed in section 7.5.2 (page 395) is recommended for reducing the calibration effort. It requires a single set of runs with optimization to obtain the best fit if β_{1f}, C_1 and C_2 are used or a set of runs for each combination of β_{2f} and β_{3f} if all five parameters are used in the calibration process. The optimization can be constrained to produce a slope of 1 to eliminate the bias.*

Due to the data limitations, calibration has been attempted only with the use of parameters β_{1f}, C_1 and C_2. The calibration process resulted in β_{1f} = 1.188, C_1 = 0.571, and C_2 = 2.277. These values provide a significant improvement over the national global calibration fit. Nevertheless, similarly to other studies, a significant number of observations can be observed along one of the axes (the observed axis in this case). Furthermore, the slope of the regression line is 0.55, which indicates that the bias has not been eliminated completely.

Performing the calibration with a restriction on the slope of the fitted line resulted in β_{1f} = 0.771, C_1 = 0.686, and C_2 = 2.506 and an observed vs. predicted line almost indistinguishable from the 45° line. Eliminating the bias in this case was considered questionable since all that was gained was a theoretical unbiasedness at the expense of significantly more scatter. The calibration does not appear to really take care of the real reason behind the under prediction for some observations. For many sections in the sample, top-down rather than bottom-up fatigue cracking is suspected to be the mechanism for several reasons: 1) cracking usually appears longitudinally (which per se may be top-down or bottom-up) but it stays like that for a relatively long time. It rarely develops into a typical alligator cracking pattern; 2) there are certain combinations of moduli that may result in minimum principal strain distributions with maximum tensile strains near the top of the surface; and 3) some of the sections are simply very thick (about 13 inches of HMA with traffic loading that is apparently not too high.) Whether the

cracking on most of the problematic data points is top-down or not is yet unknown here. Thus, until more data are obtained for a more robust calibration, it is recommended to use the values β_{1f} = 1.188, C_1 = 0.571, and C_2 = 2.277.

Recommendation 30: *(I) Until more data is obtained for a more robust calibration, it is recommended to use the values β_{1f} = 1.188, C_1 = 0.571, and C_2 = 2.277.*

Calibration attempts were also performed using the top-down fatigue equations. Similar issues were confronted. Since at present there is uncertainty about the mechanism of cracking, these results are not presented.

Recommendation 31: *(I) It is recommended to perform forensic studies on different type of pavements (soon after cracking is first detected) to determine how cracking initiates so as to better guide its modeling.*

9.2.3.3 International Roughness Index (IRI)

Simulation runs with the default coefficients performed after calibration of the cracking and rutting models presented earlier and with a default IRI_0 = 63 (default value in the MEPDG) resulted in a substantial under-prediction of roughness. Since the global calibration of the MEPDG was performed with national data, these results indicate that most of the new pavements/reconstructions in the State are being built with considerable more roughness than in the mainland US.

There is a group of pavements that have substantially more roughness than expected (roughly 70 in/mile more than other sections). The only common feature that was identified for these sections is that, in general, they are fill sections with relatively important embankments. This may indicate that the specification, materials, and construction practices of this type of embankments may need to be evaluated further.

Recommendation 32: *(I) Further study is needed to determine the cause of the substantially higher roughness on fills and embankments. Specification, materials, and construction practice of high embankments may need to be evaluated further.*

The goal of the calibration is to obtain appropriate values of C_1, C_2, C_3, and C_4 (C_3 is irrelevant for Hawaii since no transverse cracking is predicted.) It is also desirable to obtain a reasonably representative value of IRI_0 to use in the simulations. However, IRI_0 is not available for every calibration section, which poses a challenge for calibration of C_1, C_2, and C_4. This challenge was overcome by minimizing the sum of squared residuals by varying the parameters C_1, C_2, and C_4 and simultaneously varying the values of IRI_0 for each section. Thus, in addition to the three parameters C_1, C_2, and C_4, an additional value was estimated for each section. It is important to note that the only goal of this exercise was to obtain unbiased estimates of C_1, C_2, and C_4. The estimated values were $C_1 = 0.323$, $C_2 = 23.1$, and $C_4 = 0.015$ (global factor).

Recommendation 33: *(I) Until more data is obtained for a more robust calibration, it is recommended to use the values $C_1 = 0.323$, $C_2 = 23.1$, and $C_4 = 0.015$.*

Then, IRI_0 values were estimated for two groups of pavements by minimizing the sum of squared residuals with the values of $C_1 = 0.323$, $C_2 = 23.1$, and $C_4 = 0.015$ and varying the IRI_0 value for each group. These resulted in $IRI_0 = 78.0$ in/mile for "normal" sections and $IRI_0 = 150.5$ in/mile for fill sections.

Note that $IRI_0 = 78.0$ in/mile is 15 in/mile higher than the default recommended value. This again, points out that for some reason the pavements in our State appear to have larger built-in roughness. For sections in fill, the values of $IRI_0 = 150.5$ in/mile is almost double the value for other sections, which as indicated before is something that needs to be investigated in more detail.

9.2.3.4 Top-Down Fatigue Cracking

It is suspected that top-down fatigue cracking may be the main mechanism of cracking on state roads with thick HMA layers.

The variation of the HMA modulus with depth has an important bearing on the strain distribution within the HMA layers and in turn on the location with the largest fatigue damage. Computations of stresses and strains within the pavement structure for different simulated temperature profiles and the frequency of loading as computed in the MEPDG (including the effect of binder aging) indicate that there are situations in which the HMA modulus increases with depth, which results in the greatest estimated damage occuring near the top of the HMA layer next to the tire. However, for the Hawaii weather stations, the MEPDG never predicts that the modulus increases with depth. The apparent contradiction may be explained by the fact the the MEPDG simulates only five temperature profiles corresponding to the 10^{th}, 30^{th}, 50^{th}, 70^{th}, and 90^{th} percentiles. Since the conditions leading to the modulus increasing with depth correspond to the hottest temperatures in the day, they are likely to be above the 90^{th} percentile. Thus, the MEPDG modeling may be too coarse to capture these conditions, which although they occur on less than 10% of the time, may be where most of the damage occurs. The predicted strains for the situations described are much larger than those at the bottom of the layer and so are the corresponding damages despite of the lower moduli.

In order to verify the hypothesis that top-down fatigue cracking may be induced by these strains at high temperatures, monitoring of actual pavement temperatures for a few sections is desirable.

Recommendation 34: *(D) It is desirable to instrument a few pavement sections to monitor the pavement temperatures with depth.*

If the above hypothesis about the effect of temperature is correct, then it would be desirable for the MEPDG to model the environmental effects more finely at high temperatures (for example including the 95^{th} and 98^{th} pavement temperature percentiles.

Another factor worth exploring is that the modulus of the HMA is different in tension and compression. All the strains calculations are currently performed assuming a single modulus

value for each sublayer. However, for HMA elements within the pavement structure subjected to tension in some direction, a different modulus should be used in that direction. Since elements may be subjected to compression in one of the principal directions and tension in another, different moduli may be needed in different directions for the constitutive modeling, leading to some form of anisotropy. This has the potential of significantly altering the distribution of stresses and strains within the pavement structure and it is worth exploring it further. The effect of confinement, which is known to affect dynamic modulus at high temperatures and low frequencies, should also be included in the constitutive modeling.

Recommendation 35: *(D) Perform an additional study to quantify the differences of the HMA modulus in tension and compression to develop a constitutive model and study the potential effect on top-down fatigue cracking using Finite Element Analysis.*

Other theories for predicting top-down fatigue cracking exist [118] that should also be considered.

9.2.3.5 General Observations

Because of data limitations, the calibration attempt has been limited to new HMA pavements. Significant challenges have been faced with the calibration for rutting, fatigue cracking, and roughness. This first calibration attempt presents some very promising results as it shows that predictions can be within reasonable ranges. Nevertheless, considerable work is still needed for regular use of the MEPDG.

In particular, it is imperative to obtain distress and FWD information for calibration of the rehabilitation procedures for HMA pavements.

Recommendation 36: *(C) Collect reliable distress and FWD information, together with conditions before rehabilitation, to calibrate the MEPDG for rehabilitation projects.*

For PCC pavements, faulting data should be collected over time, along with other other distresses so that calibration is possible. Several years are needed to determine faulting trends.

Recommendation 37: *(C) Collect faulting data over time for PCC pavements along with other distresses to make calibration possible.*

Reliable information for a larger sample of sections is needed to obtain standard error estimates. This may be challenging in the state for new HMA or PCC pavements. However, for HMA rehabilitation projects, it should be possible to obtain samples of adequate size. Good standard error estimates are needed for reliability analysis.

Recommendation 38: *(C) Collect reliable distress information for a larger number of rehabilitation projects (including the condition before rehabilitation) to allow the determination of standard error estimates for reliability analysis.*

In addition, based on the roughness information and video logs, it is believed that in some situations the construction date may be off by up to three years, which may have adversely influenced some of the predictions. For long projects, the construction date for different sections within the project may need to be different.

Recommendation 39: *(I) Improve the communication protocols to make sure that the construction dates are accurate within each section (as opposed to a whole project).*

One of the major features of the MEPDG is the prediction of the effects of environmental factors on pavement performance. In this respect, however, to take full advantage of the MEPDG it is desirable to develop information for new weather stations to account, for example, for the differences in weather (rain, cloud cover, wind, etc.) between the different sides of the islands. Furthermore, mapping water table depths could go a long way to improve the predictions of resilient moduli of unbound materials.

Recommendation 40: *(I) Perform an additional study to develop additional weather stations within the state to take advantage of the environmental modeling capabilities within the MEPDG.*

As described in section 7.4, non-linearities create substantial uncertainty in the selection of appropriate resilient moduli for design. This may be complicated even further with the wetting and drying that occurs with soils in practice. It would be desirable to perform a study of the resilient moduli of unbound materials and soils by varying the post-compaction moisture content (as opposed to compacting the materials at different moisture contents). This could help in guiding in the interpretation of backcalculation results, particularly if non-linearities are considered. Field backcalculation studies with different load levels are also desirable to determine the effect of non-linearities on the resilient modulus of bases.

Recommendation 41: *(D) Perform a study to evaluate the effect of post-compaction moisture changes on the resilient moduli of unbound materials.*

It would also be extremely important to conduct forensic studies on thick pavements with recently formed cracks to determine where they originate and also monitor pavement temperatures so as to validate or invalidate the belief that a significant proportion of the fatigue cracking observed in the State on pavements with thick HMA layers originates near the top of the HMA at relatively high temperatures.

Recommendation 42: *(I) Conduct forensic studies on thick pavements with recently formed cracks to determine where they originate and also monitor pavement temperatures so as to validate or invalidate the belief that a significant proportion of the fatigue cracking observed in the State on pavements with thick HMA layers originates near the top of the HMA at high temperatures.*

Finally, given all the uncertainties discussed in the previous sections, it is recommended to maintain most threshold values suggested by default in the MEPDG. Once pavement conditions are determined more accurately than currently done, these can be updated.

Recommendation 43: *(I) Use the following suggested distress thresholds: 2,000 ft/mi for top-down fatigue cracking, 20% of the lane area for bottom-up fatigue cracking, 0.5 in. for total permanent deformation, 0.4 in. for permanent deformation on HMA layers and 163 inches/mi for roughness on freeways and 200 inches/mi for roughness on other roads (no threshold is provided for thermal cracking as the MEPDG never predicts the presence of this distress for Hawaii's weather.)*

9.3 Suggested Modifications to the Current HDOT Design Procedure

It is recognized that due to the need for additional calibration efforts and the learning curve to implement the MEPDG the current HDOT pavement design procedure will continue to be used for some time. However, based on the results and/or analysis of this research a few changes are recommended.

9.3.1 Permeable Base

9.3.1.1 Permeable Base Material

The gradation of the 3-Fine material used for several mixes in the State was identified as a potential alternative gradation for permeable bases since it meets the widely used Wisconsin Open Graded Base Course gradation. The 3-Fine material provides a slightly softer support than conventional bases but the differences do not appear to be substantial. Of course, with the 3-Fine material M_r is likely to change little with changes in moisture (if the base is material is kept free from intrusion of fines) but the conventional base material M_r would tend to increase significantly dry of optimum and decrease wet of optimum. In addition, the permeability values observed during laboratory tests of the 3-Fine material ranged between 36,000 and 140,000 ft/day, well above the minimum values recommended by the HDOT current design guide. This indicates that the material tested is extremely permeable.

Recommendation 44: *(I) Consider the 3-Fine base material produced at the local quarries as an alternative unbound permeable base material.*

9.3.1.2 Permeable Layer Need

The 2002 HDOT pavement design manual [13] essentially requires a permeable layer for all pavements with the exception of locations with rainfall less than 5 inches or where the basement soil is free draining (a permeability greater than or equal to 100 ft/day). Other exceptions must be justified in the structural section submittal.

On the other hand, the MEPDG provides different recommendations about the need of subdrainage for four different climatic zones of the country. Much of Hawaii falls within the Wet-No freeze climatic conditions defined in the MEPDG (Annual precipitation > 508 mm (20 in) and annual freezing index ≤ 83 °C-days (150 °F-days)). For these conditions, the MEPDG provides the recommendations in Table 6-22. These are less restrictive than the current HDOT requirements and leave more room to the designer to determine when a permeable layer is needed.

Recommendation 45: *(I) With respect to the need for a permeable layer, it is recommended to adopt the MEPDG guidelines in reference [1] (see Table 6-22, page 349), which relax the requirements of the current pavement design guide but still require a drainage layer for the conditions when it can be most cost-effective. The MEPDG also indicates that additional factors must be considered in the decision for installing permeable bases over subgrades with higher permeability. The requirement of permeable over lava flow formations should be maintained.*

9.3.1.3 Minimum Permeable Base Layer Thickness

The Hawaii Pavement Design guide currently requires a minimum of 6” of permeable base over a geotextile *permeable* separator on a 6” granular material layer to protect the permeable layer from infiltration of fines from the subgrade. In contrast, the design guides of several states (e.g., CA, FL, and MO) do not use a variable thickness of the drainage layer but rather a fixed value governed by local experience and constructability issues. Based on drainage analyses, the MEPDG recommends 4 inches as an appropriate permeable base layer thickness (maximum and minimum), allowing compaction without segregation while providing an acceptable hydraulic conduit. This justification makes good engineering sense and it is practical.

Recommendation 46: *(D) Selection of an appropriate minimum thickness should depend on the material used for constructing the permeable layer. Untreated permeable bases (UPB) with gradations in accordance with current Section 306 of the Hawaii Standard Specifications for Roads and Bridge Construction should be constructed with a thickness of 6 inches to accommodate the large aggregate sizes. For other materials with maximum aggregate sizes of 1 inch or less, a thickness of 4 inches is recommended.*

In order to address recommendation 46, it is recommended to change item *f* of page 25 of the current HDOT design procedure [13] to the following:

"If a permeable base is required, it shall have a minimum thickness of 4 inches and a maximum of 6 inches. A layer thickness of 6 inches is recommended only for materials meeting the grading requirements of Table 703.04-2 of the Hawaii Standard Specifications for Road and Bridge Construction to accommodate their large particles sizes. A thickness of 4 inches is recommended for other permeable base gradations with maximum aggregate size of 1" or smaller. Since the permeable base material is usually relatively unstable, the alternative with a 4" thickness may be more desirable."

Recommendation 47: *(D) The previous practice of fixing the subbase to a thickness of 6 inches and designing a drainage layer to absorb as much water as it can infiltrate the pavement surface is discouraged since the additional permeable material may lead to stability problems and not much benefit is obtained in terms of time-to-drain.*

In order to address this recommendation, it is recommended to change items *g* and *h* of page 25 of the current HDOT design procedure [13] to:

"When aggregate subbase or aggregate base is used as a granular layer separating the permeable base from the basement soil, the R-value of the aggregate subbase or aggregate base shall be the same as the permeable base (i.e, 55). In such cases, the thickness of the base/subbase in terms of GE is determined by subtracting the GE contribution of the permeable base (1.1 ×

t_{UPB}/12 for UPB or 1.4 × t_{TPB}/12 for treated permeable base) from the gravel equivalent required to protect the subgrade ($GE = 0.0032\ TI\ (100 - R_{subgrade})$)".

9.3.2 Structural Design

It is suggested to use the most up-to-date traffic loading information. Suggested ESALC derived in this study were presented in Table 3-24 (page 104) of section 3.6.2. Except for those road sections with more detailed WIM data for which more representative ESALC are available (as presented in Table 3-20, page 95), it is suggested to use the values of Table 3-24 (page 104) as a reasonable compromise. As discussed in section 3.6.2 (page 102), the use of the different ESALC can result in different in thicknesses of about 10%.

Recommendation 48: *(I) Use the ESALC presented in Table 3-24 (page 104) of section 3.6.2, except for those road sections for which WIM data are available in Table 3-20, page 95.*

As indicated in Section 3.7 (page 104), the Design Lane Factors in the current HDOT design procedure (commonly known as the Lane Distribution Factor or LDF) appear to be too conservative for multilane highways. It is suggested instead to use the values in Table 3-26 (page 109) for design when field data collection is not possible or when AVC data are not available. These LDF or Design Lane Factor values represent a compromise between the highly conservative values in the current HDOT design procedure [13] and the values in the MEPDG.

Recommendation 49: *(I) Use the Design Lane Factors or LDFs in Table 3-26 (page 109).*

9.4 Implementation of Pavement ME Design

Substantial progress has been made towards the calibration of the MEPDG, particularly for new pavement sections, but more work is still required on the overlay procedures and on PCC pavement designs for its full implementation. Thus, the old design procedure is expected to continue to be used for some time.

Implementation of the MEPDG will take considerable effort in terms of training and additional calibration. Thus, it is desirable for HDOT personnel to start learning it to familiarize themselves with the interface, procedures, and outputs. After training of the personnel in the use of the Pavement ME software, it is recommended to continue using the HDOT design procedure in tandem with the Pavement ME software for selected sections. These sections, for which there would be available detailed input information during the design phase (subgrade information, water table depth, base/subbase characteristics, etc.), should be carefully monitored (i.e., collecting distress information over time) to obtain the data necessary for re-calibration of the MEPDG prior to its adoption as the primary design method. This, should produce several desirable results. 1) HDOT personnel would get familiar with the Pavement ME software without the risk of designing subpar structures due to the change in design procedure; 2) detailed material, traffic, and performance data would be generated for a better calibration of the guide (for new and rehabilitated sections); and 3) gaining confidence in the use of the MEPDG will allow its use for the evaluation of new materials.

Recommendation 50: *(C) In order to transition to the use of the Pavement ME design procedure, it is recommended to use the HDOT and Pavement ME design procedures in tandem for several years so that detailed data are generated for a re-calibration and so that the personnel is thoroughly familiar with its use before the transition is completed.*

REFERENCES

[1] NCHRP 1-37A, "Guide for Mechanistic-Empirical Design of New and Rehabilitated Pavement Structures," National Cooperative Highway Research Program, Champaign, Illinois, 2004.

[2] AASHTO, "AASHTOWare Pavement ME Design," 29 June 2013. [Online]. Available: http://www.darwinme.org/MEDesign/Index.html.

[3] R. Haas, W. R. Hudson and J. Zaniewski, Modern Pavement Management, Malabar, Florida: Krieger, 1994.

[4] K. Zimmerman, "Pavement Management Systems Workshop," in *International Road Federation Asia-Pacific Regional Meeting*, 1996.

[5] K. McPherson and C. Bennett, "Success Factors for Road Management Systems," The World Bank, Washington, D.C., 2005.

[6] W. Patterson and T. Scullion, "Information Systems for Road Management: Draft Guidelines for System Design and Data Issues," The World Bank, Washington, D. C., 1990.

[7] M. Shahin, Pavement Management for Airports, Roads, and Parking Lots, 2nd Edition, Norwell, Massachusetts: Springer, 2005.

[8] Hawaii Department of Transportation, "Pavement Preservation Technical Appraisal, Hawaii Executive Summary," 2009.

[9] FHWA, Highway Performance Monitoring System - Field Manual, March 2013 ed., U.S. Department of Transportation, Federal Highway Administration, Office of Highway Poliicy Information, 2013.

[10] D. Walker, Pavement Surface Evaluation and Rating - PASER Manual - Asphalt Roads, Transportation Information Center, University of Wisconsin-Madison, 2002.

[11] A. R. Archilla and L. G. Diaz, "Development of an Inventory Processing Tool to Generate Historical Pavement Structural Information," *Proceedings of the 8th International Conference on Managing Pavement Assets*, November 2011.

[12] AASHTO, Guide for Design of Pavement Structures, Washington, D.C.: American Association of State Highway and Transportation Officials, 1993.

[13] HDOT, Pavement Design Manual, Revision March 2002, Honolulu, Hawaii: Department of Transportation, Highways Division, Materials Testing and Research Branch, 2002.

[14] R. Quinley, "WIM Data Analyst's Manual," Federal Highway Administration, Office of Pavement Technology, U.S. Department of Transportation, 2010.

[15] USDOT, "Traffic Monitoring Guide," U.S. Department of Transportation, Federal Highway Administration, Office of Highway Policy Information, Washington, D.C., 2001.

[16] NCHRP, "Traffic Data Collection, Analysis, and Forecasting for Mechanistic Pavement Design," National Cooperative Highway Research Program, Washignton, D.C., 2005.

[17] HRS §291-35, "www.capitol.hawaii.gov," 12 July 2013. [Online]. Available: www.capitol.hawaii.gov/hrscurrent/Vol05_Ch261-0319/HRS0291/HRS_0291-0035.htm.

[18] C&CH, "The Bus Fast Facts," City and County of Honolulu Department of Transit Services/Oahu Transit Services, 2013. [Online]. Available: www.thebus.org/AboutTheBus/TheBusFacts.pdf. [Accessed 12 July 2013].

[19] FTA, "Study & Report to Congress: Applicability of Maximum Axle Weight Limitations to Over-the-Road and Public Transit Buses," 2003.

[20] Metro, 12 July 2013. [Online]. Available: www.ctha.org/Rosters/Go-Metro/Gillig/C27D102N4.asp.

[21] PTI, "Partial STURAA Test, 12 Year 500,000 Mile Bus," 2002.

[22] AASHTO, Mechanistic-Empirical Pavement Design Guide - A Manual of Practice, Vols. July 2008, Interim Edition, American Association of State Highways and Transportation Officials, 2008.

[23] M. Sayers, T. Gillespie and C. Queiroz, "The International Road Roughness Experiment: Establishing Correlation and a Calibration Standard For Measurements.," World Bank Technical Paper No. 45., 1986.

[24] The Transtec Group, Inc., "PROVAL 3 User's Guide," 2013.

[25] F. Thomas, A Bayesian Approach to Retrospective Detection of Change-points in Road Surface Measurements, Stockholm: Doctoral Dissertation, Department of Statistics, Stockholm University, SE-106 91, 2001.

[26] F. Thomas, "Statistical Approach to Road Segmentation," *ASCE Journal of Transportation Engineering, Vol. 129, No. 3.*, pp. 300-308, 2003.

[27] F. Thomas, "Automated Road Segmentation Using a Bayesian Algorithm," *ASCE Journal of Transportation Engineering, Vol. 131, No. 8.* , pp. 591-598., 2005.

[28] J. Miller and W. Bellinger, "Distress Identification Manual for the Long-Term Pavement Performance Porgram," Office of Infrastructure Research and Development, Federal Highway Administration, 6300, Geogetown Pike, McLean, VA 22101-2296, 2003.

[29] G. R. Rada, C. L. Wu, R. K. Bhandari, A. R. Shekharan, G. E. Elkins and J. S. Miller, "Study of LTPP Distress Data Variability, Volume I," 6300 Georgetown Pike, McLean, Virginia 22011-2296, 1999.

[30] FHWA, "Variability in Pavement Distress Data From Manual Surveys," Turner Fairbank Highway Research Center, 6300 Georgetown Pike, McLean, Virginia 22101-2296, 2000.

[31] AASHTO, "Guide for the Local Calibration of the Mechanistic-Empirical Pavement Design Guide," American Association of State Highway and Transportation Officials, 2010.

[32] P. Fu, J. Harvey, J. Lee and P. Vacura, "New Method for Classifying and Quantifying Cracking of Flexible Pavements in Automated Pavement Condition Survey," *Transportation Research Record: Journal of the Transportation Research Board, No. 2225*, pp. pp. 99-108, 2011.

[33] J. Laurent, J. Hérbert, D. Lefebvre and Y. Savard, "Using 3D Laser Profiling Sensors for the Automated Measurement of Road Surface Conditions," in *7th RILEM International Conference on Cracking in Pavements: Mechanisms, Modeling, Testing, Detection and Prevention Case Histories*, 2012.

[34] Y. H. Huang, Pavement Analysis and Design, 2nd Edition, New Jersey: Prentice Hall, 2004.

[35] R. B. Mallick and T. El-Korchi, Pavement Engineering - Principles and Practice, Second Edition, Boca Raton, Florida: CRC Press, Taylor & Francis Group, 2013.

[36] A. T. Papagiannakis and E. A. Masad, Pavement Design and Materials, Hoboken, New Jersey: Johm Wiley & Sons, Inc., 2008.

[37] NCHRP, "NCHRP 09-29 - Simple Performance Tester for Superpave Mix Design," 2011. [Online]. Available: http://apps.trb.org/cmsfeed/TRBNetProjectDisplay.asp?ProjectID=963.

[38] R. Bonaquist, "NCHRP Report 614: Refining the Simple Performance Tester for Use in Routine Practice," National Cooperative Highway Research Program, Transportation Research Board, Washington, D.C., 2008a.

[39] R. Bonaquist, "NCHRP Report 629: Ruggedness Testing of the Dynamic Modulus and Flow Number Tests with the Simple Performance Tester.," National Cooperative Highway Research Program, Transportation Research Board, Washington, D.C., 2008b.

[40] W. Abd-Elaziz Zeiada, K. Kaloush, K. Biligiri, J. Reed and J. Stempihar, "Significance of confined dynamic modulus laboratory testing for asphalt concrete: Conventional, gap-graded, and open graded mixtures.," *Transportation Research Record 2210: Journal of the Transportation Research Board*, pp. 9-19, 2011.

[41] AASHTO, *Standard Method of Test for Determining the Dynamic Modulus and Flow Number of Hot Mix Asphalt (HMA) Using the Asphalt Mixture Performance Tester (AMPT).*, American Association of State Highways and Transportation Officials, 2012.

[42] AASHTO, *Standard Method of Test for Determining Dynamic Modulus of Hot Mix Asphalt (HMA).*, American Association of State Highways and Transportation Officials., 2011.

[43] Abatech, "Rheology Analysis Software Users Manual," Abatech Inc. Blooming Glen, PA (2011), 2013. [Online]. Available: http://www.abatech.com/documents/RHEA%20Manual%201%202011.pdf. [Accessed 28 May 2013].

[44] L. G. Diaz and A. R. Archilla, "An Easy Way to Use and Interpret the Results from the Asphalt Mixture Performance Tester," *International Journal of Pavement Research and Technology*, p. (forthcoming), 2013.

[45] A. R. Archilla, "Developing Master Curve Predictive Equation Models for Local Conditions: A Case Study for Hawaii," *Journal of the Association of Asphalt Paving Technologists,* vol. 79, pp. 325-362, 2010.

[46] A. Archilla, "Effect of Polymer Modified Asphalt Binders on the Performance of Asphalt Concrete Mixes Used in Hawaii," Honolulu, 2008.

[47] J. K. Rayapeddi Kumar, "Material Characterization in Support of the Implementation of the Mechanistic-Empirical Pavement Design Guide," Honolulu, 2012.

[48] J. Bari and M. Witczak, "Development of a New Revised Version of the Witczak E* Predictive Development of a New Revised Version of the Witczak E* Predictive Model for Hot Mix Asphalt Mixtures," *Journal of the Association of Asphalt Paving Technologists,* vol. 75, pp. 381-424, 2006.

[49] J. Bari and M. Witczak, "New Predictive Models for Viscosity and Complex Shear Modulus of Asphalt Binders For Use with Mechanistic-Empirical Pavement Design Guide," *Transportation Research Record: Journal of the Transportation Research Board, Transportation Research Board of the National Academies,* vol. 2001, pp. 9-19., 2007.

[50] A. R. Archilla, L. de Lannoy Kobayashi and L. G. Diaz, "Using Permanent Deformation Tests and the MEPDG to Quantify Permanent Deformation Improvements from Modified Binders," *Journal of the Association of Asphalt Paving Technologists,* vol. 77, pp. 1005-1036, 2008.

[51] Asphalt Institute, "Quantification of the Effects of Polymer-Modified Asphalt for Reducing Pavement Distress," Asphalt Institute, 2005.

[52] A. R. Archilla and L. G. Diaz, "Effects of Asphalt Mixture Properties on Permanent Deformation Response," *Transportation Research Record: Journal of the Transportation Research Board, No. 2210,* pp. 1-8, 2011.

[53] M. Thompson, S. Baremberg, S. Brown, M. Wilson, M. Darter, G. Larson, M. Witczak and M. El-Basyouny, "Independent Review of the Mechanistic-Empirical Pavement Design Guide and Software," *Research Results Digest 307,* 2006.

[54] D. Li and E. T. Selig, "Resilient modulus for fine-grained subgrade soils.," *Journal of Geotechnical Engineering, Vol. 120, No. 6,* pp. 939-957, 1994.

[55] P. S. Ooi, A. R. Archilla and K. G. Sandefur, "Resilient Modulus Models for Compacted Cohesive Soils," *Transportation Research Record: Journal of the Transportation Research Board. No. 1874.,* pp. 115-124, 2004.

[56] FHWA, "Study of LTPP Laboratory Resilient Modulus Test Data and Response Characteristics: Final Report.," 2002.

[57] K. George, "Prediction of Resilient Modulus from Soil Index Properties.," 2004.

[58] S. Hossain, "Characterization of Subgrade Resilient Modulus for Virginia Soils and Its Correlation with the Results of Other Soil Tests.," Report No. VTRC 09-R4. Virginia Transportation Research Council, VA, 2008.

[59] A. G. Heydinger, Q. L. Xie, B. W. Randolph and J. D. Gupta, "Analysis of Resilient Modulus of Dense and Open-graded Aggregates.," *Transportation Research Record: Journal of the Transportation Research Board, National Research Council, National Research Council, Washington, D.C., No. 1547,* pp. 1-6., 1996.

[60] T. Bennert and A. Maher, "The Development of a Performance Specification for Granular Base and Subbase Material," New Jersey Department of Transportation, Final Report, Project FHWA-NJ-2005-003, 2005.

[61] Y. Song, "Testing and Analysis of Recycled Materials for Highway Projects," Ph.D. Dissertation, University of Hawaii at Manoa, Honolulu, 2009.

[62] P. Ooi, A. Archilla and Y. S. M. Song, "Application of Recycled Materials in Highway Projects," Final Report prepared for the Hawaii Department of Transportation, Highways Division, Honolulu, 2010.

[63] D. Stolle, P. Guo and L. Y., "Unbound Resilient Modulus Testing of Granular Base, Subbase Materials in Ontario," Ontation Ministry of Transportation, Provincial Highways Management Division Report HIIFP-033, 2005.

[64] J. Mitchell and N. Sitar, "Engineering Properties of Tropical Residual Soils," *Proc., Engineering and Construction in Tropical Residual Soils, ASCE,* pp. 30-57, 1982.

[65] Sandefur, K.G, "Correlation of Resient Modulus, Mr, of Fine-Grained Soils with Common Soil Parameters for Use in Design of Flexible Pavements," M.S. Thesis, University of Hawaii at Manoa, Honolulu, 2003.

[66] S. Alavi, T. Merport, J. Wilson, J. Groeger and A. Lopez, "LTPP materials characterization program: resilient modulus of unbound materials (LTPP Protocol P46) laboratory startup and quality control procedure.," Report No. FHWA-RD-96-176, U.S. Department of Transportation, Federal Highway Administration, McLean, Virginia, 1997.

[67] A. R. Archilla, P. S. Ooi and K. G. Sandefur, "Estimation of a Resilient Modulus Model for Cohesive Soils Using Joint estimation and Mixed Effects," *Journal of Geotechnical and Geoenvironmental Engineering, Vol. 133, No. 8,* pp. 984-994, 2007.

[68] C. Zapata and C. Cary, "Integrating The National Database of Subgrade Soil-water Characteristic Curves and Soil Index Properties with the MEPDG," National Cooperative Research Program, NCHRP Project No. 9-23B, Arizona, 2012.

[69] A. Yau and H. von Quintus, "Predicting Elastic Response Characteristics of Unbound Materials and Soils.," *Transportation Research Record 1874, Transportation Research Board of the National Academies,* pp. 47-56, 2004.

[70] F. Akeroyd and B. J. Hicks, "Foamed Bitumen Road Recycling.," *Highways,* vol. 56, no. 1933, pp. 42, 43, 45, 1988.

[71] D. Munar-Castaneda, *Study of Fatigue Performance of a Mixture with Unmodified and Polymer-Modified Asphalt,* Honolulu: M.Sc. Thesis, University of Hawaii at Manoa, 2009.

[72] R. Lundstrom, H. Di Benedetto and U. Isacsson, "Influence of Asphalt Mixture Stiffness on Fatigue Failure," *Journal of Materials in Civil Engineering, ASCE,* vol. 16, no. 6, 2004.

[73] L. Diaz and A. Archilla, "Effect of Laboratory Data Range Selection in Permanent Deformation Characterization of Asphalt Mixtures," *Transportation Research Record: Journal of the Transportation Research Boad, N. 2057, Transportation Research Board of the National Academies,* pp. 126-133, 2008.

[74] A. Archilla, L. de Lannoy Kobayashi and L. Diaz, "Using permanent deformation tests and the MEPDG to quantify permanent deformation improvements from modified binders.," *Journal of the Association of Asphalt Paving Technologists,* vol. 77, pp. 1005-1035, 2008.

[75] K. Hall and J. Crovetti, "Effects of Subsurface Drainage on Pavement Performance: Analysis of the SPS-1 and SPS-2 Field Sections," National Cooperative Highway Research Program, Washington, D.C., 2007.

[76] K. T. Hall and J. Crovetti, "Performance of Drained and Undrained Flexible Pavements in the LTPP SPS-1 Experiment," in *86th Annual Meeting of the Transportation Research Board, Compendium of Papers CD-ROM*, Washington, D.C., January 21-25, 2007.

[77] B. Christopher, "Maintenance of Highway Edgedrains," National Cooperative Highway Research Program, 2000.

[78] ERES Consultants, Inc., "Pavement Subsurface Drainage Design—Reference Manual," Federal Highway Administration, Washington D.C., 1999.

[79] HDOT, "Hawaii Standard Specifications and Special Provisions for Road and Bridge Construction," Hawaii Department of Transportation, 2005.

[80] FHWA, "Drainable Pavement Systems – Participant Notebook, Demonstration Poject 87," U.S. Department of Transportation, Federal Highway Administration, 1992.

[81] H. L. Von Quintus and B. M. Killingsworth, *Design Pamphlet for the Backcalculation of Pavement Layer Moduli in Support of the Guide for the Design of Pavement Structures (AASHTO 1993)*, McLean, VA: Federal Highway Adminstration, 1997, a..

[82] H. L. Von Quintus and B. M. Killingsworth, "Design Pamphlet for the Determination of Design Subgrade Modulus in Support of the Guide for the Design of Pavement Structures (AASHTO, 1993)," McLean, VA, 1997, b.

[83] M. Sagario, "Assessing the Compactability of Recycled Concrete Aggregate and Reclaimed Asphalt Pavement," University of Hawaii at Manoa, Honolulu, 2009.

[84] H. Von Quintus and B. Killingsworth, "Analyses Related to Pavement Material Characterization and Their Effects on Pavement Performance," Federal Highway Adminstration, 6300 Georgetown Pike, McLean, VA, 1998.

[85] D. Timm, X. Guo, M. M. Robbins and C. Wagner, "M-E Calibration Studies at the NCAT Test Track," *Asphalt Pavement Magazzine*, pp. 45-51, September/October 2012.

[86] M. Darter, J. Mallela, L. Titus-Glover, C. Rao, G. Larson, A. Gotlif, H. Von Quintus, L. Khazanovich, M. Witczak, M. El-Basyouny, S. El-Badawy, A. Zborowski and C. Zapata, "Changes to th Mechanistic-Empirical Design Guide Software Through Version 0.900, July 2006," Transportation Research Board of the National Academies, 2006.

[87] I. Al-Qadi, W. Xie and M. Elseifi, "Frequency Determination from Vehicular Loading Time Pulse to Predict Appropriate Complex Modulus in MEPDG," *Journal of the Association of Asphalt Paving Technologists,* vol. 77, pp. 739-772, 2008.

[88] AASHTO, "Pavement Management Guide," American Association of Transportation Officials., Washington, D.C., 2001.

[89] A. Wolters, K. Zimmerman, K. Schattler and A. Rietgraf, "Implementing Pavement Management Systems for Local Agencies - State-of-the Art/State-of-the-Practice," Illinois Center for Transportation, Springfield, Illinois, 2012.

[90] G. Hicks, S. B. Seeds and D. Peshkin, "Selecting a Preventive Maintenance Treatment for Flexible Pavements," Foundation for Pavement Preservation, 2000.

[91] Asphalt Institute, "The Asphalt Handbook," Asphalt Institute (2007), 2007.

[92] A. Johnson, "Best Practices Handbook on Asphalt Pavement Maintenance," Minnesota Technology Trasfer (T2) Center/LTAP Program, Center for Transportation Studies, University of Minnesota, Minneapolis, Minnesota., 2000.

[93] MDOT, "Sealing and Filing of Cracks for Bituminous Concrete Pavements – Selection and Installation Procedures," Michigan Technological University in cooperation with the Michigan Department of Transportation., 1999.

[94] Deighton, Deighton, [Online]. Available: http://www.deighton.com/dtims.html. [Accessed 10 10 2013].

[95] Agile Assets, "Pavement Analyst | Advanced Pavement Management Systems (PMS) and Analysis Software," Agile Assets, [Online]. Available: http://www.agileassets.com/products/pavement-analyst/. [Accessed 26 October 2013].

[96] University of Birmingham, Highways Management Research Group,, "HDM-4 Technical Manual," Birmingham, UK, 1999.

[97] US Department of Transportation - Federal Highway Administration, "HERS-ST Highway Economic Requirements System - State Version," 2013. [Online]. Available: http://www.fhwa.dot.gov/infrastructure/asstmgmt/hersindex.cfm. [Accessed 12 2013].

[98] US Department of Transportation - Federal Highway Adminstration , "HERS-ST - Highway Economic Requirement Systems - State Version - User's Guide," Washington, D.C., 2009.

[99] US Department of Transportation - Federal Highway Adminstration, "HERS-ST: Highway Economic Requirements System - State Version - Technical Report," Washington, D.C., 2005.

[100] Metropolitan Transportation Commission., "StreetSaver Products, Regional Streets and Roads Program, 2003-2013," 2013. [Online]. Available: www.mtcpms.org/products/index.html. [Accessed 15 11 2013].

[101] MTU, "Roadsoft(R)," Michigan Technological University, [Online]. Available: http://roadsoft.org. [Accessed 30 11 2013].

[102] State of Hawaii - Office of Planning, "Hawaii Statewide GIS Program," [Online]. Available: http://planning.hawaii.gov/gis/download-gis-data/. [Accessed 30 11 2013].

[103] Colorado State University, "PAVER," [Online]. Available: http://www.paver.colostate.edu/upcoming.php. [Accessed 23 December 2013].

[104] K. McGhee, "Automated Pavement Distress Collection Techniques," National Cooperative Highway Research Program, Washington, D.C., 2004.

[105] A. Archilla, "Report on Pavement Management Practices - Adaptation of MicroPAVERTM (or PAVERTM) Input Parameters (and Guidelines) for the City and County of Honolulu," Honolulu, 2013.

[106] M. Shahin, W. Welborn, L. Hammond, S. Kim, R. Meisel, L. Cerda and S. Franzen, "User Manual – PAVERTM 6.5," US Army Corps of Engineers, Engineer Research and Development Center, Construction Engineering Research Laboratory, USACE., 2012.

[107] M. Shahin and J. Walthers, "Pavement Maintenace Management For Roads and Streets Using the PAVER System," Construction Engineering Research Laboratory, U.S. Army Corps of Engineers, 1990.

[108] CALTRANS, "Flexible Pavement Preservation Second Edition: Maintenance Technical Advisory Guide (MTAG) Volume I, Chapter 5 – Patching and Edge Repair," 2007.

[109] FHWA, "Long-Term Monitoring of Pavement Maintenance Materials Test Sites," McLean, VA, 1998.

[110] T. Wilson and A. Romine, "Materials and Procedures for Repair of Potholes in Asphalt-Surfaced Pavements – Manual of Practice," 6300 Georgetown Pike, McLean, Virginia 22101-2296, 1999.

[111] R. Wolters, "Repair of Potholes with Hot Mix Asphalt (HMA)," Minnesota Asphalt Pavement Association, 2003.

[112] T. Kuennen, "The Pothole Patching Playbook - Why potholes occur, how to patch them, and how to prevent them in the first place.," *Better Roads,* February 2004.

[113] K. Smith and A. Romine, "Materials and Procedures for Sealing and Filling Cracks in Asphalt-Surfaced Pavements – Manual of Practice," Strategic Highway Research Program, National Research Council, Transportation Research Board of the National Academies, Washignton, D.C., 1993.

[114] Y. Yildirim, A. Qatan and J. Prozzi, "Field Manual for Crack Sealing in Asphalt Pavements," 2006.

[115] D. Orr, "Pavement Maintenance, Cornell Local Roads Program, Ithaca, New York," 2006. [Online]. Available: www.clrp.cornell.edu/workshops/pdf/pavement_maintenace-web.pdf.

[116] HAPI, "HAPI Asphalt Pavement Guide," Hawaii Asphalt Pavement Industry, 2013. [Online]. Available: http://www.stmuench.com/modules/11_maint-rehab/11_maintenance.htm. [Accessed March 2013].

[117] Nebraska Department of Roads, "Pavement Maintenance Manual," 2002.

[118] R. Roque, J. Zou, Y. Kim, C. Baek, S. Thirunavukkarasu, B. Underwwod and M. Guddati, "Top Down Cracking of Hot-Mix Asphalt Layers; Models for Initiation and Propagation," February 2010. [Online]. Available: http://onlinepubs.trb.org/onlinepubs/nchrp/nchrp_w162.pdf. [Accessed 28 12 2013].

[119] B. Christopher and V. McGuffey, "Pavement Subsurface Drainage Systems," NCHRP Synthesis 239, A Synthesis of Highway Practice, Transportation Research Board, National Research Council, 1997.

[120] J. Mallela, L. Titus-Glover and M. Darter, "Considerations for Providing Subsurface Drainage in Jointed Concrete Pavements," Transportation Research Record 1709, Transportation Research Board of the National Academies, 174–180, 2000.

[121] B. Christopher, "Maintenance of Highway Edgedrains," NCHRP Synthesis of Highway Practice 285, National Cooperative Highway Research Program, 2000.

[122] T. Kuennen, "Making edge drains work : base edge drains can enhance pavement life - but only if you maintain them," *Better Roads, Volume 73, Issue 1*, 2003 .

[123] E. Harrigan, "NCHRP Research Results Digest Number 268 (Summary of key findings from NCHRP Project 1-34 "Performance of Subsurface Pavement Drainage")," National Cooperative Research Program, 2002..

[124] B. Diefenderfer, K. Galal and D. Mokarem, "Effect of Subsurface Drainage on the Structural Capacity of Flexible Pavement," Report VTRC 05-R35, Virginia Department of Transportation., 2005.

[125] M. Darter, H. Von Quintus, Y. Jiang, E. Owusu-Antwi and B. Killingsworth, "Catalog of Recommended Pavement Design Features," National Cooperative Highway Research Program, NCHRP Project 1-32, Washington, D.C., 1997.

[126] Florida State Department of Transportation, "Standard Specifications for Road and Bridge Construction," Florida State Department of Transportation, 2004.

[127] California Department of Transportation, "Standard Specifications for Construction of Local Streets and Roads," California Department of Transportation, 2002.

[128] Louisiana Department of Transportation, "Louisiana Standard Specifications for Road and Bridges," 2006.

[129] Federal Highway Administration, "Drainable Pavement Systems, Participant Notebook, Demonstration Project 87," 1992.

[130] CALTRANS, "CALTRANS Highway Design Manual," California Department of Transportation.

[131] J. P. Donahue, "Missouri Guide for Pavement Rehabilitation," Missouri Department of Transportation, Report RDT 02-013, October 2002., 2002.

[132] MnDOT, *Road Design Manual,* Developed by the Office of Project Management and Technical Support, Minnesota Department of Transportation, 2007.

[133] K. Hall and C. Correa, "Effects of Subsurface Drainage on Performance of Asphalt and Concrete Pavements," Transportation Research Board of the National Academies, Washignton, D.C., 2003.

[134] M. Bejarano and J. Harvey, "Accelerated Pavement Testing of Drained and Undrained Pavements under Wet Base Conditions," Transportation Research Record 1816, Transportation Research Board of the National Academies, 137–147, 2002.

[135] H. Melhem and R. Swart, "Evaluation of the Performance of Permeable and Semi-Permeable Unbound Granular Bases Under Portland Cement Concrete Pavement (PCCP) Slabs and Alternate Load Transfer Devices for Joint Repair," Kansas Department of Transportation, 2003.

[136] M. Elseifi, I. Al-Qadi, A. Loulizi and J. Wilkes, "Performance of Geocomposite Membrane as Pavement Moisture Barrier," *Transportation Research Record 1772, Transportation Research Board of the National Academies,* pp. 168-173, 2001.

[137] T. Winkelman, "Open Graded Drainage Layer Performance in Illinois," 2004.

[138] S. Jahangirnejad, N. Buch and A. Kravchenko, "Evaluation of Coefficient of Thermal Expansion Test Protocol and Its Impact on Jointed Concrete Pavement Performance.," vol. Vol. 106, no. 1, pp. pp 64-71., 2009.

[139] A. Neville, Properties of Concrete, New York: John Wiley and Sons, Inc., 1996.

[140] J. Mallela, A. Abbas, T. Harman, C. Rao, R. Liu and M. Darter, "Measurement and Significance of the Coefficient of Thermal Expansion of Concrete in Rigid Pavement Design," *Transportation Research Board: Journal of the Transportation Research Board,* vol. 1919, pp. 38-46., 2005.

[141] J. H. Yeon, S. Choi and M. C. Won, "Effect of Relative Humidity on Coefficient of Thermal Expansion of Hardened Cement Paste and Concrete," *Transportation Research Record: Journal of the Transportation Research Board,* vol. 2113, pp. 83-91, 2009.

[142] N. Tran, K. Hall and M. James, "Coefficient of Thermal Expansion of Concrete Materials, Characterization to Support Implementation of the Mechanistic–Empirical Pavement

Design Guide," *Transportation Research Record: Journal of the Transportation Research Board, No. 2087,* pp. 51-56, 2008.

[143] K. Shushkewich and I. Robertson, "Instrumentation of the North Halawa Valley Viaduct, Oahu, Hawaii," Progress Report prepared for the Hawaii Department of Transportation and the Federal Highway Administration, Honolulu, 1998.

[144] FORTA-Ferro. [Online]. Available: http://www.forta-ferro.com/products/macrofibers/forta-ferro/. [Accessed 9 August 2011].

[145] S. A. Havel, "Coefficient of Thermal Expansion of Concrete Mixes in Hawaii: Determination and Implications for Concrete Pavement Design," M.Sc. Thesis, University of Hawaii at Manoa, 2011.

[146] J. Tanesi, G. Crawford, M. Nicolaescu, R. Meininger and J. Gudimettla, "New AASHTO T336-09 Coefficient of Thermal Expansion Test Method How Will It Affect You?," *Transportation Research Record: Journal of the Transportation Research Board, No. 2164,* pp. 52-57, 2010.

[147] G. Crawford, J. Gudimettla and J. and Tanesi, "Interlaboratory Study on Measuring Coefficient of Thermal Expansion of Concrete," *Transportation Research Record: Journal of the Transportation Research Board, No. 2164,* pp. 58-65, 2010.

[148] S. H. Kosmatka, B. Kerhoff, N. MacLeod and R. J. McGrath, "Design and Control of Concrete Mixtures," EB101, 7th Canadian ed. Cement Association of Canada, Ottawa, Ontario, 2002.

[149] W. Navidi, Statistics for Engineers and Scientists, McGraw Hill Higher Education, New York, 2006., New York: McGraw Hill Higher Education, 2006.

[150] S. Jahangirnejad, "Evaluation of Portland Cement Concrete Coefficient of Thermal Expansion Test Protocol and the Impact of CTE on Performance of Jointed Concrete Pavements," Ph.D. Dissertation, Michigan State University, 2009.

[151] F. Wittmann and J. Lucas, "Experimental Study of Thermal Expansion of Hardened Cement Paste," *Materials and Structures,* vol. 7, no. 40, 1974.

[152] Rudeloff and Sieglerschmidt, *Deutscher Ausschuss f. Eisenbeton,* vol. 23, 1913.

[153] S. Jahangirnejad, N. Buch and A. Kravchenko, "Evaluation of Coefficient of Thermal Expansion Test Protocol and Its Impact on Jointed Concrete Pavement Performance," *ACI Materials Journal,* vol. 106, no. 1, pp. 64-71, 2009.

[154] D. T. Hartgen, M. G. Fields, E. San José and A. Moore, "20th Annual Highway Report on the Performance of State Highway Systems," 2013.

[155] "Developing Master Curve Predictive Equation Models for Local Conditions: A Case Study for Hawaii," *Journal of the Association of Asphalt Paving Technologists,* 2010.

[156] D. Muir Wood, Soil Behaviour and Critical State Soil Mechanics, Cambridge: Cambridge University Press, 1990.

[157] P. Ooi, K. Sandefur and A. R. Archilla, "Correlation of Resilient Modulus of Fine-Grained Soils with Common Soil Parameters for Use in Design of Flexible Pavements," Final Report prepared for the Hawaii Department of Transportation, Honolulu, 2006.

[158] LADOT, *Road Design Manual,* Louisiana Department of Transportation, 2009.

[159] ASTM, "Standard Test Method for Permeability of Granular Soils (Constant Head)," American Society for Testing and Materials, 221-225.

[160] "Guide for Design of Pavement Structures," AASHTO, Washington, D.C., 1993.

[161] [Online]. Available: http://www.pewcenteronthestates.org/. [Accessed 04 2011].

[162] [Online]. Available: http://www.infrastructurereportcard.org/state-page/hawaii. [Accessed 13 February 2011].

[163] Guide for Mechanistic-Empirical Design of New and Rehabilitated Pavement Structures. NCHRP Project 1-37A. Final report, Part 2., Champaign: ERES Consultants Divisions, Applied Research Associates, Inc., 2004.

[164] FHWA, Integrated Materials and Construction Practices for Concrete Pavements: A State-of-the-Practice Manual, HIF-07-004, Federal Highway Administration, U.S. Department of Transportation, 2006.

[165] L. N. Mohammad, Z. Wu, S. Obulareddy, S. Cooper and C. Abadie, "Permanent Deformation Analysis of Hot-Mix Asphalt Mixtures Using Simple Performance Tests and

2002 Mechanistic–Empirical Pavement Design Software," *Transportation Research Record: Journal of the Transportation Research Board, No. 1970,* p. 133–142, 2006.

[166] FHWA, Highway Economic Requirements System – State Version User's Guide., Washington, D.C.: US Department of Transportaiton, Federal Highway Administration, 2007.

[167] J. K. E. Tanesi, A. A. M. and R. Meininger, "Effect of Coefficient of Thermal Expansion Test Variability on Concrete Pavement Performance as Predicted by Mechanistic-Emperical Pavement Design Guide.," *In Transportation Research Record: Journal of the Transportation Research Board,* vol. 2020, pp. 40-44, 2007.

[168] M. Won, "Improvements of Testing Procedures for Concrete Coefficient of Thermal Expansion.," *In Transportation Research Record: Journal of the Transportation Research Board,,* vol. 1919, pp. 23-28, 2005.

[169] K. Hall and S. Beam, "Estimating the Sensitivity of Design Input Variables for Rigid Pavement Analysis with a Mechanistic-Empirical Design Guide.," *In Transportation Research Record: Journal of the Transportation Research Board,* vol. 1919, pp. 65-73, 2005.

APPENDIX A – LITERATURE REVIEW ON PERMEABLE BASES

A.1 Introduction

In order to update the current HDOT Pavement Design Manual, a comprehensive review of the literature was conducted regarding the practices related to the use of permeable bases in pavement design across the United States. The objective of the review was to identify and document current practices across the country, particularly those that may differ from current HDOT procedures. Experiences from other states regarding the use subsurface drainage features, particularly those involving the use of drainage layers in pavement structural sections, are emphasized in this section.

A.2 Pavement Subsurface Drainage Systems

It is widely recognized that excess moisture within the pavement system is greatly responsible for accelerated deterioration rates and subsequent diminished pavement life. Excess moisture can enter the pavement structure from surface infiltration through cracks and joints in the pavement surface, from groundwater from a high water table, interrupted aquifers and/or localized springs, and from capillary suction in the soil from the water table.

The strategies used to avoid moisture related problems in pavement systems range from use of relatively moisture-insensitive materials (e.g., some treated materials), to the construction of complete subsurface drainage systems including permeable layers within the pavement structure to evacuate infiltration water. In a study involving a survey of state highway agencies (SHA), Christopher and McGuffey [119] concluded that a preponderance of evidence supports the philosophy that "good sealing and good drainage, along with a commitment to long term maintenance will lead to optimum performance of a pavement system." Nevertheless, the same study indicated uncertainty in the cost-effectiveness of edge drains and permeable bases, and that SHA consider it as a topic that needs to be a priority for further investigations.

Mallela et al. [120] list five specific issues that must be addressed in a successful drainage design, including first the evaluation of the need for subdrainage, followed by the determination of the drainage components needed in each situation, the hydraulic and structural design of the subdrainage system within the overall pavement design process, the specifications of the materials

used in the drainage system to ensure long-term performance, and finally, the documentation of construction and maintenance considerations.

Site and design factors are commonly taken into account when deciding if subsurface drainage is required, and the criteria and level of complexity in the decision process varies among agencies. Mallela et al. [120] present an approach recommended in NHI Course 13126, which consists in assessing the need for a drainage system based in an objective ranking of both site and design conditions. A summary table for the determination of the need for subsurface drainage in jointed plain concrete pavements (JPCP) is included in [120].

The basic components of a pavement drainage system include a permeable base layer, a separator or filter layer to avoid intrusion of fines from the subgrade or subbase materials to the permeable base (usually a specifically graded aggregate layer and/or a geotextile filter fabric), and a collector system (edge drain structures and outlet pipes) to transport the intercepted water within the pavement structure to an outside drainage ditch or water sewer system. The essential components of an edge drain structure include [121]:

- A trench filled with filter-graded aggregate, open graded aggregate wrapped with a geotextile filter, or a prefabricated geocomposite drain; and
- A longitudinal conduit consisting of a perforated pipe or other hollow plastic core.

The incorporation of a drainage system into the pavement structure design introduces a wide variety of complexities related to construction practices that need to be addressed in order to ensure that the pavement structure works as originally intended in the design. NCHRP Synthesis 239 “Pavement Subsurface Drainage Systems” [119] recommends having from the start of the construction activities the presence and active participation from someone with knowledge about drain installation principles and practices.

A.3 Potential Problems with Subsurface Drainage

As indicated before, a properly designed, constructed, and maintained drainage system usually improves the performance of pavement structures. However, over time the drainage system may be affected by problems, particularly without proper maintenance.

The first indicator that problems with the drainage system are present is that there is no longer flow of water from the permeable base to the ditch. In contrast, an indication of a functioning system is the presence of deeper grass around a lateral outlet.

The majority of the problems within the drainage system are created during the construction stage, due to crushed pipes by construction equipment, and undulating drain lines that will accumulate water in depressed areas [119]. Other problems encountered with subsurface drainage systems include clogging of edge drains and outlet pipes from fine particles accumulation, rodent nests, lack of transverse drains in the lowest vertical alignment points, and backup of water from drain ditches ([119], [122]).

Video inspection of the drainage system right after construction is an excellent way to evaluate if the system is in proper operating conditions, and can also be used for work acceptance purposes [119].

When the presence of distress in the pavement surface is what suggests there are problems with the drainage system, the situation is almost always irreversible, although successful correction of the problem will slow the deterioration rate of the pavement structure. This situation stresses the idea that a well-established inspection and maintenance plan for the subsurface drainage system should be implemented [119].

A.4 Drainage System Maintenance Activities

A structured inspection and maintenance plan for the subsurface drainage of a pavement system is generally recommended in order to ensure that the system performs as designed. Some authors also suggest that if no maintenance is expected to be done, the presence of an inoperative drainage system could be more detrimental to the pavement structure than not having a system at all ([119], [120], [122], [122], [123], and [124]). The general consensus is that continuous inspection and maintenance of outlets and edge drain pipes contributes to maintain the roads in good condition.

The Christopher and McGuffey [119] study encountered different levels of maintenance activities across the United States. According to the responses received from SHA, there was not a clear maintenance policy established within the individual agencies, and the activities relied heavily on the responsible individuals in each maintenance jurisdiction. Most states reported

inspection of outlet condition in a yearly basis, and most maintenance strategies were selected with little central control. Detailed findings about the maintenance of subsurface drainage systems can be found in Chapter 5 of NCHRP Synthesis 239 “Pavement Subsurface Drainage Systems” [119].

Christopher and McGuffey [119] indicate different instances of pavement systems in Europe incorporating drainage with no maintenance that performed sometimes as if there were no drains at all after 14 years. The same report cites findings from France where operating edge drains at time of construction became inoperative after 11 years without maintenance, and showed moisture related distresses (pumping) after only 7 years under these circumstances.

It is generally accepted that if distress from subsurface drainage blockage is visible, the damage is irreversible. According to the above authors, good sealing and good drainage, along with a commitment to long-term maintenance lead to optimum pavement performance. This stresses the need for the implementation of regular inspection and preventive maintenance programs for the subsurface drainage systems.

The 1998 “Catalog Of Recommended Flexible Pavement Design Features” prepared by Darter et al. [125], describe four levels of solutions for pavement drainage problems, ranging from basic joint and crack sealing combined with proper geometrics (including side ditches on both sides of the pavement section), to more complex (and expensive) sub drainage systems including permeable bases and edge drains, to rapidly remove excess moisture that enters the pavement section before it can cause damage. They also mention the use of moisture insensitive and non-erodible materials as an effective measure to minimize moisture-induced distresses in the pavement structure.

A.5 Drainage Layer

A permeable base (or drainage layer) is a treated or untreated layer of open graded aggregate, designed with the primary function of collecting surface infiltration water in the pavement and direct it towards the edge drains within an acceptable time frame, while providing adequate support to the pavement.

There is not a unique set of requirements or specifications for the materials and construction procedures for permeable bases, as they vary from agency to agency (specification

details for CA, LA and FL can be found in [126], [127], and [128]). In general, the aggregate should come from crushed stone, with very little, if any, fine material. This is necessary to improve the interlock between the aggregate particles, critical to ensure proper stability in the drainage layer.

Permeable bases can be treated with asphalt cement (ATPB) or Portland cement (CTPB). Asphalt cement contents between 2 – 4 percent by weight of mix are common practice, although the specific amount varies from state to state. The general requirement is that 95% of the aggregate particles be fully coated with asphalt cement, as a minimum. The use of a standard permeable base thickness is common practice, usually between 75 mm to 100 mm for ATPB (CA and FL, respectively), and 105mm for CTPB (CA). These standard thicknesses have been established in most cases from local experience and constructability issues. No specific recommendations have been found for untreated permeable base thickness. However, the MEPDG documentation [1] states that "The recommended minimum and maximum thickness of permeable base layers is 4 inches. This recommendation ensures an adequate hydraulic channel for the free flow of water and places an upper limit on the thickness of this relatively unstable layer. Permeable bases could be asphalt treated, cement-treated, or untreated, depending on structural requirements".

In terms of gradation, reference [129] indicates that several states use the AASHTO No. 57 gradation for their stabilized permeable bases. This gradation and the current HDOT (and CALTRANS) specifications are shown Table A-1.

As can be observed in Table A-2, Hawaii uses by far the coarser gradation (the filler changes the gradation only in the upper part of the permeable layer). This may be explain some of the construction difficulties of permeable layers in Hawaii and it may additionally lead to higher costs. It is worth mentioning that aggregates such as 3-Fine commonly used in Hawaii typically fall within the gradation limits for the Wisconsin OGBC No. 1.

A.6 Drainage Layer Use

Literature regarding the use of permeable base in pavement construction covers published pavement design manuals from different State Departments of Transportation such as California, Florida, and Minnesota, published papers regarding controlled experimentation with permeable

base materials under accelerated loading conditions, and reports from evaluations of in-service pavements across the United States.

For untreated permeable bases, reference [129] shows the gradations used by several states. These, along with the current HDOT gradation are shown in Table A-2.

Table A-1. Gradations of AASHTO No. 57 and HDOT and CALTRANS stabilized permeable bases.

Sieve Size	Percent Passing By Weight	
	AASHTO No. 57 Gradation	**HDOT and CALTRANS Specifications**
1.5”	100	100
1”	95 – 100	100
0.75”		90 – 100
0.5”	25 – 60	35 – 65
0.375”		20 – 45
No. 4	0 – 10	0 – 10
No. 8	0 – 5	0 – 5
No. 200		0 – 2

A.7 CALTRANS Highway Design Manual

The CALTRANS Highway Design Manual is discussed first because the Hawaii pavement design guide draws heavily from earlier versions of this manual, particularly for flexible pavement design.

A.7.1 Philosophy and Standards

The state of California requires that the standards used for any project meet or exceed the minimum standards provided in their guide. Three categories for standards are used in the CALTRANS Highway Design Manual (from Chapter 80 “Application of Design Standards”, page 80-2 [130]):

"(2) ***Mandatory Standards***. Mandatory design standards are those considered most essential to achievement of overall design objectives. Many pertain to requirements of law or regulations such as those embodied in the FHWA's 13 controlling criteria (see below). Mandatory standards use the word "shall" and are printed in **Boldface** type (see Table 82.1A).

(3) ***Advisory Standards***. Advisory design standards are important also, but allow greater flexibility in application to accommodate design constraints or be compatible with local conditions on resurfacing or rehabilitation projects. Advisory standards use the word "should" and are indicated by Underlining (see Table 82.1B).

(4) ***Permissive Standards***. All standards other than mandatory or advisory, whether indicated by the use of "should" or "may", are permissive with no requirement for application intended."

Table A-2. Untreated base gradations.

Sieve Size	Iowa	Minnesota	New Jersey	Pennsylvania	Wisconsin OGBC No. 1	Hawaii	
						Coarse	Filler
2'				100		100	
1.5"			100			75 – 100	
1"	100	100	95 – 100		100	15 – 55	
0.75"		65 – 100		52 – 100	90 – 100	0 – 15	
.5"			60 – 80			-	100
0.375"		35 – 70		33 – 65	20 – 55	0 - 5	85 – 100
No. 4		20- 45	40 – 55	8 – 40	0 – 10		10 – 30
No 8	10 -35		5 – 25		0 – 5		0 – 10
N 10		8 – 25					
No. 16			0 – 8	0 – 12			0 – 5
No. 40		2 – 10					
No. 50	0 – 15		0 – 5				
No. 200	0 – 6	0 - 3		0 - 5			

The Mandatory and Advisory standards are listed in Table 82.1A and 82.1B, respectively, in reference [130], Chapter 80 "Application of Design Standards".

Proposals for the implementation of new ideas and techniques in California's highway system, particularly in the design, construction, maintenance, and materials engineering of the structural section, are encouraged. The proposed research must be first submitted to the Division of Research and Innovation, while approval and implementation of experimental construction features must be done by the Pavement Standards Team (who can also receive suggestions about

changes in design standards and research studies). They recommend the involvement of maintenance personnel in discussions related to any experimental construction features

The above discussion is introduced here because it may help in writing the standards for Hawaii, since it appears it is not always clear whether a given standard is a requirement or not. In addition, it helps in the interpretation of the summary of CALTRANS practices below.

A.7.2 Drainage Layer in Caltrans Highway Design Manual (CALTRANS Highway Design Manual)

There is no mandatory standard regarding the utilization of permeable base in the CALTRANS Highway Design Manual. However, its utilization is recommended in most cases, except when environmental or subgrade conditions do not justify it[90].

When Treated Permeable Base (TPB) is included in the design, standard thicknesses of 75 and 105mm for Asphalt Treated Permeable Base (ATPB) and Cement Treated Permeable Base (CTPB), respectively, are suggested. This differs from the current HDOT Pavement Design Manual, where the thickness of the drainage layer is based on surface water infiltration rate. In the case of California, the recommended thicknesses are based primarily on constructability, with an added allowance to compensate for construction tolerances. They indicate that the fixed TPB thicknesses will generally be more than enough to evacuate the surface infiltration water (Section 606.3 (1) [130]).

While the placement of at least 6" of an aggregate separation layer covered by a permeable geotextile between the subgrade and the TPB is currently required by HDOT (due to the amount of fines commonly encountered in subgrade soils in the state, Chapter 2, pg. 17 [13]), no mandatory standard regarding the utilization of an aggregate separation layer below the permeable base was found in the CALTRANS manual. However, they indicate that a filter fabric or other suitable membrane should be placed on top of the layer supporting the TPB when there

---

[90] From CALTRANS Highway Design Manual, Section 606.2, pg. 31.

"The structural section should include a layer of Treated Permeable Base (TPB) under the pavement except in areas where the mean annual rainfall is very low (less than 125 mm) or where the basement soil is free draining (a permeability greater than 3.53 x 10-4m/s)".

is concern that the infiltrating surface water may saturate and soften the underlying subbase or subgrade, generating migration of fines and contamination of the TPB.

For structural design purposes, no R-value is assigned to TPB materials (Section 606.3(2), pg. 600-33 [130]). Use of TPB layers thicker than the 75 or 105mm recommended (ATPB or CTPB, respectively) are only recommended under unique combination of conditions (footnote Table 604.3 in [130]). CALTRANS does not prohibit the use of other types of drainage layers, but suggests that checks for suitability regarding permeability and structural capacity should be performed.

Asphalt treated permeable base material is plant produced, and production requirements can be found in Section 29-1.04A from "Standard Specifications for Construction of Local Streets and Roads" [127]. Aggregate requirements for ATPB are included in Section 29-1.02A of the same document. It is important to note that the gradation requirements for ATPB are identical for both HDOT and CALTRANS (gradation requirements in Section 703.04 in HDOT specifications refer to Untreated Permeable Bases (UPB) alone). Even though use of drainage layers other than ATPB and CTPB is not forbidden in the CALTRANS manual, no specifications were found regarding aggregate gradation for untreated permeable bases (UPB) layers.

A.8 Drainage Layer Use in Other Design Guides

This section first discusses the information regarding drainage layer included in the mechanistic-empirical design guide documentation and then discusses the information found on the same subject on several State DOT's design guides and specifications.

A.8.1 MEPDG Drainage Layer Treatment

The use of subsurface drainage (and therefore of permeable base) is not mandatory in all cases, but rather depends on the conditions of the particular project. Table 3.1.1 in [1] gives an indication on when subsurface drainage might be required, as a function of general climatic conditions and traffic level. According to that table, for Hawaiian climatic conditions and with less than 2.5 million 20-year design lane heavy trucks, subsurface drainage is not required for subgrades with coefficients of permeability of 3 m/day (10 ft/day) and above. This is in contrast to the requirement by HDOT of 30 m/day (100 ft/day) (irrespective of traffic level and only for "pavement layers" (asphalt concrete?) placed directly on the pavement soil), which is an order of

magnitude higher than the recommended values in the new guide. This may point out situations in which the usage of a permeable layer may not be warranted.

For intermediate traffic loadings (between 2.5 and 12 million 20-year design lane heavy trucks), the MEPDG requires the use of a permeable layer for subgrades with permeability of less than 3 m/day (10 ft/day) and indicates that additional factors must be considered in the decision for installing permeable bases over subgrades with higher permeability.

For higher traffic loadings (greater than 12 million 20-year design lane heavy trucks), the MEPDG requires a drainage layer for subgrade permeability lower than 30 m/day (100 ft/day), and also indicates the consideration of additional factors for higher permeability.

In summary, the MEPDG provides conditions under which a drainage layer is not required and intermediate conditions under which it may be required depending on other factors. Unfortunately, the additional factors, which include past pavement performance and experience in similar conditions, cost differential and anticipated increase in service life, and anticipated durability and/or erodability of paving materials, may not be easy to quantify.

Also, as is the case with some other state's current design guides (CA, FL, and MO), the thickness of the drainage layer is not variable, but rather a fixed value governed by local experience and constructability issues ([126], [127], [131]).

As reported in Part 3, Chapter 1, Section 3.1.5.3 in [1], the layer thickness has the least effect on the "time-to-drain" parameter in a permeable base, while permeability has the greatest effect, as the time to drain decreases exponentially with an increase in permeability. Based on this, the MEPDG recommends 4 inches as an appropriate permeable base layer thickness (maximum and minimum), allowing compaction without segregation while providing an acceptable hydraulic conduit.

To ensure appropriate stability in an untreated permeable base, a minimum Coefficient of Uniformity (Cu) of 3.5 is required. If this cannot be achieved, the base should be asphalt or cement treated. The aggregate used for untreated permeable bases should have 98% crushed faces, and have no more than 45% loss in the Los Angeles Abrasion Test (AASHTO T96), while soundness should not exceed 12 to 18% loss (AASHTO T104). Minimum permeability of 1000ft/day is required, and fines should be non-plastic (AASHTO T90). (The MEPSG excerpted

these requirements from the "Guide Specification for Material Selection and Construction of Unstabilized Permeable Base Layers available from FHWA).

For ATPB, the asphalt cement content must be 3 ± 0.5 percent by weight of dry aggregate, and gradation should ensure mix permeability of at least 1000 ft-day. Restrictions for aggregates in CTPB are the same as those for untreated permeable bases.

Use of a separation layer is recommended to avoid penetration of subgrade fines into the permeable base, to serve as a moisture barrier to horizontally remove any excess water from the pavement to the edges, and to support construction traffic. This layer can be an untreated dense aggregate base, or a geotextile layer.

The requirements for an Untreated Dense Aggregate Separation Layer, as listed in the MEPDG [1] are:

- Fractured Faces on material retained on No. 4 sieve (98% crushed stone is preferred)
- L.A Abrasion Test below 50% (AASHTO T96)
- Loss from soundness test (AASHTO T104) should not exceed 12 to 18%
- Maximum Permeability of 15 ft/day
- Maximum % passing N200 of 12%
- Material passing N40 sieve must be no plastic (AASHTO T90)

If the edge drain pipes can resist the loads imposed during construction, it can be expected that they resist the whole design life of the pavement without crushing. The MEPDG suggests using existing state specifications for edge drain construction, and indicates that the permeability of the backfill used in edge drain trenches must be greater than or equal to the permeability of the permeable base. Appendix SS of the MEPDG [1] covers hydraulic design, material selection, and construction issues of edge drains with and without permeable bases.

A.8.2 Florida DOT

The Florida DOT Design Guide of Rigid Pavements describes the use of 100 mm of Asphalt Treated Permeable Base (ATPB) or Cement Treated Permeable Base (CTPB) as their typical drainage layer section [126]. This drainage layer is sitting on top of a 30 mm Structural Course that acts as a separation and waterproofing blanket, which is placed on top 300mm stabilization layer, which acts as a construction-working platform. The infiltration water is then

directed to the nearest outfall located on the shoulder slope, or to a storm sewer system in urban areas.

The state of Florida allows gradations with 1 and ¾" maximum nominal size to be used in ATPB layers. Other properties specified include:

- Los Angeles abrasion test Max 45% (50% for Granites)
- Soundness Max 12%
- Flat and Elongated particles Max 10%
- For Natural Stones:
    - Fractured Faces Min 85% (Retained in N4 sieve)
    - Dry Unit Weight Min 95lb/ft3 (AASHTO T19)

Detailed specifications for aggregates to be used in ATPB, including specific aggregate gradations, can be found in "Standard Specifications for Road and Bridge Construction", Section 901 [126].

Differences between FLDOT and CALTRANS compaction of ATPB include:

- Installation (spread) temperature (above 5C for CALTRANS, 10C for FL)
- Compaction Temperature Start/Finish: 65C/38C for CALTRANS; 88C/38C for Florida DOT (Both using steel 2 axle tandem roller between 8 – 12 tons).
- Use of water to cool ATPB material allowed in FL, forbidden in CA.

The gradation requirements for both CTPB and ATPB are the same (both specify use of gradations 57 or 67 from "Standard Specifications for Road and Bridge Construction", Section 901 [126]).

A.8.3 Missouri DOT

The preferred base type in Missouri for *concrete pavements* is a 2-feet, day lighted rock base, which provides a stiff platform and that is currently believed to be a very drainable layer (performance to date is reported as excellent). Missouri also uses an alternate 4" TPB over 4" of Type 5 subbase with edge drains, as indicated in the document "Missouri Guide for Pavement Rehabilitation" [131]. The daylighted recommendation is in contrast from the recommendation in [129], which states "daylighting the permeable base layer is not recommended since the

daylighted layers are subject to clogging from roadway debris and vegetation". However, the latter reference is 10 years older than the Missouri DOT reference.

A.8.4 Minnesota DOT

MnDOT does not require the use of permeable base as mandatory, but includes it in one of their pavement design standards. Consideration about the use of drainage layer in pavement structures is given in "Permeable Aggregate Base Drainage Systems Design Guidelines", 1994. The use of an impervious layer is illustrated in Figure 8-3.06A [132].

A.8.5 Louisiana DOTD (Louisiana Department of Transportation and Development)

To help prevent water from entering the pavement structure from beneath, *the design high water elevation should be 2 ft below the base course,* and roadside ditches should be set a minimum of 2 ft below the lowest part of the base course [from Section 5.1.3 in Louisiana's Road Design Manual [128].

It is apparent from Section 307 in their Standard Specifications Manual that only treated permeable bases are prescribed in their pavement designs. Thickness of the permeable base appears to be a variable in the pavement design process, in contrast with current practice in California and Florida, where the thickness of the permeable base is fixed, and based on constructability. Pavement structural section design in the state of Louisiana follows the AAHSTO design method, as specified in the Pavement Structural Design Directive EDSM II.2.1.12.

A.8.6 Reported Performance Information

A considerable amount of research has been published regarding the use of permeable bases within pavement structures. The general consensus is that properly constructed permeable bases within a well-designed subsurface drainage system contribute to extend the service life of pavements.

Use of permeable base does not appear to be necessary for Doweled JPCP, as reported in NCHRP Project 1-34 "Performance of Pavement Subsurface Drainage". However, the performance of undoweled JPCP is greatly improved with permeable base layers and edge drains. The incorporation of a permeable layer beneath the dense asphalt concrete was reported

as being the most cost-effective design. It was indicated that in any case, proper maintenance of drainage structures (permeable layers, edge drains, etc.) must be warranted, as abandoned drainage structures can lead to a more rapid failure of the pavement. This information was obtained from NCHRP Research Results Digest Number 268 [123].

A lot of confusion reported from "as designed" and "as constructed" records was reported in NCHRP Report 499, "Effects of Subsurface Drainage on Performance of Asphalt and Concrete Pavements" [133]. No statistically significant difference between the uses of drained or undrained structures was obtained from this study. The general feeling is that a permeable base (asphalt treated) improves pavement performance (measured with IRI, cracking, and rutting).

In a study of accelerated pavement testing of drained and undrained pavements under saturated base conditions, Bejarano and Harvey [134] report that the failure modes for drained and undrained pavement sections are different (bottom up fatigue for undrained while rutting for drained sections), but that similar pavement life was observed for both types of structures. They recommend the elimination of Asphalt Treated Permeable Base (ATPB) use by increasing the asphalt concrete (AC) thickness to reduce the risk of load induced cracking, and to ensure low permeability of the AC layer through proper compaction. They suggest that special steps and care needs to be taken in order to avoid stripping of the asphalt binder in the ATPB material.

In another study, after evaluating the performance of permeable and semi-permeable unbound granular bases under PCC slabs, it was concluded that PCC sections over permeable bases perform better than under semi-permeable bases [135].

Use of an impervious separator layer was investigated in Virginia by Elseifi et al [136]. They report the use of a specially designed geocomposite membrane as a moisture barrier, consisting of a low modulus polyvinyl chloride (PVC) backed on both sides with polyester nonwoven geotextile, installed under 75mm of ATPB. The researchers report prior success in the use of this membrane as an impermeable material for dams, canals, reservoirs, and hydraulic tunnels. The results from the investigation suggested that for pavement systems with low water table conditions, an impervious membrane used in combination with a permeable base layer is capable of removing surface infiltration water, and can provide a dry service condition for the underneath layers even in the event of heavy rain.

The performance of different types of drainage layers constructed during the late 80's and early 90's was evaluated by the Illinois Department of Transportation, and reported by Winkelman [137]. The report covered the construction, performance, and rehabilitation of six projects, and studied the effects of using both asphalt and cement treated permeable bases, as well as the effects of placing an aggregate separation layer between the drainage layer and the lime-modified subgrade, as opposed to placing the drainage layer directly on top of it. Pavement performance was measured by means of visual distress surveys, FWD testing, IRI values, and Condition Rating Survey (CRS) values. The use of drainage layers was evaluated in three types of rigid pavements (JPCP, JRCP, and CRCP)[91], and in one full depth Hot Mix Asphalt (HMA) pavement.

Mid panel cracks in 99% of the JRCP slabs triggered the abandonment of this type of design, and set to 15 feet the maximum joint spacing allowed for jointed concrete pavements in the state. Based on the poor performance of two CRCP projects, a moratorium on the construction of drainage layers under state maintained highways was issued in January 1996. One of the reasons identified for the poor performance of these projects was the intrusion of fine materials into the permeable base, in part due to high moisture levels within the subgrade, and the presence of silty soils that were non-reactive to the lime modification process.

[91] JPCP, JRCP, and CRCP stand for Jointed Plain Concrete Pavement, Jointed Reinforced Concrete Pavement, and Continuously Reinforced Concrete Pavement, respectively.

APPENDIX B COEFFICIENT OF THERMAL EXPANSION OF PORTLAND CEMENT CONCRETE MIXES IN HAWAII

B.1 ABSTRACT

The coefficient of thermal expansion (CTE) of Portland Cement Concrete (PCC) is a significant factor affecting the performance of concrete pavements. It is also required as a direct input in the Mechanistic-Empirical Pavement Design Guide (MEPDG). The primary objective of this study was to determine CTE values of PCC mixes used in Hawaiian pavements. A secondary objective was to study the effect that curing time has on the CTE. To achieve these objectives, forty five concrete specimens were prepared onsite at three Hawaiian concrete companies using local basaltic aggregates. For each site, 15 replicate test specimens (five sets of three) were cured in a 100% humidity room for 3, 7, 14, 28, and 56 days before determining their CTEs following AASHTO T-336. It was found that CTE values vary significantly with curing time. It was also observed that the CTEs at 28 days computed in this study, ranging from 6.1 to $6.6 \times 10^{-6}/°\text{F}$, differ significantly from the value recommended in the MEPDG Manual of Practice for concrete specimens with basaltic rock as a constituent ($5.2\times10^{-6}/°\text{F}$), which can lead to designs whose performance is overestimated. Based on the study results, it is recommended to use the CTE obtained after 28 days of curing for design. Possible implications of the results obtained in this study are illustrated with a particular Jointed Plain Concrete Pavement (JPCP) design with the MEPDG.

B.2 INTRODUCTION

The coefficient of thermal expansion (CTE) of Portland Cement Concrete (PCC), defined as the unrestrained change in unit length per degree of temperature change, has significant influence on the design of joints and temperature-related pavement deformations (expansion/contraction and curling) in jointed concrete pavements (JCPs) [138].

It has been reported that the measured CTE is affected by several factors. For example, Huang [34] states: "The thermal coefficient of expansion for PCC, α_c, depends on many factors such as the water-cement ratio, concrete age, richness of mix, relative humidity, and the type of aggregate in the mix. However, the type of coarse aggregate has the most influence." According

to Jahangirnejad et al. [138], the CTE of PCC is influenced significantly by: 1) the volume and geology of coarse aggregate present in the mixture, 2) moisture conditioning of the sample at the time of testing, and 3) the number of heating-and-cooling cycles applied to the test specimen. These authors also found the CTE to be affected by curing time.

As for the moisture condition, Neville [139] indicates that the maximum value for the CTE of a concrete specimen is found at a relative moisture content of 60% to 70% (70-80% saturated according to [138]). This condition is not practical for a large scale project due to the difficulty of accurately obtaining the same degree of saturation for hundreds of samples. Furthermore, concrete in the field typically has a relative humidity of 80% or more, except for the top portion of the slab which is dryer due to the environment [140]; therefore, using a low relative humidity may not be representative. Yeon et al. [141] reported that little difference (~3%) was observed between maximum concrete CTE at 70% - 80% relative humidity (RH) and CTE of concrete at 100% RH.

Tran et al. [142] reported that "the CTEs of PCC mixtures and cement paste specimens at the fully saturated condition determined at 7 and 28 days were not significantly different. However, these CTE values would be significantly different if the samples were not fully saturated". As a result, AASHTO T 336 requires that the concrete sample be completely saturated in limewater until approximately 100% relative moisture content is met (approximately 48+ hours).

Despite its importance, the CTE was not directly used as a design input in the AASHTO *Guide for the Design of Pavement Structures* [12]; instead, it was only employed to determine the magnitude of joint movement and sealant reservoir dimensions. However, the Mechanistic-Empirical Pavement Design Guide (MEPDG) [1], developed under NCHRP Project 1-37A, recognized it as an important factor by using it as a direct input design variable to analyze critical slab distresses and joint/crack openings. This means that in order to achieve more reliable PCC pavement designs with the MEPDG, state highway agencies need to determine the CTE for their local paving mixtures rather than taking advantage of default or recommended values. Otherwise, input of non-representative values of CTE into the MEPDG may result in larger prediction errors of distresses in PCC pavements.

There is not much information on the value of CTE of Hawaiian concrete mixes. Shushkewich and Robertson [143] reported values measured in accordance with CRD C39 for

seven sections of the North Halawa Valley Viaduct, a section of the H-3 freeway in Oahu. They found values varying between 3.78 and 6.06 microstrain/ºF with an average of 4.58 microstrain/ºF at an age of 3 days, between 4.1 and 5.34 microstrain/ºF with an average of 4.64 microstrain/ºF at an age of 28 days, and between 4.06 and 6.53 microstrain/ºF with an average of 5.33 microstrain/ºF at an age of 90 days. In addition to having being obtained with a different standard, these values display high variability for each age.

The main goal of this study is to quantify the value of the CTE of PCC mixes prepared with aggregates from quarries found throughout the state of Hawaii. A secondary objective is to study the effect that curing time has on the CTE. To achieve these objectives, forty five concrete specimens were prepared onsite at three Hawaiian concrete companies using local basaltic aggregates. For each site, 15 replicate test specimens (five sets of three) were cured in a 100% humidity room for 3, 7, 14, 28, and 56 days before determining their CTEs following AASHTO T-336.

B.3 EXPERIMENTAL WORK

B.3.1 Mixes

The CTEs of three mixes used in recent jobs by three separate Hawaiian concrete companies were studied. Two of the companies are located in the island of Oahu (Island Ready Mix and Hawaiian Cement) and one in the Island of Hawaii (West Hawaii Concrete). Mix characteristics provided by each company are shown in Table B-1. The aggregates from the three quarries consist of basaltic rock that has been crushed into a gradation with a nominal maximum aggregate size of 3/4 inch used as the coarse aggregate (3 Coarse and 3 Fine aggregates are aggregates with maximum nominal sizes of ¾"). The water/cement (w/c) ratio did vary from one mix to another, but the type (Type I/II) and source of the cement used in all three mixes was the same. According to Tran et al. [142], the type or mixture of cement (i.e. cement mixed with fly ash) does not significantly affect the CTE. Due to time constraints; the individual effects of the type or mixture of cement, the w/c ratio and other variables present in the mixes (i.e. sand, fine aggregates, and admixtures) have on the CTE were not investigated. However, it is important to point out that the amount of cement per cubic yard of three mixes is higher than normal, and particularly for the mixes from the two companies from Oahu (Island Ready Mix and Hawaiian Cement) is substantially higher than normal, which in turn may have had some effect on CTE.

FORTA-FERRO® Fibers were used in the Hawaiian Cement mix. These fibers are typically used to reduce plastic and hardened concrete shrinkage, improve impact strength, and increase fatigue resistance and concrete toughness [144]. This is noted because Hawaiian Cement is the only company that used these fibers, which could affect the measurements of the CTE on these mixes.

Other admixtures were used throughout the mix designs of each of the companies. The admixtures were used for increased strength, durability, and workability. These design aspects, along with the FORTA-FERRO® fibers, were beyond the scope of this research and therefore their individual effects were not studied.

Table B-1. Mix Characteristics

Mix	Materials Source and Type	SSD (Weight) (lbs)	Specific Gravity	Absolute Volume (ft^3)	Admixture(s) & Dosage	Water-Cement Ratio
Island Ready Mix	Hawaiian Cement (Type I/II)	799	3.15	4.06	Master Builder's Pozz 322N (Water-Reducer) @ 1-5 oz./cwt, Pozz 100XR (Set-Retarding) @ 0-5 oz./cwt, Micro Air (Air-Entraining) @ 0.1-1.0 oz./cwt	0.34
	Maui Sand	212	2.65	1.28		
	Kapaa Crushed Fine	845	2.65	5.11		
	Kapaa 3Fine	763	2.70	4.53		
	Kapaa 3 Coarse	1146	2.70	6.80		
	Water	275	1.00	4.41		
	Total	4040	-	26.19		
Hawaiian Cement	Hawaiian Cement (Type I/II)	893	3.15	4.54	Glenium 3030 (Water-Reducer) @ 54 oz./cy, DELVO (Hydration Control) @ 22 oz./cy, VMA (Viscosity-Modifier) 362 @ 17.9 oz./cy, FORTA-FERRO FIBERs (Strength Reinforcement) @ 3.5 lbs/cy	0.35
	Halawa #3 Fine Washed	1360	2.65	8.22		
	Halawa 3/8" Chips	338	2.65	2.04		
	ORCA Sand	851	2.69	5.07		
	Halawa No. 4	210	2.65	1.27		
	Water	275	1.00	4.41		
	Total	3927		25.55		
West Hawaiian Concrete	Hawaiian Cement (Type I/II)	682	3.15	3.47	Micro Air (Air-Entraining) @ 1.36%, Pozz 220N (Water-Reducer) @ 25.23 oz.	0.46
	Kona Fine Aggregate	1383	2.90	7.64		
	Waimea 3 Coarse	1650	2.65	9.98		
	Water	317	1.00	5.07		
	Total	4032		26.16		

B.3.2 Sample Preparation

Following AASHTO T23, concrete cylinders were cast and prepared on-site, and brought to the University of Hawaii at Manoa laboratory. Once in the laboratory, the specimens were cured for a predetermined amount of days (3, 7, 14, 28, and 56 days) in a 100 percent humidity room.

After the predetermined curing time was reached, the specimens were properly sawed and prepared for the CTE measurements. Once a specimen was sized, it was then placed in limewater for a minimum of 48 hours and until a change in weight of less than 0.5 percent over a 24 hour period was achieved.

Other quality control tests were performed on the fresh concrete. The details of these tests can be found in [145].

B.4 CTE Measurement

The CTE of the concrete cylinders cast on-site and cured were measured following AASHTO T 336-09. Much of the literature refers to the test protocol AASHTO TP 60-00, on which AASHTO T 336-09 is based. However, a major difference between the two test protocols is that an erroneous value of the CTE of the 304 stainless steel calibration specimen was recommended in AASHTO TP 60.

Figure B- shows the concrete thermal expansion measuring setup prepared for this study. The setup has four major parts: linear variable differential transformer (LVDT) and thermocouples, data acquisition controller, custom water bath with overflow return system, and factory built water bath with heating/cooling capabilities. A stainless steel frame and calibration specimen are seen inside the custom water bath.

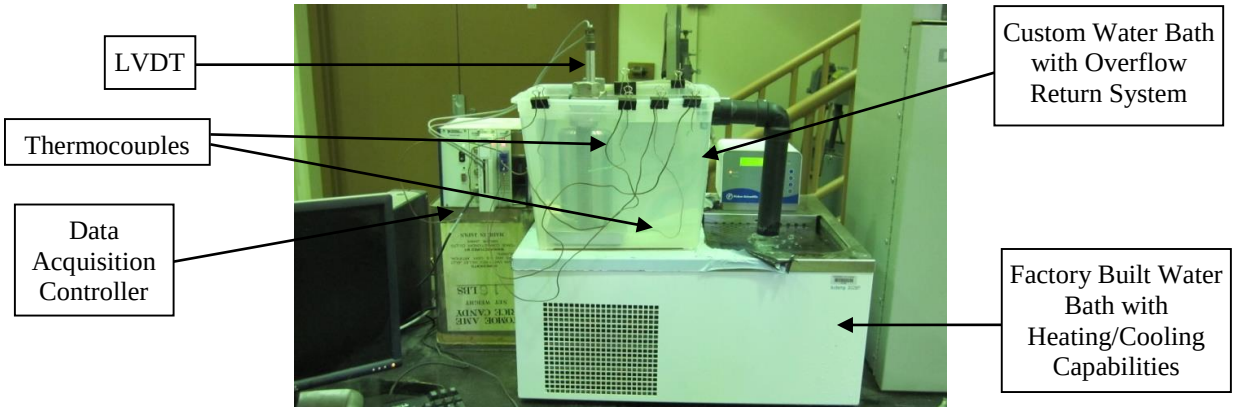

Figure B-1. Custom Water Bath Employed by UH Manoa.

To calibrate the amount of expansion or contraction of the measuring frame, a 410 stainless steel (SS) specimen was used. AASHTO T 336-09 indicates that a calibration specimen "should be composed of a material that is essentially linearly-elastic, non-corroding, non-oxidizing, nonporous, and non-magnetic, and it should have a known thermal coefficient as close as possible to that of concrete [e.g., a range of 9 to 18 x 10^{-6}/°C within the temperature range of 10 to 50°C (304 stainless steel is a suitable material)]". For this study, a 410 SS specimen was available to determine the amount of expansion and contraction of the measuring frame. A study completed by Tanesi et al. [146], reported values for a 410 SS calibration specimen obtained by two independent laboratories to be between 10.2 x 10^{-6}/°C and 10.4 x 10^{-6}/°C. The CTEs reported in this study are based on a CTE of 10.4 x 10^{-6}/°C (5.8 x 10^{-6}/°F) for the calibration specimen. Notice that the CTE of 410 SS falls within the acceptable range for AASHTO T 366-09. Tanesi et al. [146] also noted that although 410 stainless steel has a weak magnetic field that could affect the LVDT during testing, their preliminary evaluations did not show any effect on the CTE units at the FHWA Turner-Fairbank Highway Research Center or the FHWA Mobile Concrete Laboratory.

The specimen was completely submerged in the water bath. An LVDT with a minimum resolution of 0.00025 mm (0.00001 in) was mounted on the stainless frame to capture the axial length change of the specimen due to the set temperature changes. Once the specimen was centered on the frame, it was subjected to two temperature cycles: from 10 ± 1 °C (50 ± 2 °F) it was heated up to 50 ± 1 °C (122 ± 2 °F), then back down to 10 ± 1 °C (50 ± 2 °F), then up to 50

± 1 °C (122 ± 2 °F), and then finally back to 10 ± 1 °C (50 ± 2 °F). In the AASHTO T 336 standard, there is no protocol regarding the rate at which the temperature change must occur. Crawford et al. [147] studied if the rate of temperature change could significantly affect the CTE. Their results showed that the influence of the rate of temperature change on the CTE is not statistically significant. This is in an important consideration for this study since as described before the need to circulate water from the factory built water bath to the plastic water bath made the heating and cooling cycles longer than with a single bath.

The software LabVIEW SignalExpress Version 3.0 was used to process the signals from the LVDT and the thermocouples. This program, which monitors the test startup and run parameters, acquires and displays the temperature change recorded from the thermocouples and the length changes measured by the LVDT. The information retrieved from the LVDT and thermocouples were recorded at 30 second intervals so as to obtain enough points to verify that the specimen and frame were in thermal equilibrium at 10°C and 50°C. According to AASHTO T 336, thermal equilibrium is achieved when the LVDT values show consistent readings to the nearest 0.00025mm (0.00001 in) every 10 minutes over a one-half hour period. Figure 2 is a typical screenshot of LabVIEW SignalExpress Version 3.0 displaying a graph with readings from the LVDT and thermocouples. Following AASHTO T 336-09, four thermocouples were placed at various depths to ensure that temperature equilibrium was consistent throughout the water bath. This was important because of the use of a custom water bath, which was potentially susceptible to temperature differentials within the bath due to the larger than usual surface exposure. As can be observed in Figure B-, where the lines for each thermocouple practically overlap, the temperature stayed consistent throughout the depth of the bath.

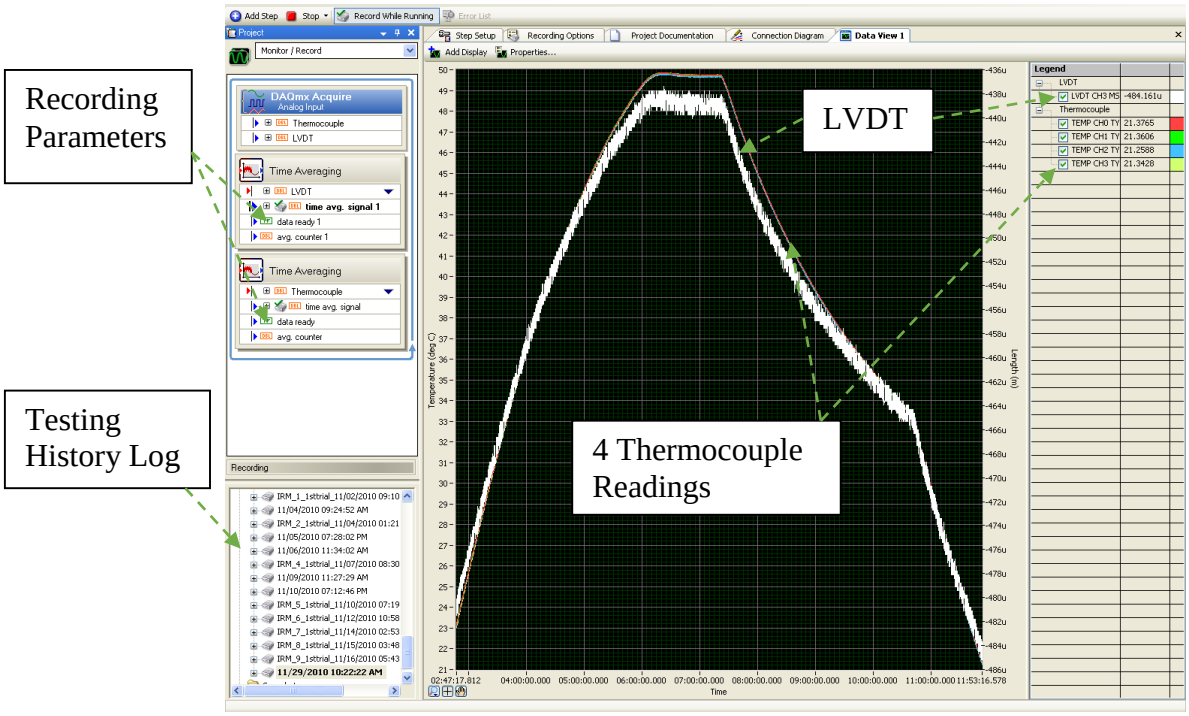

Figure B-2. Temperature and displacement measurements obtained from LabVIEW SignalExpress Version 3.0 program for one concrete specimen.

B.5 CTE TEST RESULTS

Table B-2 shows the calculated CTE values for each of the specimens. Unfortunately, the file for one of the specimens from Island Ready Mix with 3 days of curing got corrupted, so only two replicates are available for that case.

Table B-2. Coefficients of thermal expansion of the testing specimens.

Mix	Curing Time	CTE (10^{-6}/°F)			
		Replicate			Average
		1	2	3	
Island Ready Mix	3 Days	7.1	6.9	-	7.0
	7 Days	6.7	6.9	6.4	6.7
	14 Days	6.1	6.1	6.2	6.1
	28 Days	6.2	6.2	6.1	6.2
	56 Days	6.1	6.1	5.9	6.0
Hawaiian Cement	3 Days	6.1	6.4	6.4	6.3
	7 Days	6.3	6.6	6.4	6.4
	14 Days	6.1	5.9	6.0	6.0
	28 Days	6.1	6.2	6.0	6.1
	56 Days	6.2	6.3	6.0	6.2
West Hawaii Concrete	3 Days	6.9	6.9	6.9	6.9
	7 Days	7.2	6.9	6.8	7.0
	14 Days	6.9	6.8	6.8	6.8
	28 Days	6.8	6.5	6.6	6.7
	56 Days	6.6	6.4	6.5	6.5

Figure B- illustrates for each PCC mix at different curing times the averages of the CTE test results. The average values of CTE after 28 days of curing for the three Hawaiian companies range from 6.1 to 6.6 × 10^{-6}/°F (11.0 to 11.9 × 10^{-6}/°C), which are substantially higher than the 5.2 × 10^{-6}/°F (9.4 × 10^{-6}/°C) value recommended in the MEPDG Manual of Practice [22] for mixes prepared with basaltic aggregates. Common values found in the literature for PCC mixes with basaltic aggregates range from 3.3 × 10^{-6}/°F to 5.7 × 10^{-6}/°F ([139], [147], [148]), though it must be recognized that these values were obtained before the problem with the calibration specimen discussed in [146] was discovered. Hawaiian basalts are Tholeiitic basalts, which are relatively rich in silica and differ in composition from alkali olivine basalt, which occurs along continental rifts. This may partly explain the differences in the CTEs measured in this study with the values reported in the literature for mixes with basaltic aggregates.

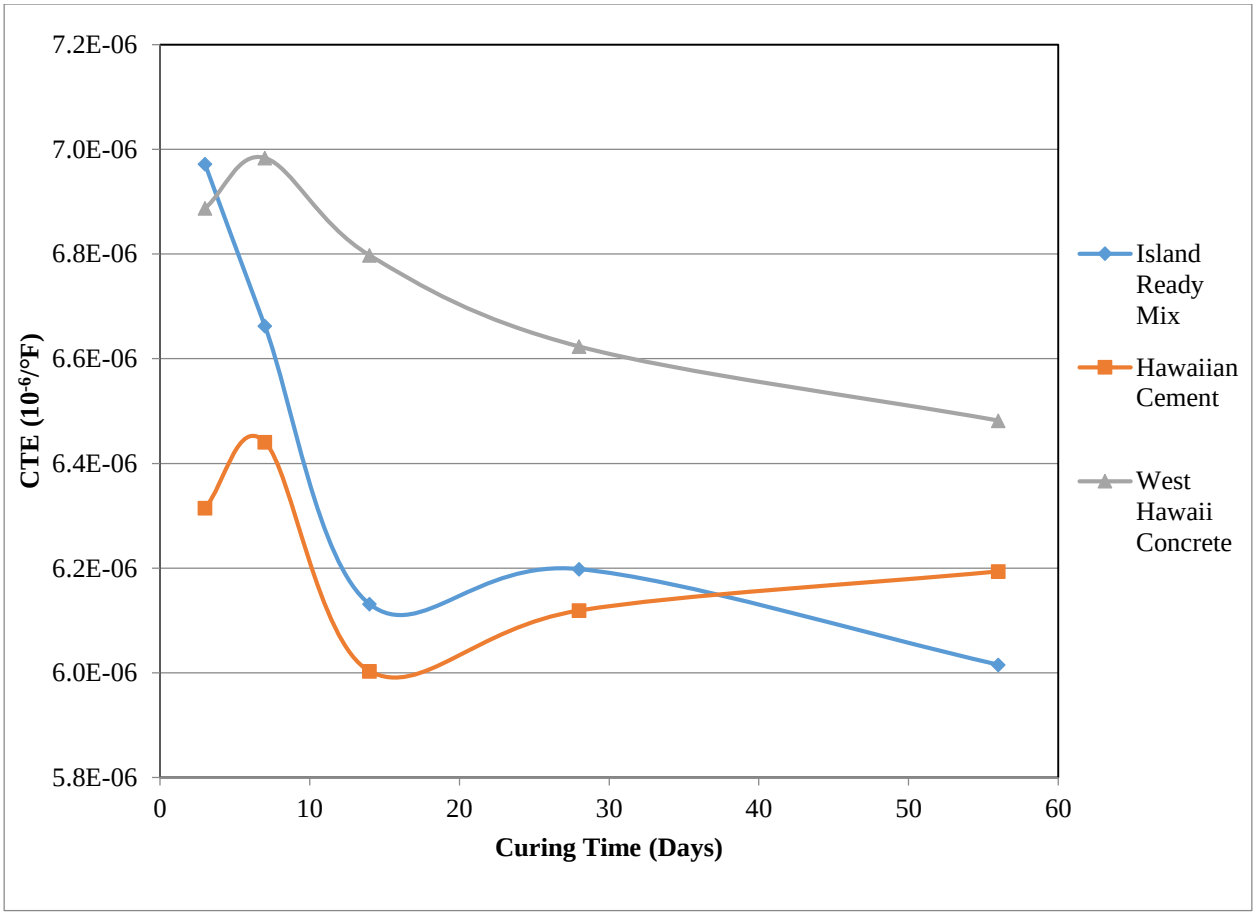

Figure B-3. Variation of the CTE with respect to curing time of concrete specimens for Hawaiian companies.

The three PCC mixes show different trends with curing times. In two of them (Hawaiian Cement and West Hawaii Concrete), the CTE first increases with 7 days curing time relative to 3 days curing time whereas for the Island Ready Mix the CTE decreases. On the other hand, the CTE values at 56 days are lower than the values at 28 days for the Island Ready Mix and West Hawaii Concrete mixes but the opposite happens for the Hawaiian Cement mix. There is no clear explanation for these discrepancies between mixes. Nevertheless, using Fisher's Least Significant Difference Method [149] to make pair wise comparisons from the results of a one factor ANOVA analysis (where the factor is curing time), it can be concluded that in all cases the values at 3 and 7 days are statistically significantly higher at a 5% significance level than those at

28 and 56 days and that the results at 28 and 56 days are not statistically significantly different from each other, also at a 5% significance level.

Notice that the CTEs at the longer curing times for the two mixes produced in Oahu are close two each other whereas the CTE for the mix produced in the Island of Hawaii is significantly higher. Although this may indicate a difference in aggregate thermal expansion characteristics between the islands it may also be related to other mix characteristics (e.g., the water cement ratio is higher for the West Hawaii Concrete mix than for the other two mixes.)

The changes in CTE with curing time, expressed as a percentage, vary depending on the values selected for comparison (3 or 7 days and 28 or 56 days) but are roughly between 5 and 10%, which are quite substantial (and as indicated earlier, statistically significant).

It must be pointed out that the trends with curing time found in this study are surprising since other researchers have found results that conflict with these. As reported in [150] Wittmann and Lukas [151] found an increase in the CTE of saturated concrete specimens around room temperature up to 56 days of age and Rudeloff and Sieglerschmidt [152] also reported increases in CTE of wet-cured specimens up to 90 days. Jahangirnejad [150] states that the effect of age on CTE is associated with proceeding hydration and change in the composition of the cement paste which in turn affects the CTE of concrete. However, except for the experimental observations, he does not provide an explanation for why the CTE should increase with curing time. In his study, he found statistically significant increases with curing time up to 365 days. However, in ([153], [150]), except for an air entraining agent (and fly ash for one of the eight mixes) no other additives were used. With so many variables that may be playing a factor, it is not clear why the results in the present study display a different trend. It may well be that with curing times longer than 56 days the CTE may increase or that other mix characteristics affect the CTE differently (e.g., the higher cement contents per cubic yard in this study). Either way, this is a subject that deserves further study.

Notice that there is no recommendation in the MEPDG regarding the most appropriate curing time to determine the CTE of concrete specimens for pavement design. The statistical results described in the previous paragraph support computing the CTE for pavement design at a curing time of 28 for days from a theoretical and practical point of view. The values at longer curing times appear not to be significantly different and demand longer waiting. On the other

hand, the values at shorter curing times produced statistically significantly higher CTEs that are probably not representative of the concrete behavior throughout most of the life the pavement.

B.6 EFFECT OF CTE ON PAVEMENT PERFORMANCE

The MEPDG [1] addresses many aspects that were missing or that were inadequately addressed in other pavement design procedures. The consideration of the CTE in the design procedure is perhaps one of the most important aspects addressed by the MEPDG. Its consideration gives the engineer a more site specific design possibility.

This section illustrates the effect of CTE on pavement performance by using the MEPDG. The effects of changes in CTE are shown for a Jointed Plain Concrete Pavement (JPCP) section with the characteristics shown in Table B-3. The purpose of the analysis is not to show absolute values of the different distresses as these may be different for different structural designs (slab thickness, use of dowels, joint spacing, etc.) and traffic and climate conditions but instead to illustrate the performance differences resulting from the different values of CTE for the different mixes and curing times. The analysis also intends to illustrate the difference between using a level 3 analysis (with a default CTE value for PCC mixes with basaltic aggregates suggested in the MEPDG manual of practice [22]) and using a level 2 analysis with the CTE value corresponding to each of the local mixes analyzed in this study.

A hierarchical method is employed in the MEPDG which includes three levels for specifying the CTE. Level-1 CTE input requires a CTE value of a mixture tested in the laboratory in compliance with AASHTO T 336 standard. In contrast, Level-3 CTE input requires the designer to estimate the most appropriate design input value of the material property based on experience with little or no testing. Published and default values are also used in this input level. Level-2 CTE inputs are estimated through correlations with other material properties that are measured in the laboratory or field. As a case in point, if the CTE values obtained here were utilized in further studies, they would have to be considered as Level-2 inputs.

Table B-3. Characteristics of the evaluation pavement section.

Parameter	Input
General	
Type of design	Jointed Plain Concrete Pavement (JPCP)
Design Life	35 years
Traffic	
Initial two-way annual AADTT	4500
Lanes in design direction	3
Operational speed	55 mph
Climate	
Location	Honolulu International Airport
Depth to water table	10 ft
Structure	
Joint spacing	15 ft
Dowels	Without and with dowels
Layers (from top to bottom)	
Portland Cement Concrete (PCC)	
Layer thickness	9 in.
Coefficient of Thermal Expansion	5.2×10^{-6} (default) and values in Table 2
Joint spacing	15 ft
Cement Stabilized	
Layer thickness	4 in.
Elastic/resilient modulus	2,000,000 psi
Crushed gravel	
Layer thickness	6 in.
Modulus	25,000 psi
Subgrade (CL)	
Layer thickness	∞
Modulus	16,000 psi

The structural design was obtained from an actual section of the H-1 freeway, near Kapolei in Oahu. The pavement section was built in 1966 and rehabilitated in 1986 (although the type of work done is not known, the original thickness in 1966 was 9" but the record for 1986 indicates a thickness of only 8.5"). Between 2010 and 2011, the section was retrofitted with dowel bars and diamond grinded. Axle load spectra, vehicle class distribution, and number of axles per vehicle were obtained from data for the Kalaeloa Weigh in Motion (WIM) station close to the section. For other traffic inputs and other variables not mentioned here, default values

were used. Except for the CTE, water cement ratio, and the amount of cement per cubic yard, all variables were held constant throughout the analysis.

For JPCP, the MEPDG provides estimates of the progression of the pavement distresses (faulting and fatigue cracking) as well as of the International Roughness Index (IRI). The controlling distress can vary from one design to the next depending on certain factors, including traffic characteristics, weather patterns, and the pavement section characteristics. For the particular design analyzed here, faulting was the limiting distress.

The effects of the estimated CTE for each mix at different curing times are the focus of the following paragraphs. Figure B-4 shows the estimated time to reach 0.12 in (0.3 mm) faulting at a 50% reliability for the design without dowel bars (i.e., it shows how long it would take to reach the threshold on average.) It can be observed that the variation in CTE caused by curing time translates directly into a high variation of the times to reach the threshold. Notice that the variation caused by curing time is similar in magnitude to the variation caused by the use of different mixes for a giving curing time. Therefore, the wide range of values presented in this graph supports the need to establish a standard curing time when determining an appropriate CTE for design.

Although the MEPDG is not yet calibrated for Hawaii and the criteria used for rehabilitating this pavement section are unknown, the estimated time to reach the threshold (~20 years at the longer curing times) does not appear unreasonable considering that the pavement received some rehabilitation after 20 years and needed to be retrofitted with dowel bars after another 24 years.

The figure also illustrates the substantial differences with the predictions obtained using the value of 5.2×10^{-6}/°F suggested in the MEPDG Manual of Practice [22] for mixes prepared with basaltic aggregates. Not surprisingly, a substantially better performance is predicted with this lower CTE value.

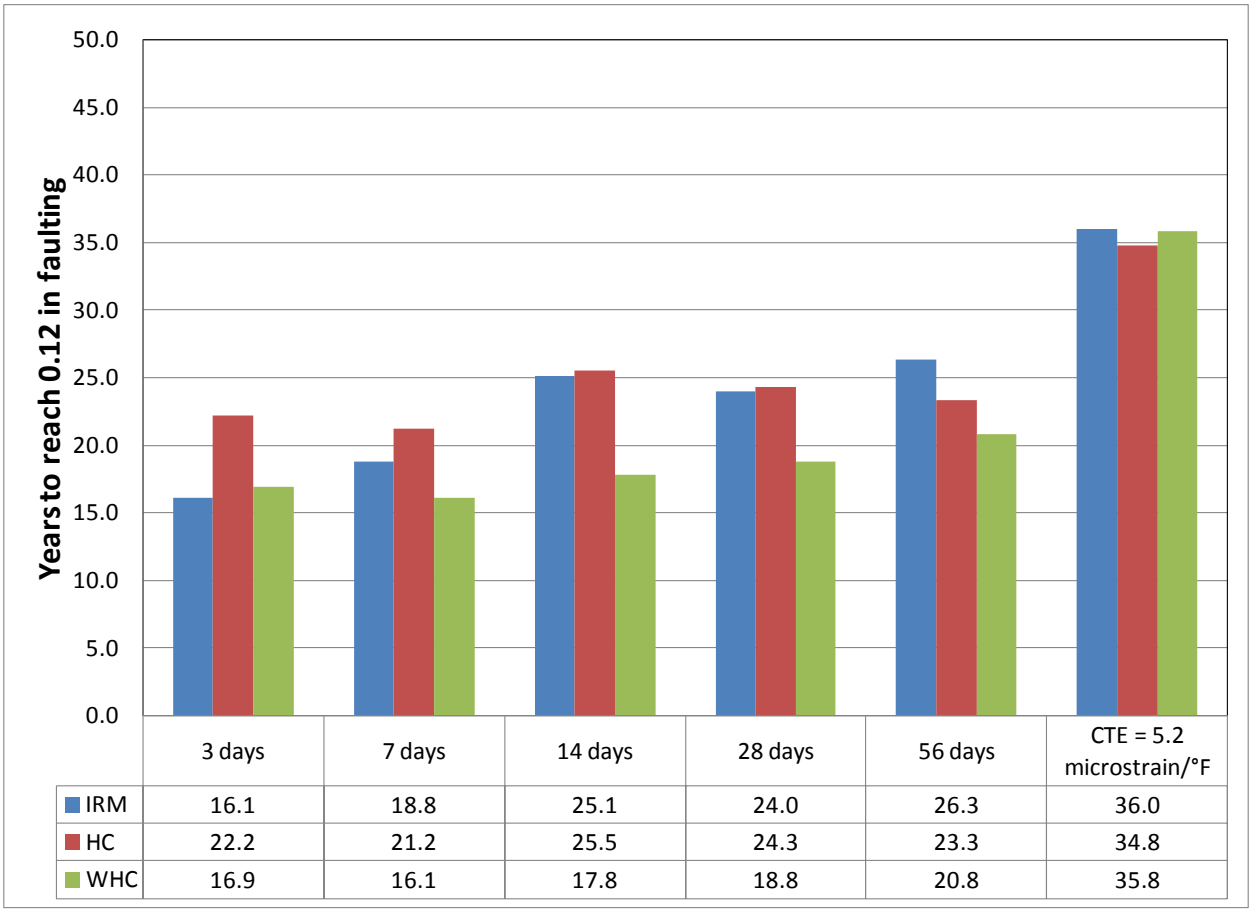

	3 days	7 days	14 days	28 days	56 days	CTE = 5.2 microstrain/°F
IRM	16.1	18.8	25.1	24.0	26.3	36.0
HC	22.2	21.2	25.5	24.3	23.3	34.8
WHC	16.9	16.1	17.8	18.8	20.8	35.8

Figure B-4. Effect of CTE on the predicted time to reach 0.12 in faulting at 50% reliability for a pavement design without dowels (IRM = Island Ready Mix, HC = Hawaiian Cement, and WHC = West Hawaii Concrete)

Figure B-5 shows the faulting values predicted after 35 years on the pavement section with dowel bars also with 50% reliability. For this particular pavement section, faulting is the governing distress with and without dowel bars. Again, the differences in the predicted values produced by different curing times are about the same order of magnitude as the differences produced by the different mixes. Furthermore, one can notice that the difference produced by the use of a not representative default value can be higher than the differences between mixes or curing times.

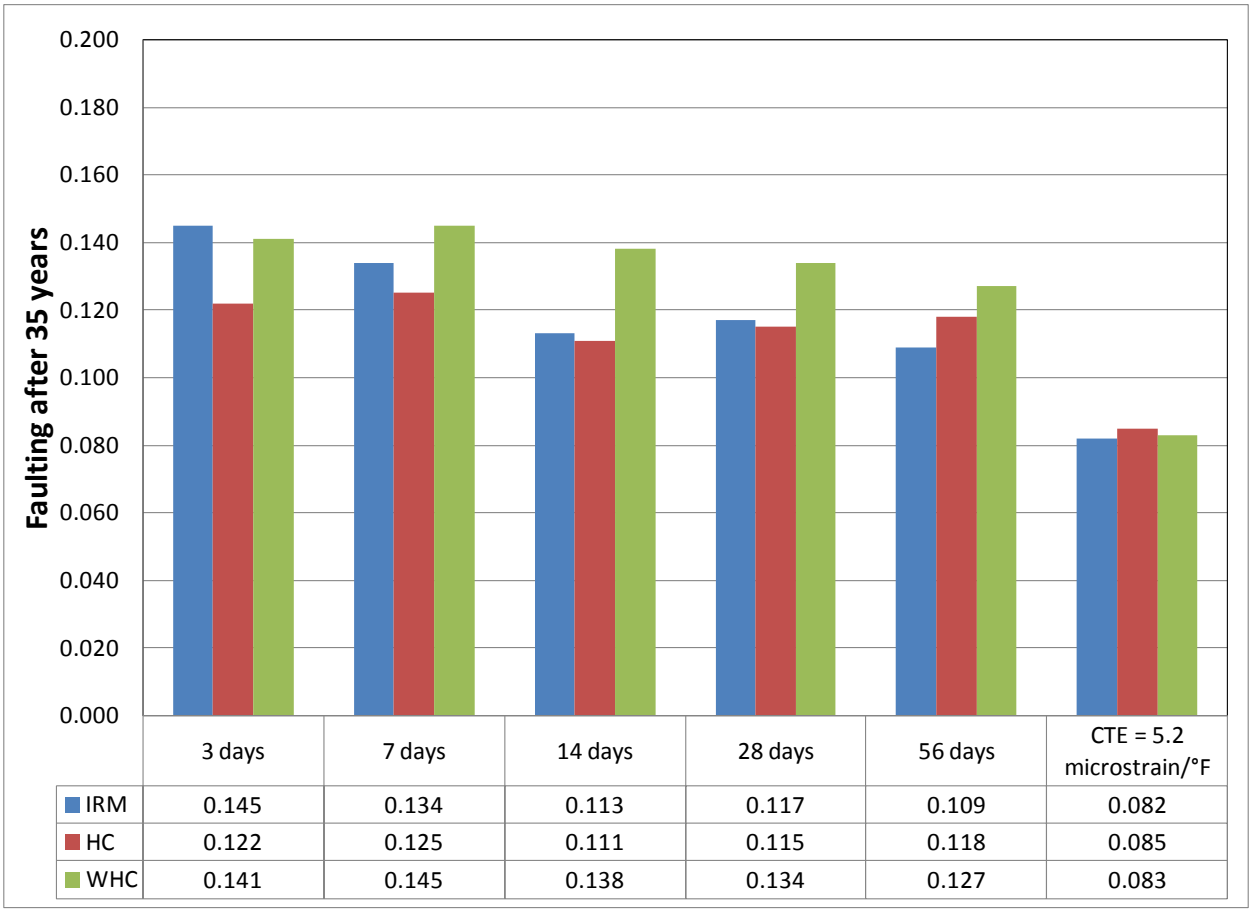

	3 days	7 days	14 days	28 days	56 days	CTE = 5.2 microstrain/°F
IRM	0.145	0.134	0.113	0.117	0.109	0.082
HC	0.122	0.125	0.111	0.115	0.118	0.085
WHC	0.141	0.145	0.138	0.134	0.127	0.083

Figure B-5. Effect of CTE on the predicted faulting at 50% reliability for a pavement design with dowels (IRM = Island Ready Mix, HC = Hawaiian Cement, and WHC = West Hawaii Concrete).

Although cracking does not govern the design in this case, it is instructive to analyze the effect of CTE on this distress as well since by changing some design parameters one could make this the critical distress. Figure B-6 illustrates the results for 90% reliability for the case with dowels. Using a 15% slabs cracked criterion, one can see that in this case a 35 years design could be considered acceptable or not depending on the mix used and on the curing time used to obtain the CTE.

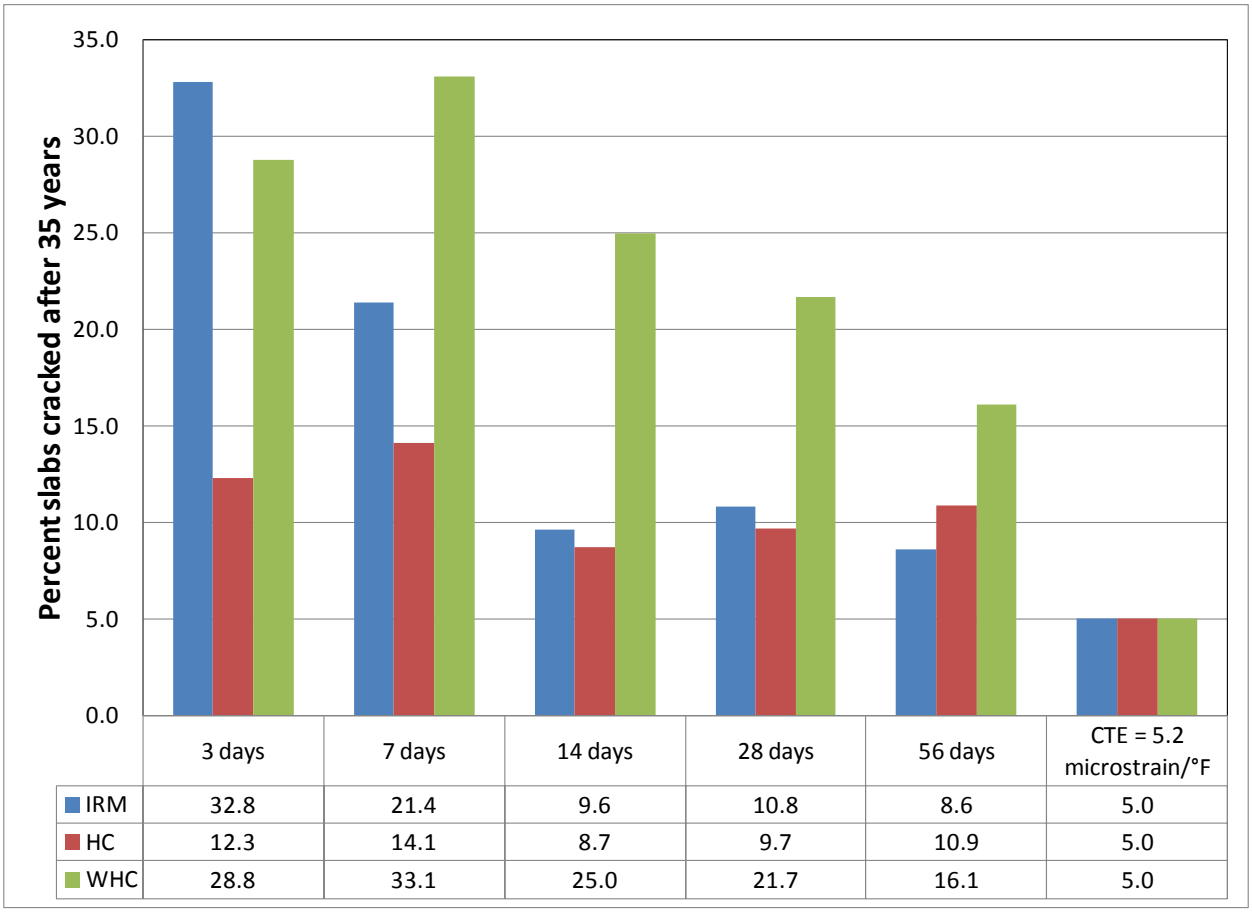

	3 days	7 days	14 days	28 days	56 days	CTE = 5.2 microstrain/°F
IRM	32.8	21.4	9.6	10.8	8.6	5.0
HC	12.3	14.1	8.7	9.7	10.9	5.0
WHC	28.8	33.1	25.0	21.7	16.1	5.0

Figure B-6. Effect of CTE on the predicted percent of slabs cracked at 90% reliability for a pavement design with dowels (IRM = Island Ready Mix, HC = Hawaiian Cement, and WHC = West Hawaii Concrete).

Similar observations can be made about the roughness output which is not presented here.

The wide range of values presented in the previous figures provides another argument towards the need to establish a standard for curing time when determining an appropriate CTE for a design.

As expected, in all cases, CTE affects the service life of the pavement, i.e. the higher the CTE, the shorter the expected service life.

B.7 CONCLUSIONS

The main conclusions of this study are:

- There is a large discrepancy between the CTE values found for Hawaiian mixes with basaltic aggregates (6.1 to 6.6 × 10-6/°F for 28 days curing) with the CTE value suggested in the MEPDG manual of practice [22] for a mix prepared with basaltic aggregates (5.2 × 10-6/°F). Use of the MEPDG suggested value would lead to significant differences in the predicted performance of the pavement.
- The MEPDG does not provide guidance about the curing time to use for the determination of the CTE. In this study, the CTE varied significantly until about the 28th day curing time and then it tended to stabilize. Thus, the value of the CTE at the 28th day curing time could be a reasonable choice for design purposes.

B.8 RECOMMENDATIONS

Although this study provides some useful information for the design of pavements in Hawaii, it also brings up additional questions. Further study could potentially focus on:

- Including more quarries to increase the reliability of the study, since due to time and economic constraints, only three of the potential quarries were studied.
- Perform a larger study to evaluate the effects of other mix characteristics.
- Study the effect of curing time more in depth so that it can be determined with more confidence whether the CTE increases with curing time, decreases with curing time, or whether the trend is affected by some other mix design variable.
- Perform a petrography analysis to study if the composition of the Hawaiian basalts can explain the larger CTE for the Hawaiian mixes when compared to mixes prepared with basaltic aggregates from the continental US.